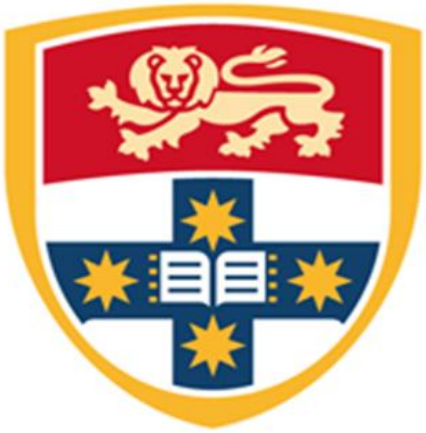

PIII treatment improves biocompatibility

by

Irina Kondyurina

A thesis submitted to fulfil requirements for the degree of
Doctor of Philosophy

At the

School of Medicine
The University of Sydney

2019

Statement of originality

The presented research in this thesis was carried out with the guidance and supervision of Prof. Shisan (Bob) Bao and Prof. Brett Hambly. **Except where specifically noted in the text, the presented work in this thesis is my primary work.**
The experimental work, analysis and writing of this thesis was undertaken between 2013 and 2017 in the School of Medicine of the University of Sydney. This study was supported by Australian Research Council and Australian Synchrotron Facility. The Raman spectra were recorded in Vibrational Spectroscopy Core Facility of University of Sydney. The NEXAFS spectra were recorded in Australian Synchrotron Facility.
The thesis is entirely my own work with advice from my supervisors except some separate study mentioned below. However, at times I have had to access equipment and resources outside Sydney University. I am grateful to the following people who have made this possible:
For Chapter 3, Dr. V. Shadrin (Institute of Continuous Media Mechanics of Russian Academy of Science, Perm, Russia) supervised and assisted when I conducted the cycling mechanical tests of my polyurethanes.
For Chapter 4, Dr. A. Kondyurin (University of Sydney) recorded the XPS spectra, Raman spectra and ellipsometry spectra for my samples. Mr. V. Chudinov (Perm State University, Perm, Russia) recorded ESR spectra for my samples.
For Chapter 6, Ms. Juichien Hung of the Heart Research Institute (Sydney) conducted the sewability of polyurethane shunt test in rat and thrombogenicity test for my samples. Implantation of the polyurethane samples into mice in University of Sydney was done with assistance from Prof. S. Bao.
Although the experiments were conducted outside of the University of Sydney, none of the material contained within this thesis has been presented for a degree at this or any other university.

My experimental preliminary work on the thesis's topic was undertaken between 1995 and 2001 in the Institute of Continuous Media Mechanics of the Russian Academy of Science (Perm, Russia) and at the Centre of secondary education "Detstvo" (Perm, Russia). It was here that for the first time the reduced immune reaction on ion beam treated polyurethane was observed. I continued the research at the Rossendorf Research Center (Dresden, Germany) from 2001-2005 where, for the first time, PIII treatment of polymers was successful for the improved cells, and protein adhesion and some biomedical applications were found. Then my studies were continued in the School of Physics at the University of Sydney from 2005-2013 where the dewetting effect of PLGA coating on drug release vascular stents was found and PIII treatment was proposed to reduce the dewetting. Boston Scientific and German Ministry of Economics supported these studies. These investigations were the foundation of the research presented in this thesis. **The results presented in Appendices are related to this thesis, but do not form a part of it.**

I certify that the intellectual content of this thesis is the product of my own work and that all the assistance received in preparing this thesis and all the sources have been acknowledged except where it is noted in the text.

Irina Kondyurina

Acknowledgements

Firstly, I would like to thank my supervisors Prof. Bob Bao and Prof. Brett Hambly for their guidance and support during my work.
I thank Prof. Marcela Bilek and Prof. David McKenzie for their advice and support of my studies before and during my PhD study in School of Physics as well as for providing employment in an equipped laboratory.
I thank Prof. Antony Wiess and Dr. Giselle Yeo for advice and support with ELISA test and providing tropoelastin in Charles Perkins Centre.
I thank Dr. Jenny Liu and Ms. Sanaz Maleki for assistance with preparation of histology samples.
I thank Prof. Wojciech Chrzanowski (Faculty of Pharmacy, University of Sydney) for advice and a possibility to measure AFM images.
I thank Dr. Ali Fathi (School of Bioengineering) for a possibility to do the mechanical test.
I thank Dr. Steven Wise and Ms. Juichien Hung for support of my cell work in Heart Research Institute and sewability test.
I also would like to thank Dr. Manfred Maitz for his assistance and support of my cell studies in Rossendorf Research Centre.
I would like to thank Dr. Reinhard Guenzel for his support and possibility to work with PIII system in Rossendorf Research Centre.
I would like to thank Prof. Valery Begishev and Dr. Vladimir Briskman for their support and advice at the beginning of my study in Institute of Continuous Media Mechanics.
I would like to thank all my colleagues for their advice, support and collaborations during my PhD study and before.
I thank Ms. Hayley Katzen for her advice and assistance with writing.
Special thanks to my son Tim Kondyurin and husband Prof. Alexey Kondyurin for their great help and patience.

Abstract

Global medical investigations have shown that cardio-vascular diseases cause 29% of all deaths that is 17 million people annually. Cardio-vascular diseases cause more deaths than car crash, cancer, tuberculosis and AIDS combined. In Australia 40% of total deaths are from cardio-vascular diseases, and the annual budget for cardio-vascular treatment is about $8.8 billion. Internationally about 80% of lethal cardio-vascular diseases occur in developing countries with low income.

In most cases of cardio-vascular disease a life can be saved by an operation that replaces organs or parts. One of the most common implants are heart implants or implants concerned with heart or vascular systems. An implantation of donor organs has many ethical problems and is limited by donor possibilities. Many patients die waiting for a donor organ to become available. Therefore, artificial implants may be the preferable way to save lives.

Modern artificial implants work successfully in organisms for more then 20 years. The success of the medical implant industry and surgery practice is proved by a high number of operations. Research has shown that 73% of people who received artificial heart implants survived after 9 years and 65% survived after 18 years, while only 48% of people who received the therapeutic treatment survived after 5 years. In the case of artificial aorta implants 85% of people survive after 5 years, while only 10% of people who received the therapeutic treatment survived after 5 years. Further development of the biomaterial science and surgery techniques can increase this difference.

Full biocompatibility of the implant with the organism is the goal. However, an intrusion of any artificial material into an organism causes a reaction of the organism's immune system. The immune reaction on the foreign body protects the organism against bacteria, viruses and injuries, and causes an isolation of the implant from the organism tissue that can break a functionality of the implant. In the worst case scenario the implant must be removed or replaced. This involves a secondary operation that increases the risk of lethality significantly, especially for elderly people who mostly need the implants. Research has shown that 100% of all artificial implants cause an immune reaction, and 35% of them require a secondary operation.

Therefore, the immune response of the organism on the artificial implant is a problem and must be solved. The artificial implant with absent or decreased immune response is necessary to save patients and to improve quality of life.

This research proves that the cross-linked non-soluble polyurethane can be synthesised so that it has adjustable mechanical properties comparable to soft tissue with low stiffness and sufficient mechanical strength, and which also has low residuals, is non-toxic and stable in the organism. We have modified the polyurethane with Plasma Immersion Ion Implantation (PIII) and created the active carbonised layer. The modified polyurethane implant was characterised with different physical and chemical methods and it was shown, that:
- Modified polyurethane has thin carbonised surface layer consisting of condensed aromatic structures like graphite or grapheme. The carbon atoms on the edge of this surface layer have unpaired electrons known as free radicals;

- These free radicals are responsible for the polyurethane implant's high hydrophilicity and high chemical activity, which allows the organism's protein to covalently attach to the implant surface forming total stable coverage.

The carbonised layer provides fast total endothelialisation of the implant surface like control TCP surface.

The polyurethane implants as disks were implanted subcutaneously in mice and the polyurethane graft replaced the abdominal aorta of a rat. The animal experiments and following histological investigations showed that the PIII treated implant causes significantly weaker immune response of the organism than the untreated implant. This is evidenced by the thinner collagen capsule ($p<0.001$), lower number and activity of macrophages ($p<0.001$), specific distribution of macrophages near the implant surface, less cell proliferation activity ($p<0.001$), less pro-inflammatory factor activity ($p<0.001$). In some cases the capsule and macrophages activity was absent. The absence of the immune reaction on an artificial soft polyurethane implant with PIII treatment is possible.

Conference presentations

1. I. Kondyurina, S. Bao, A. Kondyurin, M. Bilek, Synthesis of polyurethane materials for medical implants and improvement by plasma immersion ion implantation, USYD Pharmaceutical Student Symposium, American Association of Pharmaceutical Scientists (AAPS) Symposium, Sydney, Australia, September 16, 2016, oral presentation.
2. I. Kondyurina, S. Bao, A. Kondyurin, M. Bilek, PIII treatment of PU for medical implants, Bosch Institute Annual Scientific Meeting, ASM, July 21–22, 2016, poster.
3. I. Kondyurina, B. Bao, M. Bilek, A. Kondyurin, Polyurethane medical implants improved by plasma immersion ion implantation, Conference Condensed Matter and Materials, Wagga Wagga, Australia, 2-5 February 2016, poster.
4. I. Kondyurina, M. Bilek, A. Kondyurin, B. Bao, Polyurethane medical implants with improved biocompatibility, Inaugural CPC EMCR Symposium, Sydney, Australia, August 20-21, 2015, poster.
4. I. Kondyurina, S. Bao, A. Kondyurin, R. Bao, M. Bilek, Polyurethane medical implants improved by plasma immersion ion implantation, Bosch Institute Annual Scientific & Young Investigator's Meeting, Sydney, Australia, July 16-17, 2015, poster.
5. I. Kondyurina, A. Ngo, A. Kondyurin, B. Bao, M. Bilek, Polyurethane medical implants improved by plasma immersion ion implantation, 5th International Symposium of Surface and Interface of Biomaterials 24th and Annual Conference of the Australasian Society for Biomaterials and Tissue Engineering (ASBTE), Sydney, Australia, 7 - 10 April, 2015, oral presentation.
6. I. Kondyurina, S. Bao, A. Kondyurin, M. Bilek, Polyurethane for medical implants, Society of Plastic engineers (SPE) seminar, Sydney, Australia, October 30, 2014, poster and oral presentation.
7. I. Kondyurina, R. Bao, A. Kondyurin, M. Bilek, B. Bao, Plasma immersion ion implantation of PU biomedical implants, 12th APCPST (Asia Pacific Conference on Plasma Science and Technology) and 27th SPSM (Symposium on Plasma Science for Materials), Adelaide, Australia, August 31 – September 5, 2014, poster.
8. I. Kondyurina, R. Bao, A. Kondyurin, M. Bilek, B. Bao, Polyurethane implants improved by plasma immersion ion implantation, 5th World Congress on Biotechnology, Valencia, Spain, June 25-27, 2014, abstract and poster.

List of figures

List of Tables

Abbreviations

AFM - Atomic force microscopy
ATR – Attenuated Total Reflection
BSA – Bovine Serum Albumin
DA - 3,3'-dichlor,4,4'-diaminediphenylmethane
DBD - dibutyl dilaurate of Stannum
DMFA – dimethylformamide
EDA - ethylene diamine
ePTFE - expanded polytetrafluor ethylene
ESR - electron spin resonance
FBR - Foreign Body Reaction
FDA - Food and Drag Administration
Fg - fibrinogen
FTIR – Fourier Transform Infrared (spectroscopy)
H&E - Hematoxylin-Eosin
HCAEC - human coronary artery endothelial cells
HDFs - human dermal fibroblasts
HRP – Horseradish peroxidase
IHC - Immunohistochemistry
LAS - Laboratory Animal Services
LDPE – Low Density Polyethylene
NEXAFS - Near edge X-ray absorption fine structure
MCP – Multichannel Photo amplifier
PA - polyamide
PE - polyethylene
PEG - polyethylene glycol
PET - polyethylene terephthalate
PDMS - polydimethylsiloxane
PI - polyimide
PIII – Plasma Immersion Ion Implantation
PMMA - poly-methyl-methacrylate
PMN - polymorphonuclear
POTM - polyoxitetramethylene
POP - polyoxipropylene
PP - polypropylene
PPG - polypropylene glycol
PTFE – polytetrafluoro ethylene, Teflon
PTHF - polytetrahydrofuran
PVDF - polyvinylidene fluoride
PU - polyurethane
SDS - Sodium dodecyl sulphate
TCP - Tissue culture plastic
TDI - 2,4-toluenediisocyanate
TE – tropoelastin
TMB - 3,3,5,5'- Tetramethylbenzidine
UV - ultraviolet
vWF - von Willebrand Factor
XPS – X-ray Photoelectron Spectroscopy

Table of Contents

Chapter 1. Introduction

The results of global medical investigations show that cardio-vascular diseases are the cause of about 29% of all deaths, that is 17 million people annually. Cardio-vascular diseases cause more deaths than car crash, cancer, tuberculosis and AIDS combined. Internationally about 80% of lethal cardio-vascular diseases occur in developing countries with low income. In Australia 40% of total deaths are from cardio-vascular diseases. The treatment of cardio-vascular disease is very expensive: higher than for all other diseases. In Australia the annual budget for cardio-vascular treatment is about $8.8 billion.

In most cases an operation replacing organs or parts could save lives. One of the most common implants are heart implants or implants concerned with heart or vascular systems. An implantation of donor organs has many ethical problems and is limited by donor possibilities. The long waiting list for donor organs kills many patients. Therefore, the most preferable way is to use artificial implants.

The success of the medical implant industry and surgery practice is proved by a high number of operations. In the USA annually more than 13 million devices are implanted.

Modern artificial implants work successfully in organisms for more then 20 years. Research has shown that 73% of people who received artificial heart implants survived after 9 years and 65% survived after 18 years, while only 48% of people who received the therapeutic treatment survived after 5 years. In the case of artificial aorta implants 85% of people survive after 5 years, while only 10% of people who received the therapeutic treatment survived after 5 years. Further development of the biomaterial science and surgery techniques can increase this difference.

1.1. Materials for medical implants and biocompatibility problems

Artificial implants for soft tissue are made of polymer materials such as polyvinylidene fluoride (PVDF), polyethylene (PE), polypropylene (PP), polydimethylsiloxane (PDMS), parylene, polyamide (PA), polyimide (PI), polytetrafluoroethylene (PTFE), poly-methyl-methacrylate (PMMA) and polyurethane (PU) [1-4]. These materials satisfy the requirements for biomedical devices approved by the USA's Food and Drug Administration (FDA). Australia follows their regulations.

Following FDA classification cardiovascular implants such as pacemaker, implantable cardio defibrillator, ventricular assist device, heart valve, blood vessel, catheter are made of PP, PE, PTFE, PA, PET, PDMS; cochlear, staples and nasal implants are made of PDMS, parylene, PE; penile implant, Foley implant, urinary sphincter, hernia or vaginal mesh are made of PDMS, PE, PTFE, PA, PP; breast implant, cheek, jaw and chin implants, lip implant, hip implant are made of PP, PET, PTFE, PDMS; intrauterine device, intravaginal ring, urogynecologic mesh implant,

fetal micro-pacemaker are made of PDMS, PP, PU; retinal prosthesis, intraocular lens, glaucoma valve, orbital implant, ophthalmic implant are made of PMMA, PE, PTFE, PA.

These materials have been tested and approved by the FDA as providing an acceptable level of cytotoxicity, sensitization, irritation, acute systematic toxicity, sub-chronic toxicity, genotoxicity, hemocompatibility, chronic toxicity, carcinogenicity, reproductive developmental and biodegradation [5]. The most stringent requirements are applied to the materials used for long term implants (more then 30 days of an implant in the organism are considered as permanent) and sensitive organs such as ophthalmic devices. Materials for implants are selected based on conditions in the organism such as mechanical loading and movement, pH environment, aggressive liquids, and on the functionality of the implant such as electro-conductivity or electro-resistivity, mechanical strength, softness and elasticity, multiple cyclic loads, low or high friction, required biodegradation rate, and corrosiveness. The product of biodegradation must satisfy the biocompatible requirements too. Also the materials for implant must be sterilisable by certified methods such as ethylene oxide, steam, UV irradiation or γ-irradiation.

In practice, however, even a complete satisfaction of these requirements does not always mean a full biocompatibility. An intrusion of any artificial material into an organism will cause a reaction of the immune system of the organism [6]. This reaction on the foreign body protects the organism against bacteria, viruses and injuries. The immune reaction causes an isolation of the implant from the organism tissue and can break a functionality of the implant. Most of the implantable materials that have been approved cause acute and chronic inflammatory response. In the worst case scenario the implant must be removed or replaced. A secondary operation significantly increases the risk of lethality, especially for elderly people who mostly need the implants. Research has shown that 100% of all artificial implants cause an immune reaction, and 35% of them require a secondary operation.

Patients are selected for cardio vascular surgery based on the health of their immune systems. Patients who are rejected are left to die, never being given an opportunity to have the surgery. However, many of the people who require an operation are elderly and suffer from a number of different diseases, such as diabetes, which compromise the immune system. Whatever one's views on the prolongation of human life, cardio vascular operations can significantly improve the functionality and quality of life for the sufferer and their family.

The immune response of the organism on the artificial implant is therefore the problem that must be solved. An artificial implant with absent or decreased immune response is the simplest and cheapest way of saving patients' lives and improving quality of life.

1.2. Surface of medical implants and reaction of organism

An organism contacts the medical implant via an implant surface. The surface can be characterised by surface energy and its polar and non-polar parts, surface chemistry as active chemical groups accessible to any kind of organism molecules, surface topography and the mechanical properties of the surface layer. The surface energy of

a polymer implant is in the range from 20 to 45 MJ/m. Most of the implant materials are hydrophobic with low polar part of the surface energy. The hydrophilic implants such as hydrogels have high polar part of the surface energy due to swelling in water. However, such implants have limited application due to low mechanical properties. When an implant is placed into the organism, the implant surface contacts the organism's liquids such as blood and intercellular liquids. At this contact the proteins are firstly absorbed on the implant surface [7].

The proteins can be absorbed on the surface via intermolecular interaction of different kinds [8, 9]. The proteins have hydrophobic and hydrophilic aminoacid residuals that create a wide range of interactions depending on the protein conformation. In the water media the hydrophilic residuals are predominantly on the external side of the protein molecule. When the polymer implant is placed in the organism, the proteins contact the polymer surface and adjust their conformation to minimise the free energy [10-12].

The immune reaction is a complex of biochemical reactions and immune cell activity [13]. The insertion of the implant begins with a cut of the soft tissue. Even without the implant, the immune system reacts on the tissue damage. A few seconds after the cut the blood vessels are activated, the blood stream increases and the immune cells within the blood stream come to the wound. The interaction between blood and air changes the conformation of the blood proteins such as fibrinogen, the albumin, the laminin, the tissue factors, the complement cascade (5) and others on the surface liquid-gas due to surface tension [14].

The immune cells recognise the conformation of the proteins and release cytokines to start the intrinsic coagulation cascade, thrombosis, complement systems, platelets and leukocytes. As a result, the thrombus clot forms. In a few minutes the cells such as polymorphonuclear leukocyte (PMN), neutrophils and monocytes come and take part in the lysis process of the tissue's damaged cells. If the wound is small, the tissue can be regenerated after the lysis of the damaged cells and the cell damaging products are removed. In the case of bacterial infection or a big wound the macrophages and monocytes come to the damaged tissue and take part in the lysis of the bacterial cells creating a capsule, which isolates the damaged tissue from the rest of the organism. This can take days. The damaged tissue, the bacteria and all the products of the lysis must be removed from the blood for the immune reaction to be stopped. The worse case scenario is that scar tissue remains after the complete immune reaction.

An ideal candidate for an implant is expected to have a similar reaction of the immune system. When the implant is placed in the cut, the blood contacts the implant surface. The proteins from the blood stream come to the interface blood-implant. If the proteins do not change the conformation of this interface, the immune cells are not activated. However, the materials used for the modern implant change the conformation of the proteins due to the different interaction of proteins with the implant surface. As a result, the immune cells are activated and a cascade of immune reactions starts.

In contrast to the simple cut, the permanent presence of the implant causes a permanent immune reaction. The immune reaction on the implant has three stages. During the first stage the proteins are absorbed on the implant surface and PMN,

neutrophils and monocytes are activated and collected near the implant. In the case of a biodegradable implant, the lysing factors (enzymes, proteases, reactive oxygen species) can degrade the implant material. When the degradation of the material is complete, the immune reaction stops. However, usually the implants are made of stable materials and lysing factors cannot degrade the implant. The neutrophils release large amounts of signalling factors to attract more cells including factors to differentiate monocytes into macrophages, which play a significant role in the following stages of the immune response. During the second stage the immune reaction is characterised by the presence of macrophages, foreign body giant cells and lymphocytes and the formation of granular tissue. At this stage the macrophages, giant cells, T-lymphocyte and other cells release a number of cytokines and growth factors such as PDGF, TNF, TGF, IL-1 and others. These cytokines and growth factors regulate cell migration, differentiation and proliferation that heal wounds by growing new blood vessels with endothelial cells or collagen tissue growing with fibroblasts. If the activity of immune cells is high and the signalling factors continue to be released, the collagen capsule can grow into a thick fibrosis shell and calcify in the later stages.

Regulating immune cell activity by stopping or decreasing the release of active factors like cytokine secretion decreases the resistance of the whole organism to bacterial disease and other wound healing. The immune reaction can be minimised or stopped with medications. However, an implant with drug release to regulate immune cell activity has a limited time frame for the drug release, and a high probability of causing local bacterial infection at the time of operation. The decrease of the immune reaction intensity can be achieved with fast endothelialisation of the implant's surface [15]. However, the endothelialisation process of modern materials is not fast enough to avoid the immune reaction.

For example, two materials clinically approved are mostly used for synthetic conduits: polyethylene terephthalate (PET) and expanded polytetrafluor ethylene (ePTFE). However these materials remain thrombogenic, cause permanent immune response with chronic inflammation, and a luminal coating of endothelial cells is not formed. As a result the conduit's size is limited to a minimal diameter of 6 mm for a successful operation. The problem is that smaller diameter conduits show a significantly higher risk of occlusion [16].

Therefore, the immune response on artificial implants remains a significant problem for polymer implants.

1.3. Synthesis of medical polyurethanes

Of the various prospective biomaterials, polyurethanes (PU) are considered one of the best materials for implants. Polyurethane is a broad class of materials that always has the urethane group in its chain. Most ways of synthesis are based on poly-condensation reactions of the isocyanate group with hydroxyl, carboxyl or amine groups. Modern PUs are block copolymers with 'hard' and 'soft' domains of macromolecule, having glass transition temperatures above and below room temperature respectively. They are extensively used in medicine due to their biological inertness, low toxicity and the wide range of mechanical properties.

Modern polyurethanes are used for short-term devices such as blood and urinary catheters [17], syringe tips, pipes and bags for blood circulation system, tissue scaffolds [18, 19], as well as long-term devices such as artificial diaphragm membranes, artificial joints, meniscal prosthetics [20], breast prosthetic shells [21], artificial hearts [22, 23], bones [24] and other orthopaedic devices [25]. PU has also been widely used in the manufacture of vascular grafts [26-31], because of its ability to create compliant, durable materials. Past iterations of PU constructs have suffered from a combination of lack of appreciation of their biological destination (see below) and a failure to tune their biological interface prior to implantation [32]. The development of hybrid materials has the potential to increase biocompatibility [33].

The mechanical and biodegradation properties of polyurethanes vary depending on the selection of specific monomer groups for inclusion in the backbone [34]. Polyester oligomers used as soft blocks, are susceptible to hydrolysis facilitating the high biodegradability required for dissolving sutures and surgical glue [35]. The products of glycolysis and hydrolysis of biodegradable PU are non-toxic and released from the body in the urine. Highly stable polyurethanes, like the ones required for long-term implants, on the other hand, can be obtained by using carbonate oligomers and co-polymers [36].

The mechanical properties of PU can be varied over an extremely wide range through the chemistry of isocyanate ‘hard’ domain, the length of the polyol ‘soft’ domain, the soft/hard domain ratio and by controlling microphase separation during synthesis. The extent of microphase separation can be increased through annealing, exposure to solvents and/or the addition of plasticiser during synthesis [37, 38]. Short chain PU, with a low soft/hard domain ratio, are used for prosthetic implants where mechanical strength is required. Long chain polyols, with high soft/hard domain ratio are used for soft implants where mechanical properties similar to soft tissue are required. The large range of mechanical properties attainable makes PU a universal material suitable for augmenting the wide range of tissues and organs that can be implanted [39]. PU is particularly attractive for meeting the challenge of vascular conduits matching surrounding vessels with sufficient strength at high pressures. The tunability of PU formulations allows for close matching of these target vessels, whose mechanical properties vary depending on anatomical location.

Despite its popularity as a biomaterial, the less than ideal biocompatibility of PU still presents problems in most applications. When PU implants come into contact with body fluids the immune system recognizes them as foreign bodies and initiates an immune response. This foreign body response is typically triggered by interactions between the PU surface and proteins of the organism. The surface of polyurethane is hydrophobic and proteins that are adsorbed on the PU surface become denatured and change their conformation.

There are polyurethanes certified for medical applications including long-term implants. All these polyurethanes are much harder than the soft tissue of an organism [40-44]. The hard material causes mechanical damage in the surrounding tissues, which also causes an immune response. When very soft polyurethane is synthesised to tune the stiffness of the polyurethane implant to the stiffness of the soft tissue it is difficult to keep sufficient mechanical strength.

The modern commercial polyurethanes are mostly linear polymers or thermoplastic [45]. These polyurethanes can be softened with high temperatures in preforms or can be dissolved in selected solvents for casting. Such polyurethanes are limited. They all have a high stiffness because high mechanical strength of linear polyurethanes is associated with high stiffness. Usually polyurethane contains residuals as byproducts of the synthesis. Such residuals cannot be washed out from linear polyurethane in solvents, and an adhesion of casted or moulded linear polyurethane coating to a metal medical device is usually weak. It would be more effective to synthesise the polyurethane coating directly on medical implantable devices [46].

It follows that polyurethane synthesis suitable for medical implants in soft tissues remains a significant problem.

1.4. Plasma and ion beam methods modification of polymer materials

Plasma treatment methods are used for improvement of biocompatibility for different kinds of polymers [47-49]. The plasma's effect is based on macromolecule destruction with the formation of active groups predominantly oxygen-containing groups in the surface layer, improved wettability, developed surface roughness and hardening of the surface layer [50, 51]. An advantage of the plasma methods is the thin surface modification while the bulk polymer remains virginal. Therefore, all the polymer implant's exploitation properties remain in their initial form and only the surface can be adjusted to fulfil the requirements of biocompatibility.

The plasma methods can be classified according to the energy of ions. One of the methods, ion beam implantation, bombards ions with high energy so that the kinetic energy of ions is much higher then any chemical bond in the polymer [52, 53]. However, ion beam implantation methods require large machines with a small diameter ion beam. The most practical method is plasma immersion ion implantation (PIII), where the ion beam is formed in the plasma chamber over the polymer implant [54]. Such PIII system consists of a vacuum chamber with a rotary pump and a turbomolecular pump providing basic pressure of $1e^{-5}$ Torr, a plasma generator in high frequency (MHz) or ultrahigh frequency (GHz) range, a pulsed high voltage power supply generating pulses of high voltage (1-20 keV) in microsecond range duration. To prevent the polymer burning the total average current must be in the μA range.

Ion beam implantation and PIII have been used for the treatment of many kinds of polymers to improve adhesion, wettability, hardness, optical properties, crosslinking, stability and so on [55, 56]. Polyurethanes have also been treated by ion beam implantation and PIII to form a carbonised layer on the surface [57, 58].

Biocompatibility of polyurethanes was improved by ion beam implantation as reported by Suzuki [59] and others [60-63]. Later it was shown that the polyurethane in mammary implants can also be improved with ion beam implantation [64]. The cells and protein adsorption was improved with PIII treatment for PTFE, polyethylene, polystyrene, nylon and other polymers [65-69]. It was shown that the ion bombardment creates a carbonised layer on the surface, which is rich with condensed aromatic structures like graphene or graphite. Such structures stabilise

unpaired electrons at carbon atoms on the edges of aromatic rings [70, 71]. These carbon atoms at the edge of the aromatic structures with unpaired electrons are called free radicals and are very active to any molecule able to donor a proton [72]. The stabilised unpaired electrons can be preserved in condensed aromatic structures for a long time before they take part in chemical bond formation with protein molecules [73]. The formed chemical bond between the condensed aromatic structures and protein molecules is stable and cannot be destroyed with any detergent.

At the same time, the unpaired electrons are very energetic providing high surface energy of the carbonised layer with high contribution of polar interactions. The polar interactions provide high hydrophilicity of the carbonised surface in such a way that the protein adsorbed on such surface does not change conformation [74.]. Consequently, the high activity of the ion beam implanted surface of the polymer attaches the protein molecule to the stable covalent bond, which provides preservation of the initial conformation of protein [75]. The activity of the carbonised layer can be sufficient to provide total protein coverage of the surface. Therefore, the ion beam implantation and PIII treatment has the potential to create a carbonised surface layer, which can provide a stable bioactive protein layer totally covering the polymer surface.

This research investigated the PIII treatment of newly synthesised polyurethane and the reaction of the organism to it.

1.5. Aims of this research and structure of this thesis

The aim of this study was to develop a new polyurethane formula with adjusted mechanical properties and plasma related methods of surface modification, which decrease the immune response of the organism when the polyurethane medical device is implanted into the organism.

The study had the following stages:

1. To synthesise cross-linked non-soluble polyurethane with adjusted mechanical properties to soft tissue with low stiffness and sufficient mechanical strength so that it has low residuals, is non-toxic and stable in the organism, and then to modify the polyurethane with PIII to get an active carbonised layer with its characterisation. The synthesised material should comply with FDA and ISO 10993 standards for implantable materials suitable for long-term functionality in organisms. These results are described in Chapter 3 and 4.

2. To investigate *in vitro* the interactions of the modified polyurethane surface with biologically significant components of an organism such as proteins and cells. These results are described in Chapter 5.

3. To investigate the immune response of the organism *in vivo* to the modified polyurethane implant and to consider the applications of PIII treated polyurethane for biomedical devices. These results are described in Chapter 6.

The chemicals and experimental methods used in the present study are described in Chapter 2.

Appendices contain the supporting results and the applications of modified polyurethanes in biomedical devices.

References

1. Malmsten M., 2003, Biopolymers at Interfaces, New York: Dekker; Ratner BD. Biomaterials science : an introduction to materials in medicine. 3rd ed. Amsterdam ; Boston: Elsevier/Academic Press; 2013.
2. A. Mata, A.J. Fleischman, S. Roy, Characterization of Polydimethylsiloxane (PDMS) Properties for Biomedical Micro/Nanosystems, Biomedical Microdevices 7:4, 2005, 281–293.
3. H. Plank, I. Syre, M. Dauner and G. Egbers, Polyurethanes in Biomedical Engineering, Volume II. Elsevier, Amsterdam, 1987.
4. Materials and coatings for medical devices. Cardiovascular. Ed. By S.D.Henry. Materials Park: ASM International, 2009.
5. A.J.T. Teo, A. Mishra, I. Park, Y.-J. Kim, W.-T. Park, Y.-J. Yoon, Polymeric Biomaterials for Medical Implants and Devices, ACS Biomater. Sci. Eng., 2, 2016, 454−472.
6. W.K. Ward, A Review of the Foreign-body Response to Subcutaneously-implanted Devices: The Role of Macrophages and Cytokines in Biofouling and Fibrosis, Journal of Diabetes Science and Technology, 2, 2008, 768-777.
7. D.G. Castner, B.D. Ratner, Biomedical surface science: Foundations to frontiers, Surface Science, 500, 2002, 28–60.
8. H. Chen, L. Yuan, W. Song, Z. Wu, D. Li, Biocompatible polymer materials: Role of protein–surface interactions, Progress in Polymer Science, 33, 2008, 1059–1087.
9. M Bellion, L Santen, H Mantz, H Hahl, A Quinn, A Nagel, C Gilow, C Weitenberg, Y Schmitt, K Jacobs, Protein adsorption on tailored substrates: long-range forces and conformational changes, J. Phys.: Condens. Matter, 20, 2008, 404226 (11pp).
10. H. Noha, E.A. Vogler, Volumetric interpretation of protein adsorption: Mass and energy balance for albumin adsorption to particulate adsorbents with incrementally increasing hydrophilicity, Biomaterials, 27, 2006, 5801–5812.
11. Sethuraman A, Han M, Kane RS, Belfort G. Effect of surface wettability on the adhesion of proteins. Langmuir, 20 (18), 2004, 7779–88.
12. Nygren H, Elam JH, Stenberg M. Adsorption of coagulation proteins and adhesion and activation of platelets at the blood–solid interface. An experimental study of human whole blood. Acta Physiol Scand, 133, 1988, 573–577.
13. X. Wang, Overview on Biocompatibilities of Implantable Biomaterials, in Advances in Biomaterials Science and Biomedical Applications, http://dx.doi.org/10.5772/53461.
14. W.-J. Hu, J.W. Eaton, L. Tang, Molecular basis of biomaterial-mediated foreign body reactions, Blood, 98 (4), 2001, 1231-1238.
15. W.C. Aird, Phenotypic Heterogeneity of the Endothelium I. Structure, Function, and Mechanisms, Circ Res., 100, 2007, 158-173.
16. M.S. Lord, W. Yu, B. Cheng, A. Simmons, L. Poole-Warren, J.M. Whitelock, The modulation of platelet and endothelial cell adhesion to vascular graft materials by perlecan, Biomaterials, 30, 2009, 4898–4906.

17. P. Klement, Y.J. Du, L.R. Berry, P. Tressel, A.K.C. Chan, Biomaterials, 27, 2006, 5107-5117.
18. M.R. Williamson, R. Black, C. Kielty, Biomaterials, 27 (2006) 3608-3616.; J.Y. Zhang, B.A. Doll, E.J. Beckman, J.O. Hollinger, Tissue Engineering, 9, 2003, 1143-1157.
19. J.E. McBane, S. Sharifpoor, K. Cai, R.S. Labow, J.P. Santerre, Biomaterials, 32, 2011, 6034-6044.
20. J.H. de Groot, R. de Vrijer, A.J. Pennings, J. Klompmaker, R.P.H. Veth, H.W.B. Jansen, Biomaterials, 17, 1996, 163-173.
21. N. Handel, J. Gutierrez, Aesthetic Surgery Journal, 26, 2006, 265-274.
22. D.J. Wheatley, L. Raco, G.M. Bernacca, I. Sim, P.R. Belcher, J.S. Boyd, Polyurethane: material for the next generation of heart valve prostheses?, European Journal of Cardio-thoracic Surgery, 17, 2000, 440-448.
23. S.J. Stachelek, C. Song, I. Alferiev, S. Defelice, X. Cui, J.M. Connolly, R.W. Bianco, R.J. Levy, Localized gene delivery using antibody tethered adenovirus from polyurethane heart valve cusps and intra-aortic implants. Gene Ther, 11, 2004, 15-24.
24. M. Bil, J. Ryszkowska, P. Wosniak, K.J. Kurzydcowski, M.C. Lewandowska-Szumie, Acta Biomaterialia, 6, 2010, 2501-2510.
25. M.D. Lelah, S.L. Cooper, Polyurethanes in medicine, CRC Press, 1986, 225.
26. J.H. Ashton, J.A.M. Mertz, J.L. Harper, M.J. Slepian, J.L. Mills, D.V. McGrath, J.P. Vande Geest, Acta Biomaterialia, 7, 2011, 287-294.
27. J. Robin, S. Martinot, A. Curtil, C. Vedrinne, F. Tronc, M. Franck, G. Champsaur, Experimental right ventricle to pulmonary artery discontinuity: outcome of polyurethane valved conduits, The journal of Thoracic and Cardiovascular Surgery, 115 (4), 2007, 898-903.
28. V. Thomas, T.V. Kumari, M. Jayabalan, Biomacromolecules, 2, 2001, 588-596.
29. J.P. Theron, J.H. Knoetze, R.D. Sanderson, R. Hunter, K. Mequanint, T. Franz, P. Zilla, D. Bezuidenhout, Acta Biomaterialia, 6, 2010, 2434-2447.
30. T.-W. Chuang, K.S. Masters, Regulation of polyurethane hemocompatibility and endothelialization by tethered hyaluronic acid oligosaccharides. Biomaterials, 30, 2009, 5341-5351.
31. F. Hess, S. Steeghs, R. Jerusalem, O. Reijnders, C. Jerusalem, B. Braun, P. Grande, Patency and Morphology of Fibrous Polyurethane Vascular Prostheses Implanted in the Femoral Artery of Dogs after Seeding with Subcultivated Endothelial Cells, Eur J VascSurg, 7, 1993, 402-408.
32. A.R. Smith, J.L. Garrison, W.B. Greene, D.S. Raso, The Clinical, Histologic and Ultrastructural Presentation of Polyvinyl sponge Breast Prosthesis Removed for Massive Fluid Accumulation, Plastic and Reconstructive Surgery, 103(7), 1999, 1970-1974.
33. M. Tatterton, S.P. Wilshaw, E. Ingham, S. Homer-Vanniasinkam, Vascular and endovascular surgery, 2012.
34. K.A. Murray, J.E. Kennedy, B. McEvoy, O. Vrain, D. Ryan, R. Cowman, C.L. Higginbotham, The influence of electron beam irradiation conducted in air on the thermal, chemical, structural and surface properties of medical grade polyurethane, European Polymer Journal, 49, 2013, 1782–1795.
35. F. Saleh, B. Palmieri, D. Lodi, K. Al-Sebeih, International Journal of Medical Sciences, 5, 2008, 354-360.
36. D.J. Martin, L.A. Poole Warren, P.A. Gunatillake, S.J. McCarthy, G.F. Meijs, K. Schindhelm, Biomaterials, 21, 2000, 1021-1029.
37. Szycher M. Szychers handbook of polyurethanes. Boca Raton: CRC. Press; 1999.

38. G.E. Oertel, C. Hanser, Polyurethanes, Verlag, München-Wien, 1993.
39. J.P. Santerre, K. Woodhouse, G. Laroche, R.S. Labow, Biomaterials, 26, 2005, 7457-7470.
40. U. Braun, E. Lorenz, C. Weimann, H. Sturm, I. Karimov, J. Ettl, R. Meier, W.A. Wohlgemuth, H. Berger, M. Wildgruber, Mechanic and surface properties of central-venous port catheters after removal: A comparison of polyurethane and silicon rubber materials, J of the mechanical behaviour of biomedical materials, 64, 2016, 281-291.
41. V. Kanyanta, A. Ivankovic, Mechanical characterisation of polyurethane elastomer for biomedical applications, J of the mechanical behaviour of biomedical materials, 3, 2010, 51–62.
42. S.M. Wells, E. J. Walter, Changes in the Mechanical Properties and Residual Strain of Elastic Tissue in the Developing Fetal Aorta, Annals of Biomedical Engineering, 38 (2), 2010, 345–356.
43. K. Miller, Method of testing very soft biological tissues in compression, Journal of Biomechanics, 38, 2005, 153–158.
44. H. Saraf, K.T. Ramesh, A.M. Lennon, A.C. Merkle, J.C. Roberts, Mechanical properties of soft human tissues under dynamic loading, Journal of Biomechanics, 40, 2007, 1960–1967.
45. A. Boubakri, N. Haddar, K. Elleuch, Y. Bienvenu, Influence of thermal aging on tensile and creep behavior of thermoplastic polyurethane, C. R. Mecanique, 339, 2011, 666–673.
46. Y. Farhatnia, J.H. Pang, A. Darbyshire, R. Dee, A. Tan, A.M. Seifalian, Next generation covered stents made from nanocomposite materials: A complete assessment of uniformity, integrity and biomechanical properties, Nanomedicine: Nanotechnology, Biology, and Medicine, 12, 2016, 1–12.
47. P.K. Chu, J.Y. Chen, L.P. Wang, N. Huang, Plasma-surface modification of biomaterials, Materials Science and Engineering, 36, 2002, 143–206.
48. J. Jagielski, A. Piatkowska, P. Aubert, L. Thomé, A. Turos, A.A. Kader, Ion implantation for surface modification of biomaterials, Surface & Coatings Technology, 200, 2006, 6355–6361.
49. Pignataro B, Conte E, Scandurra A, Marletta G. Improved cell adhesion to ion beam-irradiated polymer surfaces. Biomaterials, 18, 1997, 1461–1470.
50. G. Marletta, Ion-beam modification of polymer surfaces for biological applications, in Materials science with ion beams, ed. by Harry Bernas, Springer, 2010, 345-371.
51. Ion Beams in nanoscience and technology, Ed. by R.Hellborg, H.J.Whitlow, Y.Zhang, Springer, 2009.
52. Handbook of Ion Implantation Technology, Ed. By J.F.Ziegler, Elsevier, 2003.
53. V.B. Odzhaev, I.P. Kozlov, V.N. Popok, D.B. Sviridov, Ion Implantation of Polymers. Minsk: Belorussian State University, 1998.
54. Handbook of Plasma Immersion Ion Implantation and Deposition, Ed. by A. Anders, Wiley-Interscience, 2000.
55. Fink, D., Fundamentals of Ion-Irradiated Polymers, Berlin, Springer, 2004.
56. Kondyurin, A., Bilek, M., Ion Beam Treatment of Polymers: Application Aspects from Medicine to Space. 2nd ed., Amsterdam, Elsevier, 2015.
57. J.J. Murphy, M. Patel, S.J. Powell, P.F. Smith, Volatile evolution induced by energetic He++ ions in a poly(ester) based polyurethane, Radiation Physics and Chemistry, 63, 2002, 101–108.

58. Kondyurin A.V., M.F.Maitz, V.A.Romanova, V.P.Begishev, I.V.Kondyurina, R.Guenzel, Drug release from polyureaurethane coating modified by plasma immersion ion implantation, J. Biomater. Sci. Polymer Edn., 15(2), 2004, 145-159.
59. Y. Suzuki, M. Kusakabe, J.-S. Lee, M. Kaibara, M. Iwaki, H. Sasabe, Endothelial cell adhesion to ion implanted polymers, Nucl.Instr. Meth., B65, 1992, 142-147.
60. K. Kurotobi, M. Kaibara, Y. Suzuki, M. Iwaki, H. Nakajima, S. Kaneko, Ion implantation into collagen-coated surfaces for the development of small diameter artificial grafts, Colloids and Surfaces B: Biointerfaces, 19, 2000, 227–235.
61. Melnig V, Apetroaei N, Dumitrascu N, Suzuki Y, Tura V. Improvement of polyurethane surface biocompatibility by plasma and ion beam techniques. J Optoelectron Adv Mater, 7, 2005, 2521–2528.
62. Kusakabe M, Suzuki Y, Nakao A, Kaibara M, Iwaki M, Scholl M. Control of endothelial cell adhesion to polymer surface by ion implantation. Polym Adv Technol 12, 2001, 453–460.
63. Bacakova, L., Svorcik, V., Rybka, V., Micek, I., et al., Adhesion and proliferation of cultured human aortic smooth muscle cells on polystyrene implanted with N+, F+ and Ar+ ions: Correlation with polymer surface polarity and carbonization. Biomaterials, 17, 1996, 1121-1126.
64. Begishev V., Gavrilov N., Mesyats G., Klyachkin Yu., Kondyurina I., Kondyurin A., Osorgina I., Modification of polyurethane endoprosthetics surface by pulse ion beam, Proc. of 12th Intern. Conf. on High-Power Particle Beams, Haifa, Israel, June 7-12, 1998, 2, p. 997-1000.
65. Kondyurin A., Maitz M.F., Surface Modification of ePTFE and Implants using the same, US patent WO 2007/022174 A3, 2007.
66. Bilek M., McKenzie D., Nosworthy N., Kondyurin A., Activated polymers binding biological molecules, WO 2007104107 (A1), Australian Patent Application Number 2007225021 (PCT/AU2007/000321), 2009.
67. B.K. Gan, A. Kondyurin, M.M.M. Bilek, Comparison of Protein Surface Attachment on Untreated and Plasma Immersion Ion Implantation Treated Polystyrene: Protein Islands and Carpet, Langmuir, 23, 2007, 2741-2746.
68. A.Kondyurin, N.J. Nosworthy, M.M.M. Bilek, R.Jones, P.J. Pigram, Surface Attachment of Horseradish Peroxidase to Nylon Modified by Plasma-Immersion Ion Implantation, Journal of Applied Polymer Science, vol. 120, pp. 2891–2903, 2011.;
69. A. Kondyurin, N.J. Nosworthy, M.M.M. Bilek, Attachment of horseradish peroxidase to polytetrafluorethylene (teflon) after plasma immersion ion implantation, Acta Biomaterialia, 4, 2008, 1218–1225.
70. I.C. Lewis, L.S. Singer, Electron spin resonance of stable aromatic radical intermediates in pyrolysis, Carbon, 1969, 7, 93-99; K. Yamaguchi, Theoretical studies of free radical reactions IV. Selection rules, Chemical Physics, 25, 1977, 215-235.
71. S.E. Stein, R.L. Brown, Chemical theory of graphite-like molecules, Carbon, 23(1), 1985, 105-109.
72. Mesyats G., Klyachkin Yu., Gavrilov N., Kondyurin A., Adhesion of Polytetrafluorethylene modified by an ion beam, Vacuum, 52, 1999, 285-289.
73. M.M.M. Bilek, D.V. Bax, A. Kondyurin, Y. Yin, N.J. Nosworthy, K. Fisher, A. Waterhouse, A.S. Weiss, C.G. dos Remedios, D.R. McKenzie, Free radical functionalization of surfaces to prevent adverse responses to biomedical devices, Proceedings of National Academy of Science, 108(35), 2011, 14405–14410.
74. A. Kondyurin, N.J. Nosworthy, M.M.M. Bilek, Effect of Low Molecular Weight Additives on Immobilization Strength, Activity, and Conformation of Protein Immobilized on PVC and UHMWPE, Langmuir, 27, 2011, 6138–6148.

75. Bilek, M.M.M., Biofunctionalization of surfaces by energetic ion implantation: Review of progress on applications in implantable biomedical devices and antibody microarrays. Applied Surface Science, 310, 2014, 3-10.

Chapter 2. Materials and methods

This chapter describes the general methods and materials used in this thesis. Particular materials and methods applied in experiments are described in subsequent chapters.

2.1. Materials and chemicals

Polyurethane pellets of Pellethane 2103 and Pellethane 2363-80 were purchased from Dow Chemical (Germany). Pellethane 2103 is a polyurethane for general use. Pellethane 2363-80 is a polyurethane for biomedical applications.

A co-polymer of polyoxitetramethylene (POTM) and polyoxipropylene (POP) glycol (trademark PF-OP-15, MM=2000) with an oxitetramethylene/oxipropylene monomer chain ratio of 85:15 was purchased from Kirovskiy plant (Perm, Russia). Chemicals 2,4-toluenediisocyanate (TDI), 3,3'-dichlor,4,4'-diaminediphenylmethane (DA), dibutyl dilaurate of Stannum (DBD), polytetrahydrofuran (PTHF), polyethylene glycol (PEG), ethylene diamine (EDA) and polypropylene glycol (PPG), ethylacetate, acetone, toluene, tributylphosphate and dimethylformamide (DMFA) were purchased from Aldrich (Sydney, Australia). Oligomer of polyoxypropylene glycol with MDI extender was purchased from ERA Polymers Pty Ltd (Sydney, Australia).

Polypropylene glycol terminated by toluenediisocyanate (PPG-TDI) was purchased from Aldrich (Germany). Polyglycol Lapronol 1200 was purchased from BASF (Germany).

ePTFE sheets, vascular stents with PLGA coating and PLGA pellets were provided by Boston Scientific SCIMED, USA. Polytetrafluorethylene (Teflon) film of 20 mm thickness was purchased from Galogen plant (Perm, Russia).

Stainless steel urinary catheters with variable geometry from URINAE Frommelius GmbH used in experiments were 1500 mm in length and 2 mm in wire diameter. Starting at a distance of 300 mm from the end of the catheter, the diameter decreases gradually reaching 0.2 mm at the other end.

Acrylamide with 0.1% of Tetramethylethylenediamine inhibitor of polymerization was purchased from Aldrich (Germany).

2.2. Methods for implant preparation and analysis

Ion beam treatment
The ion beam accelerator "Pulsar" (Institute of Technical Chemistry, Perm, Russia) was used for ion beam treatment of the polymers. The accelerator has a vacuum chamber with ultimate pressure of $3x10^{-3}$ Pa provided by rotary and diffusion pumps. The working pressure of $5x10^{-2}$ Pa was provided by nitrogen flux via needle valve. The plasma was generated in hollow cathode under 2 kV pulse of 300 μSec duration with 1 Hz frequency repetition. The permanent high voltage potential was applied to

the electrostatic optical system to extract the nitrogen ions from the plasma cloud and to accelerate to the polymer target with energy of 20 and 30 keV. The beam diameter with uniform current distribution was about 100 mm.

The ion current on the target was measured using Faraday cap, which has additional screening electrode under 2 kV potential to bring back secondary electrons from the bottom of the cap. Average ion current density was not higher then 1 $\mu A/cm^2$ to prevent overheating of the samples. The bulk measurements of temperature after the longest treatment time and highest ion current density 1 $\mu A/cm^2$ was not higher then 40^0C. The pressure, bias, plasma density and ion current were monitored during the treatment.

Some samples of polyurethane were treated by ion beam accelerator ILU-3 (Physical-technical Institute, Kazan, Russia). The pressure in the vacuum chamber was 10^{-3} Pa achieved by rotary and diffusion pumps. The samples were treated by nitrogen ions with energy of 20 keV and fluence range of 10^{13}-10^{16} ions/cm^2. The current density of the ion beam was 10 $\mu A/cm^2$ at the area of 100x5 mm^2. The beam was scanned on the target surface with the frequency of 10 Hz to prevent overheating. The average ion current was about 1 $\mu A/cm^2$. The temperature of the sample was lower then 40^0C.

Plasma immersion ion implantation (PIII)
The Plasma immersion ion implantation (University of Sydney, Sydney, Australia) used for treatment consists of a vacuum chamber equipped with dry scroll pump and turbomolecular pump. The pumps provide a basic pressure up to 10^{-6} Torr. The working pressure of 2 mTorrs was provided by nitrogen flux via needle valve of flow controller (MKS, USA). The plasma of 100 W was generated by rf-generator EMI (13.75 MHz). Plasma power was transported to the chamber via an inductive antenna through the glass part of the vacuum chamber. The magnetic coils were placed on the top part of the vacuum chamber made of aluminium. The coil current was adjusted to get uniform distribution of the plasma bar to intensify the treatment and to exclude aluminium deposition from the chamber walls to the polymer samples. The high voltage electrode used as a sample holder of 150 mm diameter was made of stainless steel and mounted on top of the vacuum chamber. The holder was cleaned with ethanol. The sample of polyurethane was fixed on the sample holder with springs or scotch tape. The sample was covered by mesh electrode made of stainless steel, which was electrically connected to the sample holder. The distance from mesh to the sample was 50 mm. The mesh electrode provided uniform distribution of the ion current on the sample surface. The high voltage pulse from Pulse high voltage supply (ANSTO, Sydney, Australia) was applied to the sample holder via high voltage 50 Ohm inductive resistivity cable and high voltage input. The pulse amplitude was 20 kV at 20 mSec duration and 50 Hz repetition frequency. The average current including capacitance charge current in the cable was 1.4-1.5 mA.

The fluence of the PIII treatment was estimated from UV-spectra of LDPE film of 50 mM thickness. This LDPE film was treated for different time periods with 20 keV energy nitrogen ions and calibrated using UV spectra of the same film treated by the "Pulsar" accelerator with the same parameters and known ion fluence measured with the Faraday cap. The used fluence range of $5x10^{13}$-10^{16} ions/cm^2 corresponded to 40-800 sec of the treatment time.

The same experimental setup was used for the polyurethane capillary internal treatment. The geometry and parameters of this treatment are described in Chapters 4 and 7.

Some samples of polyurethane were treated in PIII system in Rossendorf Centre (Dresden, Germany). The system consists of a vacuum chamber equipped with rotary and turbomolecular pumps providing basic pressure of 10^{-4} Pa. The working nitrogen pressure of 10^{-2} Pa was provided by the flow controller. The plasma was generated by electron cyclotron resonance source with density of 10^{10} cm^{-3} and electron temperature of 9 eV. The high voltage pulse of 20 keV energy and 5 μSec duration was applied to the sample holder. The sample of polyurethane was placed on the sample holder and covered by stainless steel mesh. The distance between the sample surface and the mesh was 30 mm.

Wettability
A contact angle device DS-10 (KRUSS, Germany) was used to measure contact angles of deionized water and diiodomethane (Aldrich, Australia) on the surface of polyurethane. The sessile drop method was used for an analysis of the drop shape. The surface energy of polyurethane was calculated using Owner-Wendt-Rabel-Kaelble method developed for total surface energy, dispersive and polar parts analysis. Rabel method parameters such as 53.6 MJ/m for polar part of surface energy and 18.7 MJ/m for dispersive part of surface energy for water and 0 MJ/m for polar part of surface energy and 50.8 MJ/m for dispersive part of surface energy for diiodomethane were used for calculation of the surface energy for polyurethanes. The measurements of the contact angle were done for a minimum of 5 drops for one sample on the smooth polyurethane surface central area. The edge area of the samples was excluded. Every new drop was placed on a virgin part of the surface to exclude any contamination from the previous drops. The drop was kept for 5-10 seconds after it was dropped to ensure the drop had a stable shape for analysis. The results of the measurements of untreated polyurethane were compared with the literature data for polyurethanes.

Fourier transform infrared spectra
Fourier transform infrared (FTIR) spectra were recorded using a Digilab FTS7000 FTIR spectrometer (Agilent, Australia) and Bomem (Toronto, Canada) FTIR spectrometer with DTGS detectors. The number of scans was 100 with a spectral resolution of 4 cm^{-1}.

Fourier transform infrared attenuated total reflection (FTIR ATR) spectra were recorded using a Digilab FTS7000 FTIR spectrometer equipped with a multi-bounce ATR accessory with a trapezium germanium crystal at an incidence angle of 45° (Harrick, USA). The number of scans was 500 with a spectral resolution of 4 cm^{-1}. Analysis of spectra was made with Grams software (Galactic, USA).

Micro FTIR ATR spectra were recorded with Vertex 70 FTIR spectrometer (Bruker, Germany) equipped with FTIR microscope and Ge prism crystal and MCT liquid nitrogen cooled detector. The sample area for the spectra recording was 100 μm diameter. The number of scans was 100 with a spectral resolution of 1 cm^{-1}.

FTIR ATR spectra were recorded at an IFS-66 spectrometer (Bruker, Germany). FTIR ATR spectra were recorded with the ATR accessory on KRS-5 and Ge crystal. The number of scans was 100 with a spectral resolution of 1 cm^{-1}. Analysis of spectra was made with the help of the OPUS program (Bruker, Germany).

FTIR ATR spectra were recorded on Nicolet Magna spectrometer with Ge ATR crystal with a 45^0 incident angle. The number of scans was 100 with a spectral resolution of 2 cm^{-1}.

Quantitative measurements of the characteristic line absorbance were conducted using Bouger-Lambert-Beer law and basic line methods. For ATR spectra the ratio of absorbance for analytical line and internal standard line was used.

X-ray photoelectron spectroscopy
X-ray photoelectron spectra (XPS) were recorded on spectrometer equipped with Al Kα X-ray source (1486.6 eV exciting line) and X-ray beam monochromator (SPECS, Germany). The X-ray source power was 200 W. PHOIBOS 150−9 MCD hemispherical analyser with a detector of 9 channeltrons working simultaneously with energy shift calibrated by the software was used. The energy was calibrated by $Au_{4f7/2}$ 83.98 eV line of the gold sample. The electron gun was used to compensate a surface charge on the surface of polyurethane sample. The survey spectra were recorded at 30 eV passing energy and 2 scans with 1 eV step in 50-1200 eV range of energy for an analysis of surface contamination. The detail spectra of C_{1s}, O_{1s} and N_{1s} regions of high spectral resolution were recorded at 23 eV passing energy and minimum 10 scans with 0.1 eV step. The peaks were fitted with Gaussian-Lorentzian components using Marquardt-Levenberg fitting procedure in CASA software. The peaks were quantified with the sensitivity factor individualised to each element and used for atomic concentration calculations. The charge shift was calibrated on C_{1s} line corresponded to C-C bond at 285 eV position.

Raman spectroscopy
Micro-Raman spectra were recorded in 180^0 degree geometry excited by Nd:YAG laser line of secondary harmonic (532.14 nm wavelength) on a diffraction double monochromators HR800 (Jobin Yvon) equipped with LabRam 010 positioning system (Lastek, Australia). Corresponding notch filters were used to exclude parasite lines and the laser beam line. The CCD matrix was used for detection of the Raman scattering signal. The optical microscope was used to focus the laser beam in thin polyurethane surface. The objective 100 was used. The laser beam power was adjusted to avoid any trace of carbonisation on the surface. The absence of burning under the laser beam was proved with repeating the spectra at the same place. The method of delay measurements was used to bleach the sample with the laser beam to exclude a fluorescence signal. The spectral resolution was 4 cm^{-1}. The spectral range of survey spectra was 100-4000 cm-1. The detail spectra were recorded in 200-2000 cm^{-1}. The number of scans between 10 and 100 and the dwelling time of 0.1-1 sec range were selected to get sufficient signal noise ratio.

Near edge X-ray absorption fine structure (NEXAFS) spectra of polyurethane
X-ray absorption spectroscopy was performed on untreated and 800 sec PIII treated polyurethane using the soft X-ray beam line of the Australian Synchrotron. The near edge X-ray absorption fine structure (NEXAFS) on the C1s and N1s regions was

recorded using the MCT detector (spectra from bulk) and channeltron detector (spectra from surface). The X-rays were polarised horizontally and the sample was tilted at an angle of 90°o to the incoming beam. Variations in X-ray intensity with energy were extracted from the measured spectra using the signal generated from a standard gold covered grid. Contributions to the C1s NEXAFS from contamination in the beam line were determined by replacing the sample with a reference photodiode and collecting a spectrum, which was then used to correct the spectra from the polyurethane samples.

Electron spin resonance spectra
The electron spin resonance spectra (ESR) were recorded using Adani electron spin resonance spectrometer (Minsk, Belarus). The polyurethane samples of 20x40 mm^2 area were rolled and placed inside a quartz capillary tube. The tube was placed into the cavity of the spectrometer. The spectrometer was calibrated using a weak pitch KCl sample. Measurements were taken in X band at 20^0C. Ten scans were taken per sample to get sufficient signal/noise ratio.

Atomic force microscopy
The surface topography of the polyurethane was measured with Atomic force microscopy (AFM) using Park System device (Park System, South Korea) in tapping mode with a speed of 1 Hz and amplitude 10 nm. Statistics from 3 to 5 different places of one sample were measured with 10x10, 1x1 mm and 0.3x0.3 mm areas. The resulting images were analysed with Gwyddion software and WM&S software.

The hardness of the surface polyurethane layer was measured with AFM Dimension 3100 (Digital Instruments Veeco Metrology Group, USA) in a contact mode. A silicon probe with a cantilever spring constant of 20 nN/nm and a resonance frequency 300 kHz was used. The tip radius of curvature was measured by imaging standard gold particles and determined to be 20 nm. The tip vibration frequency in the contact mode was 0.5 Hz. Digital Instruments' software with compensating lateral motion was used for data analysis. A silicon wafer, LDPE plate and PTFE plate were used as reference materials for analysis of the hardness of the polyurethane.

Optical microscopy
The surface of polyurethanes were analysed with optical microscope Axioplan2Imaging (Zeiss, Germany) in reflective mode with 10, 20 and 50 objectives. The microscope was equipped with CCD camera. The standard plate was used to calibrate the scale of images.

Ellipsometry
The thickness of the modified layer and the optical constants were measured with optical ellipsometry using Woollam M2000V spectroscopic ellipsometer. The spectra in 250-1000 nm wavelength were collected for 55, 60, 65, 70 and 75 degrees of the incident angle of the light beam. The number of spectral scans was selected to get sufficient signal/noise ratio. Cauchy layer was used for fitting the experimental data of the untreated polyurethane to get the optical constants. These optical constants of untreated polyurethane were used for analysis of multilayer model of the modified polyurethane.

Friction measurements

The friction experiments were done using a friction measurement system (Rossendorf Research Center, Germany). The measurements were done with a Cr6 alloy ball of 5 mm diameter that moved periodically on the polyurethane surface. Polyurethane coatings were synthesised on stainless steel for the friction measurement. The amplitude of the balls motion was 6 mm and its speed was 6 mm/s. The normal force applied to the ball was 0.65 N. The friction coefficient was averaged over the first 50–80 cycles of the indenter. Longer motion caused a damage of the polyurethane coating and was not used for analysis.

Leaching residuals from polyurethane
The polyurethane samples (0.3 mm thick) were pre-weighed and placed in deionized water for 7 days in a sealed glass beaker. Samples were then dried in air for 24 h and then in a vacuum oven for 8 h. The samples were then re-weighed and the relative mass loss attributed to leached components was calculated. For an analysis of leached components, water from the beaker was placed on a germanium ATR crystal and dried. Attenuated total reflection Fourier-transform infrared (ATR-FTIR) spectra were measured using a Digilab FTS7000 FTIR spectrometer fitted with ATR accessory. A control spectrum was taken using water from a beaker stored in the same environment but without PU.

Crosslinking test for polyurethane
Polyurethane samples were tested for swelling in a "good" solvent to assess cross-linking of macromolecules [ASTM D 471-97(1998)]. PU film samples (0.3 mm thick) were weighed, placed in dimethylformamide and hexane in sealed beakers. Samples were allowed to swell for 24 h. The samples were weighed immediately after removal from the beakers, then dried for 24 h in open air and re-weighed.

Mechanical tests for polyurethane
Mechanical properties of the polyurethanes were tested using an Instron 5943 with a 100 N load cell according to the ASTM D412-06a (ASTM International, 2006) protocol. The samples were cut to $1\times0.8\times5$ cm^3 size. Each kind of polyurethane was tested with 3 identical samples. The load sensor and extensometer were calibrated prior to the test. To prevent specimen slipping during the test, hydraulic clamps were used. The polyurethane was loaded at a constant strain rate of 500 mm/min to 100% stretch and then relaxed to 0% stretch. This cycle was repeated 3 times before the polyurethane samples were stretched to failure. The Young's modulus was obtained by calculating the slope of the stress–strain curve at 100%. The tensile strength and modulus at breakage was calculated using the maximum strain at the breaking point.

A lower load cycling test was also carried out to assess performance during loads compatible with those experienced in the vasculature. One hundred cycles up to 10% strain at a constant strain rate were applied at a frequency of 1 Hz.

2.3. Methods *in vitro* investigations

Protein attachment
The polyurethane samples were incubated in protein (Tropoelastin, Poly-L-Lysine, BSA or HRP) solution for 24 hours at room temperature in 75 mm sterile Petri dishes with the samples on the bottom totally covered with the solution. Protein was diluted

to 20 μg/ml in 10 mM sodium phosphate buffer pH 7. After incubation, the samples were removed from the Petri dish, dried with Kim-Wipe tissue for 3-5 seconds, placed into glass beakers with the buffer for 1 minute, then dried with Kim-Wipe tissue for 3-5 seconds and placed into another new Petri dish with 15 ml of wash buffer (10 mM sodium phosphate buffer pH 7) for 1 hour. After that the samples were placed into glass beakers with the buffer for 1 minute, dried with Kim-Wipe tissue for 3-5 seconds, placed into glass beakers with deionised water for 1 minute and dried with Kim-Wipe tissue for 3-5 seconds. The samples were then placed into new dry Petri dish and dried overnight. Spectroscopic analysis was then conducted on these samples.

Washing protein with detergent
The polyurethane samples were placed into falcon tubes with 45 ml of 2% sodium dodecyl sulphate (SDS) solution in deionised water. The tubes were placed into a water bath at 70^0C temperature and kept there for 1 hour. After that the samples were washed with deionised water 6 times. In some experiments the Tween 20 detergent was used instead of SDS.

Activity assay
HRP activity was measured by clamping the polyurethane samples between two stainless steel plates separated by an O-ring (inner diameter was 8 mm, outer diameter was 11 mm). The top plate contained a 5 mm diameter hole. 3,3,5,5'-Tetramethylbenzidine (TMB; Sigma T0440) was added to the hole. After 30 s TMB was removed and added to 50 μl of 2 M HCl followed by 25 μl of unreacted TMB to make up the volume to 100 μl. Optical density was then measured at a wavelength of 450 nm using UV spectrophotometer.

Cell attachment
In experiments with cells, polyurethane discs with the surface area of 0.58 cm2 ethanol sterilized were mounted in Minusheets (Minucells and Minutissue, Bad Abbach). The bovine aortic endothelial cell line GM7373 (Coriell) was used for the experiments. 4×10^4 cells in 200 μL medium (MEM-Earle supplemented with 10% fetal bovine serum (FBS), 1 × MEM vitamins, 2 mM N-acetyl l-alanyl l-glutamine, 1×amino acids) were seeded directly on the samples. They were allowed to adhere for 2 hours at standard cell culture conditions, then the medium was filled up to 1 mL per sample. Three days after seeding the cells were fixed in 0.2% paraformaldehyde in PBS and stained with rhodamine. Images were taken by fluorescent microscopy with a video camera.

2.4. Methods *in vivo* investigations

Mouse operations
In this experiment the strain "wild-type" C57Bl/6 male mice were used. The mice were provided by the Laboratory Animal Services (LAS) of Sydney University. The weight of the mice was about 20g each. An intra-peritoneal injection of Avertin of 0.125 mg per gram of mouse weight was used for anaesthesia. Sterile conditions were maintained during the surgery. The back of each mouse was shaved and smeared with a betadine solution. Polyurethane samples were implanted subcutaneously in 6 pockets (two rows side by side) on the back of each mouse. The sample order in each

mouse was done in such a way that some mice held the samples with different PIII treatment time and some mice held similar samples in different pockets. The position of the samples in mice and in the pockets was taken into account at the histological and immunohistochemistry analysis as described in Chapter 6. The cuts were sewed with silk sutures. The mice were marked on tails with non-toxic permanent marker.

After the surgery 5 mice were kept in each cage with food and water provided. All mice were housed under standard conditions in the Bosch Animal facility and observed on a day-to-day basis following the standard protocol for post-surgery. The mice were euthanized (cervical dislocation) after 7 days.

Preparation samples from the mice
Freezing and Paraffin tissue fixing:
Samples of tissue with ingrown implants (10x10 mm) from euthanized mice were collected and immediately immersed in 75% ethanol at 4^0C. The samples were left in the fridge overnight, then immersed to 100% ethanol for fixing (4 hrs at 4^0C). The samples were placed into an automated tissue processor for overnight tissue processing program.

Table. 3.1 Step by step description of automated tissue processing program.

Solution	Conditions
70% Ethanol	40 mins
80% Ethanol	40 mins
95% Ethanol	40 mins
100% Ethanol	2 change 1hr and1.5 hrs
Xylene	2 change 1hr and 1.5 hrs
Liquid paraffin under vacuum	60^0C, 4 changes 1.5hrs each

Embedding and sectioning tissue:
Fixed samples of tissue with ingrown PU disks were embedded in molten paraffin wax and hardened at room temperature. Each sample was cut on a rotary microtome into 5μm sections. The sections were lifted from the 45°C floated bath onto glass slides. The Aquadhere 5% v/v (Menzel-Glaser, Germany) was used for histochemical staining. SuperFrost Plus (Australia) was used for immunohistochemical staining. The slides were dried in an oven at 37°C overnight.

Histopathology
Transverse sections (5 μm) of the capsule with the implants were deparaffinised and hematoxylin-eosin stained (H&E) to determine total cell number in the capsule.

The protocol of H&E was followed:
- Deparaffinising slides in 2 changes of xylene for 10 mins each;
- Rehydration in alcohol 100%, 95%, 70% then in tap water of 2 mins each;
- Application of Harri's haematoxylin for 3 mins;
- Washing in tap water;
- Dipping 3 times in acid alcohol (70% of ethanol in HCl);
- Dipping in a solution of Scott's bluing for 30 secs;
- Washing in tap water;

- Checking the quality of colour with microscope;
- Dipping once in 70% ethanol solution;
- Application of Eosin twice for 30 sec each time;
- Dehydration in alcohol of 70%, 95%, 100%;
- Clearing in xylene twice for 10 mins each;
- Mounting with DPX.

Milligan's Trichrome staining:
- Deparaffinising slides in 2 changes of xylene for 10 mins each;
- Rehydration in alcohol of 100%, 95%, 70% then in tap water for 2 mins each;
- Application of Weigert's haematoxylin for 5 mins;
- Application of Scott's solution for 30 sec;
- Application of Mordant solution for 6 mins;
- Rinsing in water;
- Placing in 0.1% acid fushin solution for 6.5 mins;
- Placing in 1% phosphomolybdic acid solution for 3.5 mins;
- Placing in 2% orange G solution for 7.5 mins;
- Washing in deionized water for 8 mins;
- Placing in 1% of acetic acid for 3 mins;
- Dipping quickly into 95% of ethanol 4 times;
- Drying in air;
- Dehydration in alcohol of 70%, 95%, 100%;
- Clearing in xylene twice for 10 mins each;
- Mounting with DPX.

The micro-photos were taken with the Nikon microscope (Japan), and the software ImageJ Pro Plus 7 with macros was used for statistical analysis of the capsule thickness. The statistical analysis was done using software GraphPad Prism Version 5.0. The ANOVA analysis and Bonferroni Post-test were used to compare the results between the two groups, and in each group. The significance of the difference between the two groups was accepted at $p<0.05$ (*), $p<0.01$ (**) and $p<0.001$ (***).

Immunohistochemistry
A number of protocols were applied to the slides to analyse specific cells and their activity.

Endothelial cells Von Willebrand Factor IHC staining protocol:
- Deparaffinising slides in 2 changes of xylene for 10 mins each;
- Rehydration in 2 changes of xylene 10 mins each, in alcohol of 100%, 95%, 70% then in tap water for 2 mins each;
- Quenching for 20 mins in H_2O_2 endogenous peroxidase (solution of 49.5 ml of methanol and 0.5 ml of 30% H_2O_2);
- Washing slides in TBS (Tweens) for 3 times for 3 mins each;
- Incubating in DAKO Target Retrieval solution of pH 9.0 at 37^0C for 20 mins;
- Cooling at room temperature for 10 mins;
- Rinsing in TBS (Tweens) twice;
- Applying monoclonal rabbit anti-human VWF primary antibody at 1:200 dilution for 60 mins;
- Rinsing in TBS (Tweens) 3 times;

- Applying DAKO labelled polymer-HRP anti-Rabbit secondary antibody for 30 mins;
- Rinsing in TBS (Tweens) 3 times;
- Applying 2 drops of DAB for 6 mins;
- Stoping reaction with tap water;
- Counterstaining slides in haematoxylin (1/20 dilution) for 2 sec;
- Washing in tap water;
- Dehydrating and mounting with DPX.

F4/80 monocyte and macrophage staining IHC Protocol:
- Deparaffinising slides in 2 changes of xylene for 10 mins each;
- Rehydrating twice in xylene for 10 mins each, in alcohol of 100%, 95%, 70% and then in tap water for 2 mins each;
- Quenching for 20 mins in H_2O_2 endogenous peroxidase (solution of 49.5 ml of methanol and 0.5 ml of 30% H_2O_2);
- Washing slides in TBS (Tweens) 3 times for 3 mins each;
- Applying 1 antibody Rat anti-mouse F4-80 monoclonal antibody (1:250) for 2 hours;
- Washing slides in TBS (Tweens) twice;
- Applying 2 antibody DAKO anti-rat HRP polyclonal antibody (1:200) for 30 mins;
- Washing in TBS (Tweens);
- Applying DAB for 6 mins;
- Stoping reaction in tap water;
- Counterstaining slides in haematoxylin (1/20 dilution) for 10 sec;
- Washing in tap water;
- Dehydrating and mounting with DPX.

Proliferation Marker Ki67 staining protocol:
- Deparaffinising slides in 2 changes of xylene for 10 mins each
- Rehydrating twice in xylene for 10 mins each, in alcohol of 100%, 95%, 70% and then in tap water for 2 mins each;
- Quenching for 20 mins in H_2O_2 endogenous peroxidase (solution of 49.5 ml of methanol and 0.5 ml of 30% H_2O_2);
- Washing slides in TBS (Tweens) 3 times for 3 mins each;
- Steaming in 200ml of DAKO Target Retrieval solution of pH 9.0 for 15 mins;
- Cooling (in retrieval solution) in a cold water bath for 20 mins;
- Rinsing in TBS (Tweens) twice;
- Applying polyclonal Rabbit anti-Mouse Ki67 primary antibody at 1:2000 dilution for 60 mins;
- Rinsing in TBS (Tweens) 3 times;
- Applying DAKO labelled polymer-HRP anti-Rabbit secondary antibody for 30 mins;
- Rinsing in TBS (Tweens) 3 times;
- Applying DAB for 6 mins;
- Stoping reaction in tap water;
- Counterstaining slides in haematoxylin of 1/20 dilution for 10 sec;
- Washing in tap water;
- Dehydrating and mounting with DPX.

The micro-photos were done with the Nikon microscope (Japan). The objectives x4 for low resolution image and x20 for high resolution image were used. The low resolution images were used for general view of the sections. The sections with ruptured tissue, not contrasted or any kind of mistake were removed from the analysis. The high resolution images of selected sections were used for the analysis.
All high resolution images for each staining were recorded in one day with constant illumination and microscope setup. The software ImageJ Pro Plus 7 with macros was used for statistical analysis of the coloured area and the density of colour, which results from the amount and intensity of activity of specific cells and their components. The images of each staining were uploaded to the software and analysed simultaneously. An empty space in each image was cut away from the analytic area of the tissue image and was not used for the colour analysis.
The total number of mice use in the experiment was 15, each mice had 6 pockets with one sample in each pocket, the total number of implants was 90, minimum 3 sections from one sample were cut, selected and analysed, minimum 10 microphotos were proceeded from one section. Total number of images for one staining used for the analysis was minimum 2700. The total number of images used for the statistical analysis was minimum 13500.
The statistical analysis was conducted with the software GraphPad Prism Verion 5.0. The ANOVA analysis and Bonferroni Post-test were used to compare the results between the two groups, and in each group. The significance of the difference between the two groups was accepted at $p<0.05$ (*), $p<0.01$ (**) and $p<0.001$ (***).

Chapter 3. Synthesis of polyurethane implants and evaluation of them

The limitations of commercially available polyurethanes are evident in their mechanical properties, in the making of devices, and in biocompatibility. In particular, most of the medical grade polyurethanes are stiffer then the soft tissues of organisms. The mechanical stresses appear in the soft tissue at the point of contact with the polyurethane implant. These stresses can cause a mechanical injury of the tissue. In order to avoid the injury the modulus of the implantable polyurethane must be similar or less than the modulus of the soft tissue surrounding the implant. Moreover an elastic modulus of soft tissue is different from other tissues. Therefore, a synthesis of soft polyurethane with adjustable elasticity can avoid the mechanical injury of the soft tissue at the point of contact with the implant. However, a low stiffness is associated with a low mechanical strength and soft polyurethane does not provide integrity of the implants under mechanical loads in an organism. It is this contradiction that was solved in the present study.

The synthesis of soft polyurethane with sufficient mechanical strength was based on an investigation of the preliminary studies of the polyurethane synthesis as presented in Appendix I and II. The synthesis of different kinds of polyurethanes for a number of medical devices was considered. The synthesis of polyurethane was based on the polymerisation reaction of the isocyanate groups with amine or hydroxyl groups. The different compositions and conditions of synthesis were used for adjustment of polyurethane mechanical, chemical and biocompatible properties to particular medical devices in accordance with the requirements for each device. FDA-approved components were selected for synthesis, where possible, and the commercial availability of components was considered, bearing in mind the future availability of the materials to medical companies. On this basis the polyurethanes for drug release coating, X-ray contrast coating and catheter coating vascular grafts were synthesised as presented in Appendix I and II. These results were then used to synthesise the polyurethane with low Young's modulus and sufficient mechanical strength.

In the present study new low Young's modulus polyurethane implants have been synthesised to minimise a mechanical injury of the soft tissue at the point of contact with the implant. The surface of the implant was modified by high energy ions to improve biocompatibility of the implant. Major required tests corresponding to FDA regulations and standards have been done for the new polyurethane implants.

3.1. Synthesis of low modulus implant for soft tissues

The modern polymer implants have Young's modulus in a range of 1-10 MPa, while the organism's soft tissue has Young's modulus in a range of 10-100 kPa. Such biomechanical behaviour of soft tissue and polymer implant can lead to local injury of the tissue and cause a permanent inflammatory reaction. To adjust the biomechanics

of polymer implant to soft tissue a new, very soft polyurethane was synthesised in order to create a material with Young's modulus as close as possible to the soft tissue, and with strength, residual stresses, elongation, inertness, toxicity, bio-stability and other exploitation parameters which would satisfy the requirements for medical implants. The contradiction of the low modulus and high strength can be solved by using segmented polyurethane with hard domains to provide high mechanical strength and soft segments to provide low modulus.

To satisfy the low modulus and high strength requirements a new composition of the polyurethane is proposed. The polyurethane was synthesised from polyoxypropylene glycol (PPG) oligomer with hydroxyl groups terminated by 2,4-toluene diisocyanate (PPG-DI). Polytetrahydrofuran (PTHF) with hydroxyl end groups was used as a chain extender, as the reaction is shown (1).

$$R\text{-}N{=}C{=}O + HO\text{-}R' \rightarrow R\text{-}NH\text{-}CO\text{-}O\text{-}R' \quad (1)$$

The general formula of PPG-DI-PTHF polyurethane is shown (1).

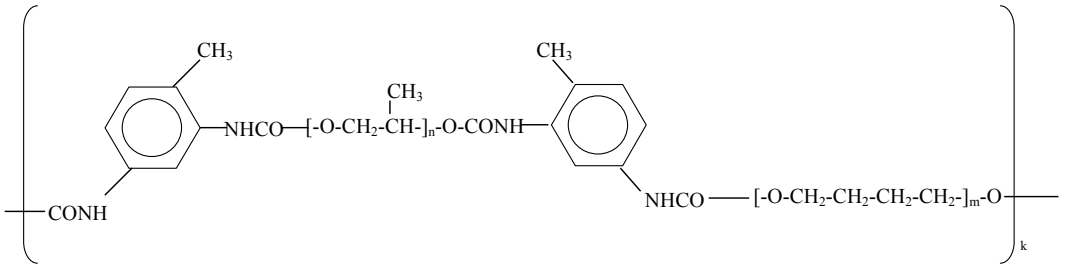

(2)

In some compositions dibutyl dilaurate stannum was used as a catalyst to accelerate the reaction. In some compositions polyethylene glycol (PEG), ethylene diamine (EDA), polypropylene glycol (PPG) and atmospheric moisture were used as a chain extender and crosslinker. For comparison, a commercial oligomer based on polyoxypropylene glycol with MDI was used for synthesis. The synthesised compositions are presented in Table.

Table.3.1. Polyurethane compositions used for synthesis.

Prepolymer	Chain extender and crosslinker	OH (or NH) / NCO ratio	Catalyst	Comments
PPG-DI	PTHF	0.35	DBD	Soft, sheets
PPG-DI	PTHF	0.35	-	Soft, sheets, tubes
PPG-DI	PTHF	0.5	DBD	Soft, sheets
PPG-DI	PTHF	0.7	DBD	Soft, sheets
PPG-DI	PEG	0.35	DBD	Soft, sheets
PPG-DI	PEG	0.5	DBD	Soft, sheets
PPG-DI	PEG	0.7	DBD	Soft, sheets
PPG-DI	Moisture	n/a		Soft, sheets
PPG-DI	EDA	1	DBD	Very hard
PPG-DI	PPG	0.7	DBD	Very hard

PPG-DI	PPG	0.9	DBD	Very hard
PEG-MDI	EDA	1		Hard
PPG-DI	TETA	0.5	DBD	Hard

The synthesis of polyurethane is sensitive to air humidity. The isocyanate groups can react with water molecules from the air to give inert products to active groups of glycols or amine [1] as shown in (3).

$$2R\text{-}N{=}C{=}O + H_2O \rightarrow 2R\text{-}NH\text{-}CO\text{-}OH \rightarrow R\text{-}NH\text{-}CO\text{-}NH\text{-}R + CO_2 \Uparrow \quad (3)$$

The study found the properties of the polyurethane cured in the open air varied widely depending on weather conditions. The sensitivity to moisture and the consequent variations of the reaction were found to be very significant: the cured polyurethane was sometimes sticky with a low mechanical strength, and sometimes very strong and hard. The influence of weather conditions and seasons on the quality of cured polyurethane was clearly observed.

These uncontrollable conditions were overcome during the synthesis by using the hermetic box (Sigma-Aldrich) with controlled humidity and temperature. For controlled synthesis of polyurethane a polyethylene box was equipped with a frame, analytical balance, temperature and humidity sensor, inlet of dry air and outlet with the regulators of the air flow, motorised support for the polyurethane preforms, gloves and isolating port. The box was placed in a permanently air-conditioned room. The components for synthesis were placed inside the box and the box was vented by dry air from Parker Dry air system for a week. The airflow rate in inlet and outlet valves was regulated to achieve sufficient positive pressure in the box to exclude air penetration through the holes and to prevent rupture of the polyethylene walls. The synthesis of polyurethane was started only when the level of humidity was 20-25% or lower. The dry air ventilation remained throughout synthesis. All operations in the box were done with inserted gloves.

The components were weighted on analytical balance, mixed in glass for 5 minutes and poured on the substrates (glass plate, Teflon plate or silicon wafer). In order to synthesise uniform coating a motorised stage of 6 continuously rotating glass tubes was designed and installed in the box. A ratio of active groups in oligomer and chain extender was selected to have residual isocyanate groups for crosslinking reaction. The ratio of isocyanate and hydroxyl or amine groups is presented in Table. The amount of mixture to cover the substrates with the requisite thickness was calculated. The mixture cured for 3 days at the stabilised temperature in the box.

After that the samples of polyurethane were taken from the polyethylene box and immediately placed into the vacuum oven, where the sample were annealed at 120^0C for 3 hours. Then the polyurethane samples were placed into mQ-water for 1 hour and peeled off from the substrate. The cured polyurethane was swollen in heptane, an approved solvent for medical application [2], for 3 hours to remove all low molecular fraction components. The amount of heptane was about 100 times higher then the polyurethane film. Then the polyurethane was dried in the open air with protection against dust for a week.

The final thickness of the polyurethane films was 100 um, 200 um, and 300 um. For mechanical tests the thick polyurethane sheets of 8 mm thickness were synthesised. Area of the films and sheets was 100x100 mm^2.

3.2. Synthesis of artificial blood vessel (shunt)

A complex shaped implant can be made by direct synthesis from liquid components in a mould. The advantage of direct synthesis was demonstrated on a synthesis of polyurethane blood vessels. The artificial blood vessel was synthesised from liquid PPG-DI and PTHF components using the procedure described above. The components were weighed and mixed in the polyethylene box under dry airflow conditions. The liquid reaction mixture of the components was poured on glass tubes. The glass tubes were turned during the pouring to cover the tubes uniformly. When necessary the reaction mixture was poured a second time to make the coating thicker. The polyurethane was cured for 3 days at room temperature and then annealed at 120^0C for 3 hours. Then the cured polyurethane tubes were swollen in hexane for 3 hours to remove all low molecular fraction components. The swollen polyurethane tubes were peeled off the glass tubes and dried in the open air with protection against dust for a week. Then the polyurethane tubes were washed for 1 hour in mQ-water and dried. The polyurethane tubes were evaluated for uniform thickness of the walls with an optical microscope and cut to the required length.

Fig.3.1. Photograph of synthesised polyurethane tubes for example. Left tube has 2 mm inner diameter, centre tube has 5 mm inner diameter, right tube has 2.5 mm inner diameter.

Finally, the polyurethane tubes of 50, 100 and 200 μm wall thickness and 6, 5, 3, 2, 2.5 and 1 mm inner diameter were synthesised (Fig.3.1). The length of the tubes was from 5 mm to 100 mm.

3.3. Mechanical evaluation of polyurethanes implants

In accordance with FDA regulations, the medical implant should provide certain mechanical parameters. The breaking stress, available elongation, Young's modulus and residual stresses are key mechanical parameters for the implant. In organisms the implant works under cycling loads without a break. To understand the mechanical behaviour of the implant in an organism the extensive mechanical tests of the newly synthesised polyurethanes were conducted.

The mechanical behaviour of polyurethane is non-linear. The polyurethanes show usually viscoelastic stress-strain curves with residual stresses. The relaxation processes have significant contribution to the stress curve. Therefore the history of the mechanical load is essential for understanding the test results. A typical strain-stress curve for PPG-DI-PTHF-0.35 is presented in Fig.3.2. The test was done with 3 preload cycles up to 100% of elongation, and a final load up to breaking point. The time dependence curve of the force during the test is presented in Fig.3.3. The strain-stress curve has 3 parts. The first part (up to 100% of strain) is strongly non-linear. The stress grows fast with the strain, and corresponds to more elastic behaviour. The second part (100-400% of strain) shows a constant slope. This part corresponds to the restructuring of the material. The stress causes flowing of the material and re-orientation of the macromolecules along the stress direction. The third part has a higher slope, and is more elastic up to breaking point.

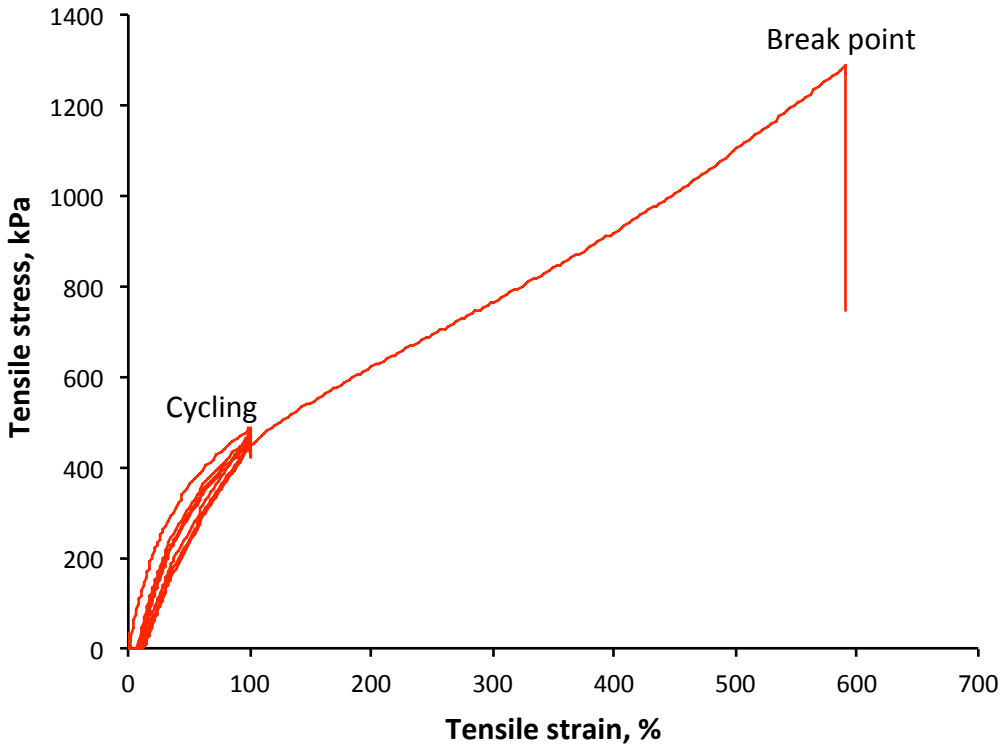

Fig.3.2. Representable strain-stress curve of PPG-DI-PTHF-0.35 polyurethane film stretched up to break with first 3 cycles of preloading. The curve shows non-linear behaviour. Low residual stresses are observed. The stress at the break is more than 1 MPa at the 600% of elongation. These are much higher values than the required values for the implant in organisms.

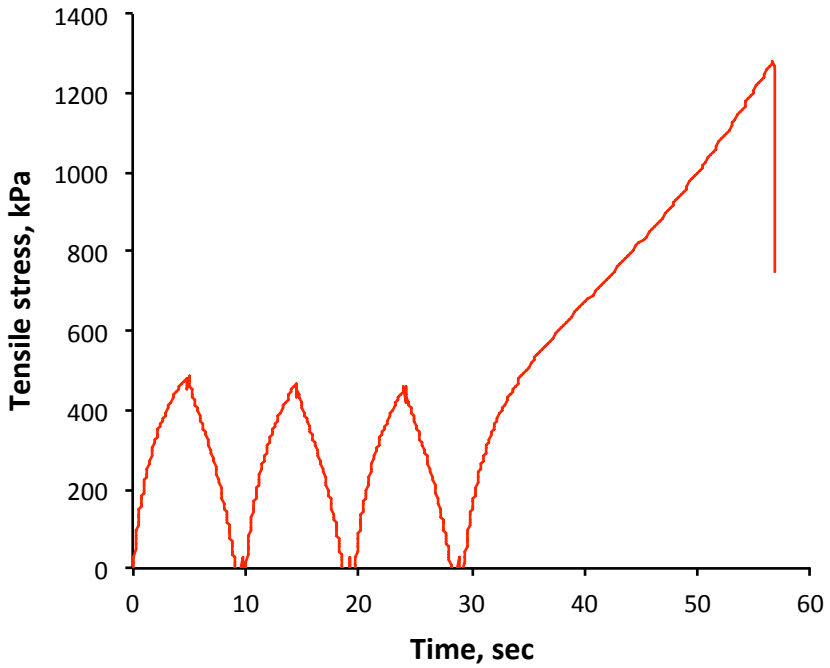

Fig.3.3. Representable time-tensile stress curve of PPG-DI-PTHF-0.35 polyurethane up to break with first 3 cycles of preloading. The stress curve shapes in the preloading 3 cycles are similar.

The cycling load up to 100% strain shows a hysteresis. The cycling part of the strain-stress curve is enlarged in Fig.3.4. The hysteresis effect is caused by restructuring and re-orientation of the polyurethane macromolecules along the stress direction, with the stress decreased with time. As a result of restructuring, the residual stresses in the polyurethane film after the load is released remain in the polyurethane. The sample remains elongated after complete release of the stress. The second and third cycle loads cause lower stress at the same strain (100%). However, the second and third cycles do not increase the residual stress significantly. The level of the residual stress remains about 10% of strain, which is in the range of the usual value for rubber materials. Consequently, the stability of the polyurethane structure is sufficient for a mechanical loading during exploitation.

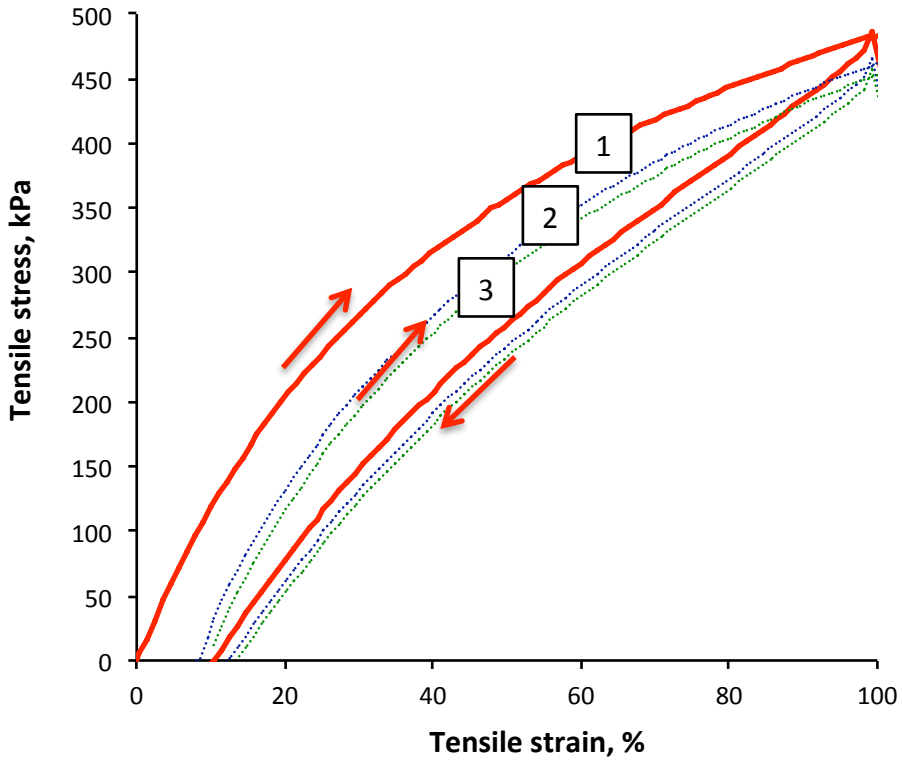

Fig.3.4. Representable cycling strain-stress curve of PPG-DI-PTHF-0.35 polyurethane with first 3 cycles of preloading. Number marks an order of the curves. The arrays show the direction of the load and release. After first loading cycle, the residual stresses remain constant at the following loads.

The strain-stress curve of PPG-DI-PTHF-0.7 has a different character (Fig.3.5). The part of the restructuring was not observed. The non-linear increase stress goes up to breaking point. The residual stresses of 12% are larger than in PPG-DI-PTHF-0.35 polyurethane. The elongation at breaking point is lower. The strength of breaking point is lower. This difference in mechanical properties is due to lower concentration of residual isocyanate groups and consequently less crosslinking of the macromolecules. For such material, the crosslinking increases the strength and elongation at breaking point. The polyurethane is stronger and shows less residual stress. Consequently, the shape of the crosslinked polyurethane recovers better after a deformation than for non-crosslinked polyurethane.

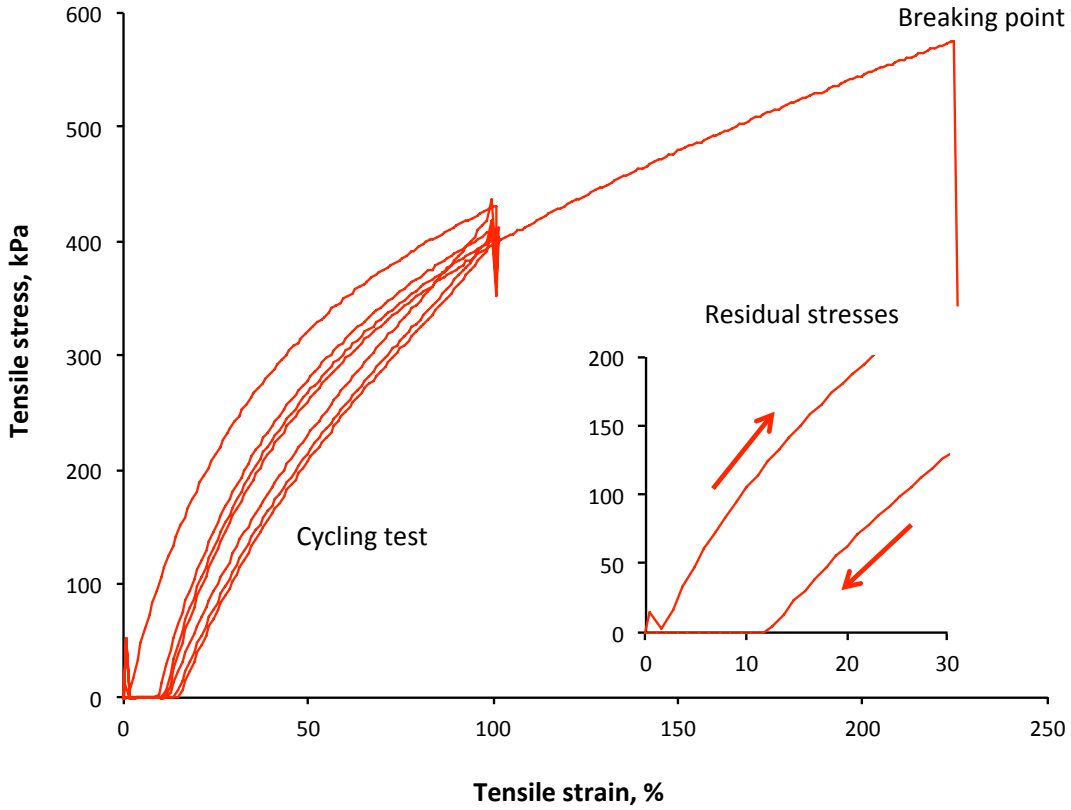

Fig.3.5. Representable strain-stress curve of PPG-DI-PTHF-0.7 polyurethane with first 3 cycles of preloading and enlarged cycling part of the curve. The residual stresses are similar, but the strength is lower.

The mechanical properties of polyurethane with PEG are worse (Fig.3.6-3.7). Character of the strain-stress curves is similar. But the tensile strength of polyurethane films is less then for polyurethane with PTHF. The residual stresses in polyurethane with PEG are larger then in the polyurethane with PTHF. In the case of PPG-DI-PEG-0.7 polyurethane the residual stresses are a quarter of the strain that is unacceptable for elastomers.

The mechanical properties of the different compositions of measured polyurethanes and the statistical analysis is presented in Fig.3.8-3.10. The strength and elongation at break point and residual elongation show that the best polyurethane with high mechanical strength and long elasticity at low residual elongation is the polyurethane PPG-DI-PTHF-0.35. This polyurethane has 1. 0±0.1 MPa tensile strength, 580±20% elongation at break, 11±1% residual elongation after 100% preload, 100±20 kPa modulus at 10% elongation and 410±50 kPa modulus at 100% elongation. This composition was accepted as a prospective material for implants and the following studies have been done with this polyurethane.

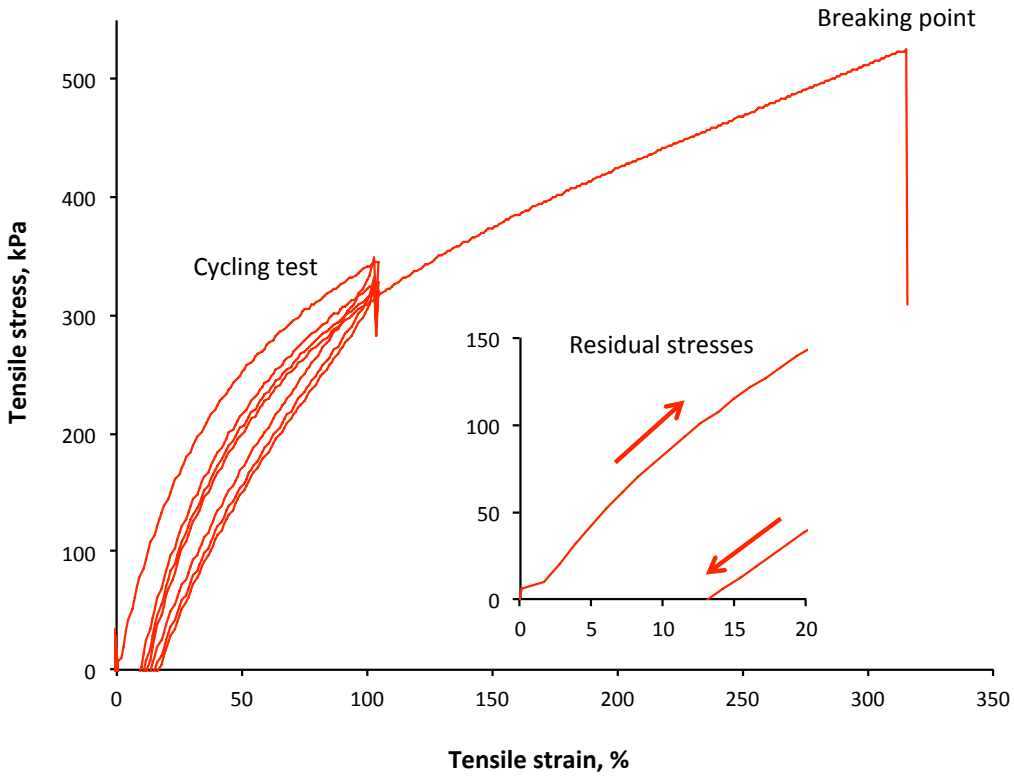

Fig.3.6. Representable strain-stress curve of PPG-DI-PEG-0.35 polyurethane with first 3 cycles of preloading and enlarged cycling part of the curve.

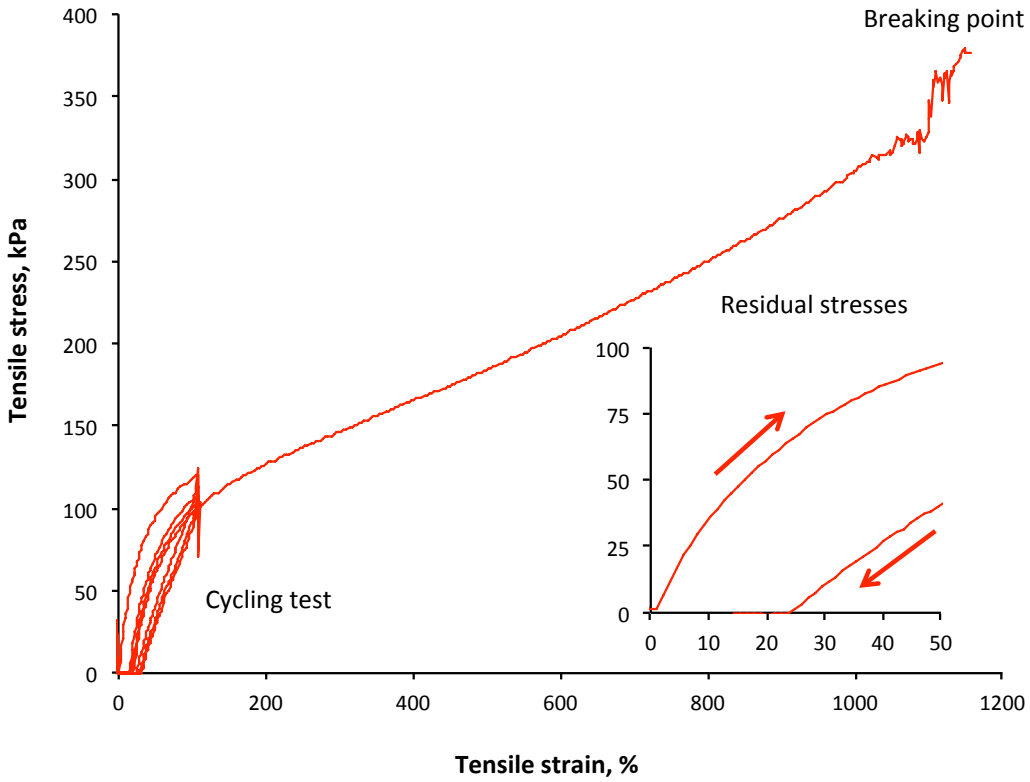

Fig.3.7. Representable strain-stress curve of PPG-DI-PEG-0.7 polyurethane with first 3 cycles of preloading and enlarged cycling part of the curve. The residual stresses are high.

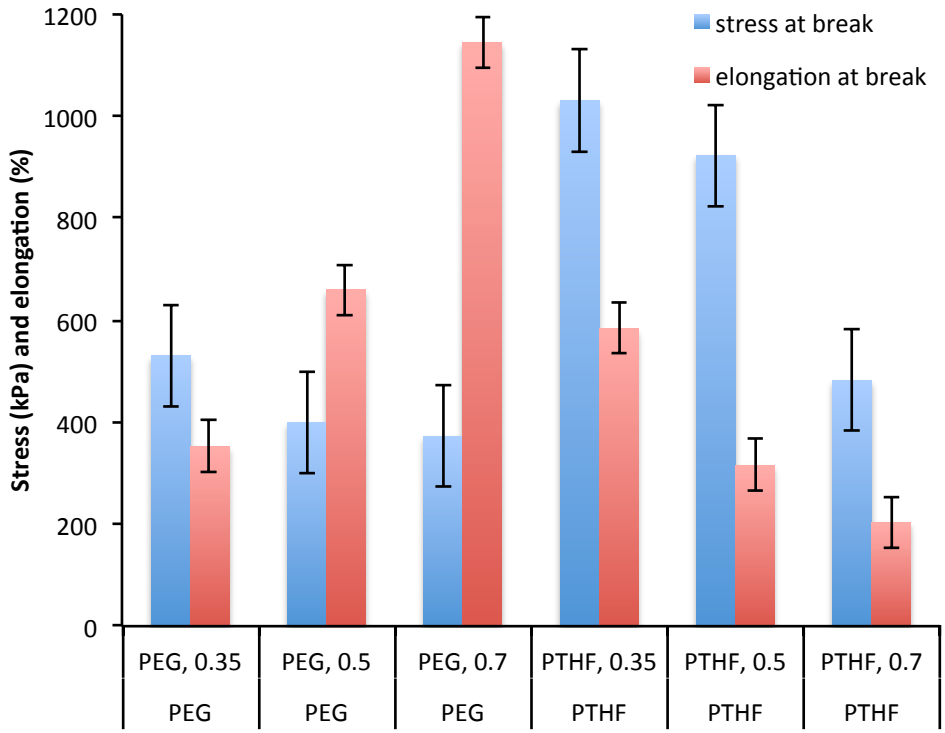

Fig. 3.8. Averaged tensile test results for different polyurethanes: stress and elongation at break point. The polyurethane PTHF,0.35 provides highest mechanical strength and longest elongation at the break with low (10%) of residual stresses (Fig.3.9).

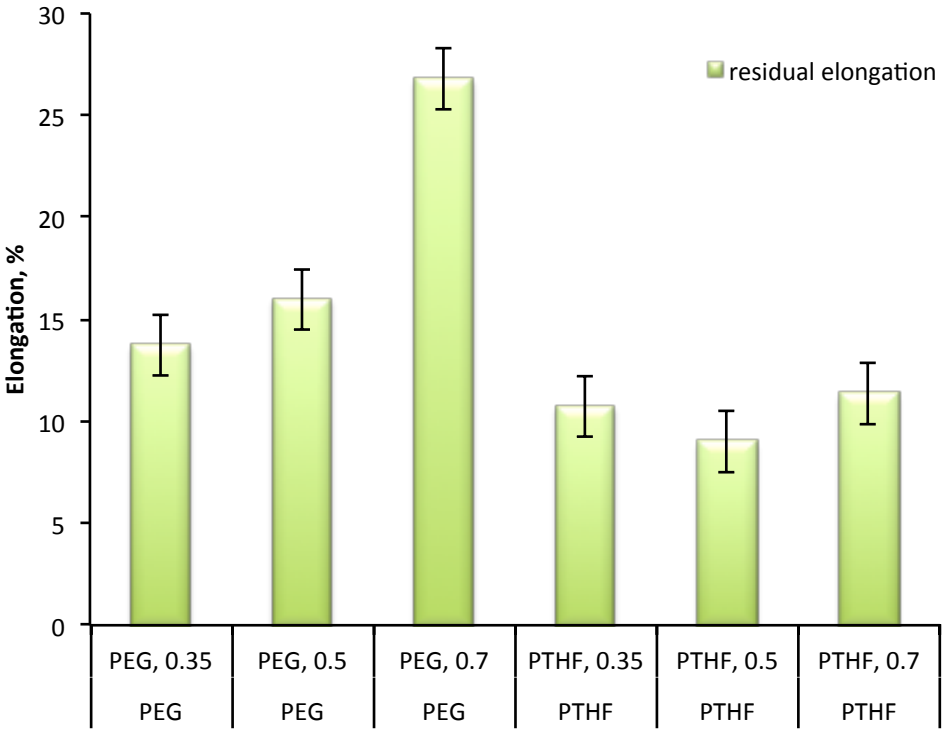

Fig.3.9. Tensile test results of polyurethanes: residual elongation after 100% elongation load. The polyurethanes based on PTHF show lowest residual elongation.

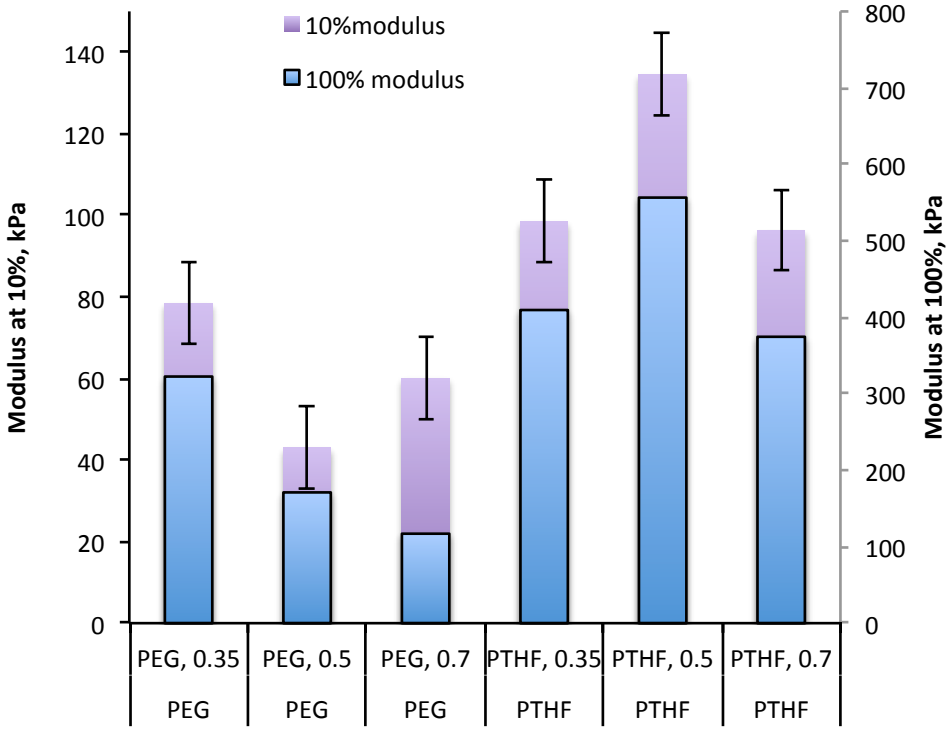

Fig. 3.10. Tensile test results of polyurethanes: Young's modulus at 10% and 100% of elongation. Despite the finding that the polyurethanes based on PEG provide the lowest modulus, the mechanical strength and residual stresses are not acceptable. Therefore, only the polyurethanes based on PTHF with higher modulus were considered for the medical implants.

The comparison of selected polyurethane with other commercial polyurethanes and other materials are presented in Fig.3.11. A rank soft tissue modulus from the literature's data is added for estimation [3-7]. Medical grade commercial polyurethanes show significantly high values. Silicon rubber has modulus, which is closer to the modulus of some tissues. New polyurethane SIBSTAR PSU shows modulus closer than the silicon rubber, but higher than the soft tissue [8]. The most promising material is TPE1. However, there is not enough experimental data on the biocompatibility of such material. The synthesised PPG-DI-PTHF-0.35 polyurethane has the closest modules to the soft tissue average modulus. For some tissues, this polyurethane has a lower modulus and an injury of implant caused by the local stresses can be expected to be negligible.

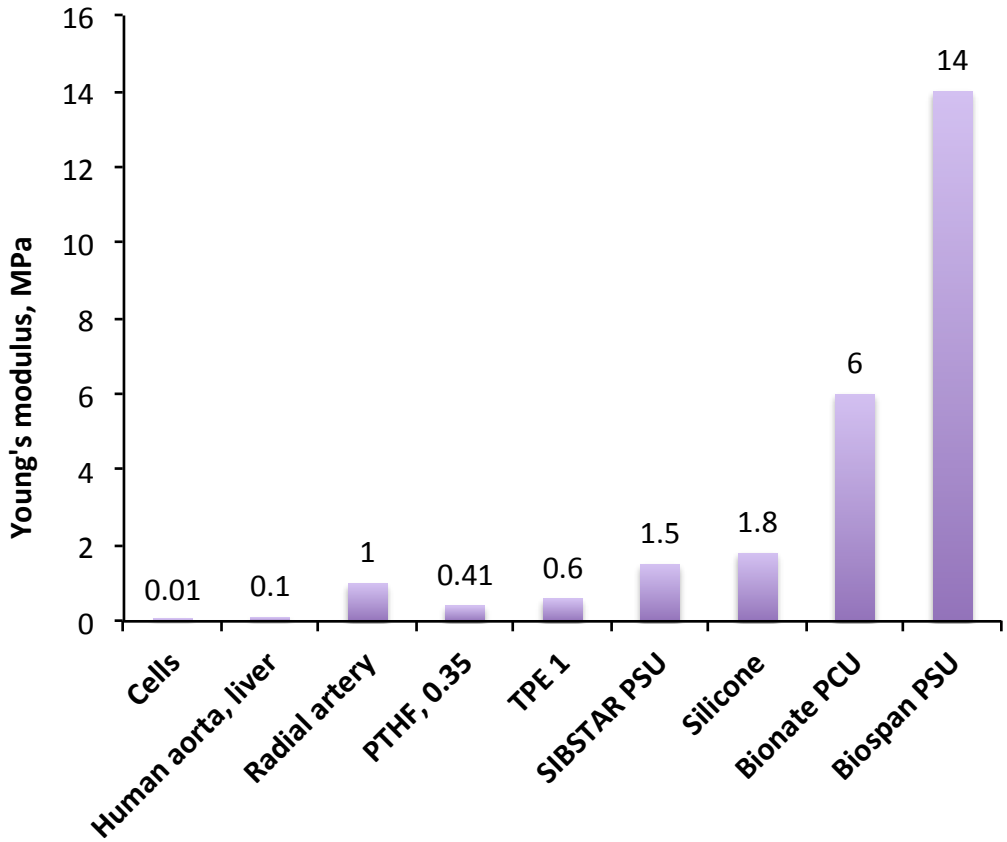

Fig.3.11. Young's modulus of medical polymers, tissues and selected polyurethane PTHF, 0.35. The synthesised polyurethane (PTHF, 0.35) has lower modulus then the used commercial polyurethanes and other materials (TPE and silicone) as well as the new polyurethane with low modulus proposed for medical applications.

3.4. Implant stability in water media

Following FDA regulations an implant material must be stable in an organism for a long time. In general, the organism's environment is aggressive for a polyurethane implant. The processes of polyurethane degradation in water are based on hydrolysis reaction of ether and urethane groups. The reactions of hydrolysis are following:

$$R\text{-}CH_2\text{-}O\text{-}CH_2\text{-}R_1 + H_2O \rightarrow R\text{-}CH_2\text{-}OH + HO\text{-}CH_2\text{-}R_1$$

$$R\text{-}O\text{-}CO\text{-}NH\text{-}R_1 + H_2O \rightarrow R\text{-}OH + HOOC\text{-}NH\text{-}R_1$$

As the result of these reactions, the polyurethane backbone is cleaved and short chain molecules are released into the water. The reaction depends on the temperature following the Arrhenius law. This fact is used for acceleration test of materials. In experiment, a polyurethane mass should decrease.

Using the FDA regulations to evaluate a stability of the polyurethanes in a water environment, the samples of polyurethanes were exposed in water with different temperatures. The newly synthesised polyurethane PPG-DI-PTHF-0.35 was tested (Fig.3.12 –Fig.3.14). For comparison the commercially available polyurethanes of medical grade Pellethane and SKU-PFL were tested as controls. The temperature

range was 40, 60 and 80 degrees. The temperature of 40 degrees was selected for the organism environment. The temperature of 80 degrees was selected as the condition close to water boiling temperature. The polyurethane PPG-DI-PTHF-0.35 was tested at 40 and 60 degrees because phase transition in this polyurethane occurs at 80 degrees. The samples were stored in individual sealed glass beakers filled with sufficient amounts of water (mass ratio of water to polyurethane sample was 20:1). The beakers were placed into the automatic ovens with stabilised temperature. The temperature variations were $\pm 1^0$C. The test was done over 3 months. In the required time periods the samples of polyurethanes were taken from the beakers, dried with Kim Wipe tissue and weighed with analytical balance. After that the samples were immediately returned to the beakers.

The results of mass loss measurements show that in the range of temperature and time the mass of the samples slightly increases due to the swelling effect of polyurethane in water during the first day. After that the mass of polyurethane samples does not change over the 3 months. Following the Van Goff law the 60 and 80 degrees tests corresponds to degradation under body temperature at 17 months and at 29 months. Therefore, the investigated polyurethane PPG-DI-PTHF-0.35 shows similar stability as the certified SKU-PFL and Pellethane polyurethanes.

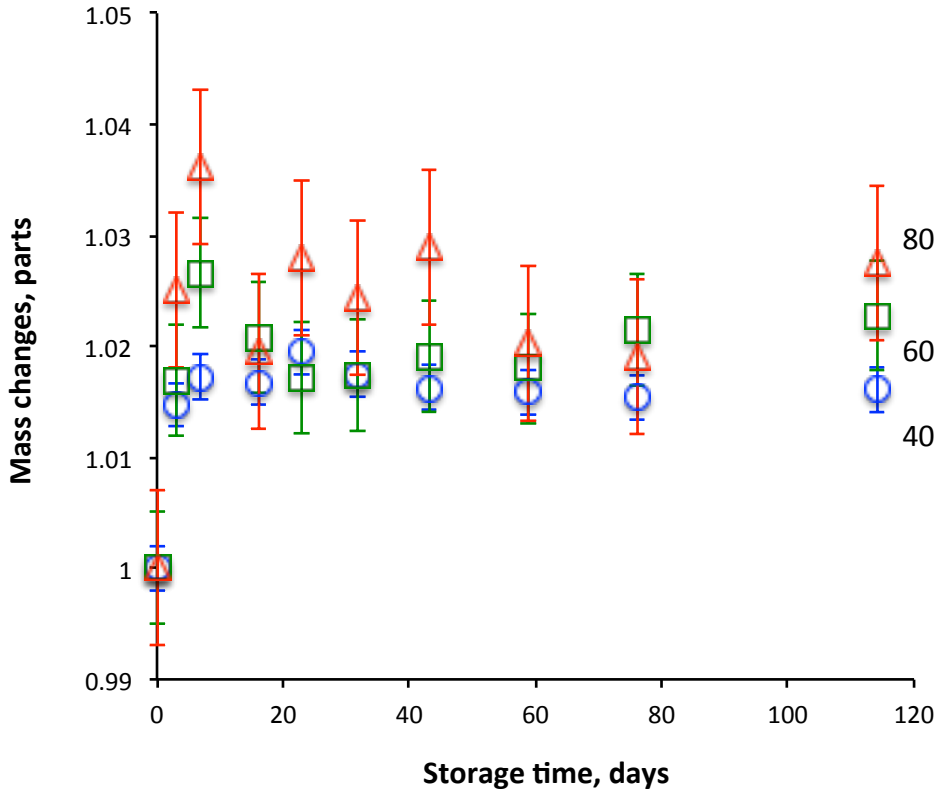

Fig.3.12. Mass change of PU Pellethane in hot water. The polyurethane swells in water in the first hour and stable thereafter. No mass loss was observed. The temperature in Celsius is noted.

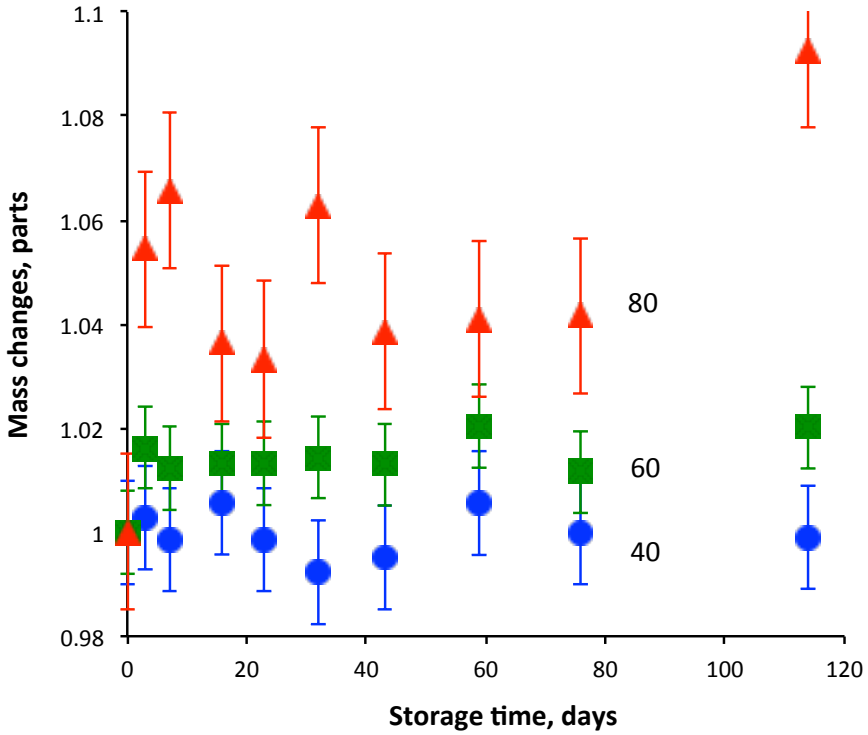

Fig.3.13. Mass change of polyurethane SKU-PFL in hot water. The polyurethane swells in water in the first hour and stable thereafter. No mass loss was observed. The temperature in Celsius is noted.

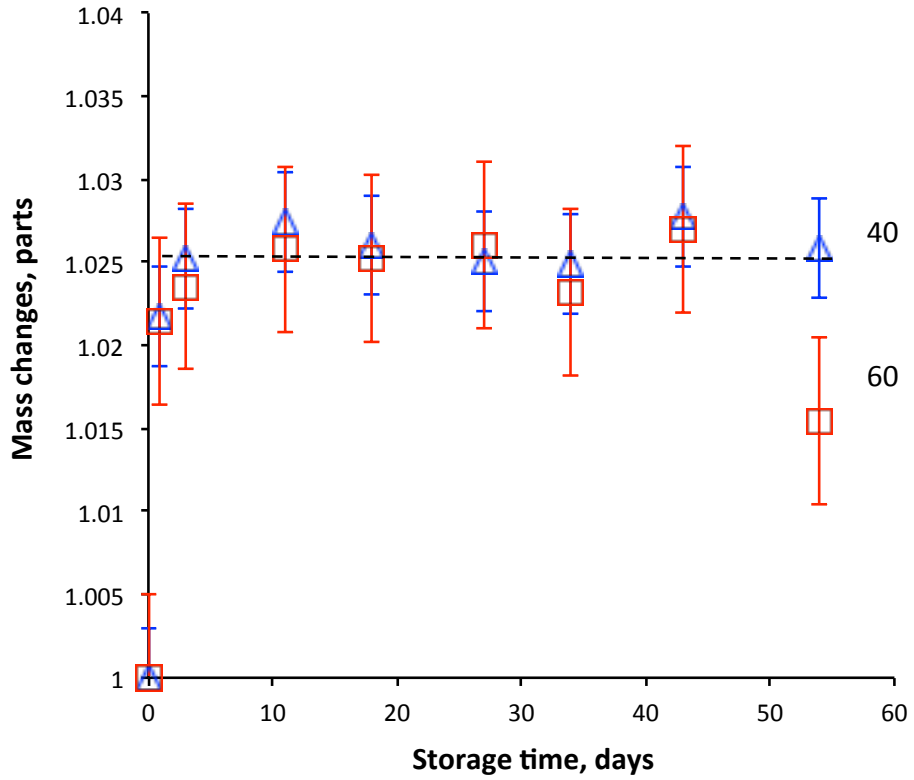

Fig.3.14. Mass change of polyurethane PPG-DI-PTHF-0.35 in hot water. The polyurethane swells in water in the first hour and is stable thereafter. No mass loss was observed. The temperature in Celsius is noted.

3.5. Leaching residuals from implant

In accordane with FDA regulations, an implanted material must not release low molecular components with toxic or carcinogenic activity. Polyurethane materials like any other material leaches some low amount of residuals into water media. For medical grade polyurethane to satisfy the biocompatibility requirements the leached components should be of a low amount and not toxic. The leaching test was done for Pellethane as the control certified medical grade polyurethane (Fig.3.15), and PPG-DI-PTHF-0.35 polyurethane (Fig.3.16). The polyurethane samples were exposed in mQ-water for 7 days at room temperature, then a drop of solution was placed on Ge ATR crystal and dried in the open air. After complete water evaporation, the spectra of FTIR ATR with the dry drop on the ATR crystal were recorded.

The Pellethane leaches residuals that are non-reactive, low molecular weight components and were not linked to the long chain molecules. The spectra of leached components from PPG-DI-PTHF-0.35 polyurethane show lines of OH group (3350 cm^{-1}), CH group (2975-2875 cm^{-1} region), carbonyl group (1728 cm^{-1}), aromatic ring (1603 cm^{-1}) and ether group (1106 cm^{-1}). The largest substance is PTHF non-crosslinked to PPG-DI component and a low amount of PTHF bonded to PPG-DI. The PPG-DI molecular fragment with active isocyanate group was not observed. No isocyanate groups were observed in the spectra of both polyurethanes. The amount of leachable components from both polyurethanes was lower than the detectable limit of the weight method, which was used for the evaluation of the medical grade materials. Therefore, the leached components and its amount from PPG-DI-PTHF-0.35 polyurethane satisfy the requirements for medical grade polymers such as certified Pellethane polyurethane.

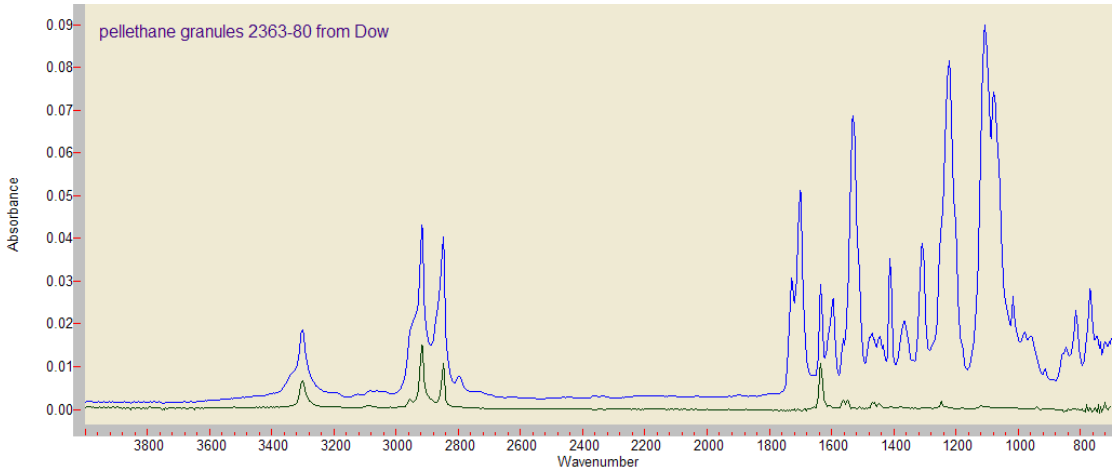

Fig.3.15. FTIR ATR spectra of polyurethane Pellethane (blue, top) and leached substrate from polyurethane Pellethane 2363-80 (Dow Chemicals) into mQ-water during 7 days (green, bottom).

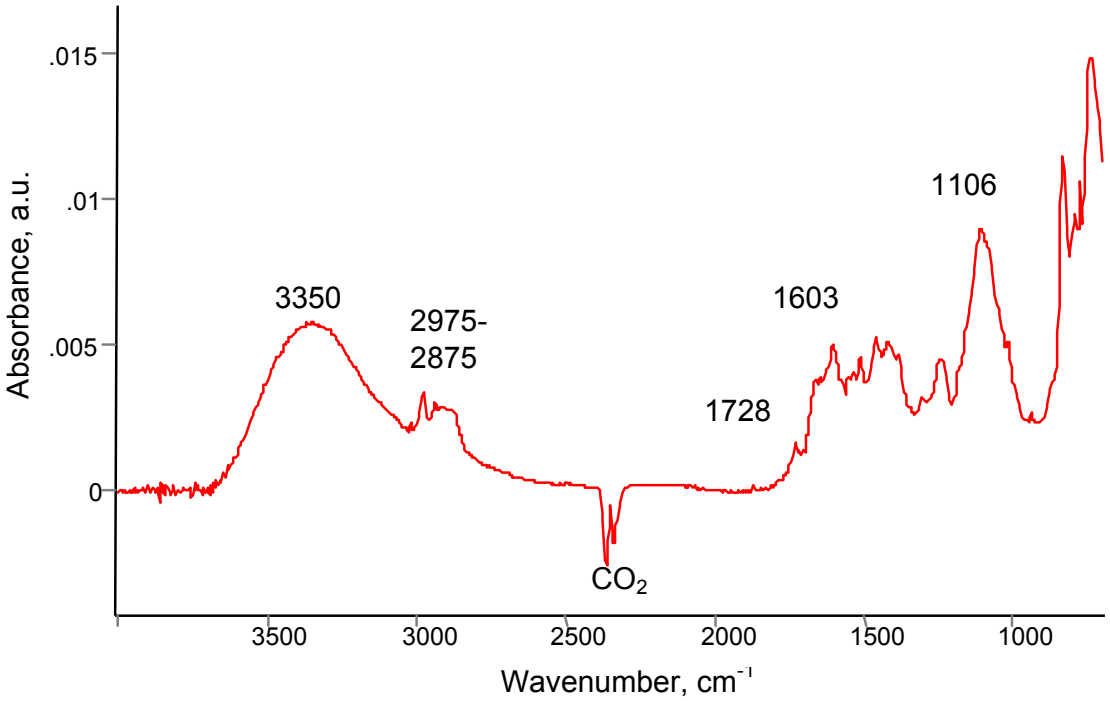

Fig.3.16. FTIR ATR spectra of leached substrate from PU PPG-DI-PTHF-0.35 into mQ-water during 7 days.

3.6. Implant non-toxicity evaluation

In accordance with FDA regulations, an implantable material must not have cytotoxicity effect. The PPG-DI-PTHF-0.35 polyurethane was tested for cytotoxicity in cell culture experiments and in organisms. In the experiment the endothelial human cells (HCAEC) were seeded on the polyurethane film and proliferated for 2 days. As the control, the tissue culture plastic (TCP) was used. The analysis of cells after staining of the attached cells showed that the cells were attached, spread and proliferated on polyurethane as on TCP. Cell bodies are elongated (Fig.3.17). Cell lysis or membrane disintegration was not observed. However, the amount of the cell after proliferation in 2 days on the polyurethane is lower then on TCP control. This indicates that the untreated polyurethane surface does not provide cell adhesion as sufficient as TCP. Therefore, the polyurethane does not show a toxicity while the cell adhesion is lower.

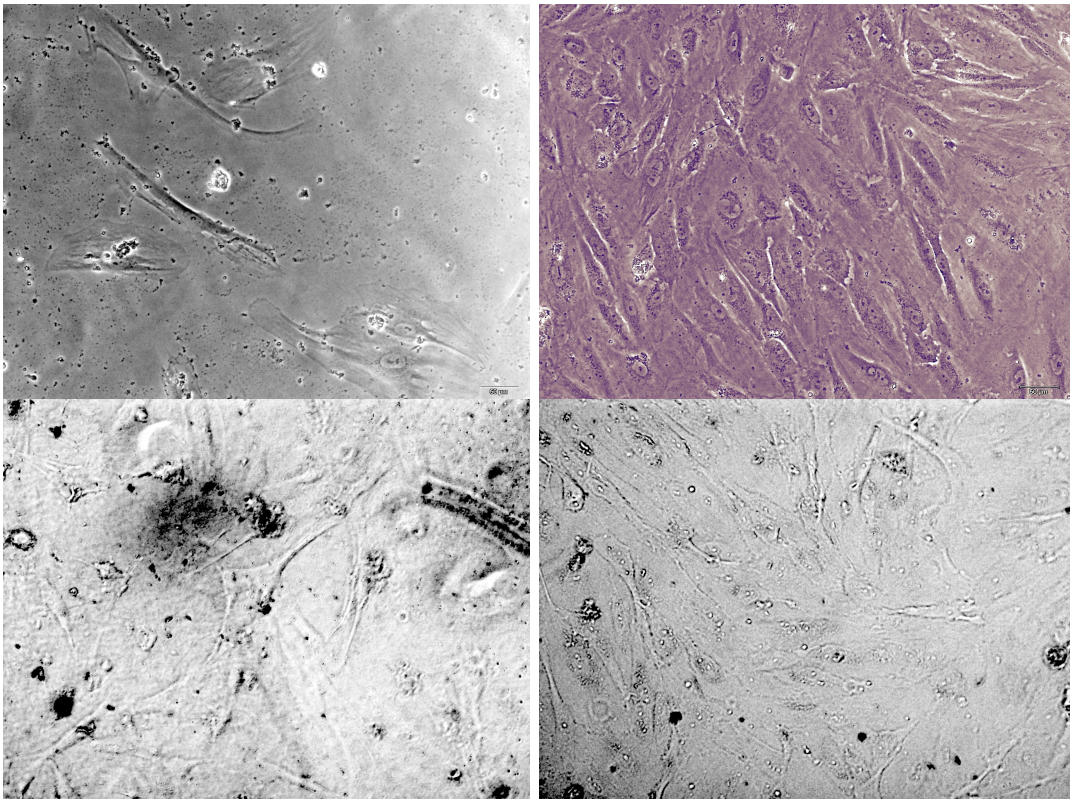

Fig.3.17. Cell images on polyurethane (left) and TCP (right) without staining. The cytotoxic effect for the polyurethane was not observed.

For toxicity tests in organisms the polyurethane films were implanted under the skin area of mice for 7 days. After 7 days the block of tissue with the implant was cut, sectioned and stained in H&E dye. The microphotos of the sections are presented in Fig.3.18. The results show that there is no toxic reaction in the surrounding tissues for all kinds of polyurethanes. The capsule with activated cells is well visible. The thickness of the capsule is equal or less then 100 μm which is normal for immune reaction. The capsule is intact which shows that the implants are strong enough in the body. No tissue necrosis was observed.

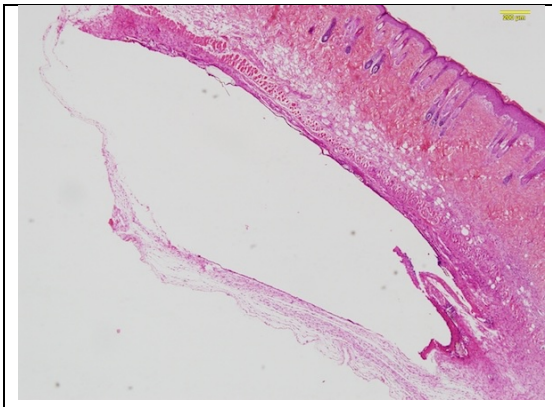

PPG-DI-PTHF-DBD (0.35)

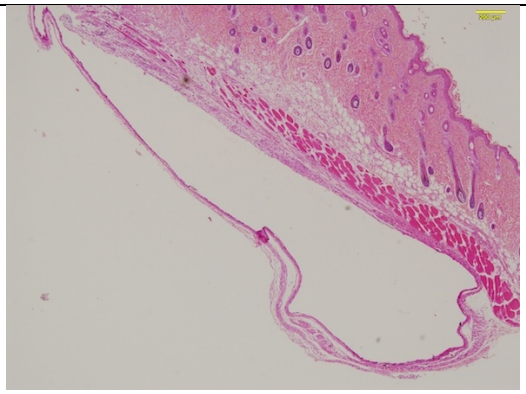

PPG-DI-PTHF-DBD (0.5)

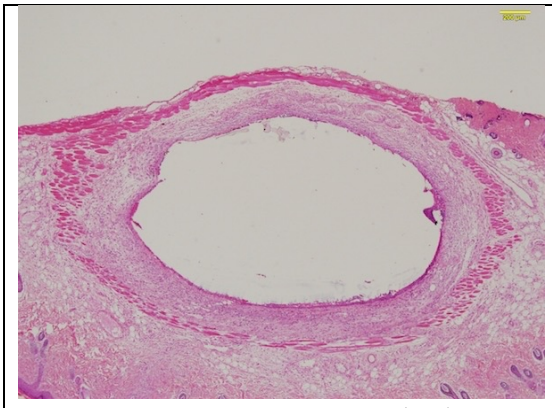

PPG-DI-PTHF-DBD (0.7)

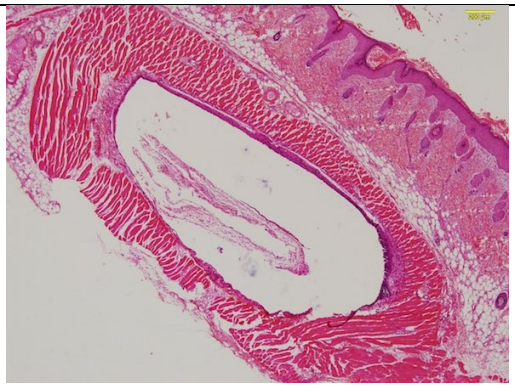

PPG-DI-PEG-DBD (0.35)

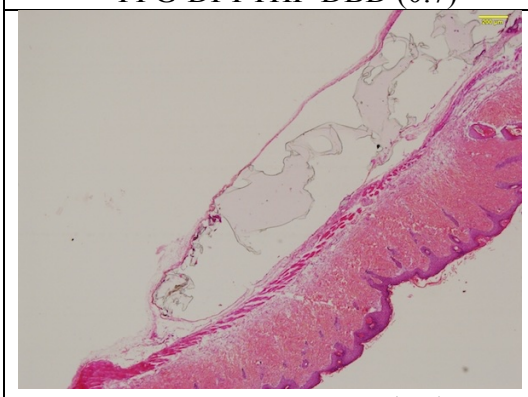

PPG-DI-PEG-DBD (0.5)

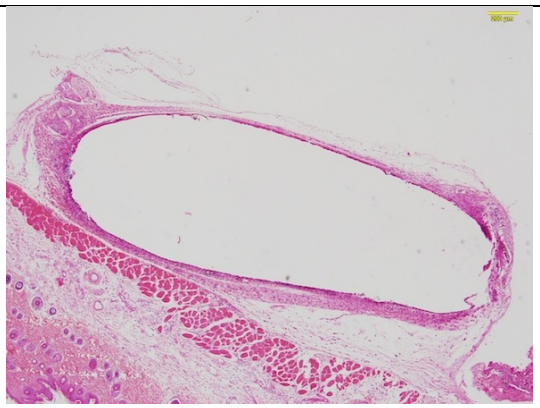

PPG-DI-PEG-DBD (0.7)

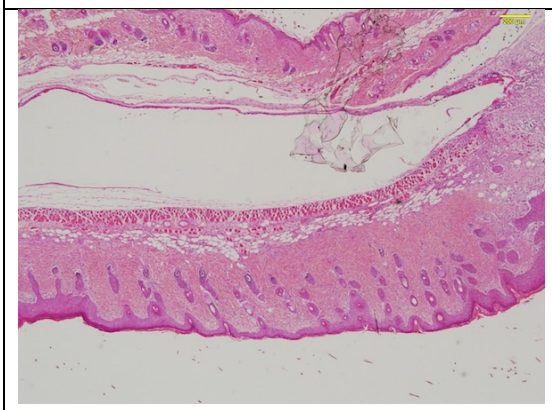

PPG-DI-PTHF-DBD (0.35). The implant has been synthesised on a silicon wafer.

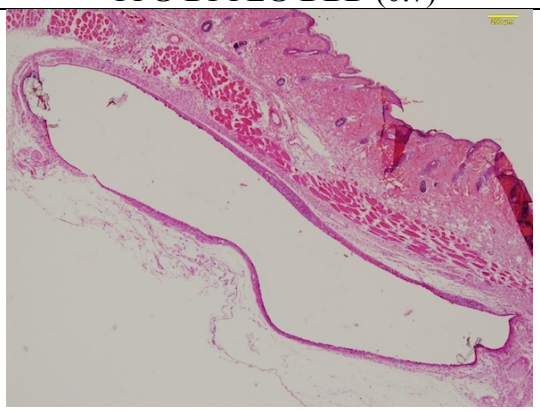

PPG-DI-PTHF (0.35). The implant has been synthesised without catalyst.

Fig.3.18. Microphotos of histological sections of mice tissue with the implant stained in Hematoxylin-Eosin. Objective is x4. The empty area surrounded by the tissue was filled by the polyurethane implants. The implant film was removed at the microtome sectioning due to high elasticity of the polyurethane implants, while in two shown samples some pieces of polyurethane implants remain and are visible as uniformly coloured films. The cytotoxic effect was not observed. The immune reaction was not strong.

The presence of catalyst DBD in the implant used for the curing reaction in polyurethane synthesis does not play a role in organism reaction. No difference was observed in the organism reactions between the polyurethane synthesised on silicon wafer or on glass plate.

For the quantitative results, the images were analysed with calculations of the capsule thickness. The results are presented in Fig.3.19. The average thickness of the capsule does not depend on the polyurethane composition. The thickness of the capsule for all polyurethane is close to the thickness of the capsule for polyethylene implant. Therefore, the synthesised polyurethane does not show the toxic effect in organisms.

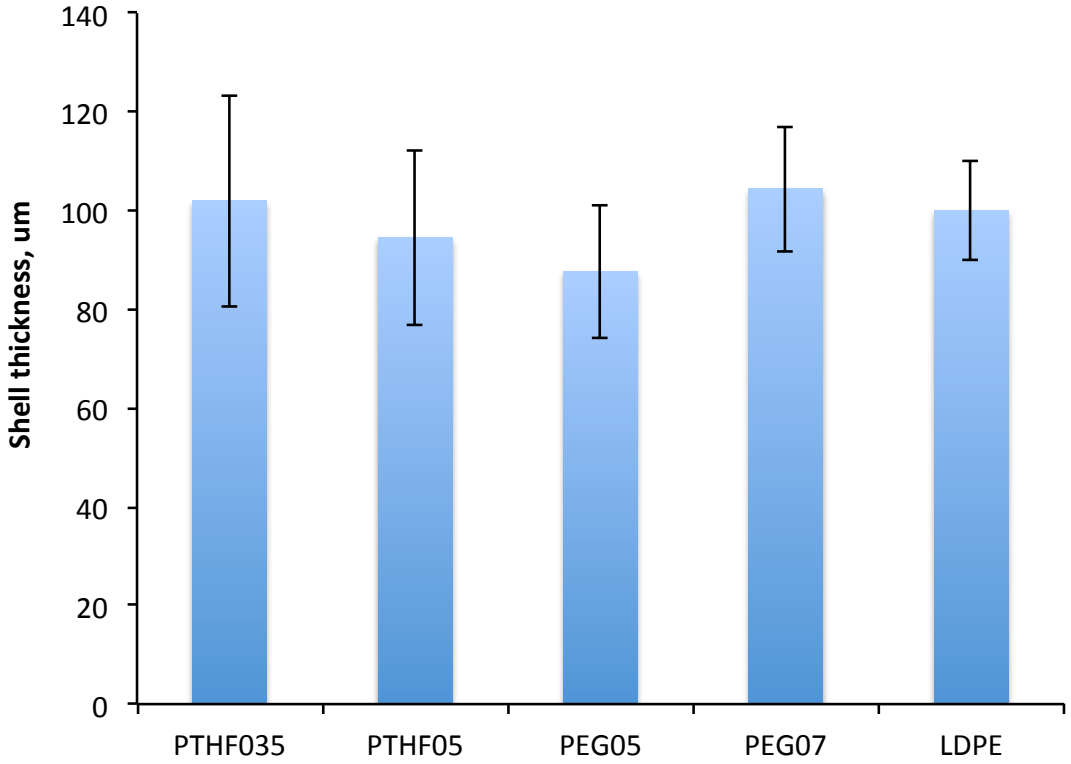

Fig.3.19. Capsule thickness around polyurethane implants of different composition. LDPE is used as a well-known standard. The average thickness of the capsule for all investigated polyurethanes is similar to the capsule around polyethylene implant as a control.

3.7. Discussion

The modern artificial materials used for soft tissue implantation have a significant problem due to the very different mechanical properties of these two materials [9-11]. As a result, the surrounding tissue is under extremely high mechanical stress near the implant surface [12, 13]. The stress causes damage to the cell membrane with consequent apoptosis and activation of an immune reaction. The continuing immune reaction leads to a chronic inflammation and, in the worst case, heavy encapsulation and calcification. However, the modern medical grade polyurethane materials do not provide a low or comparable value of the modulus to the soft tissue modulus.

With the synthesis of this new polyurethane with low modulus it was shown that the low modulus polyurethane could be synthesised from the components approved for use in an organism. The PPG-DI-PTHF-0.35 polyurethane synthesised in the present study has similar or even lower modulus than soft tissue. Therefore, the soft tissue of the organism near the polyurethane implant would be under similar mechanical stress as without the implant.

The residual stress and strain is important for functional implants such as heart valves and blood vessels [14-16]. For example, the residual stresses could significantly decrease the effectiveness of the heart valve as the insufficient closing of the valve could lead to patient death. The PPG-DI-PTHF-0.35 polyurethane has low residual stress (10% after 100% of elongation) so that the implant shape will recover sufficiently after a deformation.

The synthesised polyurethane has chemically cross-linked macromolecules. In comparison with linear polyurethane, the cross-linked polyurethane has higher mechanical strength and stability in aggressive environments such as an organism [17, 18]. Thus the diffusion of aggressive low molecular components from organisms such as enzyme ferments is lower in the cross-linked polyurethane in comparison with linear polyurethanes [19]. Intensive swelling and washing of the implant facilitates the removal of unreacted low molecular components in cross-linked polyurethane. Therefore, the leaching of residual components from the implant to the organism could be significantly decreased in comparison with the linear polyurethane where swelling and washing does not reliably remove unreacted low molecular components.

The synthesis of polyurethane directly on modern medical devices is now recognised as a prospective method for ensuring sufficient adhesion, which cannot be achieved with other methods.

The synthesised polyurethane was successfully tested for cytotoxicity and stability satisfying FDA requirements [20]. Given all these advantages of synthesised polyurethane, it could provide new medical implants with increased functionality and improved stability in organisms.

However, the synthesised polyurethane shows the usual immune reaction for the foreign body's intrusion into an organism. The next chapter shows how the plasma modification process can decrease the immune reaction of the polyurethane.

3.8. Conclusions

The results of this Chapter are:
- A number of polyurethanes for medical applications with new compositions and structures have been synthesised. The advantage of direct synthesis for complex shaped implants was shown. For example, the polyurethane tube for blood vessel shunt has been synthesised.
- The synthesised polyurethanes have been tested and compared with known polyurethanes for biomedical applications. A polyurethane based on PTHF component with low Young's module as close as possible to the soft tissue Young's module to prevent mechanical injury in the surrounding tissues was synthesised and proposed for forthcoming investigations.
- The proposed polyurethane has been tested for tensile strength, cyclic mechanical stress, completeness of the curing reaction, stability in water media, leaching of residual components, and toxicity for cells and organism reactions according with FDA requirements.
- The proposed polyurethane has low Young's module, low residual deformations, sufficient mechanical strength for using as a material for medical implants in soft

tissue, low residual components, sufficient stability in water and low or absent toxic effect in comparison with existing polyurethane for medical applications. This polyurethane was considered for medical application and used in this study.

References

1. V.P. Begishev, A.Ya. Malkin, Reactive Processing of Polymers, Chemical Technology Publishing, Toronto, 1999.
2. Note for guidance on impurities: residual solvents, European Medicines Agency, CPCM/ICH/283/95, 1998, 1-24.
3. L. Guo, Y. Lv, Z. Deng, Y. Wang, X. Zan, Tension testing of silicone rubber at high strain rates, Polymer Testing, 50 (2016) 270-275.
4. V. Kanyanta, A. Ivankovic, Mechanical characterisation of polyurethane elastomer for biomedical applications, J of the mechanical behaviour of biomedical materials, 3 (2010) 51–62.
5. S.M. Wells, E.J. Walter, Changes in the Mechanical Properties and Residual Strain of Elastic Tissue in the Developing Fetal Aorta, Annals of Biomedical Engineering, 38(2) (2010) 345–356.
6. R. Akhtar, M.J. Sherratt, J. Kennedy Cruickshank, B. Derby, Characterizing the elastic properties of tissues, Materials Today, 14 (2011) 96-105.
7. B. Ahn, J. Kim, Measurement and characterization of soft tissue behavior with surface deformation and force response under large deformations, Medical Image Analysis 14 (2010) 138–148.
8. G.T. Lim, S.A. Valente, C.R. Hart-Spicer, M.M. Evancho-Chapman, J.E. Puskas, W.I. Horne, S.P. Schmidt, New biomaterial as a promising alternative to silicone breast implants, Journal of the mechanical behavior of biomedical materials 21 (2013) 47–56.
9. Kannan R.Y., Salacinski H.J., Butler P.E., Hamilton G., Seifalian A.M. Current status of prosthetic bypass grafts: A review, Journal of Biomedical Materials Research. B. Applied Biomaterials, 74 (2005) 570-581.
10. Holst J., Watson S., Lord M.S., Eamegdool S.S., Bax D.V., Nivison-Smith L.B., Kondyurin A., Ma L., Oberhauser A.F., Weiss A.S., Rasko J.E.J. Substrate elasticity provides mechanical signals for the expansion of hemopoietic stem and progenitor cells, Nature Biotechnology 28 (2010) 1123-1128.
11. P. Moshayedi, G. Ng, J.C.F. Kwok, G.S.H. Yeo, C.E. Bryant, J.W. Fawcett, K. Franze, J. Guck, The relationship between glial cell mechanosensitivity and foreign body reactions in the central nervous system, Biomaterials, 2014; DOI: 10.1016/j.biomaterials.2014.01.038
12. Ballyk P.D., Walsh C., Butany J., Ojha M. Compliance mismatch may promote graft-artery intimal hyperplasia by altering suture-line stresses // Journal of Biomechanics. 1998. Vol. 31. PP. 229-237.
13 K. Miller, Method of testing very soft biological tissues in compression, Journal of Biomechanics 38 (2005) 153–158.
14. D.J. Wheatley, L. Raco, G.M. Bernacca, I. Sim, P.R. Belcher, J.S. Boyd, Polyurethane: material for the next generation of heart valve prostheses?, European Journal of Cardio-thoracic Surgery, 17 (2000) 440-448.
15. U. Braun, E. Lorenz, C. Weimann, H. Sturm, I. Karimov, J. Ettl, R. Meier, W.A. Wohlgemuth, H. Berger, M. Wildgruber, Mechanic and surface properties of central-venous port catheters after removal: A comparison of polyurethane and silicon rubber

materials, Journal of the mechanical behavior of biomedical materials, 64 (2016) 281–291.
16. J.S. Bergstrom, M.C. Boyce, Constitutive modeling of the time-dependent and cyclic loading of elastomers and application to soft biological tissues, Mechanics of Materials 33 2001) 523±530.
17. A. Sultan Nasar, Mitsutoshi Jikei, Masa-aki Kakimoto, Synthesis and properties of polyurethane elastomers crosslinked with amine-terminated AB2-type hyperbranched polyamides, European Polymer Journal 39 (2003) 1201–1208.
18. V. Sekkar, Comparison Between Crosslink Densities Derived from Stress–Strain Data and Theoretically Data Evaluated Through the a-Model Approach for a Polyurethane Network System Based on Hydroxyl Terminated Polybutadiene and Isophorone-Diisocyanate, Journal of Applied Polymer Science, Vol. 117, 920–925 (2010).
19. S. Desai, I. M. Thakore, Surekha Devi, Effect of Crosslink Density on Transport of Industrial Solvents Through Polyether Based Polyurethanes, Polymer International 47 (1998) 172-178.
20. A.J.T. Teo, A. Mishra, I. Park, Y.-J. Kim, W.-T. Park, Y.-J. Yoon, Polymeric Biomaterials for Medical Implants and Devices, ACS Biomater. Sci. Eng. 2016, 2, 454−472.

Chapter 4. Surface modification and characteristics of polyurethane implants

A polyurethane surface is chemically inert for proteins and other bioactive molecules. The newly synthesised polyurethane has similar inertness to proteins. Ion beam treatment and plasma immersion ion implantation methods have been used to modify the polyurethane surface. The chemical structure, topography, wettability, hardness and other parameters of the surface layer are dramatically changed after the modification. These changes depend on the parameters of the modification process and the kind of polymer. An analysis of the newly synthesised polyurethanes treated by method of plasma immersion ion implantation (PIII) is presented in this Chapter.

The following questions are considered in this Chapter:
- the physical model of ion penetration and energy transfers was used to estimate the thickness of the modified layer in dependence on the energy of ions;
- the wettability and surface energy changes of the synthesised polyurethanes are analysed in dependence on regimes of PIII and storage time after the treatment;
- the chemical structure changes in the synthesised polyurethanes in dependence on the parameters of PIII, composition of polyurethane and storage time;
- the surface topography of the synthesised polyurethane in dependence on PIII treatment regimes.

Most results are presented for PPG-DI-PTHF-0.35 while other polyurethanes are noted.

4.1. Simulation of ion penetration into polyurethane implant

A physical model of collisions between the penetrating ion into the polyurethane with electrons and atoms of the polyurethane macromolecules was used to understand the modification process in the surface layer. The penetration of a high energy ion into any polymer causes collisions with electrons and atoms of the polymer macromolecules. The simplest model of the collisions is based on ion-atom interactions developed by Ziegler and Biersack [1, 2]. The computer code SRIM/TRIM was designed for a simulation of such collisions and following physical effects in a target under ion bombardment. The model includes the physical effects such as ion/atom and ion/electron collisions, phonon excitation, atom and electron recoils and stopping of the penetrating ions (Fig.4.1). The code gives a depth and lateral distribution of these effects.

However, the code does not include chemical effects of the ion bombardment. The code also does not include an initial chemical structure of the target and structure transformation in the target with fluence of the ion bombardment. Taking into account these limitations, the simulation of ion penetration into polyurethane was done for nitrogen ions with energy of 1, 5, 10, 15 and 20 keV. The results of the calculations are presented in Fig.4.2-4.4.

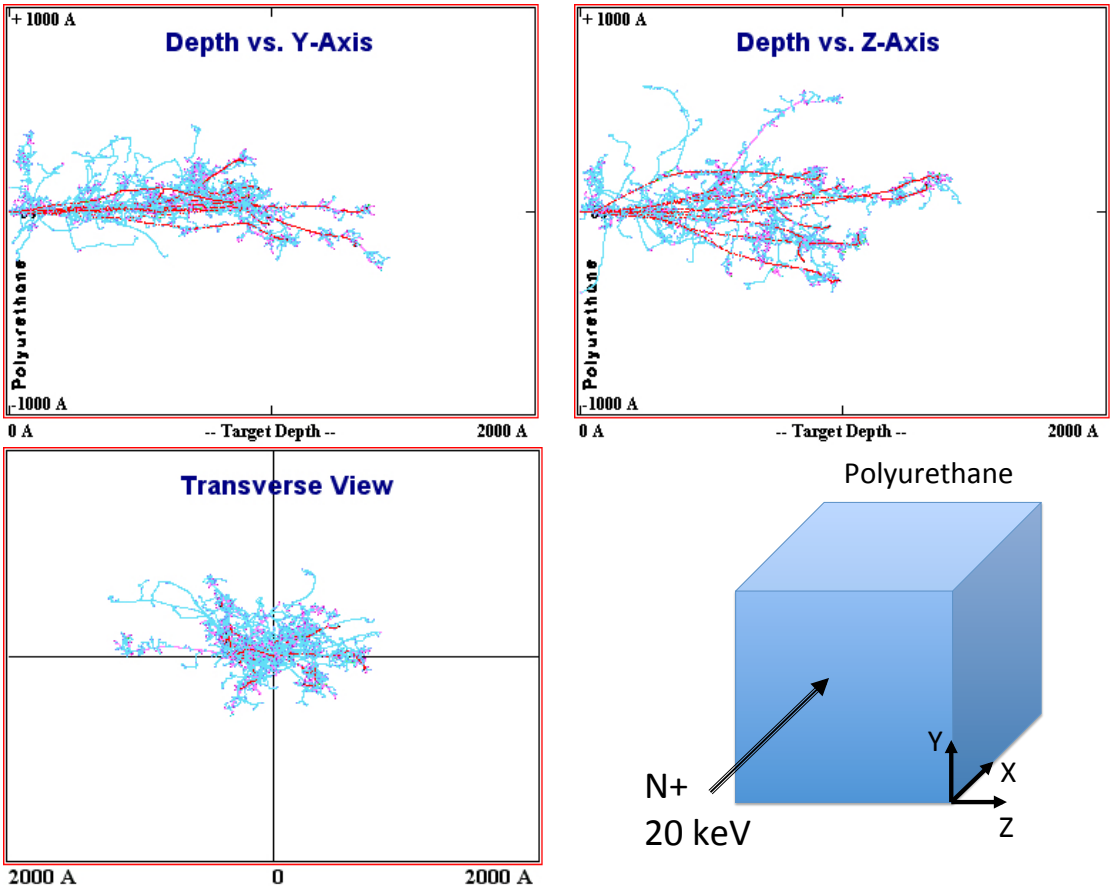

Fig.4.1. Example of SRIM calculation of nitrogen ion penetration into polyurethane and scheme of the calculation geometry. Red lines are trajectories of nitrogen ions, blue lines are trajectories of displaced hydrogen atoms, green lines are trajectories of displaced carbon atoms, pink lines are trajectories of displaced oxygen atoms, and green lines are trajectories of displaced carbon atoms in the screens from SRIM program after 10 nitrogen ion penetration. The calculations are based on Monte Carlo algorithm of the collisions. The following results are based on statistical averaging of 10000 ions penetrations.

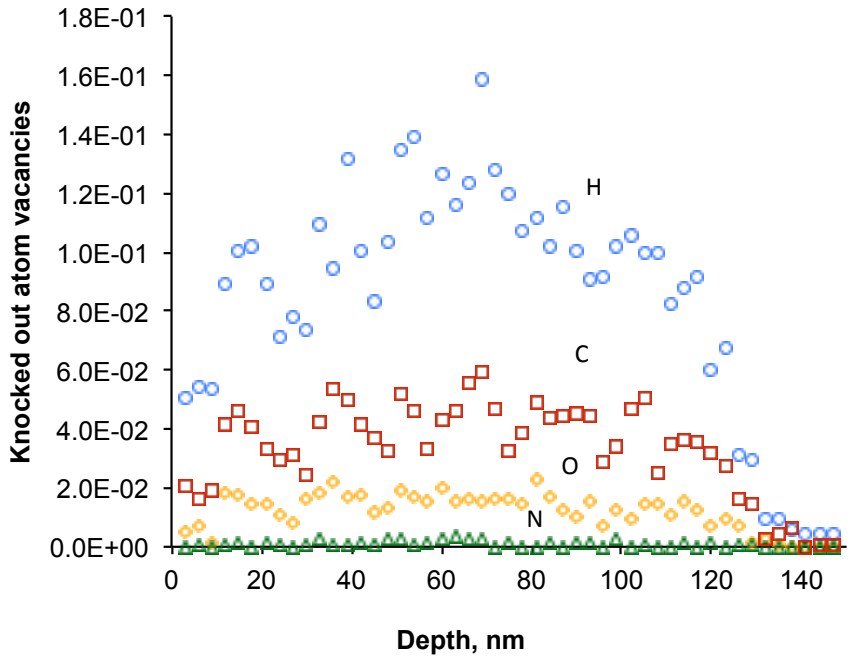

Fig.4.2. Vacancy atom distribution by SRIM calculations after 20 keV nitrogen ion bombardment caused by displacing of carbon, hydrogen, oxygen and nitrogen atoms from macromolecule of polyurethane. Mostly hydrogen atoms are displaced.

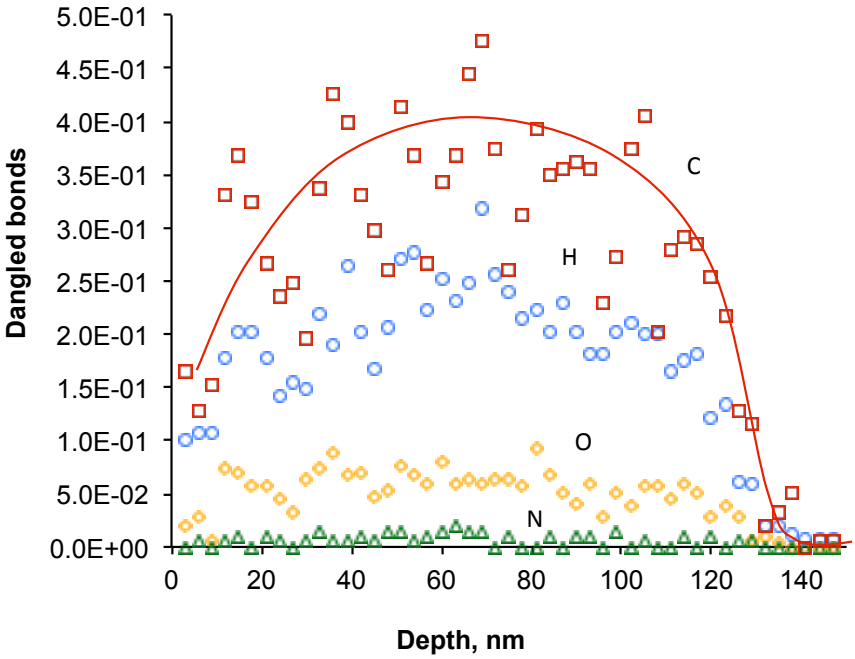

Fig.4.3. Dangled bond depth distribution caused by displaced of carbon, hydrogen, oxygen and nitrogen atoms in macromolecule of polyurethane by 20 keV nitrogen ion bombardment. The results of SRIM simulation. The most dangles bond appear after carbon atoms displacement.

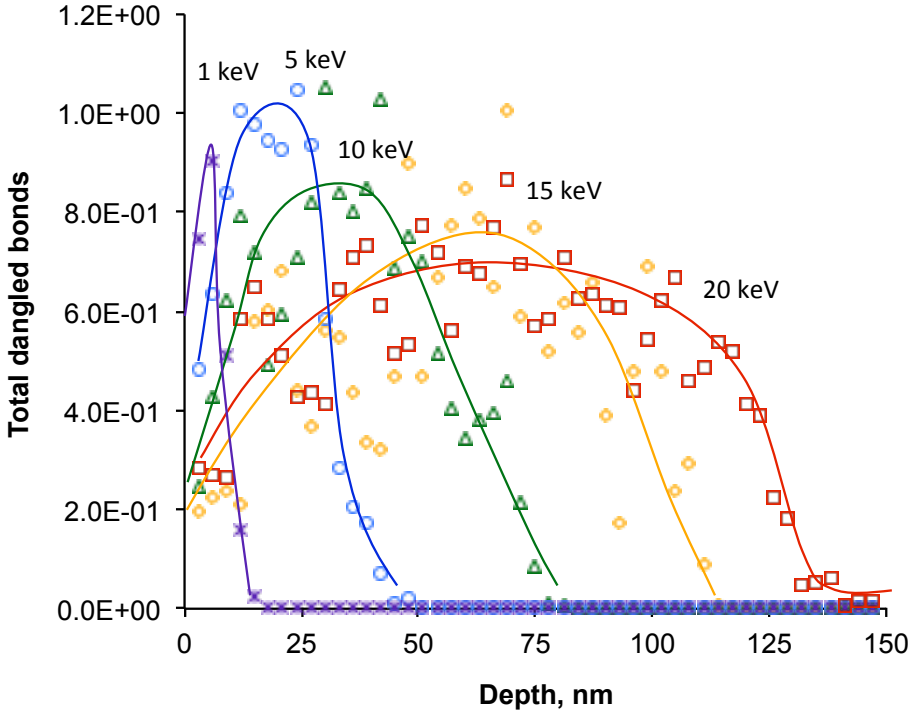

Fig.4.4. Dangled bond depth distribution (vacancy per Angstrom per Ion) in polyurethane by SRIM calculations after nitrogen ion penetration. The results of SRIM simulation. The thickness of the modified layer with dangled bonds is about 130 nm for 20 keV ion energy, 110 nm for 15 keV ion energy, 75 nm for 10 keV ion energy, 45 nm for 5 keV ion energy, 10 nm for 1 keV ion energy.

The results of calculations for 10 nitrogen ions are presented in Fig.4.1. The nitrogen ions penetrate into the polyurethane and knock the atoms of the macromolecule and transfer the kinetics energy from ions to atoms. The displaced atoms with high kinetic energy fly away from the mother macromolecule and knock another atom of macromolecules, transferring the kinetic energy to them. Each penetrating nitrogen ion removes many atoms. After cascades of collisions the kinetic energy is dissipated to phonon excitations and the process of collision finishes. The result is a number of displaced atoms, which travelled from the mother macromolecules. The area of the affected macromolecules has a shape of a large falling drop.

For quantitative estimation the calculation of 10000 ion penetrations was done. The distribution of displaced carbon, hydrogen, oxygen and nitrogen from polyurethane macromolecule with chemical formula of $C_{30.8}O_{9.88}N_{0.598}H_{58.6}$ is presented in Fig.4.2. For example, the chemical formula corresponded to PPG-DI-PTHF-0.35 polyurethane formula. The layer of about 130 nm is affected by the bombarding nitrogen ions with kinetics energy of 20 keV. Mostly the hydrogen atoms are displaced from the macromolecule, but carbon and oxygen atoms are also displaced. Nitrogen atoms are less affected. The different amounts of displaced atoms is due to different concentrations of these atoms in polyurethane macromolecule.

The displaced atoms move from the mother macromolecule over a long distance from the initial position so that each displaced atom leaves all their bonds in the mother molecule. For hydrogen atoms, one bond becomes dangled. Displaced oxygen,

nitrogen and carbon leave two, three and four dangled bonds in the mother macromolecule respectively. The displaced atoms are stopped after some collisions in new places and hold all their unpaired electrons. Therefore, these atoms bring dangled bonds to new places. Corresponding atom valencies of displaced carbon gives eight dangled bonds, nitrogen gives six, oxygen gives four and hydrogen gives two. The corresponding distribution of the displaced atoms and distribution of dangled bonds in the surface layer of polyurethane is presented in Fig.4.3. Displaced carbon atoms give the highest contribution, then hydrogen, oxygen and nitrogen. The total average number of displaced atoms from polyurethane macromolecule is 194 and the corresponding average number of dangled bonds generated by one bombarding ion of 20 keV energy is 722. All these dangled bonds are generated in a thin surface layer of about 130 nm thickness. Such a high concentration of the dangled bonds causes a number of free radical reactions immediately after the displaced atoms stop. These reactions are finalised with deep structural transformations of the surface layer.

The penetration depth of bombarding ions depends on the energy of the ions. Lower energy gives shallower modified layer Fig.4.4. The energy of 1 keV gives the thickness of the modified layer of about 5-10 nm, which is close to the size of the isolated macromolecule globule.

As a result of ion penetration and following deep molecular transformations, a chemical structure of the polyurethane surface changes dramatically after ion beam treatment. Chemical activity as well as other surface characteristics change correspondingly and are important for interactions with proteins, surrounding tissues and the organism as a whole. Therefore, efforts were made to understand the chemistry of the surface, the influence of ion beam parameters and storage kinetics after surface modification. The analysis of chemical structure was done with modern spectroscopy methods developed for a surface analysis.

4.2. Wettability and surface energy of modified polyurethane implant

One of the simplest methods of surface analysis and an important parameter for biocompatibility is wettability. Protein molecules are very sensitive to wettability of the implant. The surface of untreated polyurethane is hydrophobic. The water drop on the polyurethane surface shows the contact angle of about 90 degrees while the diiodomethane drop shows the contact angle significantly lower (Fig.4.5). This difference between drops of water and diiodomethane shows that the polar interactions on polyurethane surface are much weaker then non-polar (dispersic) interactions.

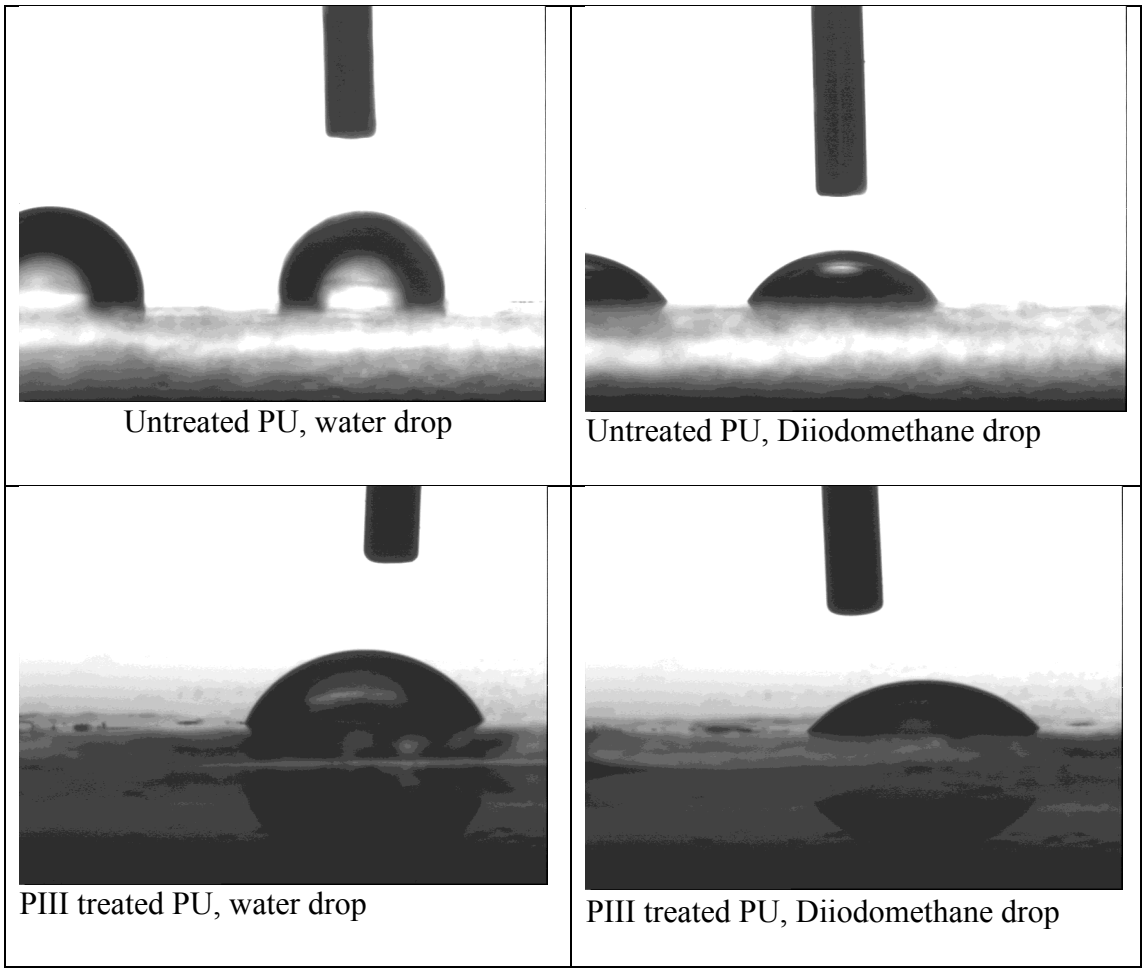

Fig.4.5. Images of water and diiodomethane drops on polyurethane surface untreated and 800 sec PIII treated after 2 weeks of ageing after the treatment. KRUSS wetting device was used for the images. The most changes caused by PIII treatment were observed for water drops.

After the PIII treatment the drops of water and diiodomethane were similar. It shows that the PIII treated surface becomes more hydrophilic and the polar interactions on the modified surface are similar to the non-polar interactions. The quantitative measurements of the drops show significant decrease of the contact angle from 93 degrees up to 35-45 degrees in 15 minutes after PIII treatment (Fig.4.6). The contact angle increases with the storage time after PIII treatment. The angle is stabilised a week after PIII treatment. The stabilised value for the treated surface is lower than for the untreated surface. These changes were observed to be in a similar statistical range for all treatment times from 40 sec to 800 sec corresponding to $5*10^{14}$ and 10^{16} ions/cm^2 fluence.

The contact angles of the water and diiodomethane were used for calculation of surface energy and its parts (Fig.4.7.). The surface energy is an energetic parameter of the surface to describe an interaction with the adsorbed molecules. The surface energy increases from 33 mN/m for untreated polyurethane to 65-67 mN/m for freshly treated polyurethane. A week after PIII treatment the surface energy decreases with stabilisation at 45-50 mN/m. The stabilized level of the surface energy is much higher then the surface energy of untreated polyurethane.

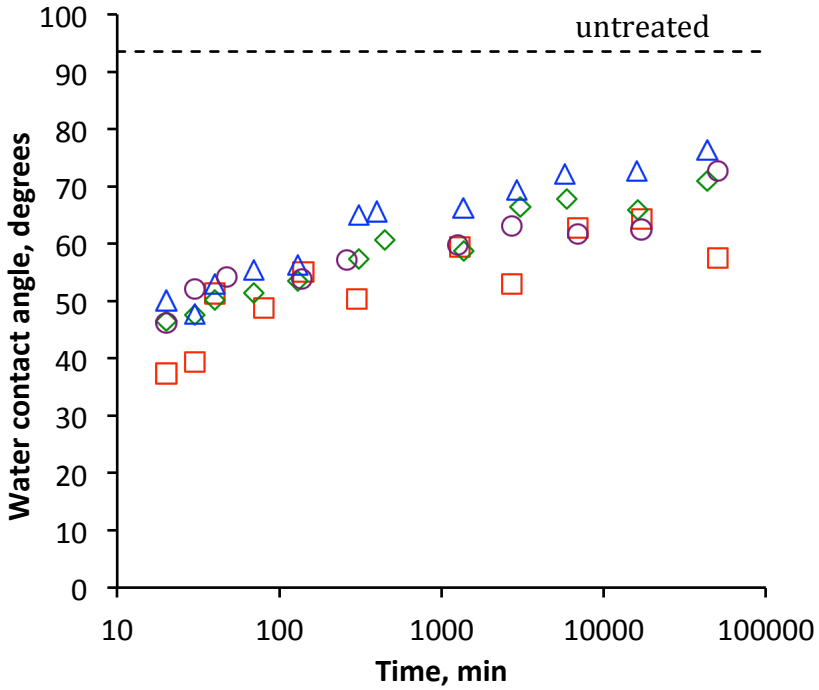

Fig. 4.6. Water contact angle of PIII treated PU as a function of storage time after the treatment. PIII treatment time is: violet circle – 40 sec, blue triangle – 80 sec, green rhomb – 400 sec, red square – 800 sec. The dashed line is untreated PU. The water contact angle decreases significantly after PIII treatment and increases with the storage time.

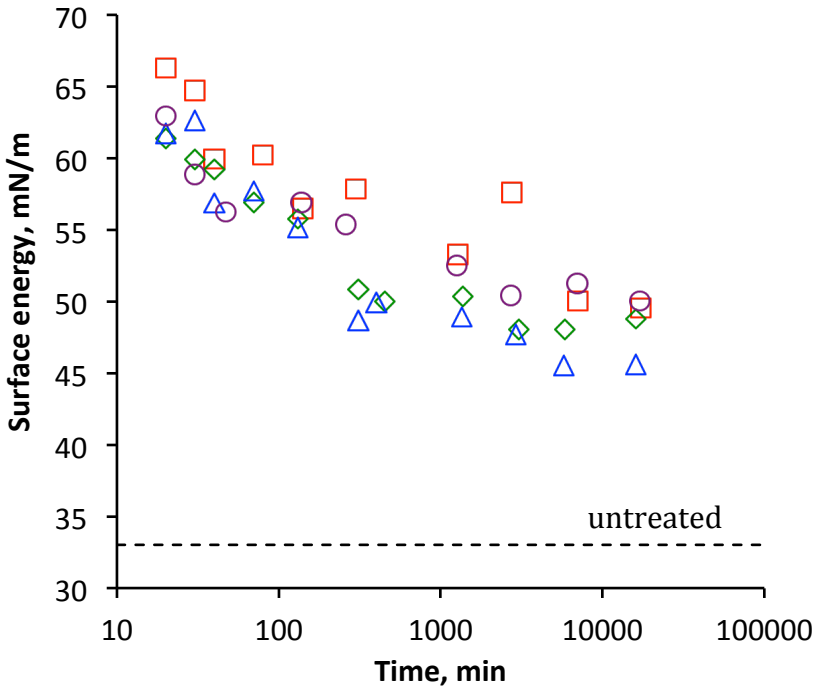

Fig.4.7. Total surface energy of PIII treated PU as a function of storage time after the treatment. PIII treatment time is: violet circle – 40 sec, blue triangle – 80 sec, green rhomb – 400 sec, red square – 800 sec. The dashed line is untreated PU.

The dispersic part of the surface energy increases from 31 mN/m to 40-44 mN/m for untreated polyurethane and decreases with storage time up to 37-39 mN/m (Fig.4.8).

The polar energy changes more dramatically (Fig.4.9). The polar part calculations show a value of 2 mN/m for untreated polyurethane. This value is usual for untreated polymers [3]. A short time after PIII treatment the polar part of surface energy increases to 17-27 mN/m and then decreases and is stabilised at 8-14 mN/m. The difference between the samples treated with different fluences is weak. There is no correlation trend of the surface energy and its parts with PIII fluence.

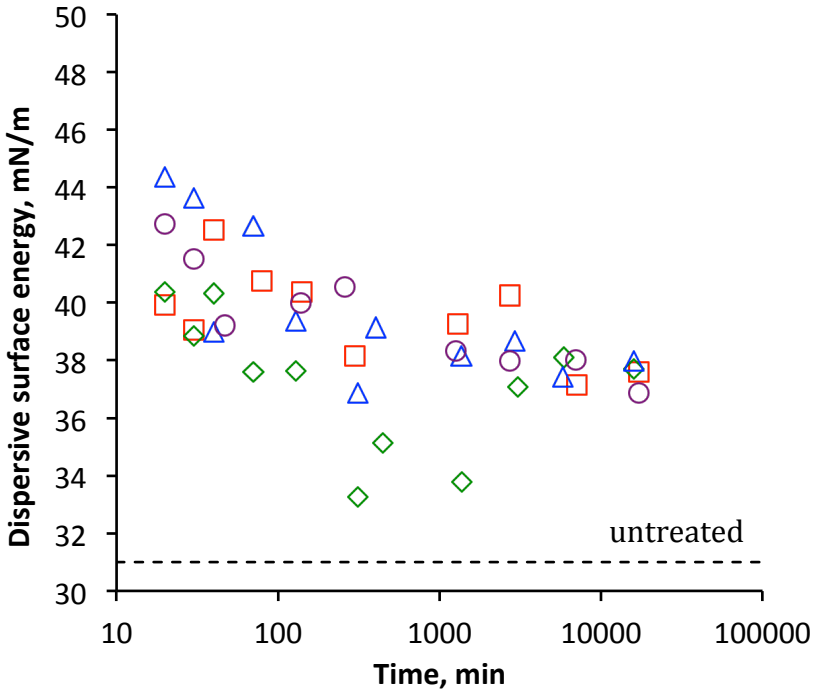

Fig.4.8. Dispersive part of surface energy of PIII treated PU as a function of storage time after the treatment. PIII treatment time is: violet circle – 40 sec, blue triangle – 80 sec, green rhomb – 400 sec, red square – 800 sec. The dashed line is untreated PU.

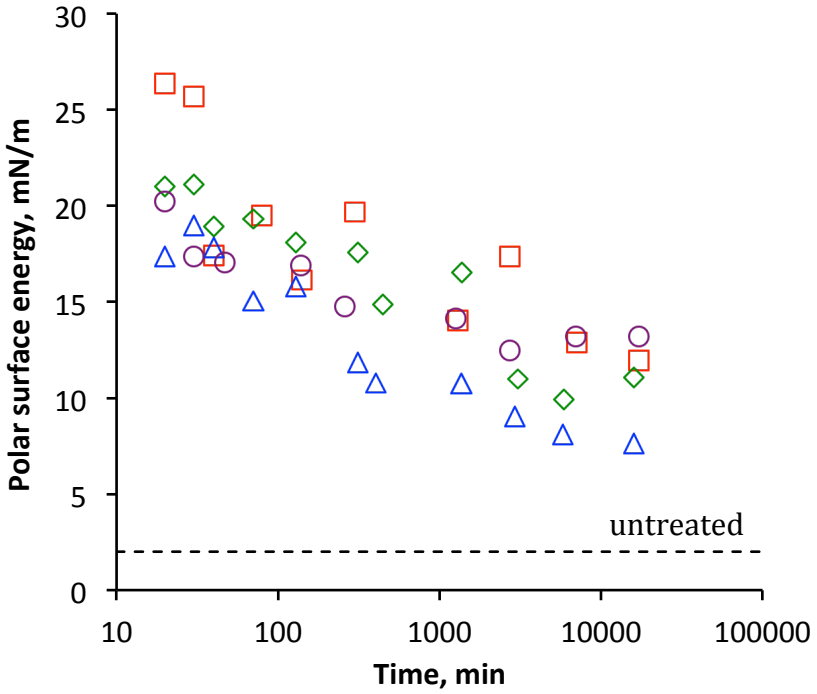

Fig.4.9. Polar part of surface energy of PIII treated PU as a function of storage time after the treatment. PIII treatment time is: violet circle – 40 sec, blue triangle – 80 sec, green rhomb – 400 sec, red square – 800 sec. The dashed line is untreated PU.

4.3. Chemical structure of the modified implant surface

To understand the chemical activity of the modified polyurethane implant surface, the analysis of the chemical groups and its stability was done. Due to the very thin modified layer (100 nm or less) of the polyurethane implant after PIII the modern methods of chemical structure surface analysis were used.

The effect of PIII treatment is visible by darkening the surface layer of polyurethane. A similar darkening previously observed for ion beam treated polymers was considered to be connected with carbonisation of the thin surface layer. The surface layer of polyurethane was analysed with X-ray photoelectron spectroscopy (XPS). XPS signal comes from very thin layer estimated as 5-10 nm of top layer. The survey spectra of the PU surface before and after PIII treatment are shown in Fig.4.10. The spectrum of untreated polyurethane shows lines of C1s of carbon, O1s of oxygen and N1s of nitrogen corresponding to the chemical formula. No other elements were detected.

After PIII treatment by nitrogen ions of 20 keV energy during 800 seconds the XPS spectrum shows the same lines of carbon, oxygen and nitrogen however the intensity ratio of the lines changed. The intensity of nitrogen lines increases following the nitrogen ion incorporation into the surface. The intensity of carbon line increases and the intensity of oxygen line decreases show the structure's changes. The treated surface becomes richer with carbon. No other elements are observed in polyurethane surface after PIII treatment.

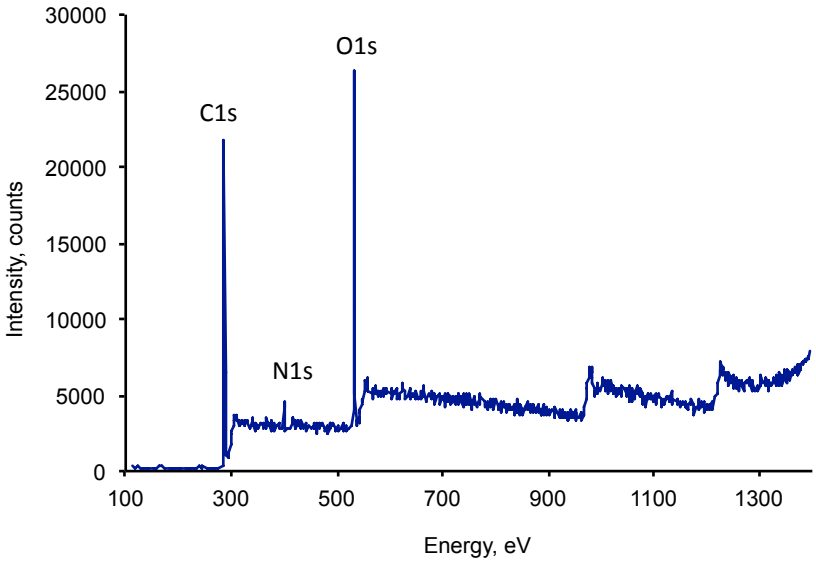

Untreated polyurethane

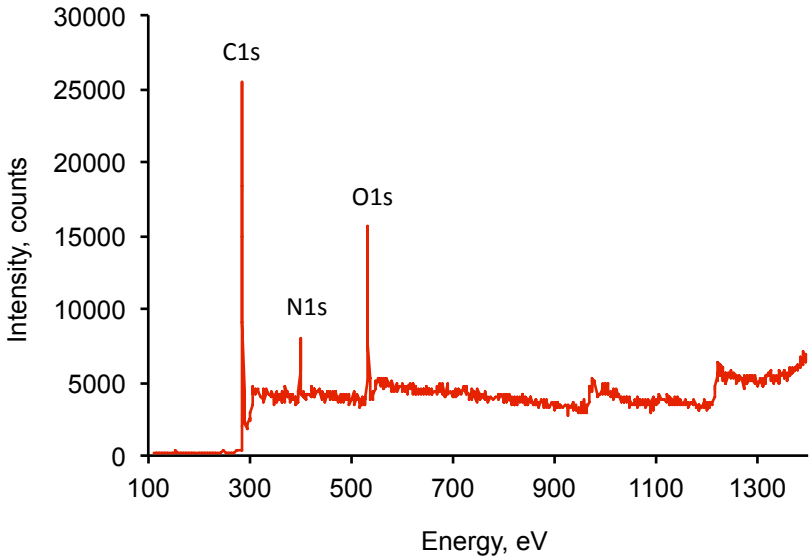

PIII treated polyurethane

Fig. 4.10. Survey XPS spectra of polyurethane untreated and PIII treated polyurethane with nitrogen ions of 20 keV energy 800 seconds.

The detailed analysis of the XPS spectra shows that the chemical structure of polyurethane has been changed after PIII treatment. For the analysis XPS spectra with high resolution were recorded and the lines were fitted with Gauss functions. The results of the analysis are presented in Fig.4.11. The C1s line contains 3 components of carbon atoms in C-C and C-H groups (284.8 eV), in C-O groups (286.3 eV) and O=CN-O groups (289.3 eV), that corresponds to polyurethane formula. The component of carbon atom in ether group is mostly intensive. After PIII treatment the line contains a minimum 4 components: 284.9 eV of carbon in C-C and C-H groups, 286.4 eV line of carbon in C-O and C-N groups, 288.0 line of carbon in C=O and C=N groups, and 288.9 line of carbon in O-C=O groups. The most intensive component is 284.9 eV of carbon in C-C and C-H groups.

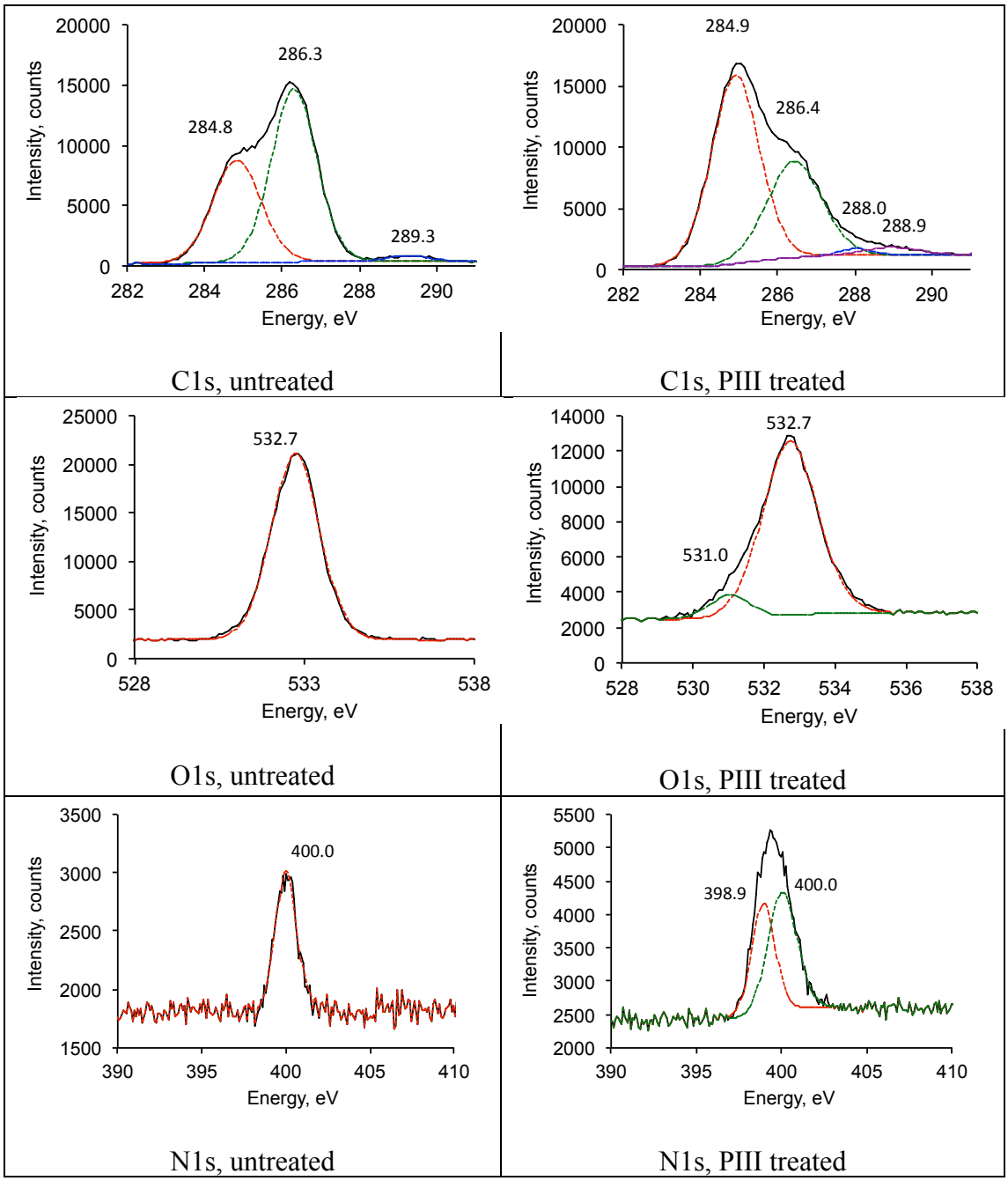

Fig.4.11. High resolution XPS lines of polyurethane before and after PIII treatment fitted with individual components.

The O1s oxygen line has been changed from the singlet line at 532.7 eV (oxygen in ether group) to doublet at 531.0 eV and 532.7 eV (oxygen in carbonyl and ether groups). The N1s nitrogen line has been changed also from the singlet line at 400.0 eV of nitrogen in urethane group to 398.9 eV and 400.0 eV of nitrogen in C=N and C-N groups. All these spectral changes show that the polyurethane structure is significantly damaged. The carbon structure with oxidation and nitrization is observed.

The optical properties of the polyurethane surface layer were analysed using spectroscopic ellipsometry. The polyurethane surface is relatively rough for precise optical measurements. Therefore the reflected light beam has a very low intensity that makes the signal noisy. An example of Ψ and delta functions of untreated polyurethane is presented in Fig.4.12. The region below 400 nm is undetectable while the region higher then 600 nm is well detectable. The Ψ and delta functions of the untreated and PIII treated polyurethane have different characters (Fig.4.12 and 4.13). The spectra of untreated polyurethane does not have interference features that show uniformity of the material by depth. The spectra of PIII treated polyurethane show features related to the interference effect due to different optical properties of surface and bulk materials. Using Cauchy model the optical properties n and k have been analysed to fit the experimental and theoretical Ψ and delta functions. The model of uniform bulk material was used for the untreated polyurethane. The PIII treated polyurethane was modelled with two layers: untreated bulk layer with the optical parameters from the spectra of untreated polyurethane, and the top layer with fitted properties.

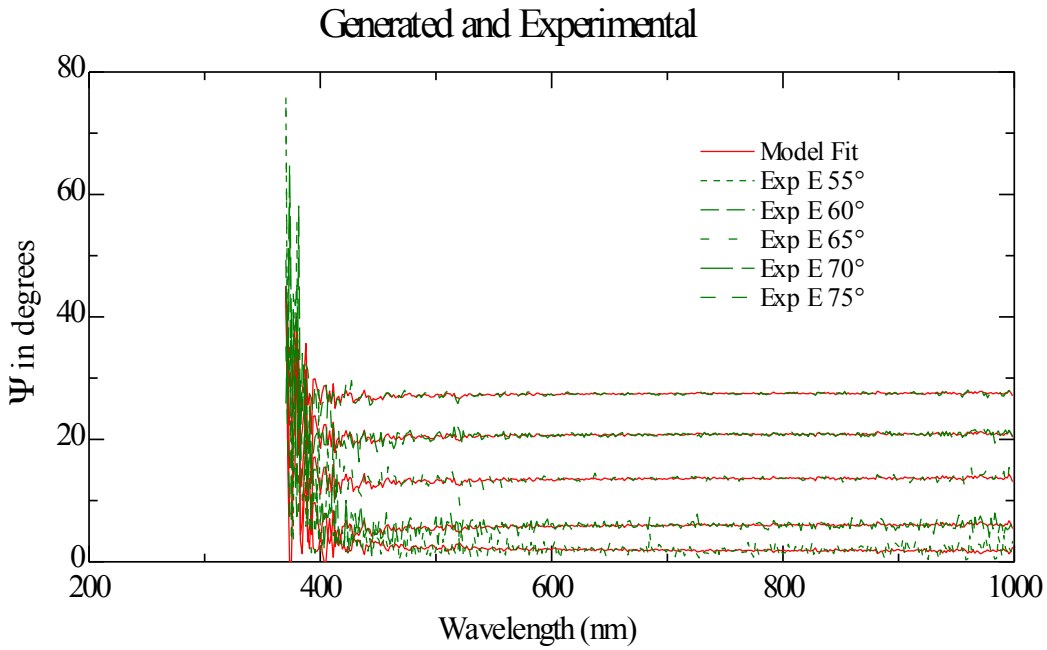

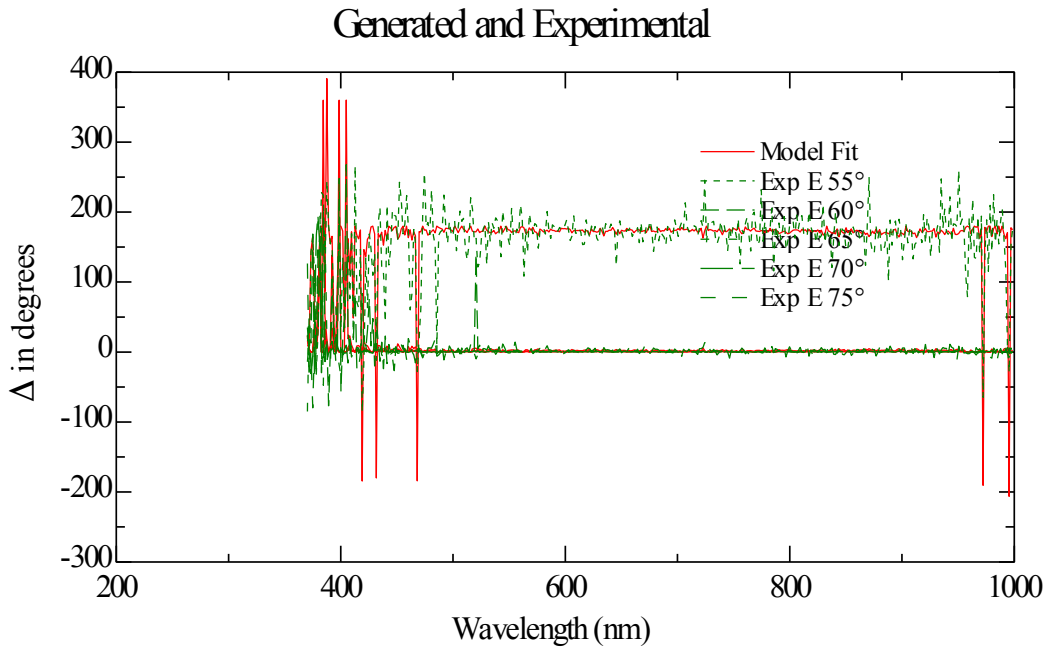

Fig.4.12. Ellipsometry Ψ and delta functions of untreated polyurethane and the model fit of bulk material.

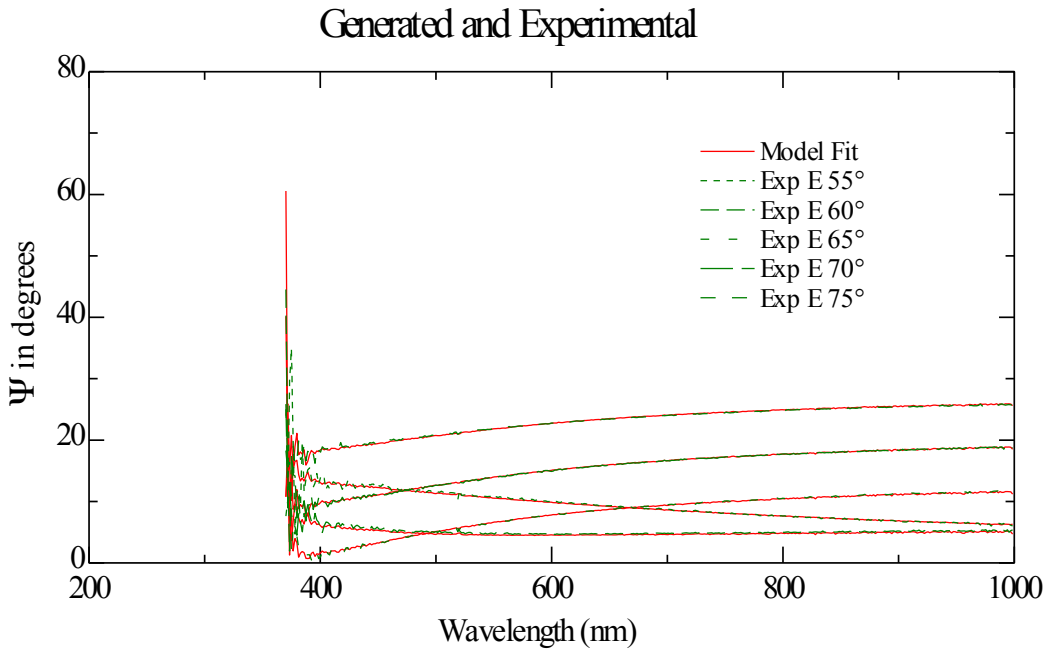

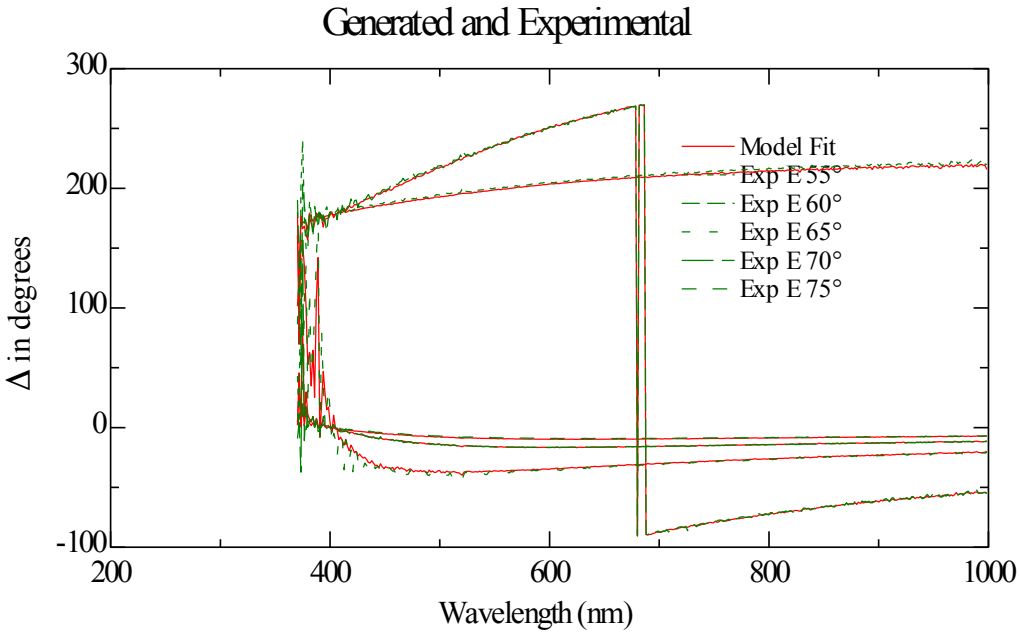

Fig.4.13. Ellipsometry Ψ and delta functions of PIII treated polyurethane with 20 keV energy nitrogen ions during 800 seconds and the model fitted with two layer materials: untreated polyurethane underneath and top fitted layer.

The results of the optical constants' fitting are presented in Fig.4.14. The thickness of the top layer on PIII treated polyurethane fitted in the model was 56 nm. The untreated polyurethane has the refractive index about 1.5 of low dispersion and no absorption in 450-1000 nm spectral region, when the PIII treated top layer has high dispersion of the refractive index between 1.7-1.8 values in 350-1000 nm region with absorption in 350-650 nm region. A similar effect of the high refractive index and absorption in short wavelength region is observed in other polymers after PIII treatment and interpreted as the carbonised top layer with condensed aromatic carbon rings like graphite or graphene. Such structures have high refractive index and high optical absorption. A similar interpretation can be used in the case of the PIII treated polyurethane. Therefore the PIII treated polyurethane has the top carbonised layer with high refractive index and optical absorption predominantly in short wavelength region of spectra.

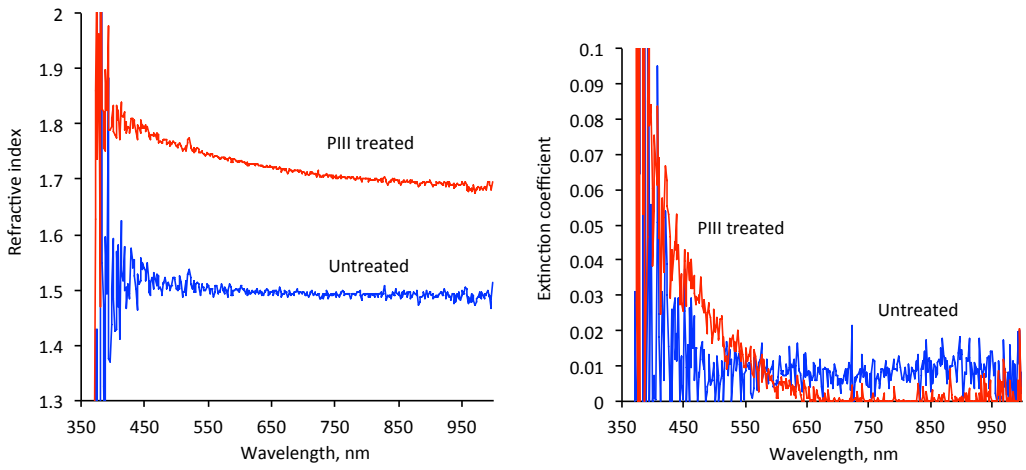

Fig.4.14. Refractive index and extinction coefficient of untreated polyurethane and 56 nm top layer of the treated polyurethane (800 sec of 20 keV nitrogen ion PIII) by ellipsometry spectra fitting.

The carbonisation of the top layer increases with the number of the bombarding ions or PIII treatment time. The spectra of the refractive index and extinction coefficient of the top polyurethane layer are presented in Fig.4.15. The refractive index spectra show the refractive index consistently increases across the whole diapason of the wavelength. The refractive index at the short wavelength increases as the saturation increases in the present range of PIII treatment time, while the refractive index at the long wavelength increases almost linearly (Fig.4.16). The extinction coefficient spectra show an increase of the absorbance in short wavelength region with PIII treatment time (Fig.4.15). The absorbance in a wavelength region longer then 500 nm does not increase with PIII treatment time. The linear character of the extinction coefficient with PIII treatment time was observed for 244 nm and 312 nm wavelength (Fig.4.16).

If the short wavelength corresponds to a low number of condensed aromatic structures, such structures appear in the top layer at shorter PIII treatment time. The long wavelength corresponds to the higher number of condensed aromatic structures and such structures need longer treatment time to be generated in the top layer of the polyurethane. The curve of the refractive index at long wavelengths and the extinction coefficient curves did not reach saturation in the diapason of the PIII treatment time that was used. However, a longer PIII treatment would probably make a larger size and number of condensed aromatic structures in the top layer of polyurethane.

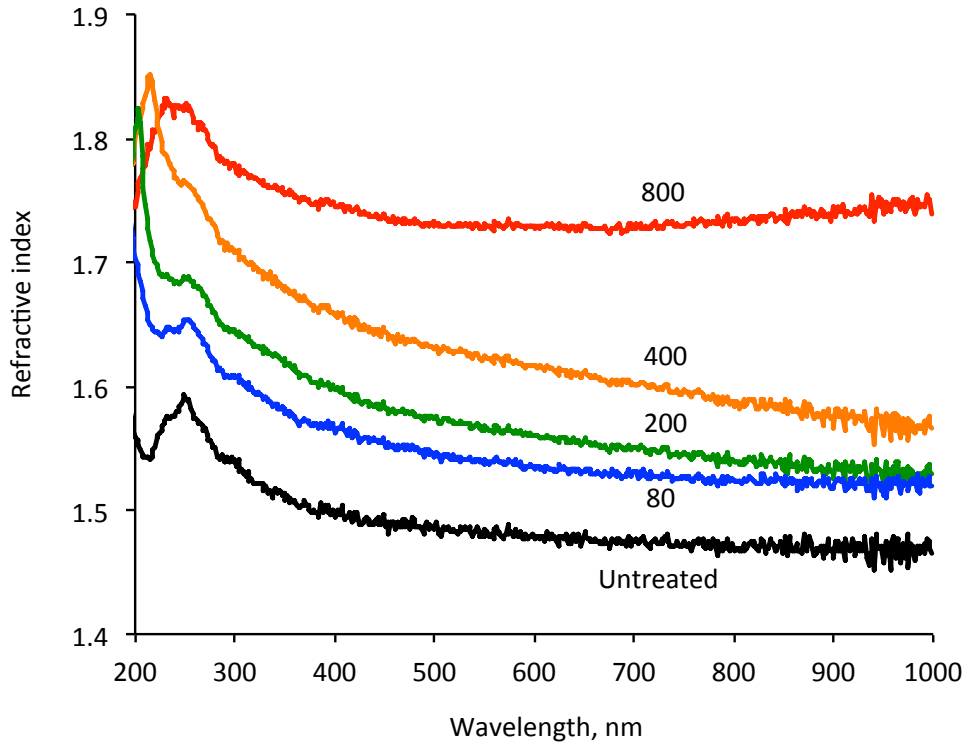

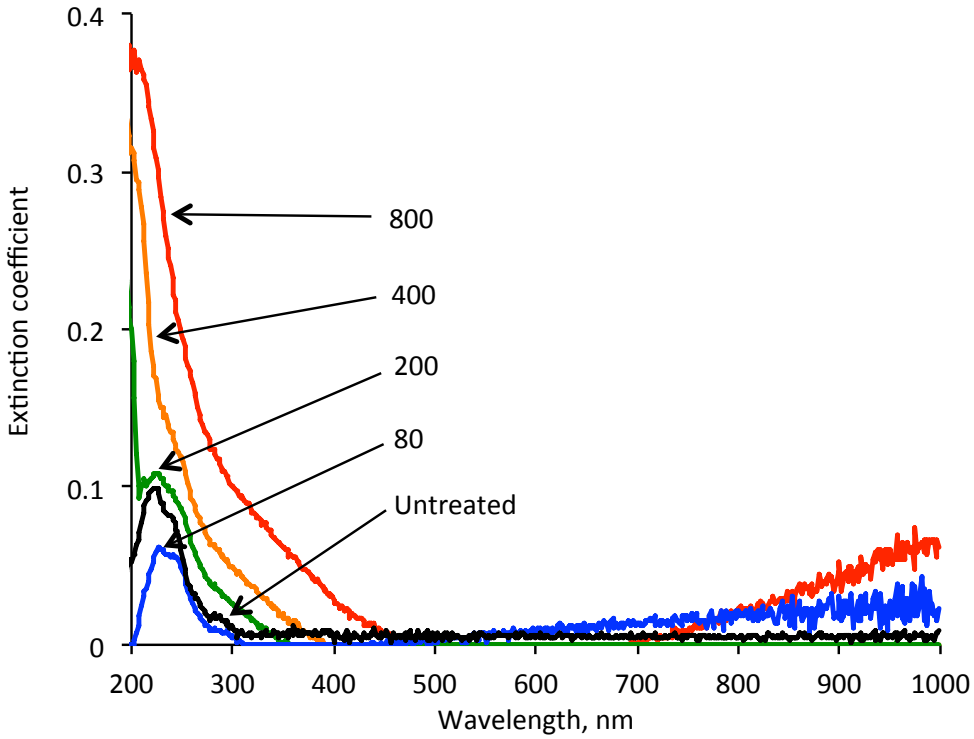

Fig.4.15. Refractive index and extinction coefficient spectra of top surface layer in 20 keV nitrogen ion PIII treated polyurethane with PIII treatment time (noted in sec) by ellipsometry fitting model.

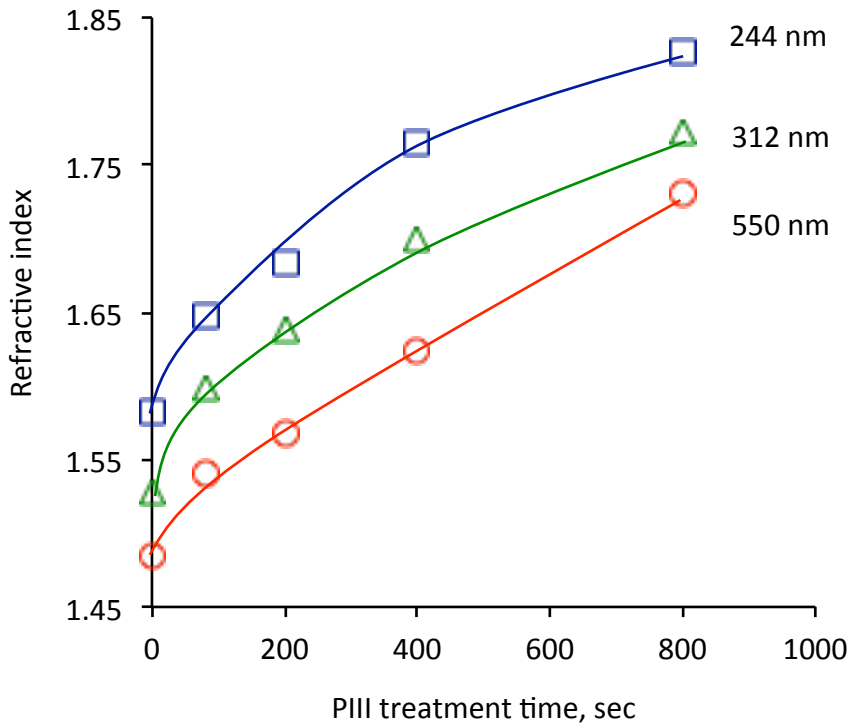

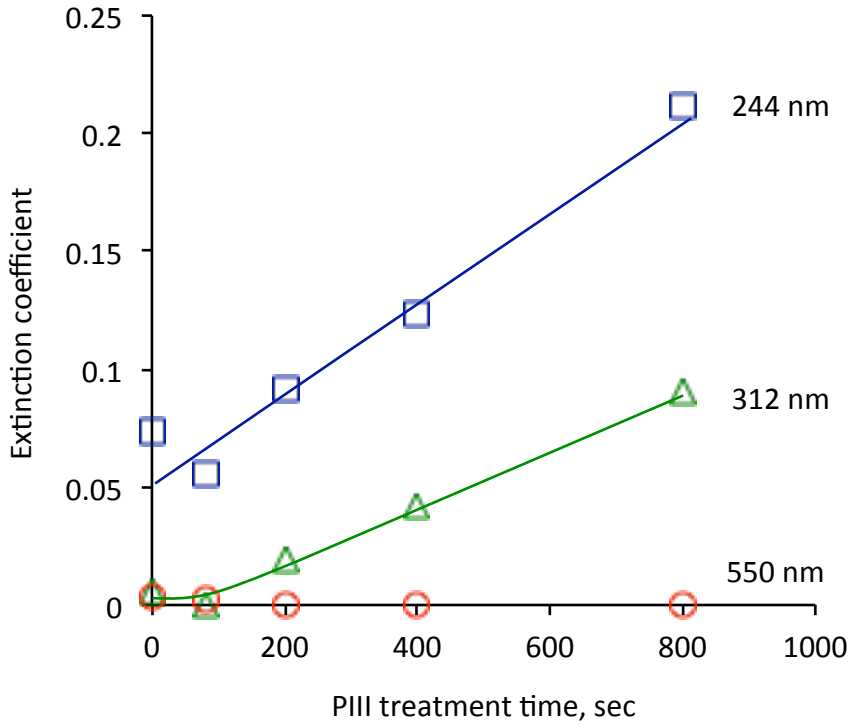

Fig.4.16. Refractive index and extinction coefficient of top surface layer in 20 keV nitrogen PIII treated polyurethane in dependence on PIII treatment time (noted in sec) by ellipsometry fitting model for different wavelength. The increase of refractive index and extinction coefficient corresponds to the transformation of the surface polyurethane layer to the surface carbonised layer with PIII treatment time.

The carbonisation of the top layer was detected using micro-Raman spectra (Fig.4.17). Spectrum of untreated polyurethane contains a number of spectral lines interpreted as vibrations of polyurethane macromolecule. The strong line at 1619 cm^{-1} is interpreted as a stretching vibration of aromatic ring, 1453 cm^{-1} and 1320 cm^{-1} lines are interpreted as bending vibrations in hydrocarbon chains. Low intensity characteristic lines are interpreted as Amide 1 vibration (1712 cm^{-1}) and Amide II vibration (1540 cm^{-1}) in urethane group, skeletal vibrations C-C (1080-1267 cm^{-1}) and aromatic ring vibrations (870 and 925 cm^{-1}).

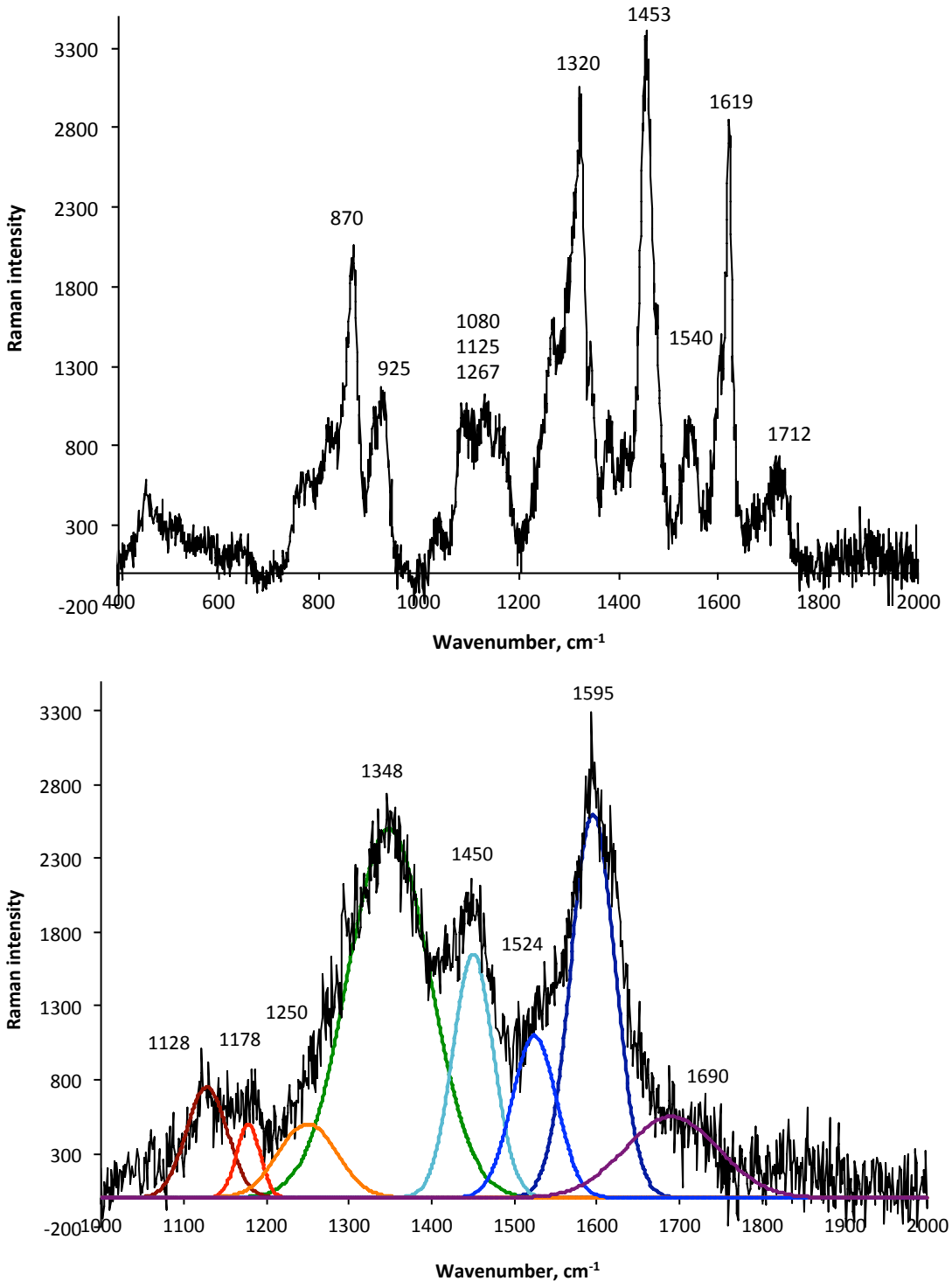

Fig.4.17. Micro-Raman spectra of untreated (top spectrum) and 20 keV nitrogen ion PIII treated polyurethane at 800 sec (bottom spectrum). Two new strong peaks at 1348 and 1595 cm^{-1} show the presence of graphite planes with defects in PIII treated polyurethane.

The spectrum of PIII treated polyurethane contains new strong lines at 1348 and 1595 cm^{-1}. These two lines are interpreted as resonance Raman lines of the carbonised top layer: D and G peaks. G-peak is E_{2g} vibrations in graphitic structure with sp^2

hybridisation of the valence electrons. D-peak is A_{1g} vibrations in graphitic structure. The mode A_{1g} is forbidden in Raman spectra of infinite ideal graphitic plane. However, due to the edges and disordering of the graphitic structure in real material, this mode becomes visible in Raman xx. This effect can be used for estimation of the irregularity of the graphitic structure. The ratio I(D)/I(G)=1.77 and G-peak position corresponds to I area in Robertson/Ferrari diagram that shows a nanocrystalline graphite with characteristic size of graphitic islands of L_a=2.5 nm separated by amorphous carbon with sp^3 hybridization.

The surface layer transformations have been detected with NEXAFS spectroscopy. The spectra of surface and bulk layers of untreated polyurethane are presented on Fig.4.18. The C1s spectrum region of the bulk layer detected by MCP detector and the surface layer detected by channeltron contain lines of 285.14 eV of C1s(C-H)→ $1\pi^*_{C=C}$ transition, 288.87 eV of C1s(C=O)→ $\pi^*_{C=O}$ transition, 291.22 eV of C1s(C-H)→ σ^*_{C-O} transition, 293.1 eV of C1s(-CH-O-)→ σ^*_{C-C} transition and broad line at about 300 eV of C1s(C-H)→ σ^*_{C-C} transition. The spectra interpretation of C1s lines corresponds to known literature data on NEFAXS spectra of polyurethanes based on TDI and polyethers.

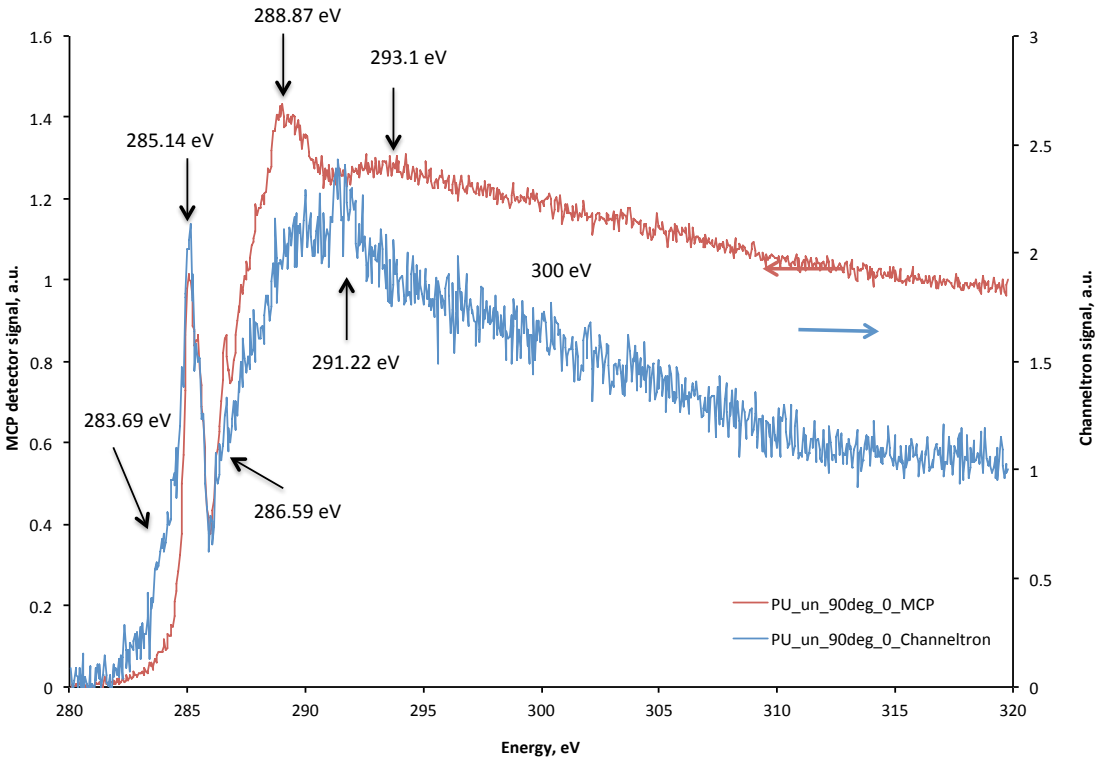

Fig.4.18. Near-edge X-ray absorption fine structure (NEXAFS) spectra of untreated polyurethane with channeltron (surface) and MCP detector (bulk) in C1s region.

The N1s spectrum of bulk layer detected by MCP detector and the surface layer detected by channeltron contain two narrow lines and broad band with two maximums (Fig.4.19). The weak narrow line at 399.0 eV can be interpreted as N1s(C-N)→ $1\pi^*_{C=C}$ transition and second narrow line at 403.3 eV can be interpreted as N1s(C-N)→ $\pi^*_{C=O}$ transition. The broad line at 407.3 eV can be interpreted as N1s(C-N)→ σ^*_{C-N} transition and broad line at 412.3 eV is interpreted as N1s(C-N)→ σ^*_{C-C} transition. This interpretation is preliminary because an interpretation of N1s

NEXAFS peaks for polyurethane has not yet been found in the literature. The present interpretation was done based on similar interpretations for C1s and O1s peaks of NEXAFS spectra of polyurethanes.

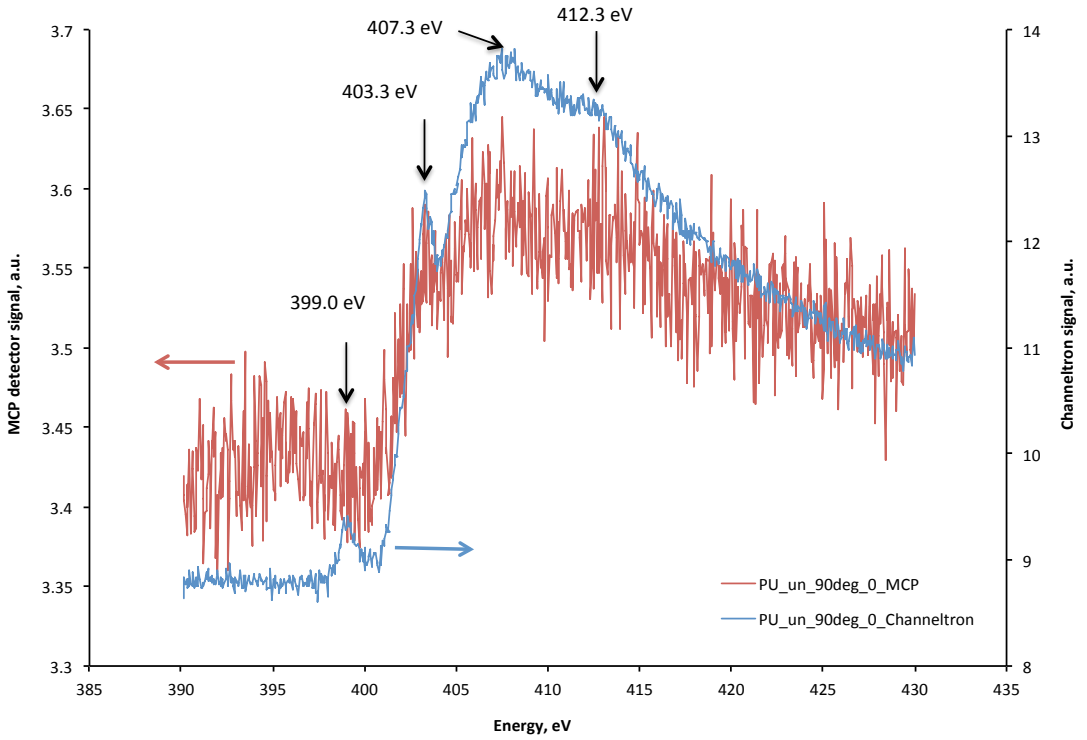

Fig.4.19. Near-edge X-ray absorption fine structure (NEXAFS) spectra of untreated polyurethane with channeltron (surface) and MCP detector (bulk) in N1s region.

The NEXAFS spectra of polyurethane after PIII treatment shows differences from the spectra of untreated polyurethane (Fig.4.20) while the NEXAFS spectra of the bulk layer in untreated and PIII treated polyurethane are identical (Fig.4.21). The intensity of 285.14 eV line decreases significantly. The intensity of 288.98 line increases. The spectrum becomes similar to a spectrum of deposited carbon. The strong coupling of C-H bond with p-orbital becomes weaker and that shows that the aromatic structures are condensed or surrounded by amorphous carbon. The line at 403.3 eV disappears and a new line at 400.0 eV appears. The first line at 403.3 corresponds to a coupling of the nitrogen with p-orbital in carbonyl bond of urethane group. Due to destruction of the urethane groups in the surface layer, the line disappears. The second line at 400.0 eV is interpreted as N1s(C=N)→ $\pi^*_{C=N}$ transition as it is observed in carbon nitride coatings. Therefore, the nitrogen is incorporated into the condensed aromatic structures of the top layer in nitrides form.

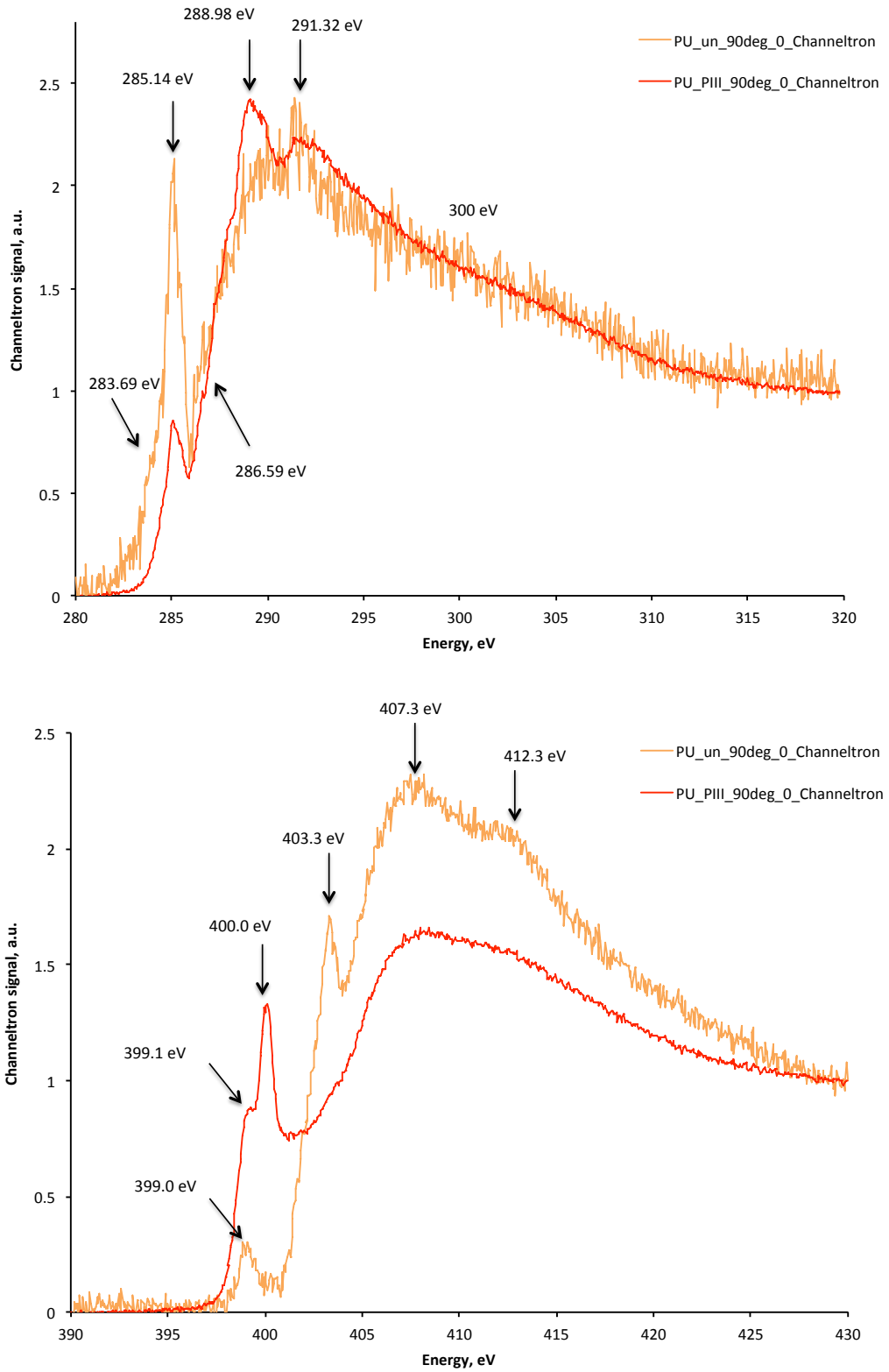

Fig.4.20. Near-edge X-ray absorption fine structure (NEXAFS) spectra with channeltron (surface) of untreated polyurethane and PIII treated polyurethane (N+ 20 keV, 800 sec) in C1s and N1s region.

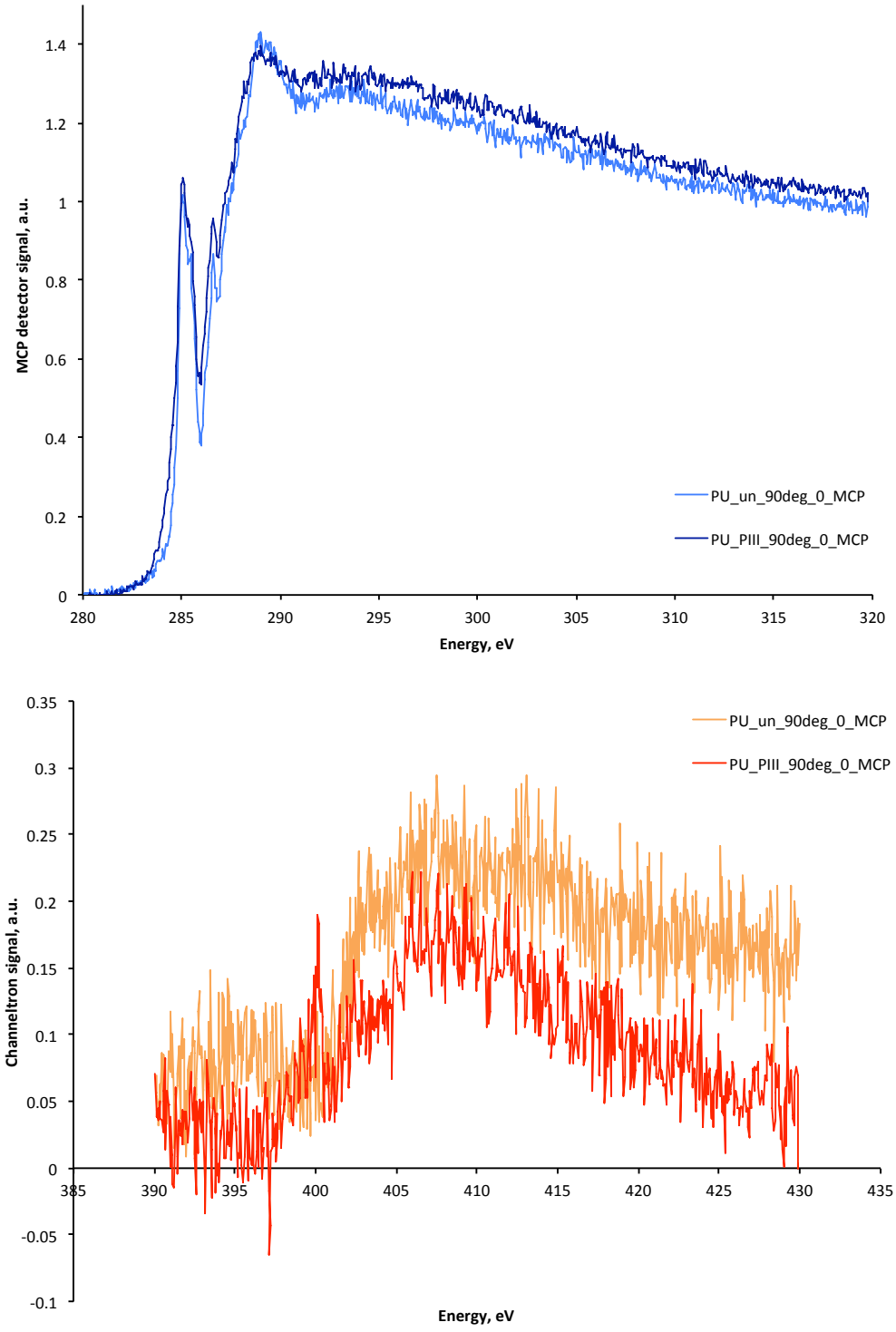

Fig.4.21. Near-edge X-ray absorption fine structure (NEXAFS) spectra with MCP detector (bulk) of untreated polyurethane and PIII treated polyurethane (N+ 20 keV, 800 sec) in C1s and N1s regions.

The modified polyurethane layer has a signal of unpaired electrons in electron spin resonance (ESR) spectra. The ESR spectra of the untreated polyurethane and the PIII treated polyurethane at 800 seconds by nitrogen ions with 20 keV energy are presented in Fig.4.22. The PIII treated sample was recorded after 3 months storage in laboratory under normal conditions (in Petri dish, in dark box, 20-25^{0}C, 50-80% of

humidity). The untreated polyurethane film does not have a signal higher than the noise level. The PIII treated film has a strong signal with g-factor about 2.0028. The signal with such g-factor corresponds to unpaired electrons of carbon free radicals at the edges of aromatic structures in graphite- or graphene-like structures [4]. The spectra show that the free radicals in the modified layer appear after PIII treatment and then remain when it is stored for a further 3 months. Such long shelf-life free radicals are probably stabilised by π-electrons of the aromatic rings of graphite-like structures. The presence of nitrogen in the aromatic structures can increase the stabilisation effect.

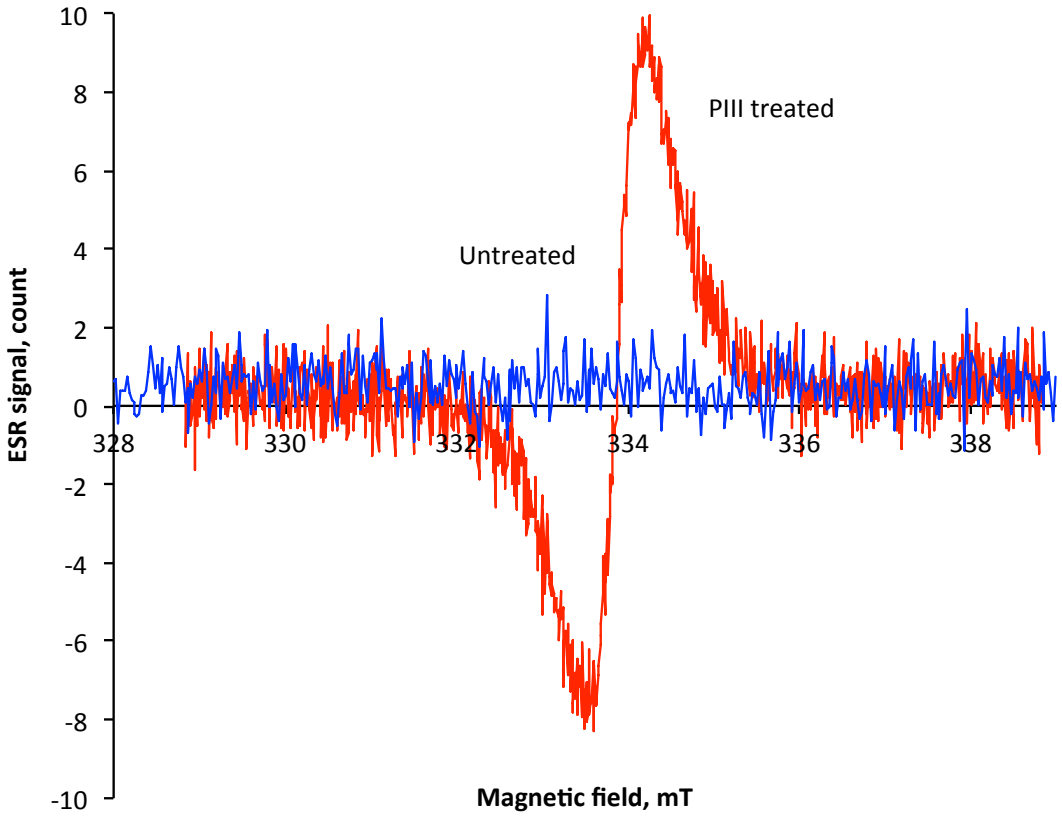

Fig.4.22. Electron spin resonance spectra of untreated polyurethane (blue) and PIII treated polyurethane (red).

The free radicals in the surface layer are able to react with a large number of molecules adsorbed on the surface including atmospheric gases like oxygen and nitrogen. The reactions of free radicals in the carbonised layer with oxygen from the atmosphere can generate a number of oxygen-containing groups [5].

The presence of new chemical groups in the modified surface layer has been observed in FTIR ATR spectra of the polyurethane surface (Fig.4.23). The spectra of untreated and PIII treated polyurethane surfaces show similar intensive lines interpreted as vibrations of the polyurethane structures: Amide A, I and II lines of urethane and urea groups, CH stretching and bending vibrations in –CH<, $-CH_2-$ and $-CH_3$ groups, aromatic ring lines, C-O vibrations in urea and ether groups as well as complex shape vibrations in finger-print regions. The spectrum of PIII treated polyurethane shows additional lines in 3500-3300 cm^{-1} region interpreted as hydroxyl group line vibrations, and 1700-1600 cm^{-1} region interpreted as carbonyl, amide and carbon-

carbon unsaturated group lines overlapped in one wide band. The intensity of these lines is low due to the thin modified layer (about 100 nm) in comparison with a depth penetration of the infrared beam to the sample from ATR crystal during the spectra recording (about 1 μm). Other spectral changes are less visible.

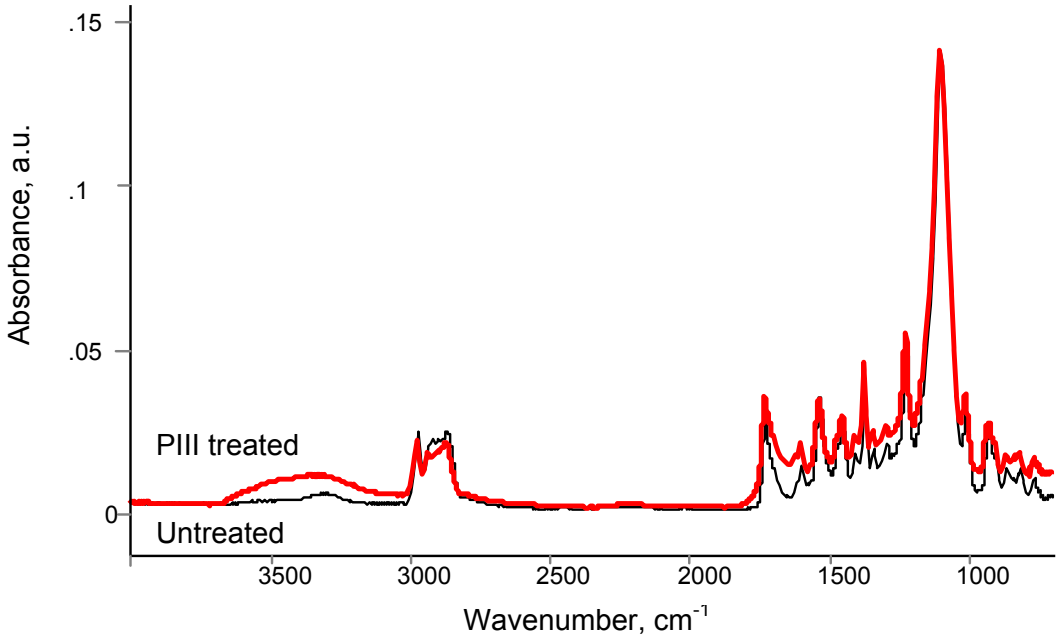

Fig.4.23. FTIR ATR spectra of PPG-DI-PTHF-0.35 polyurethane untreated (thin black bottom curve) and PIII treated during 800 seconds of 20 keV nitrogen ions (thick red top curve).

To recognise all changes, a subtraction method of the spectra is used. The spectrum of the untreated sample was subtracted from the treated sample spectrum with adjustment of the subtraction factor to minimise the spectral line intensity common for both spectra. The result of subtraction is a difference in the spectra caused by the different chemical structure of the treated and untreated polyurethane surface layer (Fig.4.24). In this way, the subtracted spectra are more sensitive and the contrast of the spectral difference is more clearly visible than is suitable for an analysis of the modified layer.

The lines of the subtracted spectra strong band in 3500-3000 cm^{-1} region have a complex shape and consist of some visible peaks with maximums at 3625, 3400, 3360 and 3220 cm^{-1}. The peaks are broad and overlayed with each other. The position of the peak maximums and width show that these peaks can be interpreted as –OH stretch vibrations of hydroxyl groups in hydrogen bonds. The shape of the line does not change much with PIII treatment time.

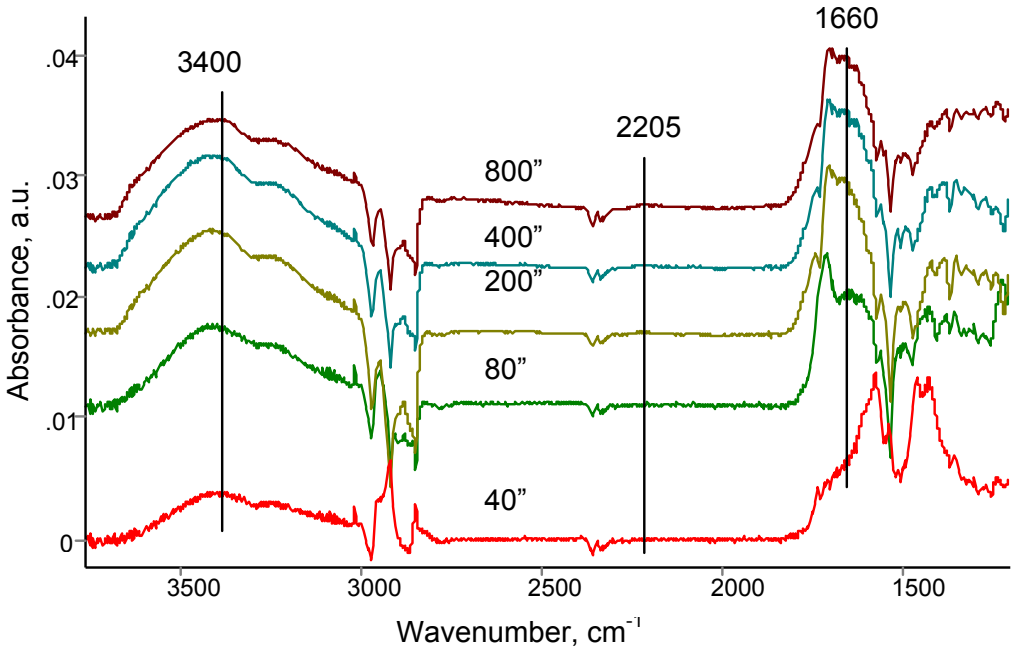

Fig.4.24. Differential FTIR ATR spectra of PPG-DI-PTHF-0.35 polyurethane after PIII of 20 keV nitrogen ions with different treatment time (shown on diagram). The spectrum of untreated PU is subtracted.

In the middle region, the strong complex lines are observed in 1800-1400 cm^{-1} region. The shape of the lines depends on the PIII treatment time. The spectrum of 40 sec PIII treated sample shows strongest peaks at 1613 cm^{-1} of C=C vibrations, 1465 and 1435 cm^{-1} of CH bending vibrations with low intensity 1740, 1715 and 1660 cm^{-1} peaks of C=O vibrations. The spectrum of 80 sec PIII treated sample and spectra of other samples with longer PIII treatment time do not show 1613, 1465 and 1435 cm^{-1} peaks, but show strong peaks at 1715 and 1660 cm^{-1} of C=O vibrations. The low intensity peak at 2205 cm^{-1} observed in spectra of these samples is interpreted as stretching vibrations CN in nitrile groups. All these peaks are not related to initial polyurethane structures but are related to the modified surface layer.

The quantitative measurements of the absorbance peaks show a dependence of the chemical changes in terms of PIII treatment time Fig.4.25-28. The intensity of hydroxyl group line was analysed on absorbance at 3400 cm^{-1} as the most intensive peak (Fig.4.25a). The -OH line absorbance was normalised on absorbance of methyl group in polyurethane at 2870 cm^{-1}, which is constant with PIII treatment time. The intensity of peak increases asymptotically with a saturation achieved after 400 sec of PIII treatment time. The saturated character of the OH absorbance shows that the maximal effect of modification of the surface layer in term of hydroxyl group formation is limited.

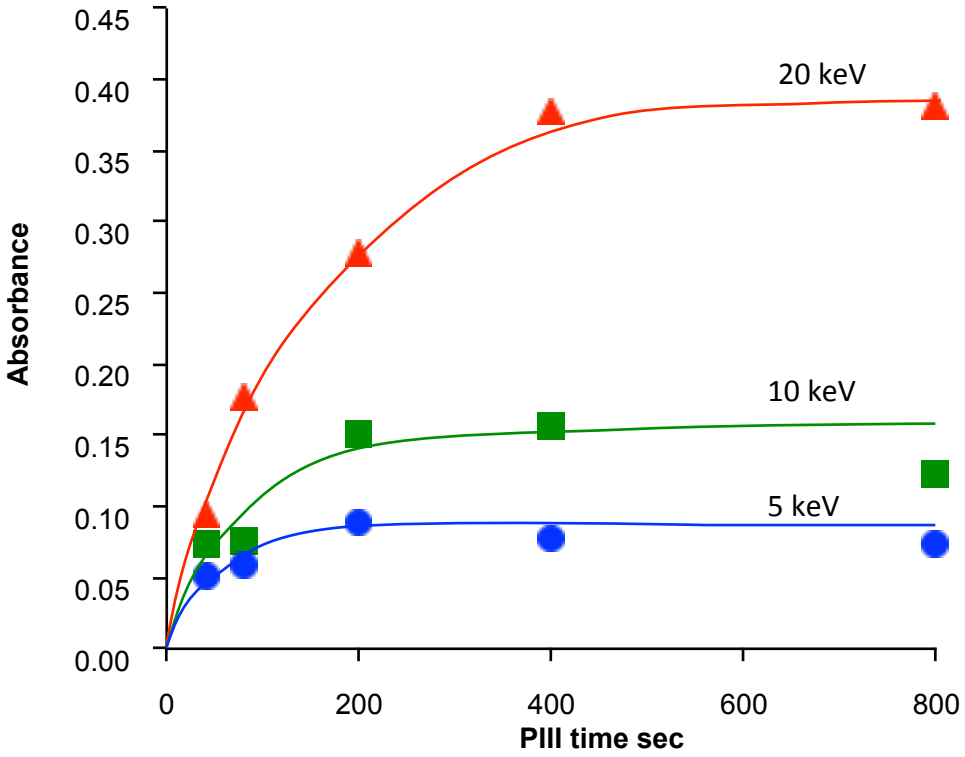
0.45
0.40
0.35
0.30
0.25
0.20
0.15
0.10
0.05
0.00
Absorbance
20 keV
10 keV
5 keV
0
200
400
600
800
PIII time sec

a

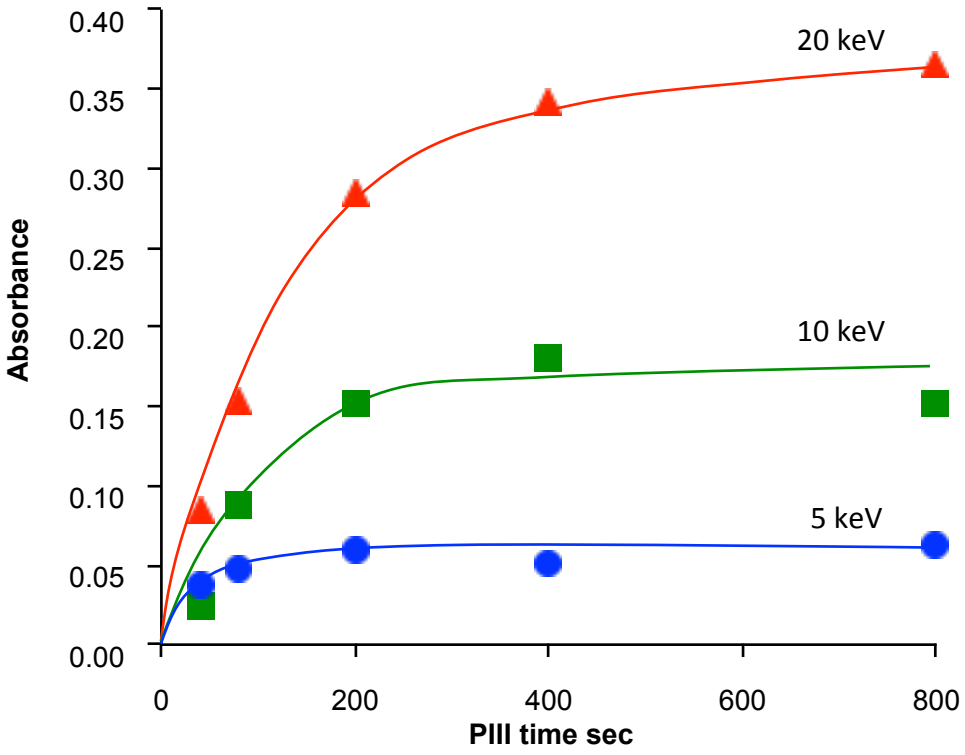
0.40
0.35
0.30
0.25
0.20
0.15
0.10
0.05
0.00
Absorbance
20 keV
10 keV
5 keV
0
200
400
600
800
PIII time sec

b

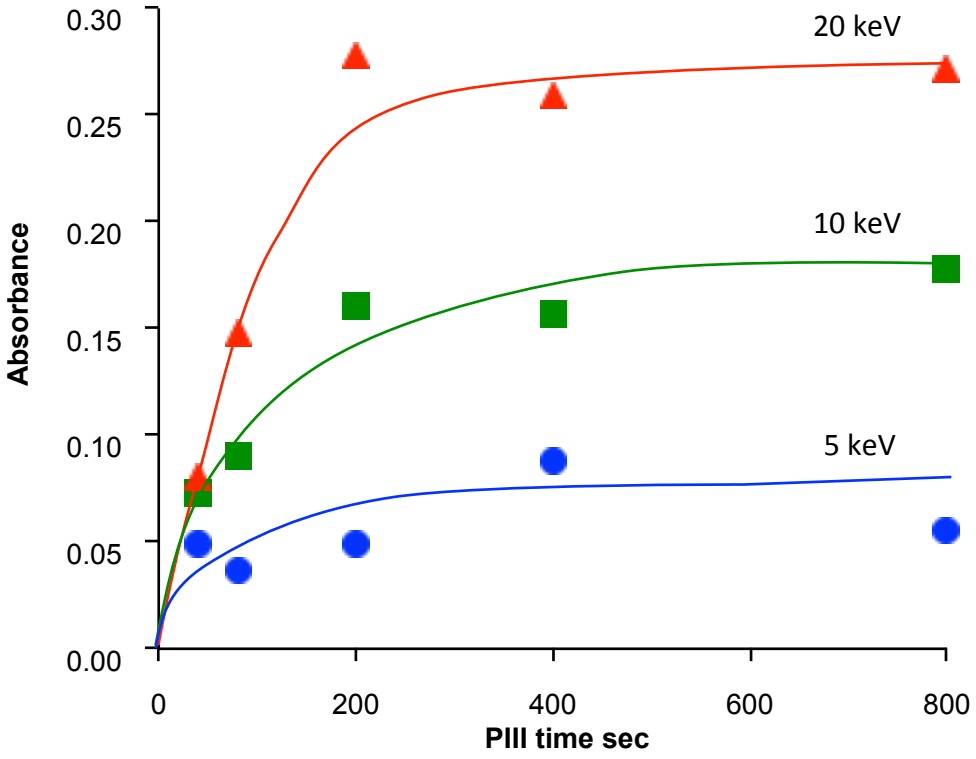

c

Fig.4.25. Absorbance of hydroxyl group (3400 cm^{-1}) normalised on absorbance of methyl group (2870 cm-1) in FTIR ATR spectra of PU as a function of PIII treatment time with 5, 10 and 20 keV energy nitrogen ions: a – PPG-DI-PTHF-0.35 polyurethane, b – PPG-DI-PTHF-0.5 polyurethane, c – PPG-DI-PTHF-0.7 polyurethane.

The maximal amount of hydroxyl groups depends on the applied bias during PIII treatment. For lower applied bias and correspondingly lower kinetics energy of bombarding nitrogen ions, the thickness of the modified layer is proportionally lower following TRIM/SRIM calculations (Fig.4.4). The bias of 10 kV and 5 kV was applied to the polyurethane samples and the FTIR ATR spectra were analysed. The frequency of bias pulses was adjusted for 10 kV and 5 kV to get the same fluence of the PIII treatment as described in Chapter 2. Similar asymptotical character of hydroxyl group absorbance is also observed for PIII treated polyurethane at lower PIII bias of 10 kV and 5 kV (Fig.4.25a). However, the maximal saturated amount of hydroxyl groups in the modified layer is proportionally lower for 10 and 5 kV bias samples in comparison with 20 kV samples. This fact shows that the hydroxyl group amount is proportional to the ion kinetics energy or thickness of the modified layer.

The asymptotical character of hydroxyl group collection and dependence on bias voltage is observed for other polyurethanes with different composition (Fig.4.25a, b and c). The polyurethanes with 0.5 and 0.7 molar ratio of NCO/OH groups at the synthesis (the synthesis is described in Chapter 3) were PIII treated and FTIR ATR spectra were analysed. The saturation effect was also observed after 400 sec of PIII treatment time. However, the saturation level of hydroxyl group absorbance was lowest for 0.7 ratio polyurethane with highest PTHF concentration (Fig.4.26). This

polyurethane has the lowest ether group concentration in comparison with polyurethanes of 0.35 and 0.5 ratios.

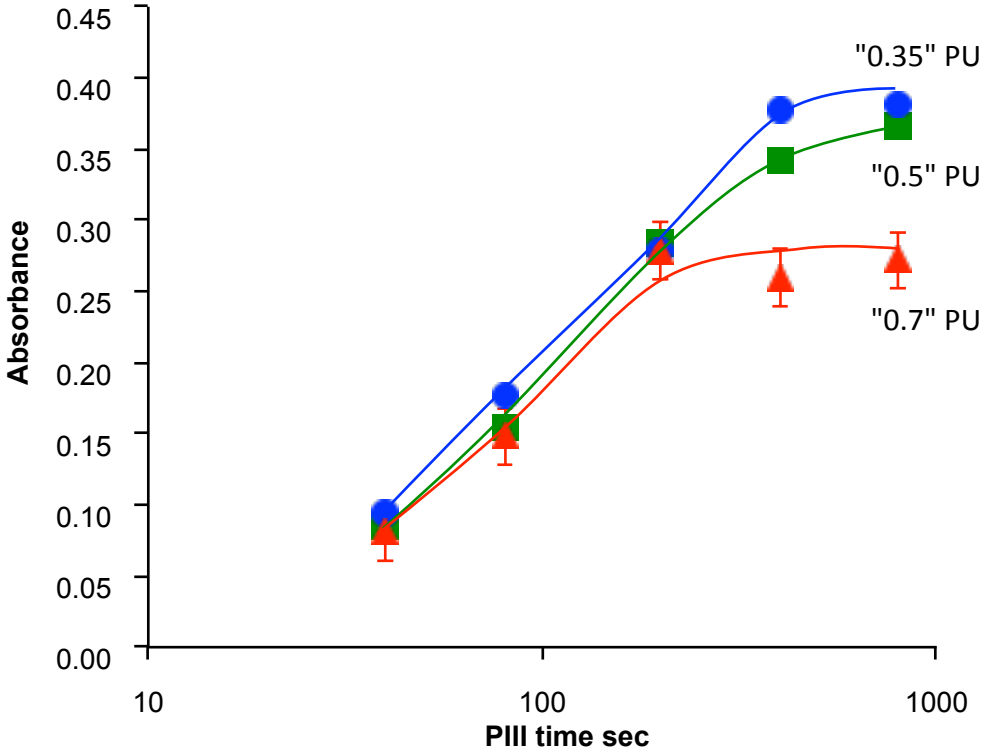

Fig.4.26. Absorbance of hydroxyl group (3400 cm^{-1}) in FTIR ATR spectra of "0.35" (PPG-DI-PTHF-0.35 polyurethane), "0.5" (PPG-DI-PTHF-0.5 polyurethane) and "0.7" (PPG-DI-PTHF-0.7 polyurethane) as a function of PIII treatment time with 20 keV energy nitrogen ions.

The absorbance of carbonyl group in the PIII treated polyurethanes was analysed by peak at 1660 cm^{-1} (Fig.4.27). Similar asymptotical character of the carbonyl group absorbance is observed for all used biases (20, 10 and 5 kV) and all polyurethane compositions (0.35, 0.5 and 0.7 NCO/OH ratios). The saturation is observed after 400 sec of the PIII treatment time for all biases and polyurethane compositions. The saturated level of the carbonyl group absorbance depends on the applied bias as it was observed for hydroxyl group absorbance: the lowest absorbance is observed for 5 kV bias treated samples, when the highest absorbance is observed for 20 kV bias treated samples. The saturated level of the carbonyl group absorbance also depends on the polyurethane composition: the lowest absorbance is observed for polyurethane with highest PTHF concentration, when the highest absorbance is observed for polyurethane with lowest PTHF concentration.

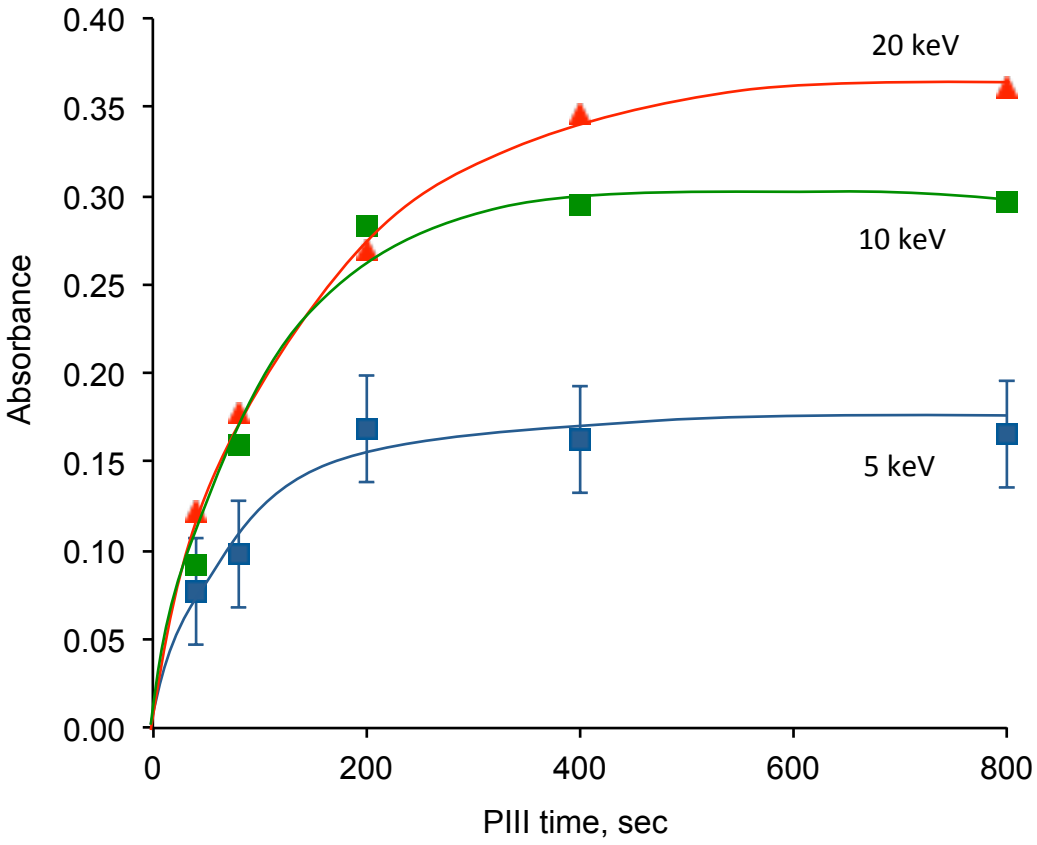
0.40
0.35
0.30
0.25
0.20
0.15
0.10
0.05
0.00
Absorbance
20 keV
10 keV
5 keV
0
200
400
600
800
PIII time, sec

a

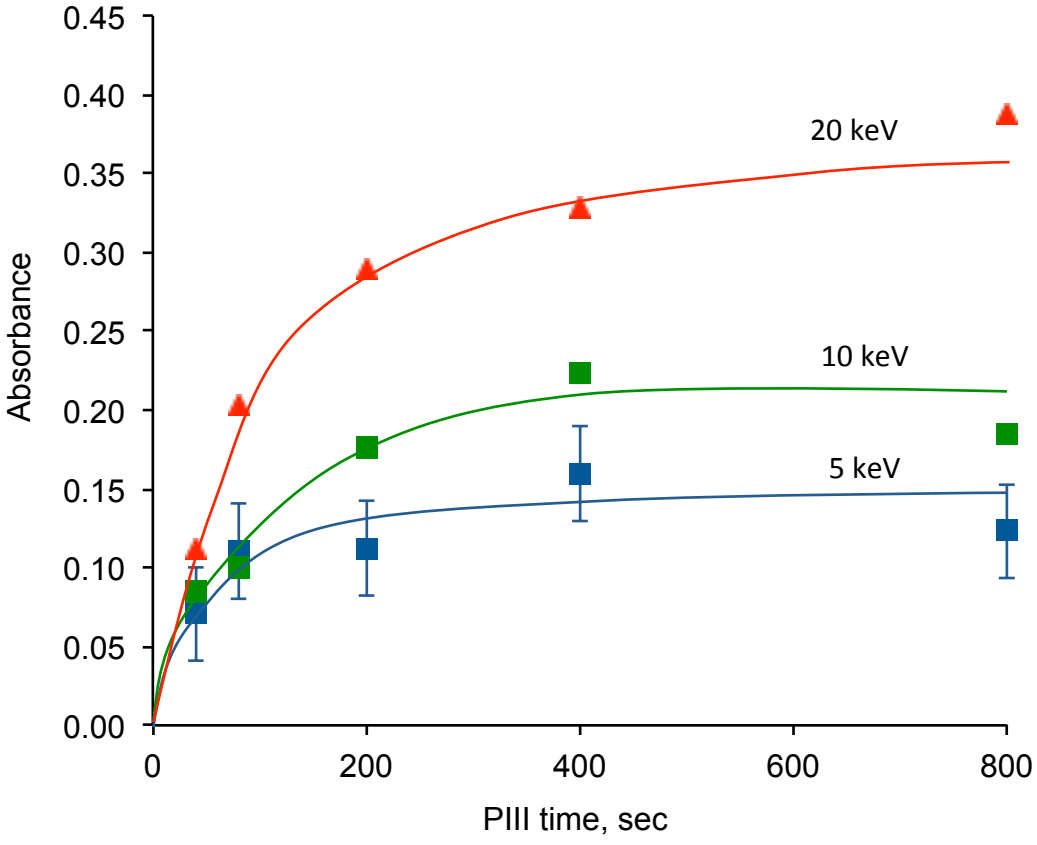
0.45
0.40
0.35
0.30
0.25
0.20
0.15
0.10
0.05
0.00
Absorbance
20 keV
10 keV
5 keV
0
200
400
600
800
PIII time, sec

b

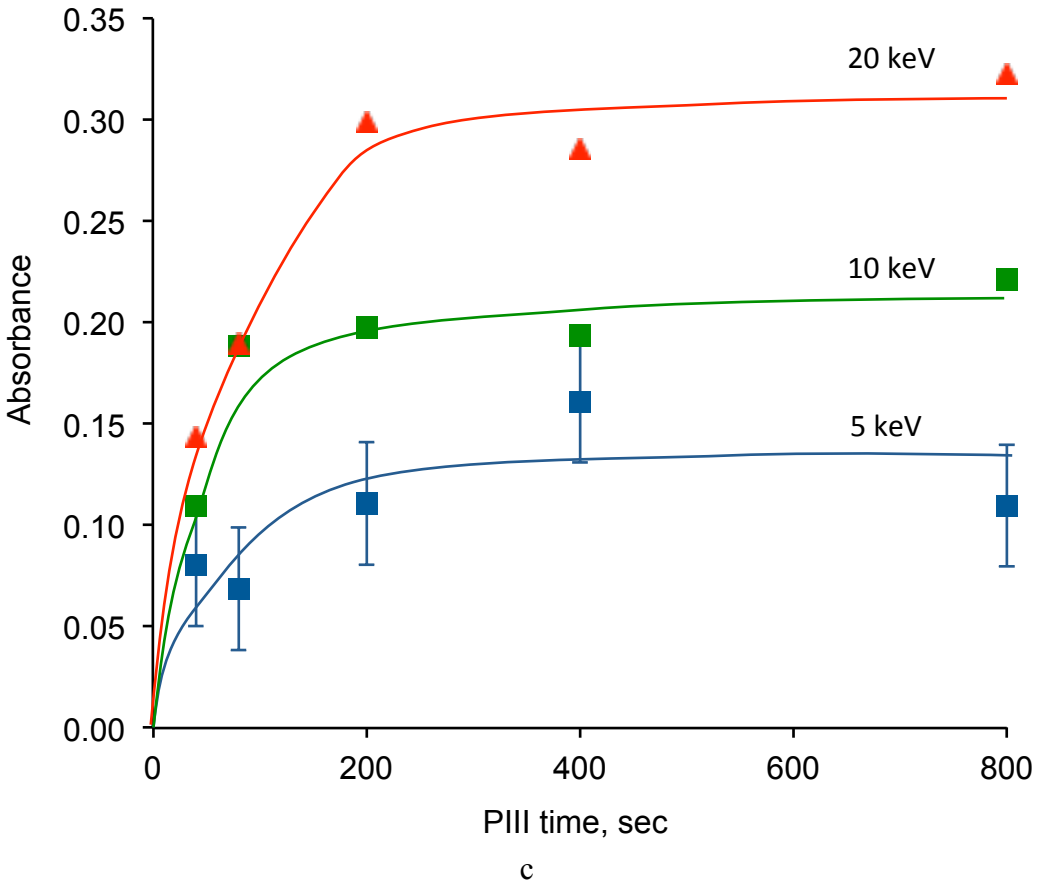

Fig.4.27. Absorbance of carbonyl groups (1660 cm^{-1}) in FTIR ATR spectra of PU as a function of PIII treatment time with 5, 10 and 20 keV energy nitrogen ions: a – PPG-DI-PTHF-0.35 polyurethane, b – PPG-DI-PTHF-0.5 polyurethane, c – PPG-DI-PTHF-0.7 polyurethane.

The absorbance of nitrile group at 2205 cm^{-1} increases with PIII treatment time as does hydroxyl and carbonyl group absorbance (Fig.4.28). However, the saturation level was not achieved when PIII treatment time exceeded 400 sec. The nitrile group absorbance curves tended to increase with applied PIII bias, but the difference between the curves for 5, 10 and 20 kV bias was not very different as with the hydroxyl and carbonyl group absorbance. Also there was no clear dependence of the nitrile group absorbance on the polyurethane composition.

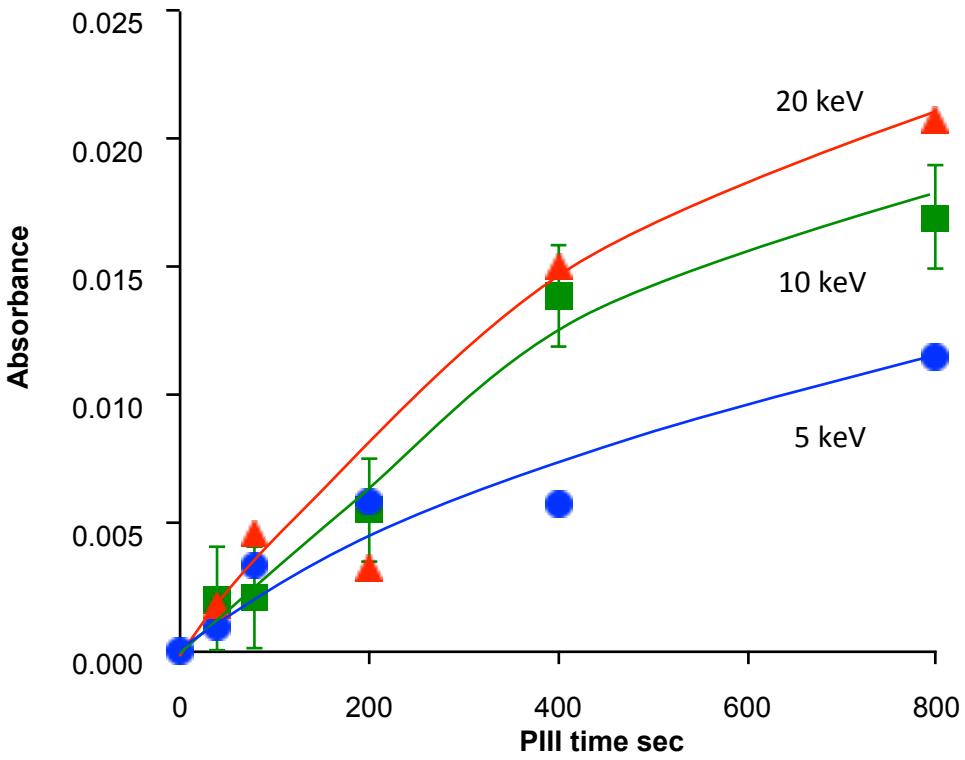
0.025
0.020
0.015
0.010
0.005
0.000
Absorbance
20 keV
10 keV
5 keV
0
200
400
600
800
PIII time sec

a

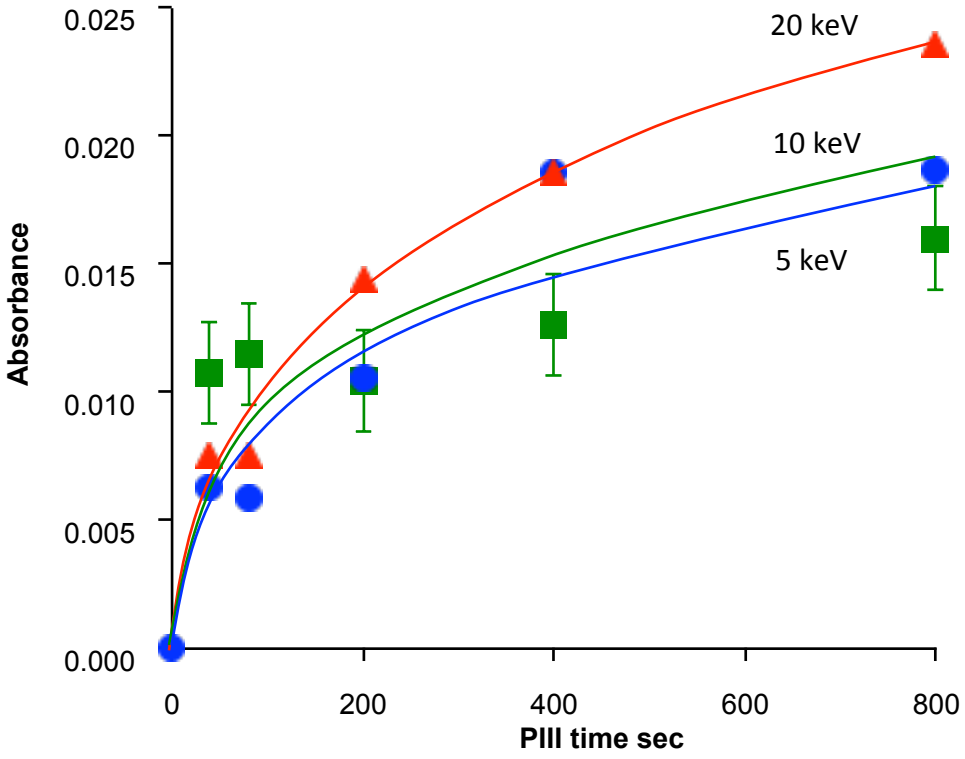
0.025
0.020
0.015
0.010
0.005
0.000
Absorbance
20 keV
10 keV
5 keV
0
200
400
600
800
PIII time sec

b

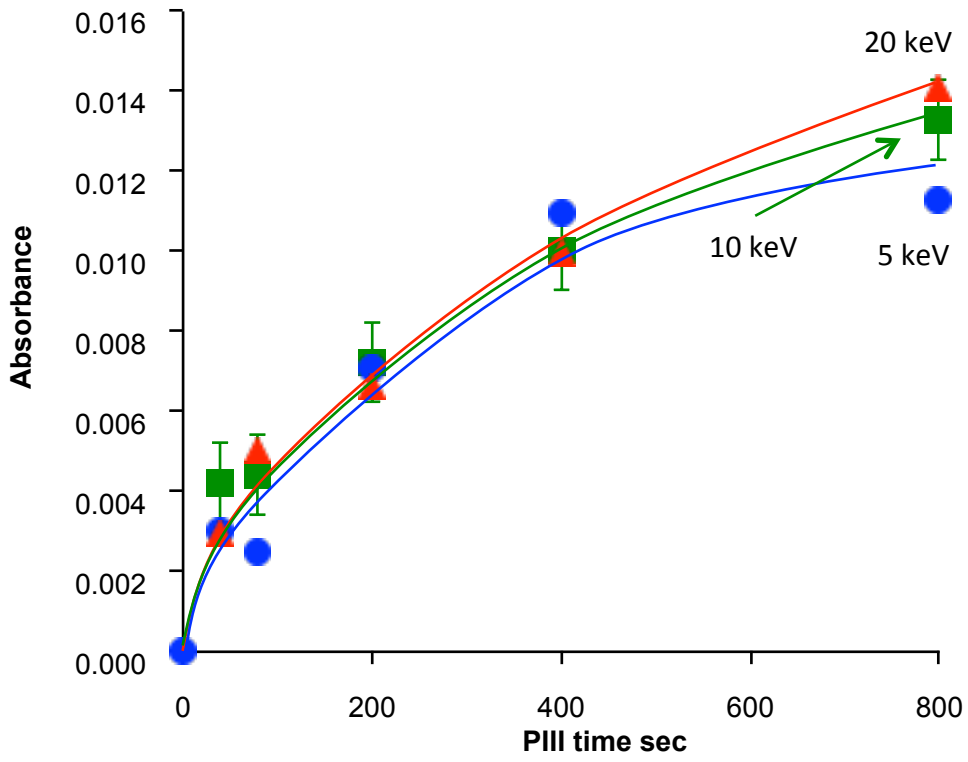

c

Fig.4.28. Absorbance of nitrile CN group in FTIR ATR spectra of PU as a function of PIII treatment time with 5, 10 and 20 keV energy of nitrogen ions: a – PPG-DI-PTHF-0.35 polyurethane, b – PPG-DI-PTHF-0.5 polyurethane, c – PPG-DI-PTHF-0.7 polyurethane.

The surface of polyurethane is unstable after PIII treatment. The above results are related to the polyurethane surface after long storage time (a month). The analysis of the surface transformation with time after PIII treatment was done using FTIR ATR spectra. The polyurethane samples were treated by PIII and the spectra were recorded immediately after removing the sample from the PIII chamber, and after a month's storage under laboratory conditions in closed Petri dishes in darkness. The treated surface was preserved against any contact with any material. Every FTIR ATR spectra was recorded with new samples that were not previously in contact with ATR crystal. The shortest time after switching off the bias voltage before the spectra were recorded was 25 minutes. The spectra recording with sufficient signal/noise ratio and resolution of 4 cm^{-1} took 2 minutes for each sample. The differential spectra of 0.35 ratio polyurethane recorded with storage time after 800 sec PIII treatment time are presented in Fig.4.29. The absorbance at selected wavenumbers of the spectra with storage time is analysed in Fig.4.30a-c.

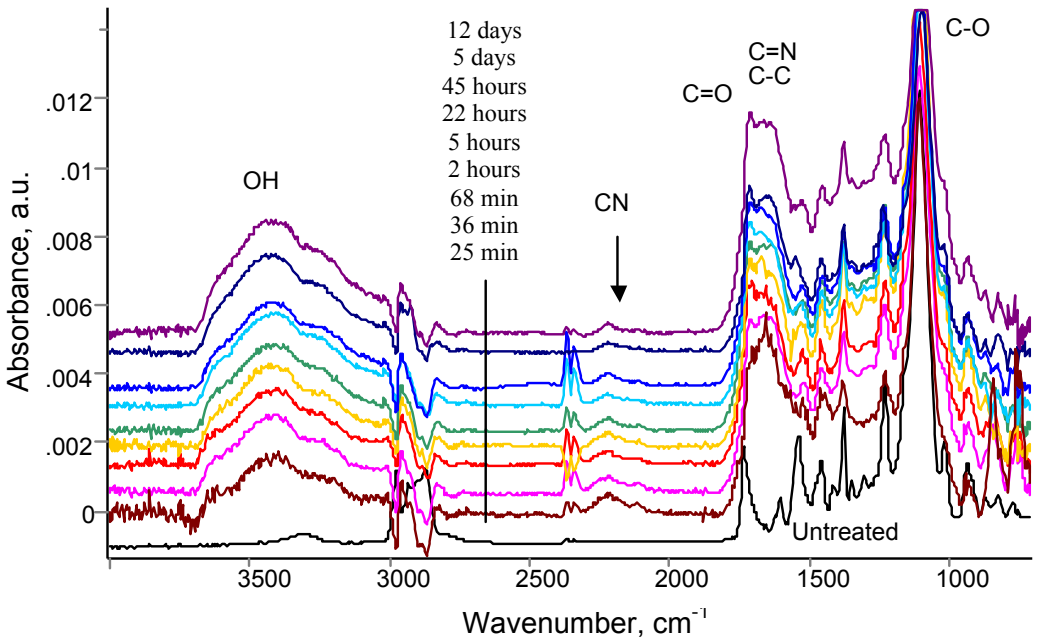

Fig.4.29. FTIR ATR spectra of PPG-DI-PTHF-0.35 polyurethane: bottom is untreated polyurethane spectrum (the spectrum is 1/20 of original intensity). The following spectra from bottom to top are differential spectra of polyurethane after PIII treatment according to the length of storage time. The treatment was done by 20 keV energy nitrogen ions for 800 seconds.

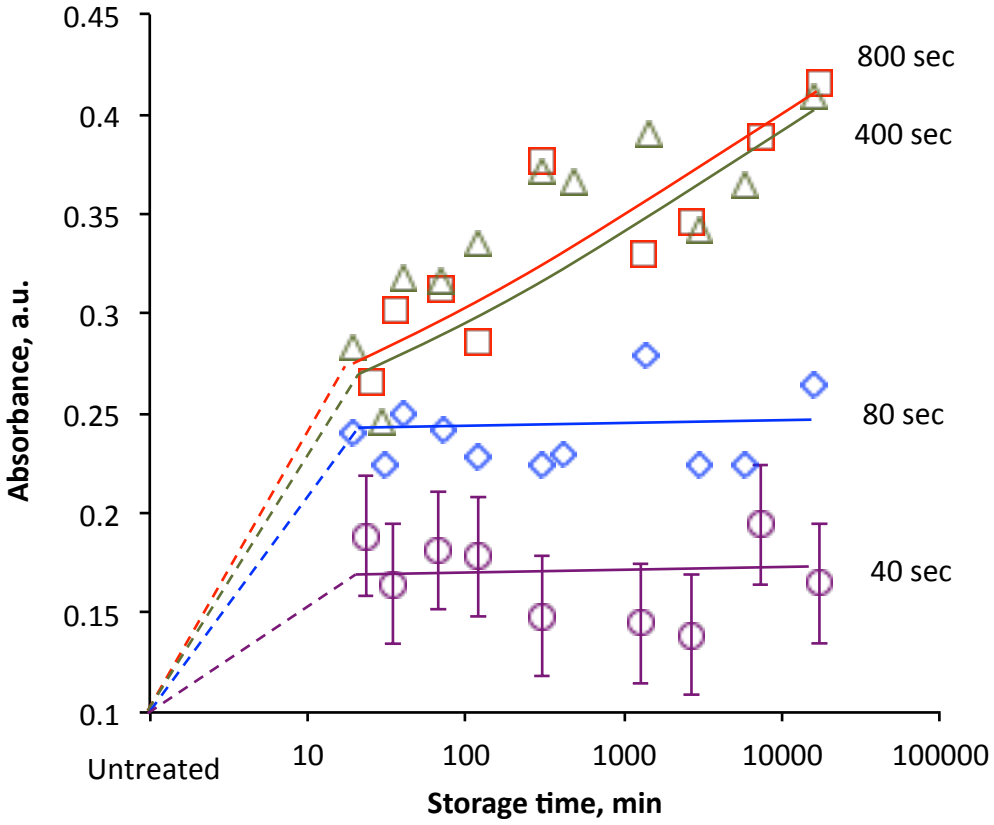

a

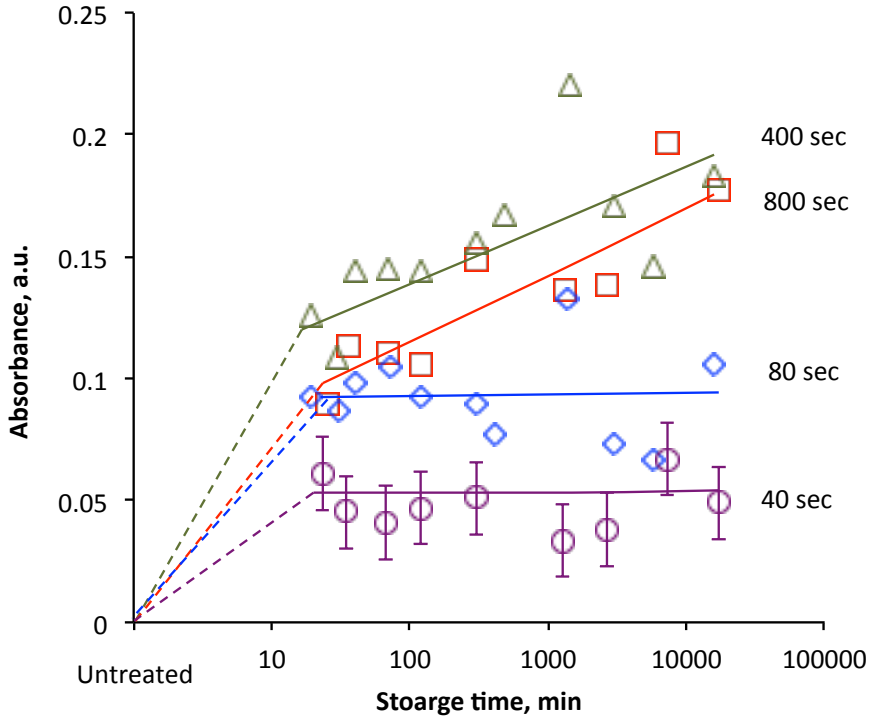

b

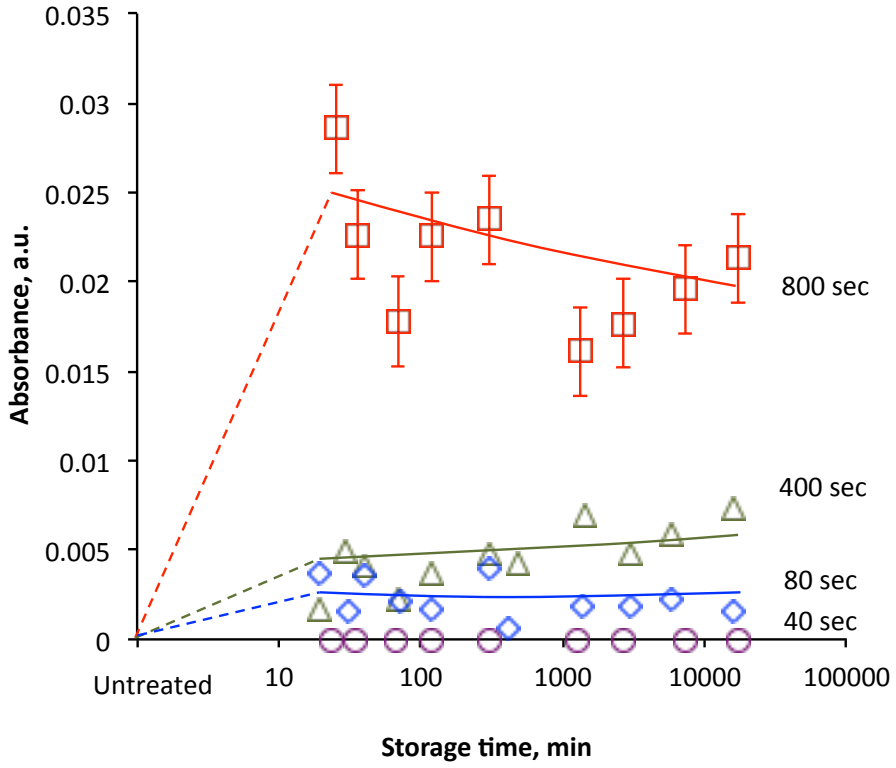

c

Fig.4.30. Absorbance of carbonyl group line at 1708 cm^{-1} (a), hydroxyl group line at 3400 cm^{-1} (b) and nitrile group line at 2205 cm^{-1} (c) in FTIR ATR PPG-DI-PTHF-0.35 polyurethane as a function of storage time after N+ PIII treatment of 20 kV bias.

The absorbance of these groups was normalised on the absorbance at 1373 cm^{-1} line of methylene group. The PIII treatment time are noted in the diagram.

The spectra show the absorbance growing in 3500-3000 cm^{-1} and 1800-1400 cm^{-1} regions corresponding to hydroxyl, carbonyl and unsaturated carbon-carbon group vibrations. The quantitative analysis was done for the absorbance at 3400 cm^{-1}, 2205 cm^{-1} and 1708 cm^{-1} wavenumbers normalised on 1373 cm^{-1} of methylene group absorbance in polyurethane which was strong and stable after PIII treatment. The normalised absorbance of hydroxyl and carbonyl groups remained constant with storage time for the polyurethane samples treated with PIII for 40 and 80 sec, while the absorbance for samples treated for 800 and 400 sec grew with the storage time two weeks after PIII treatment. The growth of the absorbance showed an increase of hydroxyl and carbonyl groups due to oxidation reactions of free radicals in the surface layer of polyurethane.

The absorbance of nitrile group vibrations remained constant for the samples treated with PIII for 40, 80 and 400 sec. For the sample treated for 800 sec, the absorbance decays with the storage time due to degradation of nitrile group under environmental conditions.

4.4. Surface topography of the modified polyurethane implant

The surface topography of the medical implant is a very important parameter for the tissue reaction in organisms. The analysis of the surface topography was done for the polyurethane implants after PIII for different treatment parameters.

The surface topography of PPG-DI-PTHF-0.35 polyurethane was changed dramatically after PIII treatment even with a short treatment time (Fig.4.31). The surface was wrinkled and cracked. After a short treatment time (40 sec) the surface became covered by wave-like structures. The direction of the wave was random. After 80 sec of PIII treatment, the cracks of the surface layer were well visible. After 800 sec of PIII treatment, the surface was totally covered by irregular wrinkles and cracks. The surface topography remained stable after a month long storage time. The topography viewed was similar to polyurethane free standing films and polyurethane coating on hard substrate (silicon wafer). Therefore the surface wrinkles and cracks are not the result of a deformation of the sample. The surface topography changes are due to the PIII treatment process.

Quantitative measurements of the surface topography were done with Atomic Force Microscopy. The untreated surface was characterised by random surface structures which were formed during the free surface synthesis under the influence of the surface tension, folding due to chemical reaction contraction and environmental artefacts like dust particles and air flow (Fig.4.32). The amplitude of the height varied across a wide range (48-150 nm in 10x10 nm^2 area). However the phase image is flat showing a uniformity of the surface chemical structure.

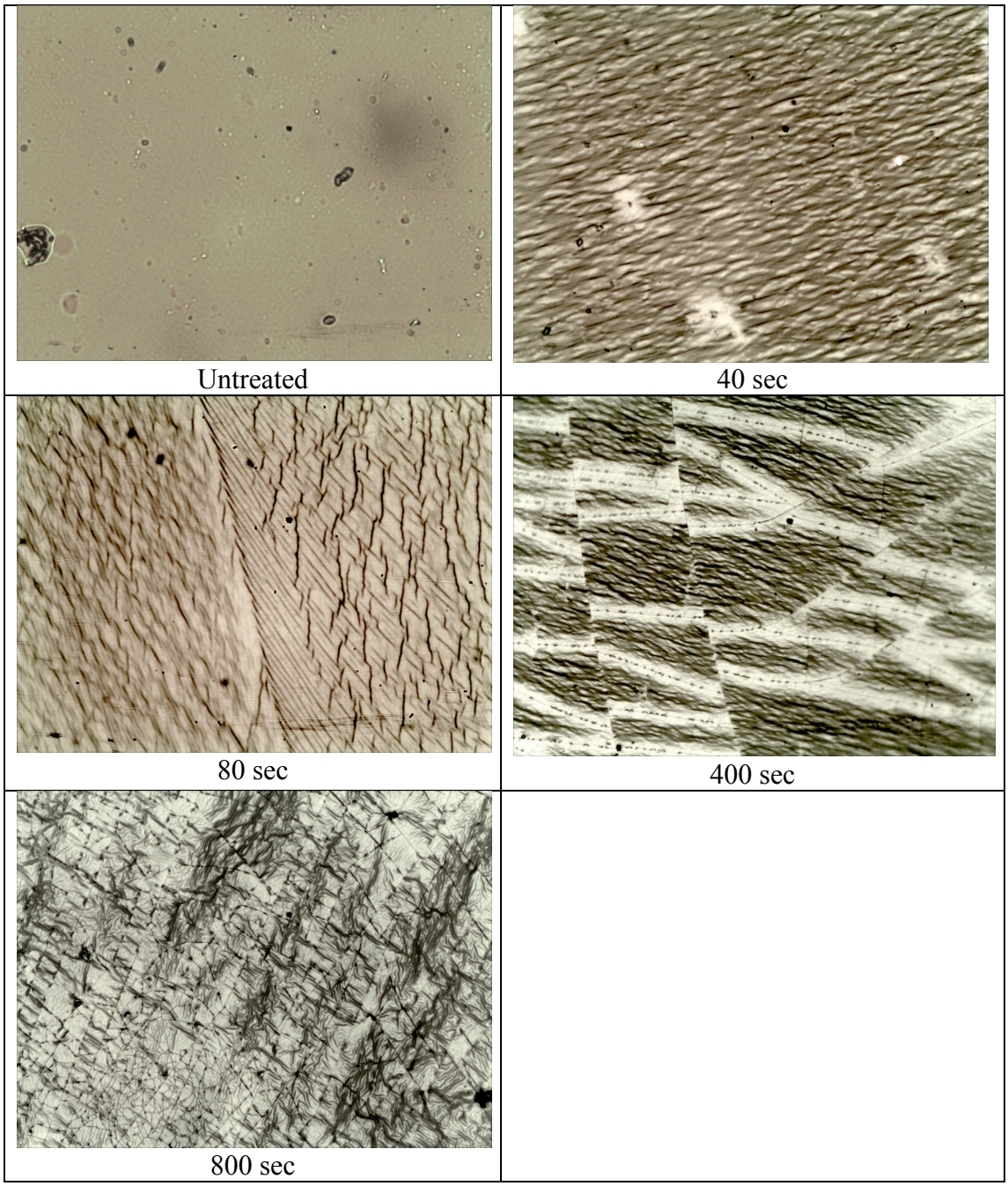

Fig.4.31. Optical microphotos of PPG-DI-PTHF-0.35 polyurethane after PIII treatment by 20 keV energy nitrogen ions. The PU was synthesised and treated on silicone wafer to exclude any deformations after the treatment. Objective is x50. The developed surface structure with waves and cracks is observed after PIII treatment.

The surface topography of the polyurethane treated with PIII for 40 sec is characterised by wave structure (Fig.4.33). The waves are distributed regularly over the whole surface (Fig.4.33a). The topography profile crossing the waves shows a periodicity of the wave structure (Fig.4.33b). The statistical analysis of the surface topography shows parameters of the surface averaged over the whole area. Power spectral density gives a peak at 0.0021 nm^{-1} wavenumber that corresponds to characteristic wavelength of 476 nm over the whole surface (Fig.4.33c). Fourier transformation 2D analysis shows definite direction of the surface waves (Fig.4.33d).

A histogram of the height events is characterised with three Gauss peaks that shows a normal distribution of the waves with two characteristic amplitudes of 30 nm and 62 nm (Fig.4.33e).

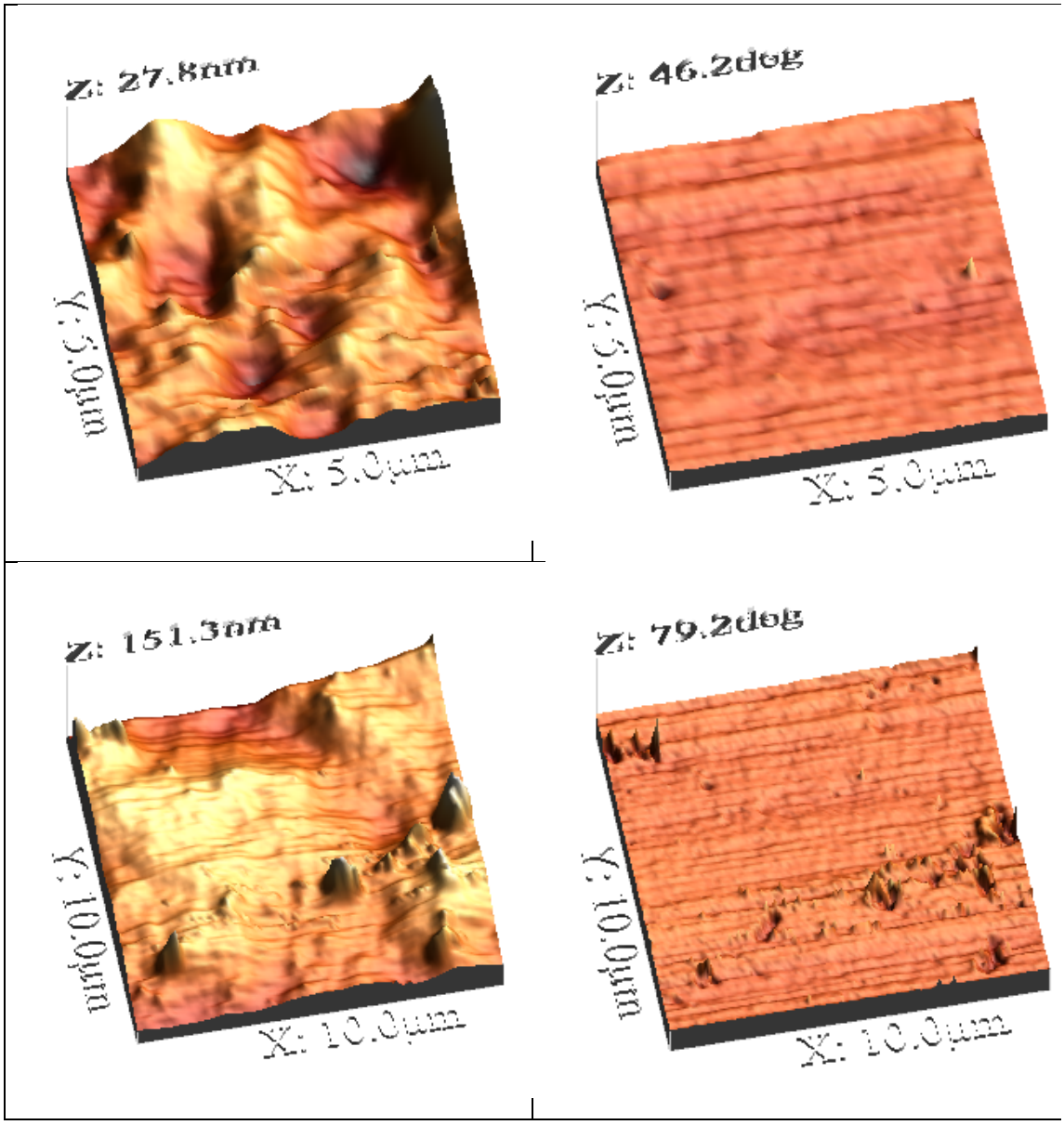

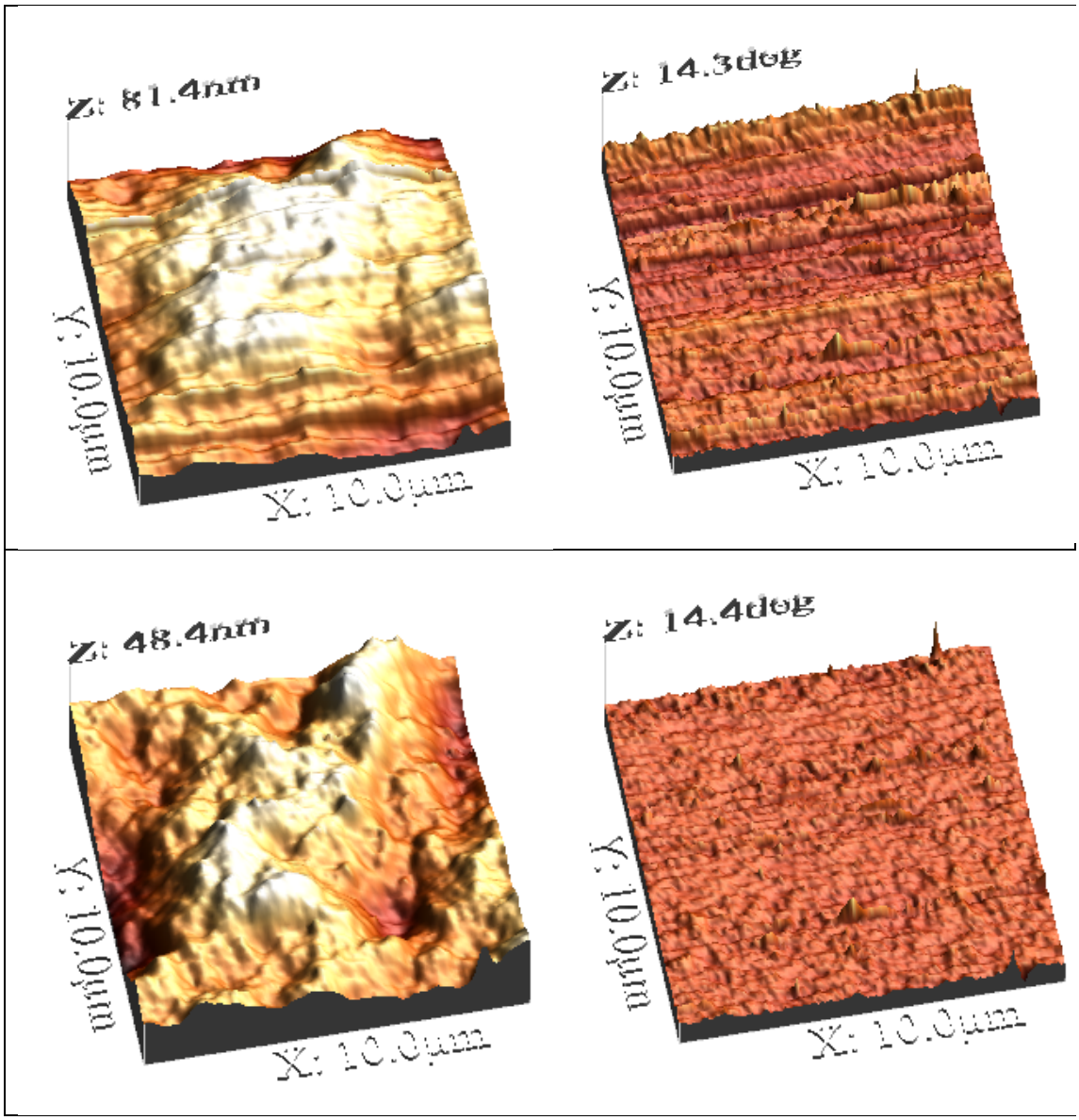

Fig.4.32. AFM image of untreated polyurethane: topography (left) and phase (right) images. The surface of the untreated polyurethane is uniformly rough with uniform chemical structure.

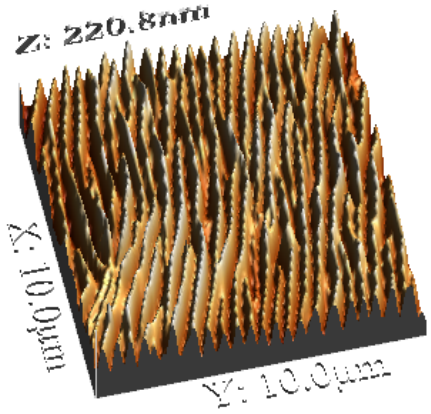

a

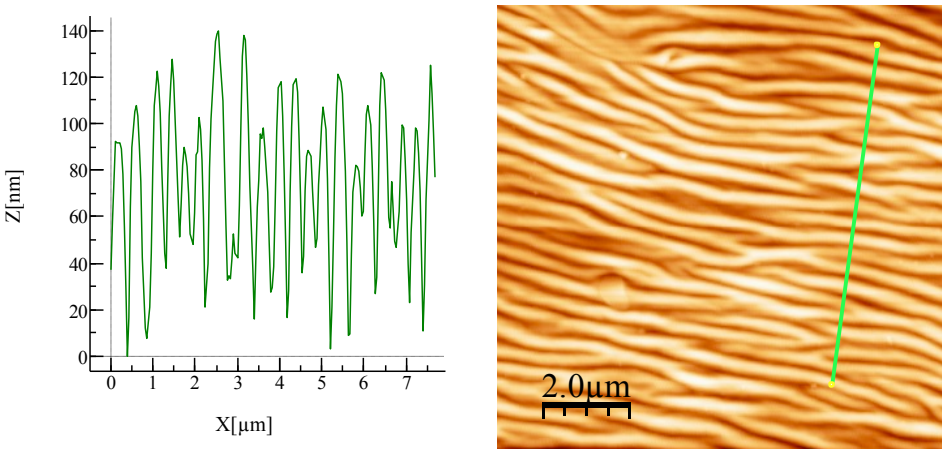

b

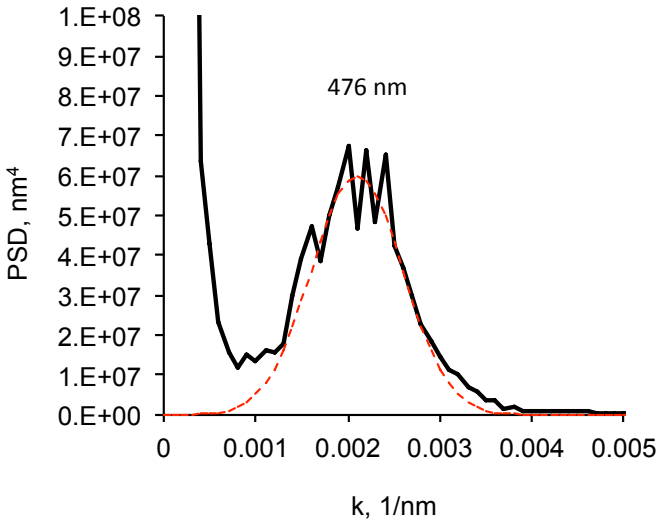

c

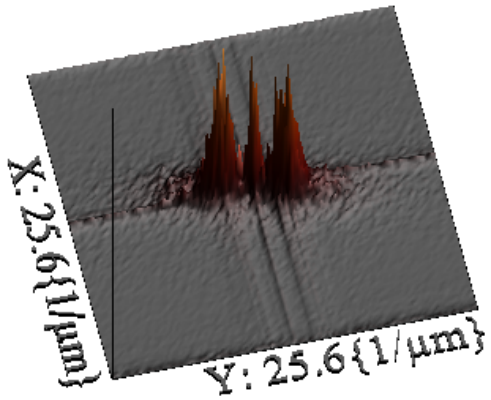

d

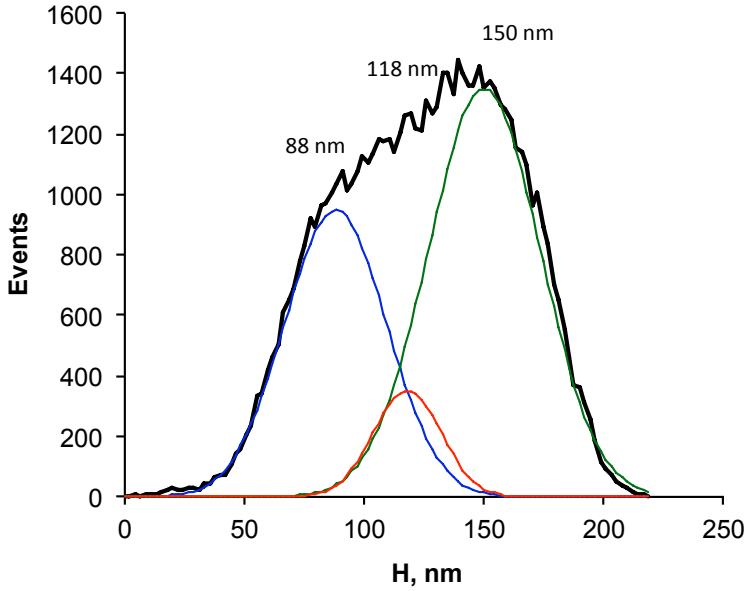

e

Fig.4.33. AFM images and statistical analysis of the polyurethane surface treated with PIII for 40 sec with 20 keV nitrogen ions: a – 3D image of 10x10 μm area; b - profile cross the wave structures; c – power spectral density analysis fitted with Gauss function; d – 2D Fourier transformation analysis; e – histogram analysis fitted with three Gauss functions. The surface shows wave structures. The waves are oriented. The waves have well defined periodicity (467 nm) and amplitudes (30 and 62 nm).

Following the treatment the polyurethane surface cracked. The AFM image of the polyurethane surface treated for 80 sec shows cracks in some areas (Fig.4.34a). The profile crossing the crack shows a depth of 250-300 nm, which is deeper then the thickness of modified surface layer of polyurethane treated with 20 keV energy nitrogen ions described above. The width of the crack is about 1.5-2 μm (Fig.4.34b). The profile on the bottom of the crack is similar to the surface profile of untreated polyurethane with random features (Fig.4.34c). The flat area near the crack shows a wave structure as observed for the 40 sec PIII treated surface (Fig.4.34d). The profile of the phase image shows that the phase characterising an interaction of the surface with AFM tip is different on the flat area near the crack and on the bottom of the crack (Fig.4.34e). This means that the surface composition on the flat area and in the crack is different. Assuming the flat area is a carbonised layer of polyurethane, the bottom of the crack can be assumed to be untreated polyurethane. The polyurethane surface treated by 200 sec, 400 sec and 800 sec became more frequently cracked and the waves became deeper (Fig.4.35).

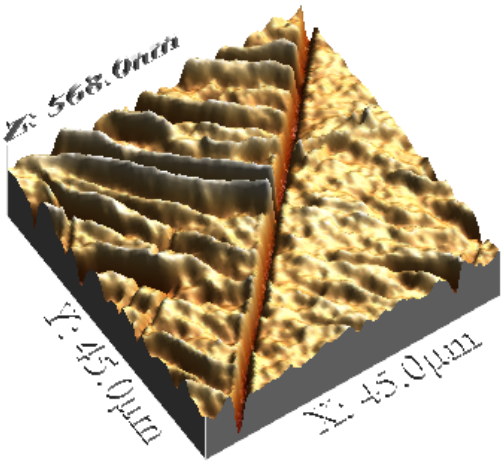
Z: 568.0nm
Y: 45.0µm
X: 45.0µm

a

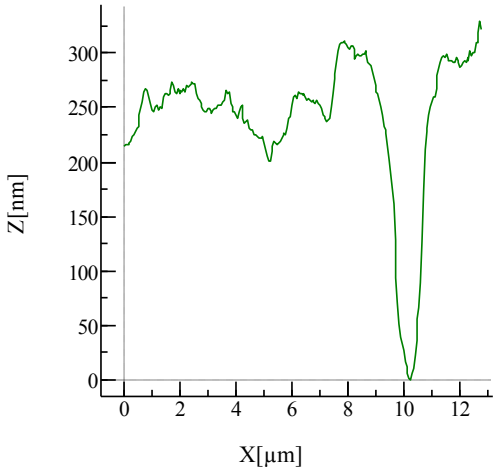
Z[nm]
X[µm]
0
50
100
150
200
250
300
0
2
4
6
8
10
12

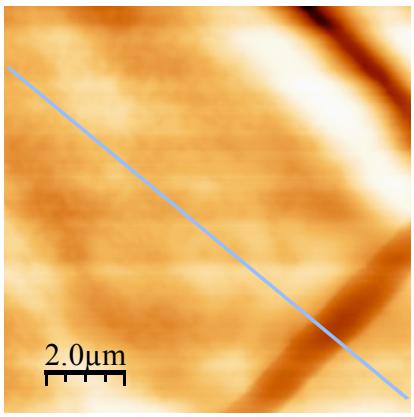
2.0µm

b

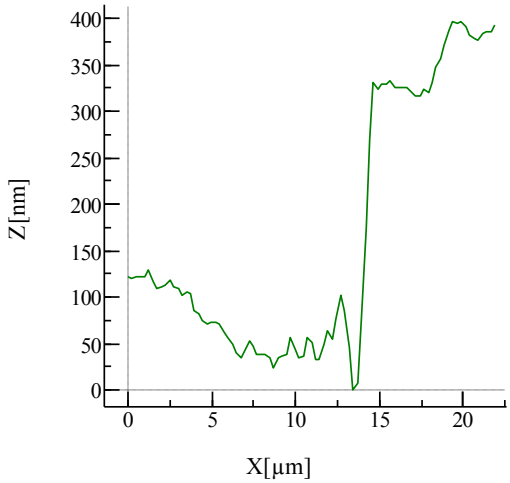
Z[nm]
X[µm]
0
50
100
150
200
250
300
350
400
0
5
10
15
20

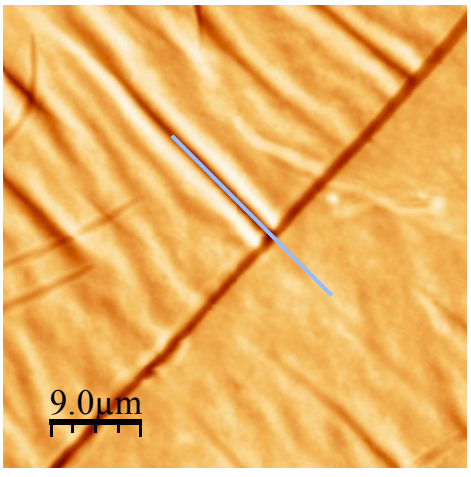
9.0µm

c

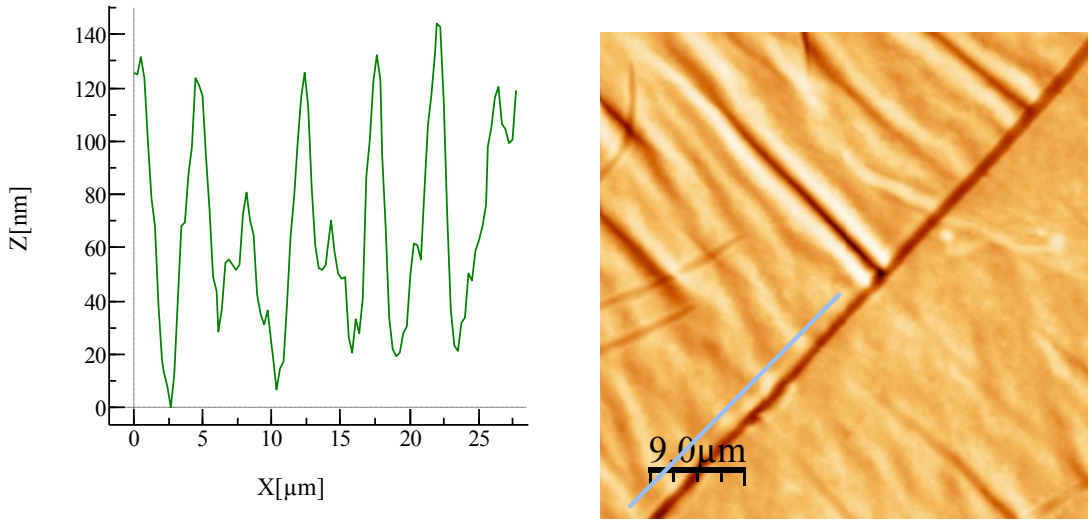

d

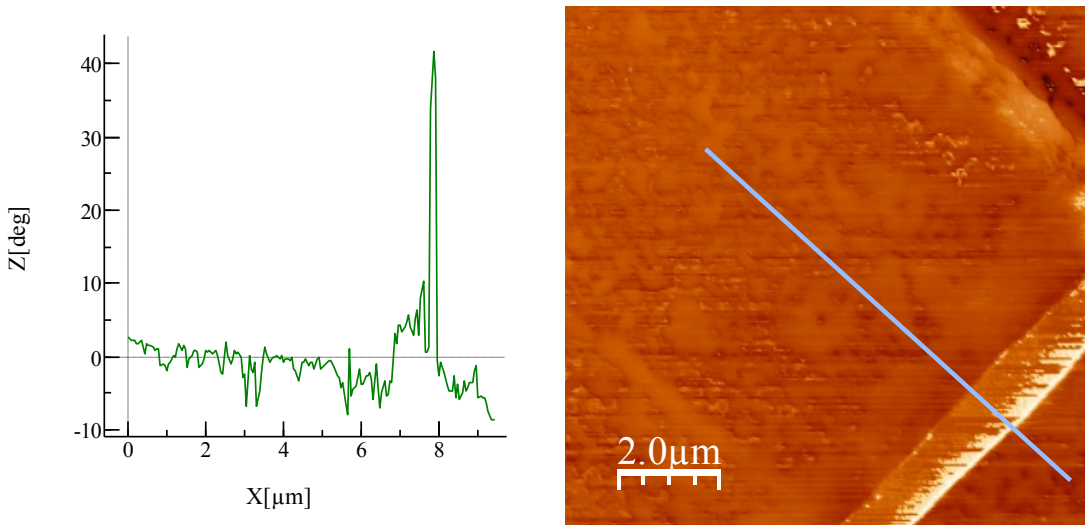

e

Fig.4.34. AFM images of the polyurethane surface treated by 80 sec PIII treatment time of 20 keV nitrogen ions: a – 3D image of 45x45 µm area; b - profile crosses the crack; c – profile along the crack bottom; d – profile crosses the wave structure; e – profile of the phase image crosses the crack. The surface shows wave and crack structures.

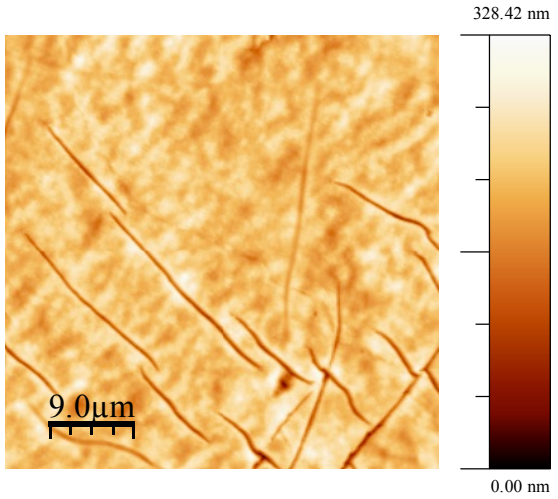

a

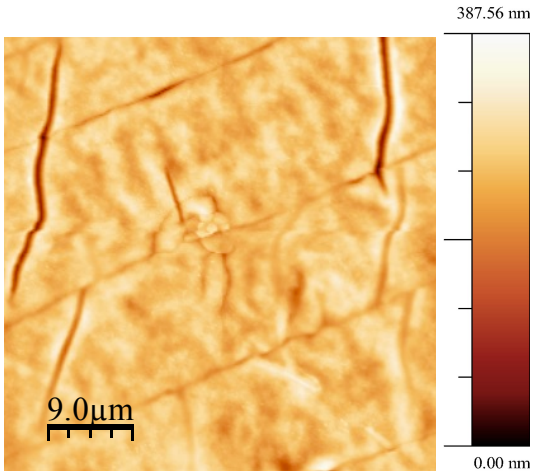

b

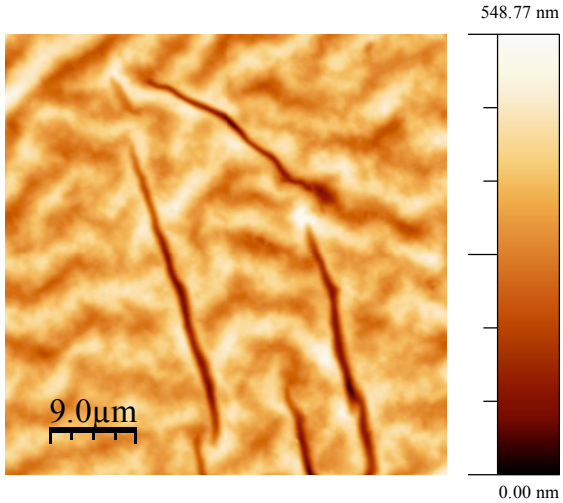

c

Fig.4.35. AFM images (45x45 µm) of the polyurethane surface treated by 200 sec (a), 400 sec (b) and 800 sec (c) PIII treatment time of 20 keV nitrogen ions.

4.5. Discussion

The PIII treatment changes the surface layer of the polyurethane significantly. The wettability of the treated PPG-DI-PTHF-0.35 polyurethane changes dramatically. The water contact angle changes from 90 degrees to 35-45 degree range 15 minutes after the treatment. Therefore the surface becomes very hydrophilic. The contact angle increases asymptotically after a week up to 60-70 degree range, but it does not reach the initial value of 90 degrees. The same changes of the water contact angle were observed for other polymers. For example, for polystyrene the water contact angle changes from 90 degrees for untreated surface to 27-36 degrees immediately after PIII treatment and stabilises in 53-68 degrees after a month [6]. The water contact angle changes are also observed for PIII treated polyurethanes of different compositions. For example, SKU-PFL polyurethane water contact angle achieves 38-48 degrees immediately after PIII and stabilises in 63-73 degrees range after a month of storage [7].

The water contact angle of PPG-DI-PTHF-0.35 polyurethane does not depend on the PIII fluence. Some polymers do not show this dependence, for example, polyetheretherketone, [8] or LDPE [9]. However, some polymers show a dependence of the contact angle on the PIII fluence, for example polystyrene [6] or polyurethane based on MDI diisocyanate [10].

The surface energy of PPG-DI-PTHF-0.35 polyurethane calculated from the contact angles of water and diiodomethane changes from 33 mN/m for the untreated surface to 65-67 mN/m for the PIII treated surface. The main contribution to these changes comes from the polar part of the surface energy, which increases from 2 mN/m to 27 mN/m. The same tendency is observed for all other polymers [11, 6, 12, 13]. However, the maximal value of the surface energy for other polymers can be as high as 75 mN/m for polystyrene [6] and as low as 50 mN/m for polyurethane based on MDI diisocyanate [10]. The increase of the surface energy is connected to the free radicals in the surface layer [13, 6, 14]. The free radical signal is also observed in the ESR spectra of PIII treated PPG-DI-PTHF-0.35 polyurethane. Therefore, the high values (65-67 mN/m) of surface energy for PIII treated PPG-DI-PTHF-0.35 polyurethane could also be caused by the presence of free radicals on the surface, because such high values cannot be explained by the presence of other chemical groups like carboxyl or hydroxyl, which appear in the surface layer of polyurethane after storage time as detected by FTIR ATR and XPS spectra.

The number of oxygen-containing groups generated by oxidation under air was observed by FTIR ATR and XPS spectra. These groups observed for all plasma, ion beam and PIII treated polymers [15] are the results of free radical reactions with air oxygen after the treated samples were removed from the vacuum chamber and exposed to open air. The kinetics of the oxygen-containing groups in PIII treated PPG-DI-PTHF-0.35 polyurethane shows that the oxidation reactions occur even a week after PIII treatment. Therefore, the surface layer remains highly active to the air oxygen a week after the treatment. Similar oxidation process was observed for other polymers including polyurethanes.

However, the kinetics of oxidation for different polyurethane compositions is different. The highest concentration of hydroxyl and carboxyl groups was observed for PPG-DI-PTHF-0.35 polyurethane and the lowest concentration of hydroxyl and carboxyl groups was observed for PPG-DI-PTHF-0.7 polyurethane. It was observed for the first time that the composition of polyurethane influences the chemical transformation process in the surface layer after PIII treatment.

Also the influence of different ion energies on the oxidation process in polyurethanes had not been observed before. The PPG-DI-PTHF-0.35 polyurethane was treated by nitrogen ions of different energy and the kinetics of the oxidation was found to be sensitive to the ion energy. The higher ion energy caused higher saturation level of the oxygen-containing group concentration, while the nitrile group concentration directly associated with the carbonised layer remains independent on the ion energy for PPG-DI-PTHF-0.7 polyurethane. These facts have not been observed before and we do not have a clear explanation for them. It could be because of the depolymerised reactions in the underneath layers where the free radicals can migrate from the carbonised layer and where the oxidation processes could be sensitive to the chemical structure of polyurethane. Further investigations are required.

The formation of the carbonised layer was observed by Raman spectra on characteristic two lines of graphite planes. These lines are narrower than the lines in the Raman spectra of other polymers irradiated by ion beam [15]. The spectra line positions and intensity ratio corresponds to the 2.5 nm characteristic size of the graphitic clusters. In comparison with other polymers [15], the 2.5 nm cluster is large. This means that the average cluster has about 200 condensed aromatic rings. The NEXAFS spectra showed the graphitic clusters contains also C=N bonds involving in sp^2 hybridization. Therefore, the graphitic clusters could have a lot of defects and disturbance of π-clouds. The strong ESR spectrum of unpaired electrons confirms that the g-factor corresponds to electrons on the edge of graphitic clusters.

The top layer of PIII treated polyurethane has higher density than the untreated polyurethane. The refractive index of the top layer achieves the value of 1.85, while the untreated polyurethane layer has the refractive index of 1.45-1.55 in visual light range of wavelength. The density of this layer is lower than for PIII treated PS [16], LDPE [11] and PC [17], and close to the refractive index of PIII treated PMMA [18].

The appearance of graphitic structures forms a hard surface layer. The underneath soft layer of polyurethane and hard layer on the top cause the cracks in the surface layer penetrating up to the deep layer of unmodified polyurethane. The AFM phase images confirm this fact. The cracks are caused by internal stresses in the carbonised layer. The thickness of the hard layer from AFM measurements (250-300 nm) is higher then the thickness of the modified layer (130 nm) calculated from SRIM model. The difference between these values corresponds to the rupture of the untreated underneath layer under the internal stresses in the carbonised layer. The thickness of the carbonised layer measured from the ellipsometry data (65 nm) is lower then these two values. The layer with high refractive index is highly carbonised and dense. Therefore, the surface layer has a complicated structure with a gradient of chemical structure and stresses.

The study proved that the surface of the PIII treated PPG-DI-PTHF-0.35 polyurethane consists of carbonised top surface layer with 2.5 nm graphitic clusters with edges rich with unpaired electrons shared with π-electron clouds of aromatic structures.

4.6. Conclusions

The PIII treatment forms the carbonised hard layer on the top of polyurethane implant. The thickness of the carbonised layer corresponds to the penetration depth of the bombarding ions. The carbonised layer consists of condensed aromatic structures like graphite. The edges of these structures are carbon atoms with unpaired electrons that are regarded as free radicals. These unpaired electrons are stabilised by π-electron cloud of the aromatic structures in such a way that the free radicals at the edges decay slowly and produce oxygen containing groups. However, these free radicals remain detectable for a long time. The kinetics of the chemical transformation with the storage time depends on the parameters of PIII treatment and the composition of polyurethane.

The surface of the modified polyurethane implant becomes highly hydrophilic immediately after the PIII but recovers up to middle value over time. The modified surface has a complicated topography and is characterised by wave and crack structures depending on PIII treatment parameters.

All these transformations show that the surface of the polyurethane implant changes dramatically after PIII, and that it can cause different interactions with protein molecules, cells and tissue of organism.

References

1. J.F. Ziegler, J.P. Biersack, in: The Stopping and Range of Ions in Solid, Pergamon, New York, 1985.
2. Ziegler, J. F.; Ziegler, M. D.; Biersack, J. P. SRIM - The stopping and range of ions in matter, Nucl. Instrum. Methods Phys. Res., B 268 (11−12), 2010, 1818−1823.
3. Encyclopedia of Polymer Science and Technology, Ed. M.F. Herman, Wiley, New York, 2004.
4. N. Emanuel, A. Buchachenko, Chemical Physics of Polymer Degradation and Stabilization, VNU Science Press, Utrecht, 1987.
5. B. Ranby, J. Rabek, Photodegradation, Photo-Oxidation and Photo-Stabilisation of Polymers, Wiley, London, 1975.
6. E. Kosobrodova, A. Kondyurin, D.R. McKenzie, M.M.M. Bilek, Kinetics of post-treatment structural transformations of nitrogen plasma ion immersion implanted polystyrene, Nuclear Instruments and Methods in Physics Research Section B: Beam Interactions with Materials and Atoms, 304, 57–66, 2013
7. R.I. Iziumov, A.Y. Beliaev, I.V. Kondyurina, I.N. Shardakov, A.V. Kondyurin, M.M. Bilek, D.R. McKenzie, Experimental investigation of plasma- immersion ion implantation treatment for biocompatible polyurethane implants production, Materials Science and Engineering 123 (2016) 012003.
8. E.A. Wakelin, A.V. Kondyurin, S.G. Wise, D.R. McKenzie, M.J. Davies, M.M.M. Bilek, Bio-Activation of Polyether Ether Ketone Using Plasma Immersion Ion Implantation: A Kinetic Model, Plasma Process. Polym., 2015, 12, 180–193.

9. Gavrilov N., D.Yakusheva, A.Kondyurin, Structure of polyethylene after pulse ion beam treatment, J. Applied Polymer Science, v.69, 1998, P.1071-1077.
10. X. Cheng, A. Kondyurin, S. Bao, M.M.M. Bilek, L. Ye, Plasma immersion ion implantation of polyurethane shape memory polymer: Surface properties and protein immobilization, Applied Surface Science, 416 (2017) 686–695.
11. A.V. Kondyurin, P. Naseri, J.M.R. Tilley, N.J. Nosworthy, M.M.M. Bilek, D.R. McKenzie, Mechanisms for Covalent Immobilization of Horseradish Peroxidase on Ion-Beam-Treated Polyethylene, Scientifica, Volume 2012, Article ID 126170, 28 pages, http://dx.doi.org/10.6064/2012/126170, 2012.
12. A. Kondyurin, N.J. Nosworthy, M.M.M. Bilek, Attachment of horseradish peroxidase to polytetrafluorethylene (teflon) after plasma immersion ion implantation, Acta Biomaterialia, 4, 2008, 1218–1225.
13. A.Kondyurin, N.J. Nosworthy, M.M.M. Bilek, R.Jones, P.J. Pigram, Surface Attachment of Horseradish Peroxidase to Nylon Modified by Plasma-Immersion Ion Implantation, Journal of Applied Polymer Science, vol. 120, pp. 2891–2903, 2011.
14. Mesyats G., Klyachkin Yu., Gavrilov N., Kondyurin A., Adhesion of Polytetrafluorethylene modified by an ion beam, Vacuum, vol.52, 1999, P. 285-289.
15. A. Kondyurin, M. Bilek, Ion Beam Treatment of Polymers. Application aspects from medicine to space, Second Edition, Elsevier, Oxford, 2014.
16. Gan B.K., M.M.M. Bilek, A. Kondyurin, K. Mizuno, D.R. McKenzie, Etching and structural changes in nitrogen plasma immersion ion implanted polystyrene films, Nuclear Instruments and Methods in Physics Research B 247 (2006) 254–260.
17. E. Kosobrodova, A. Kondyurin, W. Chrzanowski, D.G. McCulloch, D.R. McKenzie, M.M.M. Bilek, Optical properties and oxidation of carbonized and cross-linked structures formed in polycarbonate by plasma immersion ion implantation, Nuclear Instruments and Methods in Physics Research B 329 (2014) 52–63.
18. A. Kondyurin, M. Bilek, Etching and structure changes in PMMA coating under argon plasma immersion ion implantation, Nuclear Instruments and Methods in Physics Research, B 269, 1361–1369, 2011.

Chapter 5. In vitro biocompatibility of modified implants

Modified polyurethanes were investigated as a prospective material for implants into organisms. This chapter is devoted to answering whether PIII treatment can improve biocompatibility *in vitro*. A successful incorporation of an implant into an organism's tissue requires that the proteins and cells be attached to the implant's surface. For this investigation, different proteins and endothelial cells were attached on the polyurethane surface and analysed. The results of the *in vitro* experiments in this chapter are the required preliminary stage for the *in vivo* experiments.

The results in this chapter are partially published by I. Kondyurina, S.G. Wise, A.K.Y. Ngo, E.C Filipe, A. Kondyurin, A.S. Weiss, S. Bao, and M.M.M. Bilek in 'Plasma mediated protein immobilisation enhances the vascular compatibility of polyurethane with tissue matched mechanical properties', *Biomed. Mater*., 12, 2017, 045002.

5.1. Interaction of proteins with implant

The proteins selected for the investigation were albumin, fibrinogen and tropoelastin. The choice of protein was based on common attachment analysis of polyurethane surfaces, on an organism's protein environment and as a way to improve the biocompatibility of the polyurethane surface. The albumin is the most common protein in the blood stream and the intercellular matrix. An attachment of albumin can be a critical test for polyurethane implant inserted anywhere inside a body. Fibrinogen is the third primary plasma protein following serum albumin and immunoglobulins which are key proteins for biocompatibility of blood-contacting implant devices. Fibrinogen takes part in the blood coagulation cascade, where the fibrinogen fragments are ultimately cleaved to yield insoluble fibrin monomers that polymerize into an intricate cross-linking structures. Also fibrinogen plays the role of a cell adhesive protein, which is an important requirement for biocompatibility. Tropoelastin is a monomer of elastin found in the extracellular matrix of elastic tissues. Tropoelastin is used in tissue engineering because of conformational flexibility and stability under medical-grade sterilization, for example, ultraviolet light sterilization. Also tropoelastin is a good candidate protein to modulate a number of processes including adhesion, spreading, proliferation, and migration in cell types such as fibroblasts and endothelial cells. These three proteins are an example of immobilisation onto polyurethane surface, but it does not exclude other protein immobilisation for future studies.

The Bovine serum albumin (BSA) has been used in this attachment experiment. The polyurethane untreated samples and polyurethane samples treated by nitrogen ions with 20 keV energy with different fluence were used for the protein experiments. After the PIII treatment the polyurethane samples were stored for 2 weeks to stabilise the polyurethane surface before the protein attachment. The stabilisation of the PIII

treated surface was done to minimise the difference of oxidation between the sample incubated in the buffer and the sample incubated in protein solution that can mask the protein lines in the differential spectra. The polyurethane samples were incubated overnight in 50 μg/ml BSA solution in PBS buffer at 25C in 45 ml polypropylene falcon tube. Then the polyurethane samples were rinsed in 3 different falcon tubes with the 45 ml buffer solution and in 45 ml mQ-water. The samples were dried overnight in Petri dishes. The control samples were incubated in buffer solutions only. These were prepared the same way and at the same time as the protein attached samples. The buffer samples were rinsed only in mQ-water once. Then the control samples were dried overnight the FTIR ATR spectra was recorded.

The spectral lines of protein are not visible in row spectra of the samples as recorded due to high intensity of the polyurethane lines in comparison with the protein lines (Fig.5.1). The low intensity of protein lines corresponds to very thin BSA protein monolayer (about 5 nm) in comparison with the high intensity polyurethane spectrum corresponding to the infrared beam penetration depth into polyurethane (400-1000 nm in dependence on wavenumber of the spectral region). The spectra of buffer samples were subtracted from the spectra of protein samples treated at the same PIII treatment time with adjusted subtraction factor to minimise absorbance of polyurethane lines. The resulted spectra are presented in Fig.5.2.

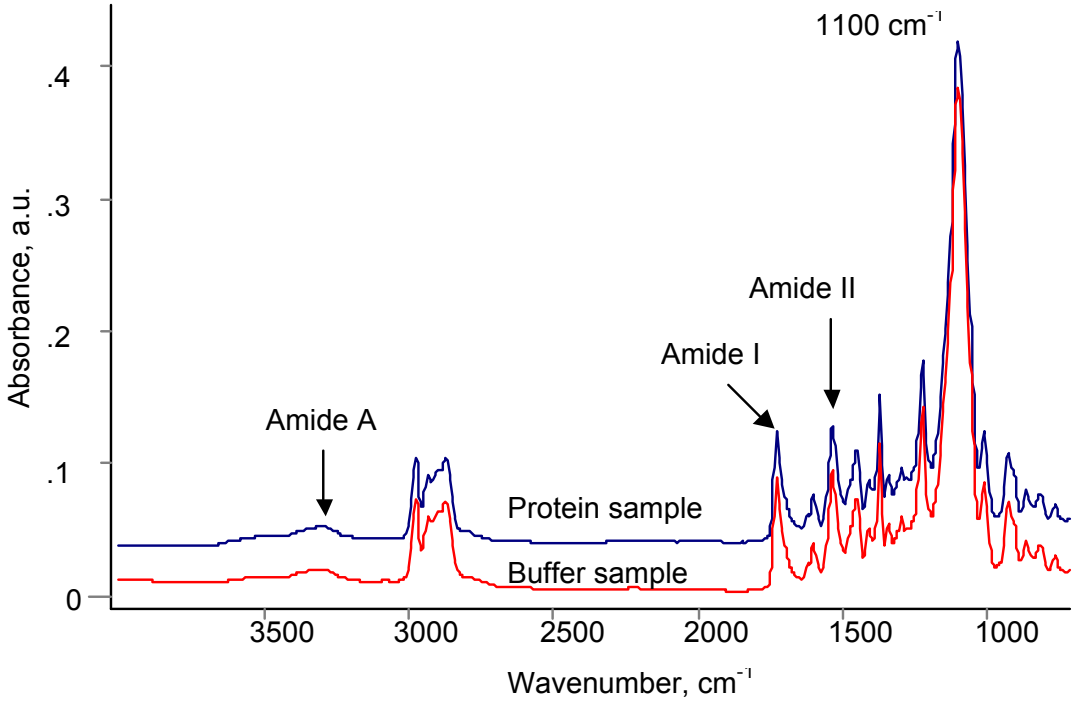

Fig.5.1. FTIR ATR spectra of untreated polyurethane PPG-DI PTHF with 0.35 NCO/OH ratio soaked in buffer solution (red) and in Fibrinogen solution (blue) as recorded.

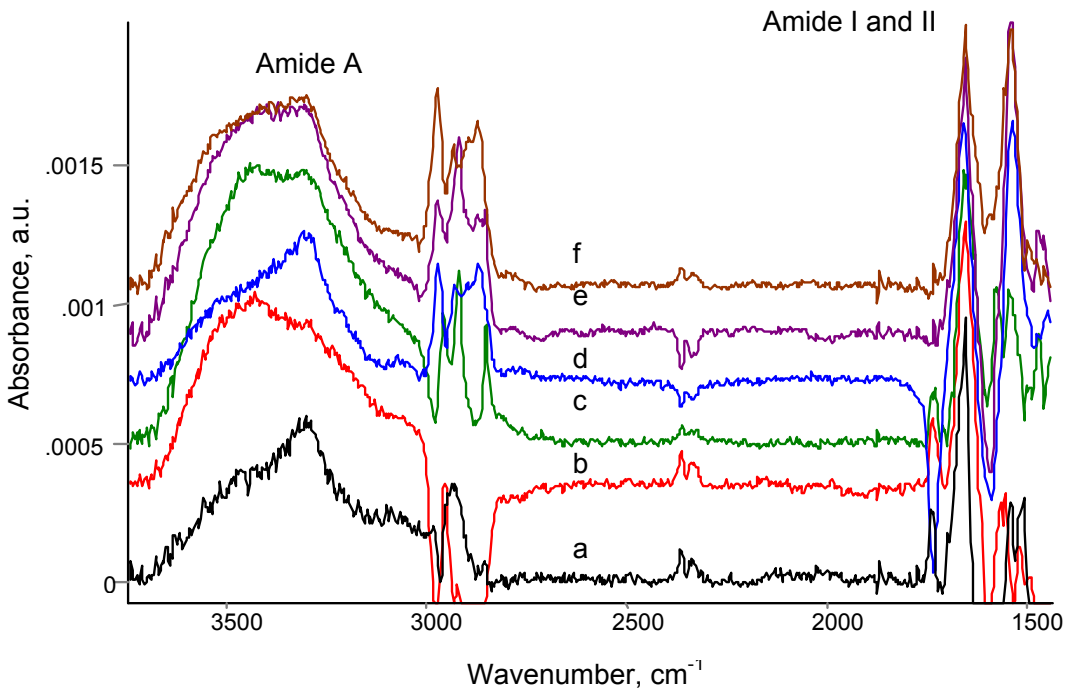

Fig.5.2. FTIR ATR spectra of attached BSA on untreated and PIII treated polyurethane of PPG-DI PTHF with 0.35 NCO/OH ratio. From bottom to top: (a) untreated polyurethane, (b) 40, (c) 80, (d) 200, (e) 400, (f) 800 s PIII treatment time with 20 keV nitrogen ions. The spectra of corresponding polyurethanes are subtracted.

The subtracted spectra show Amide A line at 3300 cm^{-1}, Amide I line at 1650 cm^{-1} and Amide II line at 1540 cm^{-1}. The line positions of Amide A and Amide II in the spectra of pure polyurethane and pure protein are similar. These lines in the subtracted spectra can be interpreted as related to both polyurethane and protein. Therefore these lines cannot be used for analysis of protein attachment. The Amide I line in the spectra of pure polyurethane was observed at 1720 cm^{-1}, and the Amide I line in the spectra of pure protein was observed at 1650 cm^{-1}. Due to these different positions, the Amide I line can be used for analysis of the protein attachment. The absorbance of Amide I line normalised on the line of polyurethane vibrations at 1100 cm^{-1} as a stable intensive line is presented in Fig.5.3 according to PIII treatment time. The amount of attached BSA increases with PIII treatment time up to saturation level. The saturation level observed after 800 seconds of PIII treatment time is double than for the untreated polyurethane.

The attachment of protein is provided due to interactions between the polyurethane macromolecules and the protein molecules on the surface. The interactions are based on physical forces (dispersic, polar and ionic) or/and can be based on chemical bonding if a reaction between the protein molecule and polyurethane macromolecule occurs. The contribution of the physical forces can be tested by washing the attached protein in strong detergent as this disturbs the physical forces. Such detergents used for washing chemicals including protein molecules are sodium dodecyl sulphate (SDS) and Tween 20. These detergents were successfully used for washing attached protein from many different surfaces. The detergent SDS was used for washing the attached BSA from the polyurethane surface.

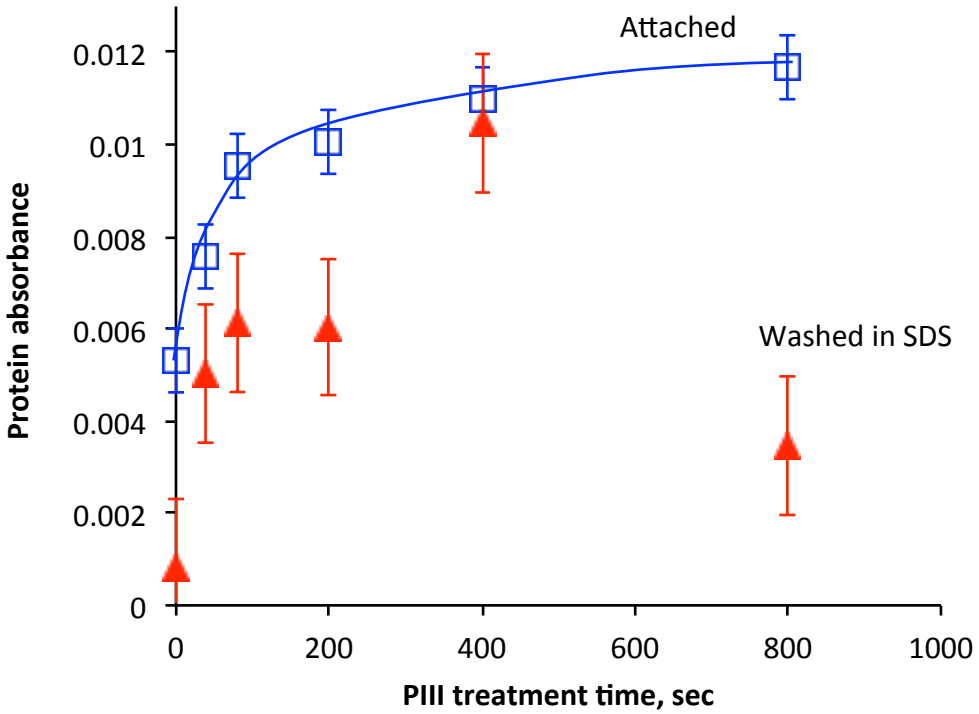

Fig.5.3. FTIR ATR spectra absorbance of Amide I line of BSA attached to polyurethane of PPG-DI PTHF with 0.35 NCO/OH ratio with PIII treatment time: blue is attached BSA, red is BSA attached and then washed off in SDS 1 hour at 70^0C. The absorbance of Amide I of protein was normalized on the absorbance of 1100 cm^{-1} line related to vibrations in polyurethane.

The experiment was done with the same samples of polyurethane after FTIR spectra recording. Both control and protein samples were washed in 45 ml of 2% SDS solution in mQ-water for 1 hour at 70^0C in individual Falcon polypropylene tubes which were placed into the water bath at controlled temperature. After washing in the detergent, all samples were rinsed in mQ-water 3 times, every time in new Falcon tubes and dried overnight in Petri dishes. Then the spectra of FTIR ATR were recorded. The spectra of buffer samples were subtracted from the spectra of protein samples as described above and presented in Fig.5.4. The absorbance of protein Amide I line was normalised on the absorbance of polyurethane 1100 cm^{-1} line and is presented in Fig.5.3.

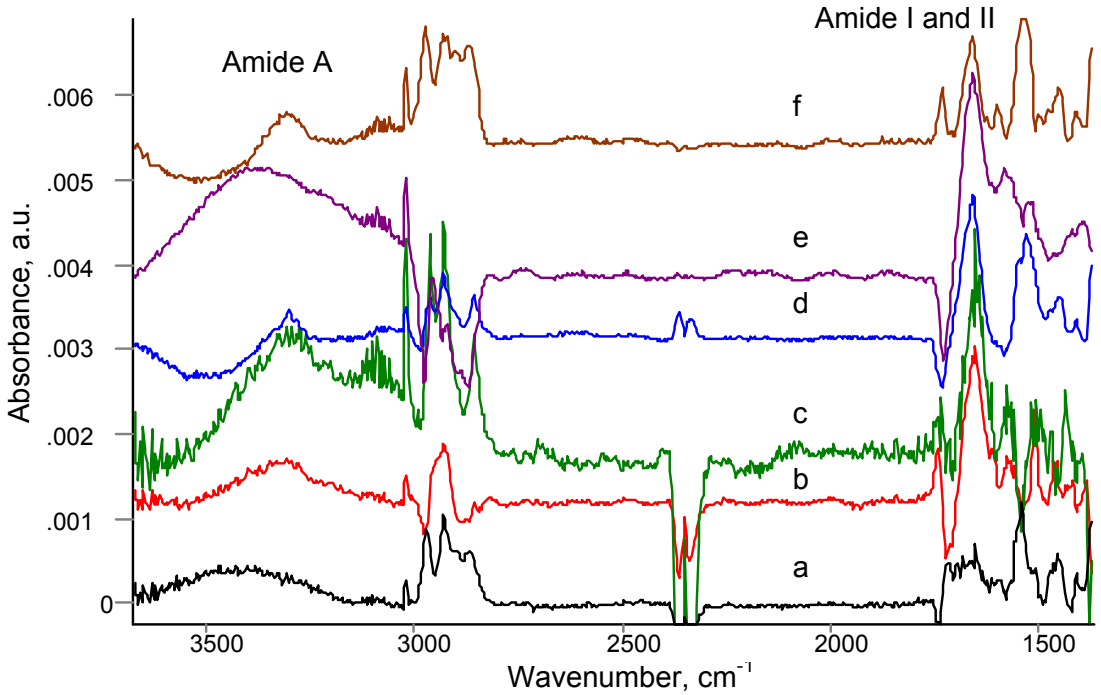

Fig.5.4. FTIR ATR spectra of attached BSA and washed off in SDS detergent on untreated and PIII treated polyurethane of PPG-DI PTHF with 0.35 NCO/OH ratio. From bottom to top: (a) untreated polyurethane, (b) 40, (c) 80, (d) 200, (e) 400, (f) 800 s PIII treatment time for 20 keV nitrogen ions. The spectra of corresponding polyurethanes are subtracted.

The spectra of SDS washed samples show the Amide I line of the attached protein only for PIII treated polyurethane. The protein lines in the spectrum of untreated polyurethane are not observed, and are under the noise level of the spectrum. Therefore the protein was almost washed from the untreated polyurethane. It shows that the protein on untreated polyurethane attached due to physical forces was disturbed by the physical forces of the detergent's molecules. Washing in detergent was sufficient to remove whole protein layers attached to the untreated surface due to physical forces.

The amount of attached protein on PIII treated polyurethane after washing in detergent solution is lower than the amount of attached protein before the washing. However, a significant portion of the attached protein remains on the surface after washing despite the detergent's physical forces. This shows that this protein is attached chemically to the surface. The ratio of attached to remained after detergent washing varies from 30% for 800 sec PIII treated sample to 95% for 400 sec PIII treated sample with average amount 63% for all PIII treated samples. This amount is consistent with previous amount of the covalently attached proteins on polyethylene [1], polystyrene [2], PTFE [3, 4], ePTFE [5], polyamide [6], polyethersulphone [7] and Polyether ester ketone [8] treated by PIII.

The attachment of Fg protein on the polyurethane surface was done as described above for BSA protein with some variations. The polyurethane samples were incubated in the Fg protein solution on the same day of the PIII treatment because a monolayer of the Fg immobilised protein is thicker then the immobilised BSA protein due to higher molecular mass of Fg protein (~340 kD) then BSA protein (~66kD).

Therefore, the signal in FTIR ATR spectra is expected to be higher for Fg protein than for BSA, and the effect of different oxidation of the polyurethane sample after PIII treatment is less important for protein detection. In addition, the concentration of Fg protein was 20 μg/ml due to higher activity of the polyurethane surface freshly treated by PIII.

The FTIR ATR spectra of Fg protein immobilised on the polyurethane surface are presented in Fig.5.5. The spectra of polyurethane was subtracted. The lines of protein backbone vibrations Amide A, I and II are clearly visible. The intensity of these lines is higher for Fg protein than for BSA protein (Fig.5.2), which corresponds to thicker Fg immobilised layer than BSA immobilised layer due to differences in size of the protein molecules.

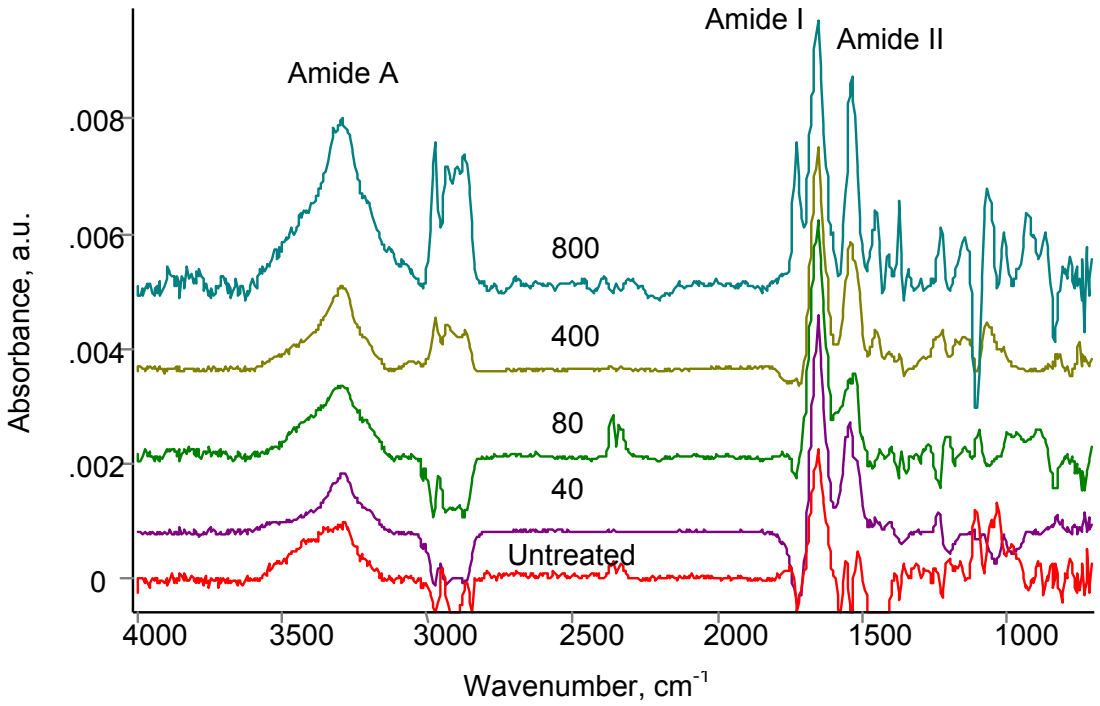

Fig.5.5. FTIR ATR spectra of attached Fibrinogen on untreated and PIII treated polyurethane of PPG-DI PTHF with 0.35 NCO/OH ratio. PIII treatment time for 20 keV nitrogen ions is noted in secs. The spectra of corresponding polyurethanes were subtracted.

The covalent immobilisation of Fg protein was analysed by FTIR ATR spectra after washing the polyurethane samples in SDS detergent. The washing conditions for Fg immobilised samples were the same as for BSA immobilised samples. The spectra of washed protein immobilised samples after subtraction of the polyurethane buffer samples spectra are presented in Fig.5.6. The lines of Amide A, I and II in the spectra of PIII treated samples are very clearly visible. In the spectra of untreated polyurethane these lines are observed at the noise level of the subtraction.

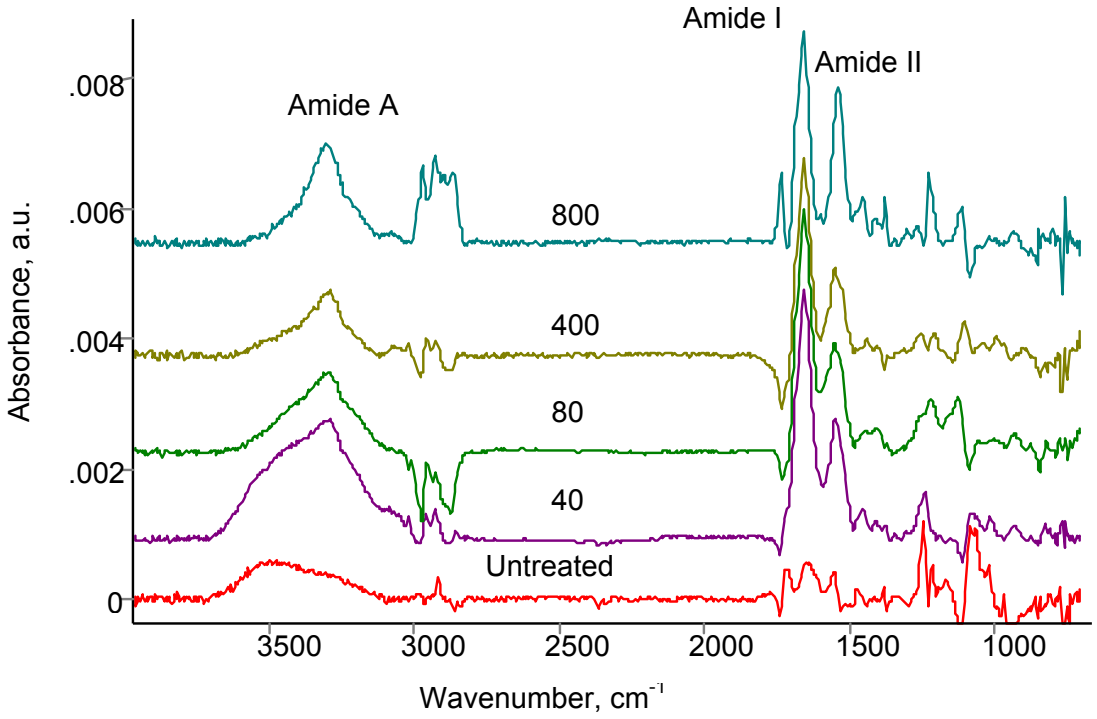

Fig.5.6. FTIR ATR spectra of attached Fibrinogen on untreated and PIII treated polyurethane of PPG-DI PTHF with 0.35 NCO/OH ratio and washed with SDS detergent. PIII treatment time for 20 keV nitrogen ions is noted in seconds. The spectra of corresponding polyurethanes are subtracted.

The quantitative analysis of the immobilised protein was done on the absorbance of Amide I line. Other Amide A and II lines are overlapped with polyurethane lines and cannot be used for the analysis. The absorbance of protein Amide I line normalised on the absorbance of polyurethane 1100 cm^{-1} line and presented in Fig.5.7. The amount of Fg protein attached to the PIII treated samples was higher than that attached to the untreated polyurethane surface. The amount of attached protein depends slightly on PIII treatment time showing the maximal amount for 80 sec PIII treatment time. However, the difference between the time points is in a range of error bars.

The amount of protein on PIII treated samples after SDS detergent washing is almost equal to the amount of attached protein. The difference between attached and remained after detergent washing is in the range of error bars. The average ratio of attached and remained protein for all PIII treated samples is ~95%. The ratio of remained protein after detergent washing on untreated polyurethane is about 26% from the attached protein amount, while the absorbance of the Amide I line is at the noise level and can be accepted as zero.

It was proved that the Fg protein is attached physically on untreated polyurethane and this protein is almost completely washable with SDS detergent. The PIII treated surface of polyurethane attaches the Fg protein covalently.

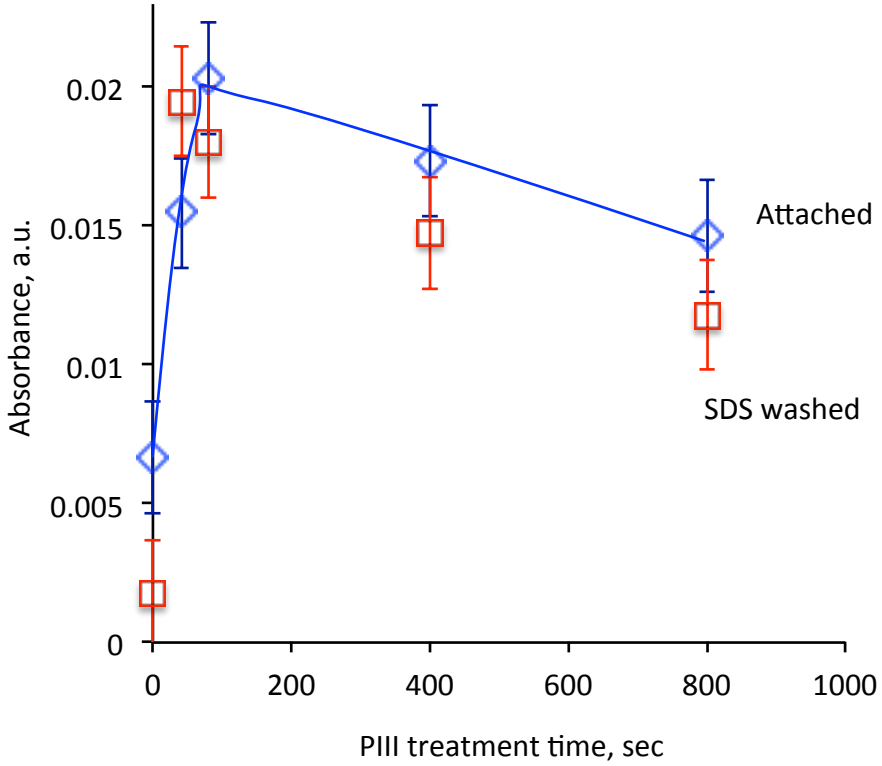

Fig.5.7. FTIR ATR spectra absorbance of Amide I line of Fibrinogen attached to polyurethane of PPG-DI PTHF with 0.35 NCO/OH ratio with PIII treatment time: blue is attached Fibrinogen, red is Fibrinogen attached and then washed off in SDS for 1 hour at 70^0C. The absorbance of Amide I of protein was normalized on the absorbance of 1100 cm^{-1} line related to vibrations in polyurethane.

The attachment of tropoelastin (TE) was detected by ELISA. The dependence of TE amount attached to untreated and PIII treated polyurethane is presented in Fig.5.8. An increase of TE concentration in the soaking solution increases the amount of attached TE up to saturation level. The saturation is achieved between 10 and 20 μg/ml concentration, consistent with the same dependence for other proteins attached on other polymers [9, 10]. The saturated level of attached TE is higher on PIII treated polyurethane then on untreated polyurethane. The concentration of TE higher then 10-20 μg/ml does not increases the amount of attached TE under applied conditions of attachment (time, temperature and volume of solution).

The strength of TE attachment was tested with washing in SDS detergent. ELISA shows that the attached TE on untreated polyurethane is washable with SDS detergent. The absorbance for untreated samples is lower then the detection level after washing of the samples in SDS solution (Fig.5.9). Under the same conditions, a part of the attached TE on PIII treated polyurethane remains on the surface.

The amount of the covalently attached TE was analysed according to different PIII treatment times (Fig.5.10). The results show that after the 40 sec of PIII treatment time point the longer treatment time does not increase the amount of the covalently attached TE in a range of error bars. The attachment of TE was done 8 days after PIII treatment.

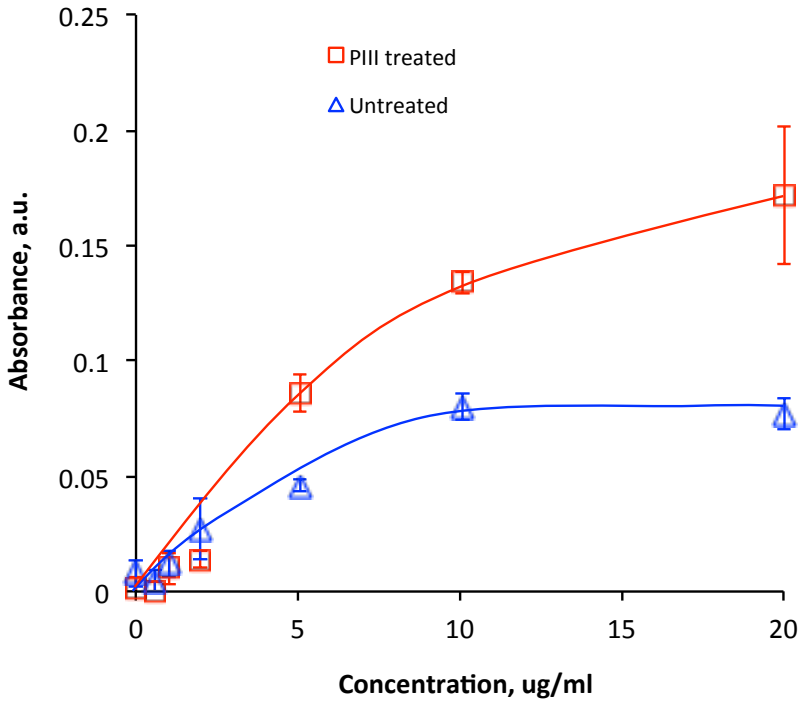

Fig.5.8. Absorbance in ELISA test of tropoelastin protein attached on untreated (blue triangles) and PIII treated (red squares, N+ ions of 20 keV energy, 800 sec PIII treatment time) polyurethane in dependence on the tropoelastin solution concentration at soaking of polyurethane.

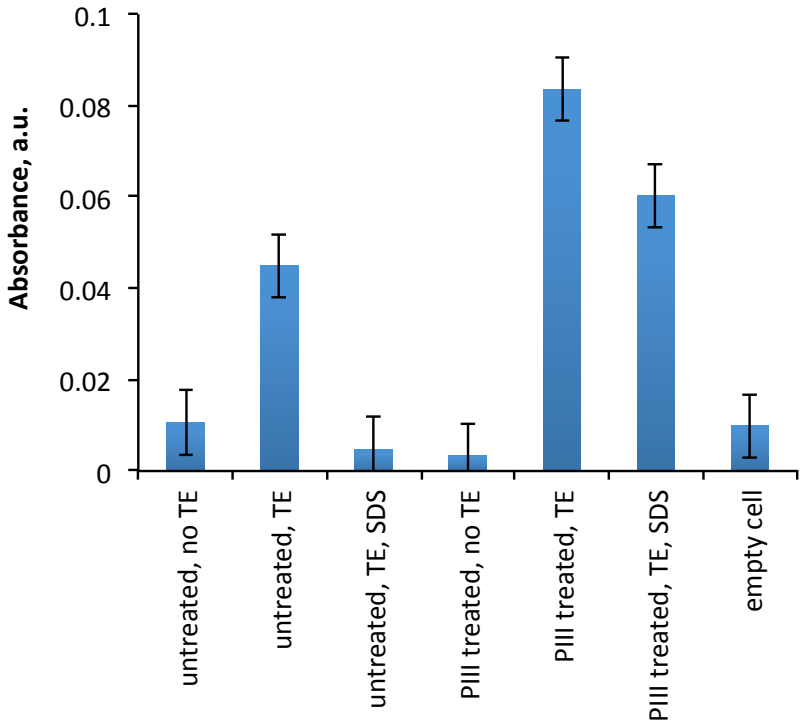

Fig.5.9. ELISA test result of tropoelastin attached to untreated and PIII treated polyurethane (20 keV N+ ions during 200 sec of PIII treatment) before and after washing in SDS detergent. The washing was done with 5% SDS (w/v) at 95°C for 30 min (black bars). The control samples results without tropoelastin are shown for comparison.

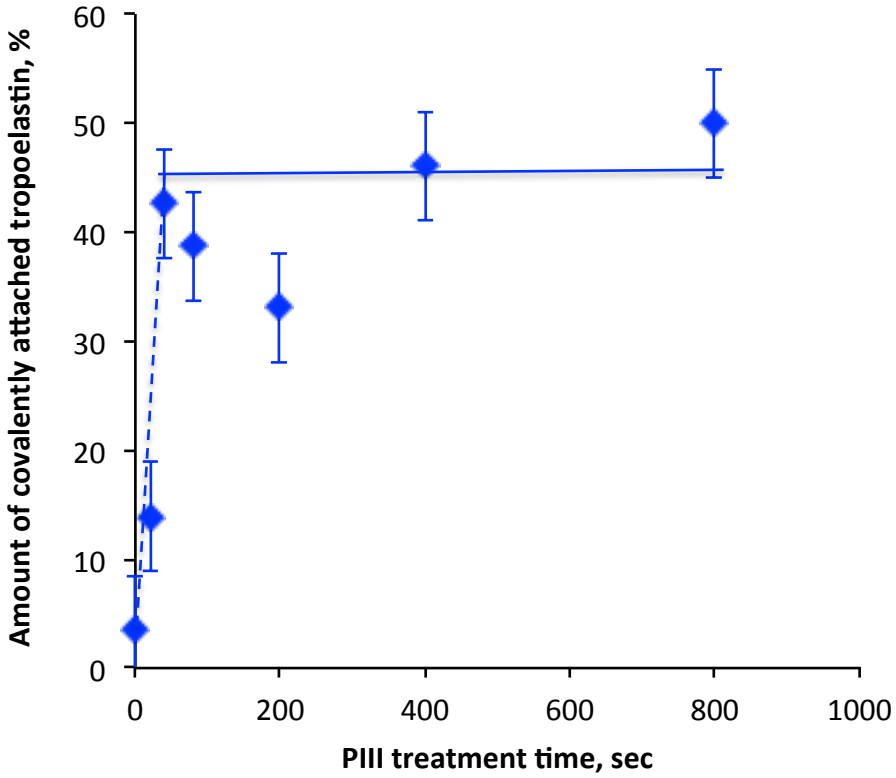

Fig.5.10. Ratio of covalently attached tropoelastin to total attached tropoelastin on polyurethane surface with time of PIII treatment by FTIR ATR data.

As observed for BSA protein, the part of covalently attached TE is lower than observed for Fg protein. The dependence of the covalent attachment on storage time, after PIII treatment and before the polyurethane was soaked in the tropoelastin solution, shows that the largest amount of covalently attached molecules occurs straight after the PIII treatment and decreases with the storage time (Fig.5.11). However, after 30 days the activity of the polyurethane surface is sufficient to attach covalently 28% of the total attached protein.

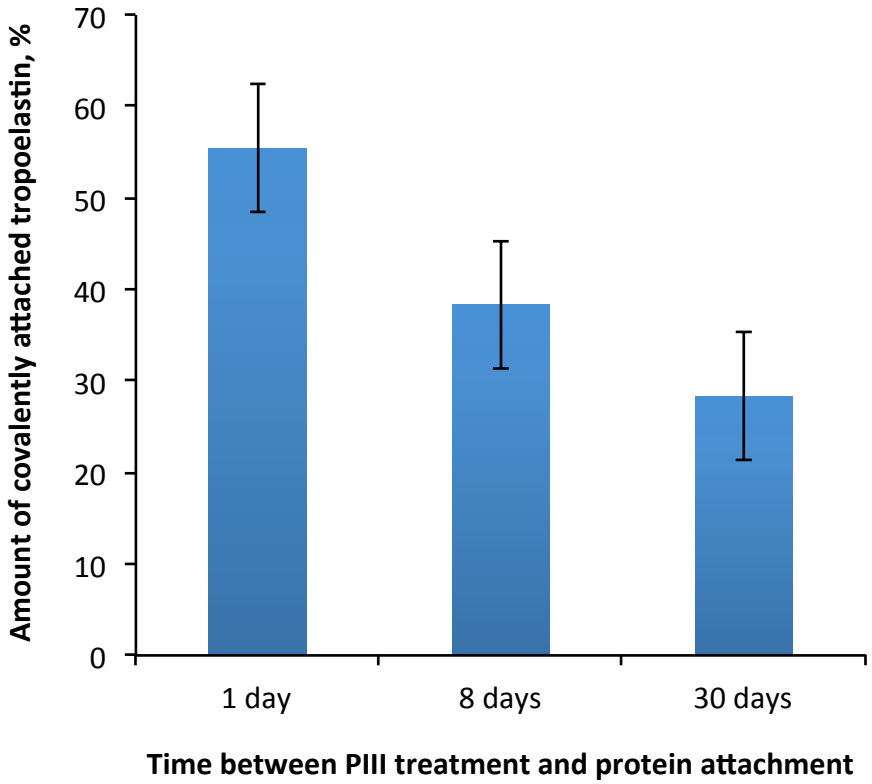

Fig.5.11. Covalently attached tropoelastin amount ratio to total attached to polyurethane surface with different time between PIII treatment and soaking in the tropoelastin solution. Polyurethane samples treated for 80 sec of PIII treatment time by nitrogen ions with 20 keV energy. Coating concentration was 10 μg/mL. SDS washing involved incubating in 5% SDS (w/v) at 95^0C for 30 min.

Therefore, the polyurethane surface becomes active to attach protein covalently after PIII treatment and maintains its activity for a minimum of one month.

5.2. Interaction of endothelial cells with implant

Endothelialisation is an important factor of biocompatibility. A total endothelialisation a short time after first contact of the organism tissue with the implant surface is required for successful integration of the implant into the organism. The endothelialisation of the polyurethane implants was tested with human cell interactions with the polyurethane surface *in vitro*. The effect of PIII treatment on cell attachment, cell spreading and cell proliferation was investigated with human dermal fibroblasts (HDFs) and human endothelial cells (HCAECs).

Polyurethane interacts with components of cell staining such as crystal violet and alcohol. This makes it difficult to get consistent results using such methods for the cell analysis.. In particular, the crystal violet assay diffuses into polyurethane and gives colour to the sample without the cells. A spectroscopic method gives false results of cell staining due to the strong variation of the background colour when the colour changes while there were no cells attached to the sample. To overcome these problems, the method of crystal violet staining was modified to exclude the colour change of the polyurethane samples due to assay diffusion into the polyurethane. The

staining time was reduced from 1 hour to 30 minutes and the washing time was increased from 3 short periods to 5 times for 30 minutes each. However, the quantitative results were not reliable. The crystal violet was washed out from polyurethane with the same speed as from cells.

The cells experiments included a step of cell staining with organic solvents such as ethanol. The polyurethane was swollen in ethanol with a strong deformation of the polyurethane samples. This deformation put the surface attached cells under mechanical stress, which led to the cells detaching from the surface at staining. The result of the cell analysis was affected by the deformation of the polyurethane film. All known protocols of cell staining used in the laboratory required ethanol or other solvent application. In some cases, when the cells were visible without staining, the analysis was done with microscopy without staining. In other cases the results of the cell analysis was considered taking into account the effect of the solvent on cell staining.

Due to the these problems with cell analysis on the polyurethane surface, the cell experiments were carried out with PTFE films treated by the same methods of ion beam implantation as a comparison. The experiments with cell adherence were started with PTFE films of 20 μm thickness which were treated by nitrogen ions of 20 keV energy.

In the cells experiment, PTFE films of 0.58 cm^2 surface area were used. The bovine aortic endothelial cell line GM7373 (Coriell) was used for the experiments. 4 x 10^4 cells in 200 μL medium (MEM-Earle supplemented with 10% fetal bovine serum (FBS), 1 x MEM vitamins, 2 mM N-Acetyl L-Alanyl L-Glutamine, 1 x Amino acids) were seeded directly on the samples. They were allowed to adhere for 2 hours at standard cell culture growing conditions. The medium was then filled up to 1 mL per sample. Three days after seeding, the cells were fixed in 0.2% paraformaldehyde in PBS and stained with rhodamine. Images were taken by fluorescent microscopy with a video camera. The cells were counted by photos and cell density was averaged on 10 photos taken randomly on the surface for each PTFE sample. The examples of the images are presented in Fig.5.12.

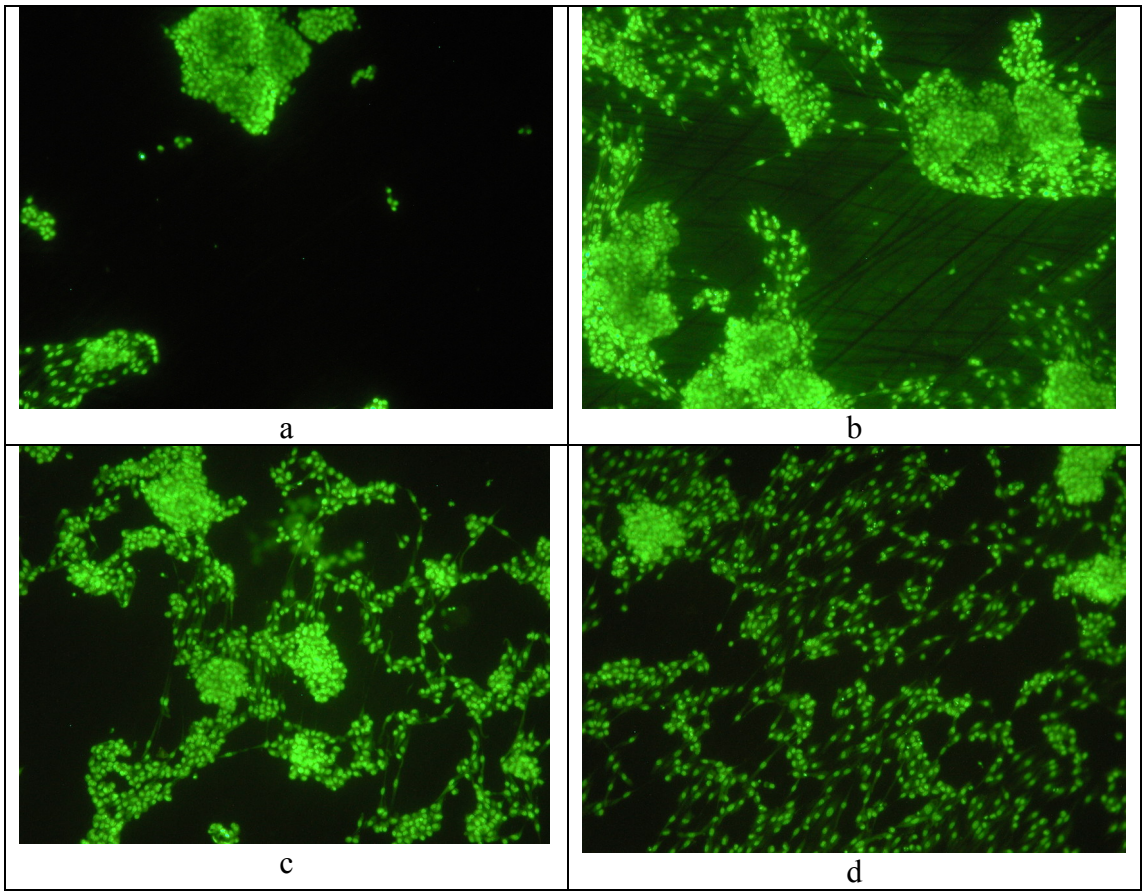

Fig.5.12. Fluorescent image of cells proliferated for 3 days on untreated (a) and ion implanted (b-d) PTFE with nitrogen ions of 20 keV energy and fluence of 6 $x10^{13}$ (b), $1x10^{14}$ (c) and $5x10^{14}$ (d) ions/cm^2.

The cells are sitting compactly on the untreated PTFE surface, and do not cover most of the surface. Cell bodies are rounded to minimise the contact with the surface. The images of the cells on ion beam treated surfaces are different. The cells are distributed on the PTFE surface. When there was a high fluence the cells formed a total cover on the surface and the cell density was mostly uniform on the overall surface. Here, the cell bodies were elongated and spread on the PTFE surface.

Quantitative results showed that the cells adhere and grow on untreated and ion implanted PTFE surface from seeded density ($0.7x10^5$ cells/cm^2). However the amount of cells on the ion implanted PTFE is higher than on untreated PTFE (Fig.5.13). The cells grew better on the PTFE treated surfaces with the lowest fluence. Similar results were expected on the PIII treated polyurethane.

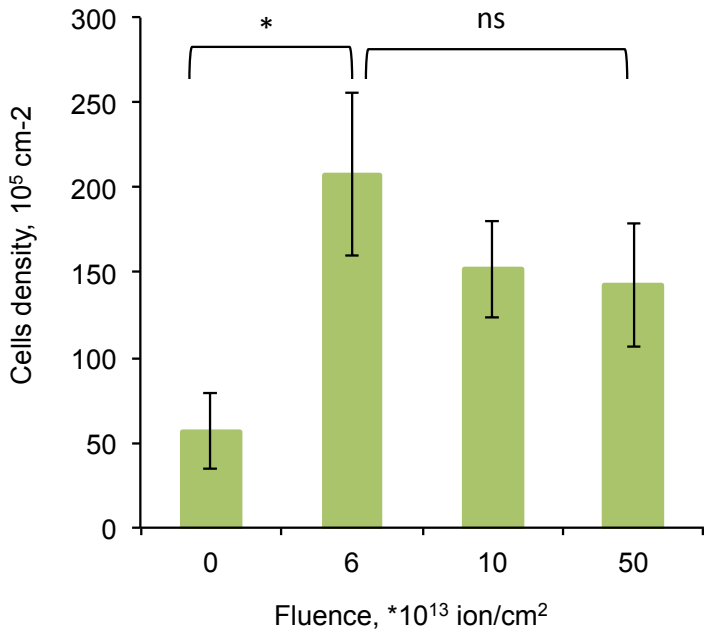

Fig.5.13. Cell density attached on PTFE after 3 days of proliferation with fluence of ion beam implantation. The mark "*" corresponds to significant difference, $p<0.05$ and "ns" to not significant difference, $p>0.05$.

The human coronary artery endothelial cells (HCAEC) were attached to the untreated polyurethane samples, to the PIII treated with different fluence, and to the Tissue culture plastic (TCP) as a control. Before the cell attachment, some samples were coated with tropoelastin as described above. For the cell attachment, 0.5 ml aliquots of cells at a density of $1x10^5$ cells/ml were added to the wells and placed at 37^0C in a 5% CO_2 incubator. The cells were proliferated for 2 days, and for 6 days, changing the media every second day. Then the cells were stained and observed with fluorescent microscopy.

For staining, the cells were fixed in ice cold 80% Ethanol and washed with PBS buffer. Then the cells were permeabilized in 1% (w/v) Triton X-100 in PBS for 5 min, washed 3 times in 1 ml with PBS 5 mins each, then blocked with 1% (w/v) BSA for 0.5 h. Cells were washed 3 times in 1 ml with PBS for 5 mins each. The cells were stained in Phalloidin-TRITC for 30 minutes in darkness. Samples were washed 3 times in 1 ml with PBS, then mounted with DAPI between glass slides, sealed and viewed using a Zeiss LSM 510 Meta confocal microscope. The fluorescence exited at 540-545 nm of light, and was observed at 570-573 nm for the cytoskeleton with actin-filament, and at 350 nm and 470 nm respectively for cell nuclei.

The selected images of the cells are presented in Fig.5.14-19. The low resolution images were used to analyse the cell density (Fig.5.14-17) and the high resolution images were used to analyse cell bodies (Fig.18-19).

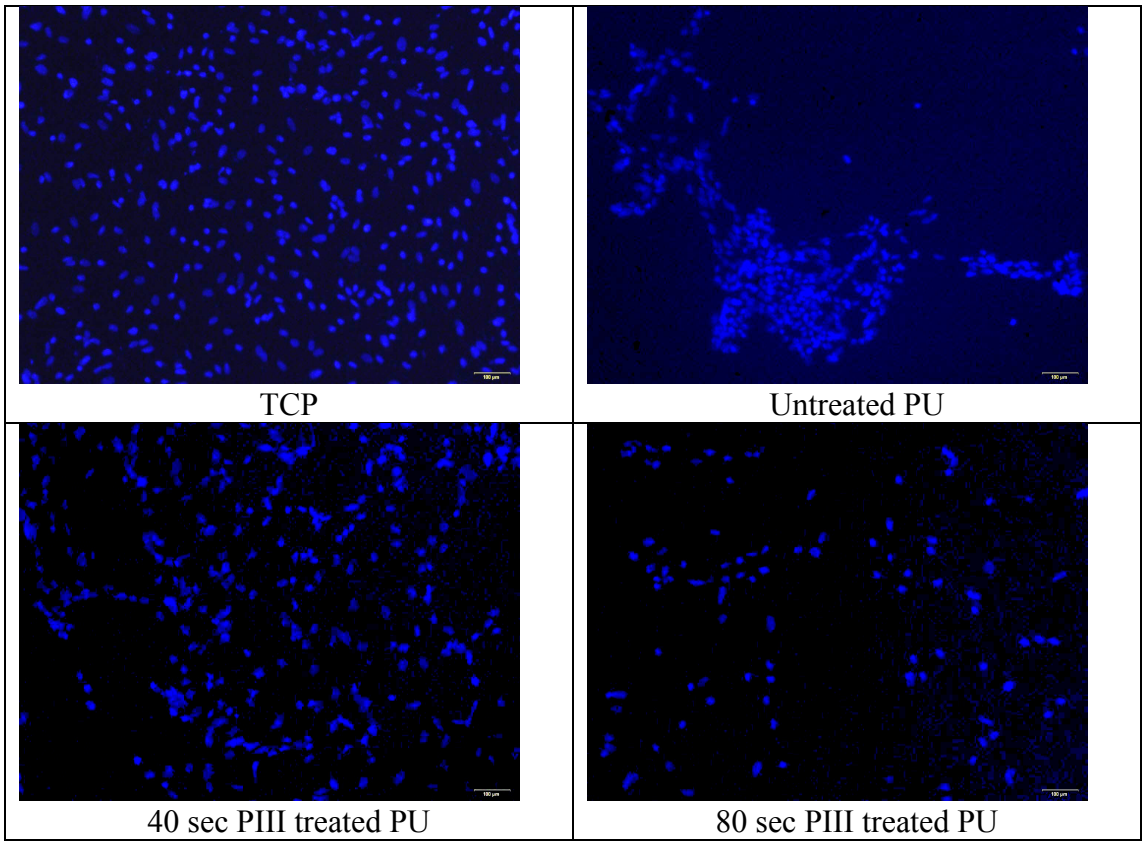

Fig.5.14. Fluorescent image of the cells adhered and proliferated in 2 days to polyurethane surface treated by PIII with different time. TCP control and untreated polyurethane samples are presented above.

The images show that the cells were differently attached and proliferated on the untreated and PIII treated polyurethane surfaces without tropoelastin. After the 2 day period the cells on the untreated polyurethane were sitting in compact clusters. However, the cells on PIII treated polyurethane were spread as they were on the TCP control. The widest spread was observed when fluence was lowest, at 40 seconds of PIII treatment.

After the 6 day period of proliferation, the surface of untreated polyurethane became totally covered by cells as they were on the TCP surface and the PIII treated polyurethane.

It follows that the presence of tropoelastin coating increases the rate of endothelialisation and the proliferation leads to total coverage of the untreated polyurethane surface by the endothelial cells.

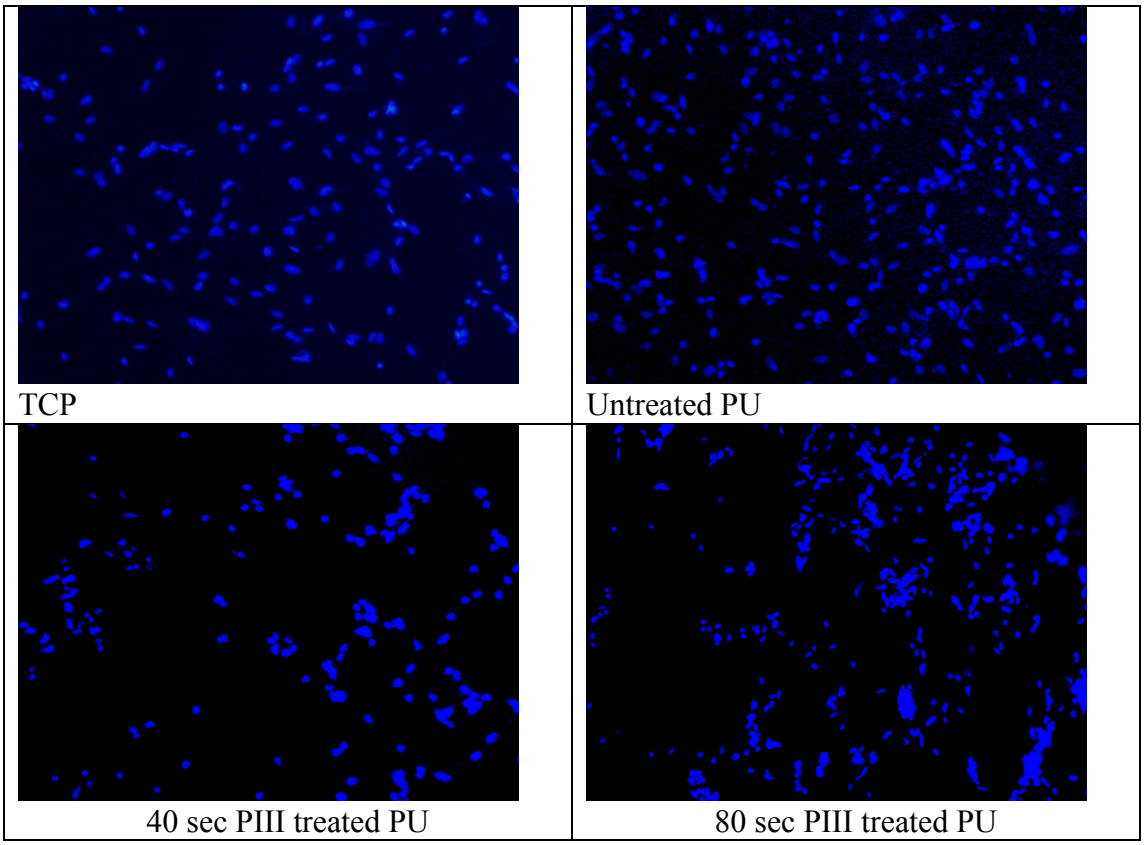

Fig.5.15. Fluorescent image of the cells adhered and proliferated for 6 days on polyurethane surface treated by PIII for different times. TCP control and untreated polyurethane samples are presented above.

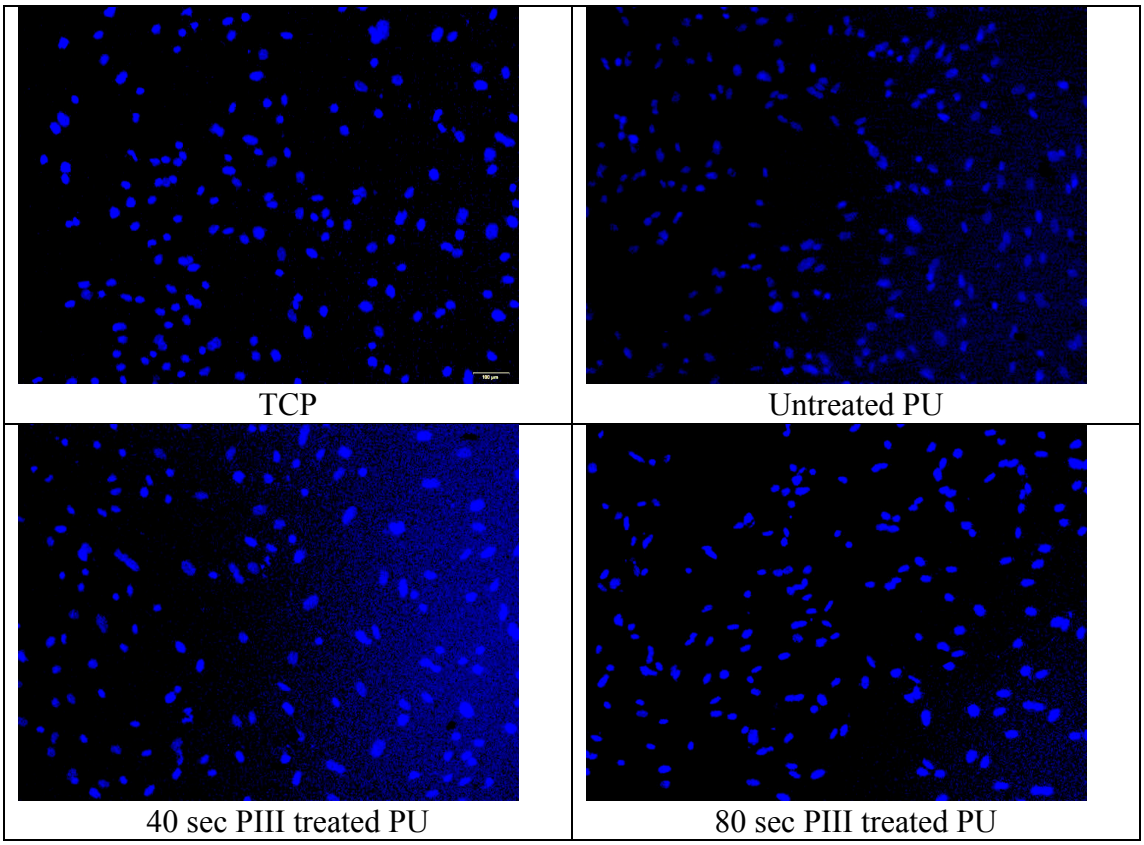

Fig.5.16. Fluorescent image of the cells adhered and proliferated for 2 days on polyurethane surface treated by PIII for different times and with tropoelastin coating. TCP control and untreated polyurethane samples are presented above.

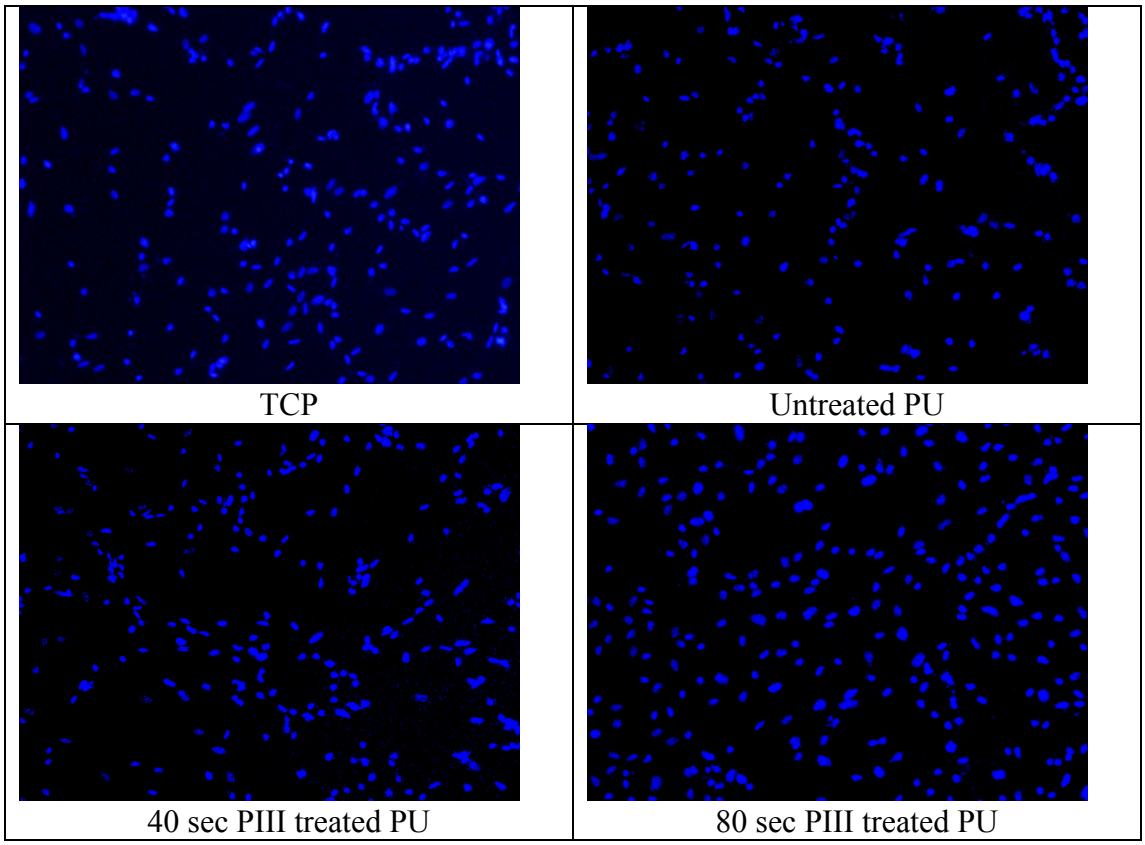

Fig.5.17. Fluorescent image of the cells adhered and proliferated for 6 days on polyurethane surface treated by PIII for different times and with tropoelastin coating. TCP control and untreated polyurethane samples are presented above.

The high resolution images (Fig.5.18-19) showed that the cell cytoskeletons were spread differently on the untreated and PIII treated polyurethanes. After 2 days of proliferation the cell bodies on the untreated polyurethane were rounded. The cells were sitting compactly to minimise contact with the untreated polyurethane surface. The cell bodies on the PIII treated polyurethane were elongated and spread on the surface.

After 6 days of proliferation the cell cytoskeletons were similarly spread on untreated and PIII treated polyurethanes. No difference was observed between the cells proliferated on TCP control surface and polyurethane.

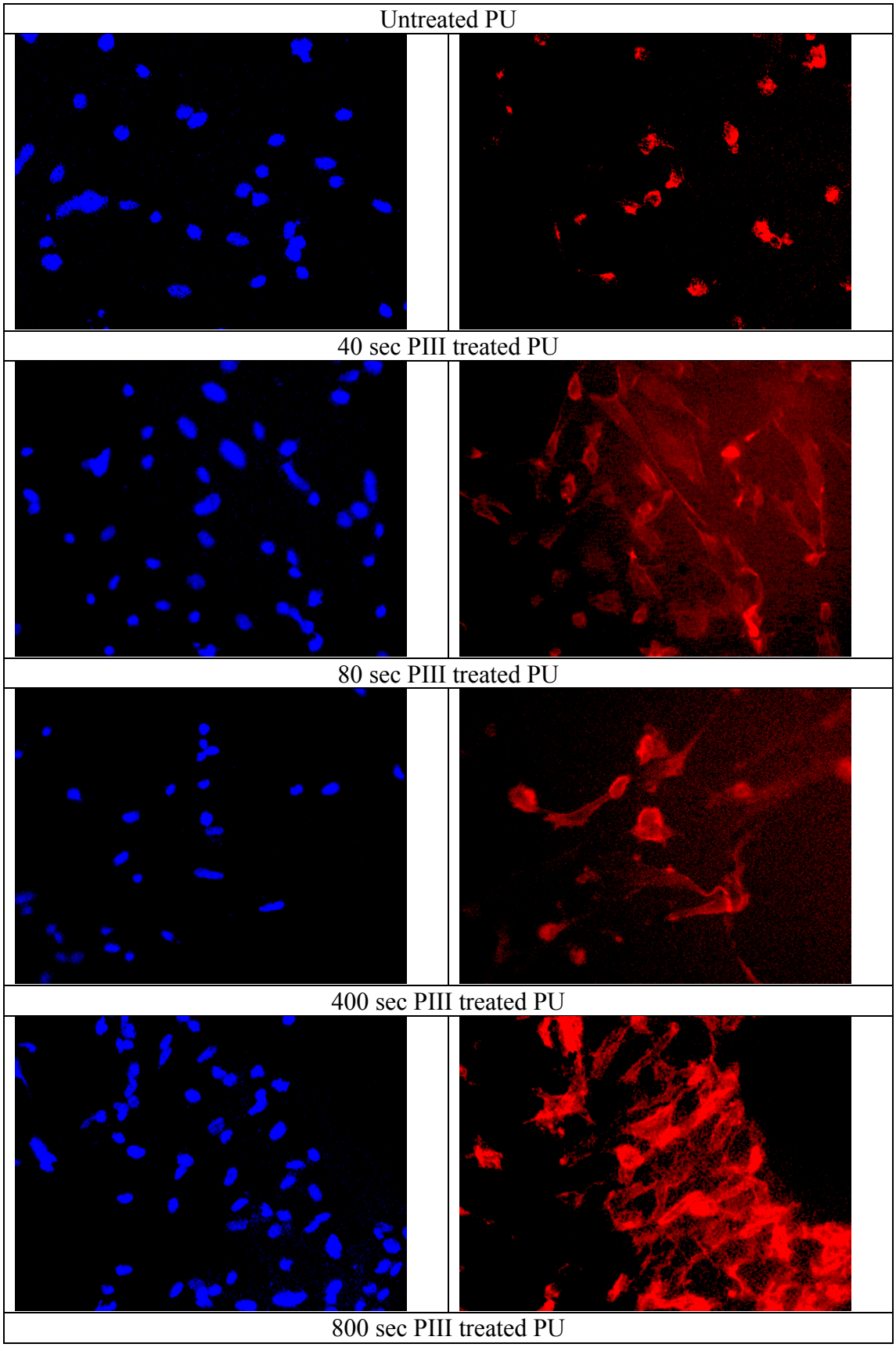
Untreated PU
40 sec PIII treated PU
80 sec PIII treated PU
400 sec PIII treated PU
800 sec PIII treated PU

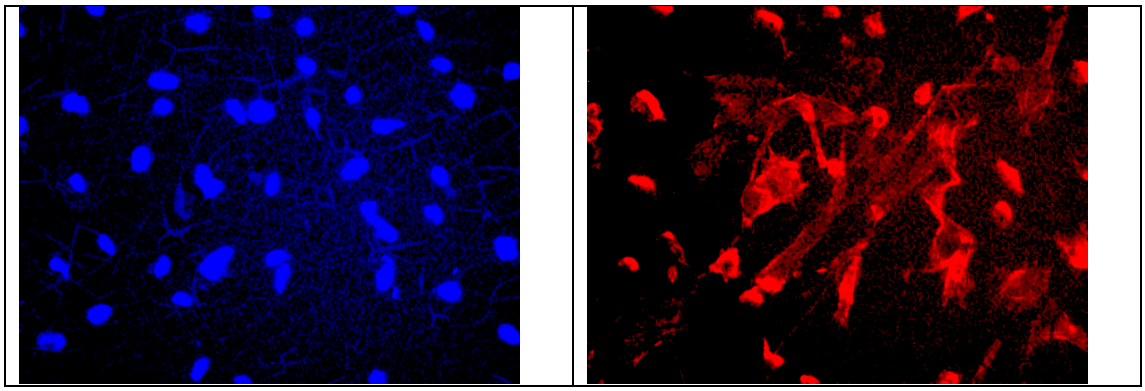

Fig.5.18. Fluorescent images of the cells adhered and proliferated for 2 days on polyurethane surface treated by PIII for different times and with tropoelastin coating. TCP control and untreated polyurethane samples are presented above. Images on the left correspond to the cell nuclei staining. Images on the right correspond to the cell cytoskeleton staining. Image size is 0.68x0.5 mm^2.

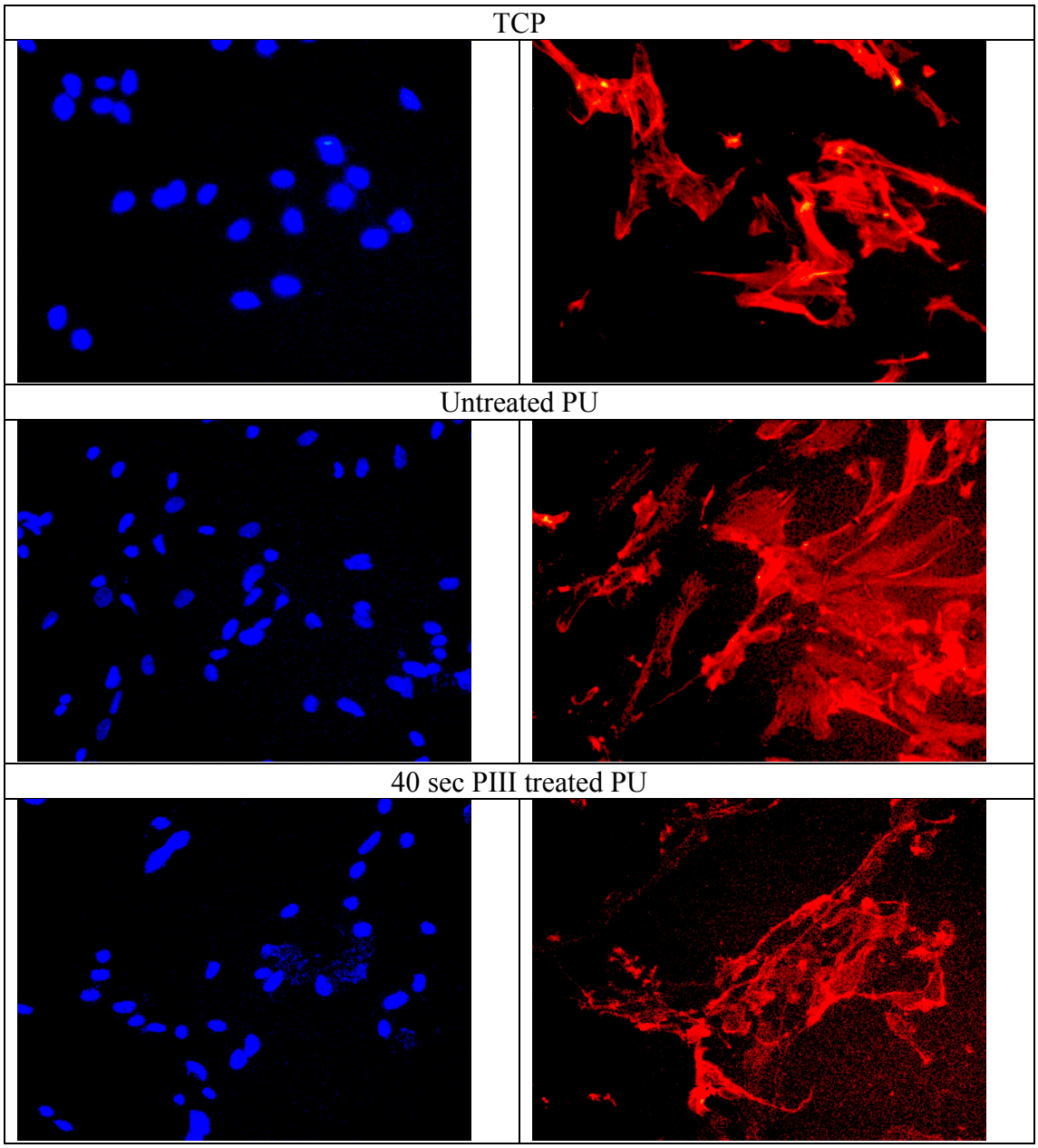

80 sec PIII treated PU

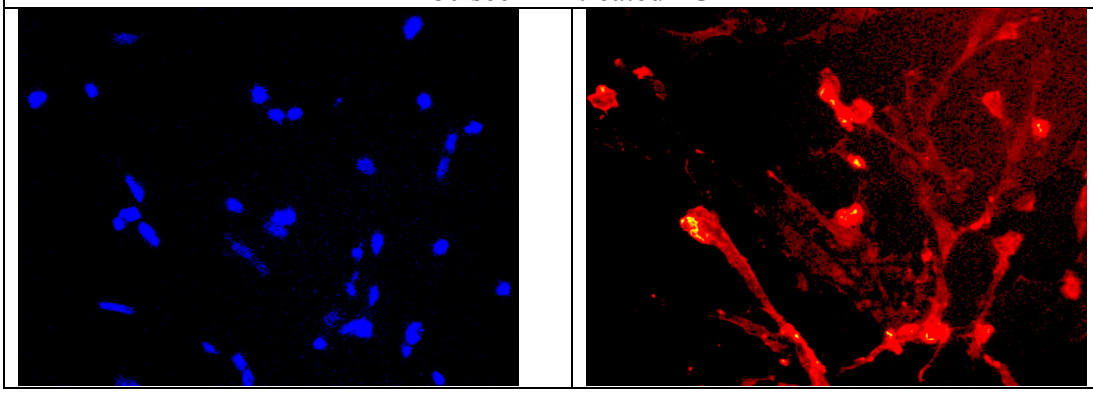

Fig.5.19. Fluorescent images of the cells adhered and proliferated for 6 days on polyurethane surface treated by PIII for different times and with tropoelastin coating. TCP control and untreated polyurethane samples are presented above. Image size is 0.68x0.5 mm^2.

The cells on high fluence PIII treated polyurethane were analysed without staining. The images are shown in Fig.5.20. The cells totally covered the 40 sec and 800 sec PIII treated polyurethane surface as they did on the control TCP surface. The cells were spread and cell bodies were elongated, providing a broad contact with the surface. The cells on the untreated polyurethane did not cover the whole surface and the cell bodies were compact and rounded, which minimised the contact with the surface. These results correspond to the staining results in Fig.5.14-5-19. Therefore, the high fluence PIII treatment does not improve the cell adherence when compared with low fluence PIII treatment.

TCP plate

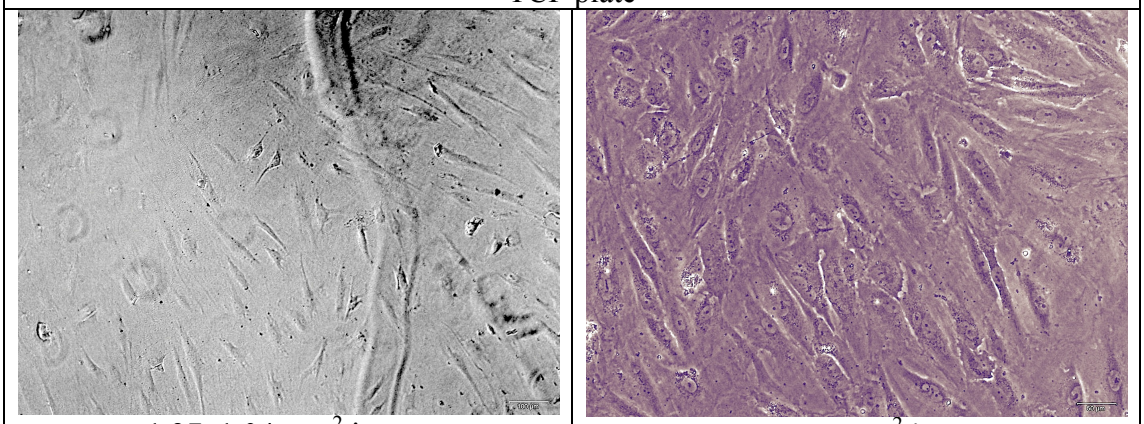

1.37x1.04 mm^2 image | 0.68x0.5 mm^2 image

Untreated PU

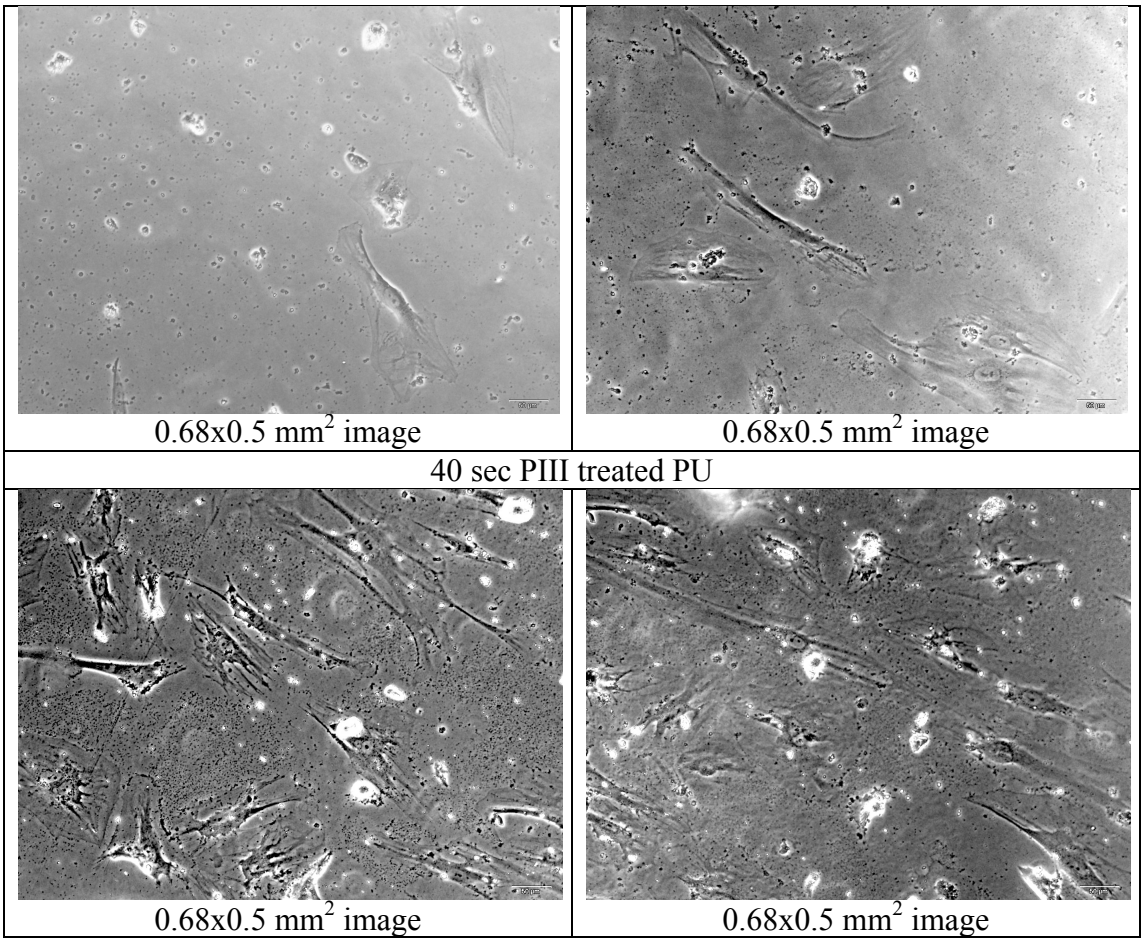

Fig.5.20. Optical microscope image of the living cells attached to polyurethane surface treated by PIII for different times. No fixing or staining was applied.

The cell density after the 2 and 6 day periods of proliferation on TCP, untreated and PIII treatment polyurethanes are shown in Fig.5.21 and Fig.5.22. The cell density after the 2 day period of proliferation on the control TCP surface and PIII treated polyurethane without tropoelastin cover was similar. The cell density on the untreated polyurethane was significantly less than on TCP and PIII treated polyurethane. The

attachment of tropoelastin on the untreated and PIII treated polyurethane provided the same cell density as on the control TCP surface.

The cell densities after the 6 day period of proliferation on the control TCP, untreated polyurethane and PIII treated polyurethane with and without the tropoelastin cover were similar.

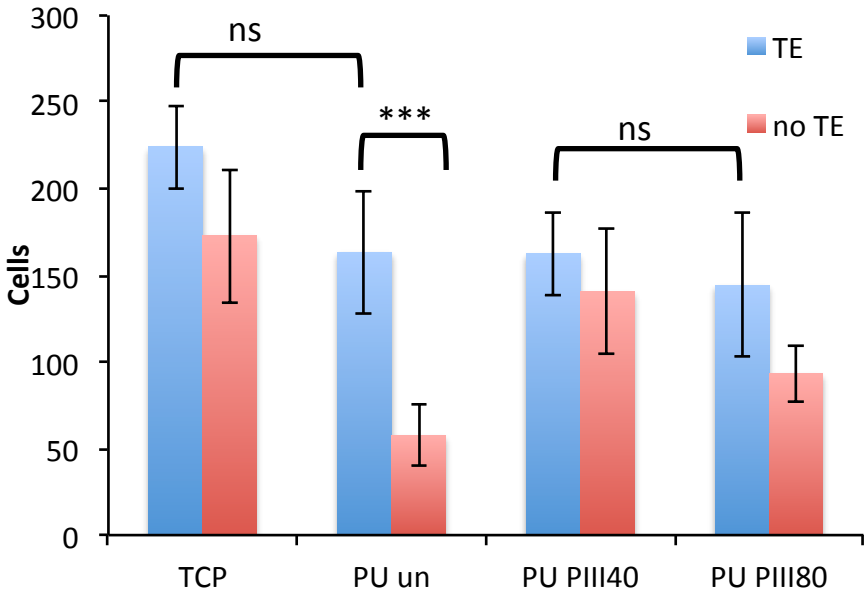

Fig.5.21. Number of cells on TCP and PU with and without tropoelastin after 2 days of attachment. The difference is significant (***), $p<0.001$ and not significant (ns), $p>0.05$.

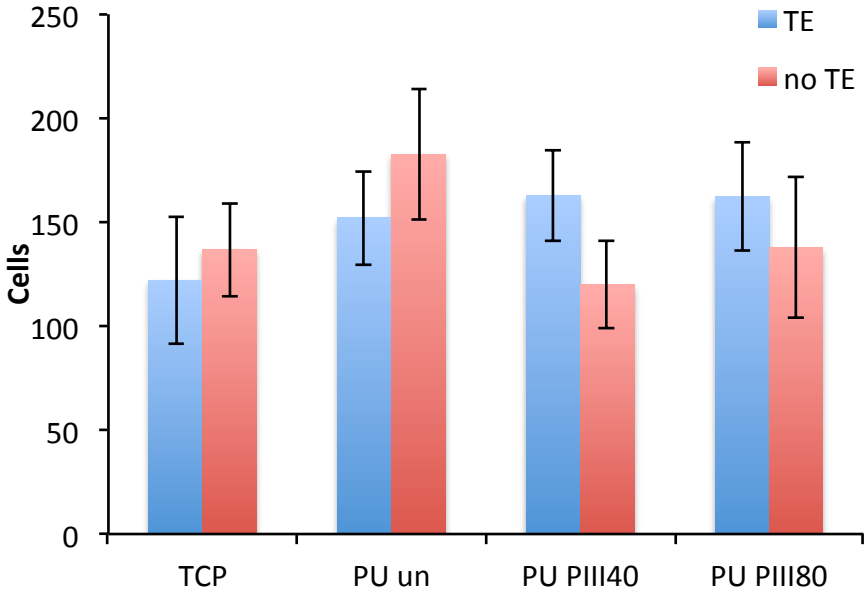

Fig.5.22. Number of cells on TCP and PU with and without tropoelastin after 6 days of attachment. The difference is insignificant, $p>0.05$.

The cell adherence and proliferation showed that the PIII treatment provided higher cell density and cell spreading on polyurethane as on the control TCP surface. The

tropoelastin cover provided faster endothelialisation on the untreated polyurethane while the PIII treated polyurethane provided the same endothelialisation with and without tropoelastin. The influence of PIII fluence on endothelialisation of PIII treated polyurethane surface with and without tropoelastin cover was not observed in the investigated range of the fluence.

5.3. Discussion

Three different proteins were attached on the polyurethane surface. The amount of attached protein was measured with FTIR ATR spectra and ELISA assay methods. All proteins were well attached on untreated and PIII treated surfaces. The BSA and tropoelastin were better attached than Fibrinogen on untreated polyurethane. The protein attachment on untreated polyurethane corresponded to the theoretical data of protein attachment on hydrophobic surfaces when the attachment is strong due to non-polar van-der-Waals intermolecular interactions between the protein molecule and polyurethane macromolecule [11-13].

In contrast with untreated polyurethane surfaces, all tested proteins were well attached on PIII treated polyurethane. The amount of attached proteins on PIII treated polyurethane is twice or more than the amount of attached proteins on untreated polyurethane. The same difference was observed for untreated and PIII treated Teflon [14, 15], polyethylene [9], polystyrene [2] and other polyurethanes [16-18].

The covalently attached protein was measured after washing in SDS detergent. The SDS detergent is widely known as a strong destroyer of physical interactions between the surface and protein molecules [19]. SDS destroys all van-der-Waals and Coulomb interactions due to both hydrophilic and hydrophobic end groups in SDS molecule. However, the covalent attachment via C-C and C-N bonds between the protein and surface cannot be destroyed by SDS detergent. The amount of protein remaining on the PIII treated polyurethane surface after strong washing in the SDS detergent shows that 40-70% of attached protein from the total attached amount was covalently bounded. For some samples, the 100% covalent attachment was observed. Similar covalent attachment was observed for PIII treated Teflon [14, 15], polyethylene [9], polystyrene [2] and other polyurethanes [16-18]. Thus, the PIII treated polyurethane surface adsorbs the proteins covalently.

The mechanism of covalent attachment as discovered in [15] is based on free radical reaction between the free radicals on the edge of the graphitic clusters and hydrogen-donating groups of protein. As a result of the reaction, the covalent bond C-C or C-N was formed and provided the stable attachment of protein to the surface. This mechanism of covalent attachment was observed for different polymers and proteins [20]. The PIII treated polyurethane contained similar graphitic clusters in the surface layer as these polymers. Therefore the formation of similar covalent bonds between the PIII treated polyurethane and attached proteins was expected. The dependence of the protein amount on PIII treatment time was not strong. The saturation of attached protein amount was observed for all proteins after short (40 or 80 sec) PIII treatment. The same saturation of the protein amount was observed for other PIII treated polymers [20]. The similar conditions of attachment, similar properties of the surface layer, similar dependence on PIII treatment parameters and similar amount of the covalently attached protein were evidence of the same covalent attachment mechanism.

The conformation of protein was not tested in the present study. The conformation of protein can be measured with FTIR spectra of Amide I line with analysis of α-helix, β-sheets, β-turns and random coils components but analysis of the strong overlapping protein and polyurethane Amide I lines does not provide useful information. However, the similar mechanism of covalent attachment of protein suggested that the conformation of the attached proteins to PIII treated polyurethane was expected to be active as observed in the attached protein to PIII treated polyethylene, polystyrene, Teflon and other polymers [20]. The high wettability of the PIII treated polyurethane supported this. Therefore, the research shows that the protein on PIII treated polyurethane attaches covalently on the mechanism of free radical reaction and its conformation is active.

The activity of the carbon surface layer usually remains for a long time. For example, PIII treated Teflon attaches protein covalently after 2 years of storage [20]. The PIII treated polyurethane shows its highest activity straight after PIII treatment, and a reduction of activity from 55% of covalent attachment after 1 day of storage up to 27% of covalent attachment after 1 month of the storage. Therefore, the polyurethane has to be used for the protein attachment as soon as possible after the PIII treatment.

The experiments with cells showed that Human dermal fibroblasts and human endothelial cells are attached and successfully proliferated at 6 days on newly synthesised polyurethane. The cells are well spread on the surface however the cell number is significantly less than on the "gold standard" TCP plastic. Also the cell bodies are characterised with minimal contact cell area indicating insufficient adhesion of the cell proteins on the surface. However, after 6 days of proliferation, the cell number on untreated polyurethane become similar to the TCP plastic. This effect of cell attachment and growing on the untreated polyurethane is significantly better than on other untreated medical grade polymers [4, 21].

The cell attachment and proliferation on PIII treated polyurethane is similar to the cell attachment and proliferation on TCP plastic. These results are similar to other PIII treated polymers [4, 21].

The preliminary attachment of tropoelastin does not improve the cell attachment on PIII treated surface. Only in the case of untreated polyurethane does the preliminary attachment of tropoelastin improve the cell attachment at the beginning (in 2 days).

Thus, the cell experiments showed that the PIII treatment improves the cell attachment and proliferation on the polyurethane surface. Therefore, the positive influence of PIII treatment on protein attachment and cell attachment and proliferation shows that the PIII treated surface is not toxic, as might be expected due to the presence of free radicals in the carbonised layer. The proteins from the cells themselves are attached to the PIII treated surface and then the cells are attached to their own protein layer. Therefore the protein that was attached to the PIII treated surface first before the cells' attachment does not help much in the cell attachment. The preliminary attachment of the proteins from the cells themselves is preferable to that of other proteins (for example, tropoelastin) because of the reduced likelihood of a foreign body reaction.

The results show that the PIII treatment provides the covalent attachment of protein and improves the cell attachment and proliferation on the PIII treated polyurethane surface. These *in vitro* results show that PIII treated polyurethane can be used for *in vivo* experiments where a positive effect of PIII treatment on biocompatibility in living organisms is expected.

5.4. Conclusions

The *in vitro* experiments showed that PIII treatment provides a covalent attachment of proteins to the modified polyurethane implant. This makes the attached protein coverage non-washable from the surface. The protein amount corresponds to the total protein coverage of the surface. However, the ability of the polyurethane surface to attach the proteins covalently decreases with the storage time after the PIII treatment.

The PIII treated polyurethane provides faster cell adherence and proliferation in comparison with the untreated polyurethane. The cell attachment on PIII treated polyurethane is the same as on the control TCP surface. For PIII treated implants, the pre-coating of the surface with tropoelastin does not improve the cell attachment and proliferation.

References

1. N.J. Nosworthy, J.P.Y. Ho, A. Kondyurin, D.R. McKenzie, M.M.M. Bilek, The attachment of catalase and poly-L-lysine to plasma immersion ion implantation-treated polyethylene, Acta Biomaterialia 3, 2007, 695–704.
2. B.K. Gan, A. Kondyurin, M.M.M. Bilek, Comparison of Protein Surface Attachment on Untreated and Plasma Immersion Ion Implantation Treated Polystyrene: Protein Islands and Carpet, Langmuir 23, 2007, 2741-2746.
3. A. Kondyurin, N.J. Nosworthy, M.M.M. Bilek, Attachment of horseradish peroxidase to polytetrafluorethylene (teflon) after plasma immersion ion implantation, Acta Biomaterialia, 4, 2008, 1218–1225.
4. I.V.Kondyurina, G.S.Nechitailo, A.V.Kondyurin, Ion beam implantation of polytetrafluorethylene and cell adhesion, Plasticheskie massi, 1, 2011, 15-21.
5. S.G. Wise, H. Liu, A. Kondyurin, M.J. Byrom, P.G. Bannon, G.A. Edwards, A.S. Weiss, S. Bao, M.M. Bilek, Plasma Ion Activated Expanded Polytetrafluoroethylene Vascular Grafts with a Covalently Immobilized Recombinant Human Tropoelastin Coating Reducing Neointimal Hyperplasia, ACS Biomater. Sci. Eng., 2, 2016, 1286−1297.
6. A.Kondyurin, N.J. Nosworthy, M.M.M. Bilek, R.Jones, P.J. Pigram, Surface Attachment of Horseradish Peroxidase to Nylon Modified by Plasma-Immersion Ion Implantation, Journal of Applied Polymer Science, 120, 2011, 2891–2903.
7. E. Kosobrodova, A. Kondyurin, W. Chrzanowski, D.R. McKenzie, M.M.M. Bilek, Plasma immersion ion implantation of a two-phase blend of polysulfone and polyvinylpyrrolidone, Materials and Design, 97, 2016, 381–391.
8. E.A. Wakelin, A.V. Kondyurin, S.G. Wise, D.R. McKenzie, M.J. Davies, M.M.M. Bilek, Bio-Activation of Polyether Ether Ketone Using Plasma Immersion Ion Implantation: A Kinetic Model, Plasma Process. Polym., 12, 2015, 180–193.
9. A.V. Kondyurin, P. Naseri, J.M.R. Tilley, N.J. Nosworthy, M.M.M. Bilek, D.R. McKenzie, Mechanisms for Covalent Immobilization of Horseradish Peroxidase on

Ion-Beam-Treated Polyethylene, Scientifica, 2012, Article ID 126170, 28 pages, http://dx.doi.org/10.6064/2012/126170.
10. D.V. Bax, D.R. McKenzie, A.S. Weiss, M.M.M. Bilek, Linker-free covalent attachment of the extracellular matrix protein tropoelastin to a polymer surface for direct cell spreading, Acta Biomaterialia, 5, 2009, 3371-3381.
11. J. Chen, Q. Luo, C.M. Breneman, S.M. Cramer, Classification of protein adsorption and recovery at low salt conditions in hydrophobic interaction chromatographic systems, Journal of Chromatography A, 1139 (2007) 236–246;;
12. N. Barnthip, P. Parhi, A. Golas, E.A. Vogler, Volumetric interpretation of protein adsorption: Kinetics of protein-adsorption competition from binary solution, Biomaterials 30 (2009) 6495–6513
13. P.M. Biesheuvel, F.A. M. Leermakers, M.A.C. Stuart, Self-consistent field theory of protein adsorption in a non-Gaussian polyelectrolyte brush, Physical Review, E 73, 011802 2006
14. I. Kondyurina, I. Shardakov, G. Nechitailo, V. Terpugov, A. Kondyurin, Cell growing on ion implanted polytetrafluorethylene, Applied Surface Science 314 (2014) 670–678.
15. Kondyurin A., Maitz M.F., Surface Modification of ePTFE and Implants using the same, US patent WO 2007/022174 A3, 2007.
16. V. S. Chudinov, I. V. Kondyurina, I. N. Shardakov, A. L. Svistkov, I. V. Osorgina, and A. V. Kondyurin, Polyurethane Modified with Plasma-Ion Implantation for Medical Applications, Biophysics (2018), 63 (3), 330–339.
17. I. V. Kondyurina, V. S. Chudinov, V. N. Terpugov, A. V. Kondyurin, Chemical Linking of Albumin to the Surface of Ion Beam Modified Polyurethane Implants, Biomedical Engineering, Vol. 52, No. 4, November, 2018, pp. 243-246.
18. X. Cheng, A. Kondyurin, S. Bao, M.M.M. Bilek, L. Ye, Plasma immersion ion implantation of polyurethane shape memory polymer: Surface properties and protein immobilization, Applied Surface Science, 416 (2017) 686–695.
19. M.M.M. Bilek, D.V. Bax, A. Kondyurin, Y. Yin, N.J. Nosworthy, K. Fisher, A. Waterhouse, A.S. Weiss, C.G. dos Remedios, D.R. McKenzie, Free radical functionalization of surfaces to prevent adverse responses to biomedical devices, Proceedings of National Academy of Science, vol. 108, no. 35, 14405–14410, 2011.
20. A. Kondyurin, M. Bilek, Ion Beam Treatment of Polymers. Application aspects from medicine to space, Second Edition, Elsevier, Oxford, 2014.
21. W. Chrzanowski, A. Kondyurin, J. H. Lee, M.S. Lord, M. M. M. Bilek, H.- W. Kim, Biointerface: protein enhanced stem cells binding to implant surface, J Mater Sci: Mater Med, DOI 10.1007/s10856-012-4687-2, 2012.

Chapter 6. In vivo biocompatibility of PIII modified polyurethanes implants

The *in vitro* experiments using the newly synthesised polyurethane implants treated with PIII produced results which provide an opportunity to predict a positive response from an organism. This Chapter presents the next step of the biocompatibility analysis: *in vivo* evaluation of the polyurethane implants. The polyurethane implant treated by PIII has been tested in animal experiments. Polyurethane films and tubes were implanted in mice and rats, and an analysis of animal reaction, tissue reactions and PIII treated and untreated implants were made and compared.

6.1. Mice surgery

The reaction of an organism on PIII treated polyurethanes films was observed in the experiment with mice. This experiment has been approved by the University of Sydney Animal Ethics Committee (protocol number K20/12-2011/3/5634) and conducted in accordance with the Australian Code of Practice for the Care and Use of Animals for Scientific Purpose. The polyurethane samples of PPG-DI-PEG and PPG-DI-PTHE with 0.35, 0.5 and 0.7 ratio of NCO/OH groups with and without PIII treatment were implanted in 15 mice. The size of the implants was 3.5 mm diameter with 0.3 mm thickness, which was estimated from the highest allowed weight for the artificial implant per weight of the average human body. The polyurethane samples were treated with PIII on the day prior to implantation.

The samples were dipped into 70% solution of ethanol and air-dried prior to insertion. The mice were rapidly induced with good muscle relaxation. No bleeding was observed at the cuts. Polyurethane samples were implanted subcutaneously. All mice rapidly recovered after the operation.

The ratio of each implant weight (5.5 mg) to mouse weight (20 g) corresponded to 275 mg of implant per kg of animal. This value is high and could potentially disturb physiological processes in the organism. The mice recovered completely 1 day after the operation as is usually observed for mice after surgery. For the following 7 days, a clinical signs was monitored daily in the mice. No obvious abnormality was observed in these mice with surgery. Dynamic activity was normal. Coordination was normal. Body weight didn't change. Breathing was normal. No change of coat or skin was observed. Eating and drinking was usual. Urine and faeces were normal. Communications between mice were normal, but mice did not show any interest in their scars. When palpated or touched no squeaking was observed. Therefore, no sign of the general physiological processes disturbance in a whole organism was observed.

Detailed histological and immunochemical analysis of the tissue near the implants are further presented in this chapter.

6.2. Rat surgery

The newly synthesised polyurethane is very soft and different from materials used for implants. The handling of very soft polyurethane required extremely gentle manipulation during surgery as the graft collapsed easily when pressed with tweezers. The polyurethane graft stuck very well to the vessel wall at first touch. This made it easy to fix the graft on the vessel, but the position of the graft had to be precise at the first contact with the vessel wall.

A polyurethane graft of 2 mm diameter and 5 mm length was implanted in a rat. The experiment has been approved by Sydney Local Heath District Animal Welfare Committee (protocol number 2014/028). For the implantation, a 5 mm segment of abdominal aorta was sectioned and the polyurethane graft was inserted and sewed with Nylon sutures. The operation was done using the operative microscope. Before the operation the heparin was administered intravenously before proximal and distal clamping below the renal arteries and above the aortoiliac bifurcation. The image of the polyurethane graft sewed with the aorta is shown in Fig.6.1.

After the insertion, the blood flow was re-established. The haemostasis was checked. After the operation no post-operative coagulators were applied. The rat was monitored for 7 days after the operation. No abnormal activity was observed.

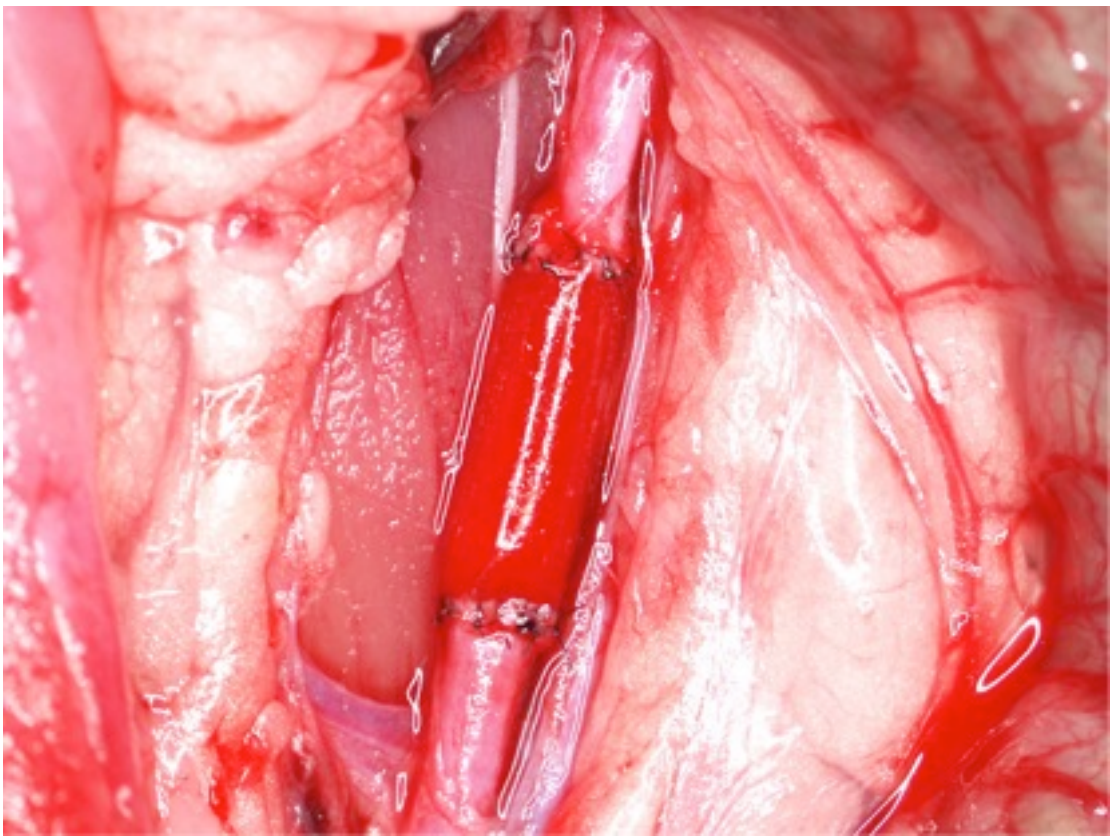

Fig.6.1. Polyurethane graft sewed with aorta in rat.

6.3. Tissue analysis and capsule thickness near the implant in mice

The histological images of the sections stained with Milligan' trichrome show that a collagen capsule is formed around all samples of the polyurethane implants (Fig.6.2). The polyurethane implants were removed at the microtome cutting due to very elastic polyurethane properties in comparison with the surrounding tissues. In all the images, the polyurethane was in the centre of the empty ovals. In some cases, the residuals of the polyurethane implants remained in the sections and stained slightly. The capsule continuously covers the implants, isolating the implant from the tissue. The observed ruptures in some capsules are due to the microtome cutting as shown by the character of the ruptures. The capsule for untreated polyurethane implants had more intensive colouring and was broader than for PIII modified implants. However, the capsule thickness appeared to be independent of what surrounded the implants, whether muscle or connectivity tissues.

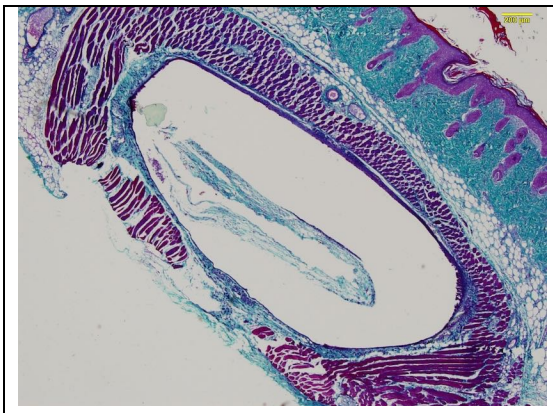

Untreated, PPG-DI-PEG-0.35

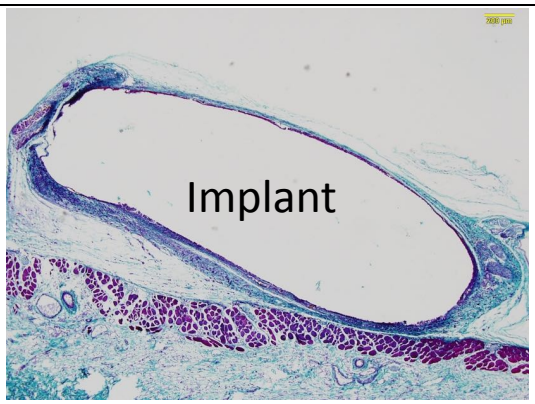

Untreated, PPG-DI-PEG-0.7

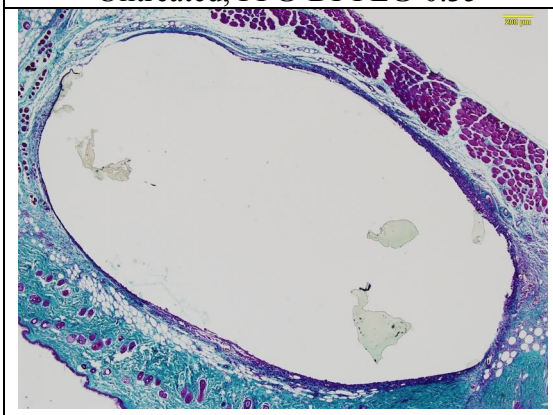

Untreated, PPG-DI-PTHF-0.35

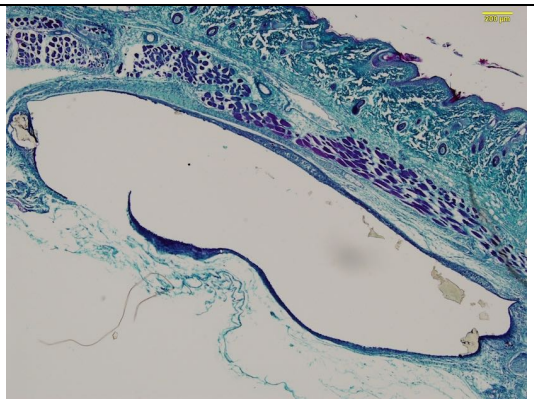

Untreated, PPG-DI-PTHF-0.7

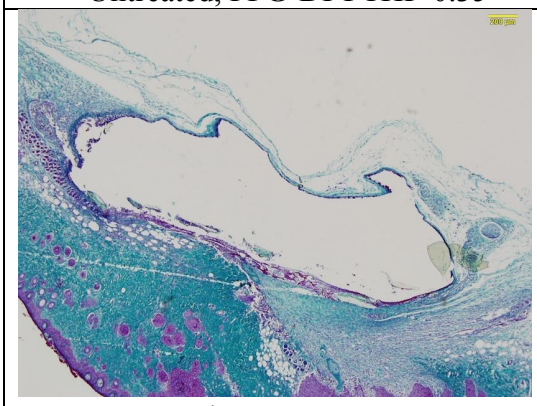

40s PIII treated, PPG-DI-PTHF-0.35

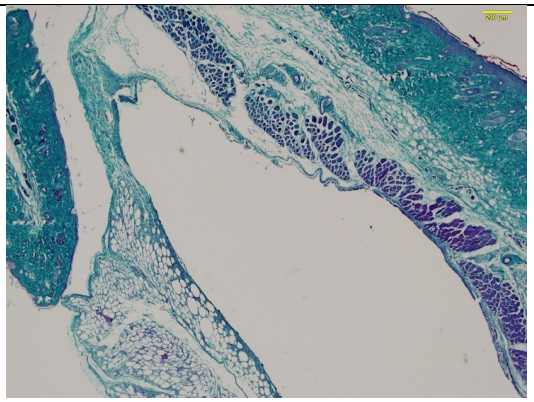

80s PIII treated, PPG-DI-PTHF-0.35

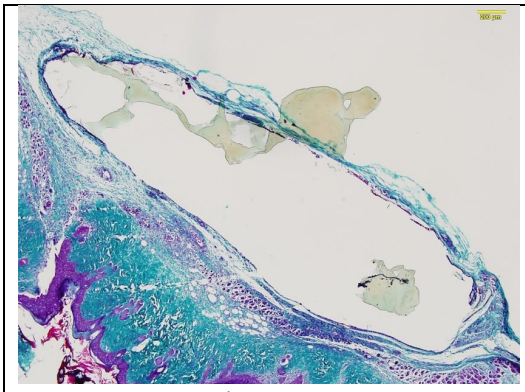

400s PIII treated, PPG-DI-PTHF-0.35

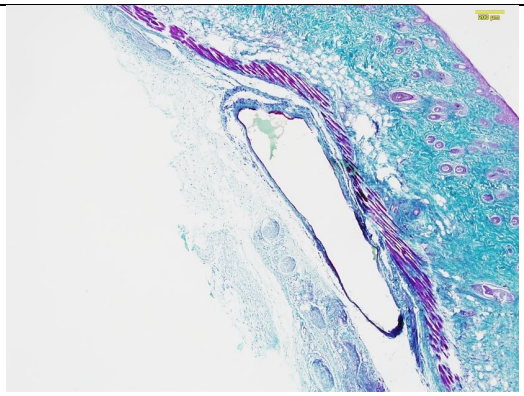

800s PIII treated, PPG-DI-PTHF-0.35

Fig.6.2. Images of the histological samples of polyurethanes stained in Milligan. Objective x4. The implant position was in the centre of the ovals. For example, the position of the implant in PPG-DI-PEG-0.7 sample is marked as "Implant". Usually, the polyurethane sample was removed at the microtome cutting, but sometimes the small pieces of the polyurethane samples remain.

The thickness of the capsule was analyzed quantitatively using the high resolution images of the tissue near the implants. The representative examples of the section stained with Milligan' trichrome in high resolution for polyurethane implants with different PIII treatment times are presented in Fig.6.3-6.8.

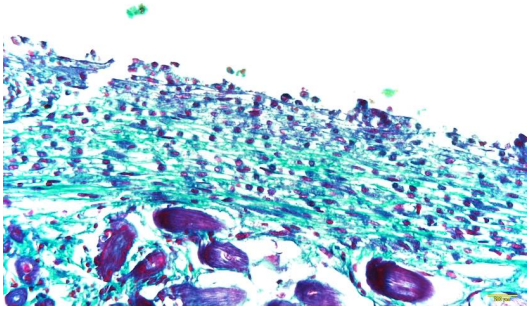

(a) mouse 12, bag 1, section 4

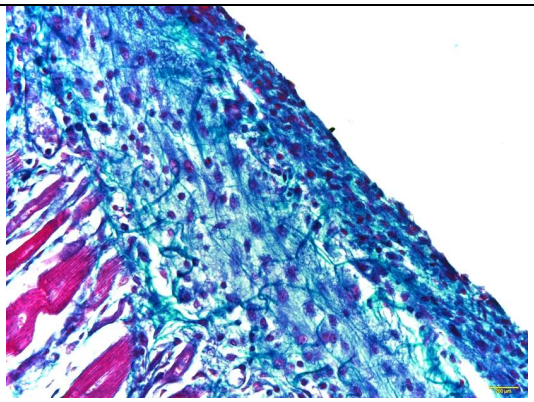

(b) mouse 12, bag 2, section 6

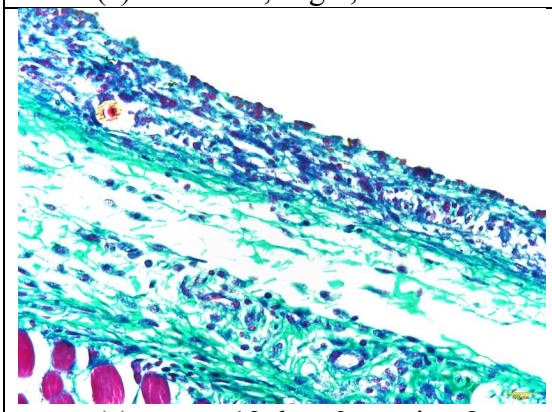

(c) mouse 12, bag 3, section 8

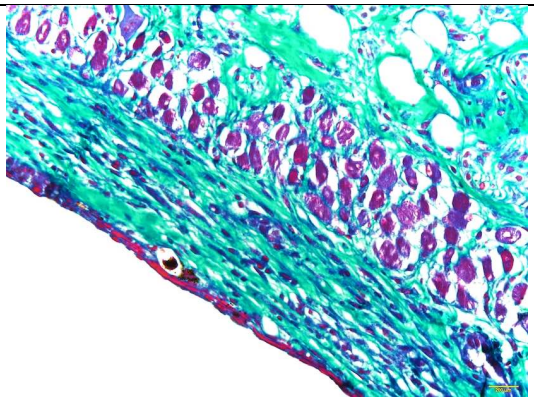

(d) mouse 12, bag 4, section 11

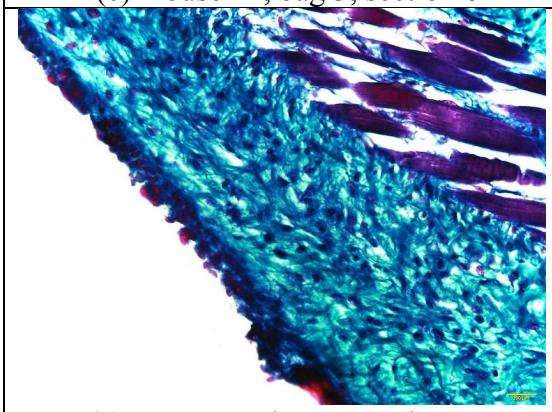

(e) mouse 12, bag 5, section 18

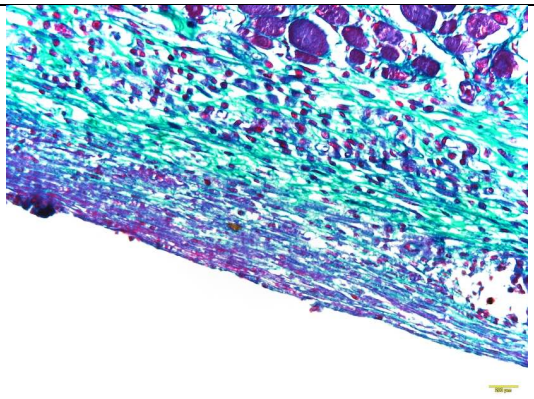

(f) mouse 12, bag 6, section 08

Fig.6.3. Microphotographs of the histological tissue samples stained in Milligan for untreated polyurethane PPG-DI-PTHF-0.35. An empty space on the figures is the implant position.

The collagen shell stained Milligan's trichrome was well developed in the tissue surrounding the untreated polyurethane implants (Fig.6.3). The collagen fibres were structured and directed parallel to the implant surface on a distance of 40-60 μm. This part of the shell was characterised by dense collagen structure. The collagen fibres were disordered at a distance of 60-120 μm from the implant surface. This part of the shell was less dense but denser than the collagen and elastin fibre structures in the normal tissue. In some samples (examples are at Fig.6.3 b and e) the very dense collagen structure was observed in the first approximately 10 μm layer from the implant surface.

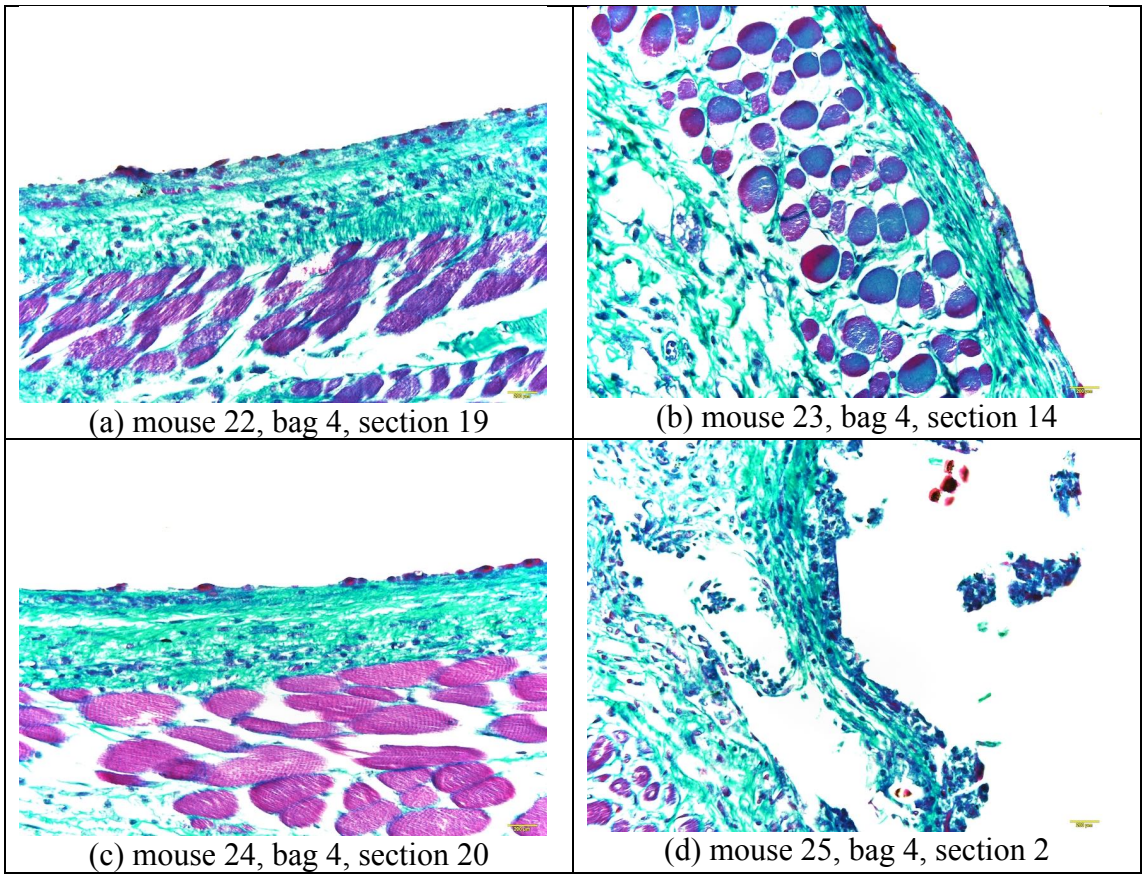

(a) mouse 22, bag 4, section 19

(b) mouse 23, bag 4, section 14

(c) mouse 24, bag 4, section 20

(d) mouse 25, bag 4, section 2

Fig.6.4. Microphotographs of the histological tissue samples stained in Milligan for 40 sec PIII treated polyurethane PPG-DI-PTHF-0.35. An empty space on the figures is the implant position.

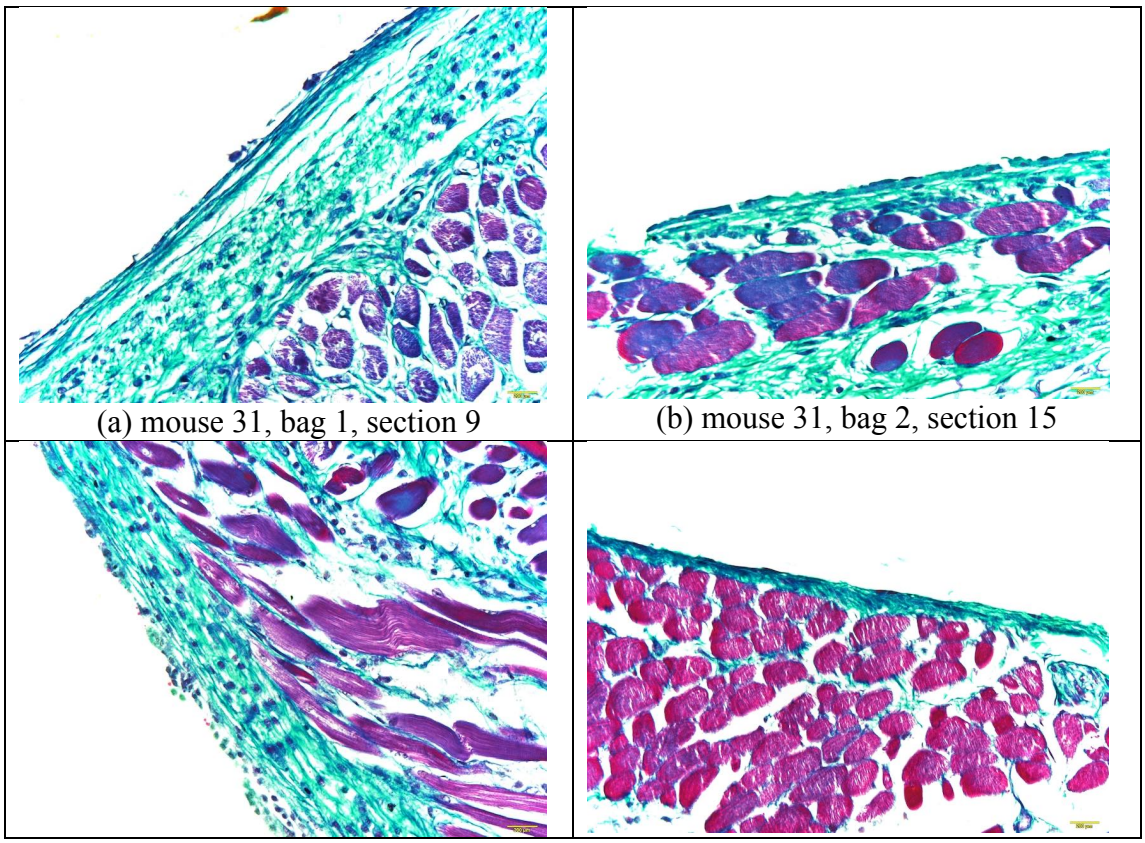

(a) mouse 31, bag 1, section 9

(b) mouse 31, bag 2, section 15

(c) mouse 32, bag 1, section 7

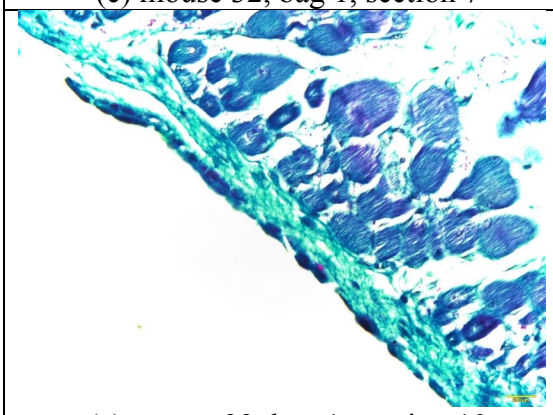

(d) mouse 32, bag 2, section 2

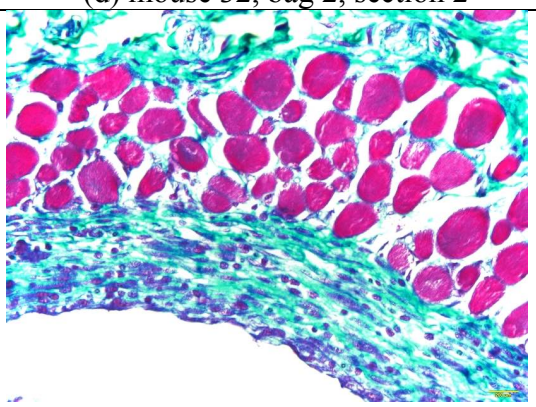

(e) mouse 33, bag 1, section 10

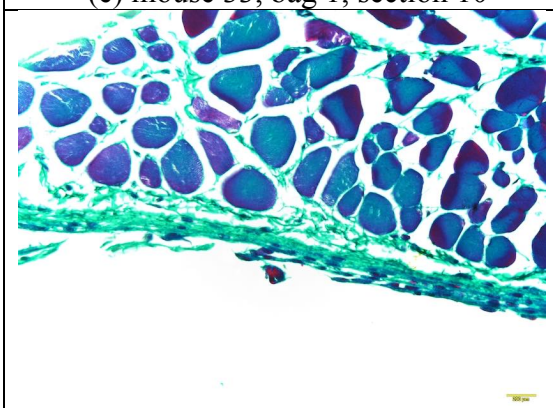

(f) mouse 34, bag 1, section 6

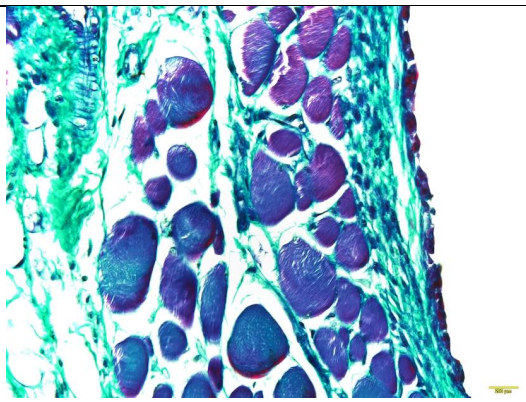

(g) mouse 34, bag 2, section 6

(h) mouse 35, bag 1, section 2

(i) mouse 35, bag 2, section 2

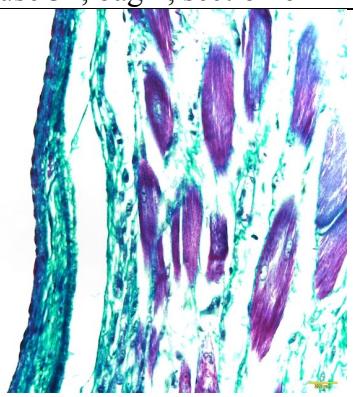

Fig.6.5. Microphotographs of the histological tissue samples stained in Milligan for 80 sec PIII treated polyurethane PPG-DI-PTHF-0.35. An empty space on the figures is the implant position.

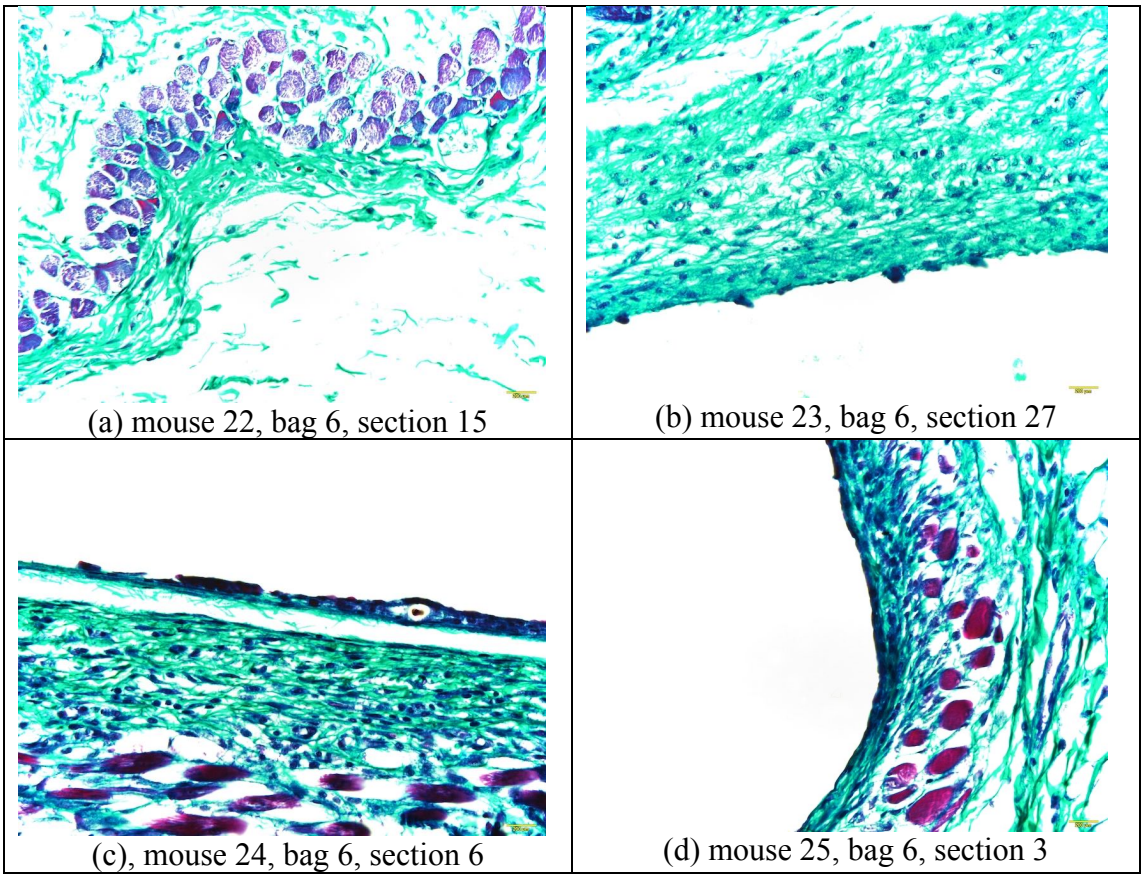

(a) mouse 22, bag 6, section 15

(b) mouse 23, bag 6, section 27

(c), mouse 24, bag 6, section 6

(d) mouse 25, bag 6, section 3

Fig.6.6. Microphotographs of the histological tissue samples stained in Milligan for 200 sec PIII treated polyurethane PPG-DI-PTHF-0.35. An empty space on the figures is the implant position.

The short PIII treatment time (40 seconds) of the polyurethane implant changed the collagen shell in the organism (Fig.6.4). The dense collagen shell was not observed. The collagen shell near the implant surface was not developed and the collagen fibres were not directed but were disordered and rare. The whole collagen shell was thinner than for the untreated polyurethane implant.

The 80 second PIII treated polyurethane implant changed the collagen further (Fig.6.5). The shell was thinner and for some samples the shell was observed in 1-2 cell layers between the implant surface and the muscle cells (Fig.6.5 d as an example). In some samples the dense collagen shell was observed in the thin surface layer (up to about 10 μm), which is in closest contact with the implant (for example, Fig.6.5 e and i). All these difference in the collagen shell were observed in different animals and are not attributed to a specific immune reaction of one mouse.

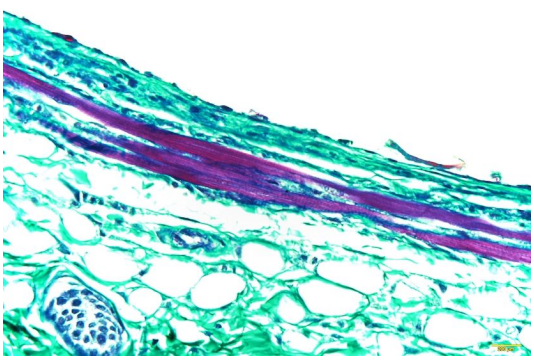

(a) mouse 31, bag 3, section 16

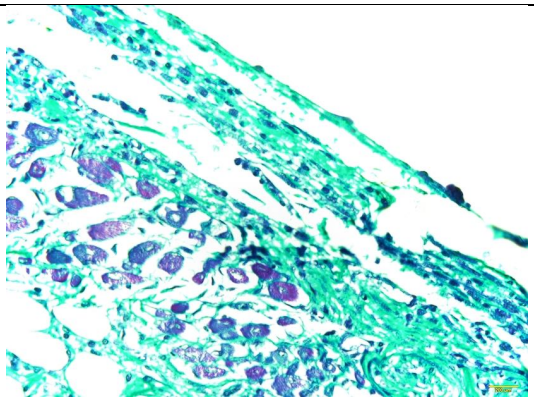

(b) mouse 31, bag 4, section 6

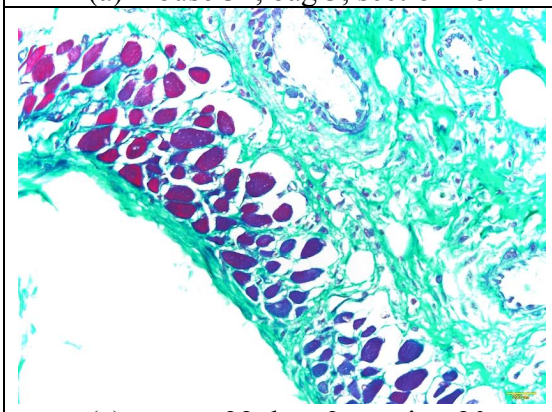

(c) mouse 32, bag 3, section 20

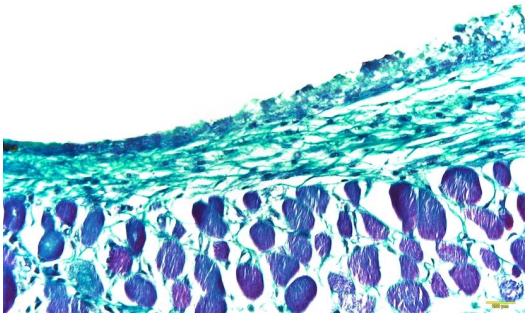

(d) mouse 32, bag 4, section 19

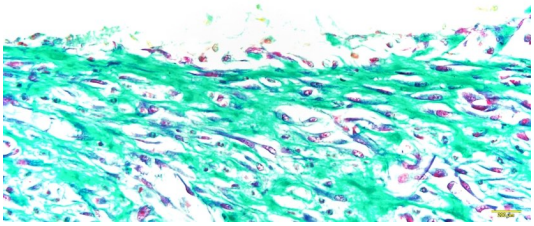

(e) mouse 33, bag 3, section 11

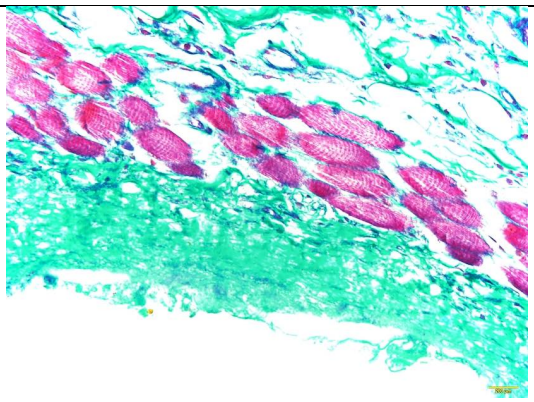

(f) mouse 33, bag 4, section 6

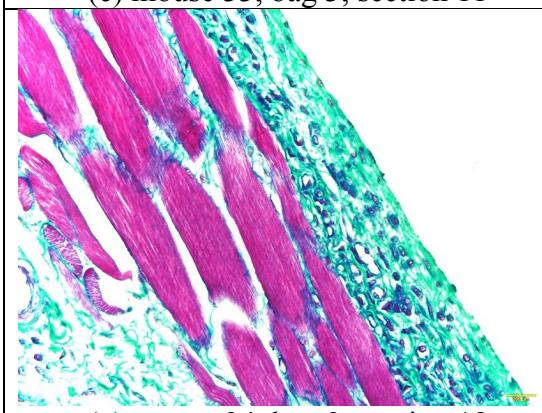

(g) mouse 34, bag 3, section 18

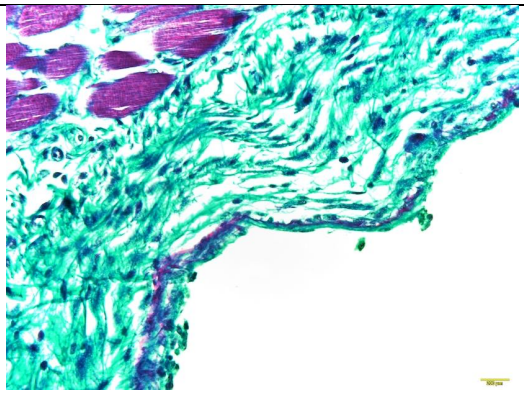

(h) mouse 34, bag 4, section 5

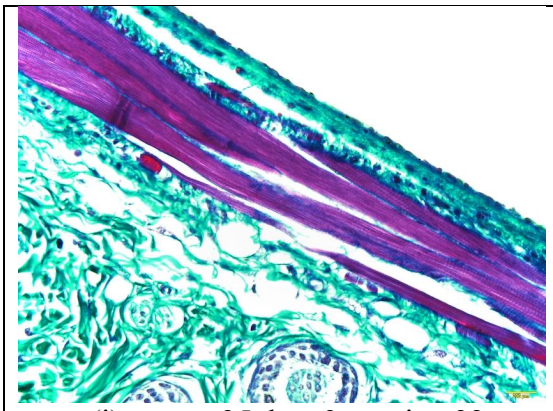

(i) mouse 35, bag 3, section 32

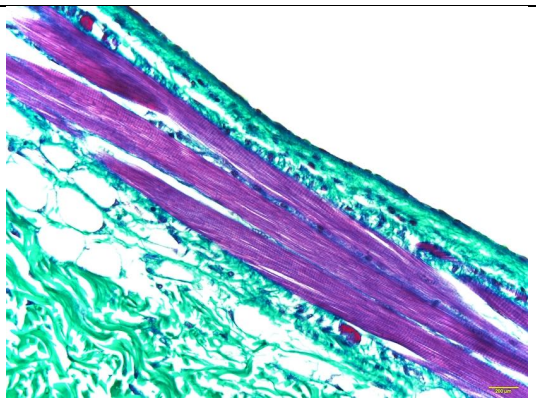

(j) mouse 35, bag 4, section 39

Fig.6.7. Microphotographs of the histological tissue samples stained in Milligan for 400 sec PIII treated polyurethane PPG-DI-PTHF-0.35. An empty space on the figures is the implant position.

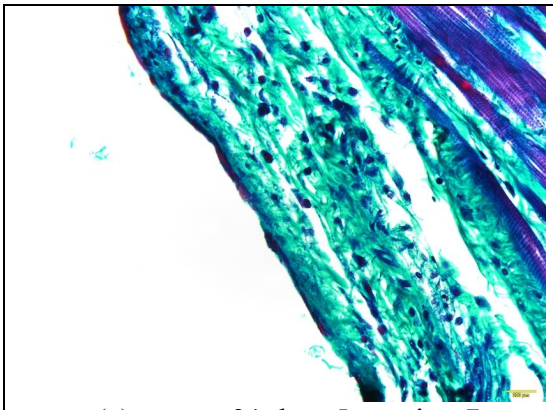

(a) mouse 31, bag 5, section 7

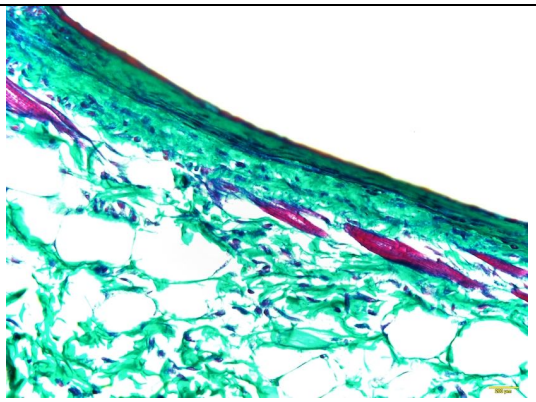

(b) mouse 31, bag 6, section 20

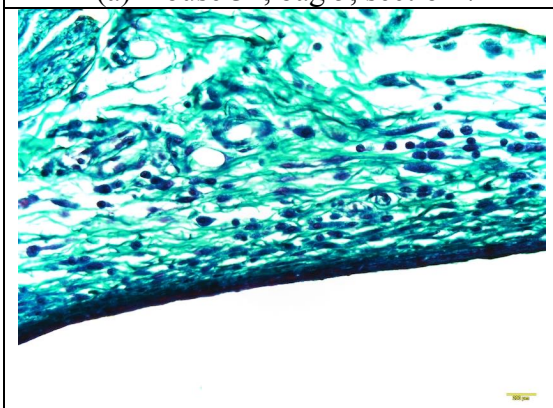

(c) mouse 32, bag 5, section 1

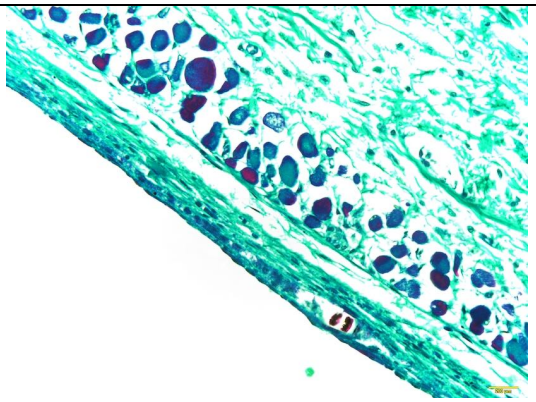

(d) mouse 33, bag 5, section 9

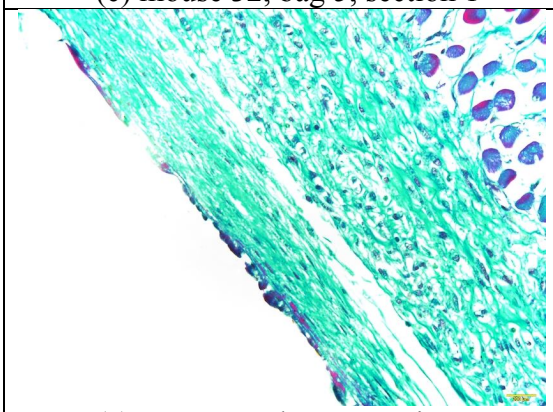

(e) mouse 33, bag 6, section 5

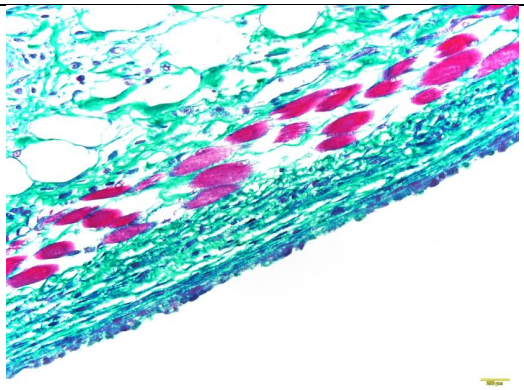

(f) mouse 34, bag 5, section 36

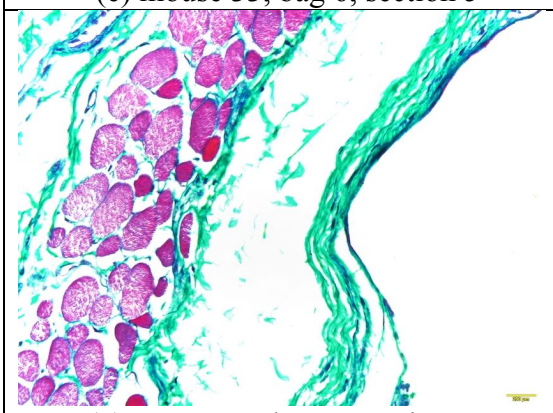

(g) mouse 34, bag 6, section 24

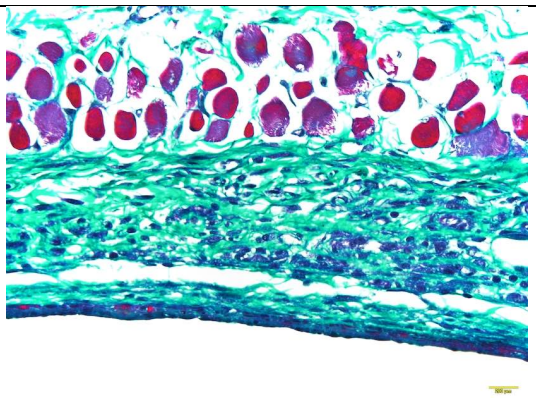

(h) mouse 35, bag 5, section 4

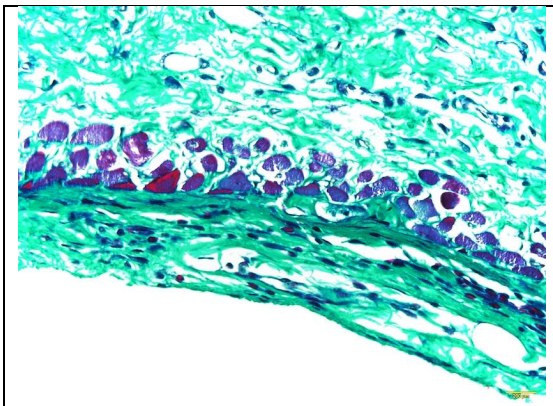

(i) mouse 35, bag 6, section 10

Fig.6.8. Microphotographs of the histological tissue samples stained in Milligan for 800 sec PIII treated polyurethane PPG-DI-PTHF-0.35. An empty space on the figures is the implant position.

When PIII treatment time was increased up to 800 seconds, the collagen shell did not change significantly. In some samples the shell was very thin, up to 1-2 cells layer between the implant and other tissues such as muscle cells (Fig.6.6 c, Fig.6.7 b and Fig.6.8 g). In some samples the collagen shell was not observed at all (Fig.6.7 c, e, f, g, Fig.6.8 e). In some samples the dense thin layer of the collagen shell was observed (Fig.6.6 c and d, Fig.6.7 d, i and j, and Fig.6.8 a, c and h). Unlike the shell for the untreated polyurethane implants, the shell was thinner and rare for all these PIII treated samples. These changes were observed for all animals. The differences between the tissues in different animals were smaller than between the treated and untreated tissue samples.

The average thickness of the collagen shell was calculated and is presented in Fig.6.9. The staining of all the slides was done in one day, the microphotographs were done in one microscope in one day with adjusted intensity and optical elements of the microscope, and the analysis of the images was done for all microphotographs simultaneously. This allowed the results between the different samples in the whole batch to be compared quantitatively.

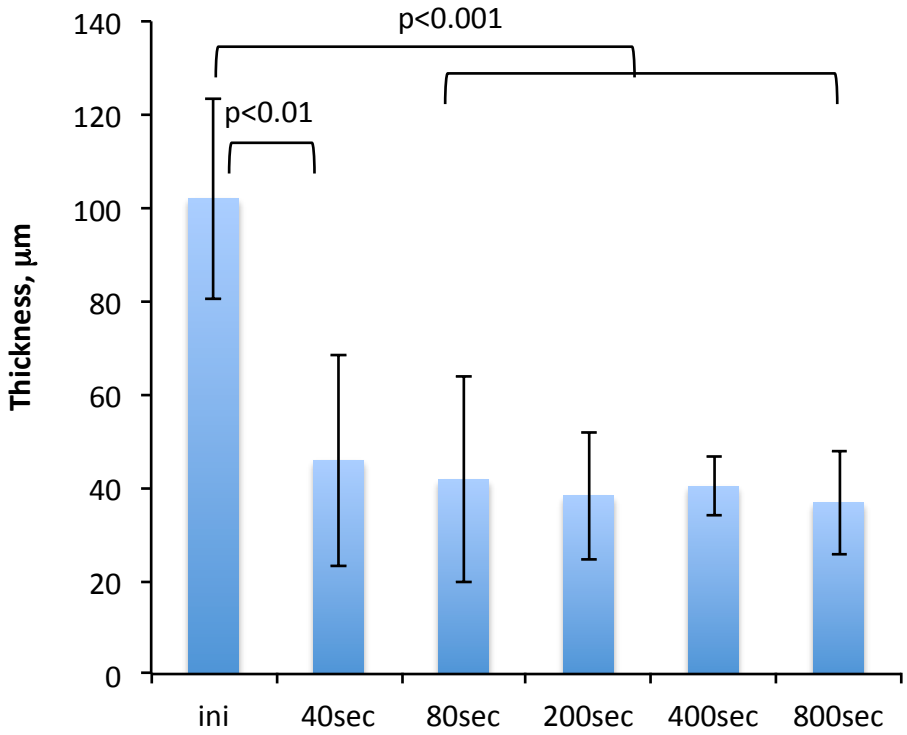

Fig.6.9. Thickness of the collagen capsule near the polyurethane implant treated by PIII with different treatment time. "Ini" means the untreated (initial) samples.

The results show that the thickness of the collagen capsule was significantly less for the PIII treated polyurethane implants (41 µm) than for untreated implants (102 µm) ($p<0.001$). The significant decrease in the thickness from 102 µm to 46 µm was observed after a short 40 second PIII treatment time ($p<0.01$). This difference between the untreated and PIII treated samples increases with the PIII treatment time.

The microphotographs of H&E stained tissue are shown in Fig. 6.10-6.15. The tissue near the untreated polyurethane implant contains macrophages, monocytes and fibroblasts (Fig.6.10). Multi-nuclear foreign body giant cells were not observed. The macrophages and monocytes were mostly distributed near the surface of the implant in the capsule. Their concentration was highest in the capsule near the implant surface. The fibroblasts were positioned mostly on a distance from the implant surface, where the collagen fibres dominate. There was no cell lysis or necrosis.

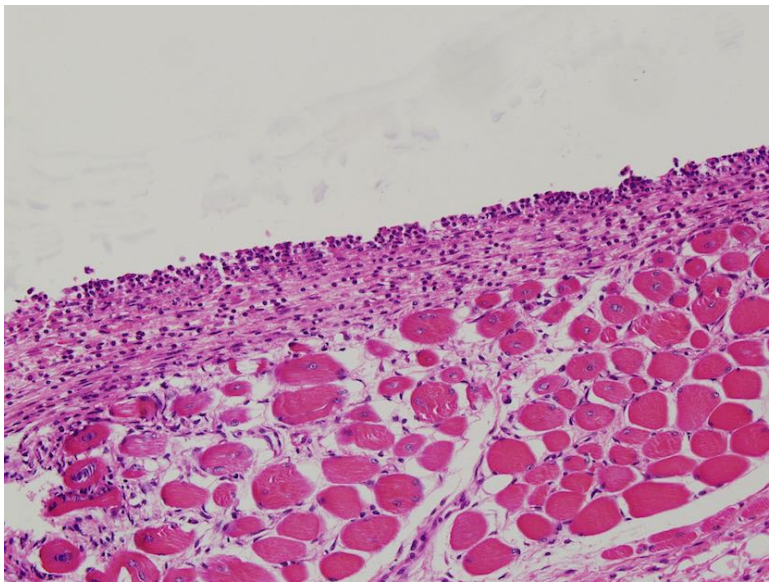

Fig. 6.10. Microphotographs of the histological tissue samples stained in Hematoxylin-Eosin for the untreated PPG-DI-PTHF-0.35 polyurethane implants. An empty space on the figures is the implant position.

The tissue near the 40 second PIII treated implant is less disturbed (Fig.6.11). Most cells in the capsule are fibroblasts and few cells were found in some spots like macrophages and monocytes (marked with arrows). The macrophages and monocytes were predominantly in the contact zone of the implant surface. In some images it is clear that the spots with macrophages and monocytes are distributed along the implant surface at the same periodicity as the cracks and waves of the polyurethane surface mentioned in Chapter 4. Similar cell distribution was observed for other PIII treated samples (Fig.6.12-6.15). Similar capsule images were observed in cases when the modified implant was in contact with the connective tissue or muscle tissue or adipocytes cells.

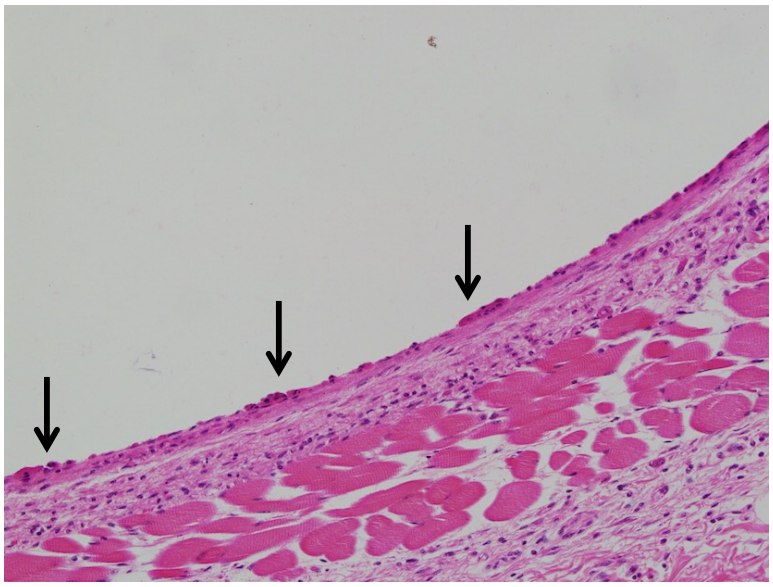

Fig.6.11. Microphotographs of the histological tissue samples stained in Hematoxylin-Eosin for the 40 sec PIII treated PPG-DI-PTHF-0.35 polyurethane implants. An empty space on the figures is the implant position. Positions of macrophages are shown with arrows.

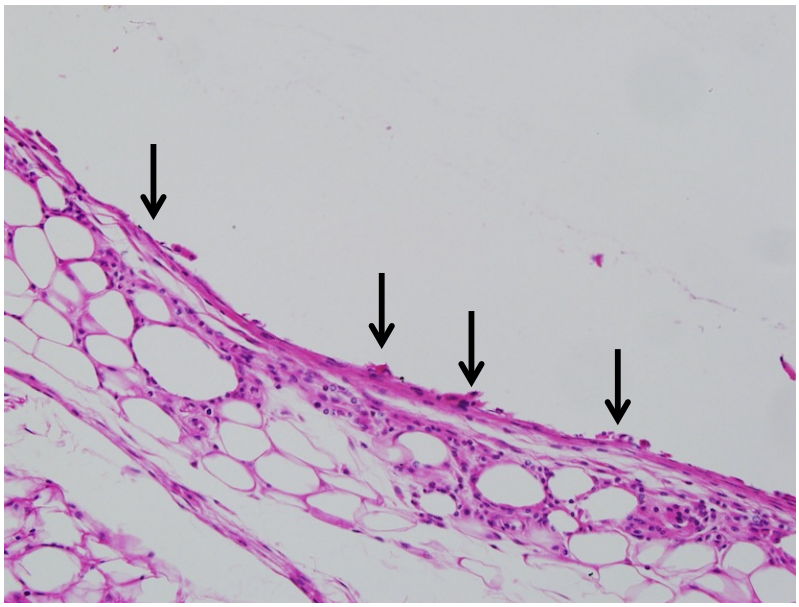

Fig.6.12. Microphotographs of the histological tissue samples stained in Hematoxylin-Eosin for the 80 sec PIII treated PPG-DI-PTHF-0.35 polyurethane implants. An empty space on the figures is the implant position. Positions of macrophages are shown with arrows.

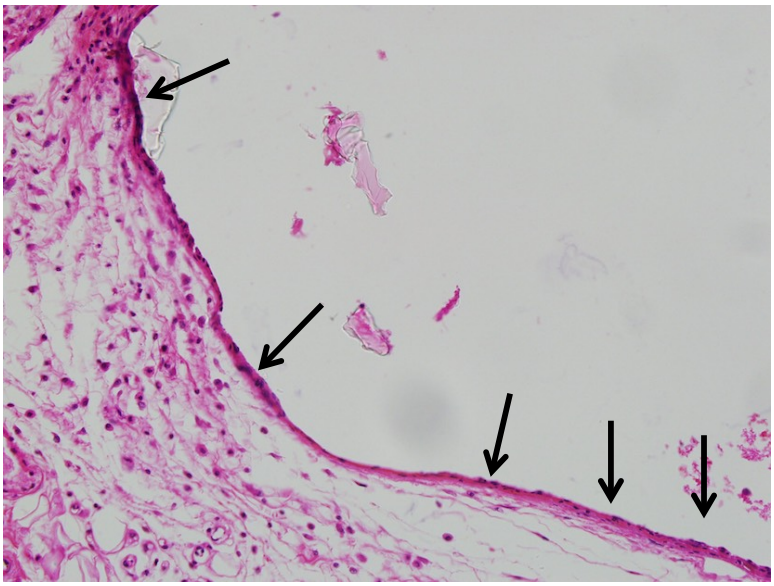

Fig.6.13. Microphotographs of the histological tissue samples stained in Hematoxylin-Eosin for the 200 sec PIII treated PPG-DI-PTHF-0.35 polyurethane implants. An empty space on the figures is the implant position. Positions of macrophages are shown with arrows.

In some places where the tissue contacted the modified implant the capsule was not observed at all. The cells, which were in contact with the implant surface, were fibroblasts or the connective tissue fibres (Fig.6.15).

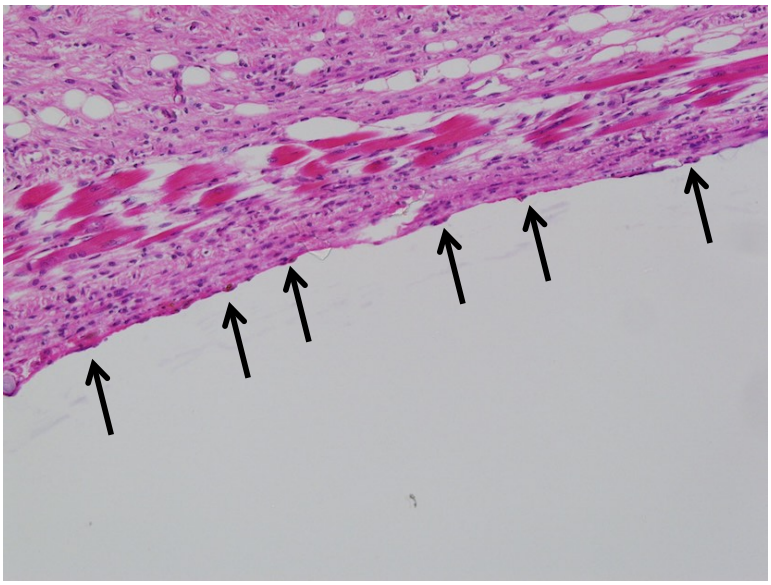

Fig. 6.14. Microphotographs of the histological tissue samples stained in Hematoxylin-Eosin for the 400 sec PIII treated PPG-DI-PTHF-0.35 polyurethane implants. An empty space on the top figure is the implant position. Positions of macrophages are shown with arrows.

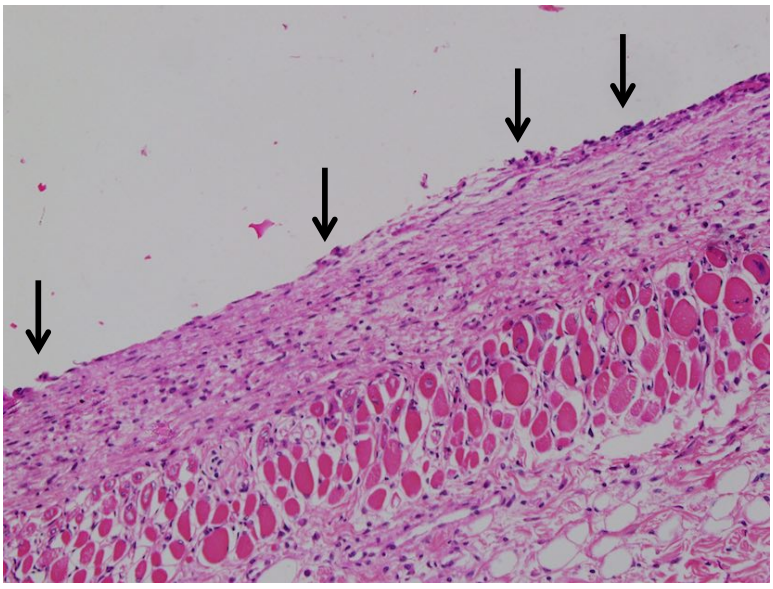

Fig.6.15. Microphotographs of the histological tissue samples stained in Hematoxylin-Eosin for the 800 sec PIII treated PPG-DI-PTHF-0.35 polyurethane implants. An empty space on the figures is the implant position. Positions of macrophages are shown with arrows.

6.4. Macrophages infiltration in the tissue

The staining with F4-80 antibody showed a presence of macrophages in the tissue surrounding the polyurethane implants (Fig.6.16). The high macrophages activity was

observed in the collagen capsule near the surface of the untreated polyurethane implant (Fig.6.16 a).

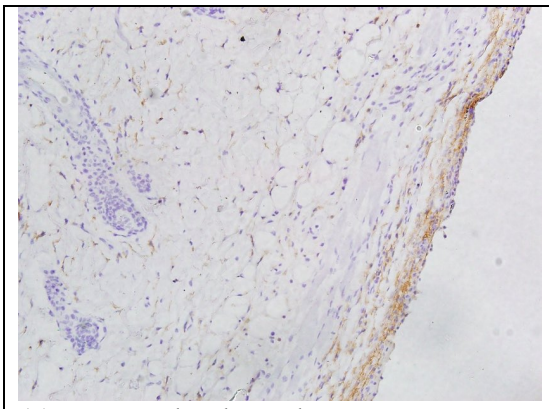

(a) untreated polyurethane, mouse 12, bag 5, section 9

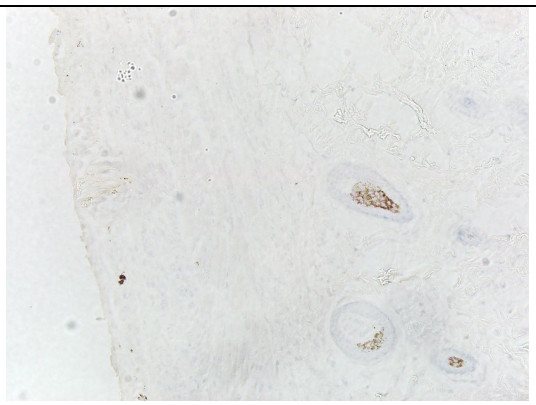

(b) 40s PIII treated polyurethane, mouse 24, bag 4, section 5

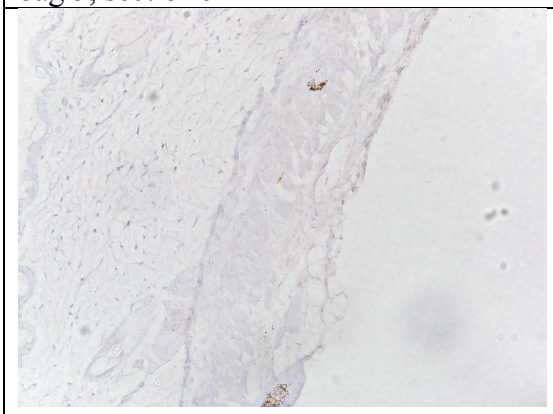

(c) 80s PIII treated polyurethane, mouse 32, bag 1, section 9

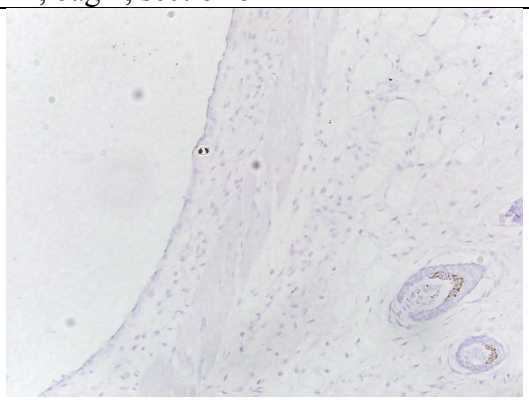

(d) 200s PIII treated polyurethane, mouse 23, bag 6, section 15

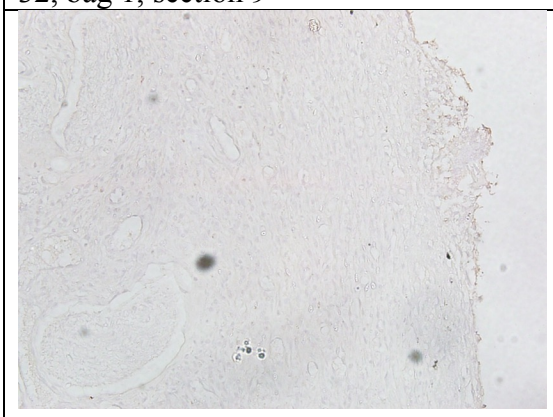

(e) 400s PIII treated polyurethane, mouse 33, bag 3, section 10

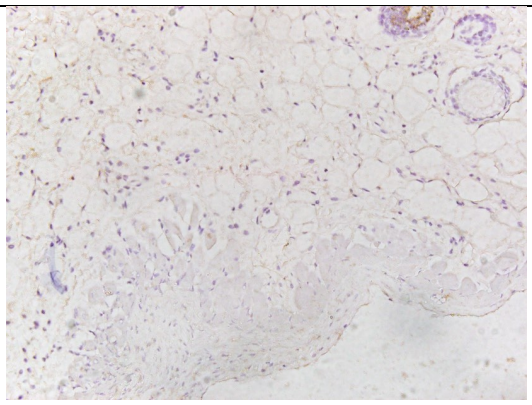

(f) 800s PIII treated polyurethane, mouse 35, bag 6, section 1

Fig.6.16. Microphotographs of the histological tissue samples stained in F4-80 antibody for the PPG-DI-PTHF-0.35 polyurethane implants. An empty space on the figures is the implant position.

The rest of the tissue outside of the collagen capsule showed low macrophages activity. The low macrophages activity was observed in the tissue surrounding the PIII treated implant (Fig.6.16 b-e) treated between 40 and 400 seconds of PIII

treatment time. For some samples (Fig.6.16 d) macrophages activity near the implant surface was not observed. The activity of macrophages in the tissue surrounding the 800 second PIII treated implant was high when the distance from the implant was greatest.

The integral area of the tissue with brown colour and the integral intensity of the colour was analysed to estimate the macrophages activity in the tissue. The results of activity macrophages dependence on the PIII treatment time is presented in Fig.6.17 and Fig.6.18. The highest macrophages activity was observed in the tissue surrounding the untreated polyurethane implant and 800 second PIII treated sample. The lowest macrophages activity was observed for 200 second PIII treated implants. The difference between the untreated and 200 second PIII treated samples is significant ($p<0.001$).

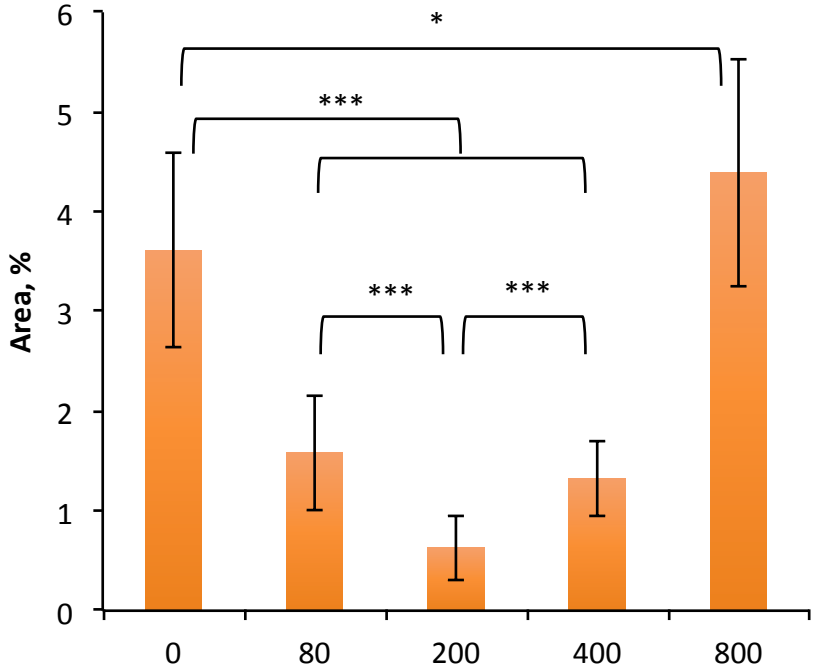

Fig.6.17. Relative area of the tissue stained by F4-80 antibody near the PIII treated polyurethane implants with time of PIII treatment (s). "0" means the untreated (initial) samples.

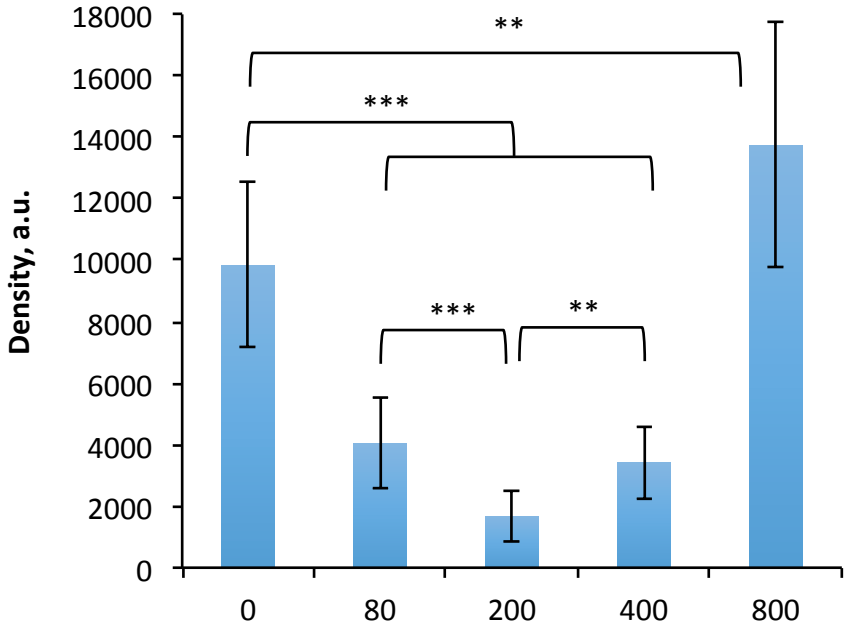

Fig.6.18. Relative staining density of the tissue stained by F4-80 antibody near the PIII treated polyurethane implants with time of PIII treatment (s). "0" means the untreated (initial) samples.

6.5. Cell proliferation in the tissue

The Ki-67 antibody was used for detection of the cell proliferation activity in the tissue surrounding the polyurethane implants. The example of characteristic images for untreated and PIII treated implants with different PIII treatment time are presented in Figs.6.19-6.24. The colour distribution and intensity shows a high cell proliferation activity in the tissue near the untreated polyurethane implants. The maximum activity is observed in the collagen capsule and the activity gradually decreases with the distance from the implant, see for example Figs 6.19 a and b). The activity was also observed in newly formed vessels a bit further away from the capsule (Fig.6.19 d).

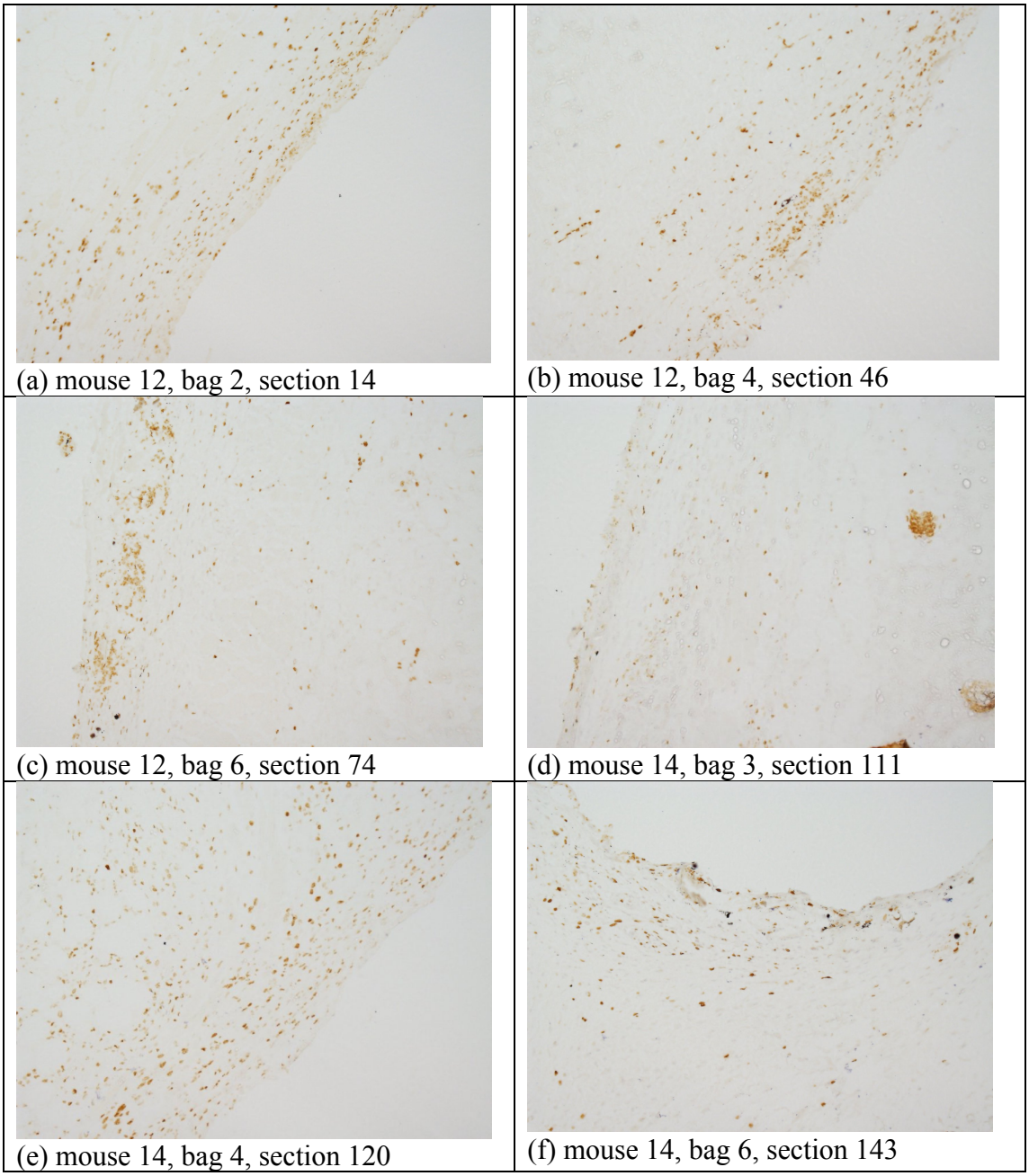

(a) mouse 12, bag 2, section 14

(b) mouse 12, bag 4, section 46

(c) mouse 12, bag 6, section 74

(d) mouse 14, bag 3, section 111

(e) mouse 14, bag 4, section 120

(f) mouse 14, bag 6, section 143

Fig.6.19. Microphotographs of the histological tissue samples stained in Ki-67 antibody for untreated polyurethane PPG-DI-PTHF-0.35. An empty space on the figures is the implant position.

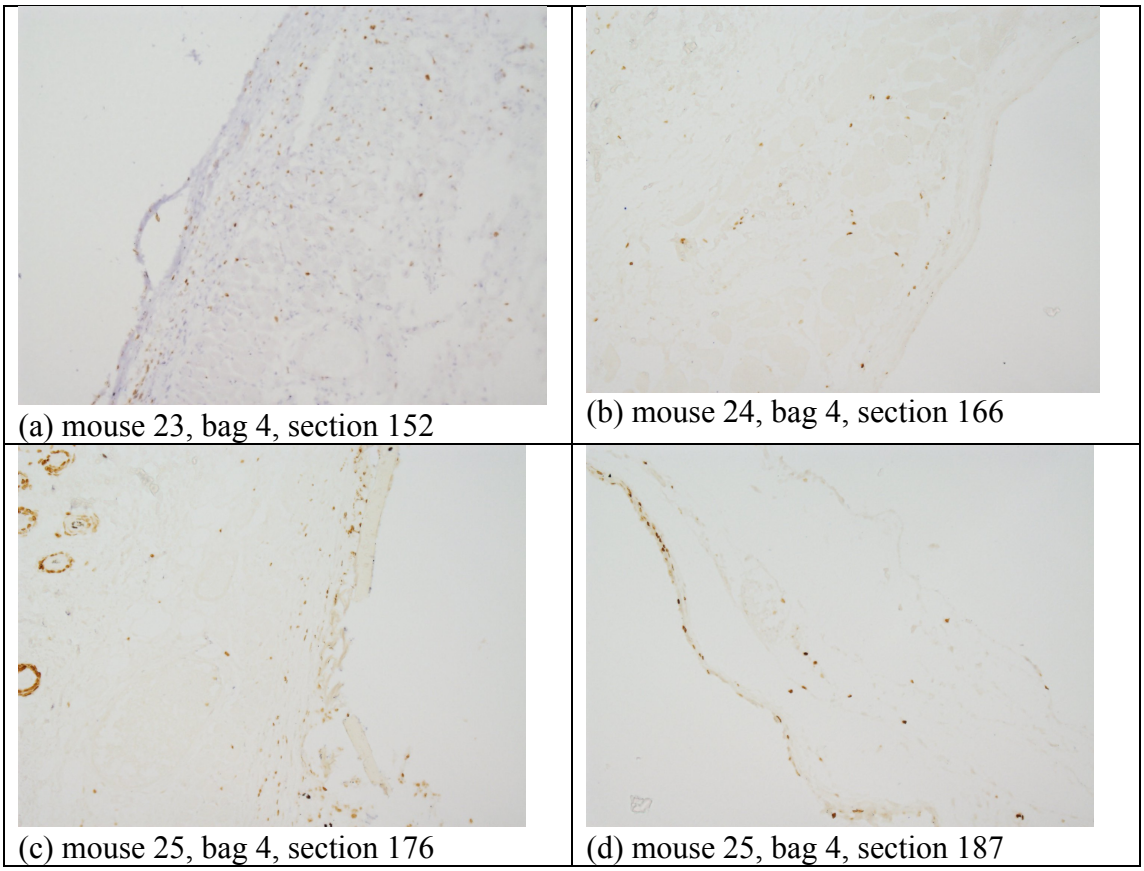

(a) mouse 23, bag 4, section 152

(b) mouse 24, bag 4, section 166

(c) mouse 25, bag 4, section 176

(d) mouse 25, bag 4, section 187

Fig.6.20. Microphotographs of the histological tissue samples stained in Ki-67 antibody for 40s PIII treated polyurethane PPG-DI-PTHF-0.35. An empty space on the figures is the implant position.

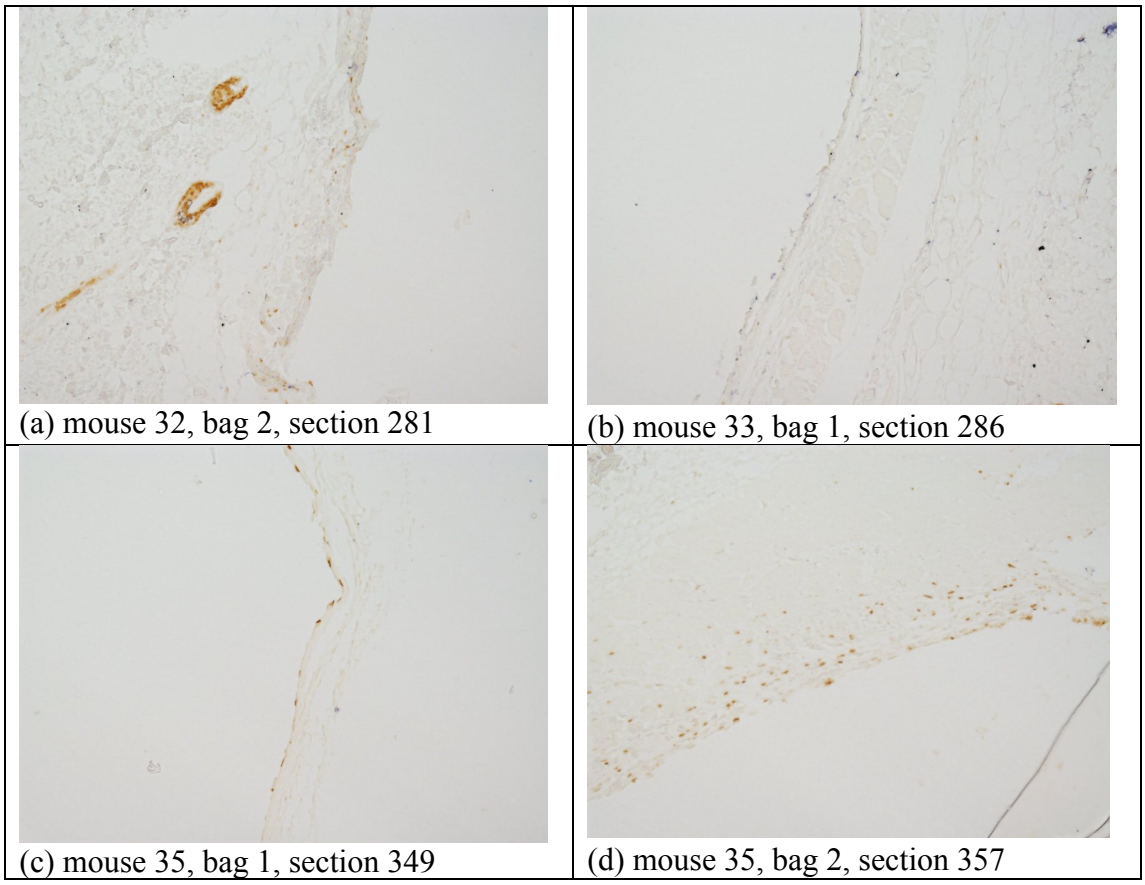

(a) mouse 32, bag 2, section 281

(b) mouse 33, bag 1, section 286

(c) mouse 35, bag 1, section 349

(d) mouse 35, bag 2, section 357

Fig.6.21. Microphotographs of the histological tissue samples stained in Ki-67 antibody for 80s PIII treated polyurethane PPG-DI-PTHF-0.35. An empty space on the figures is the implant position.

The lowest cell proliferation activity was found in 40 second PIII treated implants (Fig.6.20). In some samples the activity was observed only in a thin surface layer corresponding to the capsule thickness. Most intensive activity was observed in fields of new vessel formation. With increases in the PIII treatment time the cell proliferation activity decreased (Fig.6.21-6.24). From 200 sec PIII treatment time, the cell proliferation activity was almost not observed in the capsule although it was spread throughout the entire tissue sample (Fig.6.22). The lowest cell proliferation activity was observed in the tissue surrounding the 800 second PIII treated polyurethane implant as separate cells, as for normal tissue (Fig.6.24).

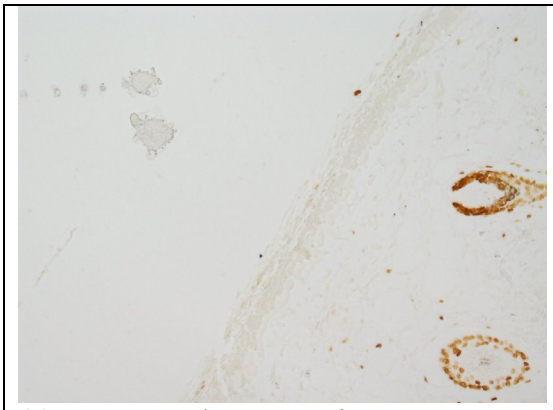

(a) mouse 22, bag 6, section 195

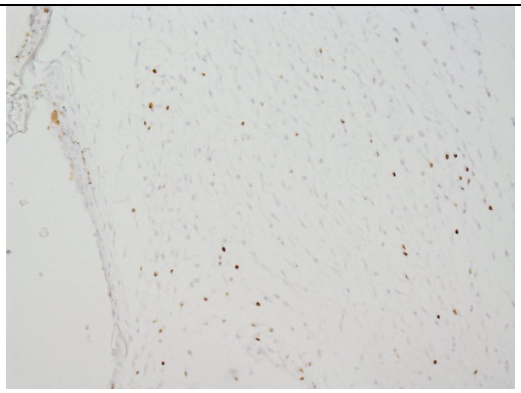

(b) mouse 23, bag 6, section 216

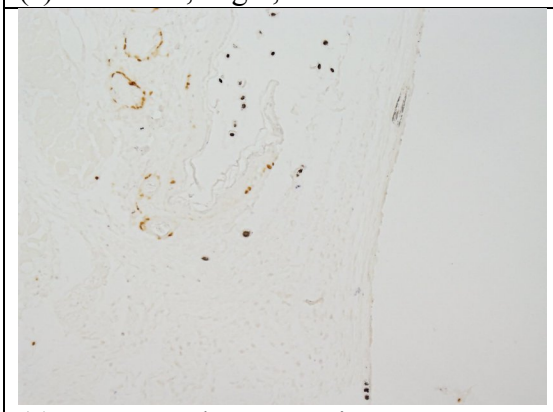

(c) mouse 24, bag 6, section 224

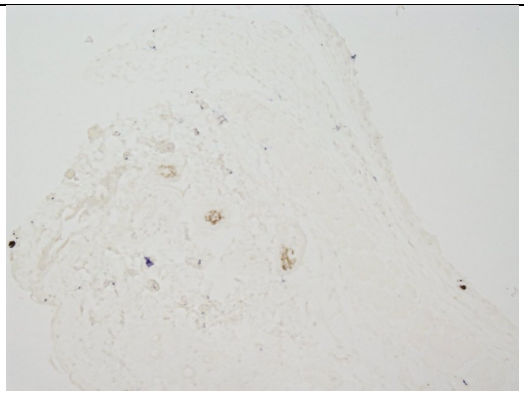

(d) mouse 25, bag 6, section 235

Fig.6.22. Microphotographs of the histological tissue samples stained in Ki-67 antibody for 200s PIII treated polyurethane PPG-DI-PTHF-0.35. An empty space on the figures is the implant position.

(a) mouse 31, bag 3, section 376

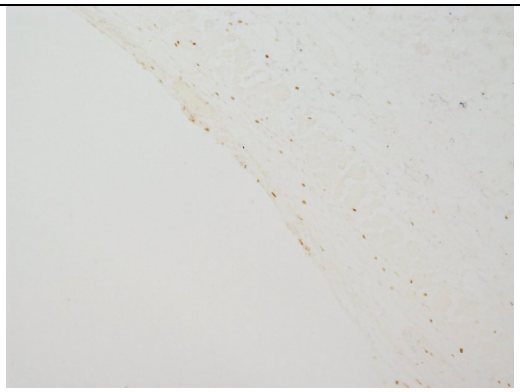

(b) mouse 32, bag 4, section 408

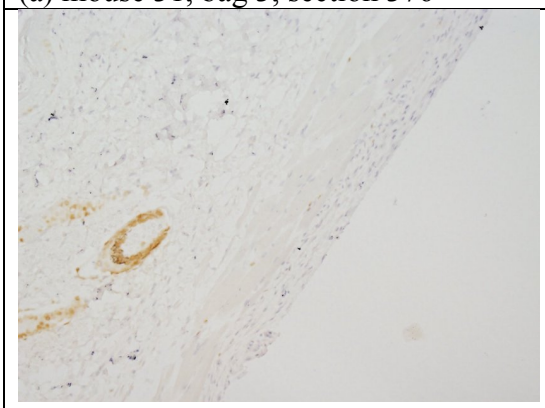

(c) mouse 34, bag 3, section 435

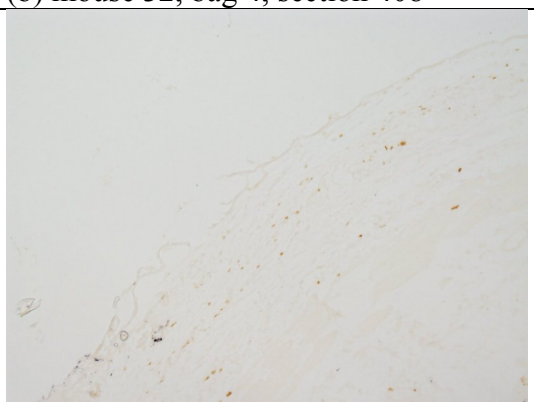

(d) mouse 34, bag 4, section 452

Fig.6.23. Microphotographs of the histological tissue samples stained in Ki-67 antibody for 400s PIII treated polyurethane PPG-DI-PTHF-0.35. An empty space on the figures is the implant position.

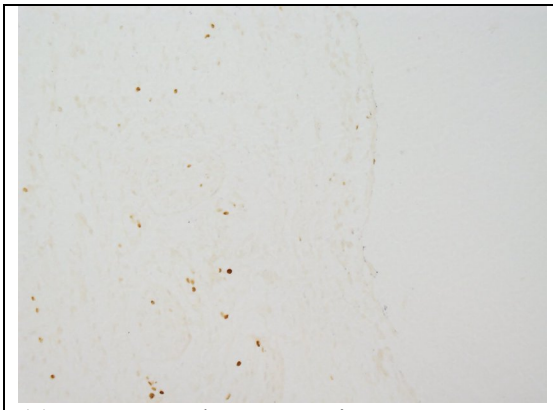

(a) mouse 31, bag 5, section 493

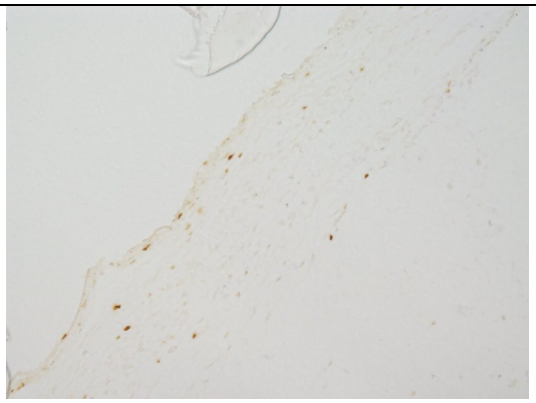

(b) mouse 33, bag 5, section 547

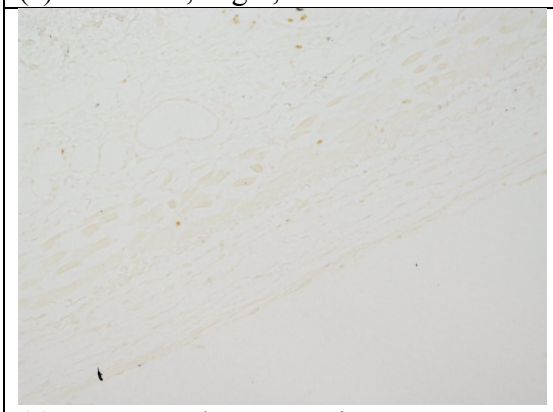

(c) mouse 34, bag 6, section 589

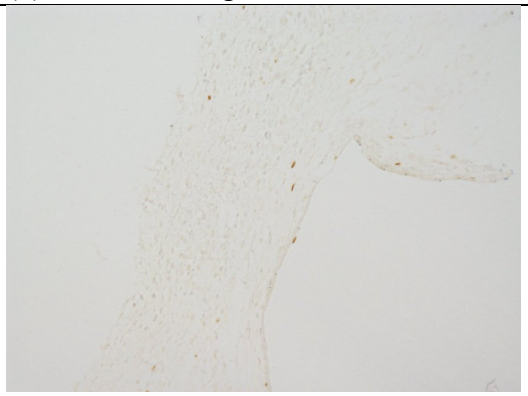

(d) mouse 35, bag 5, section 593

Fig.6.24. Microphotographs of the histological tissue samples stained in Ki-67 antibody for 800s PIII treated polyurethane PPG-DI-PTHF-0.35. An empty space on the figures is the implant position.

For a quantitative analysis of the cell proliferation activity the colour area and density of the Ki-67 staining was analysed and is presented in Fig.6.25-Fig.6.26. The activity decreases with PIII treatment time and gets a minimal value at 400 seconds of the treatment time ($p<0.001$). This trend was observed in the area and the density of stained cells.

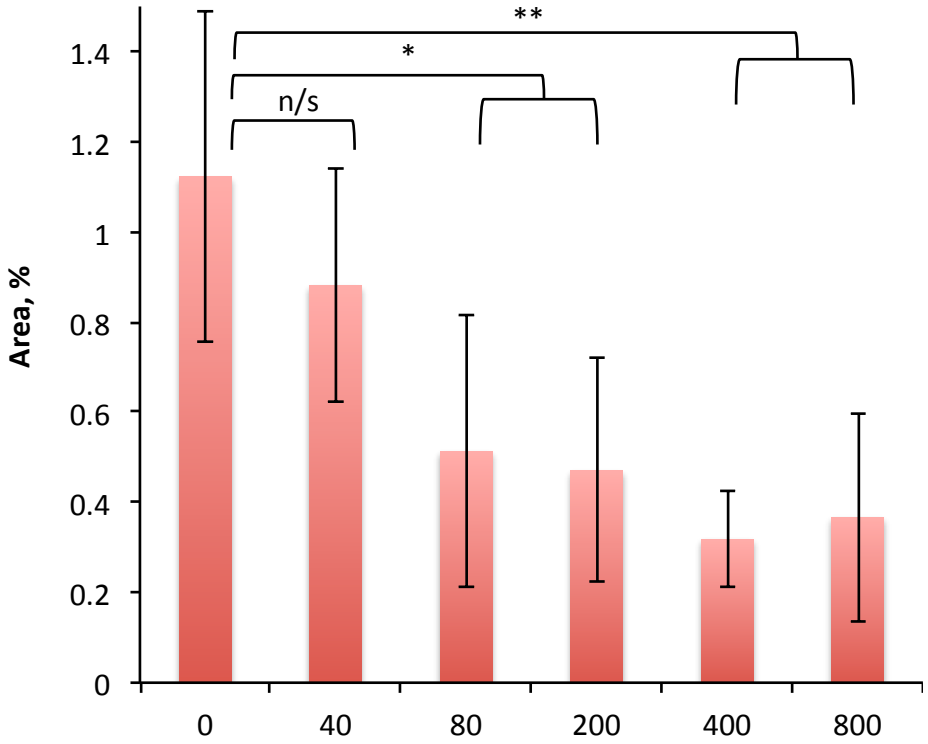

Fig.6.25. Relative area of the tissue stained by Ki-67 antibody near the PIII treated polyurethane implants with time of PIII treatment (s). "0" means the untreated (initial) samples.

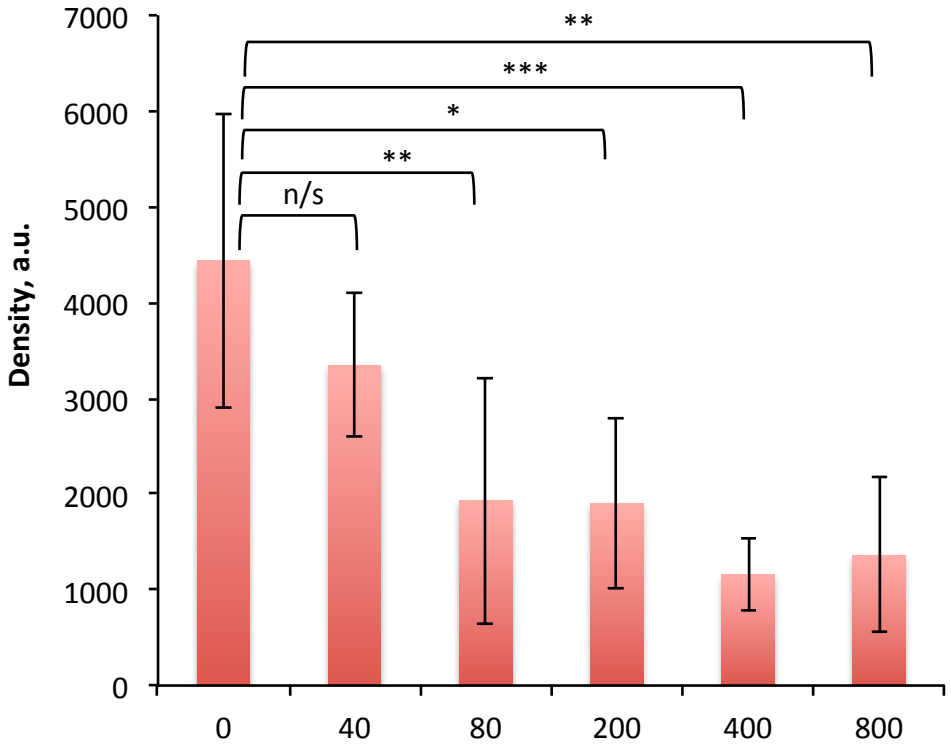

Fig.6.26. Relative staining density of the tissue stained by Ki-67 antibody near the PIII treated polyurethane implants with time of PIII treatment (s). "0" means the untreated (initial) samples.

6.6. Von Willebrand Factor activity in the tissue

Von Willebrand Factor (vWF) as a proinflammatory protein and a key player in hemostasis was analysed in the tissue surrounding the polyurethane implants. The microphotographs of the tissue stained in the vWF antibody are presented in Figs. 6.27-6.32.

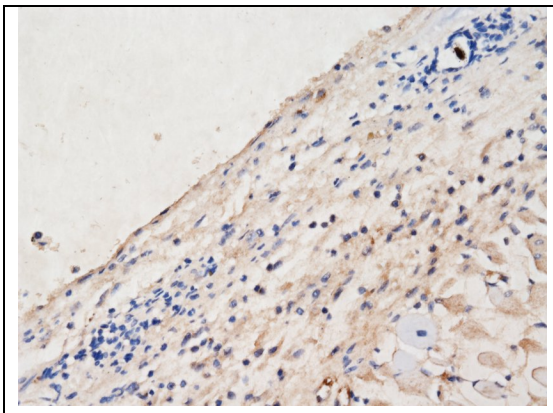

(a) mouse 12, bag 3, section 12

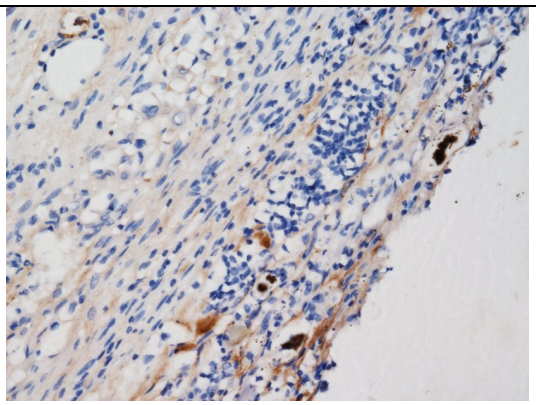

(b) mouse 12, bag 4, section 17

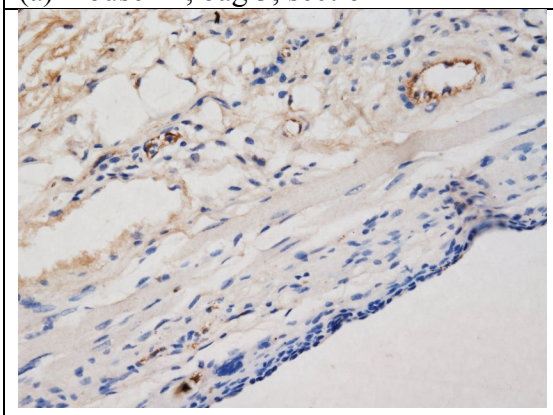

(c) mouse 12, bag 5, section 10

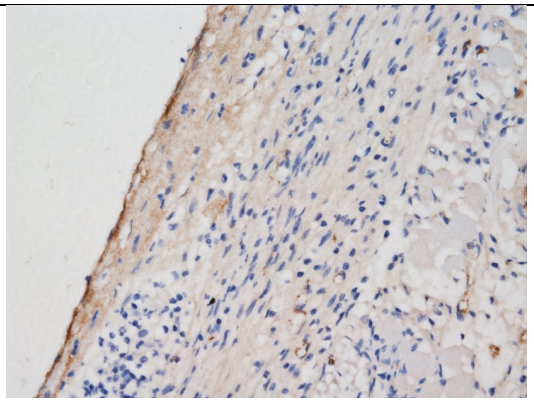

(d) mouse 12, bag 6, section 10

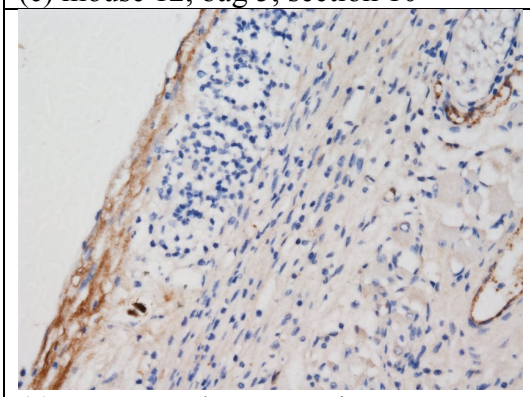

(e) mouse 12, bag 6, section 11

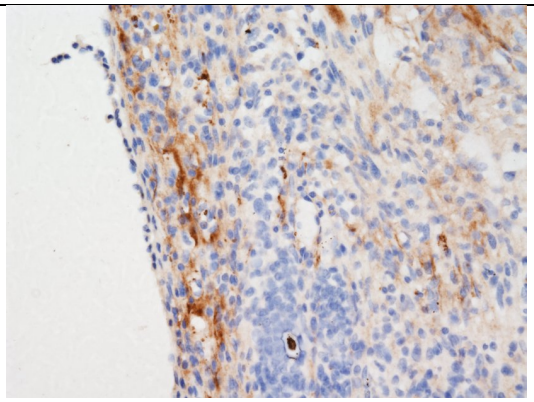

(f) mouse 12, bag 1, section 7

Fig.6.27. Microphotographs of the histological tissue samples stained in von Willebrand Factor for untreated polyurethane PPG-DI-PTHF-0.35. An empty space on the figures is the implant position.

The tissues near the untreated polyurethane implants accumulated a large amount of the vWF (Fig.6.27). Some samples show the highest concentration of the vWF in the

capsule (Figs.6.27 d and e), but some samples show a distribution of the vWF in the whole tissue far from the capsule (Figs.6.27 a, c and f). The vWF high amount was also observed in the new vessels (Figs.6.27 c, e and f).

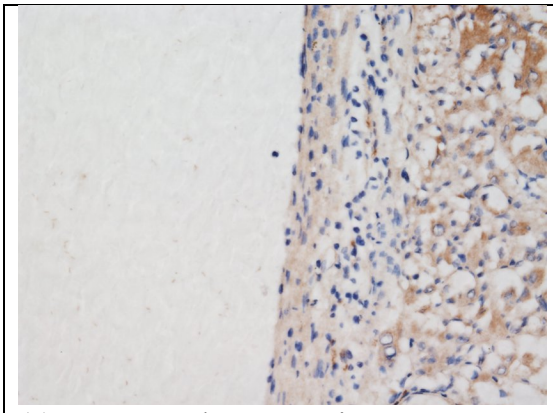

(a) mouse 23, bag 4, section 3

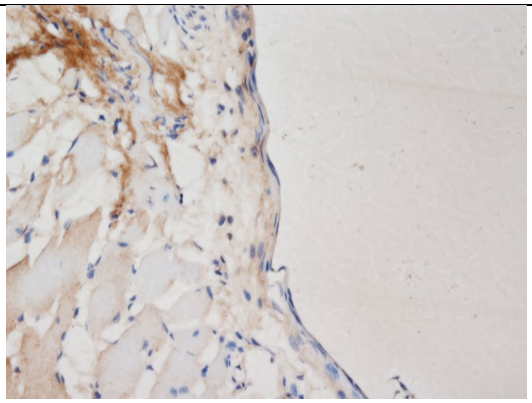

(b) mouse 24, bag 4, section 10

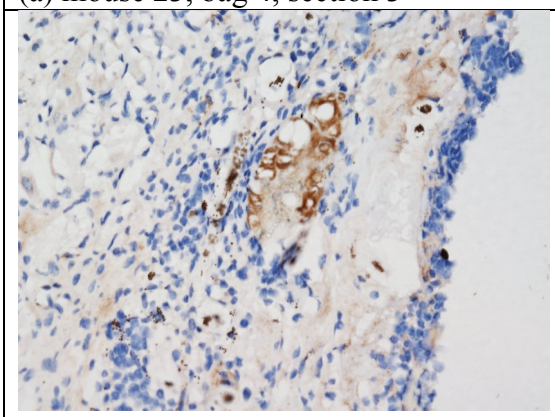

(c) mouse 25, bag 4, section 11

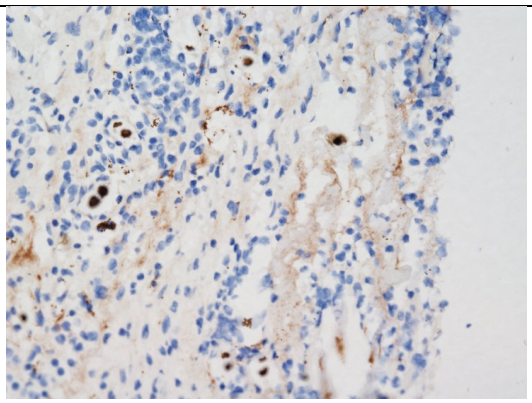

(d) mouse 25, bag 4, section 12

Fig.6.28. Microphotographs of the histological tissue samples stained in von Willebrand Factor for 40 sec PIII treated polyurethane PPG-DI-PTHF-0.35. An empty space on the figures is the implant position.

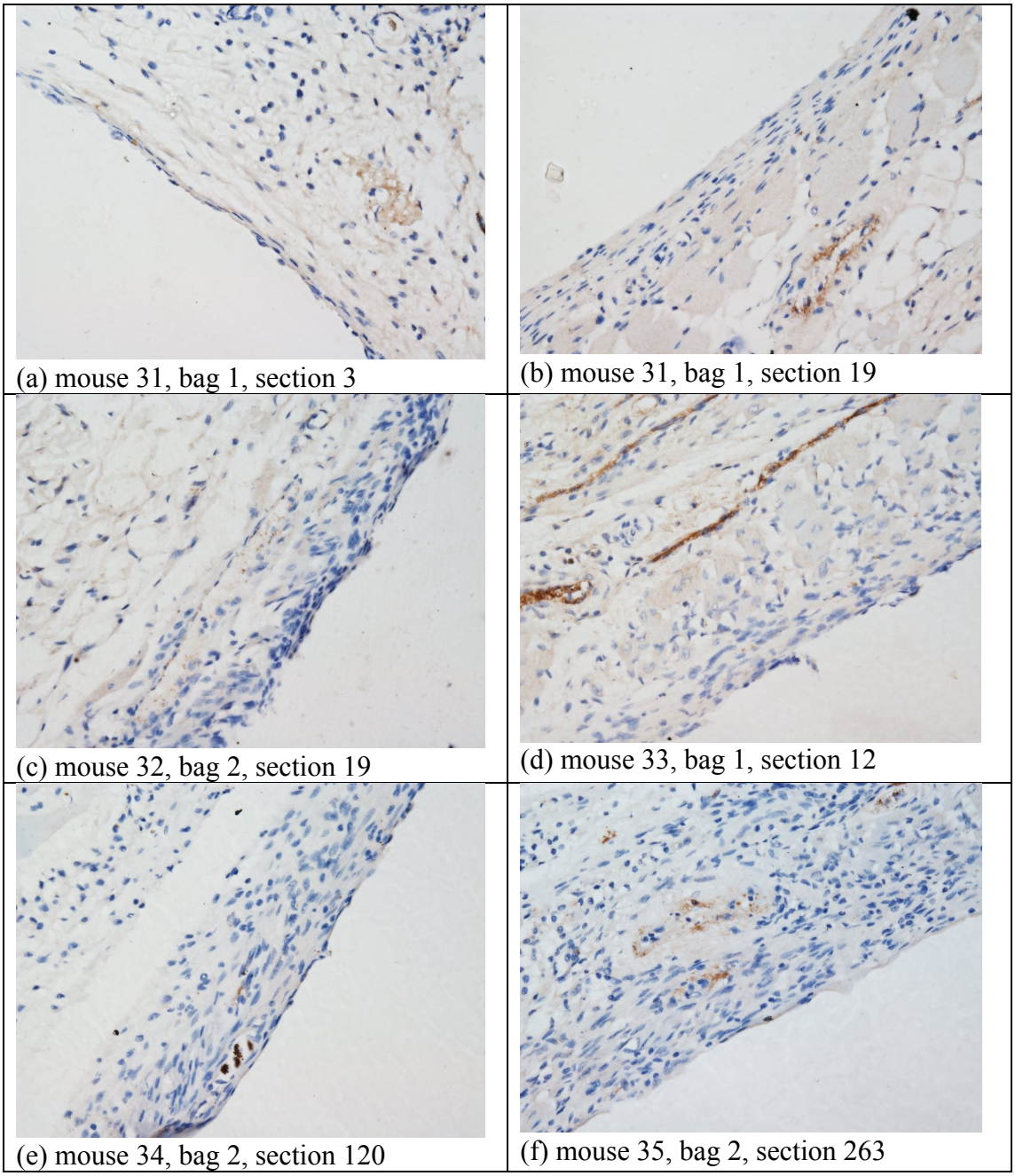

(a) mouse 31, bag 1, section 3

(b) mouse 31, bag 1, section 19

(c) mouse 32, bag 2, section 19

(d) mouse 33, bag 1, section 12

(e) mouse 34, bag 2, section 120

(f) mouse 35, bag 2, section 263

Fig.6.29. Microphotographs of the histological tissue samples stained in von Willebrand Factor for 80 sec PIII treated polyurethane PPG-DI-PTHF-0.35. An empty space on the figures is the implant position.

A similarly high amount of vWF was observed in some samples of the tissue near the 40 second PIII treated implants (Fig.6.28 a and b). In other samples the vWF was concentrated in spots outside the capsule (Fig.6.28 c and d). However, in all samples the vWF was not concentrated in the capsule as observed for the untreated polyurethane implants.

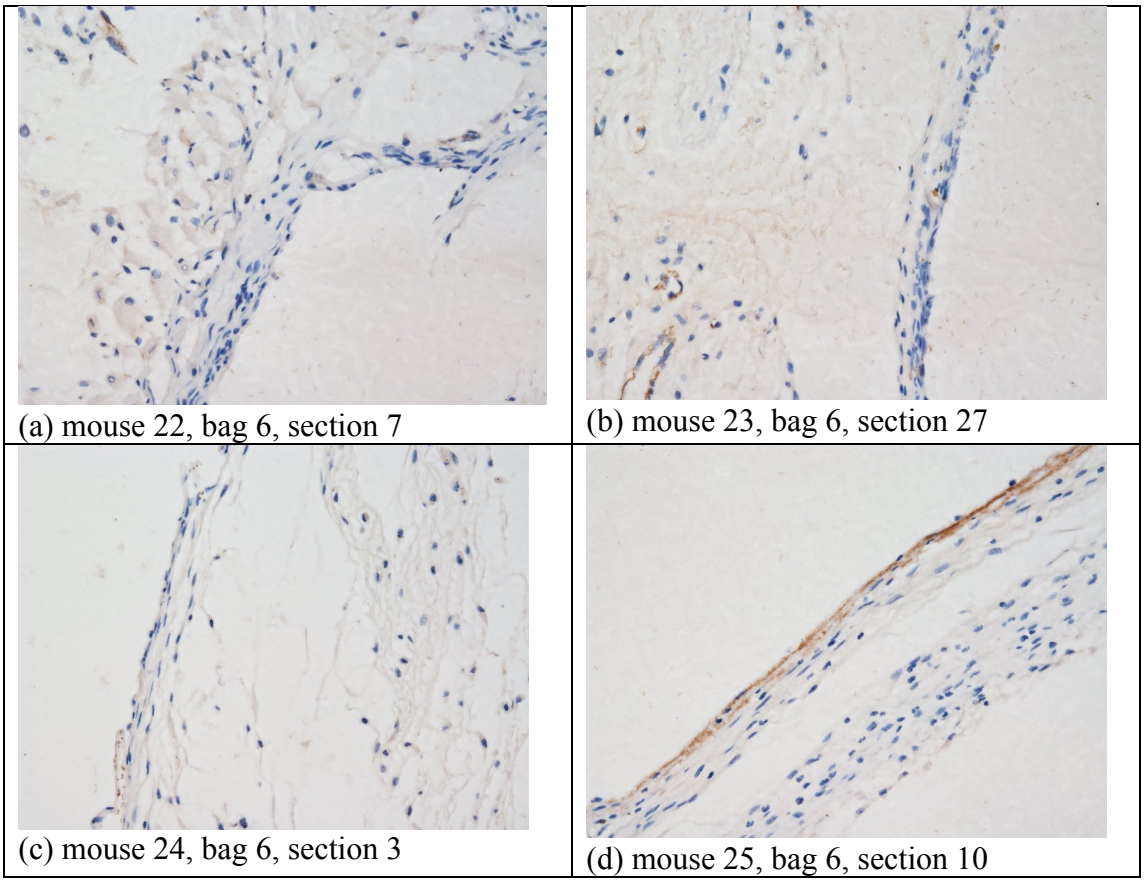

(a) mouse 22, bag 6, section 7

(b) mouse 23, bag 6, section 27

(c) mouse 24, bag 6, section 3

(d) mouse 25, bag 6, section 10

Fig.6.30. Microphotographs of the histological tissue samples stained in von Willebrand Factor for 200 sec PIII treated polyurethane PPG-DI-PTHF-0.35. An empty space on the figures is the implant position.

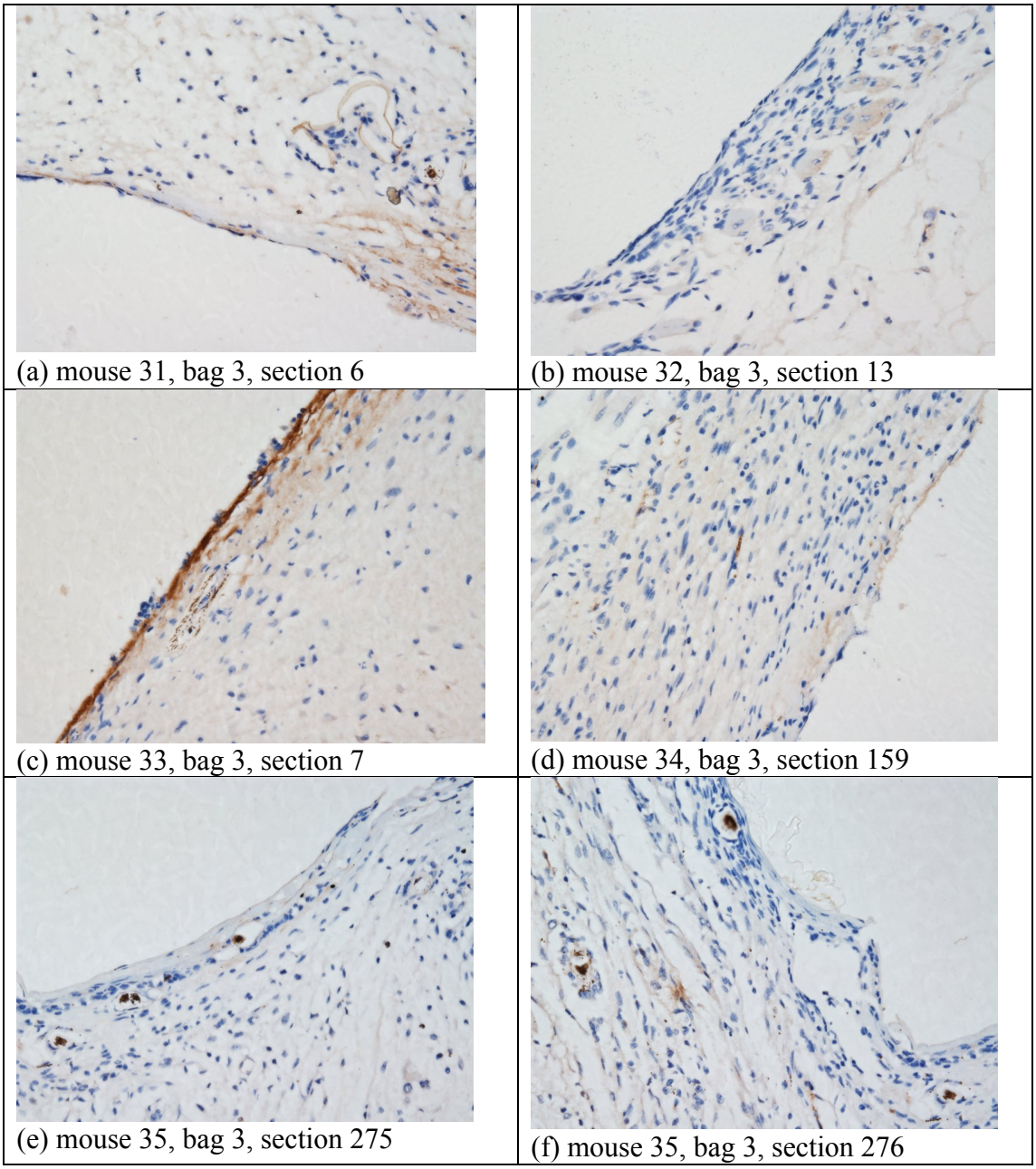

(a) mouse 31, bag 3, section 6

(b) mouse 32, bag 3, section 13

(c) mouse 33, bag 3, section 7

(d) mouse 34, bag 3, section 159

(e) mouse 35, bag 3, section 275

(f) mouse 35, bag 3, section 276

Fig.6.31. Microphotographs of the histological tissue samples stained in von Willebrand Factor for 400 sec PIII treated polyurethane PPG-DI-PTHF-0.35. An empty space on the figures is the implant position.

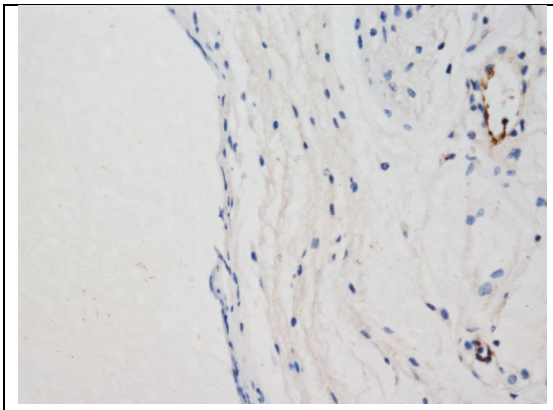

(a) mouse 31, bag 5, section 3

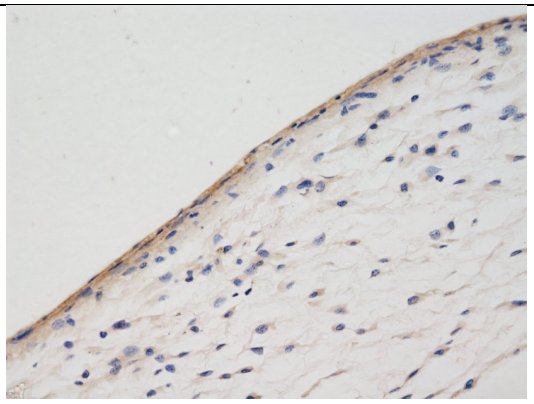

(b) mouse 31, bag 6, section 18

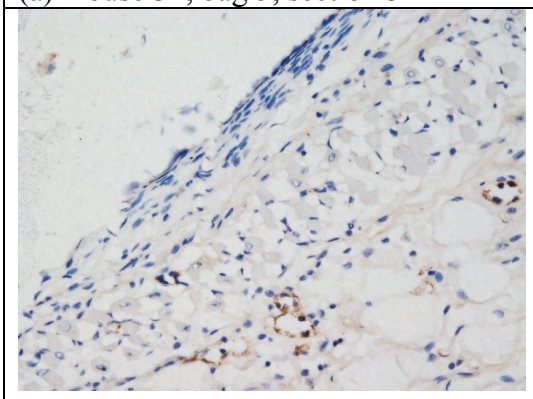

(c) mouse 32, bag 5, section 18

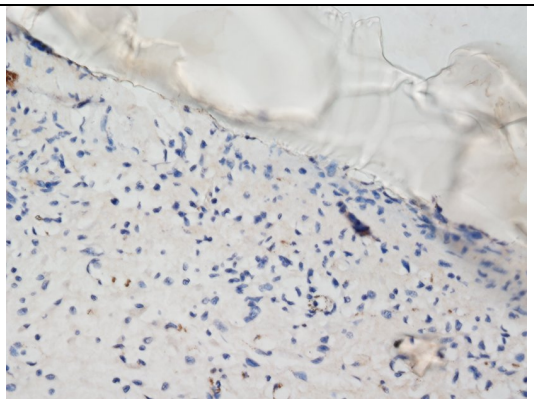

(d) mouse 33, bag 5, section 48

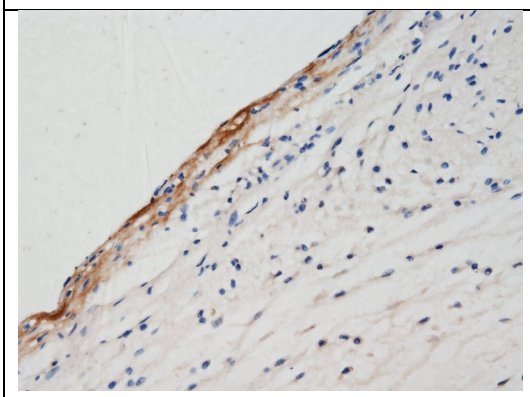

(e) mouse 33, bag 5, section 52

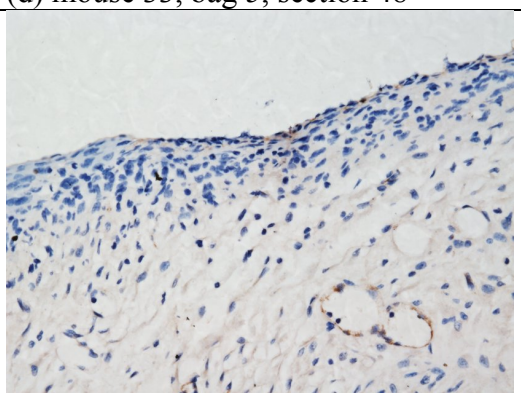

(f) mouse 34, bag 6, section 205

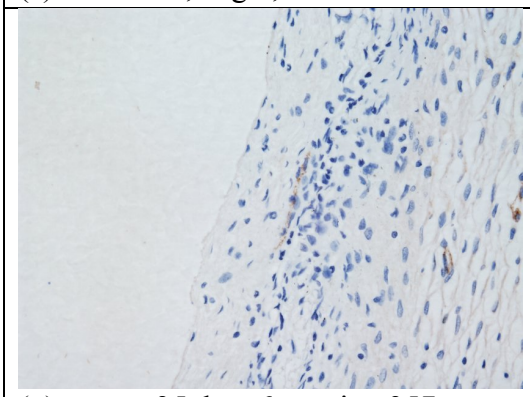

(g) mouse 35, bag 6, section 357

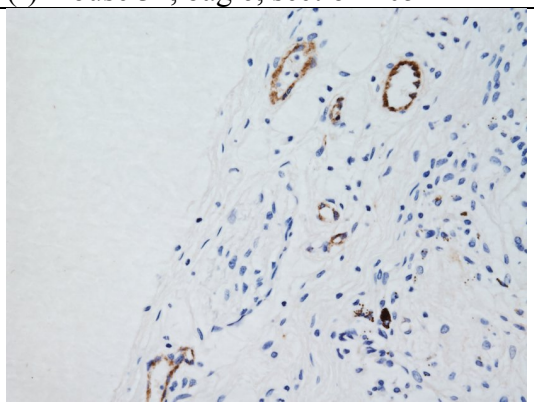

(h) mouse 35, bag 6, section 361

Fig.6.32. Microphotographs of the histological tissue samples stained in von Willebrand Factor for 800 sec PIII treated polyurethane PPG-DI-PTHF-0.35. An empty space on the figures is the implant position.

Much lower amount vWF was observed in the tissue surrounding the 80 second PIII treated polyurethane implants (Fig.6.29). There were some spots observed in the new cross-sectioned vessels (Fig.6.29 a, b and f) and in the along-sectioned vessels (Fig.6.29 d). In some samples, the coloured area was not observed at all (Fig.6.29 e). In all these samples the capsule did not contain vWF.

The stained tissues surrounding the polyurethane implants with 200 seconds, 400 seconds and 800 seconds of PIII treatment time were similar and showed very low amounts of vWF (Fig.6.30-6.32). The vWF spots were visible in areas where new vessels were formed (Fig.6.30 b, Fig.6.31 a, e, f, and Fig.6.32 a, c, h). However, in some samples a high amount of vWF was observed in a very thin layer of the tissue (1-2 cells layer), which was in contact with the polyurethane implant (Fig.6.30 d, Fig.6.31 c and Fig.6.32 b, e). This layer was much thinner than the capsule for these samples. In all other samples the capsule did not contain vWF.

For quantitative measurements the area of vWF stained tissue was calculated (Fig.6.33). The measurements show that the tissue near the implants of 80-800 s range of PIII treatment time has a significantly lower area of vWF than the tissue surrounding the untreated and 40 s PIII treated implants ($p<0.001$). The difference between the tissues near the PIII treated implants in 80 second - 800 second range was not significant ($p>0.05$).

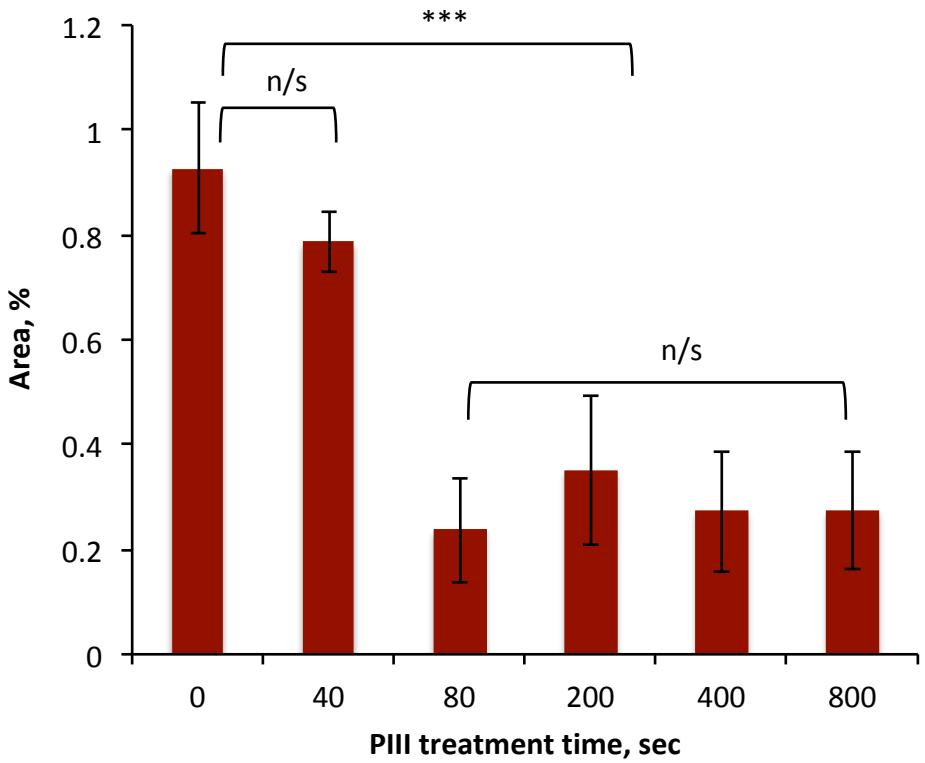

Fig.6.33. Result of von Willebrand Factor staining analysis of the tissue near the PIII treated polyurethane implants with time of PIII treatment. “0” means the untreated (initial) samples.

6.7. Discussion

The newly synthesised untreated polyurethane implant shows a minor foreign body reaction with formation of the capsule filled with macrophages and fibroblasts. The giant cells or necrosis were not observed in any samples. The thickness of the capsule of 100 μm surrounding the implant corresponded to the literature data for biocompatible implants used in medical practice [1-2]. Therefore, the newly synthesised untreated polyurethane corresponds to the biocompatible materials following the organism reaction. The softness of the new polyurethane does not influence the foreign body reaction.

However, the host response to PIII treated polyurethane was significantly reduced, showing that the average thickness of the capsule was significantly less near the treated polyurethane than near the untreated polyurethane. In some cases the capsule was not formed near the PIII treated polyurethane surface at all. In addition separate macrophages were observed on the surface with large distances between them whereas in other cases only normal tissue was observed. In some cases only one irregular layer of fibroblasts with thin not-structured collagen fibres was observed.

Acute inflammation and capsule formation are usually observed 5-7 days after surgery. Chronic inflammation is observed following this period with a formation of thick isolating capsule around the implant. However, if the capsule around PIII treated polyurethane is not observed 7 days from the operation, it is possible that the capsule might be not formed later because a delayed formation of the capsule is less likely. Therefore, there are cases when the capsule is not formed or has significantly less thickness with a significantly lower amount of immune cells.

For discussion of the histochemistry results this study considered a general scheme of immune reaction on an implant (Fig.6.34) [3] where the reaction is characterised by stages of the organism response, which becomes more complicated and intensive with time up to the total isolation of the implant from the body.

The histochemistry results showed the significant difference in immune response of the mice organism on untreated and PIII treated polyurethane implants. At first, Von Willebrand Factor concentration in the tissue near the PIII treated implants differed from that near the untreated implants. The literature [4] demonstrates that the Von Willebrand Factor is closely related to recruitment of the neutrophils in the injured tissue near the implant. When the Von Willebrand Factor concentration increases, the neutrophils are collected in the injured tissue and activated. The images of Von Willebrand Factor assay in the tissue near the untreated polyurethane implant correspond to a moderate immune reaction on the implants as seen in the literature [5-6]. The lower Von Willebrand Factor concentration in the tissue near the PIII treated implant means that there is a less intensive inflammation and lower concentration and activity of neutrophils. Therefore the stage 2 has lower intensity for PIII treated implant than for the untreated implant.

The macrophages are recruited at the next stage of the immune reaction. The role of macrophages is to remove the foreign body and/or to utilise the cell apoptosis products. The macrophages are recruited and activated via expression of cytokines released by neutrophils when the foreign body could not be destroyed in the body.

The concentration and activity of the macrophages near the untreated implant show a moderate reaction of an organism consistent with the literature data [7-10]. The lower concentration and activity of macrophages in the tissue near the PIII treated implant means that the macrophages are recruited and activated with much fewer signals from the neutrophils. Therefore the stage 3 of the immune response has a lower intensity.

The new vessels formation and cell proliferation at the next stage provide a transport of immune cells to the injured tissue. These processes are ignited by released cytokines from the immune cells, which could not exclude the foreign body. At this stage the immune response includes deep transformation of surrounding tissues, which become involved into the healing process. The organism prepares to intensify the immune attack. The cell proliferation process in the tissue surrounding the untreated implant is much more intensive than in the tissue far away from the implant. The intensity at this stage is consistent with the literature on other implanted materials [7-10]. However, the cell proliferation activity in the tissue surrounding PIII treated implant is much less. The cell proliferation is not detected, suggesting that the organism does not recognise the implant as a foreign body.

With time the implant is encapsulated with collagen fibres. The fibroblasts are activated and build a cross-linked collagen capsule around the implant. At this stage the organism tries to isolate the foreign body from the tissues. The immune response is transformed to chronic inflammation. The thickness of the capsule depends on the intensity of the foreign body reaction. The capsule around the untreated polyurethane implant is about 100 μm, which corresponds to the moderate immune reaction for most of polymer implants [1-2].

The capsule surrounding the PIII treated implants is much thinner. This collagen capsule consists of rare disordered fibres whereas a capsule of dense ordered collagen fibres surrounds the untreated implant. In some cases the capsule near the PIII treated implant was not observed at all. Therefore, the host does not recognise the PIII treated implant as a foreign body, which must be isolated.

All these observations are related to acute inflammation observed in the 7 days after the operation. According to the literature [1-2], capsule thickness for untreated implants grown after the acute stage, increases during the chronic stage. In addition, previous long-term investigations with ion beam treated hard polyurethane showed the absence of immune response in the organism after 6 months. Because of this absence in these long-term experiments with the new polyurethane, we predict that the intensive chronic inflammatory reaction on PIII treated polyurethane is unlikely due to the low inflammatory reaction during the acute stage. Therefore, the low and absent foreign body reaction is achievable.

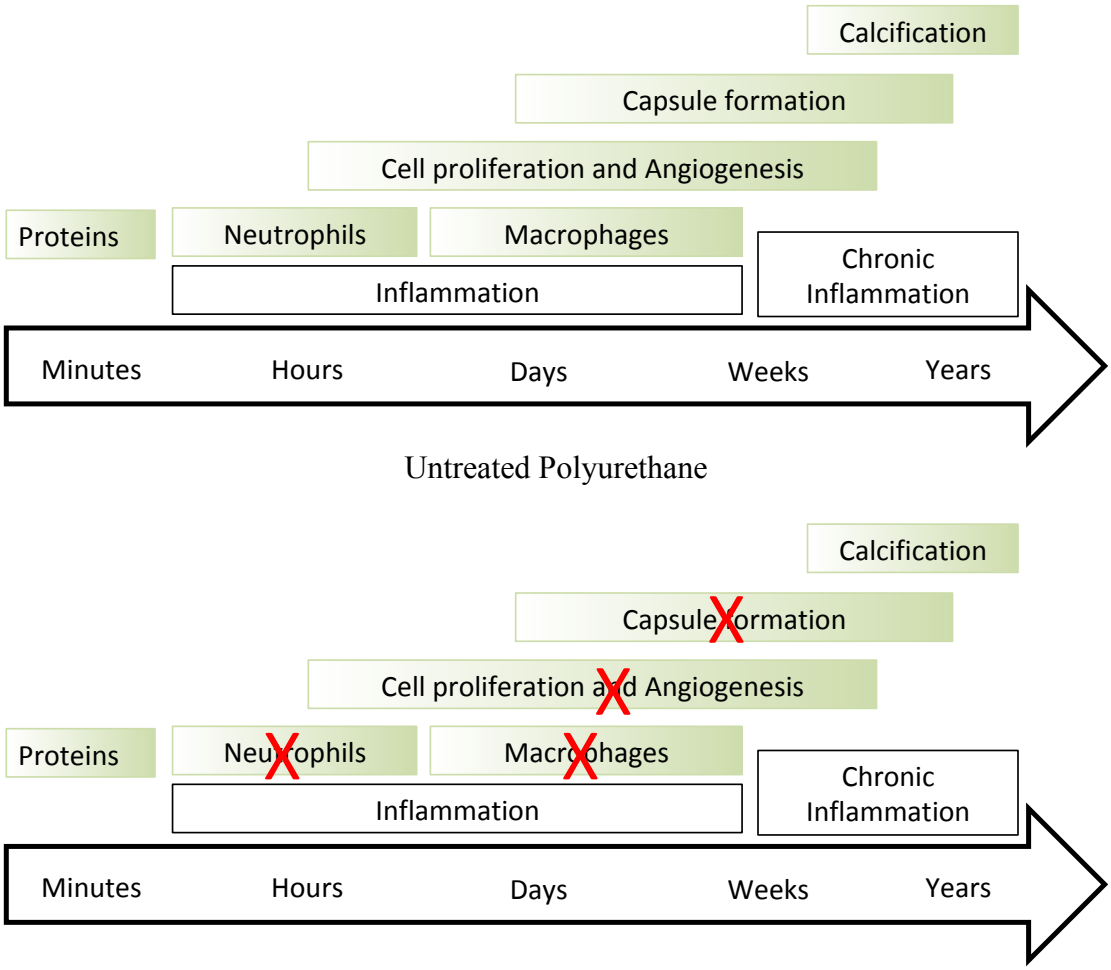

Fig.6.34. Scheme of foreign body reaction with main stages from the time of first contact of the implant with organism tissue. The scheme is adapted from literature data [3] for untreated and PIII treated polyurethane. Red crosses show low or absent activity observed in the experiments with PIII treated implants.

6.8. Conclusions

The investigations of the host response on the untreated and PIII treated polyurethane implant show that all implants do not cause physiological dysfunctions in the mice or rats. The polyurethane graft was successfully implanted as a vascular graft in the rat. The polyurethane graft is sewable and sticky, easily adhering to the vessel wall.

The PIII treated implants in mice show a weaker immune response of the organism, in particular:
1. The capsule around the PIII treated implant is significantly thinner ($p<0.01$).
2. The macrophages activity near the PIII treated implants is significantly weaker ($p<0.001$).
3. The cell proliferation activity near the PIII treated implants is significantly weaker ($p<0.001$).
4. The pro-inflammatory activity by vWF test is much weaker near the PIII treated implants ($p<0.001$).

Therefore, the changes in the organism response on PIII treated implant in comparison with the untreated polyurethane implant are statistically significant.

References

1. M.N. Avula, A.N. Rao, L.D. McGill, D.W. Grainger, F. Solzbacher, Foreign body response to subcutaneous biomaterial implants in a mast cell-deficient $Kit^{w\text{-}Sh}$ murine model, Acta Biomaterialia 10 (2014) 1856–1863.
2. M. Kastellorizios, F. Papadimitrakopoulos, D.J. Burgess, Prevention of foreign body reaction in a pre-clinical large animal model, Journal of Controlled Release 202 (2015) 101–107.
3. S. Franz, S. Rammelt, D. Scharnweber, J.C. Simon, Immune responses to implants e A review of the implications for the design of immunomodulatory biomaterials, Biomaterials 32 (2011) 6692-6709.
4. C. Hillgruber, A.K. Steingraber, B. Poppelmann, C.V. Denis, J. Ware, D. Vestweber, B. Nieswandt, S.W. Schneider, T. Goerge, Blocking Von Willebrand Factor for Treatment of Cutaneous Inflammation, Journal of Investigative Dermatology (2014) 134, 77–86.
5. B. Horvath, D. Hegedus, L. Szapary, Z. Marton, T. Alexy, K. Koltai, L. Czopf, I. Wittmann, I. Juricskay, K. Toth, G. Kesmarky, Measurement of von Willebrand factor as the marker of endothelial dysfunction in vascular diseases, Exp Clin Cardiol. 2004 Spring; 9(1): 31–34.
6. K.M. Provchy, Von Willebrand Factor Expression in Vascular Endothelial Cells of Cage Control and Antiorthostatic Cage Suspension Golden Hamster Ovaries, Senior Honors Thesis, East Tennessee State University, 2010.
7. L. Sheng, Q. Yu, F. Xie, Q. Li, Foreign body response induced by tissue expander implantation, Molecular Medicine Reports, 9 (2014) 872-876.
8. W.-J. Hu, J.W. Eaton, T.P. Ugarova, L. Tang, Molecular basis of biomaterial-mediated foreign body reactions, Blood, 98 (2001) 1231-1238.
9. W.K. Ward, A Review of the Foreign-body Response to Subcutaneously-implanted Devices: The Role of Macrophages and Cytokines in Biofouling and Fibrosis, J Diabetes Sci Technol 2 (2008) 768-777.
10. J.A. Jones, D.T. Chang, H. Meyerson, E. Colton, I.K. Kwon, T. Matsuda, J.M. Anderson, Proteomic analysis and quantification of cytokines and chemokines from biomaterial surface-adherent macrophages and foreign body giant cells. J Biomed Mater Res A. 83 (2007) 585-596.

Chapter 7. General discussion and prospective

Foreign Body Reaction (FBR) is a key problem for modern artificial implants [1]. It does not only limit the implant development but it limits the number of patients to whom the implants can be applied. An absence or reduction in the FBR would significantly improve the implant's capacity to save life. However, despite how all modern implants satisfy physical and chemical stability, non-immunogenicity and non-toxicity requirements [2], all these implants still cause an immune response in an organism. This is why there is a widely held opinion that FBR cannot be avoided [3]: "All materials implanted into humans and animals elicit 'foreign body' interactions, surrounding the materials with a protective capsule."

Attempts to avoid or decrease the immune reaction on artificial implants can be found in the literature [4-6]. All these attempts were based on stopping the immune reaction at some stage. For example, systemic corticosteroids decreases immune function and fibrosis, in particular it decreases the number of myofibroblasts [7]. However, our knowledge of the mechanism of the immune reaction is limited. The immune reaction is complicated and self-regulated with multiple ways and steps. Blocking one step in the immune response will not prevent the protective capsule formation.

The histology results in this thesis on the untreated polyurethane correspond to the results discussed above. The analysis of the tissue surrounding the untreated polyurethane implant shows a classical picture of the immune reaction. The macrophages' activity clearly increased near the implant. The cell proliferation increased. The vWF was released in the tissue near the implant. The collagen capsule formed.

The observed reaction on unmodified polyurethane implant has moderate character, which shows a moderate immune response on the implant. It corresponds to the literature on polyurethane implants. There are no giant cells, there is no necrosis or high level of cell lysis. However, the thick collagen capsule forms as a usual tissue response to a foreign body.

The immune reaction on PIII treated polyurethane implants is different (Chapter 6). The capsule is significantly thinner than for the untreated implant. In some cases, the capsule is not observed at all or only one layer of cells can be attributed to the capsule. The macrophages' activity is much lower or negligible for some samples. The cell proliferation activity is significantly lower than for the untreated implant and in some cases the proliferation activity is observed at the level of undisturbed tissue. The level of expressed vWF is much lower for PIII treated implant than for the untreated implant. In some cases, the level of vWF is the same for undisturbed tissue. Most significantly, the FBR in this study was shown to be much lower or negligible.

The thin capsule on ion beam treated implant is observed from the implant side (Appendix II). The collagen capsule is well attached to the untreated polyurethane

implant. However, the capsule is not found on ion beam implanted polyurethane surfaces with the carbonised top surface. The collagen structures are observed in the bottom of the crack of the carbonised layer, where the patches of untreated polyurethane are accessible by host proteins, phagocytes and fibroblasts.

A similar weak immune reaction was observed for ion beam treated polyurethanes in the experiments of Suzuki and colleagues [8]. Polyurethane treated by Ar+ were implanted into a rabbit for 16 days and a weak intensity of inflammatory reaction was observed. A similar effect of biocompatibility of polymer materials after the ion beam treatment was observed in vivo experiments with ePTFE grafts. ePTFE graft was treated by an ion beam and implanted in dogs' femoral artery. The control sample showed thrombosis after 3 days, where the modified was clear after 180 days [9]. However, the mechanism responsible for the weak immune reaction was not discovered at that time.

In the present study the attempt to prevent the phagocyte activation is based on the knowledge of specific adsorption of the host proteins on the PIII treated implant surface.

It is clear now that the immune response of an organism starts from a specific adsorption of host proteins on the surface of the artificial implant [10]. Then the phagocytes recognise the adsorbed proteins on the implant surface and become activated. The activated phagocytes release specific cytokines, chemokines, interleukins and other factors, which ignite the next steps of the inflammation reaction. The activation of phagocytes is a complex process and includes local cytokine expression, transformation of the macrophages and giant cells. At some stage the fibroblasts are activated, proliferated and ignited to produce collagen to form a capsule around the implant.

The host proteins in organisms exist in hydrophilic environment such as cytoplasm, extracellular liquids, blood and lymph. The biologically active conformation of the protein molecule is optimised for such an environment. When the host proteins come in contact with a surface of the artificial implant, the environment for the host proteins is changed: the protein is in contact with the implant, not with water molecules [11]. The protein molecule is adsorbed on the implant surface and changes the conformation due to different intermolecular interactions with the implant surface in comparison with the organism (hydrophilic) environment [12]. The conformation of absorbed protein depends on the surface properties [13]. However, all artificial implants have a surface energy in a range of 20-45 MJ/m^2 corresponding to the surface energy of the implant material [14]. This is much lower than the water surface energy of 72 MJ/m^2. Therefore, the protein conformation changes to adjust the hydrophobic interactions with the implant.

In contradiction with the untreated polyurethane, the PIII treated polyurethane implant is highly hydrophilic. The contact angle of the carbonised surface is 35-45 degrees for freshly treated PPG-DI-PTHF-0.35 polyurethane. The surface energy of the treated polyurethane 10 minutes after PIII treatment is 60-65 MJ/m^2. Such a high surface energy and hydrophilicity is enough to absorb the water molecules and keep the hydrophilic intermolecular interactions with proteins in such a way that the protein is surrounded by water molecules and does not change the initial conformation at the

point of absorption. This effect of hydrophilicity was observed for other polymers after PIII, ion beam treatment and plasma treatment [15]. For example, the literature shows a surface energy of 71 MJ/m^2 for the freshly PIII treated Nylon [16] and 77.9 MJ/m^2 for the freshly treated polyvinyl chloride (PVC) [17]. It maintains the conformation of the absorbed protein and its activity. For example, the conformation of Horseradish peroxidase (HRP) attached to PIII treated polyethylene remains unchanged or close to the biologically active conformation as observed by Amide I line in the FTIR ATR spectra [18]. The enzyme activity of the HRP attached on PIII treated Teflon remains high [19].

At the same time protein is attached covalently to the PIII treated polyurethane implant. The covalent attachment is key to the strong anchoring of the protein to the implant surface. The protein attachment to the untreated implant can be provided with different kinds of intermolecular interactions. The van-der-Waals forces, dispersic interactions, dipole-dipole interactions, ionic interactions or hydrogen bonds can hold the protein on the surface. However, these interactions are flexible and can be easily replaced with water-protein interactions. The more hydrophilic the surface, the easier the protein can be washed with detergent or just a buffer [20.]. Such a weakness of the intermolecular interaction is a reason for the Vroman effect where the proteins can be easily replaced with other proteins in the protein mixture solutions or in an organism [21]. Such a flexibility of the protein adsorption can lead to unpredictable attachment of proteins, including signal proteins for igniting the immune reaction.

The covalent attachment of protein is available with artificial chemical linkers [22-24]. The linker molecule is designed in such a way that one reactive group fixes the linker molecule on the surface and the second reactive group anchors the protein molecule to the linker. However, the chemistry of linker molecules is complicated. In most cases the linker molecules are toxic and cannot be used in an organism. Also the effectiveness of the linkers to bind the protein is much less than the total coverage. In such cases, part of the surface is not covered and the immune system can recognise the surface as foreign body.

The PIII treated polyurethane surface can be covered completely. The protein monolayer forms a total coverage (carpet) on the PIII treated polymer surface [25] including polyurethane. The protein layer covalently attached to the PIII treated polyurethane implant is not washable. The protein molecules covalently attached to the PIII treated surface cannot be replaced with other proteins and the Vroman effect is observed [26].

The covalent attachment of protein on PIII treated polyurethane is provided via the reactions of free radicals which are formed when the polyurethane macromolecule is destroyed under high energy ion bombardment with formation of condensed aromatic structures like grapheme or graphite. The free radicals are observed in the polyurethane implant after a long period of storage (Chapter 4). The free radicals on the edges of the graphitic planes can be stabilised by π-electrons of the aromatic structure [27-28] and remain active before the protein molecule approaches the modified surface. The literature shows that the reaction of free radicals appeared in polyethylene after ion beam treatment with aminoacids [29]. When the free radicals react with the protein molecule a covalent bond is formed [18]. As a result, the protein

molecule bonds to the carbonised surface layer of the PIII treated polyurethane implant.

The molecules with free radicals in solution are widely considered to accelerate aging of an organism because the host protein molecules can be damaged in free radical reactions [30]. The result of the protein damaging and oxidation can accelerate cell lysis and necrosis. These effects were not observed in surrounding implant tissue. The effect of free radicals on the protein requires the free radicals to be mobile in a solution. The free radicals in the polyurethane implant are associated with the condensed aromatic structures which are stable in polyurethane, and cannot propagate in the solution. When the protein is bonded with the surface, the protein does not migrate into the solution. The damaging of protein or decay of the protein activity was also not observed. Therefore, the free radicals in the polyurethane surface do not influence the organism's tissues.

The endothelialisation of the implant surface is one of the important factors of the biocompatibility [31]. Endothelialisation is considered a method of reducing the immune response [32]. The attachment of active protein can significantly improve cell adhesion [33]. A fast and total endothelialisation in an organism is the primary aim for the biocompatibility of implants.

In the case of the newly synthesised polyurethane, the endothelial cells are spread and proliferate on the surface without PIII treatment. The endothelial cells also grow well on the PIII treated polyurethane surface. However, the untreated polyurethane is observed totally covered with the endothelial cells only after 6 days, while the PIII treated polyurethane is totally covered after 2 days as observed on the control tissue culture plastic (TCP).

Similar cell attachment and proliferation was observed for other ion beam and PIII treated polymers. For example, the ion beam treatment of polystyrene by Na and Ne ions of 150 keV energy improved the endothelial cell spreading, attachment, proliferation and resistance to detaching with tripsin [34]. However, this research did not explain the mechanism by which this occurred. The adhesion and proliferation of endothelial cells and astrocytes on polyether sulphone and polyurethane by ion beam due to carbonisation of the polymer surface was reported in [35]. The endothelial cell adhesion and proliferation on PIII treated polyurethane was reported in [36]. The mechanism of improved cell adhesion via protein attachment due to free radical reactions was proposed in [37]. Thus, the attachment of protein with biologically active conformation leads to faster endothelialisation of the PIII treated polyurethane implant.

The observed improvement of the polyurethane implant with PIII treatment can be considered for future soft tissue implants such as breast implants, testicular implants, cardiovascular implants, vascular grafts, diaphragms, finger joints, ear implants, nose implants and others. The mechanism for reducing the immune response based on free radical reaction is critical to successful implantation.

First, the free radicals reduce with time after PIII treatment. Therefore, the best result for implantation is expected when the implant is treated by plasma and installed immediately. Therefore, implants should be treated just before surgery.

Second, the free radicals are sensitive to any surface contamination after the PIII treatment. Specific environmental conditions and limited contact with any other materials and devices are required before implantation into an organism.

Third, the sensitivity of free radicals limits sterilisation methods. Sterilisation by chemicals or gases reduces the concentration of free radicals and consequently the success of the implantation. Therefore, the sterilisation of the implant would be preferred before the PIII treatment. Taking into account that a plasma method is used for sterilisation [38], the PIII treatment can be done in sterile environments such as an operating theatre.

The polyurethane can be used as a coating on existing and new medical devices (see Appendix IV and V). The PIII treatment of these devices can be useful not only for the immune response decay, but also for drug release regulation (Appendix IV) to stop dewetting of the coatings (Appendix VII) and improve cell growth (Appendix VIII).

To develop further the PIII treated polyurethane implants will need an optimisation of the PIII treatment regimes, long-term animal experiments, optimisation of surgery methods, clinical studies and corresponding approval.

In general, the potential of implants without FBR cannot be overestimated. Cardiovascular implants including heart valve, blood vessel, catheter, pacemaker and defibrillator which do not generate FBR can be applied without immunosuppressants. Patients would not be at a risk of infection after implantation. A category of patients, who are at risk of corresponding diseases and for whom the implantation has not been recommended, will be able to be treated with the implants. The risk of inflammation and thrombosis can be significantly reduced. The breast, lips and other cosmetic implants would not cause contracture. Implants with electrical connection to the tissue such as cochlear, spine neurostimulator, implantable brain stimulator, different sensors in organs and blood would never lose electrical conductivity through the fibrotic capsule in an organism. The implantable drug release devices would never lose the drug penetration rate through the fibrotic capsule. Only insulin permanent releasing devices will save millions of patients with diabetes. Consequently, these improvements affect some millions of patients and can significantly influence our health, medical treatment and medical industry.

References

1. W.K. Ward, A Review of the Foreign-body Response to Subcutaneously-implanted Devices: The Role of Macrophages and Cytokines in Biofouling and Fibrosis, J Diabetes Sci Technol, 2(5), 2008, 768-777.
2. A.J.T. Teo, A. Mishra, I. Park, Y.-J. Kim, W.-T. Park, Y.-J. Yoon, Polymeric Biomaterials for Medical Implants and Devices, ACS Biomater. Sci. Eng., 2, 2016, 454−472.
3. J.E. Puskas, M.T. Luebbers, Breast implants: the good, the bad and the ugly. Can nanotechnology improve implants? WIREs Nanomed Nanobiotechnol, 2011. doi: 10.1002/wnan.164.

4. Yung LY, Lim F, Khan MM, Kunapuli SP, Rick L, Colman RW, Cooper SL. Neutrophil adhesion on surfaces preadsorbed with high molecular weight kininogen under well-defined flow conditions. Immunopharmacology, 32 (1-3), 1996, 19-23.
5. Yung LY, RW Colman, Cooper SL. Neutrophil adhesion on polyurethanes preadsorbed with high molecular weight kininogen. Blood, 94(8), 1999, 2716-2724.
6. Mazaheri MK, Schultz GS, Blalock TD, Caffee HH, Chin GA. Role of connective tissue growth factor in breast implant elastomer capsular formation. Ann Plast Surg. 50(3), 2003, 263-268.
7. Miller M, Cho JY, McElwain K, McElwain S, Shim JY, Manni M, Baek JS, Broide DH. Corticosteroids prevent myo broblast 51. accumulation and airway remodeling in mice. Am J Physiol Lung Cell Mol Physiol., 290(1), 2006, L162-169.
8. V. Melnig, N. Apetroaei, N. Dumitrascu, Y. Suzuki, V. Tura, Improvement of polyurethane surface biocompatibility by plasma and ion beam techniques, Journal of Optoelectronics and Advanced Materials, 7(5), 2005, 2521 – 2528.
9. M. Iwaki, Ion surface treatments on organic materials, Nuclear Instruments and Methods in Physics Research, B 175-177, 2001, 368-374.
10. H. Chen, L. Yuan, W. Song, Z. Wu, D. Li, Biocompatible polymer materials: Role of protein–surface interactions, Progress in Polymer Science, 33, 2008, 1059–1087.
11. A. Krishnan, Y.-H. Liu, P. Cha, D. Allara, E.A. Vogler, Interfacial energetics of globular–blood protein adsorption to a hydrophobic interface from aqueous-buffer solution, J. R. Soc. Interface, 3, 2006, 283–301.
12. W.-J. Hu, J.W. Eaton, T.P. Ugarova, L. Tang, Molecular basis of biomaterial-mediated foreign body reactions, Blood, 98, 2001, 1231-1238.
13. M. Bellion, L. Santen, H. Mantz, H. Haehl, A. Quinn, A. Nagel, C. Gilow, C. Weitenberg, Y. Schmitt, K. Jacobs, Protein adsorption on tailored substrates: long-range forces and conformational changes, J. Phys.: Condens. Matter, 20, 2008, 404226 (11pp).
14. Encyclopedia of Polymer Science and Technology, Ed. By Herman, Wiley, New York, 2004.
15. A. Kondyurin, M. Bilek, Ion Beam Treatment of Polymers. Application aspects from medicine to space, Second Edition, Elsevier, Oxford, 2014.
16. A. Kondyurin, N.J. Nosworthy, M.M.M. Bilek, R. Jones, P.J. Pigram, Surface Attachment of Horseradish Peroxidase to Nylon Modified by Plasma-Immersion Ion Implantation, Journal of Applied Polymer Science, 120, 2011, 2891–2903.
17. A. Kondyurin, N.J. Nosworthy, M.M.M. Bilek, Effect of Low Molecular Weight Additives on Immobilization Strength, Activity, and Conformation of Protein Immobilized on PVC and UHMWPE, Langmuir, 27, 2011, 6138–6148.
18. A.V. Kondyurin, P. Naseri, J.M.R. Tilley, N.J. Nosworthy, M.M.M. Bilek, D.R. McKenzie, Mechanisms for Covalent Immobilization of Horseradish Peroxidase on Ion-Beam-Treated Polyethylene, Scientifica, 2012, Article ID 126170, 28 pages, http://dx.doi.org/10.6064/2012/126170.
19. A. Kondyurin, N.J. Nosworthy, M.M.M. Bilek, Attachment of horseradish peroxidase to polytetrafluorethylene (teflon) after plasma immersion ion implantation, Acta Biomaterialia, 4, 2008, 1218–1225.
20. Kiaei D, Hoffman AS, Horbett TA, Tight binding of albumin to glow discharge treated polymers. J Biomater Sci Polym Ed, 4, 1992, 35–44.
21. A. Krishnan, Y.-H. Liu, P. Cha, D. Allara, E.A. Vogler, Interfacial energetics of globular−blood protein adsorption to a hydrophobic interface from aqueous-buffer solution, J. R. Soc. Interface, 3, 2006, 283-301.

22. W. Khan, M. Kapoor, N. Kumar, Covalent attachment of proteins to functionalized polypyrrole-coated metallic surfaces for improved biocompatibility, Acta Biomaterialia, 3, 2007, 541–549.
23. C. Mateo, V. Grazu, J. M Palomo, F. Lopez-Gallego, R. Fernandez-Lafuente, J.M. Guisan, Immobilization of enzymes on heterofunctional epoxy supports, Nature Protocols, 2(5), 2007, 1023.
24. C.D. Hodneland, Y.-S. Lee, D.-H. Min, M. Mrksich, Selective immobilization of proteins to self-assembled monolayers presenting active site-directed capture ligands, PNAS, 99, 2002, 5048-5052.
25. B. K. Gan, A. Kondyurin, M.M.M. Bilek, Comparison of Protein Surface Attachment on Untreated and Plasma Immersion Ion Implantation Treated Polystyrene: Protein Islands and Carpet, Langmuir, 23, 2007, 2741-2746.
26. Hirsh, S., McKenzie, D., Nosworthy, N., Denman, J., Sezerman, O., Bilek, M., The Vroman effect: Competitive protein exchange with dynamic multilayer protein aggregates. Colloids And Surfaces B: Biointerfaces, 103, 2013, 395- 404.
27. S. E. Stein, R. L. Brown, Chemical theory of raphite-like molecules, Carbon, 23, 1985, 105-109.
28. G. Mesyats , Yu. Klyachkin , N. Gavrilov , A. Kondyurin, Adhesion of Polytetrafluorethylene modified by an ion beam, Vacuum, 52, 1999, 285—289.
29. V. Svorcik, V. Hnatowicz, P. Stopka, L. Bacakova, J. Heitze, R. Ochsner, H. Ryssel, Amino acids grafting of Ar+ ions modified PE, Radiation Physics and Chemistry, 60, 2001, 89–93.
30. M.J. Davies, The oxidative environment and protein damage, Biochimica et Biophysica Acta, 1703, 2005, 93–109.
31. M.S. Lord, W. Yu, B. Cheng, A. Simmons, L. Poole-Warren, J. M. Whitelock, The modulation of platelet and endothelial cell adhesion to vascular graft materials by perlecan, Biomaterials, 30, 2009, 4898–4906.
32. J.H. Pang, Y. Farhatnia, F. Godarzi, A. Tan, J. Rajadas, B.G. Cousins, A.M. Seifalian, In situ Endothelialization: Bioengineering Considerations to Translation, Small, 11 (47), 2015, 6248–6264.
33. J.G. Steele, T.A. Savolainen, A. Dalton, L. Smith, G.J. Smith, Adhesion to Laminin and Expression of Laminin in Clonally Related Transformed and Control Sublines from an Alveolar Epithelial Cell Strain, Cancer research, 50, 1990, 3381-3389.
34. J.-S. Lee, M. Kaibara, M. Iwaki, H. Sasabe, Y. Suzuki, M. Kusakabe, Selective adhesion and proliferation of cells on ion-implanted polymer domains, Biomaterials, 14(12), 1993, 958.
35. B. Pignataro, E. Conte, A. Scandurra, G. Marletta, Improved cell adhesion to ion beam-irradiated polymer surfaces, Biomoterials, 18, 1997, 1461-1470.
36. N. Ozkucur, E. Richter, C. Wetzel, R.H.W. Funk, T.K. Monsees, Biological relevance of ion energy in performance of human endothelial cells on ion-implanted flexible polyurethane surfaces, J Biomed Mater Res, 93A, 2010, 258–268.
37. Kondyurin A., Maitz M.F., Surface Modification of ePTFE and Implants using the same, US patent WO 2007/022174 A3, 2007.
38. M.Y. Alkawareek, Q.Th. Algwari, G. Laverty, S.P. Gorman, W.G. Graham, D. O'Connell, B.F. Gilmore, Eradication of Pseudomonas aeruginosa Biofilms by Atmospheric Pressure Non-Thermal Plasma, PLoS ONE 7(8): e44289. doi:10.1371/journal.pone.0044289.

Appendices

The Appendices presented in this thesis are my unpublished and published work done prior to admission to the University of Sydney for PhD study. **The results presented in Appendices are related to this thesis, but do not form a part of it.** However, the results of this previous work are connected to this PhD thesis as they led me to this research.

Appendix 1 and 2 contain unpublished work carried out at the Institute of Continuous Media Mechanics and Children Centre "Detstvo" in Perm, Russia in 1995-2001. Appendix 3 contains a published article that presents work also carried out at this time. Appendix 4 and 5 contains published articles that present work carried out at the Rossendorf Research Centre Dresden, Germany in 2001-2003. The published articles in Appendices 6-10 present work carried out at the University of Sydney before and during my PhD study in 2005-2017.

Appendix I
Surface of polyurethane implant exposed in human organism

An usual study of the artificial implants in organism includes an analysis of the organism reaction such as immune response, toxicity, functionality, etc. Less attention is paid to the implant after the functionality of the implant is successfully provided. However, the analysis of the implants after it has been in an organism can be informative to understand the reaction of the organism. In particular, we have analysed the polyurethane implants after exposure in the living organisms. The investigations have been done in Perm State University in cooperation with Perm Medical Academy and Institute of Continuous Media Mechanics (Perm, Russia). The samples of implants after human organism were received from Perm Medical Academy (Prof. S. Plaksin). The sample investigations were done with approval of Ethics Committee of Perm Medical Academy.

The polyurethane has been synthesised from polyglycol based on polyoxitetramethylene (POTM) and polyoxipropylene (POP) glycols (trademark PF-OP-15, MM=2000) with an oxitetramethylene/oxipropylene monomer chain ratio of 85:15. The polyglycol hydroxyl groups were terminated with toluene diisocyanate (TDI). Then hardener 3,3'-dichlor,4,4'-diaminediphenylmethane (DA) with dibutyl dilaurate of Stannum (DBD) as catalyst was used to cure the polyurethaneurea shell. The shell was used for breast implants. The trade name of the polyurethane shell is SKU-PFL. The shell was filled with medical grade silicone resin and glued. The implants and production process were certified for medical usage in the human body for long-term use. The implants were successfully installed in the patients. The operations and following post-operational periods up to 25 years showed satisfying results of implantation and a stable functionality of the implants.

The implants used for the investigation were removed for different reasons from the patients at different times after implantation. The implants were permitted for an investigation following patient agreement. After removing the implant from the patient the implant was washed out in a buffer solution, dried and tested with FTIR ATR spectra, XPS, optical microscopy and scanning electron microscopy. The polyurethane shell stored under the same time in normal conditions and newly synthesised polyurethane shells were used as the control samples.

FTIR ATR spectra show that the polyurethane shell exposed in organism is covered by the collagen cover (Fig.1). It is well observed by disappearance of the Amide I line of polyurethane (1727 cm^{-1}) and appearance of Amide I line of

protein (1640 cm^{-1}). The ratio of Amide I lines related to polyurethane and protein molecules can be used for quantitative analysis of the collagen cover. The dependence of this ratio is shown in Fig.2. The relative intensity of the collagen cover increased with time in an organism during the first 5 months and then it was stabilised. However the variation of the protein line intensity from sample compared to the sample is high.

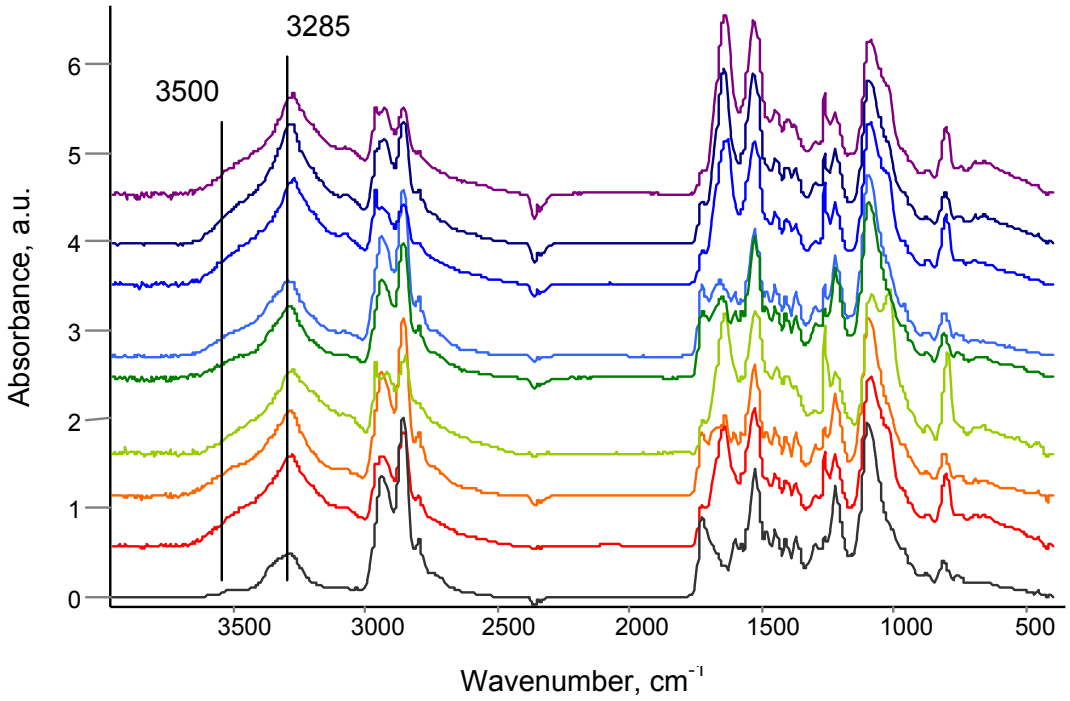

Fig.1. FTIR ATR spectra (KRS-5 ATR crystal) of polyurethane SKU-PFL after human organisms. Initial, 1 month, 4 months, 10 months, 34 months, 36 months, 46 months, 56 months, 56 months (other patient).

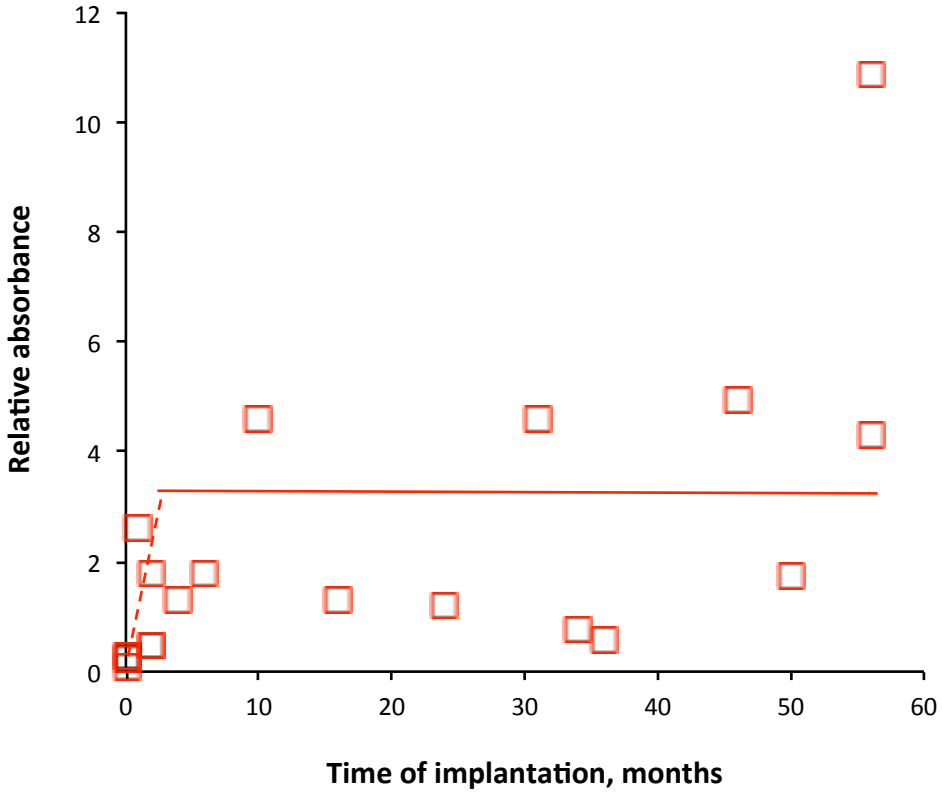

Fig.2. Ratio of Amide I line absorbance of the collagen shell (1640 cm^{-1}) to the Amide I line absorbance of polyurethane (1727 cm^{-1}) by FTIR ATR (KRS-5) spectra of polyurethane SKU-PFL after implantation in human organisms.

The collagen cover on the polyurethane surface is robust and cannot be removed by washing it in buffer, detergents or organic solvents. The spectra of the washed implants show the same spectra, just like the unwashed sample.

A successful decay of the protein line intensity was observed when the implant was treated by sodium hydroxide solution, which degraded the collagen cover on hydrolysis mechanism (Fig.3). The intensity of the protein Amide I line decreased with NaOH treatment time. However, after 10 hours in the NaOH solution, the collagen Amide I line remained in the spectrum that shows the collagen cover has a strong adhesion to the polyurethane surface. The adhesion is stronger then the collagen molecule itself.

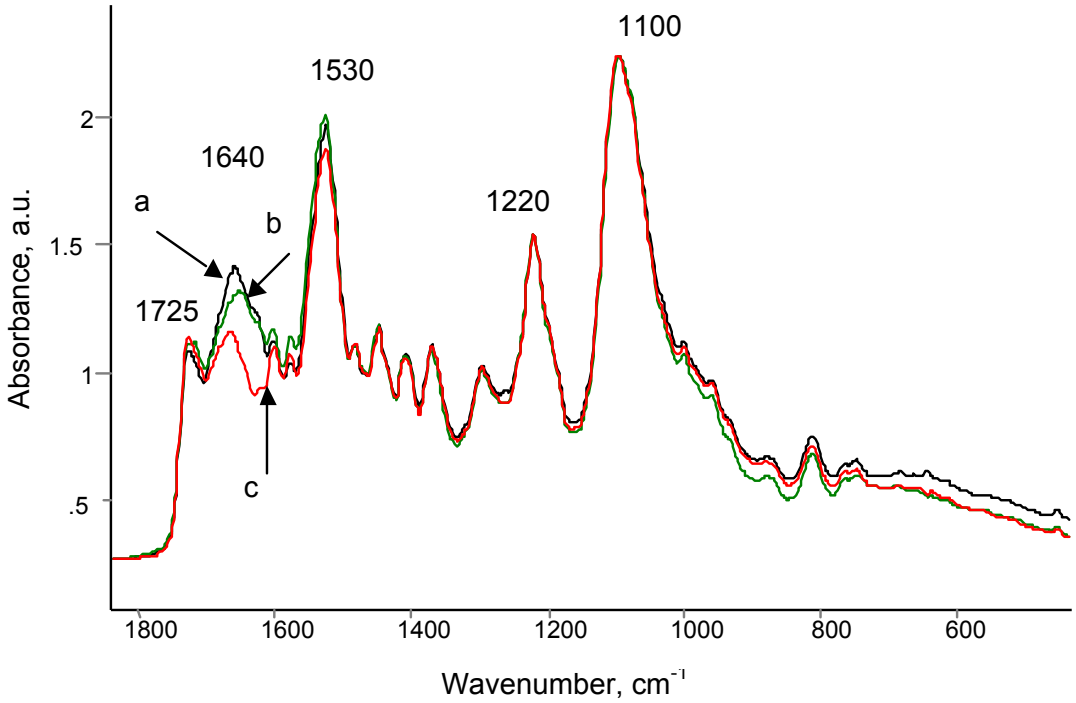

Fig. 3. FTIR ATR spectra of SKU-PFL shell of the breast implant after 2 years in human organism. Black (a) is water washed and dried implant. Green (b) is the implant after 10 min in 10% NaOH water solution. Red (c) is the implant after 10 hours in 10% NaOH water solution.

Therefore, the surface of the untreated polyurethane in the human organism becomes covered with a collagen. The collagen cover is strong enough that it can be removed by degrading the collagen molecules only.

Appendix II

Surface of ion beam treated polyurethane implant exposed in organism

The analysis of the implants after some exposure to an organism can give additional information about the immune response of the organism. We have analysed the polyurethane implants after the exposure of the implant in rats. The investigations were done in Perm State University in cooperation with Children Centre "Detstvo", Institute of Technical Chemistry and Institute of Continuous Media Mechanics (Perm, Russia) in 1995-1997. The investigations with animals were done as a required stage for an approval of biomedical implants for the following clinical studies in the human body.

The polyurethane has been synthesised from polyglycol based on polyoxitetramethylene (POTM) and polyoxipropylene (POP) glycols (trademark PF-OP-15, MM=2000) with an oxitetramethylene/oxipropylene monomer chain ratio of 85:15. The polyglycol hydroxyl groups were terminated with toluene diisocyanate (TDI). Then hardener 3,3'-dichlor,4,4'-diaminediphenylmethane (DA) with dibutyl dilaurate of Stannum (DBD) as catalyst was used to cure the films on glass substrate. Crosslinking the polyurethane was done by annealing the films at 120^0C for 3 hours in a vacuum oven. After peeling off and washing it from unreacted residuals, the films have been treated by nitrogen ions of 20 keV energy in a Pulsar ion beam implanter from both sides. The size of the films was 5 mm diameter with a 0.2 mm thickness. Straight after the treatment the films were implanted subcutaneously to the rats. The polyurethane samples with and without the ion beam treatment were implanted. The samples were sterilised in 70% solution of ethanol and dried in air prior to inserting. All the rats rapidly recovered after the operation.

The rats after operation completely recovered within a day, which is usual for rats after a surgery. In the following 5 months after the surgery, clinical signs severity score protocol was used for the rats monitoring on the every day basis. The rat dynamic activity was normal. The coordination was normal. The body weight didn't change. Breathing was normal. No change of coat or skin was observed. The eating and drinking was usual. Urine and faeces were normal. Communications between animals were normal. When palpated or touched no squeaking was observed. Therefore, it was a sign that a disturbance of the general physiological processes in whole organism was not shown by the rat.

The polyurethane films were removed after 5 months. After removing the implants from the rats, the films were washed out in a buffer solution, dried and tested with FTIR ATR spectra, optical microscopy and scanning electron microscopy. The polyurethane films with and without the ion beam treatments were stored for the same time under normal conditions as the control samples.

FTIR ATR spectra of the control polyurethane film with and without ion beam treatment show Amide I peak at 1725 cm^{-1} corresponding to urethane group vibrations (Fig.1, top). The spectra of untreated polyurethane film show Amide I peak at 1640 cm^{-1} corresponding to protein vibrations (Fig.1, bottom). The protein layer corresponds to a collagen covering on the polyurethane surface, it is observed after implantation into human organism.

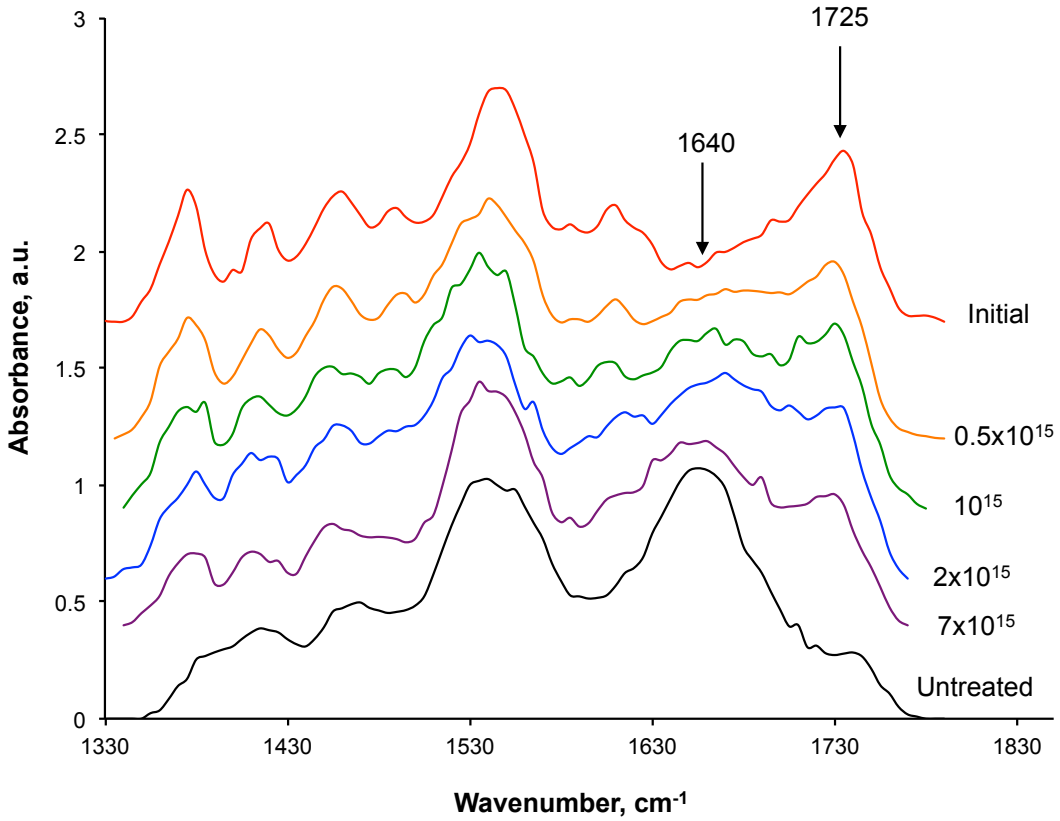

Fig.1. FTIR ATR spectra of ion beam treated Polyurethane SKU-PFL after implantation in rat for 5 months. The fluence of 20 keV nitrogen ions is shown in ions/cm^2. The curve marked as initial corresponds the polyurethane sample before the operation. The arrows mark the positions of Amide I lines for protein and polyurethane macromolecules.

The spectra of ion beam treated polyurethane films after being in the organism show these two lines with different ratio of the intensity. The spectra of the polyurethane treated with highest fluence is closer to the spectra of the untreated polyurethane after organism. The spectra of the polyurethane treated with lowest fluence is closer to the spectra of initial polyurethane before the organism. The quantitative measurement of this ratio in dependence on ion beam treatment fluence is presented on Fig.2. It is clear that the ion beam

treatment preserve the ratio from the organism influence. It means, the collagen covering is less seen by ion beam treated polyurethane, than for untreated polyurethane.

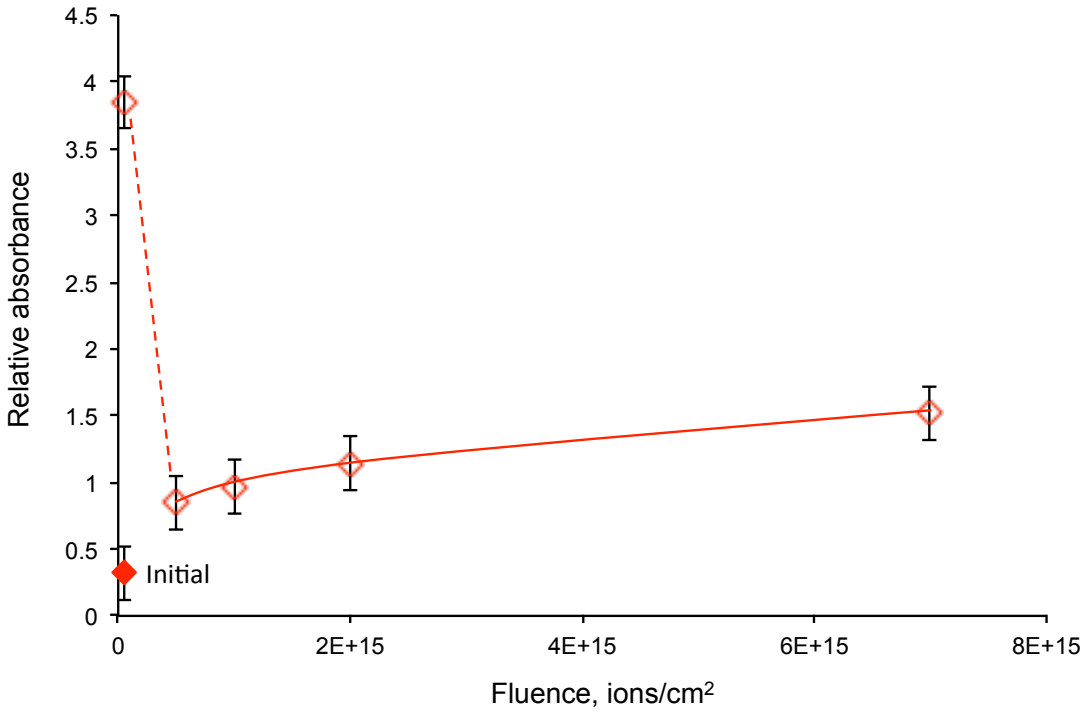

Fig.2. Ratio of absorbance of Amide I line of collagen shell and absorbance of Amide I line of polyurethane in FTIR ATR spectra of ion beam treated Polyurethane SKU-PFL after implantation in rat for 5 months. The fluence of 20 keV nitrogen ions is shown in ions/cm^2. The full sign (initial) corresponds the polyurethane sample before the operation.

Similar results were observed in optical microphotographs of the polyurethane films before and after being in the organism (Fig.3). The surface of initial polyurethane is sufficiently smooth in the scale of the image. The microphotograph of the untreated polyurethane after 5 months in rat organism shows a developed surface structure, which is interpreted as the collagen coating.

The microphotographs of the ion beam treated polyurethane before the organism show the crack structure, which corresponds to the cracking of brittle carbonised top layer. High fluence treatment gives deeper and frequent cracks on the surface than the low fluence treatment.

After the organism the surface of the ion beam treated polyurethane does not show the collagen covering. The surface of the ion beam treated polyurethane does not show any changes after the organism implantation.

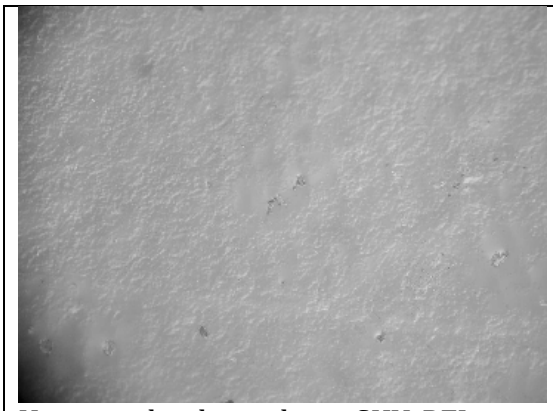

Untreated polyurethane SKU-PFL, no organism.

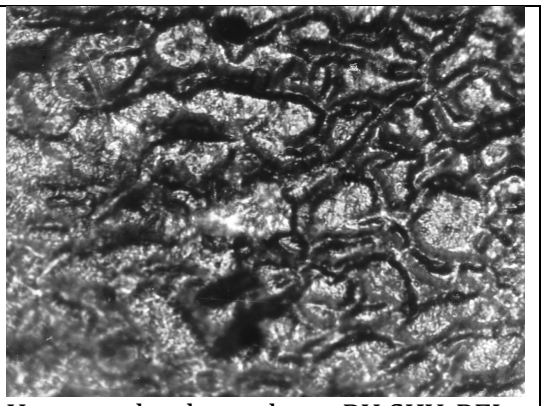

Untreated polyurethane PU SKU-PFL, implanted in rat for 5 months

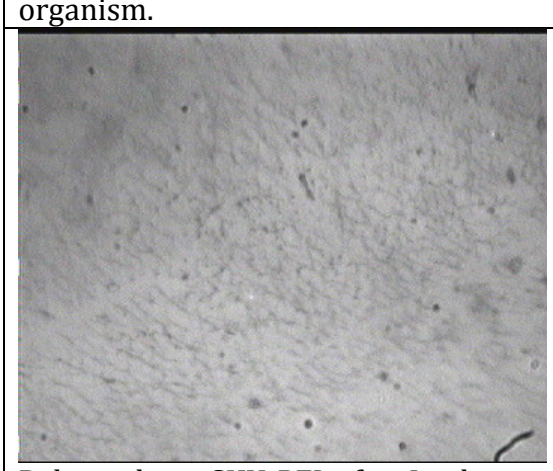

Polyurethane SKU-PFL after Ion beam treatment with 10^{13} ions/cm^2 fluence of 20 keV nitrogen ions, no organism.

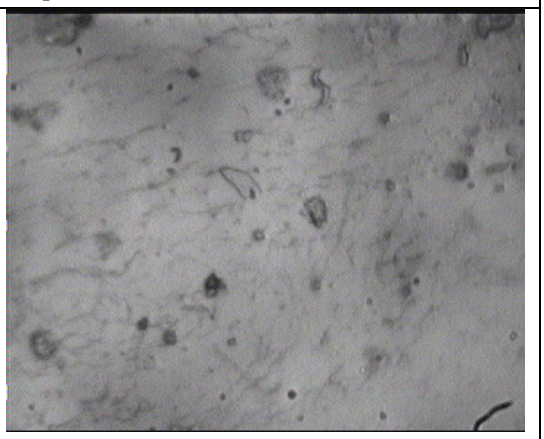

Polyurethane SKU-PFL after Ion beam treatment with 10^{13} ions/cm^2 fluence of 20 keV nitrogen ions, implanted in rat for 5 months.

Fig.3. Optical microscopy images of polyurethane after ion beam treatment implanted to rat for 5 months.

The scanning electron microscopy (SEM) images show similar results (Fig.4). The untreated polyurethane becomes covered by the collagen, while the ion beam treated polyurethane keeps the same surface like it was before it was implanted into the organism. However, the bottoms of each crack show the attached layer. Corresponding to FTIR ATR spectra the attached layer in the crack bottoms is probably the collagen coverage, which appeared during the exposure in organism, because the crack bottoms are untreated bulk polyurethane, where the organism cells can contact the untreated polyurethane.

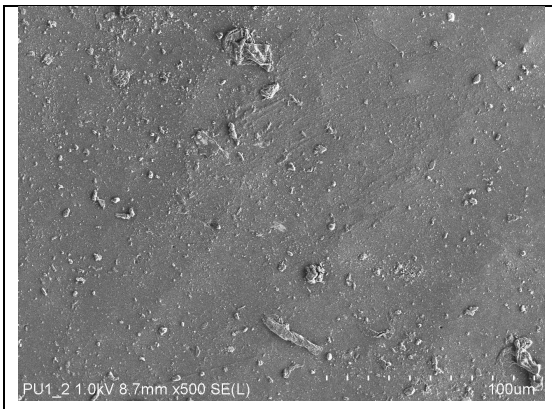

a. Initial untreated polyurethane

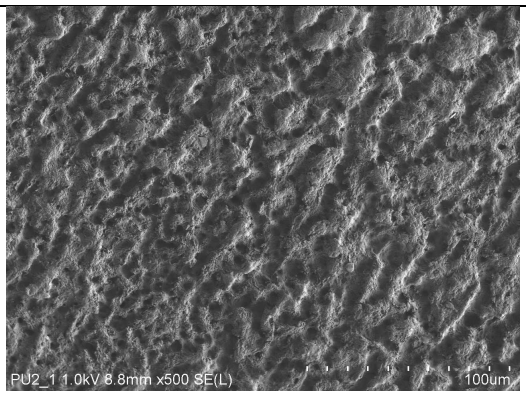

b. Untreated polyurethane after 5 months in rat organism

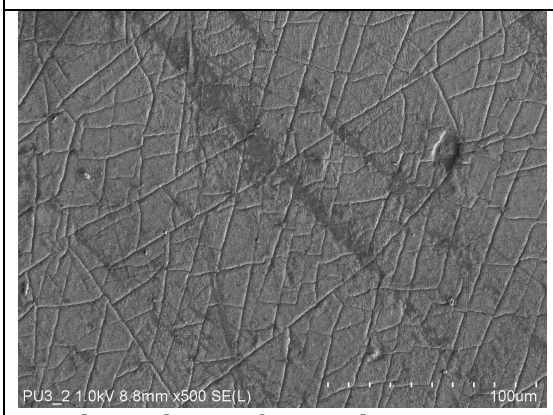

c. Polyurethane after ion beam treatment with 10^{16} ions/cm^2 fluence of 20 keV nitrogen ions

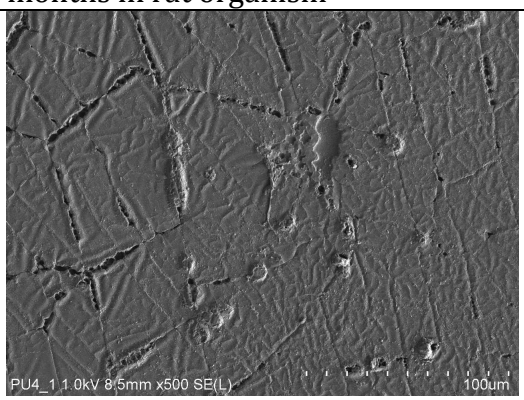

d. Polyurethane after ion beam treatment with 10^{16} ions/cm^2 fluence of 20 keV nitrogen ions and after 5 months in rat organism

Fig.4. Scanning electron microscopy (SEM) images of polyurethane after ion beam treatment and implantation in rat for 5 months.

The results of the investigations show that the untreated polyurethane causes a formation of the collagen covering as a result of immune response of the organism. The ion beam treatment decreases the collagen coverage on the polyurethane surface. Only the bottoms of the cracks in the carbonised layer where the untreated polyurethane is accessible to the organism cells, is covered by the collagen.

12th INTERNATIONAL CONFERENCE
ON HIGH-POWER PARTICLE BEAMS

BEAMS'98

HAIFA, ISRAEL, JUNE 7-12, 1998

PROCEEDINGS - VOLUME II

EDITED BY:
MEIR MARKOVITS
AND
JOSEPH SHILOH

IEEE

RAFAEL

Modification of polyurethane endoprostetics surface by pulse ion beam

[1]V. Begishev, [2]N. Gavrilov, [2]G.Mesyats, [3]Yu. Klyachkin, [4]I. Kondyurina, [1]I. Osorgina, [3]A. Kondyurin

[1]Natural - Scientific Institute, Perm State University, Perm, Russia
[2]Institute of Electrophysics, Russian Academy of Science, Ekaterinburg, Russia
[3]Institute of Technical Chemistry, Russian Academy of Science, Perm, Russia, kond@icmm.perm.su
[4]21a M.Ribalko st., Apt.17, Perm 614101, Russia

Implantation of any artificial prosthetics to an organism causes a foreign body reaction. Intensity of reaction depends on nature of the implanted material. Determination of foreign prosthetics material and initiation of reaction takes place on molecular level during interaction of body cells with prosthetics surface. In addition, a polymer surface layer is able to be destroyed under the organism medium action. On the other side, the usage of a carbon material as endoprosthetics induces the low reaction intensity of an organism [1]. So, the carbon coating of polymer endoprosthetics surface is preferred for decreasing of negative reaction of an organism.

Formation of carbon coating is possible by methods of vacuum deposition. But in this case the adhesion problem of carbon coating and polymer substrate appears. Similar problem appears in the case of chemical methods for carbon coating formation. More simple method for carbon coating on polymer substrate can be realized with the ion beam treatment. As it is well known, the ion beam treatment of polyethylene, polypropylene, polyimide and other polymers leads to carbon layer formation on polymer surface due to destruction processes in polymer surface layer under the action of the ion beam [2]. Therefore, this carbon layer has a good joint with polymer substrate.

In this paper, the influence of white rats organism medium on polymer endoprosthetics treated by ion beam is discussed. Medical polyurethane based on polyether, diisocyanate and diamin as films with 400 μ thick have been studied. Ion beam treatment was performed on the pulse ion source "Pulsar" (Institute of Electrophysics). The source generated the nitrogen ion beam with square of 100 cm^2, pulse current density of 5 mA/cm^2, pulse duration was 0.3 mS, frequency repetition was 1 Hz. Ion energy was 20 keV. Vacuum was created by oil vacuum pumps, the initial vacuum being $3 \cdot 10^{-3}$ Pa and vacuum under operating regime of the source being $5 \cdot 10^{-2}$ Pa. Polyurethane films were treated with dose from 10^{14} to 10^{16} ions/cm^2.

The polyurethane films were implanted to white rats for a 6 month period. The treated films aged in rat organisms and nearest to prosthetic tissues were studied by different spectral and histological methods. IR ATR spectra were recorded by using an UR-20 and Specord M-82 spectrometers (Carl Zeiss Jena, Germany) with ATR accessory on KRS-5 crystal (trapezium, 45^0 incident angle, 25 reflection number). Microphotographs of polyurethane surface were made with using of microscope MBS-10 (LOMO, Russia) with Zenit accessory.

The action of living organism tissue on polyurethane is the attack of organism active ferments to polyurethane prosthetic surface [3]. In the condition of active medium the hydrolysis of polyurethane leading to destruction of macromolecules and formation of low-weight products exists. At this case, durability of polyurethane film decreases and prosthetic loses its functional ability. Besides that, some products of reaction liberated into organism medium can have cancerogenic activity to organism [4]. Medical polyurethane has decreased

ability to hydrolysis. But hydrolysis of surface layer of this polyurethane exists with low speed of process [5].

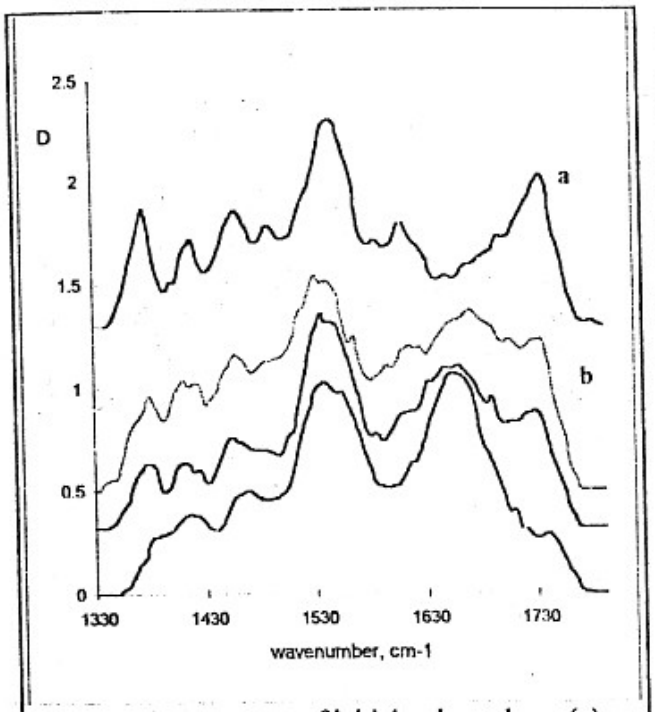

Fig.1. IR ATR spectra of initial polyurethane (a) and after action of organism (b) with increasing dose of ion bean treatment from 5 10^{14} to 7 10^{15} ion/cm^2.

Changes of polyurethane structure at hydrolysis in organism medium are observed in IR ATR spectra of polyurethane film surface as decreasing of spectral line intensity attributed to piece of macromolecules destructed in hydrolysis reaction. For the studied polyurethane, this piece of macromolecule is urethane fragment as the reminder of a toluenediisocyanate molecule. Hydrolysis reaction leads to formation of the second amine group and hydroxyl group with liberation of toluenediamine to organism medium. Decreasing of toluenediisocyanate reminder concentration were analyzed by 1375, 1415, 1490 and 1608 cm^{-1} lines intensity (Fig.1). Besides that, reaction of formation of guanidine group is observed by disappearing of carboxylic line in IR ATR spectra and appearing of intensive ν(C=N) line at 1665 cm^{-1}.

The ion beam treatment leads to carbon coating formation on polyurethane film surface. In differential IR ATR spectra the wide complex band of C=C groups vibrations in different positions and of C–O groups vibration appears (Fig.2). Similar changes of spectra were observed for polyethylene after the ion beam treatment [6]. Taking into consideration great difference between extinction coefficients of ν(C=C) and ν(C=O) lines in IR spectra, one can conclude that carbon layer is formed mainly consisting of a wide number of not saturated C=C bonds in different conjugations. The silvery shade of polyurethane surface which can be observed after the ion beam treatment characteristic of graphite covering, confirms it.

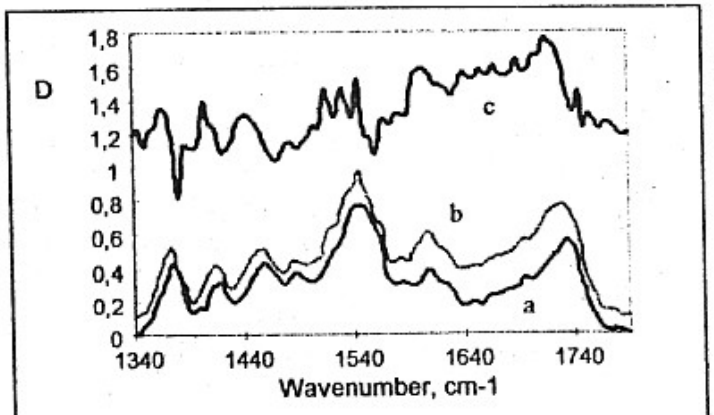

Fig.2. IR ATR spectra of (a) initial polyurethane, (b) after ion beam treatment and (c) their differential spectra.

Our observation of polyurethane surface with the help of microscope shows, that after the ion beam treatment polyurethane surface becomes covered by cracks (Fig.3). Cracks formation is explained by significant difference of stiffness of carbon covering and initial polyurethane. The carbon layer has thickness near the projected range of ion, which is about 757 Å in our experiments, so weak deformation of polyurethane film

leads to breaking of carbon covering and crack formation. Depth of cracks increases with the increase of a treatment dose.

The organism action on polyurethane samples after the ion beam treatment changes IR ATR spectra too. But intensity of these changes is weaker and depends on a treatment dose (Fig.1). The weakest spectral changes in comparison with the spectra of initial polyurethane are observed for samples with the lowest ion beam treatment dose. In the other words, low doses of ion beam treatment leading to thin carbon covering formation are more effective for the delay of hydrolysis processes. The analysis of stability of 1490 cm^{-1} line intensity in spectra of treated polyurethane showed that the hydrolysis processes at 5 10^{14} ions/cm^2 treatment dose are delayed 4 times as compared with untreated samples of polyurethane.

With the further increase of ion beam treated dose, the formation of thick carbon covering leads to formation of deeper cracks on polyurethane surface and hydrolysis of polyurethane under the action of organism medium takes place at these cracks. This is well observed by microphotographs of polyurethane surface after ion beam treatment at high dose and action of organism (Fig.3).

So, at low doses the ion beam treatment of polyurethane leads to carbon covering formation and can be the method for protection of polyurethane in organism medium.

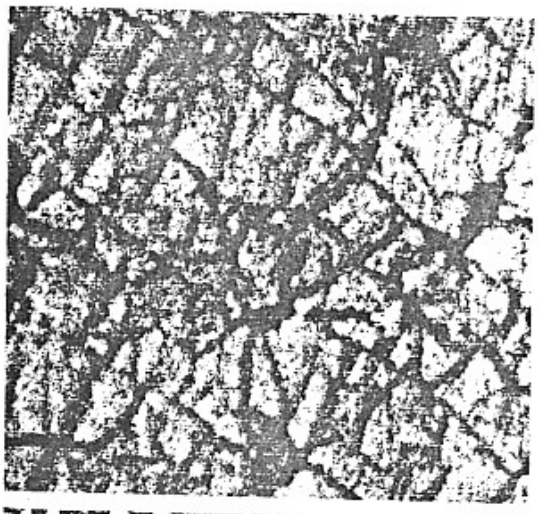

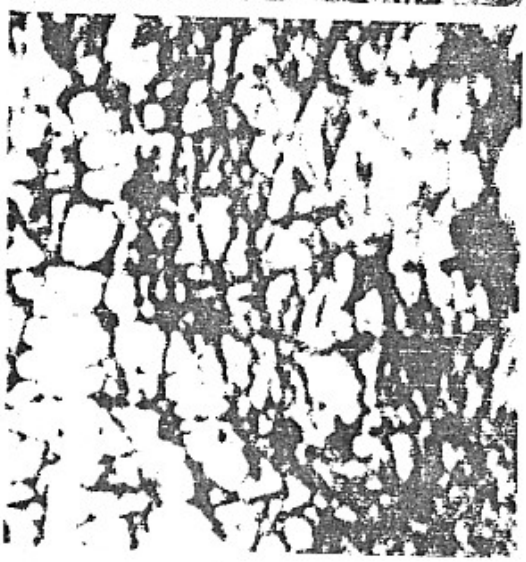

Fig.3. Microphotographs of polyurethane surface: after 5 10^{14} ion/cm^2, after 7 10^{15} ion/cm^2, after 7 10^{15} ion/cm^2 and organism action

References

[1] D.S.Borkos, Ceramics international, 9 (1), 3 (1983).

[2] L.Calcagno, G.Compagnini and G.Foti, Nucl. Instr. and Meth., B65, 413 (1992).

[3] T.E.Lipatova, G.A.Phakadze, Polymers in endoprostetics, Naukova Dumka, Kiev, 1983 (in Russian).

[4] W.J.Rea, Chemical Sensitivity, vol.1, Lewis publishers, Boca Raton, 1992.

[5] I.V.Osorgina, S.A.Plaksin, A.V.Kondyurin, V.P.Begishev, M.V.Subbotin, Posters, 3rd Int. Conf. "Modern approaches to the development of effective dressings, suture materials and polymer implants", May 26-27, 1998, A.V.Vishnevsky Institute of surgery, Moscow, p.254.

[6] G.A.Mesyats, Yu.S.Klyachkin, N.V.Gavrilov, V.N.Mizgulin, R.M.Yakushev, A.V.Kondyurin, Vacuum, 47 (9), 1085 (1996).

J. Biomater. Sci. Polymer Edn, Vol. 15, No. 2, pp. 145–159 (2004)
© VSP 2004.
Also available online - www.vsppub.com

Drug release from polyureaurethane coating modified by plasma immersion ion implantation

A. V. KONDYURIN[1,*], M. F. MAITZ[2], V. A. ROMANOVA[3], V. P. BEGISHEV[3], I. V. KONDYURINA[2,4] and R. GUENZEL[5]

[1] *Institute of Polymer Research, Dresden 01069, Germany*
[2] *Institute of Ion Beam Physics and Material Research, FZR, Dresden 01314, Germany*
[3] *Natural Scientific Institute, Perm State University, Perm 614600, Russia*
[4] *Institute of Continuous Media Mechanics, Perm 614013, Russia*
[5] *APT GmbH, Dresden 01314, Germany*

Received 14 February 2003; accepted 8 October 2003

Abstract—A crosslinked polyurethanurea (PUU) coating was synthesised from a solution on metal vascular stents. In the model system the glucocorticoid prednisolone was inserted into the film by the equilibrium swelling method; after this plasma immersion ion implantation (PIII) was applied to modify the coating for improved release kinetics. This treatment causes the formation of oxygen-containing and unsaturated carbon–carbon groups in the PUU and a destruction of the drug in the surface layer. As a consequence, the release rate of prednisolone to water becomes more stable with time than it is at the untreated coating. In this drug release system PIII treatment prevents an initial toxically high release of the drug. By this it allows the incorporation of a higher amount of the drug and an extended action.

Key words: Stent; polyurethane; drug release; plasma.

INTRODUCTION

The application of stents in combination with angioplasty of arteriosclerotic blood vessels has become a standard technique which is widely equivalent to by-pass surgery [1]. However, the application of a stent in the body often induces a local inflammatory reaction, proliferation of the smooth muscle cells and neointima formation [2–4]. This reaction can be reduced by application of a stent with polymer coating which contains anti-inflammatory or antiproliferative drugs. These drugs are released over a long time and reach effective concentrations only locally [5, 6]

*To whom correspondence should be addressed. Tel.: (49-351) 4658-528. Fax: (49-351) 4658-298. E-mail: kond@mailcity.com

at the vessel, without achieving effective concentrations systemically. One possible polymer for the coating is polyurethane, which has a high elasticity and a high strength. The residual deformation is low, high adhesion on metal, high resistance to water and to biological media can be obtained, further polyurethanes already have a good application as material for endoprosthetics [7]. As coatings on stents nowadays a linear polyurethane is used [8].

Drugs, like antibiotics [9], already have been incorporated in polyurethanes with good success. Usually this is done by adding the drug to a solution of the polyurethane. After evaporation of the solvent a layer of polyurethane incorporating the drug is formed. In particular, this technology is used for intravascular catheters. Catheters have a high risk of bacterial infection and polymers with antibiotics decrease the probability of catheter-associated infections.

An alternative method for inserting the drug is swelling of a linear polyurethane in a solution of the drug. In this case the swelling must be carefully controlled because the polyurethane may be dissolved and the coating destroyed [10]. This technology leads to an inhomogeneous distribution of the drug in the polyurethane and the kinetics of the drug release also will be non-uniform by time. Besides that, the linear polymer may become dissolved by blood lipids and soluble compounds are released into the blood flow [11].

A further technology to insert the drug is possible for a drug molecule, which is not reactive with the isocyanate groups of the prepolymer of the polyurethane. In this case the drug can be added to the reactive mixture before the reaction of the isocyanate groups of prepolymer with the active hydrogen group of the hardener [12]. In this case the distribution of the drug will be homogeneous in the polyurethane. By changing the reaction conditions the structure of the polyurethane and drug release kinetics can be modified. Further, the polyurethane can be synthesised with crosslinks, making it insoluble in any solvent and lipids.

The kinetics of drug release from a polymer to blood is generally described by the so-called ‘frontal process’ of water diffusion into the polymer. According to this model the release process is determined by the water front, which penetrates into the PUU film when it is exposed to water. The rate of the frontal process depends on the water diffusion coefficient into the PUU film, on the maximal swelling of PUU in water and on the solubility of prednisolone in water.

The first theoretical model of the drug release process was developed by Higuchi [13]. By experimental estimation, 80% of the drug is released by the frontal law and 20% of the drug amount is released by diffusion [14]. In general, the kinetics of the drug release from a swelling polymer are very complex. They depend on the solubility and the swelling of the polymer in water, the concentration limit of the drug in water and the distribution of the drug in the polymer [15]. Therefore, for real polymer–drug systems an experimental study is more preferable.

The regulation of the drug release is an important point for the development of a polymer-drug system. This regulation is possible by coating of the polymer with another polymer with a lower diffusion coefficient for water and the drug [16]. For

this technology a diffusion barrier layer slows down the drug release process from the polymer to the blood, so the drug release can be regulated by modification of the diffusibility and thickness of the barrier layer.

A change of the diffusion coefficient can also be achieved by various methods of polymer surface treatment [17]. In particular, ion-beam treatment of the polymer surface seems to be promising [18]. In this case, a very thin polymer layer is modified. The thickness of the modified layer can be adjusted by the ion species and their energy. Besides the diffusion coefficient regulation, it has been show that the ion-beam treatment can also increase the biocompatibility and the blood compatibility of polymers [19, 20]. Ion-beam treatment of polystyrene and polyurethane leads to a carbonisation of the surface layer, an increased wettability, improved adhesion of adherent growing cells and reduced blood-clotting activation. A similar structure formation is observed in polymers after plasma immersion ion implantation (PIII) as an alternative method of ion implantation [21, 22].

Therefore, the application of PIII treatment of polymer coating is promising for both the aspect of biocompatibility, as well as for the regulation of the diffusion of drug through polymer surface. In this study it is intended to insert a drug to a polyurethaneurea (PUU) coating of vascular stents and to study the drug-release kinetics before and after PIII treatment of the polyurethane surface. Prednisolone has been chosen as a model drug that decreases inflammatory reactions of the vessel wall in contact with the stent; however, the technique will be applicable also for some other, more effective drugs. The use of PIII treatment to obtain a smoother drug release profile should work also for other drug/polymer combinations.

MATERIALS AND METHODS

Synthesis of polyurethane

The synthesis of polyurethaneurea was made in two steps [23]. As a first step a prepolymer with active isocyanate groups was synthesised. A co-polymer of polyoxitetramethylene (POTM) and polyoxipropylene (POP) glycol (PF-OP-15, MM = 2000, Russia) with an oxitetramethylene/oxipropylene monomer chain ratio of 85 : 15 was used. Before synthesis the co-polymer was dried under $CaCl_2$. A 2,4-toluenediisocyanate (TDI) of industrial purity was used. This copolymer was a colourless transparent liquid without sediment. The purity of 2,4-toluenediisocyanate was determined by IR spectra. The synthesis of the prepolymer from the PF-OP-15 copolymer and 2,4-toluenediisocyanate was made in a vacuum chamber at 45°C over 6 h. After synthesis the prepolymer was stored refrigerated in closed glass container. The concentration of isocyanate groups in the prepolymer was determined by IR spectra and by titration.

As a second step a polyurethaneurea film was prepared from the synthesised prepolymer and 3,3′-dichlor,4,4′-diaminediphenylmethane (DA). The DA was recrystallised from benzene and stored light protected. For synthesis a reaction mixture of

DA and the prepolymer was prepared with a NCO/NH_2 molar ratio of 1 : 0.7. After mixing the composition was dissolved in distilled ethylacetate to a concentration of 10–30%, then the solution was applied on stents, glass, metal or Teflon substrates. After evaporation of the solvent the PU film was dried at 22°C and 50% moisture during 24 h. The film was put into a thermobox at 120°C to complete the polymerisation reaction. After annealing crosslinking of the polyurethaneurea was verified by swelling in tributylphosphate and dimethylformamide.

The synthesised polyurethaneurea has the following structure:

$$\text{-[POTM]}_n\text{-[POP]}_m\text{-CO-NH-[TDI]-NH-CO-NH-[DA]-NH-CO-NH-[TDI]-}$$

where $n = 24.31$ and $m = 4.29$.

Polyurethane films based on butylglycol (BGly), diphenylmethandiisocyanate (MDI) and ethylendiamine (EDA) with crosslinked and linear structures were used as polyurethaneurea coating for comparison. Contamination and characteristics of films of different PUU are presented in Table 1.

The PUU films with wide range of thickness were synthesised for different experiments. The thickness of PUU coating on metal stents could be done as low as 5–7 μm. PUU films for swelling and drug-release experiments with 400 μm thickness were prepared on glass substrate. The PUU films for strength test experiments were synthesised with thickness from 100 μm to 800 μm on glass, metal and Teflon substrates. The roughness of PUU surfaces was about 1 μm by electron microscopy measurements, their homogeneity was observed by optical microscopy. FT-IR spectra were used to control the PUU film structure between the different batches. In the experiment with different ion treatment dose, the PUU films were taken from a single batch. The swelling measurements of the films in alcohol were done in triplicate. A control of the swelling measurements was made for every sample at drug inserting procedure. The presence of the solvent in PUU film was checked by its characteristic spectral lines in the IR spectra. For drug release experiments, three samples of PUU for each of the 6 PIII different dose treatments were used.

Table 1.
Composition and characteristics of polyurethaneurea films

N	Formula	Polymer network	Concentration of hard blocks (% of MM)	Maximal swelling in ethanol (%)
1	BG+TDI+DA	crosslinked	12.6	90
2	BG+MDI+ED	crosslinked	17.2	75
3	BG+MDI+ED	linear	20.0	55, destroyed
4	BG+MDI+DA	crosslinked	22.0	50
5	PF-OP15+TDI+DA	crosslinked	12.0	40

Drug incorporation

For prednisolone incorporation the PUU film was swollen to equilibrium state in a solution of prednisolone in ethanol. Ethanol was chosen as solvent, because it has the following properties: a good solvent for prednisolone, a sufficient compatibility with the polyurethaneurea film for swelling but no dissolution of the PUU, good evaporation from the polyurethaneurea film and no toxicity. Prednisolone-21-hydrogensuccinate (Solu-Decortin, Merck, Darmstadt, Germany) was used as solution of the powder in ethanol. For this method, a chemical reaction of prednisolone with active groups of polyurethane was excluded because a drug is inserted into the inert PUU. As the film showed maximum swelling and the solvent was at equilibrium concentration through the whole thickness of the film, the distribution of prednisolone was more uniform than for non-equilibrium swelling.

After the synthesis, the polyurethane samples were allowed to swell in ethanol. Swelling was observed by measuring the mass of polyurethane disks with 35 mm diameter and 300 μm thickness. Weight measurements were made on an analytical balance (Sartorius). A kinetics curve of swelling is presented in Fig. 1. The rate of swelling and the maximal swelling depends on the type of polyurethane. All PUUs have sufficient compatibility with ethanol and swell to 40–100% by mass. The linear polyurethane did not dissolve in ethanol either, but due to swelling the internal stresses in film lead to cracks and destruction of the sample. In the case of polyurethane coating an increase in thickness of the polyurethane film leads to

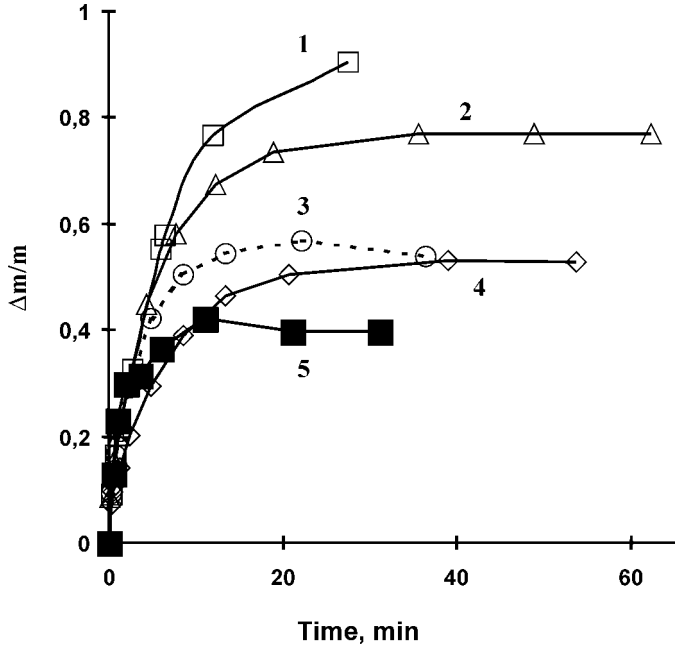

Figure 1. Swelling of polyurethane films in ethanol. The number of the curves corresponds to the PUU number in Table 1.

the formation of internal stresses in the coating and peeling of the coating from the substrate. Therefore, for the following experiments the polyurethaneurea based on PF-OP15 with lowest swelling in ethanol was chosen.

Before incubation with the drug the polyurethane samples were swollen in pure ethanol for 24 h and dried from ethanol to continuous weight. This treatment is intended to wash out low molecular products which could remain after the synthesis of the polyurethane. To incorporate the drug, a polyurethane was swollen in an ethanol solution of prednisolone with the prednisolone concentration of 1% by mass. The prednisolone concentration was calculated from a high-dose systemical treatment with 250 to 1000 mg per 70 kg body weight. The local prednisolone concentration in vessel wall of 14.2 μg/g was used for a calculation of the prednisolone concentration in PUU. This concentration should allow a prednisolone concentration available locally at the drug release system to be in the same range as it would be at medium to high systemic therapeutic application. For the calculation the maximum swelling of polyurethane in ethanol and a medium to high therapeutic concentration of prednisolone in the blood flow was used. However, real dose-finding studies must be subject of animal and clinical studies, as the distribution in blood and vessel wall may be not equal depending on the hydrophily of the drug.

Plasma immersion ion implantation

Plasma immersion ion implantation (PIII) was used for the treatment [24, 25] of the PUU coating on stents and PUU films. The PIII treatment is a well known method for modification of wide range of materials. The PIII treatment differs from usual plasma treatment due to high energy of ions [21]. By action of high energetic ions the PIII treatment has similar effects as ion beam treatment [22]. At PIII treatment a polymer sample is placed on an electrode in a high vacuum chamber. After evacuation to a base pressure of 10^{-3} Pa, a nitrogen plasma discharge is generated by a microwave source and negative high-voltage pulses are applied to the electrode with the samples, which is immersed in the plasma. The ions from the plasma get accelerated towards the electrode by the high-voltage pulses and bombard the polymer sample. The equipment of PIII is cheaper compared with ion beam accelerators. PIII already has industrial application for surface treatment.

For these experiments a nitrogen plasma was generated by a plasma source based on electron cyclotron resonance (ECR), with the density of 10^{10} cm^{-3} and an electron temperature of a few electron volts. The gas pressure during the treatment was 10^{-2} Pa. High-voltage pulses of 20 kV were applied to the sample holder which was immersed into the plasma. The PUU film were treated on both sides. The current density during the pulses was 16 mA/cm^2, the pulse duration was 5 μs, the frequency of pulse repetition was varied from 0.3 to 50 Hz, the dose of treatment was varied from 10^{13} to 10^{16} ion/cm^2.

Structure analysis

Optical microphotographs of the polyurethane surface were made (Axioskop, Carl Zeiss Jena with CCD camera, KS-100-3.0 Zeiss software). ATR–FT-IR spectra were recorded with Ge and KRS-5 crystals (trapezium, 450 reflection angle, 18 reflection number) at Bruker IFS-66s and Nicolet Magna 750 spectrometers with the corresponding software OPUS and OMNIC.

Determination of prednisolone release from polyurethane

For kinetics analysis a film of polyurethane was incubated in definite volumes of distilled water for a definite period of time. After that, the film was placed in the next aliquot of water and so on. Due to the low concentration of prednisolone in each volume of water solution (less than 10^{-4} mol/l) this method is close to the real blood flow, where the concentration of prednisolone does not influence the drug release kinetic.

A 300-μl droplet of each water aliquot after eluting the drug was posited on the Ge ATR crystal, distributed on the crystal surface and dried in a thermobox with air flow at 40°C. After evaporation of the drop the ATR–FT-IR spectra of the crystal were recorded. For quantitative analysis a calibrated curve was prepared with standard solutions with a defined concentration of prednisolone.

The intensity of the lines at 1720.7 cm^{-1} of carbonyl group vibration, at 1656.1 cm^{-1} and 1581.6 cm^{-1} of unsaturated C=C group vibrations, at 2936.5 cm^{-1} of C—H group vibration and at 3400 cm^{-1} of O—H group vibration for prednisolone, were used to determine the concentration. Calibrated curves by line intensity are presented in Fig. 2. From the drop volume and the concentration of prednisolone in the calibrated solutions it can be calculated that the thickness of the prednisolone layer in this study is lower than the penetration of the IR beam [26] and a linear part of the calibration curve is observed for this concentration range. In this study the linear part of the calibrated curve from 0.001 to 0.01 of FT-IR spectra optical density was used to determine the prednisolone concentration. At these concentrations the Bouger–Lambert–Beer law for optical density can be used for the quantitative analysis by intensity of IR spectral lines. At a high prednisolone concentrations (>0.1%), a thick layer is formed on the Ge crystal, so that the IR beam does not penetrate this film and the calibration curve looses its linear character. The average Prednisolone concentration was calculated from optical density of all analysed spectral lines. The signal/noise level of spectra for analysed lines was varied from 8 for spectra with lowest intensity to 100 for spectra with highest intensity. The repetition of FT-IR spectra showed that the optical density of analysed lines was reproducible with errors in the range of the background noise.

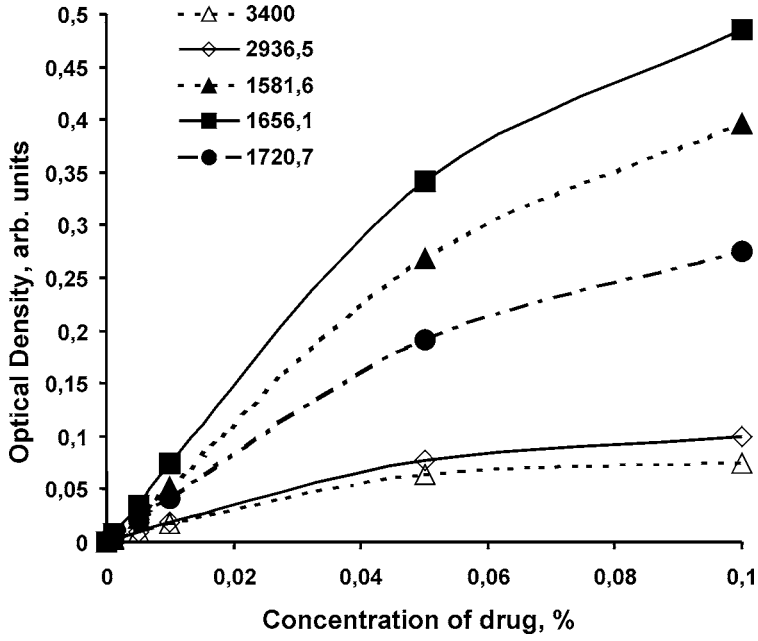

Figure 2. Calibration curve for different spectral lines (cm^{-1}) of ATR–FT-IR spectra of prednisolone from an aqueous solution.

RESULTS AND DISCUSSION

Kinetics of prednisolone release

Spectra of the sample volumes are presented in Fig. 3. The spectra of the probes contain the lines of the prednisolone at 1720.7, 1656.1 and 1581.6 cm^{-1}. This corresponds to the initial structure of the prednisolone molecules released from PUU. The first spectra of the sample volumes contain some additional lines in the regions of 1750–1550 cm^{-1} and 1470–1420 cm^{-1}, corresponding to low-weight molecules of PUU, which were formed during the polymerisation. These products appear in water only during the first day of elution; however, their concentration is too low for quantification. In the probes of the following days the low-weight PUUs were no more observed. The spectral lines of the prednisolone molecule and of the low-weight polyurethane molecules are clearly distinct, so the prednisolone concentration in the sample volumes can be determined by comparing with the standard.

The kinetics curve of the prednisolone release has a non-linear character with a very high concentration in the first sample volume (Fig. 4). In other words, the release rate is not constant, but it is highest in the beginning (Fig. 5). The kinetics curve of the prednisolone release corresponds to the frontal process of the drug release from a solid matrix by the theoretical model of Higuchi [13]. According to the frontal process theory, the non-uniform release of prednisolone into water is observed due to a quick diffusion of prednisolone from surface layer of PUU.

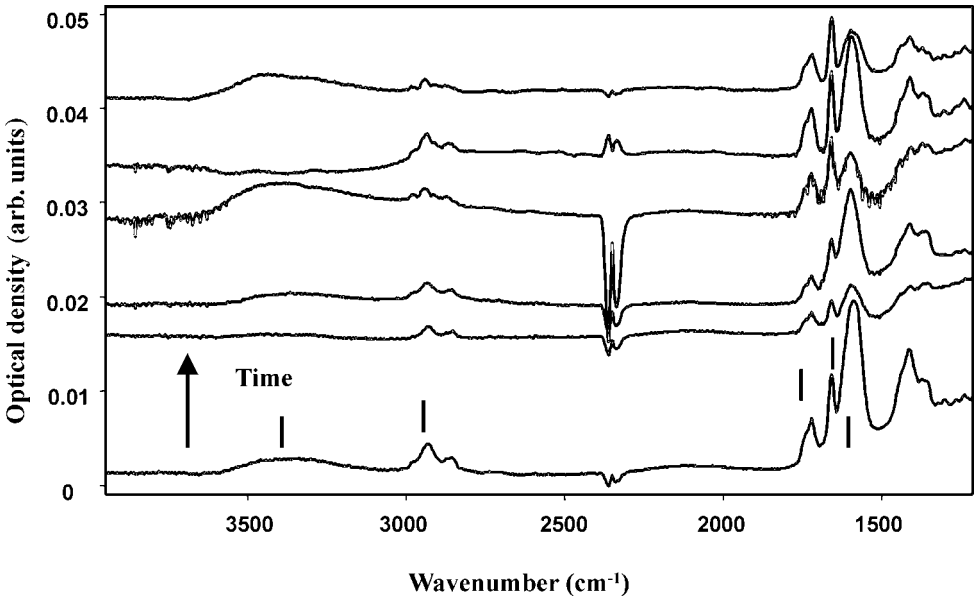

Figure 3. ATR–FT-IR spectra of prednisolone released from initial PUU to water at different points of time (from bottom to top): between 0 and 1 h, between 2 and 4 h, between 4 and 8 h, between 8 and 23 h, between 126 and 146 h, and between 263 and 341 h. The strokes show 3400, 2936.5, 1720.7, 1656.1 and 1581.6 cm^{-1} lines.

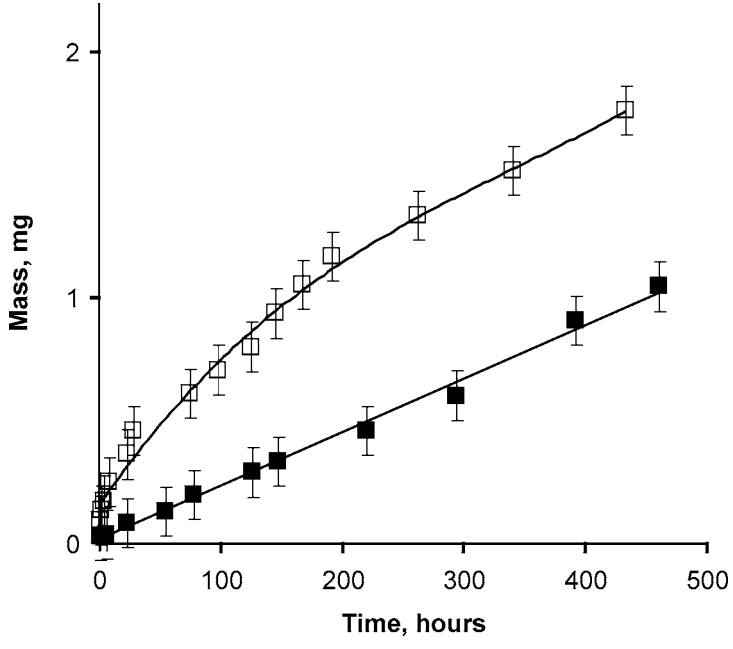

Figure 4. Kinetics of the drug release from PUU: light, initial PUU; full, PIII-treated PUU, dose is 10^{16} ions/cm^2.

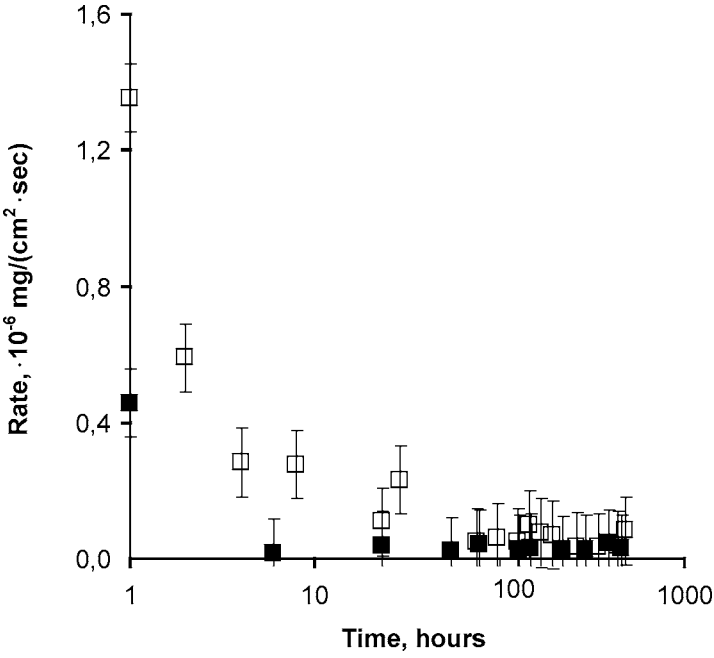

Figure 5. Rate of drug release from PUU: light, initial PUU; full, PIII-treated PUU, dose is 10^{16} ions/cm^2.

The principle of these drug-eluting stents is that a highly toxic drug is applied at high concentration only at the place where it is needed. At some distance the dilution is already so high, that there is no more toxic effect. In order to obtain long-term effective concentrations below the toxic threshold, a regulation of drug release, especially in the first period of time, is necessary.

PIII of polyurethaneurea

The PUU surface gets a metallic colour after plasma immersion ion implantation at doses of 10^{15} ions/cm^2 and higher, what is a common effect for carbon-chain polymers at ion-beam treatment [21]. It indicates the carbonisation of the PUU surface layer by PIII.

At increasing PIII doses the characteristic lines of PUU in the ATR–FT-IR spectra loose intensity (Fig. 6). An additional shoulder appears in the spectra at the 1730 cm^{-1} line of amide 1 vibrations in the region 1730–1600 cm^{-1} after normalisation of the spectra of PIII-treated PUU by the intensity of carbonyl and ether groups lines. The intensity of this shoulder increases with the dose of PIII treatment. In analogy to the spectra of carbon-chain polymers after PIII treatment, this shoulder indicates the appearance of new oxygen-containing and unsaturated carbon–carbon groups. These groups result from the destruction of the PUU macromolecules by the ion beam. With appearance of this shoulder, there is no obvious change in the ratio of ether, urethane and urea groups, indicating a weak

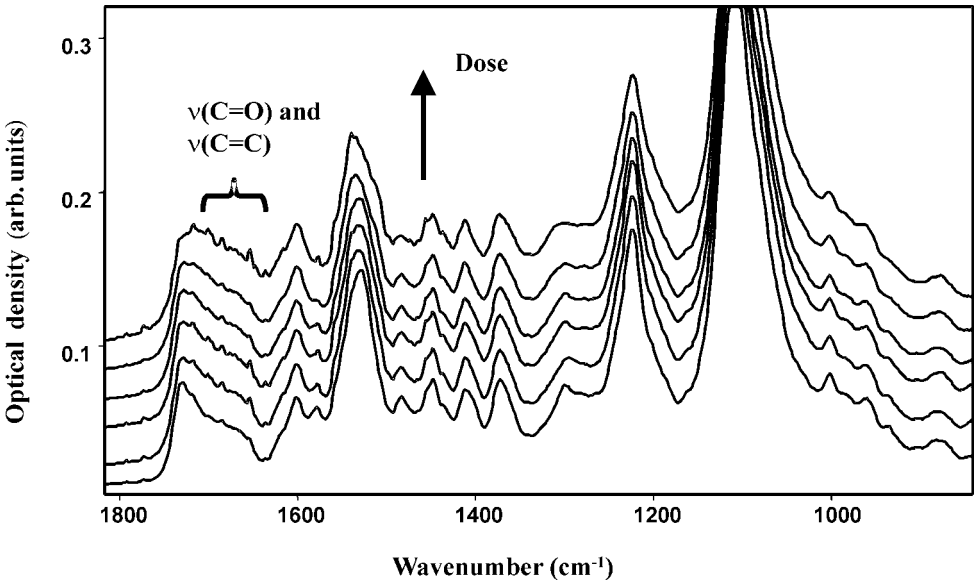

Figure 6. ATR–FT-IR spectra of PUU after PIII: not-treated, 10^{14}, 5×10^{14}, 10^{15}, 5×10^{15} and 2×10^{16} ions/cm^2.

selectivity of the destruction processes by PIII. This is in contrast to the destruction of polyurethane by environment factors like UV-light and thermal treatment, where defined reactions of depolymerisation and destruction of polyurethane by urea and urethane groups occur [28].

However, there are some small differences in the intensity of the different lines. A slight relative increase of the 1456 cm^{-1} line intensity is observed with increase of the PIII dose above 10^{15} ion/cm^2. This line corresponds to the deformation vibration of methyl and methylene groups in the ether part of the PUU macromolecule. The increase shows the higher stability of methyl and methylene groups in comparison to urea and urethane groups with heteroatoms in the main chain of the macromolecule. This corresponds to the inferior stability of polymer macromolecules with heteroatoms in the main chain under destructive conditions [29].

The intensity of the 1500 cm^{-1} line, corresponding to the vibration of aromatic rings at urea and urethane groups, has a slight tendency to decrease compared with the other lines. The decrease demonstrates the more intensive destruction of aromatic compounds near urea and urethane groups than of other groups. In the high-frequency region of the spectra the intensity of the 2937 cm^{-1} line, corresponding to methylene group vibrations and the intensity of 2917 cm^{-1} line, corresponding to methyl group vibrations, show an increase of branch numbers in macromolecules. Lines at 3000–3100 cm^{-1}, which correspond to C—H vibrations in aromatic structures, do not appear. Obviously, in the case of PUU the formation of condensed aromatic groups occurs without a significant formation of C—H groups.

This is in contrast to the behaviour of polyethylene at PIII and ion beam treatment. In the region of 3600–3100 cm^{-1} a very wide band which overlaps with the stretch ν(NH) vibration lines (amide A) appears. This band corresponds to the vibrations of hydroxyl groups, which appear in the surface layer of PUU after PIII. At high dose of PIII the spectral lines become wider in all regions of the spectra. This indicates an increased concentration of structural defects and a breakdown of periodical structures in the PUU macromolecules.

These structural changes of polyurethane are different from the usual reaction of polyurethane degradation by the ways of substitution and exchange reactions [28]. The destruction reactions in polyurethane under PIII are not selective due to extremely high local energy transformations and high concentration of free radicals in the track region of the penetrated ions. Therefore, at PIII treatment the reactions of depolymerisation to oligomers and monomers are not possible, what otherwise happens for polyurethanes. The surface layer of treated PUU has a higher concentration of carbon structures with condensed aromatic groups and oxygen-containing groups than other types of polymers. The concentration of hydroxyl groups in the treated PUU, as observed by the intensity of the ν(OH) line is higher than, for example, in treated polyethylene [22]. Obviously, this high concentration of OH groups is caused the by high concentration of oxygen in the macromolecule of the polyurethane. The hydroxyl groups in PUU under PIII are formed mainly by a substitution reaction and only to a minor degree by free radicals reactions with air oxygen, what would be the usual way for carbon-chain polymers under PIII and ion-beam treatment. The thickness of PUU layer modified by PIII was estimated from calculation by TRIM codes as 100 nm.

In conclusion, after PIII the surface layer of PUU has a very different structure compared with the initial PUU structure. These huge changes of the structure may also change the diffusibility of the film surface of PUU for prednisolone.

Kinetics of prednisolone release from the modified polyurethaneurea

ATR–FT-IR spectra of water samples after immersion of PIII-treated PUU with prednisolone are presented in Fig. 7. As in sample volumes of initial PUU, in these spectra the lines of the released prednisolone are observed. The positions and the intensity of the prednisolone lines correspond to the spectra of the initial drug. In the spectra there are no additional lines, which would indicate degradation products of the prednisolone molecule or of the PUU. The reason for missing lines of destruction products may be the degradation of the drug molecule to very small products. These products can evaporate to the vacuum chamber at PIII. Besides that, some parts of the prednisolone molecule can be crosslinked with the carbonised PUU layer during the PIII, so that they can not be released into the water.

The kinetics of the prednisolone release from the modified PUU still has a non-linear character, as was observed for the initial PUU (Fig. 4). The frontal character of the release kinetics remains, but the release rate in the beginning is lower. This is caused by the destruction of the prednisolone molecules in the surface layer of PUU,

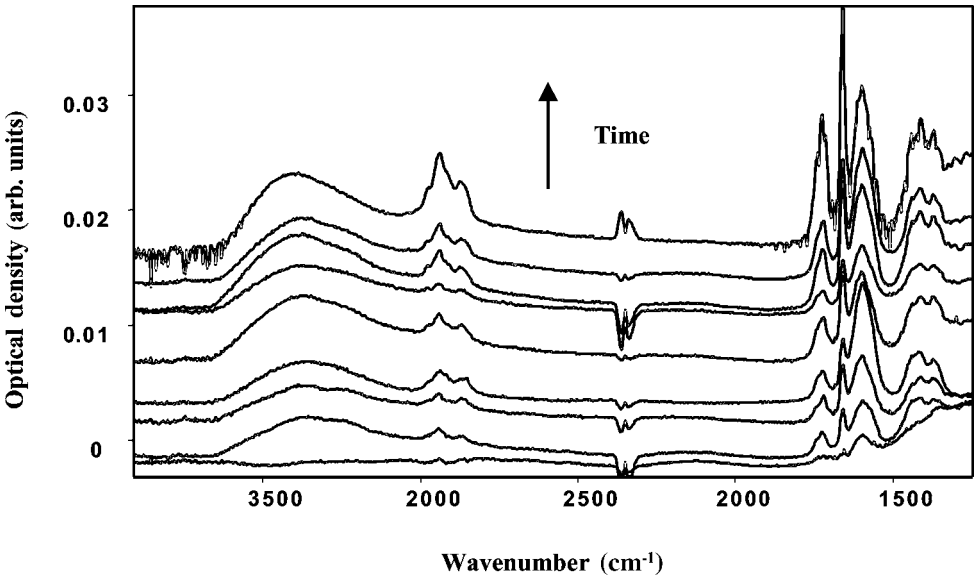

Figure 7. ATR–FT-IR spectra of prednisolone released from modified PUU to water at different times. From bottom to top: between 0 and 1 h, between 2 and 4 h, between 4 and 6 h, between 6 and 15 h, between 47 and 71 h, between 71 and 95 h, between 151 and 248 h, between 248 and 343 h, and between 416 and 482 h.

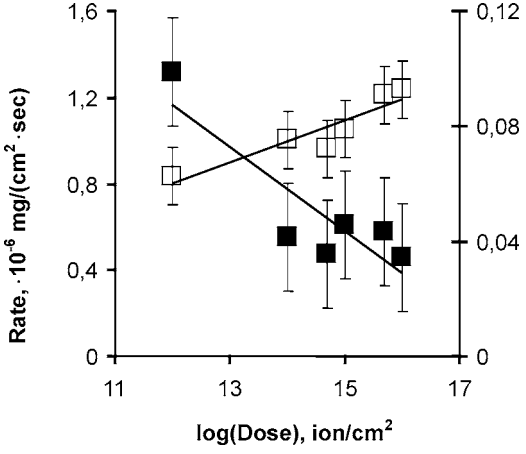

Figure 8. Dependence of the prednisolone release rate from PUU from the ion dose. Filled squares, at 2 h in water (left scale); open squares, at 400 h in water (right scale).

so at the first period of water diffusion no prednisolone molecules are available to be washed out. In consequence the rate of prednisolone release from the treated PUU the first period is suppressed in comparison to the untreated PUU (Fig. 5). The release rate in the first period of the drug release is relatively independent from the ion dose used (Fig. 8). Obviously, already at a low treatment dose most of

the surface of prednisolone molecules are destroyed and an increase of the PIII treatment dose can not further decrease the release rate.

The long-term release rate of prednisolone from PUU increases with the treatment dose of PIII (Fig. 8). The reason may be in an increased diffusion coefficient of water through the surface layer of the modified PUU. The carbonised and oxidised layer of PUU is more hydrophilic than the initial PUU, this facilitates the penetration of water and the release of prednisolone molecules.

The decrease of the prednisolone release rate at the first period of the kinetics and the increased long term release rate leads to a more homogeneous release of the drug. The concentration of the released prednisolone from the PIII-treated PUU to water or to the organism of a patient will be more stable than from non-treated PUU. Thus, even a higher concentration of prednisolone can be incorporated in the PUU to assure therapeutic level for a longer time without initial toxic concentrations. This will be important especially for other drug/polymer combinations currently under investigation.

CONCLUSIONS

This study showed that the technology of synthesis of crosslinked polyurethaneurea from solution can be used to create an elastic, drug-containing coating on stents. The model drug prednisolone can be incorporated in the coating by the method of equilibrium swelling in a solution of the drug. The drug release kinetics has a frontal character corresponding to the model of Higuchi [13]. By means of plasma immersion ion implantation a carbonised surface layer of the PUU is formed, which allows a more constant drug release rate with time. This will permit to increase the concentration of prednisolone in coating and to reach a longer action of the drug.

Acknowledgements

The study was supported by grant of WTZ RUS01/225 and RUS00/218 of German Ministry of Science and Russian Ministry of Science and by Alexander von Humboldt Foundation in the part of plasma immersion ion implantation of polymers.

REFERENCES

1. P. W. Serruys, P. de Jaegere, F. Kiemeneij, C. Macaya, W. Rutsch, G. Heyndrickx, H. Emanuelsson, J. Marco, V. Legrand, P. Materne, J. Belardi, U. Sigwart, A. Colombo, J. J. Goy, P. van den Heuvel, J. Delcan and M.-A. Morel, *New Engl. J. Med.* **331**, 489 (1994).
2. R. S. Schwartz, J. G. Murphy, W. D. Edwards, A. R. Camrud, R. E. Vliestra and D. R. Holmes, *Circulation* **82**, 2190 (1990).
3. J. A. Bittl, *New Engl. J. Med.* **335**, 1290 (1996).
4. E. J. Topol and P. W. Serruys, *Circulation* **98**, 1802 (1998).
5. M.-C. Morice, P. W. Serruys, J. E. Sousa, J. Fajadet, E. Ban Hayashi, M. Perin, A. Colombo, G. Schuler, P. Barragan, G. Guagliumi, F. Molnar, R. Falotico and the RAVEL Study Group, *New Engl. J. Med.* **346**, 1773 (2002).

6. F. Liistro, G. Stankovic, C. Di Mario, T. Takagi, A. Chieffo, S. Moshiri, M. Montorfano, M. Carlino, C. Briguori, P. Pagnotta, R. Albiero, N. Corvaja and A. Colombo, *Circulation* **105**, 1883 (2002).
7. H. Plank, I. Syre, M. Dauner and G. Egbers, *Polyurethanes in Biomedical Engineering, Volume II*. Elsevier, Amsterdam (1987).
8. P. W. Serruys and M. J. B. Kutryk (Eds), *Handbook of Coronary Stents,* 2 edn. Martin Dunitz, London (1998).
9. W. Marconi, I. Francolini, A. Piozzi and R. Di Rosa, *J. Bioact. Compat. Polym.* **16**, 393 (2001).
10. T. L. Lambert, US Patent 385373 (1995).
11. A. Takahara, K. Takahashi and T. Kajiyama, *J. Biomater. Sci. Polymer Edn* **5**, 183 (1993).
12. M. Grigorieva, I. Gladir and N. Galatenko, *J. Bioact. Compat. Polym.* **16**, 307 (2001).
13. T. Higuchi, *J. Pharm. Sci*. **52**, 1145 (1963).
14. B. C. Anderson and S. K. Mallapragada, in: *American Physical Society Meeting March 2000*, Minneapolis, MN, C9.002 (2000) (Abstract).
15. D. S. Cohen and T. Erneux, *SIAM J. Appl. Math*. **58**, 1193 (1998).
16. D. Yang, J. L. Stanslaski, L. Wang and S. R. Smith, US Patent No. 346975 (2001).
17. C. Zhao and M. N. de Pinho, *Polymer* **40**, 6089 (1999).
18. D. Fink, S. Ghosh, R. Klett, K. K. Dwivedi, Y. Kobayashi, K. Hirata, J. Vacik, V. Hnatowicz, J. Cervena and L. T. Chadderton, *Nucl. Instr. Methods B* **146**, 486 (1998).
19. Y. Suzuki, M. Kusakabe, J. S. Lee, M. Kaibara, M. Iwaki and H. Sasabe, *Nucl. Instr. Methods B* **65**, 142 (1992).
20. L. Dejun, Z. Jie, G. Hanqing, L. Mozhu, D. Fuqing and Z. Qiqing, *Nucl. Instr. Methods B* **82**, 57 (1993).
21. A. Kondyurin, V. Karmanov and R. Guenzel, *Vacuum* **64**, 105 (2002).
22. G. A. Mesyats, Y. S. Klyachkin, N. V. Gavrilov, V. N. Mizgulin, R. M. Yakushev and A. V. Kondyurin, *Vacuum* **47**, 1085 (1996).
23. V. Romanova, V. Begishev, V. Karmanov, A. Kondyurin and M. F. Maitz, *J. Raman Spectrosc.* **33**, 769 (2002).
24. S. Mandl, J. Brutscher, R. Guenzel and W. Moller, *J. Vac. Sci. Technol. B* **14**, 2701 (1996).
25. S. Mandl, J. Brutscher, R. Guenzel and W. Moller, *Surf. Coat. Technol.* **93**, 234 (1997).
26. N. J. Harrick, *Internal Reflection Spectroscopy.* Harrick Scientific, New York, NY (1987).
27. N. Gavrilov, D. Yakusheva and A. Kondyurin, *J. Appl. Polym. Sci*. **69**, 1071 (1998).
28. N. Grassie and G. Scott, *Polymer Degradation and Stabilization.* Cambridge University Press, Cambridge (1985).
29. B. Renby and J. F. Rabek (Eds), *Photodegradation, Photo-oxidation and Photostabilization of Polymers.* Wiley, London (1975).

Crosslinked Polyurethane Coating on Vascular Stents for Enhanced X-ray Contrast

ALEXEY KONDYURIN,[1,*] VALENTINA ROMANOVA,[2] VALERY BEGISHEV,[2] IRINA KONDYURINA,[3] REINHARD GUENZEL[4] AND MANFRED F. MAITZ[5]

[1]*Institute of Polymer Research Dresden, Hohe Strasse 6, Dresden 01069, Germany*

[2]*Natural Scientific Institute, Perm State University, Perm 614600, Russia*

[3]*Institute of Continuous Media Mechanics, Perm 614013, Russia*

[4]*APT GmbH, Dresden 01314, Germany*

[5]*Institute of Ion Beam Physics and Materials Research, FZR, Dresden 01314, Germany*

ABSTRACT: A coating of polyurethaneurea was made from a solution on the surface of metal stents. The influence of cleaning, etching, chemical and ion beam modification (plasma immersion ion implantation) of the metal surface on the adhesion strength of the polyurethaneurea was analysed. Polyurethaneurea films imbedded with tantalum particles as a radiopaque filler maintained their strength and elasticity and produced clear X-ray contrast images of vascular stents.

KEY WORDS: stents, polyurethane, polyurethaneurea, coatings, tantalum, X-ray, ion beam.

INTRODUCTION

The application of stents in combination with angioplasty of arteriosclerotic blood vessels has become a standard procedure that is now widely used instead of bypass surgery [1]. The success of the stent technology is the result of improved devices and application techniques

*Author to whom correspondence should be addressed.
E-mail: kond@mailcity.com

0883-9115/05/01 0077–17 $10.00/0 DOI: 10.1177/0883911505049896
© 2005 Sage Publications

[2–7]. For stents to work well, sufficient mechanical stability in the blood vessel and good biocompatibility are basic requirements. However, some problems still need to be solved, such as local inflammatory reactions [8,9], the proliferation of vascular smooth muscle cells, neointima formation [10] and, technically, compatibility with diagnostic imaging techniques [11,12].

One approach to overcome these problems was to apply a polymer coating on the metal stent [4–7]. The polymer coating acted as a drug release system to decrease the restenosis [13] and, with the use of advanced drugs, these stents have became the state-of-the-art technology [14,15].

X-ray visibility of the stent is considered important, more for the follow up, than for implanting the stent [12]. For this, radiopaque stents were made of pure tantalum [16–18]; however, the mechanical properties of this metal are lower than those of steel, and the stents did not receive high acceptance in the field. Coating the stainless steel stents with gold, as an X-ray dense material, was done to combine both properties [19,20]; however, increased restenosis rates were found for these stents in clinical applications [21].

In this study, to increase the X-ray contrast, tantalum particles were added [22] to the polymer coating. In contrast to a thick coating of tantalum metal, the polymer added flexibility to the properties of the stent. However, there were problems with these polymer coatings. For example, highly filled polymers usually lost elasticity [23], which caused problems at the high deformations needed during stent implantation. Furthermore, the bonding of these coatings to the stent was weak. Therefore, the maximum concentration of tantalum filler in the stent coating is limited.

For applications in blood, good adhesion of a coating on the stent is required to prevent migration of water into the interface. Usually, polymer adhesion to a metal surface is low and not sufficient for constructions that undergo high deformations. Therefore, an interactive bond is needed between the stent and polymer coating.

In this study, polyurethane coatings were synthesized directly on the stent surface [24,25]. Polyurethanes have good elasticity and have wide biomedical applications as materials for endoprostheses [26–28]. Using composition and synthesis conditions, physical and chemical properties of polyurethanes can be adjusted for biocompatibility. A polyurethane subclass, polyurethaneurea (PUU) has urea groups in the macromolecule that form a hard domain structures. These structures improve the strength of the polymer without significant change in the elasticity, thus opening a wide field of mechanical applications.

MATERIALS AND METHODS

Polyurethaneurea was synthesized in a two-step process [29]. The first step involved preparing a prepolymer with active isocyanate groups from a copolymer of poly(tetramethylene-propylene glycol) (PF-OP-15, Mw = 2,000); the ratio of tetramethylene to propylene chains was 85:15. The copolymer was dried over $CaCl_2$ before synthesis. The industrial grade 2,4-toluenediisocyanate (TDI) used was a colorless, transparent liquid without sediment; the purity was verified by IR spectroscopy. The PF-OP-15 copolymer and toluene dissocynate (TDI) were reacted in a vacuum chamber at 45°C for 6 h. The prepolymer obtained was stored in a closed glass tube and refrigerated. The concentration of isocyanate groups in the prepolymer was determined by IR spectra and by titration.

In the second step, a polyurethaneurea film was prepared using the prepolymer and 3,3'-dichloro-4,4'-diaminediphenylmethane (diamine was recrystallized from benzene and stored light protected) in the molar ratio of 1:0.7 NCO:NH_2. After mixing, the composition was dissolved in distilled ethyl acetate to produce a series of concentrations (10–30%). At this stage tantalum powder (100–1000 nm) was added to the reaction mixture as a filler. This mixture was applied to the surface of glass and metal substrates. After evaporation of the solvent, the film was dried at 22°C and 50% humidity for 24 h. Then polymerization was carried out at 120°C. After annealing, the polyurethaneurea crosslinked polymer network was verified by swelling in tributylphosphate.

The PUU coatings were also synthesized on carotis stents made of stainless steel and nitinol 4.5 and 6.5 mm diameter and a strut diameter of 400 μm (Optimed, Germany). These stents were coated in the expanded shape. The thickness of the PUU coating with tantalum particles was 10 μm, and the thickness of the PUU coatings without filler could be adjusted from 5 to 30 μm. Complete coating of the stents (including the holes) were performed with PUU at a thickness of 100–120 μm.

The PUU films were synthesized on glass substrates to test the polymer strength. After polymerization, the films were peeled from the glass surface and stored for 14 days at room temperature of 20°C. Strips 100 × 10 × 0.3 mm were tested on a tensile stress machine R-500 (analog Instron, Russia) at a deformation speed of 200 mm/min. The strength of the tantalum filled PUU films 50 × 5 × 0.3 mm in size was determined on a Z010 (Zwick, Germany) at the same testing parameters.

For adhesion testing, symmetrical joints of PUU–stainless steel foil–PUU were prepared with metal foils 50 μm thick. The surface of the metal foil was pre-treated by cleaning with ethanol, etching with phosphoric acid, coating with toluene diisocyanate, ion implantation and by combinations of these methods. PUU coatings 50 μm thick were synthesized on the metal foil after surface treatment. Strips (50 × 4 mm) were cut and peel tested. The adhesion strength was determined from a strain–stress diagram at the plateau of maximum values. Accelerated ageing of the adhesion joints was performed in a water bath at 70°C for 96 h.

Ion implantation of the metal foil was performed in a plasma immersion implantation (PIII) chamber. Nitrogen plasma (density of 10^{10} cm^{-3}) and electrons were generated by a plasma source based on electron cyclotron resonance. The gas pressure during treatment was $5 \cdot 10^{-1}$ Pa. The foil was conductively mounted on a sample holder and immersed in the plasma. High voltage pulses of 20 kV with 5 μs pulse duration were applied to the sample holder. The current density during the pulse was 16 mA/cm^2, and the total treatment dose was 10^{15} ion/cm^2.

FTIR spectra were recorded on an IFS-66 spectrometer (Bruker, Germany). FTIR ATR spectra were recorded with an ATR accessory on a KRS-5 and Ge crystal. Analysis of the spectra was made with the OPUS program (Bruker, Germany). Spectral analyses were made on the basis of deconvolution and their second derivation.

The evaporation of the solvent was measured with a thermogravimetric analyzer Q-1500D (MOM, Hungary). The solution was placed in an open cell and the mass loss rate was recorded at constant temperature without air movement. The evaporation rate was calculated on the open area of the cell, initial mass and the mass loss with time.

The rate of the second step of the polymerization process at different temperatures was followed by viscosity. A RHEOTEST-2 viscometer with a cylinder-in-cylinder cell thermo-stabilized by silicon oil flow from a thermostat was used. The experimental viscosity rates were recorded to the gel-point of the mixtures.

X-ray imagines of the stents were made on an AXL Multix Top X-ray Analyser (Siemens, Germany) at 40 keV, 5 cm distance from the CCD detector.

RESULTS

Polyurethaneurea films were synthesized from a prepolymer mixture; an ethyl acetate solution was applied as a thin coating on the

metal stents, it adhered to the surface by the interfacial energy. The thickness of the film depended on concentration and viscosity of the solution. A lower concentration led to lower viscosity and thinner coatings. During the synthesis the solvent evaporated, in-parallel polycondensation and film structure formation took place. The synthesis is a complex physical–chemical process that determines the quality of the polyurethaneurea film. The steps in this process were investigated in order to optimise the coating.

The synthesized polyurethaneurea has the following structure:

—[PF—OP—15]—CO—NH—[TDI]—NH—CO—NH—[DA]—
NH—CO—NH—[TDI]—

Solvent Evaporation

The evaporation of the solvent was measured in an open cell under conditions close to those of the stent surface; the rate of the mass loss was recorded.

Shown in Figure 1 is a fast increase in the concentration up to

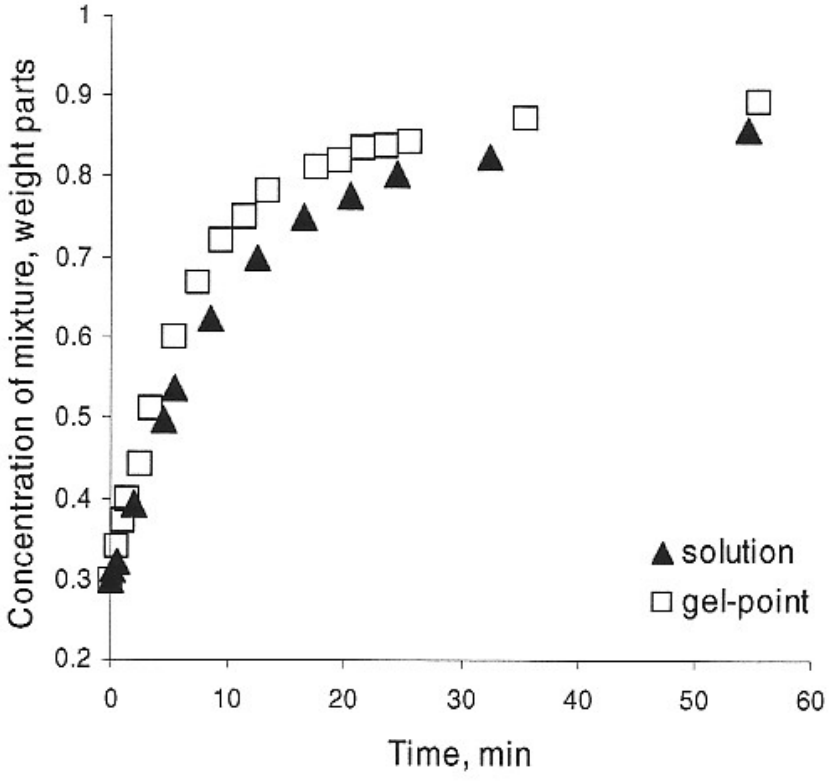

Figure 1. Evaporation of ethyl acetate from the reaction mixture during polymerization: evaporation was allowed to start at immediately after mixing (triangle) or the evaporation started when the gel point was achieved (square).

60–70% at first, and then the increase slowed. The fast increase is due to evaporation from the film, which was found to be close to the evaporation rate of the pure liquid. In the second phase, the evaporation was limited by the diffusion of the solvent from the polymer matrix. Due to the lower evaporation rate, some solvent remained in the reaction mixture during the polymerization. At the gel-point the solvent phase separated from the PUU phase and the evaporation rate increased again.

The time of the solvent evaporation increased with the thickness of the polymer solution coating (Figure 2). Therefore, 700 μm thick films still contained some solvent during the polymerization, whereas thinner films (200 μm) did not.

Polymerization Rate

The rate of polymerization was followed by the FTIR transmission for isocyanate at 2273 cm^{-1} (Figure 3) and by viscosity at 60°C for different concentrations of the reaction mixtures that are shown in Figure 4. The polymerization was found to be second order. At 0.56,

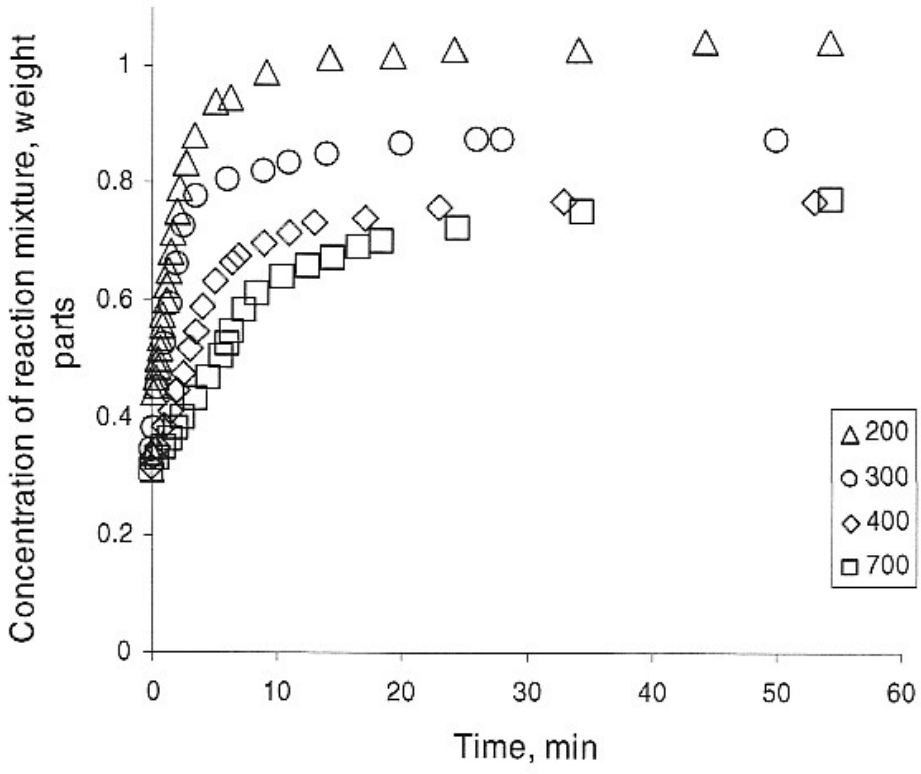

Figure 2. Evaporation of ethyl acetate from the reaction mixture of different layer thickness (μm).

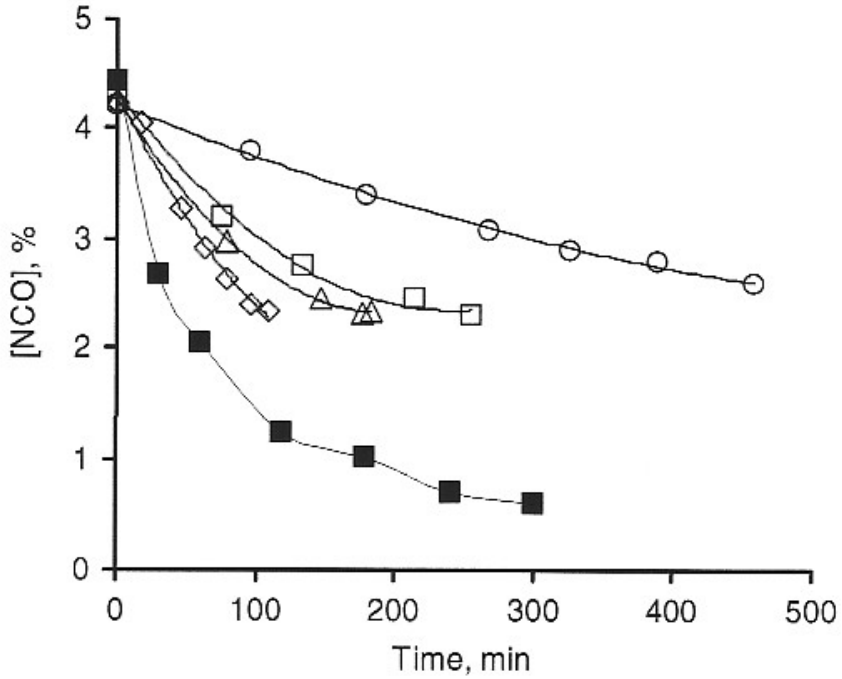

Figure 3. Rate of the NCO group increases during the polymerization reaction in solutions with different concentrations of the prepolymer mixture: circles – 30%, square – 50%, triangles – 70%, rhombus – 80% and full square – 100%.

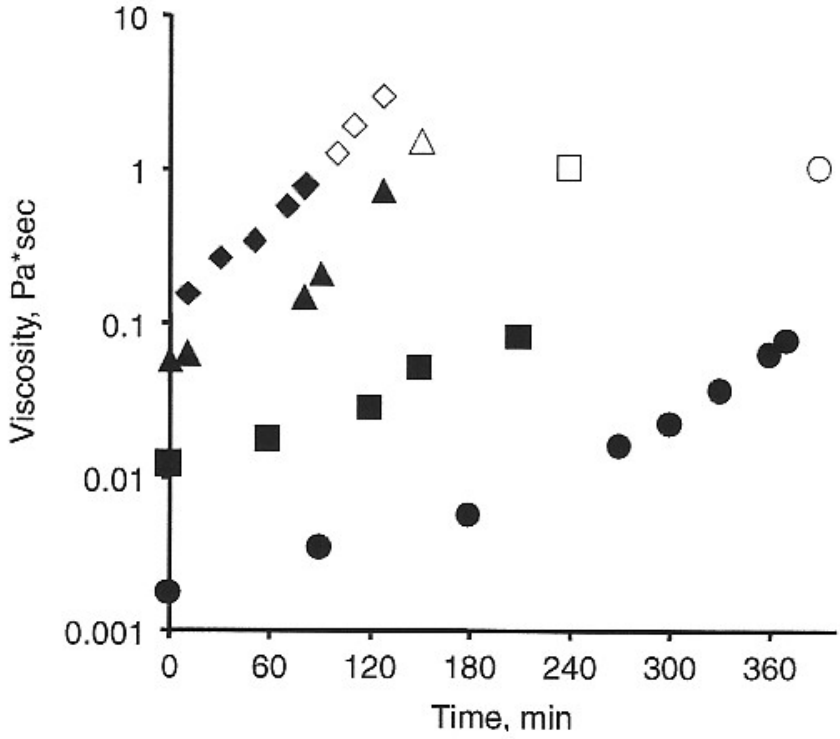

Figure 4. Viscosity of the PUU solution during the polymerization reaction. Symbols indicate different concentrations of the prepolymer solution: circles – 30%, square – 50%, triangles – 70%, rhombus – 80%. Empty symbols indicate the gel-formation.

conversion of the isocyanate groups and the viscosity increased sharply with the formation of a gel in the reactor. This gel point is where the two incompatible phases separate (the high molecular weight polymers from the solvent). In the FTIR spectra this point correlates with a sharp decline in the isocyanate absorption. The conversion at gel point was not dependent on concentration of solution, but on the composition of the reaction mixture.

The polymerization continued after evaporation of the solvent. The isocyanate group absorption in the FTIR completely disappeared during annealing at 120°C. During the annealing process, the isocyanates reacted with urethane and urea with the formation of multifunctional allophanate and biurethe groups in the polymer network. These reactions formed a crosslinked polymer network that made the PUU film insoluble.

Chemical Structure of the PUU Films

The FTIR spectra of the PUU films correspond to known spectra of polyurethanes (Figure 5). The amide A peak for amine stretch, amide 1 peak for carbonyl stretch, amide 2 peak for amine deformation, peaks

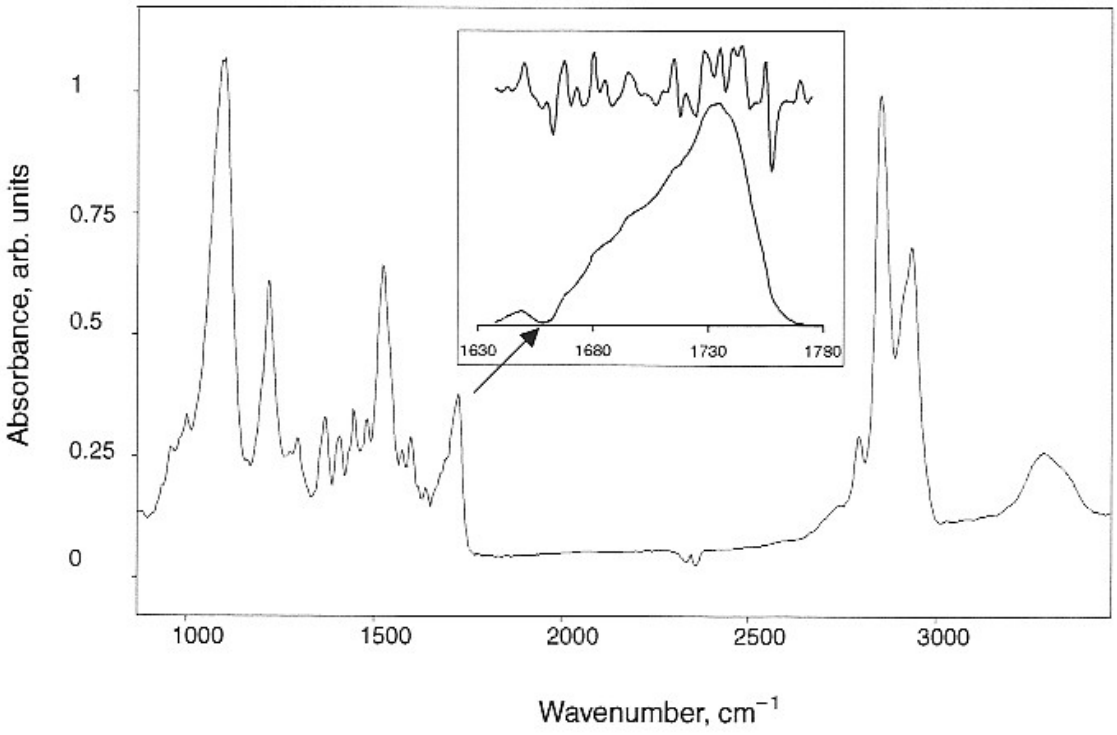

Figure 5. Exemplary FTIR ATR spectrum of a PUU film. The insert shows the amine 1 peak with its second derivative.

for the ether moiety, methyl groups, aromatic ring of toluene diisocyanate and diamine groups were observed. The peak for isocyanate was not observed. A detailed analysis for amide 1 carbonyl peaked for films is described elsewhere [29]. The structure of this spectral line is complex and components show the presence of some carbonyl groups in different intermolecular associations, such as amorphous soft phases and hard domains of macromolecules. The integrated intensity of the peaks corresponding to a hard domain phase was approximately 30% of the amide 1 peak; this means that the PUU synthesized contained hard domain phase that corresponds to segmented elastomer polyurethanes.

Insertion of Tantalum

To increase X-ray contrast, tantalum particles were suspended in the polymer coatings. Tantalum has a high X-ray absorption (due to its high density) as well as good biocompatibility (due to its stable natural oxide surface) and low thrombogenicity *in vivo* [16,30,31]. The strength of the films decreased and the modulus increased as the tantalum content was increased from 10 to 20% (v/v) (Table 1). This concentration range for tantalum was considered the critical concentration that can be applied in PUU films without a significant decrease in strength and elasticity. To determine the radiopacity of the nitinol wires (400 μm in diameter), X-ray contrast imaging requires 7 μm of pure tantalum coating or 35 μm of PUU filled with 20% tantalum. This thickness was then applied to all the stents studied.

Adhesion to the Metal Substrate

The adhesion strength was determined by peel testing the PUU–steel–PUU bond. Before PUU coating the steel surface was cleaned with alcohol, treated by plasma immersion ion implantation

Table 1. Mechanical parameters of PUU films with tantalum particles.

Concentration of tantalum particles (%)	Strength, MPa	Module, MPa	Elongation at breaking, (%)
0	10.2 ± 1.2	33.0 ± 4.8	290 ± 24
10	10.3 ± 1.6	33.9 ± 3.7	312 ± 52
20	7.3 ± 0.8	42.4 ± 2.9	244 ± 32
30	7.3 ± 0.6	55.0 ± 1.1	230 ± 47

(PIII), etched by phosphoric acid or treated with toluene diisocynate (TDI). The results of the peeling tests are in Table 2. The maximal adhesion strength was observed after PIII and TDI treatment.

DISCUSSION

The formation of a thin, strong and elastic polymer coating on metal wires requires prepolymers with a very low viscosity. For this study, a prepolymer solution was used to prepare a polymer with segmented polyurethanes and polyurethaneureas that exhibited strong intermolecular interactions between the hard domains of the macromolecules. The addition of a solvent to the reaction mixture during the synthesis induced some physical–chemical processes that influenced the structure and the properties of the polymer. The basic processes depend on the arrangement of the polar groups of the macromolecules in the solvent. This involved conformational freedom of the macromolecules or the macromolecular domains compatible with the solvent as well as the phase separation, conformational freezing of macromolecules and their domains that are incompatible with the solvent. The influence of the solvent on the process depends on the reaction conditions. The thermodynamic properties of the solvent (dipole moment and Haggin's parameter) on the structure of prepolymers has been reported for polyurethaneurea [32]; this report indicated that the solvent has a high impact on the structure and properties of polyurethaneurea [33,34].

The compatibility of the prepolymer with the solvent also changes as a function of the reaction process and solvent evaporation. A gel forms during curing, at which time the hard segments of the polyurethaneurea macromolecules assemble into hard domains. The phase separation is significant enough to stop the polymerization by separating the isocyanate groups in the gel fraction from the amine groups in the sol fraction.

Table 2. Adhesion strength of PUU coating on a stainless steel surface at different modifications of the metal surface.

Method of pre-treatment	Initial strength (N/m)	Strength after aging in hot water (N/m)
Cleaning by alcohol	203 ± 39	256 ± 41
H_3PO_4 etching	210 ± 26	173 ± 6
PIII	230 ± 36	236 ± 10
PIII and H_3PO_4	263 ± 48	248 ± 29
PIII and TDI	303 ± 42	283 ± 11

The hard domain structure of PUU forms at the time of the phase separation if the concentration of the hard segments is sufficiently high and the viscosity of the solution is still low enough to allow structure transformation. Ethyl acetate has a high compatibility with the prepolymer, with an evaporation rate close to the polymerization rate, as well as a low compatibility with the hard domain phase of PUU [29]. During annealing, after the evaporation of the solvent, the PUU film structure is formed. The isocyanates form crosslinks between the macromolecules. In this way thin elastic polyurethaneurea films were synthesized as crosslinked, segmented polyurethaneurea with a hard domain structures.

A major requirement for the PUU coating is the adhesion to the metal stent surface. Generally polyurethane bonding to metals is low [35]. After various surface modifications of the metal were applied to improved adherence, a bonding surface that reacted with isocyanate groups of the prepolymer was achieved when the PUU film was synthesized directly on the metal surface.

Plasma immersion ion implantation (PIII) carbonizes any organic contamination on metal surfaces to amorphous carbon [36]. After the stent was sputtered to produce a clean surface, it was treated with toluene diisocynate (TDI). The surface-adsorbed water reacted with the isocyanate groups of TDI with the formation of urea groups [37]:

$$2\,R_{TDI}—NCO + H_2O \rightarrow U—NH—CO—NH—R_{TDI} + CO_2$$

After coating the surface with a reactive prepolymer mixture, TDI was reacted with proton-donor groups of the prepolymer:

$$R_{TDI}—NCO + NHR_{PUU}R'_{PUU} \rightarrow U—NH—CO—NR_{PUU}R'_{PUU}$$

$$R_{TDI}—NCO + NH_2—R_{PUU} \rightarrow U_{TDI}—NH—CO—NH—R_{PUU}.$$

These reactions, on the substrate surface, have been discussed previously [38] and result in the formation of a highly crosslinked network in the interface region. As a result, a stiff urea structure is formed between the metal surface and the PUU film with a high concentration of chemical bonds between the macromolecules. The stiffness of this layer can be similar to that of the metal. This bound, hard layer formed on the PIII/TDI treated surface prevents water penetration in the interface and delamination of the coating.

Based on this technology, PUU coatings in different variants were prepared on commercial stents. First, a thin PUU film was synthesized

only on the wires of the stent without filler. In the second case, a thin PUU film was synthesized with tantalum particles on the struts of the stent. In the third case, a thick PUU film without tantalum particles was synthesized on the stents, closing completely all the voids in the stent meshwork. This latter process may be useful as a palliative treatment to prevent occlusion of a blood vessel by tumor infiltration. Finally, the latter coating was produced with tantalum particles. Images of these stents in visual light and in X-rays are presented on Figures 6 and 7. The tantalum particles in the PUU strongly enhanced the X-ray contrast.

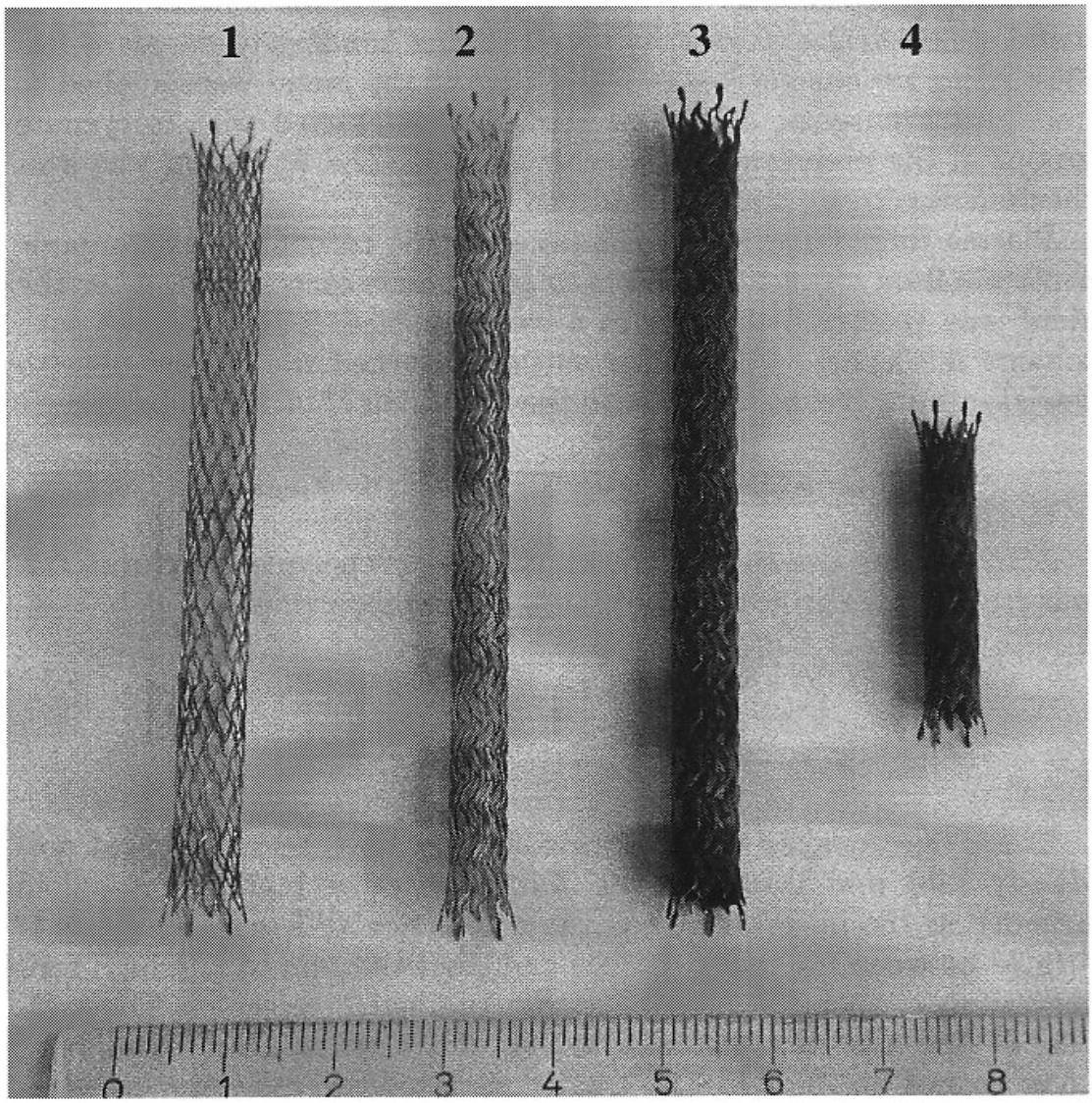

Figure 6. Photography of stents without a coating (1) and with (2–4) polyurethane coatings. In the case of (3) and (4) the polyurethane contained tantalum particles (the samples with the complete coating of wires and holes are presented).

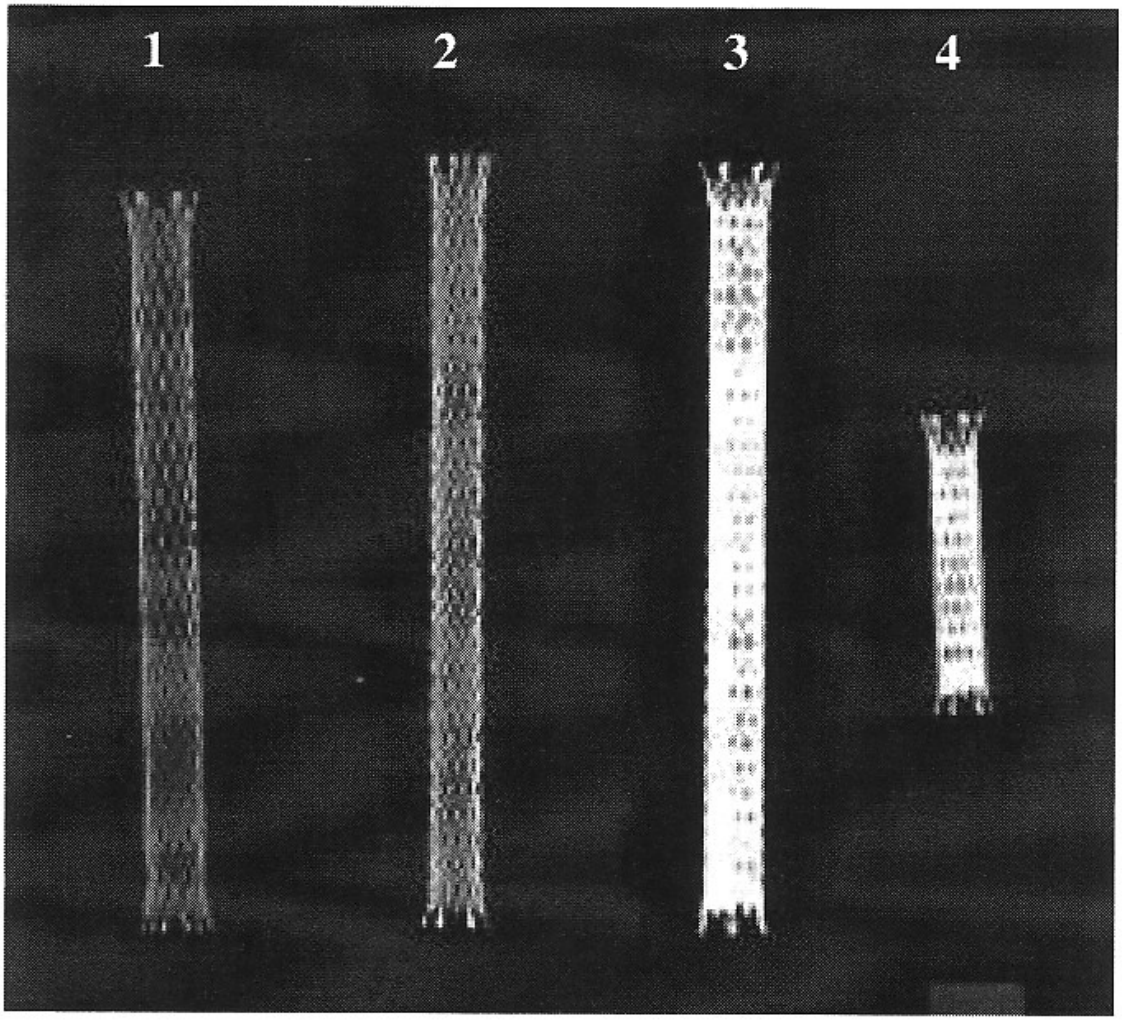

Figure 7. X-rays images of stents without (1) and with (2–4) polyurethane coating. In the case of (3) and (4), the polyurethane contained tantalum particles.

CONCLUSIONS

In the present study, a polyurethaneurea film was synthesized on vascular stents under conditions of solvent evaporation. The processes of solvent evaporation, polymerization and phase separation were investigated. The film consisted of crosslinked, segmented polyurethaneurea with a hard domain structure, high strength and elasticity. Good adhesion of polyurethane film on the stent surface was achieved by using a combination of plasma immersion implantation and toluene diisocyanate treatment of the stent surface. In selected cases, tantalum particles were suspended in the solution for an enhanced X-ray contrast. The coating could be prepared only on the wires or completely on wires and hollows

ACKNOWLEDGMENTS

The authors thank Uta Reuter for strength tests (Institute of Polymer Research), Dr. Wihsgott and Ms. Helldorf for X-ray images of the stents. This study was supported by grants from BMBF-WTZ Rus 00/218, Rus 01/225 and by the Alexander von Humboldt Foundation (A. Kondyurin).

REFERENCES

1. Diegeler, A., Thiele, H., Falk, V., Hambrecht, R., Spyrantis, N., Sick, P., Diederich, K.W., Mohr, F.W. and Schuler, G. (2002). Comparison of Stenting with Minimally Invasive Bypass Surgery for Stenosis of the Left Anterior Descending Coronary Artery, *N. Engl. J. Med.*, **347**: 561–566.
2. Serruys, P.W., de Jaegere, P., Kiemeneij, F., Macaya, C., Rutsch, W., Heyndrickx, G., Emanuelsson, H., Marco, J., Legrand, V., Materne, P., Belardi, J., Sigwart, U., Colombo, A., Goy, J.J., van den Heuvel, P., Delcan, J. and Morel, M.-A. (1994). A Comparison of Balloon-Expandable-Stent Implantation with Balloon Angioplasty in Patients with Coronary Artery Disease, *N. Engl. J. Med.*, **331**: 489–495.
3. van de Ven, P.J., Kaatee, R., Beutler, J.J., Beek, F.J., Woittiez, A.J., Buskens, E., Koomans, H.A. and Mali, W.P. (1999). Arterial Stenting and Balloon Angioplasty in Ostial Atherosclerotic Renovascular Disease: A Randomised Trial, *Lancet*, **353**: 282–286.
4. Lambert, T.L., Dev, V., Rechavia, E., Forrester, J.S., Litvack, F. and Eigler, N.L. (1994). Localized Arterial Wall Drug Delivery from a Polymer-Coated Removable Metallic Stent. Kinetics, Distribution, and Bioactivity of Forskolin, *Circulation*, **90**: 1003–1011.
5. Sheth, S., Dev, V., Jacobs, H., Forrester, J.S., Litvack, F. and Eigler, N.L. (1994). Prevention of Stent Subacute Thrombosis by Segmented Polyurethaneurea-Polyethylene Oxide-Heparin Coating in the Rabbit Carotid, *J. Am. Coll. Cardiol.*, **23**: 187A.
6. Holmes, D.R., Camrud, A.R., Jorgenson, M.A., Edwards, W.D. and Schwartz, R.S. (1994). Polymeric Stenting in the Porcine Coronary Artery Model: Differential Outcome of Exogenous Fibrin Sleeves Versus Polyurethane-Coated Stents, *J. Am. Coll. Cardiol.*, **24**: 525–531.
7. Lincoff, A.M., Furst, J.G., Ellis, S.G., Tuch, R.J. and Topol, E.J. (1997). Sustained Local Delivery of Dexamethasone by a Novel Intravascular Eluting Stent to Prevent Restenosis in the Porcine Coronary Injury Model, *J. Am. Coll. Cardiol.*, **29**: 808–816.
8. Virmani, R., Liistro, F., Stankovic, G., Di Mario, C., Montorfano, M., Farb, A., Kolodgie, F.D. and Colombo, A. (2002). Mechanism of Late In-Stent Restenosis After Implantation of a Paclitaxel Derivate-Eluting Polymer Stent System in Humans, *Circulation*, **106**: 2649–2651.

9. Carlier, S.G., van Damme, L.C.A., Blommerde, C.P., Wentzel, J.J., van Langehove, G., Verheye, S., Kockx, M.M., Knaapen, M.W.M., Cheng, C., Gijsen, F., Duncker, D.J., Stergiopulos, N., Slager, C.J., Serruys, P.W. and Krams, R. (2003). Augmentation of Wall Shear Stress Inhibits Neointimal Hyperplasia After Stent Implantation: Inhibition Through Reduction of Inflammation? *Circulation*, **107**: 2741–2746.
10. Topol, E.J. and Serruys, P.W. (1998). Frontiers in Interventional Cardiology, *Circulation*, **98**: 1802–1820.
11. Amano, Y., Ishihara, M., Hayashi, H., Gemma, K., Kawamata, H., Amano, M. and Kumazaki, T. (1999). Metallic Artifacts of Coronary and Iliac Arteries Stents in MR Angiography and Contrast-Enhanced CT, *Clin. Imaging*, **23**: 85–89.
12. Fischell, T.A. (2000). Visible Stents: All That Glitters ... Is It Gold? *J. Invasive Cardiol.*, **12**: 233–235.
13. Kondyurin, A.V., Maitz, M.F., Romanova, V.A., Begishev, V.P., Kondyurina, I.V. and Guenzel, R. (2004). Drug Release from Polyureaurethane Coating Modified by Plasma Immersion Ion Implantation, *J. Biomater. Sci.: Polym. Ed.*, **15**: 145–159.
14. Weintraub, W.S. (2004). Economics of Sirolimus-Eluting Stents: Drug-Eluting Stents Have Really Arrived, *Circulation*, **110**: 472–474.
15. Teirstein, P.S. (2004). A Chicken in Every Pot and a Drug-Eluting Stent in Every Lesion, *Circulation*, **109**: 1906–1910.
16. van der Giessen, W.J., Serruys, P.W., van Beusekom, H.M.M., Van Woerkens, L.J., van Loon, H., Soei, L.K., Strauss, B.H., Beatt, K.J. and Verdouw, P.D. (1991). Coronary Stenting with a New, Radiopaque, Balloon-Expandable Endoprosthesis in Pigs, *Circulation*, **83**: 1788–1798.
17. De Jaegere, P.P., Serruys, P.W., Bertrand, M.E., Wiegand, V., Kober, G. and Marquis, J.F. (1992). Wiktor Stent Implantation in Patients with Restenosis Following Balloon Angioplasty of a Native Coronary Artery, *Am. J. Cardiol.*, **96**: 598–602.
18. Tepe, G., Duda, S.H., Hanke, H., Schulze, S., Hagmeier, S., Bruck, B., Schott, U., Betz, E., Schmahl, F.W. and Claussen, C.D. (1996). Covered Stents for Prevention of Restenosis. Experimental and Clinical Results with Different Stent Designs, *Invest. Radiol.*, **31**: 223–229.
19. Tanigawa, N., Sawada, S. and Kobayashi, M. (1995). Reaction of the Aortic Wall to Six Metallic Stent Materials, *Acad. Radiol.*, **2**: 379–384.
20. Cremonesi, A., Benit, E., Carlier, M., Colombo, A., Piva, R., Probst, P., Wirtzfeld, A., Pico-Bourdonnec, L. and Corcos, T. (2000). Multicenter Registry to Evaluate the Efficacy of the NIROYAL Stent in De Novo or Restenotic Coronary Stenosis, *J. Invasive Cardiol.*, **12**: 225–232.
21. Kastrati, A., Schömig, A., Dirschinger, J., Mehilli, J., von Welser, N., Pache, J., Schühlen, H., Schilling, T., Schmitt, C. and Neumann, F.-J. (2000). Increased Risk of Restenosis After Placement of Gold-Coated Stents: Results of a Randomized Trial Comparing Gold-Coated with

Uncoated Steel Stents in Patients with Coronary Artery Disease, *Circulation*, **101**: 2478–2483.

22. Henke, B.L., Gullikson, E.M. and Davis, J.C. (1993). X-ray interactions: photoabsorption, scattering, transmission, and reflection at E = 50–30000 eV, Z = 1–92, *Atomic Data and Nuclear Data Tables*, **54**: 181–342.
23. Wolf, R.E. (1979). In: Morton, M., *Introduction to Rubber Technology*, pp. 213–255, Reinhold Publishing, New York.
24. Plank, H., Syre, I., Dauner, M. and Ebgers, G. (1987). *Polyurethanes in Biomedical Engineering II*. Elsevier, Amsterdam.
25. Romanova, V.A., Begishev, V.P., Guenzel, R., Maitz, M., Kondyurin, A.V. and Kondyurina, I.V. (2002). Synthesis of Polyurethane Coating with Drug Compounds on Metal Stents, *Oligomers 2002*. Chernogolovka, Russia.
26. Wheatley, D.J., Bernacca, G.M., Tolland, M.M., O'Connor, B., Fisher, J. and Williams, D.F. (2001). Hydrodynamic Function of a Biostable Polyurethane Flexible Heart Valve After Six Months in Sheep, *Int. J. Artif. Org.*, **24**: 95–101.
27. Peckham, S.M., Turitto, V.T., Glantz, J., Puryear, H. and Slack, S.M. (1997). Hemocompatibility Studies of Surface-Treated Polyurethane-Based Chronic Indwelling Catheters, *J. Biomater. Sci.: Polym. Ed.*, **8**: 847–858.
28. Marconi, W., Francolini, I., Piozzi, A. and Di Rosa, R. (2001). Antibiotic Releasing Urethane Polymers for Prevention of Catheter Related Infections, *J. Bioact. Compat. Polym.*, **16**: 393–407.
29. Romanova, V., Begishev, V., Karmanov, V., Kondyurin, A. and Maitz, M.F. (2002). Fourier Transform Raman and Fourier Transform Infrared Spectra of Cross-Linked Polyurethaneurea Films Synthesised from Solutions, *J. Raman. Spectr.*, **33**: 769–777.
30. Black, J. (1994). Biological Performance of Tantalum, *Clin. Mater.*, **16**: 167–173.
31. Matsuno, H., Yokoyama, A., Watari, F., Uo, M. and Kawasaki, T. (2001). Biocompatibility and Osteogenesis of Refractory Metal Implants, Titanium, Hafnium, Niobium, Tantalum and Rhenium, *Biomaterials*, **22**: 1253–1262.
32. Romanova, V.A., Begishev, V.P., Kondyurin, A.V. and Solodnikova, O.A. (2002). Elastomer Films of Crosslinked Segmented Polyurethaneurea Cured from Solutions, *First All-Russian Conference on Rubber and Gummy*. Moscow, Russia.
33. Vishnevskaya, I.A. and Morozova, N.I. (1993). *Zhurnal Prikladnoi Khimii*, **66**: 186–192.
34. Rogovina, L.Z. (1997). Dependence of Polymer Network Characteristics on Condition of Curing for Oligomers in Solution, *Oligomers 1997*. Chernogolovka, Russia.

35. Kinloch, A.J. (1994). *Adhesion and Adhesives. Science and Technology*. London, Chapman & Hall.
36. Kondyurin, A., Karmanov, V. and Guenzel, R. (2002). Plasma Immersion Ion Implantation of Polyethylene, *Vacuum*, **64**: 105–111.
37. Saunders, J.H. and Frisch, K.C. (1962). *Polyurethane Chemistry and Technology, Part 1: Chemistry*. Interscience, New York.
38. Kondyurin, A.V. and Klyachkin, Y.S. (1994). Vibrational Spectra of Some Diisocyanates in the Liquid State or on EPDM-40 Rubber Surface, *J. Appl. Polym. Sci.*, **54**: 1358–1393.

100. (WO2009006679) PATTERN TRANSFERRING BY DIRECT CURRENT PLASMA BASED ION IMPLANTATION AND DEPOSITION

Latest bibliographic data on file with the International Bureau

Pub. No.: WO/2009/006679 **International Application No.:** PCT/AU2008/000995
Publication Date: 15.01.2009 **International Filing Date:** 07.07.2008

IPC: ***C23C 14/48*** (2006.01), ***H01L 21/266*** (2006.01)

Applicants: **THE UNIVERSITY OF SYDNEY** [AU/AU]; Business Liaison Office, John Woolley Building A20, Cnr Manning Road & Western Avenue, Sydney, New South Wales 2006 (AU) *(For All Designated States Except US)*.
KWOK, Dixon, T., K. [AU/AU]; (AU) *(For US Only)*.
SUTHERLAND, Duncan, A [AU/AU]; (AU) *(For US Only)*.
KONDYURINA, Irina [AU/AU]; (AU) *(For US Only)*.
CHAIWONG, Chanokporn [TH/AU]; (AU) *(For US Only)*

Inventors: **KWOK, Dixon, T., K.**; (AU).
SUTHERLAND, Duncan, A; (AU).
KONDYURINA, Irina; (AU).
CHAIWONG, Chanokporn; (AU)

Agent: **SHELSTON IP**; 60 Margaret Street, Sydney, NSW 2000 (AU)

Priority Data: 2007903675 06.07.2007 AU

Title
(EN) PATTERN TRANSFERRING BY DIRECT CURRENT PLASMA BASED ION IMPLANTATION AND DEPOSITION
(FR) TRANSFERT DE MOTIF PAR DÉPÔT ET IMPLANTATION IONIQUE À BASE DE PLASMA À COURANT CONTINU

Abstract:

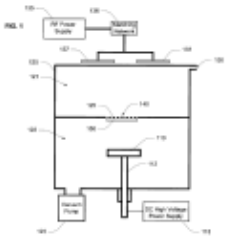

(EN)A method and apparatus is disclosed for pattern transferring by direct current plasma based ion implantation and deposition. The apparatus comprising: a vacuum chamber divided into a first part and a second part; the first part and a second part have a connecting aperture; a means for producing a plasma of charged ions in the first part; a multi-perforated grid proximal to the aperture for limiting expansion of the ion sheath beyond the grid; an ion target; a means for biasing the ions toward the target for providing a controlled trajectory therebetween; and a pattern mask within the ion trajectory for transferring the pattern to the target.
(FR)L'invention concerne un procédé et un appareil permettant de transférer un motif par dépôt et implantation ionique à base de plasma à courant continu. L'appareil comprend : une chambre à vide divisée en une première partie et une seconde partie; la première partie et la seconde partie sont pourvues d'un orifice de raccordement; un moyen permettant de produire un plasma d'ions chargés dans la première partie; une grille à perforations multiples, disposée à proximité de l'orifice, destinée à limiter l'expansion de la gaine ionique au-delà de la grille; une cible ionique; un moyen de polarisation des ions par rapport à la cible permettant de commander la trajectoire desdits ions; et un masque à motif sur la trajectoire ionique pour le transfert du motif sur la cible.

Designated States: AE, AG, AL, AM, AO, AT, AU, AZ, BA, BB, BG, BH, BR, BW, BY, BZ, CA, CH, CN, CO, CR, CU, CZ, DE, DK, DM, DO, DZ, EC, EE, EG, ES, FI, GB, GD, GE, GH, GM, GT, HN, HR, HU, ID, IL, IN, IS, JP, KE, KG, KM, KN, KP, KR, KZ, LA, LC, LK, LR, LS, LT, LU, LY, MA, MD, ME, MG, MK, MN, MW, MX, MY, MZ, NA, NG, NI, NO, NZ, OM, PG, PH, PL, PT, RO, RS, RU, SC, SD, SE, SG, SK, SL, SM, ST, SV, SY, TJ, TM, TN, TR, TT, TZ, UA, UG, US, UZ, VC, VN, ZA, ZM, ZW.
African Regional Intellectual Property Org. (ARIPO) (BW, GH, GM, KE, LS, MW, MZ, NA, SD, SL, SZ, TZ, UG, ZM, ZW)
Eurasian Patent Organization (EAPO) (AM, AZ, BY, KG, KZ, MD, RU, TJ, TM)
European Patent Office (EPO) (AT, BE, BG, CH, CY, CZ, DE, DK, EE, ES, FI, FR, GB, GR, HR, HU, IE, IS, IT, LT, LU, LV, MC, MT, NL, NO, PL, PT, RO, SE, SI, SK, TR)
African Intellectual Property Organization (OAPI) (BF, BJ, CF, CG, CI, CM, GA, GN, GQ, GW, ML, MR, NE, SN, TD, TG).

Publication Language: English (EN)

Filing Language: English (EN)

Journal of Cardiology 62 (2013) 265–266

Contents lists available at ScienceDirect

Journal of Cardiology

journal homepage: www.elsevier.com/locate/jjcc

Letter to the Editor

With reference to article: "Impact of the first-generation drug-eluting stent implantation on periprocedural myocardial injury in patients with stable angina pectoris". Dewetting problem

Biodegradable polymers are used as an effective matrix for drug-eluting coating on vascular stents [1]. Such polymers degrade in the human organism with a hydrolysis reaction that releases drugs and products of polymer degradation. The released drugs prevent an inflammatory reaction and thrombosis, suppress neointimal hyperplasia, and reduce the risk of restenosis. The organism metabolizes the released products of polymer degradation safely. Due to these advantages, drug-eluting stents have found a wide application in vascular surgery in comparison with bare metal stents. However, the question of whether drug-eluting stents show significant improvement in comparison with uncoated bare stents remains and is discussed (for example, Okada et al. reported that [2]: "...use of [drug-eluting stents] has not improved mortality in patients with [angina pectoris] in spite of their notable suppressive effect for neointimal hyperplasia compared to that of [bare metal stents]").

One reason for the contradiction could be due to a particularity of the biodegradation process in polymer coating on metal surface. A polymer coating has significantly different surface energy than a metal surface on the stent. Therefore, these two substances will minimize the contact area. The reason is a dewetting effect of polymer coating on all metal surfaces including metal stents [3,4].

We investigated vascular drug-eluting stents with poly(lactic-co-glycolic acid) (PLGA) coating (polymer base for drug) as well as a model PLGA coating on silicon wafer (http://arxiv.org/pdf/1101.0659v1). The initial PLGA coating on silicon wafer is smooth and stable. After exposure in water solution the PLGA coating swells with water, becomes soft and mobile. As result of mobility, the PLGA coating becomes ruptured, the ruptured parts move and collect as separate drops with naked metal areas between them (Fig. 1A). With time the drop sizes decrease due to biodegradation of PLGA. The dewetting process takes about 1–3 days and the biodegradation process takes 2–3 weeks. Therefore, the coating stands on stents as separate drops during most of the time of biodegradation.

Kinetics of dewetting depends on thickness of the coating, difference between surface energy of coating and metal, surface tension of polymer, geometry of the surface, density, and viscosity of the coating [3,4]. The distribution of the drops shows that the dewetting occurs by spinodal mechanism. That means the coating is unstable on the metal due to a difference in surface energy of the metal and PLGA coating.

The separation of PLGA coating to small drops, a peeling off of the drops from the stent surface, and a move to periphery vessels, where the PLGA drops can block blood flow, is strongly possible. The metal surface of the stent comes into direct contact with blood after a short time in water solution. These changes could cause periprocedural myocardial injury (PMI) as it was suggested by Okada et al. [2]: "we hypothesized that [drug-eluting stent] implantation may be associated with a higher incidence of PMI and affect the clinical outcome after [percutaneous coronary intervention]".

The dewetting of PLGA coating on metal substrates can be stopped. We used ion beam implantation to modify the PLGA coating. During modification, high energy ions cause damage to a number of chemical bonds in PLGA and replace atoms from polymer macromolecules in the trace of ions. Replaced atoms join together to each other and join to residual macromolecules so that the modified coating becomes highly crosslinked. The film becomes immovable. Dewetting stops (Fig. 1B).

The ion beam modified PLGA coating remains smooth and stable during the complete time of biodegradation. The coating is fully crosslinked and does not dewet. The degradation process occurs uniformly.

The same effect of dewetting is observed on metal stents. The initial coating before biodegradation is smooth. After biodegradation the untreated stent has a ruptured coating and part of the stent surface is naked up to metal (Fig. 1C). The ion beam treated coating remains stable on stents during biodegradation (Fig. 1D). The dewetting forces cannot break crosslinked PLGA coating, but the drug is released freely.

The study was supported by Boston Scientific, Natick, MA, USA.

0914-5087/$ – see front matter © 2013 Japanese College of Cardiology. Published by Elsevier Ltd. All rights reserved.
http://dx.doi.org/10.1016/j.jjcc.2013.04.011

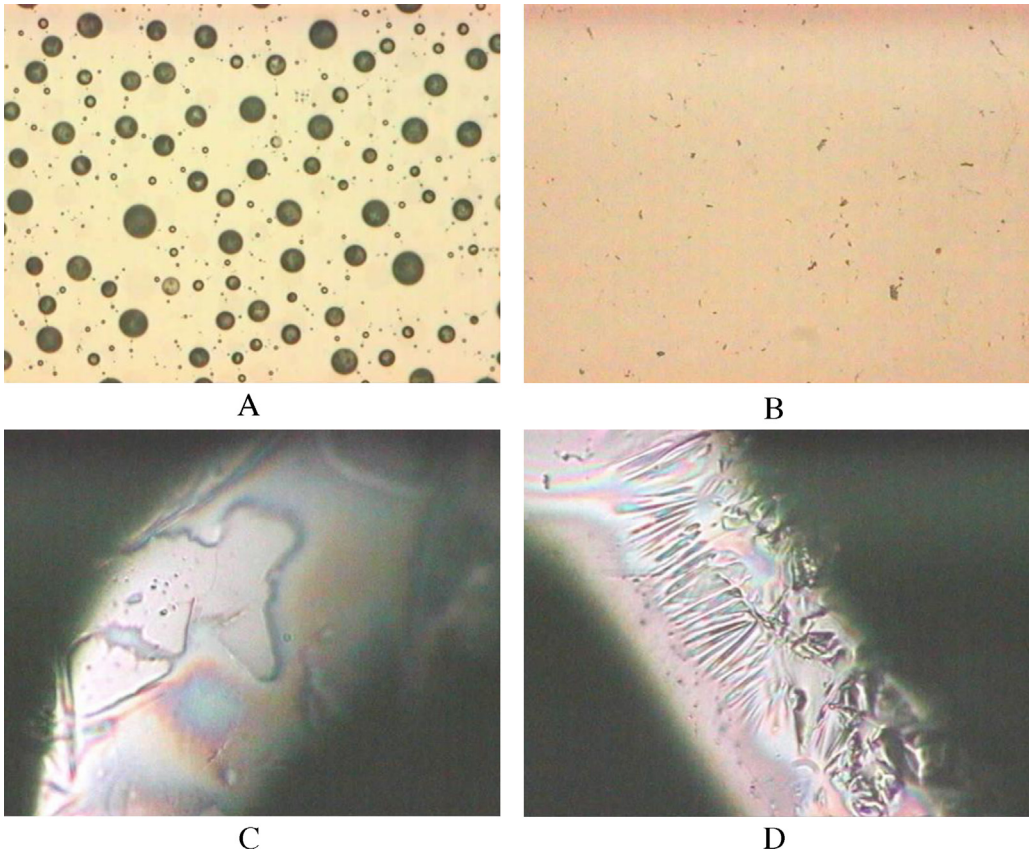

Fig. 1. Microphotographs of silicon wafer ((A) and (B), size of photos is 1.2 mm × 0.95 mm) and stents ((C) and (D), size of photos is 0.24 mm × 0.19 mm) with poly(lactic-co-glycolic acid) coating. (A) The untreated coating is dewetted to separate drops after biodegradation; (B) the ion beam treated coating remains smooth after biodegradation; (C) the untreated coating on stent is dewetted to non-regular structures after biodegradation; and (D) the PIII-treated coating on stent is crosslinked and wrinkled, but remains continuous.

References

[1] Holmes Jr DR. Interventional cardiology: a new drug-eluting stent that does not live up to its promise. Nat Rev Cardiol 2009;6:500–1.
[2] Okada T, Yoshikawa D, Ishii H, Matsumoto M, Hayakawa S, Matsudaira K, Tanaka M, Kumagai S, Hayashi M, Ando H, Amano T, Murohara T. Impact of the first-generation drug-eluting stent implantation on periprocedural myocardial injury in patients with stable angina pectoris. J Cardiol 2012;60:264–9.
[3] Becer J, Gruen G, Seenann R, Mantz H, Jacobs K, Mecke KR, Blossey R. Complex dewetting scenarios captured by thin-film models. Nat Mater 2003;2:59–63.
[4] Volodin P, Kondyurin A. Dewetting of thin polymer film on rough substrate: I. Theory. J Phys D: Appl Phys 2008;41:065306.

A. Kondyurin*
I. Kondyurina
M. Bilek
Applied and Plasma Physics, School of Physics (A28), University of Sydney, Sydney, NSW 2006, Australia

*Corresponding author. Tel.: +61 293512484.
E-mail address: kond@mailcity.com (A. Kondyurin)

31 January 2013
Available online 25 June 2013

Applied Surface Science 314 (2014) 670–678

Contents lists available at ScienceDirect

Applied Surface Science

journal homepage: www.elsevier.com/locate/apsusc

Cell growing on ion implanted polytetrafluorethylene

I. Kondyurina[a,*], I. Shardakov[b], G. Nechitailo[c], V. Terpugov[d], A. Kondyurin[e]

[a] School of Medicine, University of Sydney, Sydney, Australia
[b] Institute of Continuous Media Mechanics, Russian Academy of Science, Perm, Russia
[c] Institute of Biochemical Physics, Russian Academy of Science, Moscow, Russia
[d] Perm State University, Perm, Russia
[e] School of Physics, University of Sydney, Sydney, Australia

ARTICLE INFO

Article history:
Received 24 February 2014
Received in revised form 10 July 2014
Accepted 10 July 2014
Available online 18 July 2014

Keywords:
Surface
Plasma
Biocompatibility
PTFE
Cell

ABSTRACT

Polytetrafluorethylene (PTFE and ePTFE) substrates were treated by ion implantation with nitrogen ions of 20 keV energies and 10^{13}–10^{16} ions/cm^2 ion fluences. The modification of the polymer surface was analyzed by FTIR and XPS spectroscopy, water wetting angle measurements and AFM images. The surface morphology, wettability and chemical activity were changed due to surface modification. The growing of endothelial cells of modified surfaces was improved in comparison with untreated PTFE and ePTFE substrates. The improved cell adherence on the modified surface is based on the improved adhesion of cell proteins.

© 2014 Elsevier B.V. All rights reserved.

1. Introduction

Polytetrafluorethylene (PTFE) is known for its excellent chemical and bio stability and its bio inertness. The mechanically stretched, expanded form (ePTFE) is microscopically porous, possessing otherwise the properties of standard PTFE [1]. ePTFE found a large number of applications in surgery as flaps in herniorrhaphy, craniosurgery, etc., mainly because of its bioinertness, biostability, both flexibility and mechanical stability. However, a main domain is in vascular surgery for as prostheses for smaller, i.e. infrainguinal blood vessels, artificial AV shunts, as coating of vascular stents or heart valve rings.

Despite of wide applications, there are still two main problems with ePTFE implant: thrombosis and anastomosis stenosis by intima hyperplasia. The hemodynamic and a mismatch of the elastic properties of the graft and native vessel were considered as reasons for graft failure [2]. These problems could not be solved by improved surgical techniques but are considered as materials related. Especially thin vessel grafts are susceptible for these problems.

The extreme hydrophobicity of ePTFE and the low toxicity is regarded as the reason for the good performance in bigger vessels, but a superhydrophobic modification of ePTFE failed for small diameter grafts and in bigger vessels it showed a higher platelet adsorption than standard ePTFE grafts [3]. Additional surface coating with biologically designed surfaces such as heparin or hirudin can reduce platelet adherence and the intima proliferation but has the problem of a physiological decay in biological activity and in some cases iatrogenic inactivation by protaminsulfate [4–6].

Endothelial cells as the inner lining of blood vessels are known to provide the best hemocompatible surface. All PTFE-like materials do not support endothelialisation in vivo [7]. There is a concept is in vitro tissue engineering, seeding of autologous endothelial cells on the implant surface prior to implantation [8]. Various attempts have been made to achieve an adherent layer of endothelial cells on the surface. Seeding the cells in a system with dynamic pressure and flow [9,10] has been described as the easiest way to obtain an endothelial lining, which resists the shear stress of physiological blood flow, an effect which also works in other systems [11].

Some ways of surface modification of ePTFE have been successfully attempted based on plasma method of modification [12]. An improved cell adherence and proliferation over untreated ePTFE was found as graft for intracranial arteries. In the latter case an increased adhesion of fibrin-glue was found, which allows better anchorage of the flap. The trend is to surface modification, which provides specific cell adherence. These cells adhere via protein receptors at the extracellular matrix (ECM) and their basement membrane. The native extracellular matrix

* Corresponding author. Tel.: +61 2 93512484.
E-mail address: i.kondyurina@gmail.com (I. Kondyurina).

http://dx.doi.org/10.1016/j.apsusc.2014.07.057
0169-4332/© 2014 Elsevier B.V. All rights reserved.

[13] or selected ECM proteins, collagen [14], fibronectin [15], and laminin [16] should be adsorbed on the ePTFE surface. The interaction of these proteins with the integrin is provided by a special, highly conservative functional group of the ligand, the RGDS sequence as well as a peptide of this individual sequence should be immobilized [15]. In all cases endothelial cells were seeded in vitro and an improved growth of the cells have been demonstrated.

The preparation of PTFE surface for the increased growth of endothelial cells can be achieved by ion beam implantation [17,18]. The method is based on structural modification of a thin surface layer of a polymer under the bombardment by high energy ions [19–21]. The effect of the modification is caused by the penetration of the high energy ion into the polymer, cascades of collisions with atoms of macromolecules and transfer of the kinetic energy of penetrating ion to atoms and electrons of polymer macromolecules. The transferred energy is high enough that atoms and electrons leave macromolecules and fly away with high kinetic energy causing new collisions with nearest macromolecules. As result, breaking of chemical bonds, ionization, formation of free radicals, electron and phonon excitation of macromolecules are observed [22]. The field of such strong structure changes of polymer is named an ion track and the size of ion track depends on ion energy, kind of ion and polymer. This is a first stage of the ion beam implantation of polymers.

After ion penetration, the track field of polymer has a very high concentration of free radicals, ionized and highly excited parts of macromolecules. These active particles cause a number of chemical reactions. As result, amorphous carbon, aromatic condensed structures, stable and semi-stable free radical structures appear. The properties of the polymer surface after ion beam implantation are mostly connected with this second stage. The morphology of the surface changes dramatically with formation of rough structures [23]. The water contact angle of PTFE and ePTFE surface after modification is observed higher [24] and lower [25], than the initial. The vibrational spectra show a number of new chemical groups [26].

In general, the kinetics of free radicals takes sufficiently long time (from minutes to days) then the first stage (part of second) due to long kinetics of free radical reactions in PTFE [27,28]. The presence of free radicals in PTFE causes chain reactions of fluorine cleaving from initial macromolecules, chain breaking and crosslinking [29–31]. Due to migration of free radicals, the modified area can be shifted to significantly deeper layers then the track of ion [32]. In air the free radical reactions of modified polymer layer are carried out with participation of oxygen when the stable oxygen-containing groups appear in polymer [28]. Such modified polymer surface is used for different applications [33] including medical devices [21,34–36]. However, the structure transformation of ion implanted PTFE and ePTFE and a biological response on the modified PTFE have not been fully investigated as required for medical applications.

In present investigation the ion implantation was applied to PTFE and ePTFE surfaces. The structure changes in PTFE and ePTFE after ion implantation were investigated and linked to the improved cell adherence.

2. Experiment

ePTFE sheets were provided by Boston Scientific SCIMED, USA. PTFE films of 20 μm were provided by Halogen, Perm, Russia. The PTFE films were cleaned by ethanol and dried before using. The ePTFE samples were used as provided and handled between protective coatings to prevent contamination of the surface. Acrylamide with 0.1% of Tetramethylethylenediamine inhibitor of polymerization (Aldrich) was dissolved in deionized water with a concentration of 100 g/L.

Ion implantation of PTFE was done on Pulsar implanter described in [37]. The beam of nitrogen ions with 20 keV energy, current density of 5 mA/cm^2 in a pulse of 300 ns duration with pulse-repetition frequency of 1 Hz was applied. The fluence of ions was measured with Faraday-cup.

For acrylamide attachment the modified samples were soaked in 10% acrylamide water solution during 2 h at room temperature. After soaking the samples were washed by deionized water 3 times and dried on air overnight.

Plasma immersion ion implantation was used for modification of the PTFE and ePTFE substrates. The samples were placed on the high voltage electrode and covered by stainless steel mesh. The distance between mesh and sample surface was 30 mm. The mesh had the same electrical potential as electrode. The plasma chamber was vacuumed up to 10^{-3} Pa and filled by nitrogen up to 5×10^{-1} Pa. Plasma discharge was generated by RF-frequency generator of 200 W power at 13.75 MHz frequency. The high voltage pulsed biases of 20 kV was used. The pulse of 5 μs duration with 50 Hz frequency of repetition was applied to high voltage electrode. Ion fluence estimates for the plasma immersion ion implantation were obtained in an experiment on polyethylene using a procedure described in [21]. The fluence of one high voltage pulse was determined by comparing UV transmission spectra from polyethylene films after the plasma immersion ion implantation to samples implanted with known ion fluences in Pulsar ion implanter experiments where the fluence was measured with a Faraday cup. The pulse duration, pulse repetition frequency, average current, kind and energy of ions were adjusted to match the both experiments. One high voltage pulse of the plasma immersion ion implantation under the present conditions was found to correlate with a fluence of 2.8×10^{11} ions/cm^2. The PTFE and ePTFE samples were treated with 35–35,000 pulses, corresponding to implantation ion fluences of 10^{13}–10^{16} ions/cm^2. The plasma immersion ion implantation of PTFE has shown similar results as for ion implantation of PTFE with Pulsar implanter.

Fourier transform infrared attenuated total reflection (FTIR ATR) spectra were recorded on Nicolet Magna spectrometer with Ge ATR crystal with 45° of incident angle. Number of scans was 100, spectral resolution was 2 cm^{-1}.

The contact angles between a PTFE and ePTFE sample surface and de-ionized water were measured using a Kruss contact angle analyzer DS10 employing the sessile drop method.

X-ray photoelectron spectra (XPS) were recorded on Scanning Auger electron spectrometer Microlab 310F (Fisons) with accessory XPS-unit (Al/Mg – X-ray tube). Scanning step was 0.2 eV.

An atomic force microscope DI-3100 (Digital instruments Ins., Santa Barbara) was used for surface morphology analysis of the PTFE samples before and after ion implantation. The measurements were carried out in a tapping mode. Silicon probes with 75 kHz resonant frequency, 1.5–3.7 N m^{-1} spring constant and 10 nm curvature radius were used. The initial PTFE film was too rough for AFM measurement. To get smooth PTFE surface, the initial PTFE film was pressed between Silicon wafers before the ion implantation. A surface topology of the PTFE film after pressing was similar to the silicon wafer surface topology.

In cells experiment, ePTFE discs with the surface area of 0.58 cm^2 were mounted in Minusheets (Minucells and Minutissue, Bad Abbach) and steam sterilized at 120 °C. The bovine aortic endothelial cell line GM7373 (Coriell) was used for the experiments [38]. 4×10^4 cells in 200 μL medium (MEM-Earle supplemented with 10% fetal bovine serum (FBS), 1 × MEM vitamins, 2 mM N-acetyl L-alanyl L-glutamine, 1 × amino acids) were seeded directly on the samples. They were allowed to adhere for 2 h at standard cell culture conditions, then medium was filled up to 1 mL per sample. 3

days after seeding the cells were fixed in 0.2% paraformaldehyde in PBS and stained with rhodamine. Images were taken by fluorescent microscopy with video camera and the color was inverted for better observation.

3. Results

Visually the effect of ion implantation for PTFE and ePTFE is observed less than for hydrocarbon polymers like polyethylene and polystyrene. The ion beam implantation changes the color of the samples only at high fluences (from 5×10^{15} ions/cm^2 and higher). Both PTFE and ePTFE samples become gray at fluence of 10^{16}–10^{17} ions/cm^2. The distribution of the color on the PTFE and ePTFE samples shows uniform fluence distribution on the sample surface. In all our cases the fluence was homogeneously distributed, excluding corners where the samples were mounted to the sample holder. The corner areas of the samples were excluded from subsequent analysis of structure and cell experiments.

The analysis of the PTFE surface with using of atomic force microscopy shows that the surface of PTFE becomes significantly rough after ion implantation when the initial PTFE surface is smooth (Fig. 1a–c). The character and shape of the holes on ion implanted PTFE surface are similar to the etched surface at plasma and ion implantation observed earlier [26,30]. The untreated PTFE surface is smooth with Root Mean Square (RMS) roughness of 0.59 that is close to the silicon wafer roughness. The ion implanted PTFE with 10^{15} ions/cm^2 ion fluence shows RMS roughness of 12 nm and PTFE with 10^{16} ions/cm^2 ion fluence shows RMS roughness of 20 nm. The histogram of the surface images (Fig. 1d) shows significant broadening of the frequency events of the height. The narrow histogram of the untreated PTFE is transformed into broad curve with maximum at 55 nm after 10^{15} ions/cm^2 ion fluence and broad curve with maximum at 87 nm after 10^{15} ions/cm^2 ion fluence. The single maximum curves observed for all samples show, that the surface features height have a random character corresponding to normal distribution. The analysis of first neighbor distance (FND) as average distance between hills gives a characteristic size (diameter) of the holes is about 210 nm for 10^{15} ions/cm^2 fluence and about 440 nm for 10^{16} ions/cm^2 fluence. The Fourier filtering (FFT) of the surface image used for the image frequency components analysis (Fig. 1a–c) gives narrow peak for untreated PTFE while the ion implanted PTFE peaks are broader. The FFT image for all samples are unidirectional that shows the unidirectional character of the surface features. As the result of surface morphology changes, the effective area of the PTFE surface increases to 1.06–1.07 times after ion implantation.

The etching effect influences on the ePTFE surface structure. The untreated ePTFE has a fibril structure with micron-size nodes (Fig. 2). The ion implantation breaks some fibrils and round the edge of the nodes on the top surface layer. However, the fibril structure of ePTFE surface remains.

The new lines in 1750–1650 cm^{-1} region appear in the FTIR ATR spectra of ion implanted PTFE (Fig. 3). The modification of the polymers at ion implantation affects only a thin surface layer and the new lines have weak intensity in FTIR ATR spectra. The changes of FTIR transmission spectra of PTFE are invisible for all regimes of treatment. The new lines are interpreted as stretching vibrations of C=O and C=C groups in oxidized and carbonized PTFE surface layer. The intensity of these lines increases with the ion implantation fluence that corresponds to increase a concentration of carbonized and oxidized structures. The carbonization of the surface layer is due to a loosing of fluorine atoms in the PTFE macromolecule at ion implantation and a conjugation of carbon atoms in aromatic structures. The appearance of oxygen-containing structures is caused by reactions of free radicals with atmospheric oxygen after exposure of the treated PTFE samples on air. Due to the strong etching effect of the modified surface layer of PTFE, the concentration of new groups in the modified PTFE and ePTFE surface layer is lower in comparison with hydrocarbon polymers such as polyethylene or polystyrene at the same conditions of ion implantation.

The element composition of the PTFE surface changes after ion implantation as it is observed by XPS data (Table 1). The spectrum of untreated PTFE shows only C1s and F1s lines in ratio corresponding the chemical formula of PTFE macromolecule. The experimental value of carbon (39%) is slightly higher than theoretical value (33%), and the experimental value of fluor (61%) is slightly lower than the theoretical value (67%). The additional lines of O1s and N1s are observed in the spectra of ion implanted PTFE. The concentration of carbon atoms increases dramatically (60–70%) after ion implantation due to defluorination and carbonization of the surface layer. The fluorine concentration in PTFE significantly reduces from 61% for untreated PTFE to 4% after low fluence of 10^{13} ions/cm^2 and recovers up to 21% with high fluence of 10^{16} ions/cm^2. The nitrogen and oxygen lines are observed in all spectra of ion implanted PTFE. At low fluence, the surface layer of PTFE contains significant concentration of oxygen (14%) and nitrogen (11%) atoms and keeps it the same with higher fluence. These XPS data show that the PTFE surface layer becomes carbonized, nitrized and oxidized after ion implantation. At highest fluence (10^{16} ions/cm^2) the element content becomes closer to the initial PTFE with higher fluor (21%), lower carbon (60%), nitrogen (8%) and oxygen (10%). It supports AFM results showing the modified layer is etched significantly at high fluence and the virgin bulk layer comes to the top.

The water wetting angle of PTFE changes from 120° for untreated PTFE to about 70–80° for ion implanted PTFE (Fig. 4). The lowest contact angle (73°) is observed for the lowest ion fluence (10^{14} ions/cm^2). At high fluence (10^{16} ions/cm^2) of nitrogen ions the wetting angle increases.

The increase of the contact angle was observed in PTFE after ion implantation and laser ablation treatment [39,40]. A reason of the increase is a roughness of the PTFE surface, which increases due to etching of the PTFE macromolecules [41]. The regime of the ion implantation influence on the etching and consequently on wettability of the ion implanted PTFE surface [42].

The initial surface of ePTFE is extremely hydrophobic. The wetting angle of water drop on ePTFE initial surface is 145°. The water contact angle of ion implanted ePTFE decreases up to 120–140° range without clear tendency of fluence. These results of the wetting angles on ePTFE surface (Fig. 4) cannot be used directly for wettability analysis, because of the fibril morphology of the material (see Fig. 2). The drop partly contacts the polymer fibers and partly the air between the fibers. Therefore, the fibers obviously cannot influence on the wetting angle significantly. After ion implantation, when the ePTFE fibers become more hydrophilic, the water can penetrate between the fibers to fill the space between fibers. When it is happened, the drop of water on the ion implanted ePTFE surface contacts the fibers and the water between the fibers. In this case the contact angle is extremely low about 20–30°. These cases were excluded from these results for ion implanted ePTFE. Therefore, the results of ePTFE film wetting angle cannot be used directly. Because of equal chemical structure of PTFE and ePTFE, the wettability properties of PTFE can be transferred to ePTFE fibers.

The ion implantation changes a chemical activity of the PTFE and ePTFE surface. To test it, the ion implanted PTFE was immersed in acrylamide solution at presence of an inhibitor of polymerization (Tetramethylethylenediamine) without initiator of polymerization. Then the samples were washed in deionized water to remove the acrylamide and dried. The FTIR spectra of PTFE surface show new lines at 2994, 2960, 2924, 2854 cm^{-1} interpreted as stretch vibrations and 1465, 1452 cm^{-1} interpreted as deformation vibrations of C—H bonds of a polyacrylamide attached on the PTFE

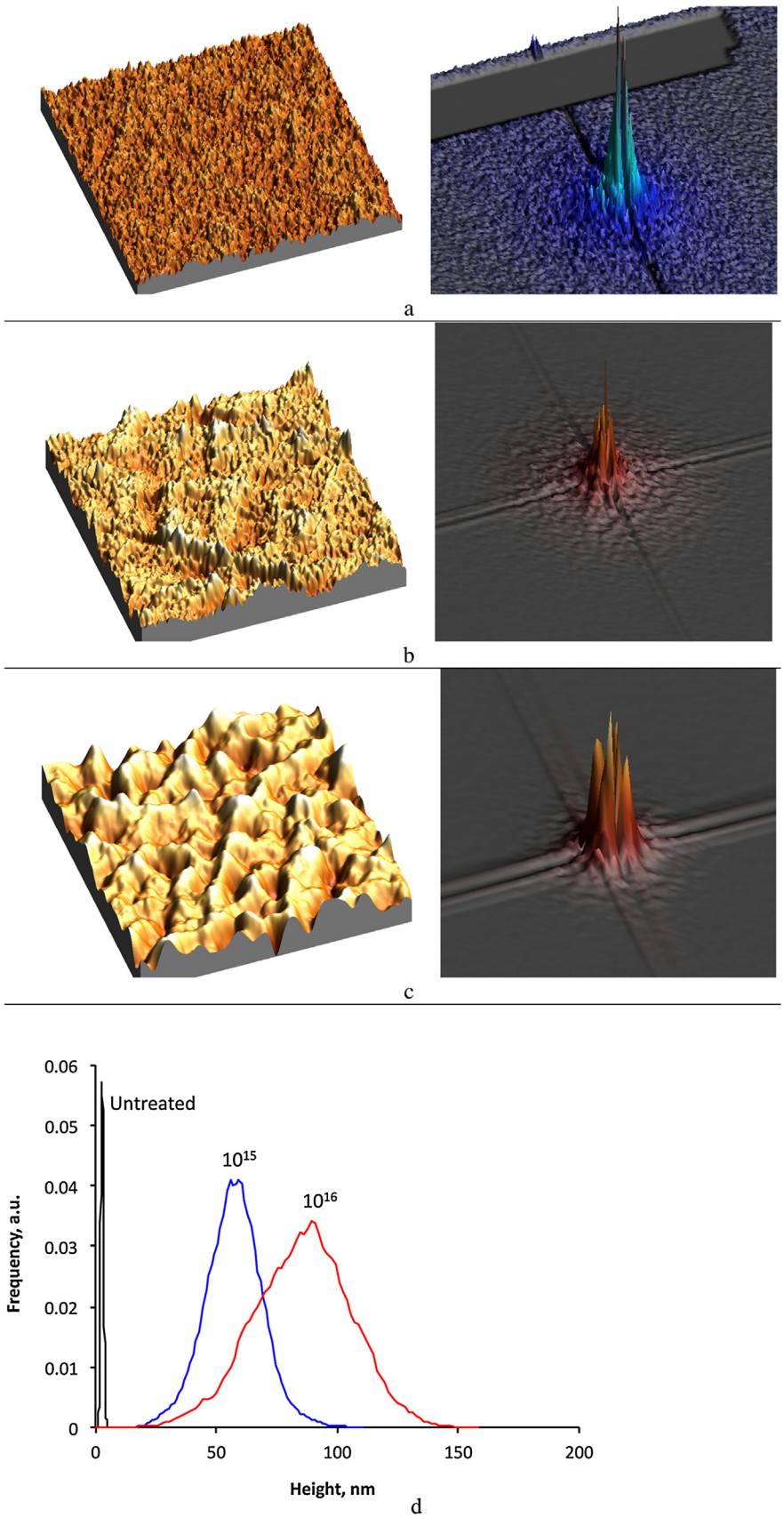

Fig. 1. AFM image of PTFE surface and statistical analysis. The ion implantation of 20 keV energy nitrogen ions is done with following fluence: (a) untreated surface, (b) 10^{15} ions/cm^2, (c) 10^{16} ions/cm^2. The graphs (a–c) are AFM images (left) and FFT images (right). The graphs (d) is a histogram of the height event of the images. The roughness and effective area increase with ion implantation fluence.

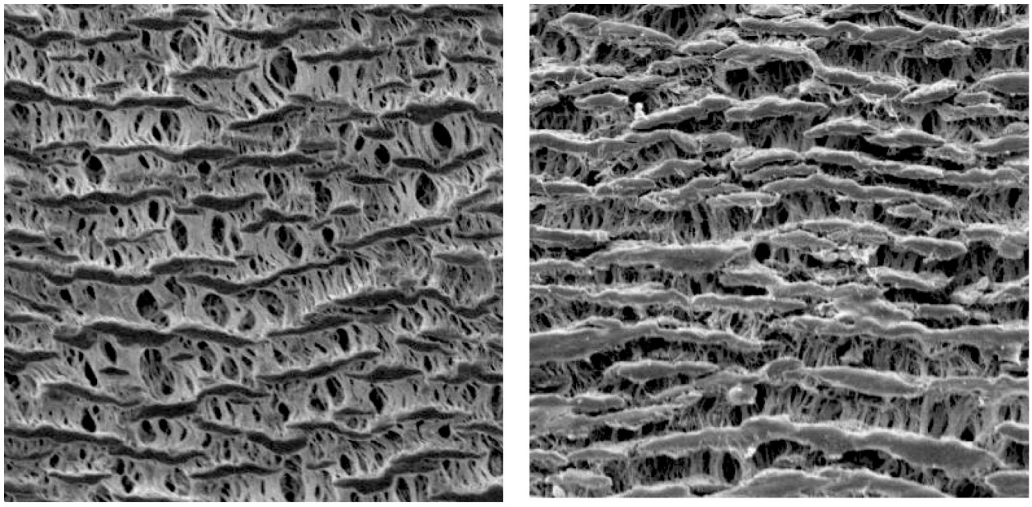

Fig. 2. SEM image of (a) untreated and (b) ion implanted ePTFE. The ion implantation is done with 20 keV energy nitrogen ions of 10^{15} ions/cm^2 fluence. The size of images is 0.3 × 0.3 mm^2. The sharp edges become smoother after ion implantation due to etching PTFE, but the fiber structure remains.

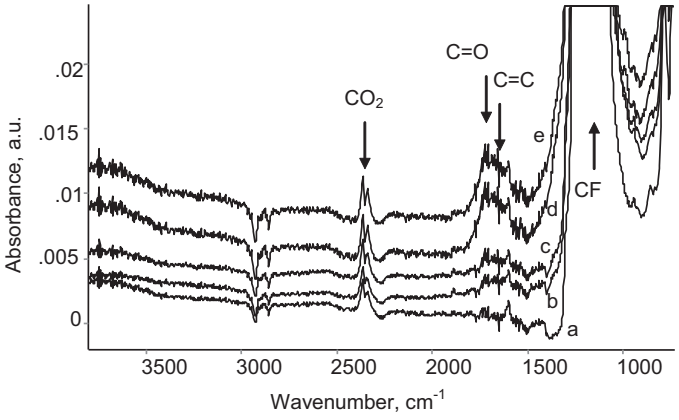

Fig. 3. FTIR ATR spectra of PTFE treated by nitrogen ions of 20 keV energy with different fluence: (a) untreated, (b) 5×10^{14}, (c) 5×10^{15}, (d) 2×10^{16}, (e) 5×10^{16} ions/cm^2. The CO_2 line corresponds to carbon dioxide in FTIR spectrometer. The spectra are zoomed to view the weak lines of oxidized and carbonized structures, while the C–F vibration line is overload.

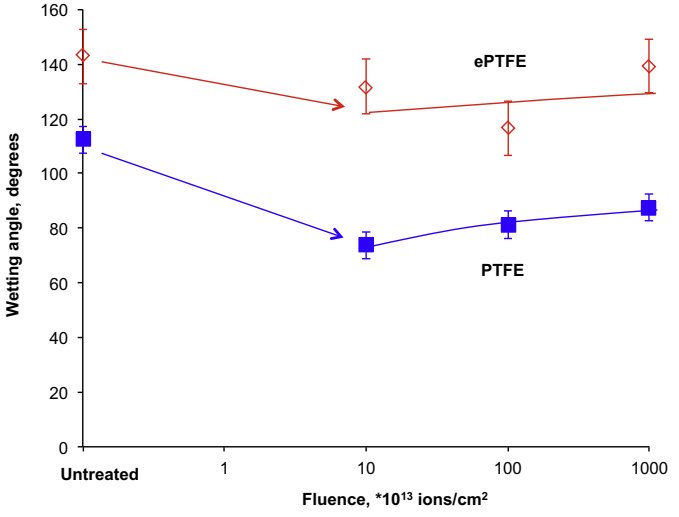

Fig. 4. Wetting angle ePTFE (empty rhomb) and PTFE (full square) after nitrogen ion implantation of 20 keV ion energy.

Table 1
Element content (%) in PTFE surface after ion implantation by 20 keV nitrogen ions. The integral intensity of C1s, N1s, O1s and F1s, lines in XPS spectra and theoretical values by formula were used for the analysis.

Elements	Formula of PTFE	Untreated	Fluence (ions/cm^2)			
			10^{13}	10^{14}	10^{15}	10^{16}
C	33	39	70	71	63	60
N	0	0	11	11	12	8
O	0	0	14	14	14	10
F	67	61	4	4	10	21

surface (Fig. 5). A strong line of C=C vibrations in acrylamide at 1630 cm^{-1} is not observed, while this is mostly intensive line in a spectra of the acrylamide monomer. The weaker lines of C=O carbonyl and NH amine groups can be overlapped with the C=O and OH lines of the modified layer of PTFE. The water contact angle of modified PTFE after soaking in acrylamide solution decreases from 80° to 51° showing hydrophilic layer of the polyacrylamide. The spectra of the untreated PTFE soaked in acrylamide solution and washed in water do not show the lines of acrylamide. The water contact angle of untreated PTFE soaked in acrylamide solution and washed in water does not change. Because the presence of inhibitor and

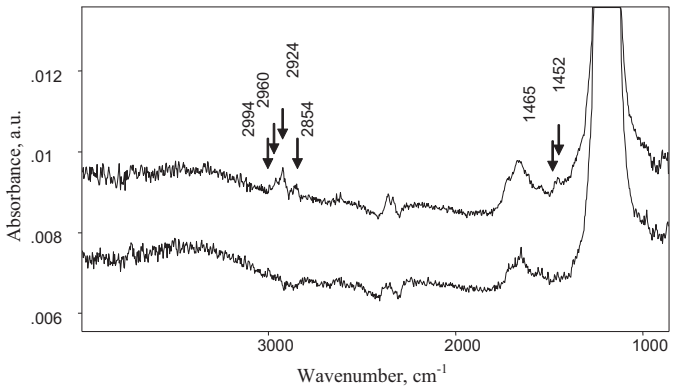

Fig. 5. FTIR ATR spectra of PTFE treated by nitrogen ions of 20 keV energy with 10^{16} ions/cm^2 fluence (bottom) and post-treated in acrylamide solution (top). Arrays show additional lines appeared after acrylamide post-treatment. The C=O and N—H acrylamide peaks are masked with C=O and OH peaks of oxidized PTFE layer and are not used for acrylamide analysis.

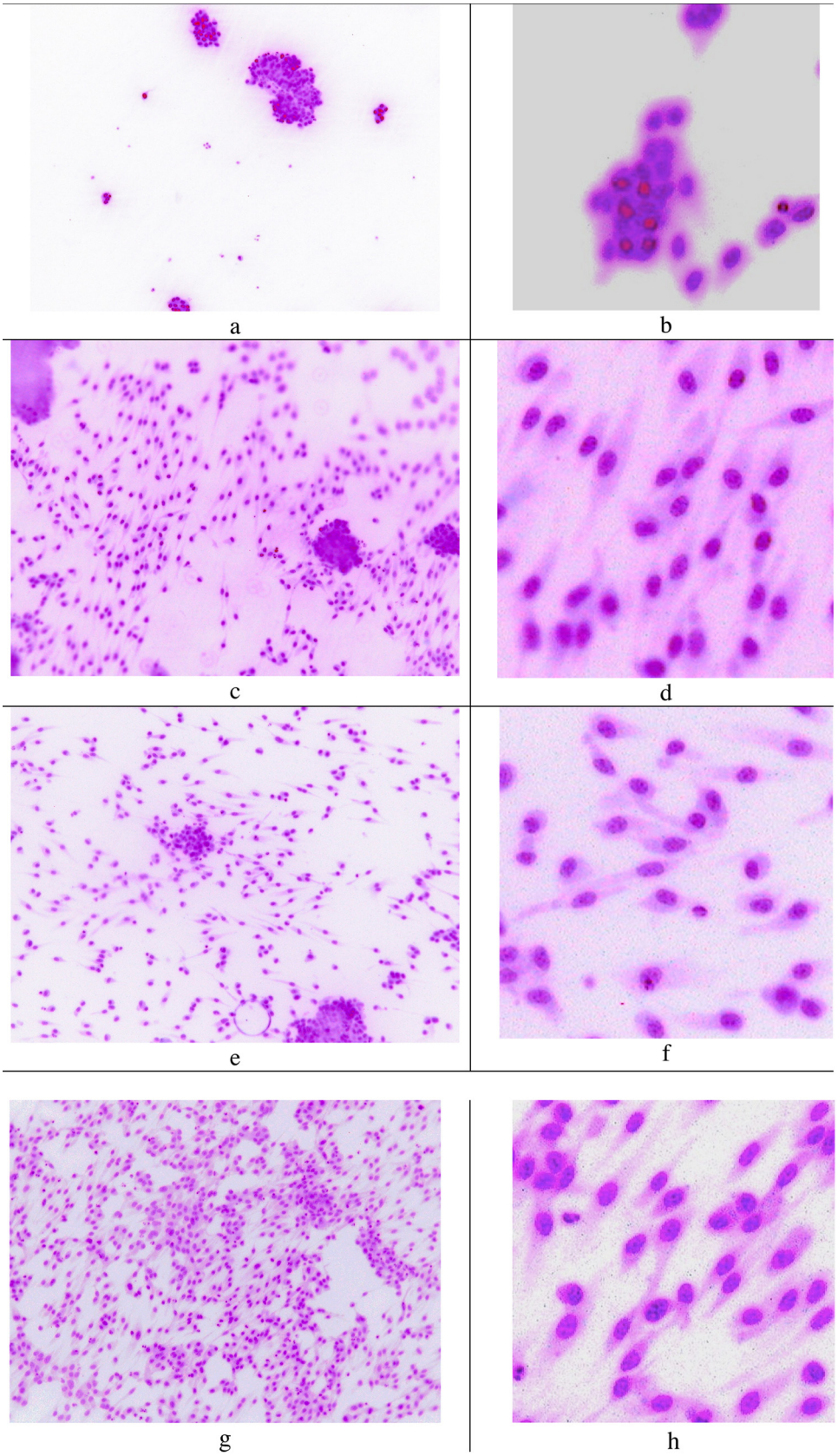

Fig. 6. Microphoto of cells grown 3 days on untreated (a, b) and ion implanted (c–h) PTFE. The treatment was done by nitrogen ions of 20 keV energy with 6×10^{13} (c, d), 1×10^{14} (e, f) and 5×10^{14} (g, h) ions/cm^2. The cells form a compact colony on untreated PTFE (low resolution image a). Cell body is circled, compact to minimize a contact area with untreated PTFE surface (high resolution image b). The cells are distributed uniformly on ion implanted PTFE (low resolution image c, e and g). The cell body is elongated to maximize a contact with the ion implanted PTFE (high resolution image d, f and h). The original color was inverted for better observation.

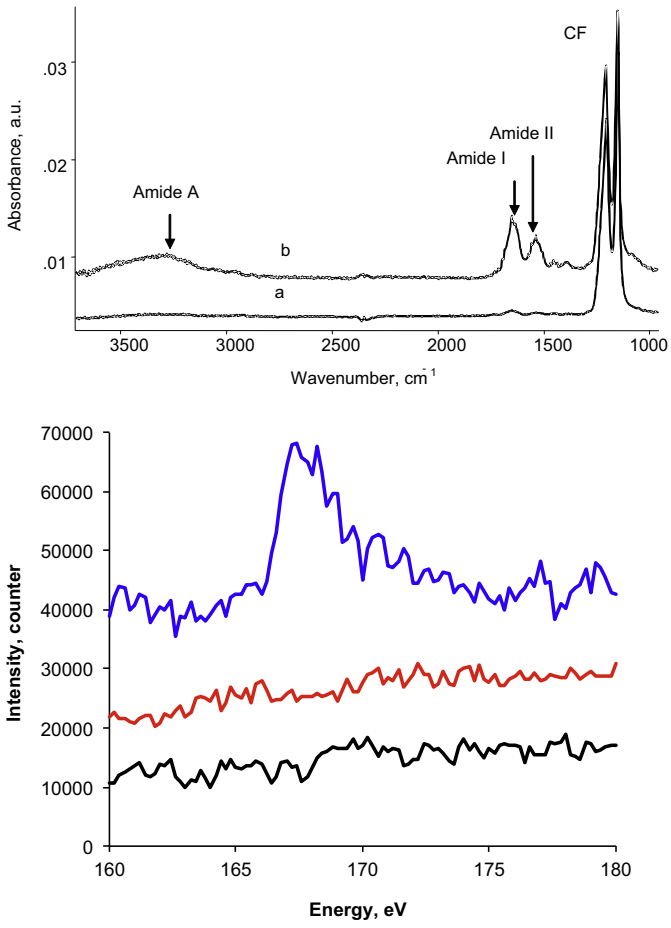

Fig. 7. Proteins are observed on the PTFE and ePTFE modified surface after cell attachment and removing. Top spectra are FTIR ATR spectra of ePTFE surface after cell growing and removing: (a) untreated, (b) ion implanted. The arrays show Amide A, Amide I and II lines of proteins. The C–F lines of ePTFE are marked with "CF". Bottom spectra are XPS spectra of PTFE in S2p region of energy: bottom (black) is untreated PTFE, middle (red) is ion implanted PTFE, top (blue) is ion implanted PTFE after cells growing. The cells have been removed. The S2p line in spectrum of ion implanted PTFE after cell growing indicates a presence of attached ECM proteins. (For interpretation of the references to color in this figure legend, the reader is referred to the web version of the article.)

absence of initiator of polymerization in the acrylamide solution prevents a spontaneous polymerization of acrylamide monomer, the polymerization of acrylamide on the ion implanted PTFE surface is available only due to reactions of acrylamide monomer with active groups in the modified surface. The absence of C=C in the attached layer shows that this group was spent for the attachment. Similar reaction of C=C group is a polymerization reaction of acrylamide with free radicals of initiator. In present experiment, the initiator of polymerization could be free radicals of the modified layer of PTFE, which were detected active in previous study [33].

Following the surface modification of PTFE, the cells adhere and grow differently on untreated and ion implanted PTFE surface. The cells adhere and grow on both untreated and ion implanted PTFE, however the amount of cells on the ion implanted PTFE is significantly higher, than on untreated PTFE (Table 2). The cells are growing better on PTFE treated with lowest fluence (6×10^{13}), while on high fluence treated PTFE (5×10^{14} ions/cm^2) the amount of cells is higher significantly that on untreated PTFE. Similar improvement of cell adherence was observed for rat smooth muscle cells on PTFE after dielectric barrier discharge [43] and vascular smooth muscle cells on PTFE with deposited carbon coating [44].

Table 2
Density of endothelial cells distribution on PTFE after 3 days growing.

Fluence of the treatment	Cell density (μm^{-2})
Seeded cell density for all samples	4×10^4
Untreated	$(490 \pm 100) \times 10^4$
6×10^{13} ions/cm^2	$(2100 \pm 500) \times 10^4$
10^{14} ions/cm^2	$(1500 \pm 300) \times 10^4$
5×10^{14} ions/cm^2	$(1400 \pm 400) \times 10^4$

The cells are distributed differently on untreated and ion implanted PTFE surfaces. The cells on untreated PTFE surface are joined to compact colony and most surface remains free of cells (Fig. 6). The cell density in the colony is high. The cell bodies are small and round.

The cells cover whole surface of the ion implanted PTFE. The cell density is mostly uniform overall surface. The cell bodies are elongated and spread on the PTFE surface. Similar uniform cell spreading is observed on the ion implanted ePTFE fibrils. Such cell improved picture is observed for low (6×10^{13}) and high (5×10^{14}) fluence of ion implantation.

The specific contact of cells with ion implanted ePTFE was supported by FTIR ATR and XPS spectra of the ePTFE surface after cell culture (Fig. 7). The substrates after the cell culture were washed with buffer and distilled water. The FTIR ATR spectra showed the presence of intensive lines at 3300, 1650 and 1540 cm^{-1} related to Amide A, Amide I and Amide II vibrations of peptide groups. Such groups are attributed to proteins, which were in contact with PTFE surface when cells were adhered. After removing of the cells, these proteins remain attached on the ion implanted ePTFE surface. The spectrum of untreated ePTFE shows these lines with lower intensity. The proteins after cell attachment were also observed by the XPS spectra of modified ePTFE (Fig. 7). The lines of S2p at 169.8 and 172.8 eV are attributed to sulfur atom of proteins. Spectrum of untreated ePTFE after cell growing does not show S2p line or its intensity is undetectable. Both kinds of spectra show, that the ion implanted ePTFE surface provides a strong protein attachment from the cells when cells are adhered and grown.

4. Discussion

The total cell coverage of the implant surface is critical for organism respond. The integration of polymer implants into organism needs a hosting for organism cells on the implantable material. The materials of implant are selected to provide the functionality of the medical device, when the surface of the material should provide adherence, differentiation, viability of the cells for a long period of time. The interaction of cell with the substrate surface is complex and proceeds through a number of protein-surface interactions and protein transformations in cell wall. The first reaction of extracellular matrix (ECM) protein on a presence of the substrate is adsorption on the surface and a conformation of the protein reports about suitability of the surface for the cell adherence. Therefore, the respond of the ECM protein should correspond to the natural cell functionality.

The untreated PTFE is hydrophobic materials with water contact angle of 120°. When a cell approaches the surface and the cell wall protein is attached on the hydrophobic surface, the conformation of the protein is adopted to maximize the hydrophobic interactions, while before the protein was surrounded by water and its hydrophilic interactions were maximized. To switch to hydrophobic interactions, the protein should change a conformation. As result, the cell could get a signal that the ECM protein changes the conformation. The squashed cell shape, compact cell distribution and low cell growing rate on untreated PTFE and ePTFE show, that the hydrophobic interactions on the untreated PTFE surface are not favorable for the cells.

The ion implantation changes the chemical structure of the PTFE and ePTFE surface layer dramatically. The surface becomes chemically active with appearance of free radicals, oxygen-containing and nitrogen-containing groups. The water contact angle decreases to 70–80°. When the protein molecule approaches this hydrophilic surface, the rest of protein molecule remains surrounded by water molecule and the water molecules remain in the interface between the surface and attached protein molecule. The water core preserves the protein hydrophilic interactions and consequently the conformation, while the protein attachment is based on a free radical activity of the modified layer. It provides a strong attachment of protein as it was shown in other studies [18,21,45–47]. According the active protein conformation, the cell gets right signal and spreads on the surface. The total coverage of the modified polymer with growing active cells gives a new opportunity for the medical implants in future.

5. Conclusions

The ion implantation changes significantly the structure of ePTFE and PTFE surface layer. The PTFE surface becomes rough due to etching of polymer surface layer under ion bombardment. The ePTFE fibrils become thinner. The surface layer becomes carbonized, oxidized and nitrized. As result, the surface becomes hydrophilic and chemically active with free radicals, as it is observed by polymerization free radical reaction of acrylamide. The cell adherence to ion implanted PTFE and ePTFE is enhanced through the attached proteins from cells. The results on cell adherence and growing show, that ion implanted PTFE and ePTFE can be suitable materials for cell growing and cell spreading on the surface, when a medical implant is required to be totally coated by the cells.

Acknowledgments

The study was supported by Boston Scientific SCIMED Inc. (USA), Ministry of Science of Germany (WTZ RUS01/225 and WTZ RUS00/218) and RFBR (13-01-96009 r_ural_a). This work benefited from the International Research Group Program supported by Perm region Government. One of the authors (A.K.) gratefully acknowledges financial support from the Alexander von Humboldt Foundation (Germany). Authors thank Dr. Manfred Maitz (Institute of Polymer Research, Germany) for his contribution in cell experiments, useful discussions and help. Authors thank Ms. Elke Quaritsch (Rossendorf Research Center, Germany) for XPS spectra recording and Dr. Darina Manova (Leibniz Institute of Surface Modification) for assistance in ion implantation of PTFE samples in Leipzig Institute.

References

[1] C. Batich, P. Leamy Biopolymers, Standard Handbook of Biomedical Engineering & Design (Myer Kutz), McGraw-Hill, New-York, 2003.
[2] T.C. Hodges, M.F. Fillinger, R.M. Zwolak, D.B. Walsh, F. Bech, J.L. Cronenwett, Longitudinal comparison of dialysis access methods: risk factors for failure, J. Vasc. Surg. 26 (6) (1997) 1009–1019.
[3] G.J. Toes, K.W. van Muiswinkel, W. van Oeveren, A.J.H. Suurmeijer, W. Timens, I. Stokroos, J.J.A.M van den Dungen, Superhydrophobic modification fails to improve the performance of small diameter expanded polytetrafluoroethylene vascular grafts, Biomaterials 23 (1) (2002) 255–262.
[4] P.H. Lin, C. Chen, R.L. Bush, Q. Yao, A.B. Lumsden, S.R. Hanson, Small-caliber heparin-coated ePTFE grafts reduce platelet deposition and neointimal hyperplasia in a baboon model, J. Vasc. Surg. 39 (6) (2004) 1322–1328.
[5] M.D. Phaneuf, S.A. Berceli, M.J. Bide, W.G. Quist, F.W. LoGerfo, Covalent linkage of recombinant hirudin to poly(ethylene terephthalate) (Dacron): creation of a novel antithrombin surface, Biomaterials 18 (10) (1997) 755–765.
[6] S.A. Berceli, M.D. Phaneuf, F.W. LoGerfo, Evaluation of a novel hirudin-coated polyester graft to physiologic flow conditions: hirudin bioavailability and thrombin uptake, J. Vasc. Surg. 27 (6) (1998) 1117–1127.
[7] J. Murray-Wijelath, D.J. Lyman, E.S. Wijelath, Vascular graft healing. III. FTIR analysis of ePTFE graft samples from implanted bigrafts, J. Biomed. Mater. Res. B: Appl. Biomater. 70B (2) (2004) 223–232.
[8] K.J. Pawlowski, S.E. Rittgers, S.P. Schmidt, G.L. Bowlin, Endothelial cell seeding of polymeric vascular grafts, Front. Biosci. 9 (2004) 1412–1421 (Landmark edition).
[9] T.R. Dunkern, M. Paulitschke, R. Meyer, R. Büttemeyer, R. Hetzer, G. Burmester, M. Sittinger, A novel perfusion system for the endothelialisation of PTFE grafts under defined flow, Eur. J. Vasc. Endovasc. Surg. 18 (2) (1999) 105–110.
[10] E. Vinard, G. Lesèche, B. Andreassian, D. Costagliola, In vitro endothelialization of PTFE vascular grafts: a comparison of various substrates, cell densities, and incubation times, Ann. Vasc. Surg. 13 (2) (1999) 141–150.
[11] I.E. Birchall, V.W.K. Lee, V. Ketharanathan, Retention of endothelium on ovine collagen biomatrix vascular conduits under physiological shear stress, Biomaterials 22 (23) (2001) 3139–3144.
[12] D.Y. Tseng, E.R. Edelman, Effects of amide and amine plasma-treated ePTFE vascular grafts on endothelial cell lining in an artificial circulatory system, J. Biomed. Mater. Res. 42 (2) (1998) 188–198.
[13] K.R. Kidd, V.B. Patula, S.K. Williams, Accelerated endothelialization of interpositional 1-mm vascular grafts, J. Surg. Res. 113 (2) (2003) 234–242.
[14] A. Lu, R. Sipehia, Antithrombotic and fibrinolytic system of human endothelial cells seeded on PTFE: the effects of surface modification of PTFE by ammonia plasma treatment and ECM protein coatings, Biomaterials 22 (11) (2001) 1439–1446.
[15] K.P. Walluscheck, G. Steinhoff, S. Kelm, A. Haverich, Improved endothelial cell attachment on ePTFE vascular grafts pretreated with synthetic RGD-containing peptides, Eur. J. Vasc. Endovasc. Surg. 12 (3) (1996) 321–330.
[16] S.P. Massia, S.S. Rao, J.A. Hubbell, Covalently immobilized laminin peptide TYR-ILE-GLY-SER-ARG (YIGSR) supports cell spreading and colocalization of the 67-kilodalton laminin receptor with alpha-actinin and vinculin, J. Biol. Chem. 268 (11) (1993) 8053–8059.
[17] N. Takahashi, H. Ujiie, Y. Suzuki, M. Iwaki, T. Hori, Ion-beam irradiated ePTFE for an artificial dura mater, No Shinkei Geka 10 (2003) 1081–1088.
[18] A. Kondyurin, M.F. Maitz, Surface modification of ePTFE and implants using the same, Patent WO 022174 A3, 2007; US Patent 7597924.
[19] V.B. Odzhaev, I.P. Kozlov, V.N. Popok, D.B. Sviridov, Ion Implantation of Polymers, Belorussian State University, Minsk, 1998.
[20] D. Fink, Fundamentals of Ion-Irradiated Polymers, Springer, Berlin, 2004.
[21] A. Kondyurin, M. Bilek, Ion Beam Treatment of Polymers, Elsevier, Oxford, 2008.
[22] L. Calcagno, G. Compagnini, G. Foti, Structural modification of polymer films by ion irradiation, Nucl. Instrum. Methods B 65 (1992) 413–422.
[23] J. Zhang, X. Zhang, H. Zhou, Effect of aging on surface chemical bonds of PTFE irradiated by low energy Ti ion, Appl. Surf. Sci. 205 (2003) 343–352.
[24] J. Zhang, X. Zhang, H. Zhou, Surface-restructuring behavior of aged PTFE irradiated by a high-flux nitrogen ion beam, Surf. Coat. Technol. 187 (2004) 250–256.
[25] C.-Y. Tu, C.-P. Chen, Y.-C. Wang, C.-L. Li, H.-A. Tsai, K.-R. Lee, J.-Y. Lai, Acrylamide plasma-induced polymerization onto expanded poly(tetrafluoroethylene) membrane for aqueous alcohol mixture vapor permeation separation, Eur. Polym. J. 40 (2004) 1541–1549.
[26] Y. Zhang, A.C.H. Huan, K.L. Tan, E.T. Kang, Surface modification of poly(tetrafluoroethylene) films by low energy Ar^+ ion-beam activation and UV-induced graft copolymerization, Nucl. Instrum. Methods Phys. Res. B 168 (2000) 29–39.
[27] A. Oshima, T. Seguchi, Y. Tabata, ESR study on free radicals trapped in crosslinked polytetrafuoroethylene (PTFE) – II radical formation and reactivity, Radiat. Phys. Chem. 55 (1999) 61–71.
[28] K. Schierholz, U. Lappan, K. Lunkwitz, Electron beam irradiation of polytetrafluoroethylene in air: investigations on the thermal behavior, Nucl. Instrum. Methods Phys. Res. B 151 (1999) 232–237.
[29] T.R. Dargaville, D.J.T. Hill, A.K. Whittaker, An ESR study of irradiated poly(tetrafluoroethylene-co-perfluoropropylvinylether)(PFA), Radiat. Phys. Chem. 62 (2001) 25–31.
[30] M. Adami, L. Guzman, B.Y. Man, A. Miotello, P.M. Ossi, High temperature ion beam erosion of polytetrafluoroethylene, Thin Solid Films 459 (2004) 318–322.
[31] A. Oshima, T. Seguchi, Y. Tabata, ESR study on free radicals trapped in crosslinked polytetrafluoroethylene (PTFE) – II radical formation and reactivity, Radiat. Phys. Chem. 55 (1999) 61–71.
[32] N. Gavrilov, D. Yakusheva, A. Kondyurin, Structure of polyethylene after pulse ion beam treatment, J. Appl. Polym. Sci. 69 (1998) 1071–1077.
[33] G. Mesyats, Yu. Klyachkin, N. Gavrilov, A. Kondyurin, Adhesion of Polytetrafluorethylene modified by an ion beam, Vacuum 52 (1999) 285–289.
[34] Y. Suzuki, M. Iwaki, S. Tani, G. Oohashi, M. Kamio, Ion implantation into ePTFE for application of a dural substitute, Nucl. Instrum. Methods Phys. Res. B 206 (2003) 538–542.
[35] R.L. Clough, High-energy radiation and polymers: a review of commercial processes and emerging applications, Nucl. Instrum. Methods Phys. Res. B 185 (2001) 8–33.
[36] V.P. Begishev, R., Guenzel, M., Maitz, A.V., Kondyurin, I.V., Kondyurina, V.A., Romanova, M. Pham, Method of preparation of drug release material, Patent RU 2223793 C1, 2002.
[37] G.A. Mesyats, Yu.S. Klyachkin, N.V. Gavrilov, V.N. Mizgulin, R.M. Yakushev, A.V. Kondyurin, Ion beam modification of polyethylene and adhesion to epoxy adhesive, Vacuum 47 (1996) 1085–1087.
[38] J.B. Grinspan, S.N. Mueller, E.M. Levine, Bovine endothelial cells transformed in vitro by benzo(a)pyrene, J. Cell Physiol. 114 (1983) 328–338.

[39] J. Zhanga, X. Yua, H. Lia, X. Liu, Surface modification of polytetrafluoroethylene by nitrogen ion implantation, Appl. Surf. Sci. 185 (2002) 255–261.
[40] H.Y. Kwong, M.H. Wong, Y.W. Wong, K.H. Wong, Superhydrophobicity of polytetrafluoroethylene thin film fabricated by pulsed laser deposition, Appl. Surf. Sci. 253 (2007) 8841–8845.
[41] Y. Chen, Z. Zhao, J. Dai, Y. Liu, Topological and chemical investigation on superhydrophobicity of PTFE surface caused by ion irradiation, Appl. Surf. Sci. 254 (2007) 464–467.
[42] K. Kereszturi, A. Toíth, M. Mohai, I. Bertoíti, J. Szépvölgyi, Nitrogen plasma-based ion implantation of poly(tetrafluoroethylene): effect of the main parameters on the surface properties, Appl. Surf. Sci. 256 (2010) 6385–6389.
[43] Y.K. Cho, D. Parka, H. Kim, H. Lee, H. Park, H.J. Kim, D. Jung, Bioactive surface modifications on inner walls of poly-tetra-fluoro-ethylene tubes using dielectric barrier discharge, Appl. Surf. Sci. 296 (2014) 79–85.
[44] T. Hubácek, J. Siegel, R. Khalili, N. Slepicková-Kasálková, V. Svorciík, Carbon coatings on polymers and their biocompatibility, Appl. Surf. Sci. 275 (2013) 43–48.
[45] M.M.M. Bilek, D.V. Bax, A. Kondyurin, Y. Yin, N.J. Nosworthy, K. Fisher, A. Waterhouse, A.S. Weiss, C.G. dos Remedios, D.R. McKenzie, Free radical functionalization of surfaces to prevent adverse responses to biomedical devices, Proc. Natl. Acad. Sci. 108 (2011) 14405–14410.
[46] A.V. Kondyurin, P. Naseri, J.M.R. Tilley, N.J. Nosworthy, M.M.M. Bilek, D.R. McKenzie, Mechanisms for covalent immobilization of horseradish peroxidase on ion-beam-treated polyethylene, Scientifica (2012), http://dx.doi.org/10.6064/2012/126170, Article ID 126170.
[47] A. Kondyurin, N.J. Nosworthy, M.M.M. Bilek, Attachment of horseradish peroxidase to polytetrafluorethylene (teflon) after plasma immersion ion implantation, Acta Biomater. 4 (2008) 1218–1225.

IOPscience iopscience.iop.org

Home Search Collections Journals About Contact us My IOPscience

Experimental investigation of plasma-immersion ion implantation treatment for biocompatible polyurethane implants production

This content has been downloaded from IOPscience. Please scroll down to see the full text.

2016 IOP Conf. Ser.: Mater. Sci. Eng. 123 012003

(http://iopscience.iop.org/1757-899X/123/1/012003)

View the table of contents for this issue, or go to the journal homepage for more

Download details:

IP Address: 220.244.130.46
This content was downloaded on 12/06/2016 at 23:28

Please note that terms and conditions apply.

IOP Conf. Series: Materials Science and Engineering **123** (2016) 012003 doi:10.1088/1757-899X/123/1/012003

Experimental investigation of plasma-immersion ion implantation treatment for biocompatible polyurethane implants production

R I Iziumov, AY Beliaev[1], I V Kondyurina[2], I N Shardakov[1], A V Kondyurin[3], M M Bilek[3] and D R McKenzie[3]

[1]Institute of Continuous Media Mechanics UB RAS, Perm, Russia
[2]School of Medicine, University of Sydney, Sydney, Australia
[3]School of Physics, University of Sydney, Sydney, Australia

E-mail: izumov@icmm.ru

Abstract. Modification of the surface layer of polyurethane with plasma-immersion ion implantation (PIII) and studying its physical and chemical changes have been discussed in this paper. The goal of the research was to obtain carbonized layer allowing creating biocompatible polyurethane implants. The experiments of PIII treatment in various modes were performed. The investigation of the modified surface characteristics was carried out by observing the kinetics of free surface energy for two weeks after treatment. The regularities between treatment time and the level of free surface energy were detected. The explanation of high energy level was given through the appearance of free radicals in the surface layer of material. The confirmation of the chemical activation of the polyurethane surface after PIII treatment was obtained.

1. Introduction

The necessity of restoring or substitution the damaged human tissues by artificial device produced using different polymers or metal alloys, has determined the development of a separate section of modern medicine – the implantology.

The main purpose of such type of surgery is to restore lost characteristics and properties of tissue or, if possible, its improvement. The most important requirements to the characteristics of the implantable material are biocompatibility, mechanical properties (strength, elasticity or hardness, coefficient of friction, durability), chemical properties (corrosion resistance, the absence of toxic emissions), the weight and the economic aspect [1].Nowadays many research groups are carried out investigations aimed at studying the possibility of applying polymer materials in medicine (food grade polypropylene (Anulon-92) [2], polystyrene [3], polymethylpentene [4, 5], polyethylene [6, 7], polyethylene terephthalate (PET) [8], thermo-plastic polyurethane (Elastollan ® 1180A50) [9], polyhydroxybutyrate (PHB), poly-L-lactic acid (PLLA) [10, 11], polytetrafluoroethylene (PTFE) [12], biodegradable polymer [13]). Polymeric materials are becoming more popular due to the fact that it satisfies almost all specified requirements [14-16]. Its surface may provide immobilization of biologically active molecules and living cells, however, this quality requires significant improvements [17,18]. Rational way to solve this problem is to develop a technique of treatment the outer layer, modifying it so that it becomes a safe, friendly, biocompatible capsule for the body and the inner part of the implant would have the rest of the required parameters.

Content from this work may be used under the terms of the Creative Commons Attribution 3.0 licence. Any further distribution of this work must maintain attribution to the author(s) and the title of the work, journal citation and DOI.
Published under licence by IOP Publishing Ltd

Among a number of ways to modify the surface (chemical exposure, temperature processing, the corona discharge, ultraviolet irradiation [19, 20]), one of the most promising areas of research is also the use of plasma-immersion ion implantation (PIII). With this technology, it is possible to create on the material surface the layer having the property of biocompatibility; moreover the process itself is clean and leaves no traces on the surface of by-products. Also, comparing with other conventional techniques, PIII advantage consists in the ability to precisely control the surface modification, regardless of its geometry [21].

In numerous papers related to the study the possibilities of PIII technology, it is shown that the structure and surface chemical properties of the treated polymer are dependent on the gas from which the plasma is generated, and the time and intensity of treatment. It is considered the application of the following gases and its mixtures: helium [22], nitrogen [8], oxygen, argon and argon + oxygen mixture [23]. There is often the interest to analyse the influence of the experimental parameters within some range (the pressure of the plasma, gas flow, power, time of treatment). In our experiments we performed the treatment in the nitrogen plasma with ion energy of 20keV. Treatment time was varied from 80 to 800 seconds that corresponds to$5\cdot10^{14}$– 10^{16} ions/cm^2.

To analyse the effect of ion-plasma treatment on the surface of the material it is often used a combination of several methods of experimental studies such as optical microscopy [3], atomic force microscopy (AFM) [2, 4], scanning electron microscopy (SEM) [2, 3], x-ray photoelectron spectroscopy (XPS) [3, 4], infrared spectroscopy (FTIR) [2], the study of the surface energy by measuring the contact angle [2, 4], tensile test [2], thermal analysis (Differential Scanning Calorimetry TA) [2], spectrophotometry [2], Rutherford backscattering spectroscopy (RBS) [4], electrokinetic analysis [4], goniometry [4], ablation of PMP surface layers determined by gravimetry [4].For biocompatibility study experiments with mouse embryonic fibroblasts [2, 6], human osteosarcoma cells [3] and human blood (haemolytic potential, thrombogenicity) [2, 8] are performed. In our work, we have applied the analysis of the kinetics of the surface energy, including its polar and dispersive components, as a function of the past time after treatment; in addition we plan to take advantage of XPS and infrared spectroscopy.

The above studies have shown that, depending on the purpose, in one case, ion-plasma treatment can dramatically increase the number of adhered cells or bioactive molecules as well as positively affect the uniform distribution of cells on the surface of the material and their viability. In another case, decrease of platelet adhesion is confirmed that causes the improvement of the blood compatibility.

2. Materials and methods

2.1. PIII treatment of PU samples

For the treatment on PIII device we used the samples of size 1×2 cm^2. Experimental investigations include set of PIII-treatments of polyurethane samples for 40, 80, 400 and 800 s (corresponding to an ion fluency of $5\cdot10^{14}$, 10^{15}, $5\cdot10^{15}$, 10^{16} ions/cm^2). The source of ions was inductively coupled radio-frequency nitrogen plasma powered at 13.56 MHz. The nitrogen gas used for PIII was 99.99% pure. The plasma power was 100W with reverse power of 12W when matched. The plasma density during treatment was monitored by a Langmuir probe with rf-block from Hiden Analytical Ltd. The base pressure was 10^{-6}Torr ($\sim10^{-4}$ Pa); the pressure of nitrogen during implantation was $2\cdot10^{-3}$Torr ($\sim4.4\cdot10^{-2}$ Pa).

The samples were treated in plasma chamber by ion beam, which was extracted from plasma by the application of high voltage (20kV) at a frequency of 50Hz with duration of pulses of 20μs. The polyurethane samples were placed on a holder with a mesh. The mesh was electrically connected to the holder and held in front of the sample on the distance of 5 cm.

2.2. Contact angles and surface free energy

The contact angles of two liquids (de-ionized water and diiodomethane) on the surface of PU were measured by contact angle analyzer Kruss DS10 based on the sessile drop technique. For calculating the surface free energy and its polar and dispersive components the Rabel model with regression method was used. There was a set of 11 measurements of 5 drops of each liquid per sample. After ion-plasma treatment the kinetics was being monitored during 2 weeks (20, 30, 40 minutes, 1, 2, 5, 7, 23 hours, 2, 4, 11 days after treatment).

3. Results

The first contact angle measurement was carried out immediately after extracting the sample from the PIII device, which process included injection of air into a vacuum chamber and took 20 minutes. The obtained data showed an inverse dependence between the values of contact angles of water and treatment time. The contact angle for the sample treated for 40 seconds was equal to 48±2º, for 80 seconds: 47±1.5º, for 400 seconds: 45±0.9º, for 800 seconds: 38±0.4º.After 2 weeks the contact angle has increased and reached a stable value. For the sample treated for 40 seconds, the contact angle became equal to 63±2.3º, for 80 seconds: 73±1.7º, for 400 seconds: 66±1.3º, for 800 seconds: 64±1.4º (figure 1).

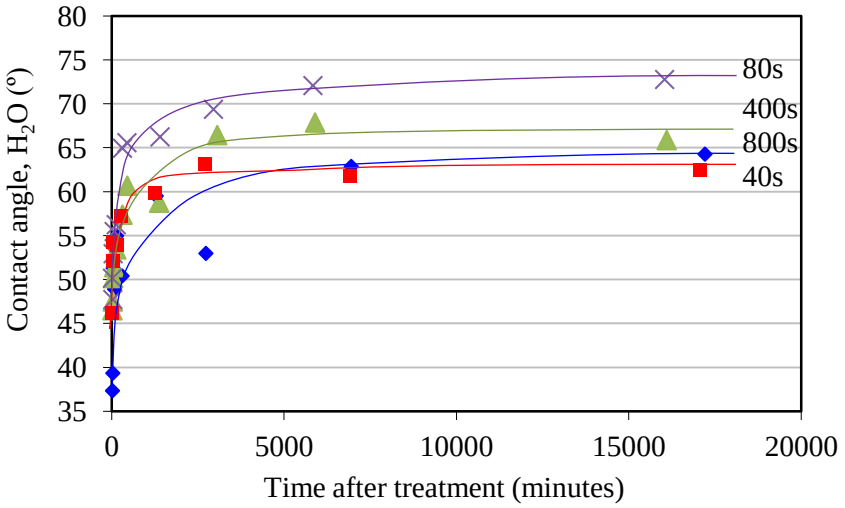

Figure 1. Kinetics of water contact angle after treatment samples in 4 modes of PIII

In this case, the correlation between the treatment time and the contact angle remained only for three treatment modes (80, 400, 800 seconds). The sample treated over the shorter time of 40 seconds, has showed the lowest value of the contact angle, standing out from the overall trend.

Kinetics of diiodomethane contact angle was significantly different from water and it was nonmonotonic. Although as in the case of water the treatment also decreased the contact angle but to a lesser degree. The correlation between the angle and the plasma treatment time is not observed, and after two weeks after treatment the contact angle has reached the level of 44±0.5° for all the samples, regardless of treatment time (figure2).

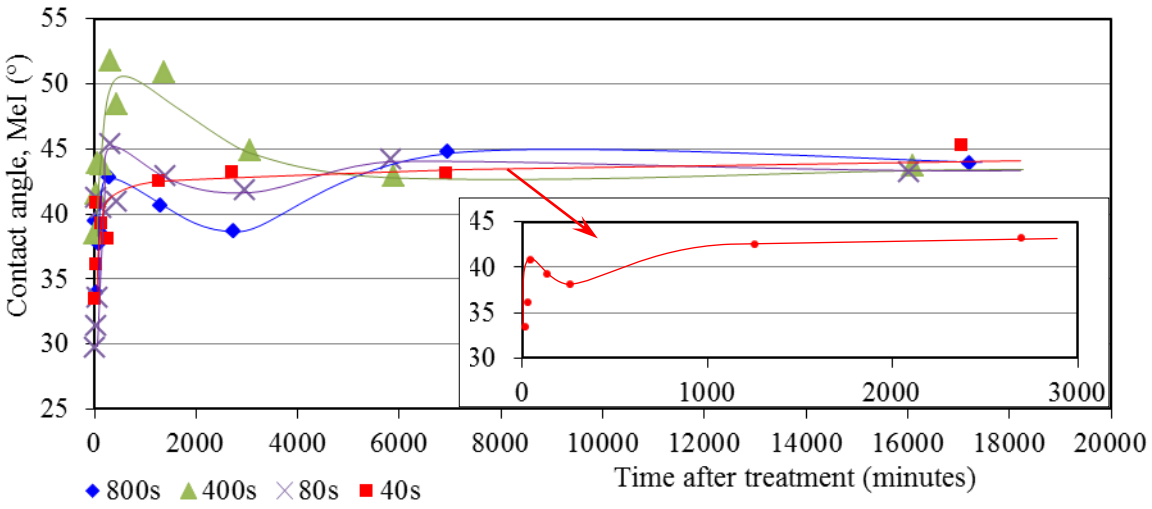

Figure 2. Kinetics of diiodomethane contact angle after PIII treatment during two weeks

The dependence between the total free energy and the treatment time has the correlation similar to the dependence of water contact angle. After 2 weeks for 3 PIII modes there was a direct dependence between the treatment time and energy value: the sample treated for 80 seconds had 45.5 mJ/m^2, for 400 seconds: 48 mJ/m^2, for 800 seconds: 49.5 mJ/m^2. But the treatment during 40 seconds gave the highest value: 50.5 mJ/m^2.

Analysis of the experimental data was carried out by approximation (figure3) using a function (equation (1)) represented as a sum of two exponential functions:

$$f(t) = a_0 + a_1 \exp(-t / k_1) + a_2 \exp(-t / k_2) \quad (1)$$

where f is a total free energy;t is time after PIII treatment; $k_1$and $k_2$are the rate constants of the two characteristic stages; a_0, $a_1$and $a_2$are the constants to be defined.

The effectiveness of such method of approximation was demonstrated in [24], in which the observed phenomenon isqualitatively similar.

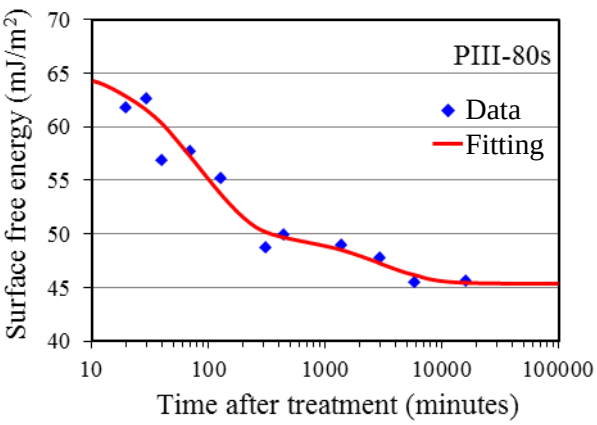

Figure 3. Exampleof data and its fitting

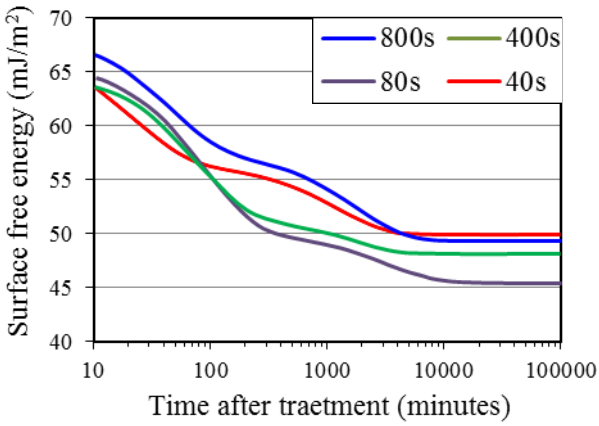

Figure 4. Kinetics of total surface free energy

Analysis of the kinetics of the surface free energy (figure4) revealed that after PIII treatment of PU two characteristic relaxation processappeared, the first of which was predominant over the second one, but faded rapidly,after which only the second process occurred.This is confirmed by the fact that the characteristic time for the first process (k_1) although has a large spread (from 24.3 to 45 min) but

comparing to the second one ($k_2$variesfrom 1258.5 to 3177.8 min) has significantly (by two orders of magnitude) smaller value (Table 1).

Table 1. The constants of fitting function and its values in limiting cases fortotal surface free energy

Time of treatment, s	$f(0)$, mJ/m^2	$f(\infty)$, mJ/m^2	k_1, min	k_2, min
40	67±1.1	50±0.7	24.3±5.3	1258.5±438.3
80	65.5±0.9	45.5±0.5	89.9±14.3	3177.8±1805.9
400	65±0.5	48±0.2	80.5±9.6	1638.6±841.7
800	66±1.2	49.5±0.5	45±10.8	1789.9±815.2

Extrapolation of the data allows determining the value of free energy at the time immediately after treatment, f (0) (Table 1). This value is essentially independent of the treatment time and equals 66±1mJ/m^2. Similar way we determined the level, which energy reached at the expiration of arbitrarily large period of time, $f(\infty)$. It is equal to 50.5, 45.5, 48, 49.5 mJ/m^2, respectively for 40, 80, 400, 800 seconds oftreatment.

The qualitative behavior of the total energy is caused by polar component, because a dispersivecomponent remains during two weeks practically constant.Its value was inside the range of 40±5 mJ/m^2 and had no dependence on the treatment time.

Polar component after 2 weeks decreased significantly (by 35-55%).Moreover, there was a direct correlation between the reduction of energy and the PIII mode: for the sample treated for 40 seconds, reduction was 35% (from 20 to 13 mJ/m^2) for 80 and 400 seconds: 53% (8 to 17 mJ/m^2 and from 21 to 10 mJ/m^2, respectively) for 800 seconds: 55% (from 26 to 12 mJ/m^2).

After 2 weeks remaining values of polar components were 3, 8, 10, 12 mJ/m^2, respectively for 40, 80, 400, 800 sec. Thus, we can trace the situation similar to total free energy, where the 40 seconds treatment is out from theoverall trend (Table 2).

Table 2. The constants of fitting function and its values in limiting cases for polar component of the surface free energy

Time of treatment, s	$f^P(0)$, mJ/m^2	$f^P(\infty)$, mJ/m^2	k_1^P, min	k_2^P, min
40	24±0.4	13±1.1	20±4.8	767±388.1
80	20.5±0.3	7.5±0.5	107±21.2	3121±1265.3
400	23±0.8	10±0.7	42.9±16.8	2224±574.5
800	28±0.5	12±1.3	43.8±16.9	5494.2±4559.4

4. Conclusion

In this work the investigation of polyurethane modification to create chemically activesurface layer in material was performed. By monitoring the kinetics of surface free energy and its polar and the dispersivecomponents itwas established that treatment of the material leads to significant and irreversible changes in the surface layer.It results in a sharp increase of the surface energy after PIII treatment and preserving its sufficiently high, in comparison with untreated PU, level thatreflectssignificant chemical changes on the surface of polymers.At the same time, such a considerable increase of energy (up to a level of about 67 mJ/m^2)and behavior of its polar and dispersive components can be attributed to only the appearance of free radicals in the material, which in turn makes it possibleto add, using existing techniques, to polyurethane the property of biocompatibility.Using a level $f(\infty)$, which is reachedby energy after a sufficiently long period of time, as a criterion of selecting a treatment mode, we can make the assumption thatamong all variants of treatment the briefest one (40s) may be the most preferable for us by the fact that stored energy and, therefore, the concentration of free radicals onto the surface has the highest level among all the considered variants.

At this stage of research it can be claimedthat the application of PIII technology has enabled to activatesurface layer of polyurethanethat offers the prospect of further modification of the surface to the level of biocompatibility.

5. Acknowledgements

The work was supported by the Russian Foundation for Basic Research (grant 13-01-96009_r_ural_a and grant 14-08-96003_r_ural_a)and the Ministry of Education of Perm Region under agreement (S-26/632).

6. References

[1] Gomathi N, Sureshkumar A and Neogi S 2008 *Curr. Sci.* **94** 1478–1486.
[2] Gomathi N, Rajasekar R, Babu R, Mishra D and Neogi S 2012 *Mat. Sci. and Eng.* C **32** (7) 1767
[3] Recek N, Mozetič M, Jaganjac M, Milkovič L, Žarkovic N and Vesel A 2013 *Vacuum* **98** 116
[4] Slepička P, Trostová S, Slepičková Kasálková N, Kolská Z, Malinský P, Macková A, Bačáková L and Švorčík V 2012 *Polymer Degradation and Stability* **97** 1075
[5] Michaljaničová I, Slepička P, Slepičková Kasálková N, Sajdl P and Švorčík V 2014 *Vacuum* **107** 184
[6] Rimpelová S, Slepičková Kasálková N, Slepička P, Lemerová H, Švorčík V and Ruml T 2013 *Mat. Sci. and Eng.* C **33** 1116
[7] Kondyurin A, Naseri P, Fisher K, McKenzie D R and Bilek M M 2009 *Polymer Degradation and Stability* **94** 638
[8] Junkar I 2013 *Vacuum* **98** 111
[9] Alves P, Cardoso R, Correia T R, Antunes B P, Correia I J an Ferreira P 2014 *Colloids and Surfaces* B **113** 25
[10] Slepičková KasálkováN, Slepička P, Bačáková L, Sajdl P and Švorčík V 2013 *Nuclear Instruments and Methods in Physics Research Section B* **307** 642
[11] Slepicka P, Trostová S, Slepicková Kasálková N, Kolská Z, Sajdl P and Švorcík V 2012 *Plasma Processes Polym*. **9** 197
[12] Reznícková A, Kolská Z, Hnatowicz V, Stopka P and Švorcík V 2011 *Nucl. Instr. Meth*. B **269** 83
[13] Morent R, De Geyer N, Desmet T, Dubruel P and Leys C 2011 *Plasma Processes Polym.* **8** 171
[14] Silva E A and Mooney D J 2004 *Current Topics in Developmental Biology* **64** 181
[15] Shin H, Jo S and MikosA G 2003 *Biomaterials* **24** 4353
[16] Ma Z, Kotaki M, Yong T, He W and Ramakrishna S 2005 *Biomaterials* **26** 2527
[17] Küttel O M, Martinu L, Poitras D, Klemberg-Sapieha J E and Wertheimer M R 1992 *Materials Science and Engineering* B – Advance 321
[18] Aflori M, Drobota M, Timpu D and Barboiu V 2008 *Journal of Optoelectronics and Advanced Materials* **2** 291
[19] Behnisch J, Hollander A and Zimmermann H 1993 *Surf. Coat. Technol*. **59** 356
[20] Mirabedini S M,, Rahimi H, Hamedifar S and Mohseni M 2004 *Int. J. Adhes*. **24** 163
[21] Boenig H V 1882 Plasma Science and Technology, *Cornell University Press,* Ithaca, New York
[22] Aflori M, Drobota M, Dimitriu D, Stoica I, Simionescu B and Harabagiu V 2013 *Mat. Sci. and Eng.* B **178** 1303
[23] Chen Y, Gao Q, Wan H, Yi J, Wei Y and Liu P 2013 *Applied Surface Science* **265** 452
[24] Kosobrodova E, Kondyurin A, McKenzie D R and Bilek M M M 2013 *Nuclear Instruments and Methods in Physics Research* B **304** 57

IOPscience iopscience.iop.org

Home Search Collections Journals About Contact us My IOPscience

Plasma mediated protein immobilisation enhances the vascular compatibility of polyurethane with tissue matched mechanical properties

This content has been downloaded from IOPscience. Please scroll down to see the full text.

2017 Biomed. Mater. 12 045002

(http://iopscience.iop.org/1748-605X/12/4/045002)

View the table of contents for this issue, or go to the journal homepage for more

Download details:

IP Address: 129.78.139.29
This content was downloaded on 18/08/2017 at 06:16

Please note that terms and conditions apply.

You may also be interested in:

A compliant and biomimetic three-layered vascular graft for small blood vessels
Y Zhang, X S Li, A G Guex et al.

Development of segmented polyurethane elastomers with low iodine content exhibiting radiopacity and blood compatibility
S Dawlee and Muthu Jayabalan

Development of a gelatin-based polyurethane vascular graft by spray, phase-inversion technology
Paola Losi, Luisa Mancuso, Tamer Al Kayal et al.

Heparinized poly(vinyl alcohol)--small intestinal submucosa composite membrane for coronary covered stents
Tao Jiang, Guixue Wang, Juhui Qiu et al.

Influence of hydroxyl-terminated polydimethylsiloxane on high-strength biocompatible polycarbonate urethane films
Rong Zhu, Xinyu Wang, Jing Yang et al.

Biofilm formation, bacterial adhesion and host response on polymeric implants
D Pavithra and Mukesh Doble

Biomedical Materials

PAPER

RECEIVED
16 August 2016

REVISED
5 April 2017

ACCEPTED FOR PUBLICATION
24 April 2017

PUBLISHED
4 July 2017

Plasma mediated protein immobilisation enhances the vascular compatibility of polyurethane with tissue matched mechanical properties

Irina Kondyurina[1,8], Steven G Wise[2,3,4,8,9], Alan K Y Ngo[4], Elysse C Filipe[2,3], Alexey Kondyurin[1], Anthony S Weiss[4,5,6,10], Shisan Bao[3,5,6,7,10] and Marcela M M Bilek[1,9,10]

[1] School of Physics, University of Sydney, NSW 2006, Australia
[2] The Heart Research Institute, Sydney, NSW 2042, Australia
[3] Sydney Medical School, University of Sydney, NSW 2006, Australia
[4] School of Life and Environmental Sciences, University of Sydney, NSW 2006, Australia
[5] Bosch Institute, University of Sydney, NSW 2006, Australia
[6] Charles Perkins Centre, University of Sydney, NSW 2006, Australia
[7] Discipline of Pathology, University of Sydney, NSW 2006, Australia
[8] Equal first authors.
[9] Authors to whom any correspondence should be addressed.
[10] Joint senior authors.

E-mail: steve.wise@hri.org.au **and** marcela.bilek@sydney.edu.au

Keywords: polyurethane, vascular graft, plasma immersion ion implantation, tropoelastin

Supplementary material for this article is available online

Abstract

Polyurethanes are a diverse class of polymers, with independently tunable mechanical and biodegradation properties making them a versatile platform material for biomedical implants. Previous iterations have failed to adequately embody appropriate mechanical and biological properties, particularly for vascular medicine where strength, compliance and multifaceted biocompatibility are required. We have synthesized a new polyurethane formulation with finely tuned mechanical properties, combining high strength and extensibility with a low Young's modulus. Additional cross-linking during synthesis enhanced stability and limits leaching. Under cyclic testing, hysteresis was minimal following completion of the initial cycles, indicating the robustness of the material. Building on this platform, we used plasma immersion ion implantation to activate the polymer surface and functionalized it with recombinant human tropoelastin. With tropoelastin covalently bound to the surface, human coronary endothelial cells showed improved attachment and proliferation. In the presence of heparinized whole blood, tropoelastin-coated polyurethane showed very low thrombogenicity in both static and flow conditions. Using this formulation, we synthesized robust, elastic prototype conduits which easily retained multiple sutures and were successfully implanted in a pilot rat aortic interposition model. We have thus created an elastic, strong biomaterial platform, functionalized with an important regulator of vascular biology, with the potential for further evaluation as a new synthetic graft material.

1. Introduction

Modern polyurethanes (PUs) are block copolymers with 'hard' and 'soft' blocks, having glass transition temperatures above and below room temperature respectively. They are extensively used in medicine due to their biological inertness and the wide range of mechanical properties and biodegradation rates that can be attained [1]. Modern PUs are used for short term devices such as blood and urinary catheters [2], syringe tips, pipes and bags for blood circulation systems, tissue scaffolds [3], as well as long term devices such as artificial diaphragm membranes, artificial joints, meniscal prosthetics [4], breast prosthetic shells [5], artificial hearts [6], bone and other orthopaedic devices [7].

© 2017 IOP Publishing Ltd

PU has also been widely used in the manufacture of vascular grafts [8–11], benefiting from the opportunity to create compliant, durable materials. Past iterations of PU constructs have suffered from a combination of the lack of appreciation of their biological destination and a failure to tune their biological interface prior to implantation [12]. PUs that have polyester soft segments degrade rapidly [13] and so are used for applications where a temporary presence is required, such as wound closure adhesives. PUs that have polyether soft segments degrade more slowly in the body and are used for longer term implants [3]. Most of these types of polyurethanes contain methylene diphenyl diisocyanate as the hard segment and have a high strength and a high Young's modulus. A reduction in strength and Young's modulus is obtained by using toluene diisocyanate (TDI) as the hard segment [14]. However, even this does not provide a Young's modulus low enough to avoid biomechanical failure at locations where the implant material contacts with soft tissue. Soft tissue moduli in a range between 2 and 1000 kPa have been reported [15–17], while modern medical grade polyurethanes have moduli in a range of 4.7–80 MPa [18, 19] and other polymers that have been used or proposed have moduli in the range 1.5–1200 MPa [20–22]. None of the modern polymers that are suitable for use as biostable medical implants has low enough Young's modulus. Although a recently proposed arborescent block copolymer, TPE1, has a Young's modulus (0.6 MPa) in the appropriate range [23], the need for new long-term biostable polymers with low Young's modulus for long-term, soft-tissue implants remains significant.

For applications in vascular medicine, there are also important biological requirements, including favorable cell interactions and low thrombogenicity. Current synthetic vascular graft materials, including Dacron and expanded polytetrafluoroethylene (ePTFE), are intrinsically unsuited to implantation as they are highly thrombogenic, fail to recover a functional endothelial cell layer and invoke a profound immune response [24]. In the long-term, uncontrolled smooth muscle cell proliferation inexorably contributes to a gradually occluded conduit, accentuated at the suture points where synthetic materials join the native vasculature. This lack of vascular compatibility and mismatched mechanical properties together translate to the uniform failure of commercial synthetic conduits for small diameter (<6 mm) grafting applications [25].

The compatibility and integration of artificial grafts with native tissue can be improved with surface modification of the graft. Ion implantation with energetic ions has been found to be a successful method for the surface modification of polymer materials. More recently, it has been shown that ion implantation can provide the polymer surface with an ability to covalently immobilise bioactive compounds on its surface without any further chemistry [26]. Compared to using traditional linker chemistry to achieve biological functionality, the plasma immersion ion implantation (PIII) approach is environmentally friendly and achieves biological functionalisation without degradation of the bulk polymer. This is a relatively new technology with emerging applications and good prospects for the practical production of biocompatible materials [27].

As the energetic ions implant into a polymer, they break chemical bonds in the polymer macromolecules and displace atoms and electrons. As a result volatile components are evolved from the structure, leaving a carbonized and densified surface layer [28] that contains sufficiently long-lived radicals to react with protein molecules upon contact such that they become covalently attached to the treated polymer surface [26]. Due to the dense monolayer of covalently immobilized protein, cells do not recognize the polymer material underneath as foreign. We have demonstrated these effects for a number of polymer materials including polyethylene, polystyrene and Teflon. Here we apply this method to activate the surface of polyurethane as a prospective material for a biomedical implant.

We show here the synthesis and characterization of a new polyurethane formulation combining tensile strength with elasticity, using non-toxic precursors. We used PIII to activate its surfaces so that they can be easily functionalized in one simple step. After using PIII to activate the polymer, we covalently immobilized recombinant human tropoelastin (rhTE) to the surface by incubation in buffer solution. We chose this vascular matrix protein because it is known to be a potent multi-faceted regulator of vascular biology [29], promoting endothelial cell adhesion and growth [30] while inhibiting smooth muscle cell proliferation [31]. There is also increasing evidence for the haemocompatibility of elastin and its derivatives [32], demonstrated *in vitro* and in clinically relevant models of prostheses thrombogenicity [33, 34]. This combination of properties suggests its usefulness for blood-contacting materials such as cardiovascular grafts. Hence, we propose that this combination will yield a suitably elastic and strong synthetic polyurethane with the potential to regulate important aspects of vascular biology.

2. Materials and methods

2.1. Chemicals

rhTE corresponding to amino acid residues 27–724 of GenBank entry AAC98394 (gi 182020) was expressed and purified as previously described [35]. Polyurethane precursors poly(propylene glycol), tolylene 2,4-diisocyanate terminated (PPG-TDI), polytetrahydrofuran (PTHF) and dibutyltin dilaurate (DBD) were purchased from Sigma-Aldrich (USA). Human

coronary artery endothelial cells (HCAEC) were purchased from Cell Applications (San Diego, CA, USA).

2.2. Polyurethane synthesis

Pre-polymers PPG-TDI and PTHF were mixed in molar ratios of 1:0.35, 1:0.5 and 1:0.7 in the presence of DBD as a catalyst (0.01% of the mixture), and applied to a glass surface in a humidity controlled environment (under $CaCl_2$). Polymerization proceeded at room temperature for 3 days, and then at 100 °C for 2 h in a vacuum oven. The thickness of the film was 0.3 mm. To remove any unreacted products and catalyst, the PU films were swollen in toluene for 24 h, dried in air for an additional 24 h and finally in a vacuum oven for 2 h at room temperature.

2.3. Leaching analysis

PU samples were pre-weighed and placed in milli-Q water (MQW) for 7 days in a sealed glass beaker. Samples were then dried in air for 24 h and then in a vacuum oven for 8 h. The samples were then re-weighed and the relative mass loss attributed to leached components was calculated. For an analysis of leached components, water from the beaker was placed on a germanium ATR crystal and dried. Attenuated total reflection Fourier-transform infrared (ATR-FTIR) spectra were measured using a Digilab FTS7000 FTIR spectrometer fitted with a multi-bounce ATR accessory with a trapezium germanium crystal at an incidence angle of 45°. To obtain sufficient signal/noise ratio and resolution of spectral bands, 500 scans were taken at a resolution of 1 cm^{-1}. A control spectrum was taken using water from a beaker stored in the same environment but without PU.

2.4. Swelling

PU film samples (0.3 mm thick) were weighed before swelling in dimethylformamide and hexane in sealed beakers, to assess cross-linking efficacy. Samples were allowed to swell for 24 h. The samples were weighed immediately after removal from the beakers, then dried for 24 h in open air and re-weighed.

2.5. Mechanical testing

Mechanical properties of synthesized polyurethanes ($1 \times 0.8 \times 5$ cm, $n = 3$) were tested using an Instron 5943 with a 100 N load cell according to the ASTM D412-06a (ASTM International, 2006) protocol. The load sensor and extensometer calibrations were performed prior to the test. To prevent specimen slipping during the test, hydraulic clamps were used. The PU was loaded at a constant strain rate of 500 mm min^{-1} to 100% stretch and then relaxed to 0% stretch. This cycle was repeated 3 times, before the PU samples were stretched to failure. The Young's modulus was obtained by calculating the slope of the stress–strain curve at 100%. The tensile strength and modulus at breakage was calculated using the maximum strain at the breaking point. A lower load cycling test was also carried out to assess performance during loads compatible with those experienced in the vasculature. One hundred cycles up to 10% strain at a constant strain rate were applied at a frequency of 1 Hz.

2.6. PIII treatment

The PU samples were placed on a stainless steel holder with a mesh made of the same material. The mesh was electrically connected to the holder and held in front of the sample parallel to its surface. The distance between the sample and the mesh was 5 cm. Plasma ions were accelerated by the application of high voltage (20 kV) bias pulses of 20 μs duration at a frequency of 50 Hz, drawing an average current of 1.2 mA to the substrate holder and its mesh. The PU samples were treated for 40–800 s corresponding to ion implantation fluences of 5×10^{14}–10^{16} ions cm^{-2} and subsequently stored in air at room temperature. The penetration depth of the nitrogen ions (20 keV) into the PU film and the distribution of displaced hydrogen and carbon atoms were calculated using SRIM software. ATR-FTIR spectra were measured using a Digilab FTS7000 FTIR spectrometer as described above.

2.7. Surface characterization

PU samples were sputter coated with a 20 nm gold film and imaged with a Zeiss EVO 50 scanning electron microscope. The contact angles between the PU surface and two liquids (de-ionized water and diiodomethane) were measured using a Kruss contact angle analyzer DS10 employing the sessile drop method. The surface free energy and its polar and dispersive components were calculated using the Owens–Wendt–Rabel–Kaelble model.

2.8. Tropoelastin coating and detection

Polymer samples were incubated with various concentrations of tropoelastin (from 0 to 50 $\mu g\,ml^{-1}$) in phosphate buffered saline (PBS) at 4 °C overnight. For ELISA, untreated and PIII-treated polyurethanes were cut into 0.6×0.8 cm samples and placed into wells of a 48-well plate, and treated as previously described [36]. Covalent attachment was determined using stringent washing in 5% sodium dodecyl sulfate (SDS), incubated for 10 min at 90 °C. Non-specific binding was blocked with 3% BSA (w/v) and tropoelastin detected with anti-tropoelastin primary antibody BA-4 (1:2000 dilution). A secondary anti-mouse IgG antibody conjugated with HRP (1:5000 dilution) was used for visualization, in conjunction with ABTS. The plate was agitated and the absorbance read at 405 nm with a microplate reader (Biorad Model 680).

2.9. Cell culture

For attachment studies, 300 cells mm^{-2} were allowed to attach for 90 min in Dulbecco's Modified Eagle Medium. In proliferation assays, 150 cells mm^{-2} were plated for 3 and 5 days. Attachment and proliferation of cells to untreated and PIII-treated polyurethane were analyzed, with no protein, and coated with rhTE. Samples were blocked with 1% heat-denatured bovine serum albumin (dBSA) where indicated. At each time point, cells were washed, fixed with 3.7% formaldehyde and stained with 0.1% (w/v) crystal violet solution for 1 h at room temperature [37]. The dye was washed with distilled H_2O, solubilized with 10% (v/v) acetic acid, and the absorbance measured at 570 nm. Results were normalized to day 3 PU only surfaces.

2.10. Thrombogenicity assessment

Whole blood was obtained from healthy, non-smoking male volunteers who had not consumed aspirin two weeks prior to donation, with informed consent in accordance with the Declaration of Helsinki. Approval for this work was granted by The University of Sydney, Human Research Ethics Committee (protocol 05-2009/11668). Experiments were conducted in triplicate with blood from different donors. Samples of untreated and PIII-treated polyurethane were incubated overnight at 4 °C in PBS for non-protein treated and 20 $\mu g\,ml^{-1}$ tropoelastin for protein-coated samples. Surfaces were rocked with heparinized whole blood (0.5 $U\,ml^{-1}$) for up to 60 min at 37 °C as previously described [38]. Evaluation of surface thrombogenicity was also performed using a modified Chandler loop [39]. Pre-weighed surfaces were inserted into loops constructed of Tygon S-50-HL tubing (SDR, Australia). Loops were filled with heparinized human whole blood (0.5 $U\,ml^{-1}$), enclosed with 1 cm silicon connectors and rotated at 34 rpm at 37 °C for 60 min to simulate mean coronary artery flow rate (85 $ml\,min^{-1}$). Surfaces and thrombi were removed, surfaces rinsed in PBS and dried before re-weighing. Alternatively, heparinized whole blood (0.5 $U\,ml^{-1}$) was centrifuged for 15 min at 1000 rpm in swinging rotors. The supernatant, platelet rich plasma (PRP) was mixed in equal volumes with PBS and fluorescently labeled (Alexa Fluor® 488) fibrinogen from human plasma to a final concentration of 25 $\mu g\,ml^{-1}$, before assessment in the Chandler loop, also for 60 min.

2.11. Conduit production and burst pressure testing

Conduits were produced on glass rods of 2 mm diameter, cured for four days at room temperature (23 °C) in low humidity (5%–10%), annealed for 2 h at 120 °C under vacuum, washed in toluene for 1 h and dried on open air for 24 h. 2.5 cm conduit sections were fixed to an 18 G cannula and connected to a pressure transducer (Cambridge Electronic Design, UK) and bio-amplifier (BMA-931; Cambridge Electronic Design, UK). Pressure in the graft was increased by increasing volumes of saline introduced into the graft at a rate of 0.5 $ml\,min^{-1}$. The pressure was recorded as a continuous wave-form using Spike2 acquisition and analysis software (version 8.03; Cambridge Electronic Design, UK) and digitised at 250 Hz.

2.12. Pilot *in vivo* implantation

Study approval was obtained from Sydney Local Heath District Animal Welfare Committee (protocol number 2014/028). PU conduits (1.5 mm by 10 mm length) were implanted as rat aortic interposition grafts in male Sprague-Dawley rats [40]. Briefly, heparin (100 $U\,kg^{-1}$) was administered intravenously, before proximal and distal clamping, just below the renal arteries and above the aorto-iliac bifurcation. A 1 cm segment of the abdominal aorta was resected, before grafts were inserted with 10-0 nylon interrupted sutures under sterile conditions using an operative microscope of X25 magnification. Flow was re-established and haemostasis checked. Following completion of implantation, the wound was irrigated with saline and the skin closed with subcutaneous and subcuticular sutures. No post-operative anti-coagulation was used and grafts were explanted after 1 week. At the time of retrieval, grafts were flushed with normal saline only.

2.13. Statistical analysis

All data were expressed as mean ± standard error of the mean (SEM) and analyzed using statistical software in GraphPad Prism Version 5.0 (GraphPad Software, CA, USA). Student's *t*-tests and two-way ANOVA with a Bonferroni post-test were used to compare between groups and within groups respectively. Statistical significance was accepted as $p < 0.05$.

3. Results

3.1. Polyurethane synthesis and mechanical characterization

PPG-TDI and PTHF precursors were combined in three different stoichiometric ratios, 1:0.35, 1:0.50 and 1:0.70. Each of the synthesized PUs formed a flexible transparent film. The chemical structure after the first stage of the synthesis is shown in figure 1(a). In the second stage, when the films are annealed, the reaction of residual isocyanate groups with urethane groups leads to the formation of allophanate groups (figure 1(b)).

Instron mechanical testing produced characteristic stress-stain curves for PTHF 0.35, 0.50 and 0.70 (figure 2(A)). Young's modulus values were derived from these curves and showed each of the newly synthesized PUs to be significantly more elastic than several currently used medical polyurethanes and silicones (figure 2(B)). PTHF 0.35 (0.41 ± 0.07 MPa), 0.50 (0.56 ± 0.03 MPa) and 0.70 (0.37 ± 0.06 MPa),

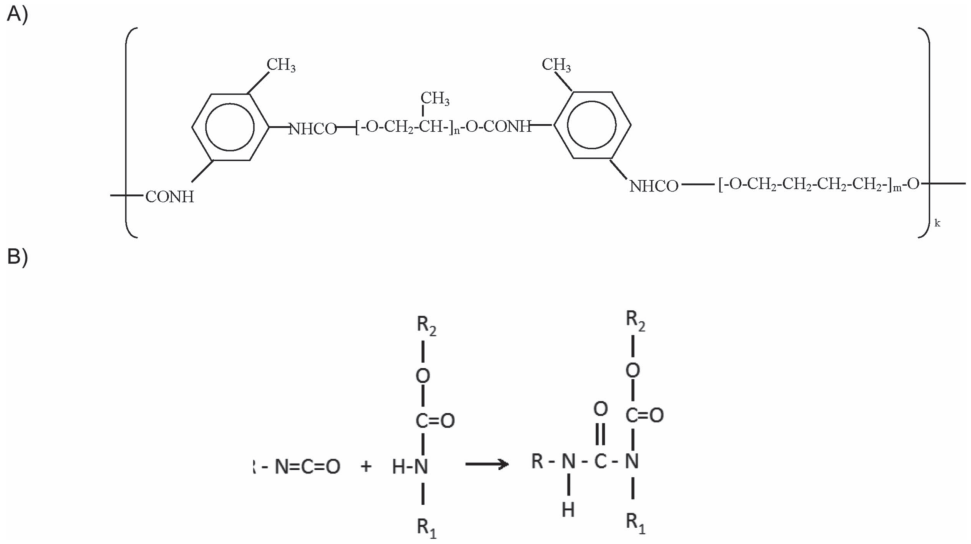

Figure 1. (a) PU chemical formula, containing a polypropylene glycol terminated tolylene diisocyanate as the pre-polymer. The pre-polymer was cured with polytetrahydrofurane as a chain extender. (b) The cross-linking of the backbone chains occurs during annealing which promotes the formation of allophanate groups.

were close to published values for soft tissue (0.01–0.1 MPa) and TPE 1 (0.60 MPa), and significantly more elastic than silicone (1.8 MPa) and commercial polyurethanes such as Sibstar PSU (1.50 ± 0.1 MPa), Bionate PCU (6 MPa) and Biospan PSU (14.0 MPa). The Young's moduli of our three synthesized PUs were not significantly different to each other.

However, clear differences in stress at break, and elongation were observed (figure 2(C)). PTHF 0.35 had the highest stress at breakage (1030 ± 250 kPa), greater than either PTHF 0.5 (924 ± 158 kPa) or PTHF 0.70 (482 ± 90 kPa). Similarly, elongation at breakage was also reduced with increasing PTHF ratio, from a high of 583 ± 1% (PTHF 0.35), down to 316 ± 62% (PTHF 0.5) and 204 ± 19% (PTHF 0.70). This difference is a result the linear macromolecules crosslinking into a 3D polymer network due to the presence of residual isocyanate groups at the second stage of the synthesis. The crosslinking is increased as the concentration of residual isocyanate groups increases, resulting an increase in the mechanical strength of the film and the Young's modulus. The increased strength and extensibility of PTHF 0.35 for a comparable Young's modulus led us to favor this variant for further investigation.

Repeated cycling of PTHF 0.35 up to 100% tensile strain for three cycles shows a nonlinear character of the stress–strain curve and mechanical hysteresis after relaxation of the load (figure 2(D)). After the first cycle the residual elongation was 11% and did not change over the following cycles. Minimal changes in strain–stress curve and hysteresis were seen in the second and third cycles. Repeated cycling of PTHF 0.35 up to 10% strain to simulate physiological conditions for 100 cycles was carried out to determine the resilience of the material and the degree of hysteresis. After 100 cycles the load for 10% tensile strain decreased by 10% showing the relaxation of the PU structure (figure 2(E)). Minimal changes in strain–stress curve and hysteresis were seen after the first ten cycles (figure 2(F)).

3.2. Leaching and cross-linking

Leaching over seven days into MQW showed that the leached components were less than 0.1% of the sample weight. The FTIR ATR spectra of the leached components (figure 3) found in solution showed that the main leached component is non-reacted PTHF—lines at 3350 cm^{-1} (OH group); in the 2975–2875 cm^{-1} region (CH groups); and at 1106 cm^{-1} (ether group). There are some low intensity lines related to vibrations of PTHF bonded to PPG-TDI appear also at 1728 cm^{-1} (carbonyl group) and at 1603 cm^{-1} (aromatic ring). No isocyanate components were seen (absence of signal at 2270 cm^{-1}) indicating that these potentially toxic components were not leached from the material. The swelling test showed that the PU films were not dissolved and rather swelled in DMFA to 874.4 ± 1.3% and in hexane to 121.9 ± 1.8%. This indicates that the PU film was robustly chemically cross-linked.

3.3. Effect of PIII treatment

One of the main advantages of PIII surface treatment is that it preserves the bulk properties of the surface modified materials. For the ion energy used in our work, the thickness of the modified layer, as calculated by TRIM/SRIM simulations, is about 70 nm [41]. Since the thickness of the PU film used for mechanical testing is 8 mm, the contribution of the modified layer is not detectable by the Instron mechanical test (5%–

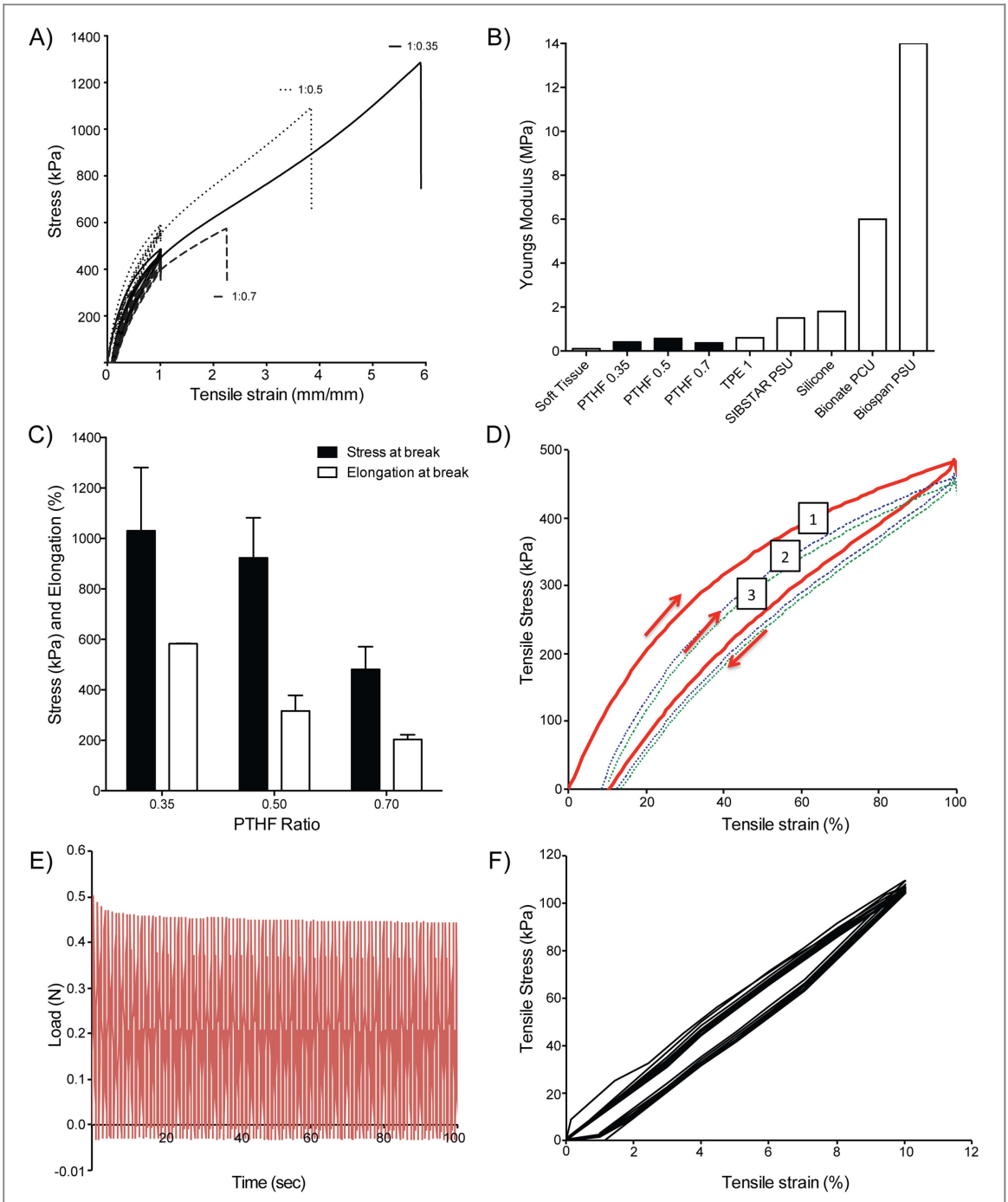

Figure 2. Mechanical testing of PU films. (A) Typical tensile stress–strain curves for three PU candidates of various NCO/OH ratio; a 1:0.35 ratio shows a combination of the highest strength and low Young's modulus. (B) Young's modulus of synthesized PU films compared with reference data for soft tissue and medical grade polymers including TPE1, SIBSTAR PSU, Silicone, Bionate PCU and BIOSPAN PSU. (C) Stress and elongation of PU films at break. (D) Cyclic testing up to 100% tensile strain for PTHF-PPG-TDI 0.35 PU. The observed nonlinear curve, mechanical hysteresis and residual stress are discussed in the text. (E) 100 cycles at tensile strain of 10%. After the first cycles, the load curves are similar for the remaining 90 cycles. (F) Strain–stress curves for first ten cycles. The mechanical hysteresis decreased after the first cycle and was maintained over subsequent cycles.

10% accuracy). Similarly, the thickness of a subsequently immobilized protein layer is about 5 nm, so its influence on the mechanical properties of polyurethane film is also not detected.

PIII treatment reduced the hydrophobicity of the PU surface from a starting contact angle of 95.3 ± 2.5° (untreated), to a minimum of 70.8 ± 2.7° after a treatment of 80 s. The contact angle remained close to this value for treatment times beyond 80 s, measured as 73.5 ± 1.4° (figure 4(A)) after a treatment of 800 s. SEM imaging following PIII treatment revealed that all of the surfaces were generally featureless and smooth, with some local imperfections. Following PIII treatment, some surface fracturing was observed, increasingly so with increasing treatment duration (figure 4(B)).

ATR-FTIR spectra of PU revealed significant changes in the surface layer after PIII treatment. The

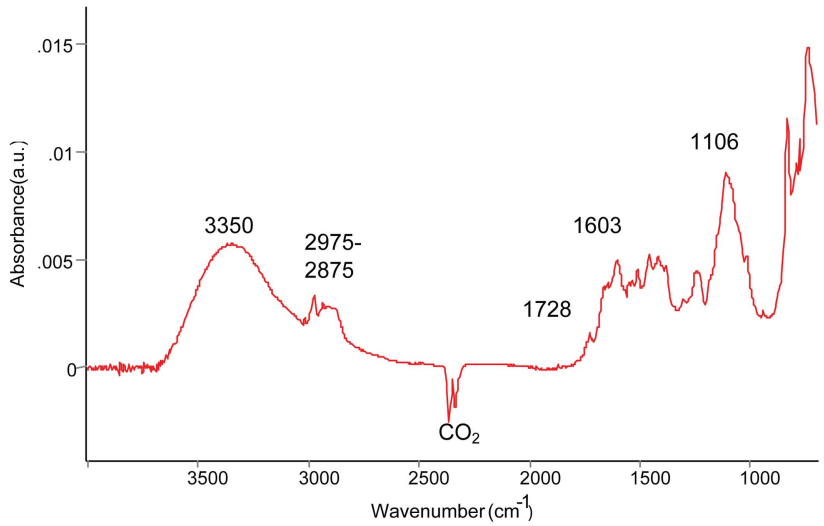

Figure 3. FTIR ATR spectra of components leached from PU into MQW over 7 days. Lines were identified for OH (3350 cm^{-1}), CH (2975–2875 cm^{-1} region), carbonyl (1728 cm^{-1}), aromatic ring (1603 cm^{-1}) and ether (1106 cm^{-1}) groups. The most abundant substance was non-crosslinked PTHF to PPG-TDI component, with a low amount of PTHF bonded to PPG-TDI. The PPG-TDI with an active isocyanate group was not observed.

spectra of untreated PU showed lines at 3300 cm^{-1} (Amide A), 1720 cm^{-1} (Amide I), 1530 cm^{-1} (Amide II) corresponding to vibrations of the urethane group, as well as a number of vibrations in the polyether and aromatic rings of the macromolecule (figure 4(C), red). After PIII treatment, broad bands in the 3600–2700 cm^{-1}, 1800–1600 $cm^{-1}$and 1450–900 cm^{-1} regions of the spectra appeared (figure 4(C), black). These bands were clearer in the differential spectrum (figure 4(C), green), with features from the untreated PU subtracted from the spectrum of the PIII treated sample. Shoulders at 3604, 3425 and 3237 cm^{-1} corresponding to hydroxyl group vibrations, 1744 and 1710 cm^{-1} for carbonyl group vibrations and 1620–1590 cm^{-1} for unsaturated carbon–carbon group vibrations were observed. The center spectral region contained broad, overlapping lines, such that clear separation of individual lines was not possible. These changes were attributed to the appearance of hydroxyl and carbonyl groups as well as new sp^2 and sp^3 carbon structures.

3.4. Covalent binding of tropoelastin

The binding of tropoelastin to the polyurethane surfaces was characterized. Untreated and PIII-treated polyurethane surfaces were incubated with increasing tropoelastin concentrations and the relative amount of adsorbed protein determined using ELISA (figure 5(A)). A steady increase in the amount of bound tropoelastin up to 20 $\mu g\,ml^{-1}$ for both untreated and PIII-treated PU surfaces was observed. This increase was steeper for PIII-treated surfaces compared to untreated samples. PIII-treated surfaces bound a greater amount of rhTE at each concentration compared to the respective untreated surface.

The covalent binding of rhTE to untreated and PIII-treated polyurethane was examined using an ELISA specific for rhTE, combined with stringent SDS washing (figure 5(B)). PU surfaces without rhTE were used as negative controls. After SDS washing the amount of rhTE present on untreated PU returned to baseline levels, while in contrast, 72.3 ± 4.8% of the rhTE was retained on PIII treated PU.

3.5. Endothelial cell interactions

3.5.1. Attachment

Adhesion of endothelial cells to polyurethane was quantified using crystal violet staining (figure 6(A)). In the absence of protein coating, untreated polyurethane had relatively poor cell adhesion (28.7 ± 3.5%). This was significantly improved by PIII-treatment to 48.1 ± 3.3% ($p < 0.01$). BSA blocking of PU returned cell adhesion to less than 20%, irrespective of PIII treatment. Tropoelastin coating of untreated polyurethane, subsequently BSA blocked, improved cell attachment relative to blocked PU (33.0 ± 4.6%). Further, tropoelastin coating of PIII-treated PU, subsequently BSA blocked, significantly improved cell attachment (56.0 ± 11.1%, $p < 0.01$), showing that increased endothelial cell adhesion facilitated by PIII treatment is further augmented by the presence of tropoelastin.

3.5.2. Proliferation

Compared to untreated polyurethane, after 3 days in culture, all PIII treated, protein coated surfaces supported elevated levels of cell growth (figure 6(B)). Tropoelastin coating of the PIII treated PU surface resulted in a 31.2 ± 5.2% increase, relative to PU only, not significantly different to fibronectin (25.3 ± 10.4% increase) coated on the PIII-treated PU, on day 3. After

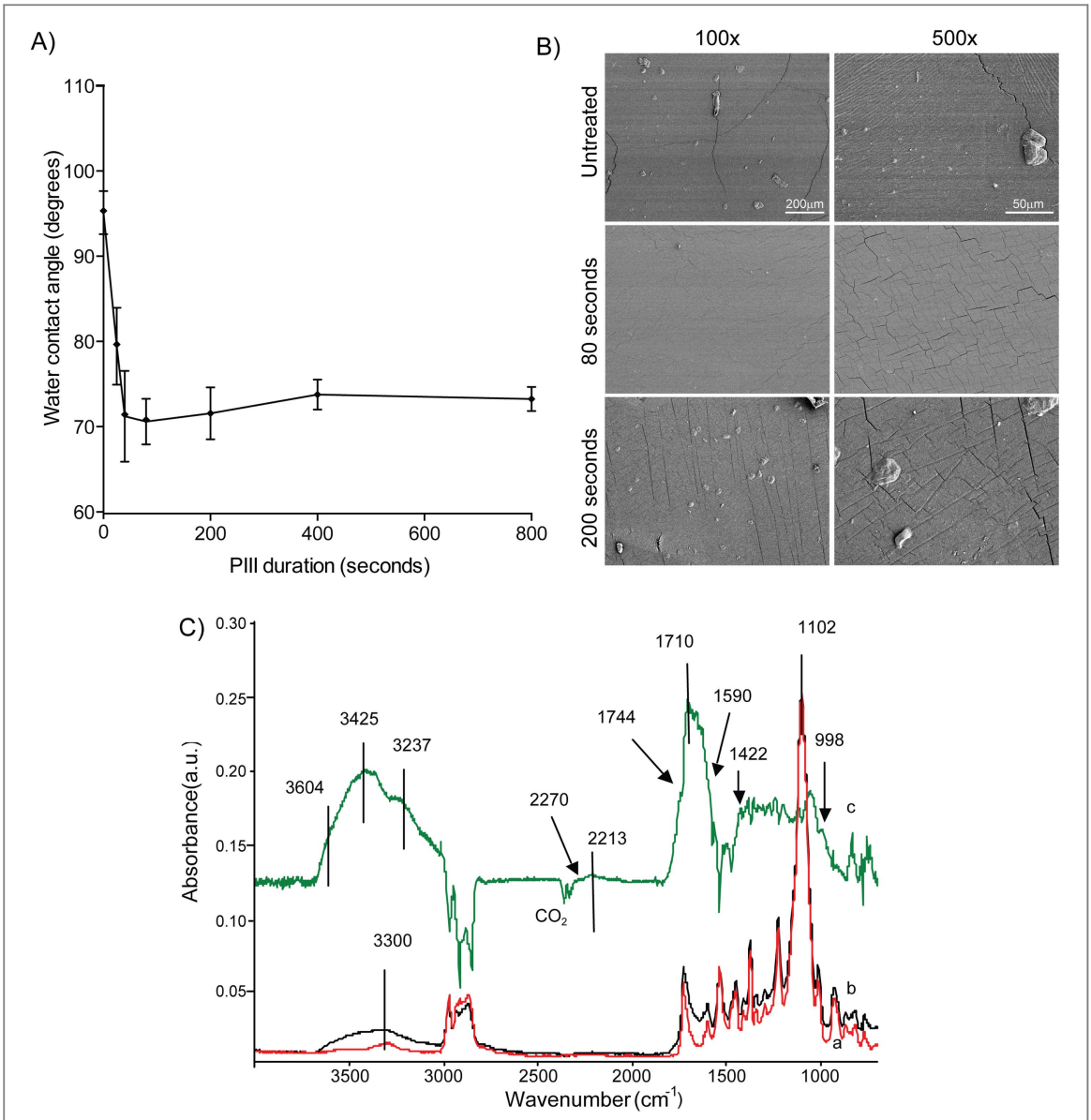

Figure 4. The effect of PIII treatment of the PU surface. (A) Water contact angle of the PU film with PIII treatment time showing that the surface became increasingly hydrophilic after PIII. The duration of PIII did not significantly influence the water contact angle. (B) SEM images of the PU surface with time of PIII treatment. Scale bars represent 200 and 50 μm as indicated in the image. (c) FTIR ATR spectra of PU before (red, bottom) and after PIII treatment (black, middle). A difference spectrum (green, top) revealed OH, CN, C=O, CH and CH in –C= groups.

5 days in culture, there was a further increase in cell numbers for all conditions. Endothelial cell proliferation on PIII+rhTE polyurethane was 54.4 ± 17.3% higher than on PU only, which did not significantly differ from fibronectin-coated PIII-treated PU on day 5 (66.7 ± 13.3% higher than the PU only control).

3.6. Blood compatibility

3.6.1. Static

The relative thrombogenicity of untreated and PIII-treated surfaces, with and without tropoelastin was assessed using heparinized whole blood. Following 90 min rocking at 37 °C, untreated PU surfaces displayed a small amount of clotting, which was not improved by tropoelastin coating. However, PIII-treated surfaces were extremely thrombogenic with almost uniform coverage of coagulated blood. Tropoelastin coating dramatically reduced the incidence of this, back to the baseline level (figure 7(A)).

Scanning electron microscopy demonstrated patchy coverage of erythrocytes on untreated polyurethane. PIII-treated polyurethane displayed a dramatic rise in thrombus formation, with large amounts of erythrocytes and associated fibrin deposition completely obscuring the underlying surface (supplementary figure 1, available online at stacks.iop.org/BMM/12/045002/mmedia). When coated with tropoelastin, untreated surfaces displayed patchy areas of thrombus constituents as well as blood cell adhesion. In contrast, PIII-treated surfaces with tropoelastin coating resulted in the majority of the surface being

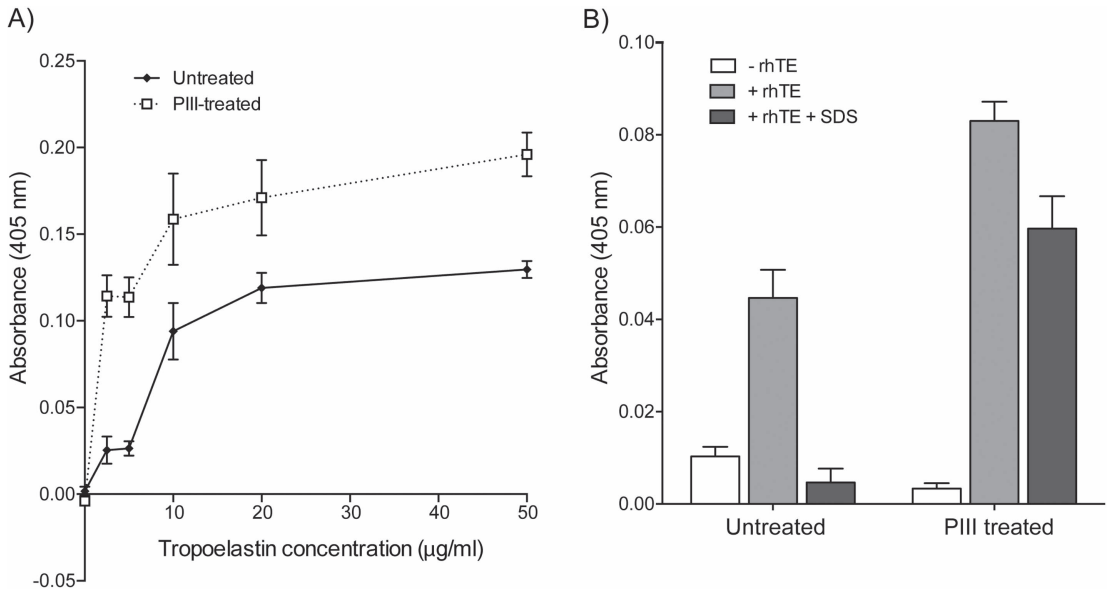

Figure 5. (A) ELISA detection of tropoelastin on untreated (solid line) and PIII-treated (dashed line) polyurethane surfaces coated in increasing concentrations of tropoelastin. (B) ELISA detection of tropoelastin bound to untreated or PIII-treated polyurethane following washing with 5% SDS at 95 °C for 30 min, without SDS washing and a no tropoelastin control.

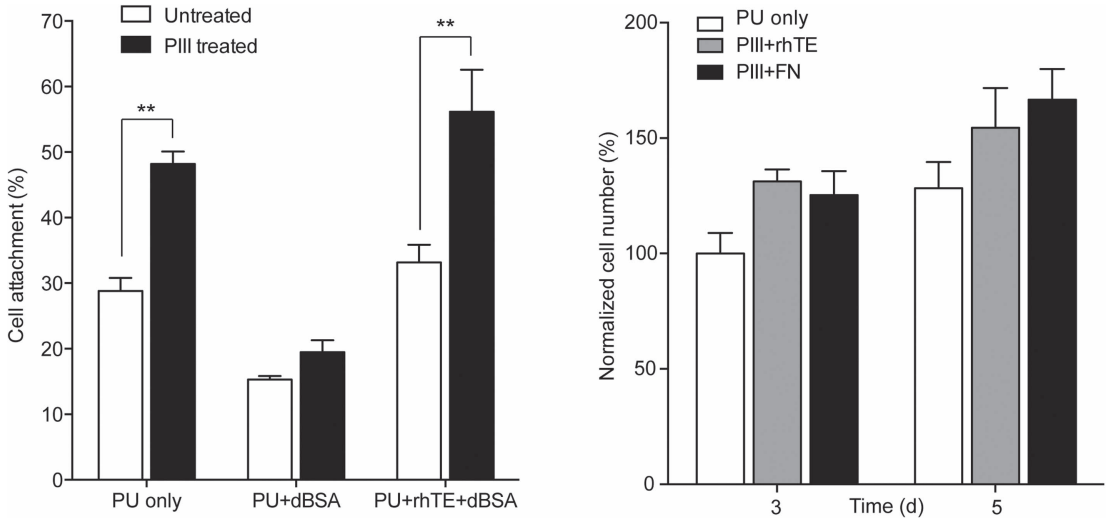

Figure 6. Endothelial cell interactions. (A) The percentage HCAEC attachment in the presence or absence of tropoelastin and dBSA blocking was measured after 90 min incubation on untreated and PIII PU. (B) Relative cell proliferation on polyurethane surfaces at days 3 and 5 is shown on PU only, PU+rhTE and PU + FN. $^{**} = p < 0.01$.

clear of blood components, with only occasional erythrocytes present (figure 7(A)).

3.6.2. Coronary artery flow using a Chandler loop

Thrombogenicity of surfaces under dynamic conditions was assessed using a modified Chandler loop assay, which aims to model coronary artery flow conditions. Untreated polyurethane surfaces displayed low clotting (15.0 ± 1.5 mg thrombus weight), but PIII treatment increased the thrombogenicity (30.0 ± 3.2 mg). However, tropoelastin coating of PIII-treated surfaces resulted in restoration of non-thrombogenicity (10.4 ± 4.1 mg, figure 7(B)).

3.7. Translation for vascular grafting

PU conduits were generated by curing the polymer on a cylindrical mandril. The resulting tubes were transparent, smooth and appeared homogenous along the length of the mandril (figure 8(A). SEM imaging confirmed the uniformity, demonstrating smooth outer and luminal surfaces and consistent wall thickness (figure 8(B)). Under increasing load, PU conduits achieved a burst pressure of 384.1 ± 17.3 mmHg, well in excess of physiological forces. To demonstrate the feasibility of testing our new conduit *in vivo*, we performed a pilot implantation in a rat aorta model. The PU conduits handled well and retained ten interrupted sutures at each anastomoses. Following

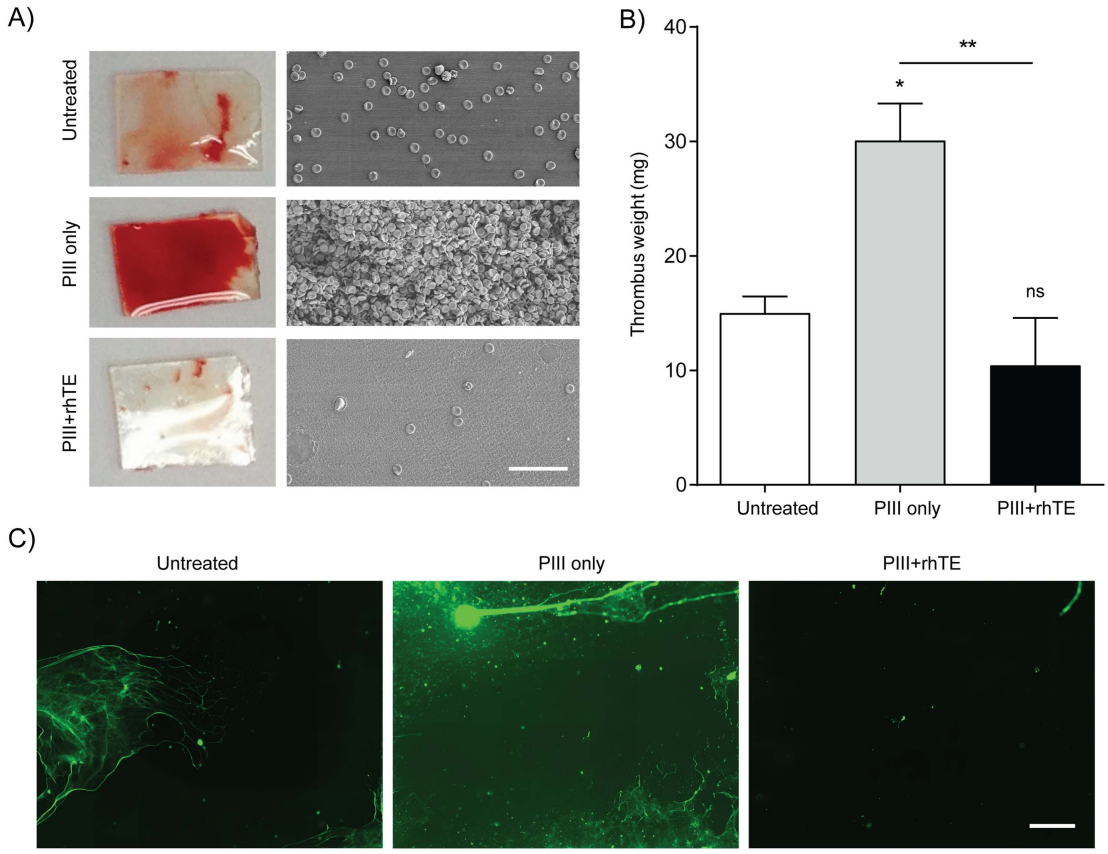

Figure 7. (A) Macroscopic and representative SEM images of surfaces following 90 min incubation with heparinized whole blood. Scale bar denotes 50 μm. (B) Thrombus weight from Chandler loop analysis on untreated polyurethane, PIII-treated polyurethane and PIII-treated polyurethane with tropoelastin coating. Statistics are relative to untreated polyurethane. (C) Fluorescently labeled fibrinogen demonstrates the same trends, increased on PIII only but substantially reduced on untreated and PIII+rhTE samples. Scale bar represents 100 μm.

removal of surgical clamps, normal blood flow resumed, observed through the transparent graft material (figure 8(C)). Rats recovered normally after surgery and showed no signs of abnormal behavior for up to one week following the procedure.

4. Discussion

We aimed to synthesize new polyurethane formulations demonstrating a combination of elasticity and mechanical strength, suitable for development as synthetic vascular grafts. The diversity in mechanical properties of polyurethanes is derived both from the ability to select various hard or soft segment precursors, and to introduce additional cross-links between the polymer chains. Classically, the hard segment provides mechanical strength while the soft segment imparts the elastomeric properties [42]. In this study, we selected polyoxypropylene glycol, tolylene diisocyanate terminated (PPG-TDI) as the hard segment and polytetrahydrofuran (PTHF) as the soft segment. PPG-TDI itself contains a polyol soft segment, poly (propylene glycol), making our PU effectively bi-soft segmented, allowing for enhanced tunability of mechanical properties [43–45]. To further strengthen the PU, an additional cross-linking reaction between the isocyanate groups and urethane groups of the prepolymers was performed at the annealing stage of the synthesis.

Traditional PUs have a much higher Young's modulus and are stiffer than native soft tissue. Developing PUs with an increase in elasticity while maintaining a high strength has been an ongoing challenge. The optimal molar ratio of the isocyanate and hydroxyl groups in the current study of 1:0.35, in combination with additional cross-linking was found to produce a PU with a Young's modulus of (0.41 $\pm$ 0.1 MPa), close to the reported range for soft tissue (0.01 to 0.1 MPa) [46]. In contrast, other new polyurethanes including TPE1 (0.6 MPa), SIBSTAR 103 T (1.5 MPa) are less elastic, while medical grade PUs such as Bionate (6 MPa) and Biospan (14 MPa) are stiffer still [23].

Importantly, this highly elastic PU is also mechanically strong, with a stress at breakage of 1030 $\pm$ 250 kPa, and an elongation at breakage of 583%. These values of breakage stress and strain greatly exceed the loads expected for soft tissue (3%–8% strain) [47], and the mechanical properties we determined are similar to those of native human vessels such as the femoral vein which has a tensile strength of

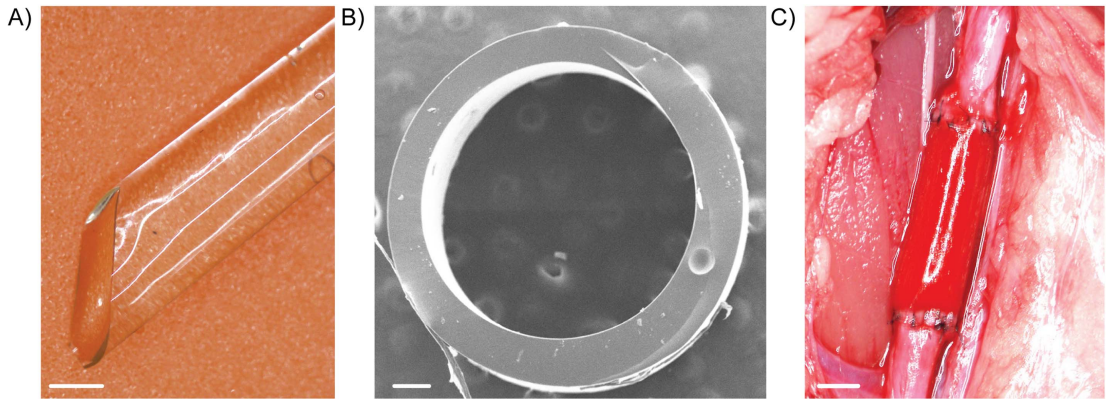

Figure 8. (A) Macroscopic photograph of a PU conduit. Scale bar denotes 500 μm. (B) Representative SEM image of conduit cross-section showing smooth inner and outer surfaces and uniform wall thickness. Scale bar denotes 200 μm. (C) Image of PU conduit implanted as a rat aortic interposition graft, following the removal of the surgical clamps and resumption of blood flow. Scale bar denotes 1 mm.

2–3 MPa, and a Young's modulus of 0.16–0.42 MPa [48]. The residual strain in the PU after 100% elongation is about 11%, which is an expected value for a segmented PU [49]. Further, our PU swells in DMFA to 874.4 $\pm$ 1.3% and in hexane to 121.9 $\pm$ 1.8%, indicating robust chemical cross-linking. Washing with toluene removed unreacted precursors and reagents, with the amount of washable low molecular fractions was found to be approximately 3%. Cross-linking also prevented leaching of PU side reaction products, as confirmed by FTIR spectra that showed no residual isocyanate groups (2270 cm^{-1} line) or any toxic residue in a sample of water in which the PU was incubated for 24 h.

Our PU was further modified with PIII to generate radicals embedded in the surface, to facilitate covalent binding of active biomolecules. Following PIII treatment, the water contact angle on PU decreased markedly from 95.3 $\pm$ 2.5° (untreated), to a minimum of 70.8 $\pm$ 2.7° after a treatment of 80 s. This effect was driven by atmospheric oxidation of radicals emerging at the surface, generating oxygen-containing groups, such as carbonyls and carboxyls on the surface layer, imparting polarity and a net negative charge, and has been well described for many polymers [50–52]. Using scanning electron microscopy we observed some surface cracking after long treatment times, predominantly due to surface carbonization [53], but this was minimal for the 80 s treatment time.

The surface of PU was subsequently functionalized with tropoelastin, increasingly accepted to favorably modulate multiple facets of vascular biocompatibility [54]. Covalent retention of tropoelastin, optimally at 20 $\mu g\,ml^{-1}$, was inferred after stringent washing in SDS [51, 55], before a comparative evaluation of interactions with human vascular endothelial cells and heparinized whole blood. SDS is a detergent that unfolds proteins [56]. It interferes with the physical forces that result in the physisorption of proteins but does not attack covalent bonds, leaving the protein's primary structure intact. SDS washing has been used as a method to test whether biological molecules are covalently attached to surfaces [57–59] and to detect covalently bound drug–protein adducts [60]. In some situations where there is a thick coverage of denatured and aggregated protein blocking access to the interface with the surface, steric hindrance may prevent SDS from accessing all of the sites where physical forces bind the protein. Because our PIII-treated surfaces are relatively hydrophilic compared to the untreated polymer controls from which our SDS wash successfully removes all of the protein, it is unlikely that steric hindrance could be responsible for the SDS-resistant binding observed on the PIII-treated surfaces. We therefore deduce that the high proportion of tropoelastin still adsorbed after SDS cleaning is covalently bonded to the surface. The mechanism for this covalent binding of the protein has been shown to be reaction with embedded radicals in the ion implanted surface layer that diffuse to the surface [26].

In its untreated form, PU supported only low levels of endothelial cell attachment and spreading, consistent with previous studies [61, 62]. PIII-treatment only, improved cell adhesion, consistent with the observed reduction in hydrophobicity, facilitating greater cell contact with the surface. rhTE immobilization on PIII treated PU further improved endothelial cell interactions, augmenting attachment and supporting proliferation, in agreement with previous studies showing this benefit [29, 63]. For proliferation studies, we also compared tropoelastin with fibronectin, which is a well-known cell adhesive extracellular matrix protein featuring a canonical RGD cell binding motif [64]. While fibronectin coatings drive improved cell interactions, they also initiate thrombus formation, attracting and activating platelets, while exerting no inhibitory effect on smooth muscle cells [65]. This makes fibronectin a poor candidate for the multi-faceted regulation of vascular compatibility [54].

Heparinized whole blood *in vitro* assays were used to assess the blood response to PU, with and without tropoelastin-coating. In several previous studies assessing the relative thrombogenicity of new biomaterials we have validated the use of heparinised whole blood assays [38, 66, 67]. The assays demonstrate changes relative to control, as absolute measurements of blood compatibility *in vitro* remain elusive. In a recent study [39] we showed that the whole blood assays used in this paper were consistent with systems using fewer components (e.g. isolated platelets, PRP) which have limitations recognised by the leaders in the blood/material interface community [68]. In both static and flow conditions, clinically used materials including stainless steel and ePTFE have demonstrated clotting profiles consistent with their behaviour in patients. Similar whole blood assays are recognised as appropriate for testing of the most promising new biomaterials surfaces [69].

Untreated polyurethane showed some adhesion of blood components, in agreement with the generally accepted short-term blood compatibility of untreated polyurethanes [70, 71]. In contrast, uncoated PIII treated surfaces generated a large network of blood clot, resulting from reduced hydrophobicity of the surface and the overall negative surface charge, which may stimulate the activation of the plasma coagulation system [72]. Tropoelastin coating of PIII treated PU, however, resulted in a clot-free surface with only occasional red blood cell adhesion. These results were confirmed under flow, in a modified Chandler loop, with untreated polyurethane displaying low thrombogenicity, forming little thrombus. PIII treatment resulted in an even coverage of coagulated blood, which was brought down to levels similar to untreated surfaces, following tropoelastin coating. Representative images of fluorescently labeled fibrin also clearly demonstrate the effects of PIII treatment, and subsequent improvement in the presence of tropoelastin. This is consistent with previous reports showing the low thrombogenicity of tropoelastin-coated surfaces [38, 63].

Having developed a new PU formulation with physical and biological properties optimized for vascular applications we sought to demonstrate the feasibility of producing conduits suitable for future *in vivo* evaluation. Uniform grafts were produced with smooth luminal and outer surfaces and uniform wall thickness. The first iteration of our PU grafts were non-porous and demonstrated a burst pressure greater than three times human physiological blood pressure, but below the levels previously published for other PU formulations such as Pellethane 2363 80A (>550 mmHg) [10], Carbothane PC3575A (1330 mmHg) and Chronoflex 80A (1680 mmHg) [73] and for native saphenous veins (1250 ± 500 mmHg) and coronary arteries (2000 mmHg) [74]. We expect that further optimization of the manufacturing process, including screening of the best ratio of diameter to wall thickness would improve this parameter. Nevertheless, our untreated PU conduit performed well in pilot testing in a rat aortic interposition model. The grafts handled and sutured well, blood flow was re-established and no signs of aneurysm or leak were detected. Rats recovered well and behaved normally out to sacrifice at one week. The high flow of the aorta precludes clot formation in this model, even for highly thrombogenic materials such as ePTFE. Re-endothelialisation is only meaningful at three weeks, while neointimal hyperplasia at this early timepoint is minimal. Accordingly, at the 1 week time point of our pilot study, our findings demonstrate appropriate handling, suturability and physical survival of the graft. The promising results justify the full assessment of our PU conduits, including those functionalized with PIII and rhTE in an appropriately powered study for up to 6 months in this well-established model [75].

5. Conclusions

Our results demonstrate a new PU platform with a combination of strength and elasticity tuned to match those of native soft tissue. We have shown that plasma treatment followed by covalent immobilization of tropoelastin on this material is sufficient to satisfy the requirements for vascular applications of positive cell interactions and blood compatibility. We propose that this promising composite material could be developed further into a synthetic vascular graft, benefiting from customizable mechanical properties and favorable modulation of vascular biology. Our PU platform combines high strength with a low Young's modulus, finely tuned to be suitable for vascular biomaterial applications. PIII treatment facilitates an enhanced biointerface, by enabling direct covalent immobilization of tropoelastin to promote endothelial cell interactions while maintaining good blood compatibility. We propose that the combination of a mechanically matched substrate with improved vascular biocompatibility could ultimately address the deficiencies known for current synthetic graft materials.

Acknowledgments

We acknowledge funding from the Australian Research Council (MMMB, SB and ASW); Perm region Government (MMMB, AK); and National Institutes of Health (EB014283 and HL107503; ASW). ASW is the Scientific Founder of Elastagen Pty Ltd The authors also acknowledge the facilities as well as scientific and technical assistance at the Australian Centre for Microscopy and Microanalysis.

References

[1] Janik H and Marzec M 2015 A review: fabrication of porous polyurethane scaffolds *Mater. Sci. Eng.* C **48** 586–91

[2] Klement P, Du Y J, Berry L R, Tressel P and Chan A K C 2006 Chronic performance of polyurethane catheters covalently coated with ATH complex: a rabbit jugular vein model *Biomaterials* **27** 5107–17

[3] McBane J E, Sharifpoor S, Cai K, Labow R S and Santerre J P 2011 Biodegradation and *in vivo* biocompatibility of a degradable, polar/hydrophobic/ionic polyurethane for tissue engineering applications *Biomaterials* **32** 6034–44

[4] de Groot J H, de Vrijer R, Pennings A J, Klompmaker J, Veth R P H and Jansen H W B 1996 Use of porous polyurethanes for meniscal reconstruction and meniscal prostheses *Biomaterials* **17** 163–73

[5] Handel N and Gutierrez J 2006 Long-term safety and efficacy of polyurethane foam-covered breast implants *Aesthet. Surg. J.* **26** 265–74

[6] Stachelek S J, Song C, Alferiev I, Defelice S, Cui X, Connolly J M, Bianco R W and Levy R J 2000 Localized gene delivery using antibody tethered adenovirus from polyurethane heart valve cusps and intra-aortic implants *Gene Ther.* **11** 15–24

[7] Bil M, Ryszkowska J, Woźniak P, Kurzydłowski K J and Lewandowska-Szumieł M 2010 Optimization of the structure of polyurethanes for bone tissue engineering applications *Acta Biomater.* **6** 2501–10

[8] Ashton J H, Mertz J A M, Harper J L, Slepian M J, Mills J L, McGrath D V and Vande Geest J P 2011 Polymeric endoaortic paving: mechanical, thermoforming, and degradation properties of polycaprolactone/polyurethane blends for cardiovascular applications *Acta Biomater.* **7** 287–94

[9] Thomas V, Kumari T V and Jayabalan M 2001 *In vitro* studies on the effect of physical cross-linking on the biological performance of aliphatic poly(urethane urea) for blood contact applications *Biomacromolecules* **2** 588–96

[10] Theron J P, Knoetze J H, Sanderson R D, Hunter R, Mequanint K, Franz T, Zilla P and Bezuidenhout D 2010 Modification, crosslinking and reactive electrospinning of a thermoplastic medical polyurethane for vascular graft applications *Acta Biomater.* **6** 2434–47

[11] Chuang T-W and Masters K S 2009 Regulation of polyurethane hemocompatibility and endothelialization by tethered hyaluronic acid oligosaccharides *Biomaterials* **30** 5341–51

[12] Smith A R, Garrison J L, Greene W B and Raso D S 1999 The clinical, histologic, and ultrastructural presentation of polyvinyl sponge (Ivalon) breast prostheses removed for massive fluid accumulation *Plast. Reconstr. Surg.* **103** 1970–4

[13] Howard G T 2002 Biodegradation of polyurethane: a review *Int. Biodeter. Biodegr.* **49** 245–52

[14] Petrović Z S and Ferguson J 1991 Polyurethane elastomers *Prog. Polym. Sci.* **16** 695–836

[15] Akhtar R, Sherratt M J, Cruickshank J K and Derby B 2011 Characterizing the elastic properties of tissues *Mater. Today* **14** 96–105

[16] Ahn B and Kim J 2010 Measurement and characterization of soft tissue behavior with surface deformation and force response under large deformations *Med. Image Anal.* **14** 138–48

[17] Wells S M and Walter E J 2010 Changes in the mechanical properties and residual strain of elastic tissue in the developing fetal aorta *Ann. Biomed. Eng.* **38** 345–56

[18] Kanyanta V and Ivankovic A 2010 Mechanical characterisation of polyurethane elastomer for biomedical applications *J. Mech. Behav. Biomed. Mater.* **3** 51–62

[19] Gorna K and Gogolewski S 2003 Molecular stability, mechanical properties, surface characteristics and sterility of biodegradable polyurethanes treated with low-temperature plasma *Polym. Degr. Stab.* **79** 475–85

[20] Teo A J T, Mishra A, Park I, Kim Y-J, Park W-T and Yoon Y-J 2016 Polymeric biomaterials for medical implants and devices *ACS Biomater. Sci. Eng.* **2** 454–72

[21] Mata A, Fleischman A J and Roy S 2005 Characterization of polydimethylsiloxane (PDMS) properties for biomedical micro/nanosystems *Biomed. Microdevices* **7** 281–93

[22] Guo L, Lv Y, Deng Z, Wang Y and Zan X 2016 Tension testing of silicone rubber at high strain rates *Polym. Test.* **50** 270–5

[23] Lim G T, Valente S A, Hart-Spicer C R, Evancho-Chapman M M, Puskas J E, Horne W I and Schmidt S P 2013 New biomaterial as a promising alternative to silicone breast implants *J. Mech. Behav. Biomed. Mater.* **21** 47–56

[24] Kapadia M R, Popowich D A and Kibbe M R 2008 Modified prosthetic vascular conduits *Circulation* **117** 1873–82

[25] Hoenig M R, Campbell G R, Rolfe B E and Campbell J H 2005 Tissue-engineered blood vessels: alternative to autologous grafts? *Arterioscler. Thromb. Vasc. Biol.* **25** 1128–34

[26] Bilek M M, Bax D V, Kondyurin A, Yin Y, Nosworthy N J, Fisher K, Waterhouse A, Weiss A S, dos Remedios C G and McKenzie D R 2011 Free radical functionalization of surfaces to prevent adverse responses to biomedical devices *Proc. Natl. Acad. Sci. USA* **108** 14405–10

[27] Bilek M M M 2014 Biofunctionalization of surfaces by energetic ion implantation: review of progress on applications in implantable biomedical devices and antibody microarrays *Appl. Surf. Sci.* **310** 3–10

[28] Bilek M M M, Kondyurin A, Dekker S, Steel B C, Wilhelm R A, Heller R, McKenzie D R, Weiss A S, James M and Möller W 2015 Depth-resolved structural and compositional characterization of ion-implanted polystyrene that enables direct covalent immobilization of biomolecules *J. Phys. Chem.* C **119** 16793–803

[29] Wise S G, Liu H, Kondyurin A, Byrom M J, Bannon P G, Edwards G A, Weiss A S, Bao S and Bilek M M 2016 Plasma ion activated expanded polytetrafluoroethylene vascular grafts with a covalently immobilized recombinant human tropoelastin coating reducing neointimal hyperplasia *ACS Biomater. Sci. Eng.* **2** 1286–97

[30] Sims F H, Chen X and Gavin J B 1993 The importance of a substantial elastic lamina subjacent to the endothelium in limiting the progression of atherosclerotic changes *Histopathology* **23** 307–17

[31] Karnik S K, Brooke B S, Bayes-Genis A, Sorensen L, Wythe J D, Schwartz R S, Keating M T and Li D Y 2003 A critical role for elastin signaling in vascular morphogenesis and disease *Development* **130** 411–23

[32] Waterhouse A, Wise S G, Ng M K and Weiss A S 2011 Elastin as a nonthrombogenic biomaterial *Tissue Eng.* B **17** 93–9

[33] Woodhouse K A, Klement P, Chen V, Gorbet M B, Keeley F W, Stahl R, Fromstein J D and Bellingham C M 2004 Investigation of recombinant human elastin polypeptides as non-thrombogenic coatings *Biomaterials* **25** 4543–53

[34] Jordan S W, Haller C A, Sallach R E, Apkarian R P, Hanson S R and Chaikof E L 2007 The effect of a recombinant elastin-mimetic coating of an ePTFE prosthesis on acute thrombogenicity in a baboon arteriovenous shunt *Biomaterials* **28** 1191–7

[35] Wu W J, Vrhovski B and Weiss A 1999 Glycosaminoglycans mediate the coacervation of human tropoelastin through dominant charge interactions involving lysine side chains *J. Biol. Chem.* **274** 21719–24

[36] Santos M, Filipe E C, Michael P L, Hung J, Wise S G and Bilek M M 2016 Mechanically robust plasma-activated interfaces optimized for vascular stent applications *ACS Appl. Mater. Interfaces* **8** 9635–50

[37] Bax D, Rodgers U, Bilek M and Weiss A 2009 Cell adhesion to tropoelastin is mediated via the c-terminal grkrk motif and integrin $\alpha_v\beta_3$ *J. Biol. Chem.* **284** 28616–23

[38] Waterhouse A, Yin Y B, Wise S G, Bax D V, McKenzie D R, Bilek M M M, Weiss A S and Ng M K C 2010 The immobilization of recombinant human tropoelastin on metals using a plasma-activated coating to improve the biocompatibility of coronary stents *Biomaterials* **31** 8332–40

[39] Wise S G, Michael P L, Waterhouse A, Santos M, Filipe E, Hung J, Kondyurin A, Bilek M M and Ng M K 2015 Immobilization of bioactive plasmin reduces the thrombogenicity of metal surfaces *Colloids Surf.* B **136** 944–54

[40] de Valence S, Tille J C, Mugnai D, Mrowczynski W, Gurny R, Moller M and Walpoth B H 2012 Long term performance of polycaprolactone vascular grafts in a rat abdominal aorta replacement model *Biomaterials* **33** 38–47
[41] Biersack J P and Ziegler J F 1982 *Ion Implantation Techniques: Lectures given at the Ion Implantation School in Connection with 4th Int. Conf. on Ion Implantation: Equipment and Techniques (Berchtesgaden, Fed. Rep. of Germany, 13–15 September 1982)* ed H Ryssel and H Glawischnig (Berlin: Springer) pp 122–56
[42] Guelcher S A, Gallagher K M, Didier J E, Klinedinst D B, Doctor J S, Goldstein A S, Wilkes G L, Beckman E J and Hollinger J O 2005 Synthesis of biocompatible segmented polyurethanes from aliphatic diisocyanates and diurea diol chain extenders *Acta Biomater.* **1** 471–84
[43] Campos E, Cordeiro R, Santos A C, Matos C and Gil M H 2011 Design and characterization of bi-soft segmented polyurethane microparticles for biomedical application *Colloids Surf.* B **88** 477–82
[44] Besteiro M C, Guiomar A J, Gonçalves C A, Bairos V A, De Pinho M N and Gil M H 2010 Characterization and *in vitro* hemocompatibility of bi-soft segment, polycaprolactone-based poly(ester urethane urea) membranes *J. Biomed. Mater. Res.* A **93** 954–64
[45] Niesten M and Gaymans R J 2001 Tensile and elastic properties of segmented copolyetheresteramides with uniform aramid units *Polymer* **42** 6199–207
[46] Levental I, Georges P C and Janmey P A 2007 Soft biological materials and their impact on cell function *Soft Matter* **3** 299–306
[47] Currier Dean P and Nelson Roger M (ed) 1992 *Dynamics of Human Biologic Tissues* (Philadelphia, PA: F.A. Davis)
[48] Okamoto R J, Wagenseil J E, DeLong W R, Peterson S J, Kouchoukos N T and Sundt T M III 2002 Mechanical properties of dilated human ascending aorta *Ann. Biomed. Eng.* **30** 624–35
[49] Qi H J and Boyce M C 2005 Stress–strain behavior of thermoplastic polyurethanes *Mech. Mater.* **37** 817–39
[50] Nosworthy N J, Ho J P Y, Kondyurin A, McKenzie D R and Bilek M M M 2007 The attachment of catalase and poly-L-lysine to plasma immersion ion implantation-treated polyethylene *Acta Biomater.* **3** 695–704
[51] Kondyurin A, Nosworthy N J and Bilek M M M 2008 Attachment of horseradish peroxidase to polytetrafluorethylene (teflon) after plasma immersion ion implantation *Acta Biomater.* **4** 1218–25
[52] Tran C T H, Kondyurin A, Chrzanowski W, Bilek M M M and McKenzie D R 2013 Influence of pH on yeast immobilization on polystyrene surfaces modified by energetic ion bombardment *Colloids Surf.* B **104** 145–52
[53] Kosobrodova E, Kondyurin A, McKenzie D R and Bilek M M M 2013 Kinetics of post-treatment structural transformations of nitrogen plasma ion immersion implanted polystyrene *Nucl. Instrum. Methods Phys. Res.* B **304** 57–66
[54] Wise S G, Waterhouse A, Michael P and Ng M K 2012 Extracellular matrix molecules facilitating vascular biointegration *J. Funct. Biomater.* **3** 569–87
[55] Yin Y B *et al* 2009 Covalent immobilisation of tropoelastin on a plasma deposited interface for enhancement of endothelialisation on metal surfaces *Biomaterials* **30** 1675–81
[56] Laemmli U K 1970 Cleavage of structural proteins during the assembly of the head of bacteriophage T4 *Nature* **227** 680–5
[57] Shlyakhtenko L S, Gall A A, Weimer J J, Hawn D D and Lyubchenko Y L 1999 Atomic force microscopy imaging of DNA covalently immobilized on a functionalized mica substrate *Biophys. J.* **77** 568–76
[58] Hodneland C D, Lee Y S, Min D H and Mrksich M 2002 Selective immobilization of proteins to self-assembled monolayers presenting active site-directed capture ligands *Proc. Natl. Acad. USA* **99** 5048–52
[59] Vandenberg E, Elwing H, Askendal A and Lundström I 1991 Protein immobilization of 3-aminopropyl triethoxy silaneglutaraldehyde surfaces: characterization by detergent washing *J. Colloid Interface Sci.* **143** 327–35
[60] Zhou S 2003 Separation and detection methods for covalent drug–protein adducts *J. Chromatogr.* B **797** 63–90
[61] De S, Sharma R, Trigwell S, Laska B, Ali N, Mazumder M K and Mehta J L 2005 Plasma treatment of polyurethane coating for improving endothelial cell growth and adhesion *J. Biomater. Sci. Polym. Ed.* **16** 973–89
[62] Lee J S, Kaibara M, Iwaki M, Sasabe H, Suzuki Y and Kusakabe M 1993 Selective adhesion and proliferation of cells on ion-implanted polymer domains *Biomaterials* **14** 958–60
[63] Wise S G, Byrom M J, Waterhouse A, Bannon P G, Ng M K and Weiss A S 2011 A multilayered synthetic human elastin/polycaprolactone hybrid vascular graft with tailored mechanical properties *Acta Biomater.* **7** 295–303
[64] Kubow K E, Vukmirovic R, Zhe L, Klotzsch E, Smith M L, Gourdon D, Luna S and Vogel V 2015 Mechanical forces regulate the interactions of fibronectin and collagen I in extracellular matrix *Nat. Commun.* **6** 8026
[65] Maurer L M, Tomasini-Johansson B R and Mosher D F 2010 Emerging roles of fibronectin in thrombosis *Thromb. Res.* **125** 287–91
[66] Hiob M A, Wise S G, Kondyurin A, Waterhouse A, Bilek M M, Ng M K and Weiss A S 2013 The use of plasma-activated covalent attachment of early domains of tropoelastin to enhance vascular compatibility of surfaces *Biomaterials* **34** 7584–91
[67] Hajian H *et al* 2014 Immobilisation of a fibrillin-1 fragment enhances the biocompatibility of PTFE *Colloids Surf.* B **116** 544–52
[68] Reviakine I, Jung F, Braune S, Brash J L, Latour R, Gorbet M and van Oeveren W 2017 Stirred, shaken, or stagnant: what goes on at the blood-biomaterial interface *Blood Rev.* **31** 11–21
[69] Leslie D C *et al* 2014 A bioinspired omniphobic surface coating on medical devices prevents thrombosis and biofouling *Nat. Biotechnol.* **32** 1134–40
[70] Ozdemir Y, Hasirci N and Serbetci K 2002 Oxygen plasma modification of polyurethane membranes *J. Mater. Sci., Mater. Med.* **13** 1147–51
[71] Wilson D J, Rhodes N P and Williams R L 2003 Surface modification of a segmented polyetherurethane using a low-powered gas plasma and its influence on the activation of the coagulation system *Biomaterials* **24** 5069–81
[72] Werner C, Maitz M F and Sperling C 2007 Current strategies towards hemocompatible coatings *J. Mater. Chem.* **17** 3376–84
[73] Nezarati R M, Eifert M B, Dempsey D K and Cosgriff-Hernandez E 2015 Electrospun vascular grafts with improved compliance matching to native vessels *J. Biomed. Mater. Res.* B **103** 313–23
[74] L'Heureux N *et al* 2006 Human tissue-engineered blood vessels for adult arterial revascularization *Nat. Med.* **12** 361–5
[75] Pektok E, Nottelet B, Tille J C, Gurny R, Kalangos A, Moeller M and Walpoth B H 2008 Degradation and healing characteristics of small-diameter poly(epsilon-caprolactone) vascular grafts in the rat systemic arterial circulation *Circulation* **118** 2563–70